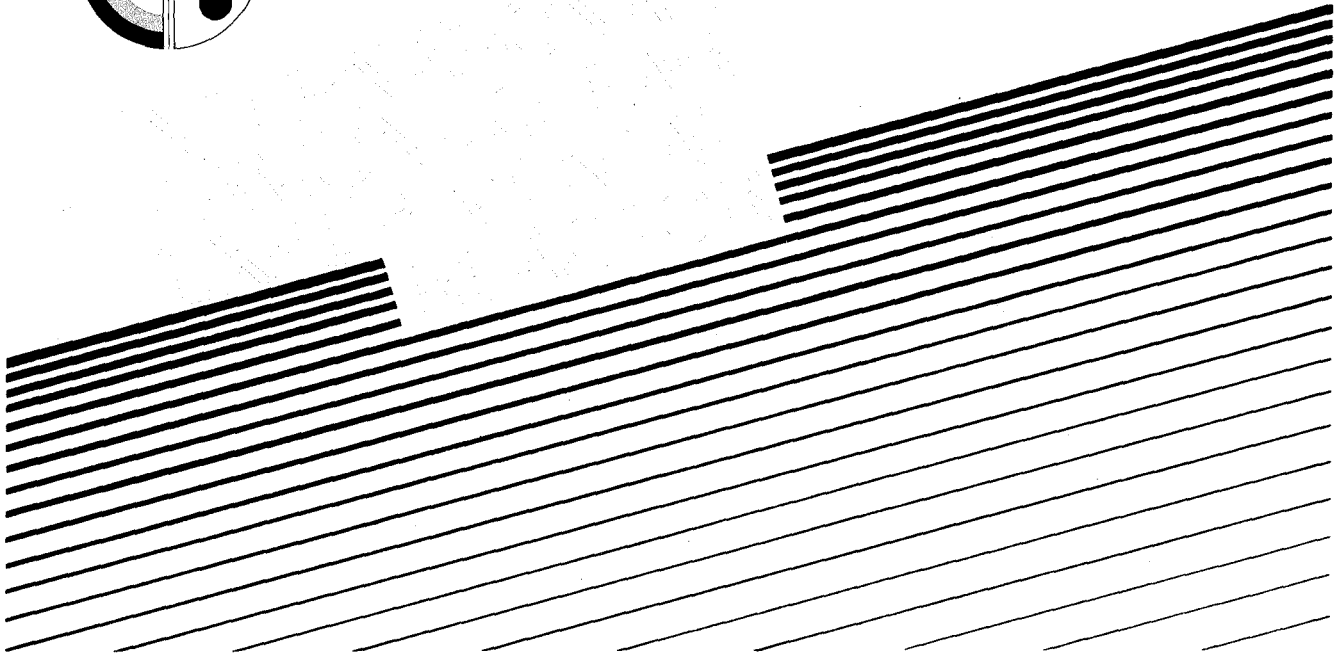




XA0102521-522,
534

ITER EDA DOCUMENTATION SERIES No. 19



TECHNICAL BASIS FOR THE ITER-FEAT OUTLINE DESIGN



INTERNATIONAL ATOMIC ENERGY AGENCY, VIENNA, 2000

32 / 34

**PLEASE BE AWARE THAT
ALL OF THE MISSING PAGES IN THIS DOCUMENT
WERE ORIGINALLY BLANK**

ITER EDA DOCUMENTATION SERIES No. 19

International Thermonuclear Experimental Reactor
(ITER)

Engineering Design Activities
(EDA)

TECHNICAL BASIS FOR THE ITER-FEAT OUTLINE DESIGN

INTERNATIONAL ATOMIC ENERGY AGENCY, VIENNA, 2000

TECHNICAL BASIS FOR THE ITER-FEAT OUTLINE DESIGN

IAEA, VIENNA, 2000
IAEA/ITER EDA/DS/19

© IAEA, 2000

Printed by the IAEA in Austria
November 2000

FOREWORD

Development of nuclear fusion as a practical energy source could provide great benefits. This fact has been widely recognized and fusion research has enjoyed a high level of international co-operation. Since early in its history, the International Atomic Energy Agency has actively promoted the international exchange of fusion information.

In this context, the IAEA responded in 1986 to calls at summit level for expansion of international co-operation in fusion energy development. At the invitation of the Director General there was a series of meetings in Vienna during 1987, at which representatives of the world's four major fusion programmes developed a detailed proposal for co-operation on the International Thermonuclear Experimental Reactor (ITER) Conceptual Design Activities (CDA). The Director General then invited each interested Party to co-operate in the CDA in accordance with the Terms of Reference that had been worked out. All four Parties accepted this invitation.

The ITER CDA, under the auspices of the IAEA, began in April 1988 and were successfully completed in December 1990. The information produced within the CDA has been made available for the ITER Parties and IAEA Member States to use either in their own programmes or as part of an international collaboration.

After completing the CDA, the ITER Parties entered into a series of consultations on how ITER should proceed further, resulting in the signing of the ITER EDA (Engineering Design Activities) Agreement and Protocol 1 on July 21, 1992 in Washington by representatives of the four Parties. The Agreement entered into force upon signature of the Parties, with the EDA conducted under the auspices of the IAEA. Protocol 1 expired on March 21, 1994. On this very day representatives of the ITER Parties signed in Vienna Protocol 2, which entered into force upon signature. This Protocol covers the remaining part of the EDA.

As part of its support of ITER, the IAEA is pleased to publish the documents summarizing the results of the Engineering Design Activities.



XA0102534

CONTENTS

TECHNICAL BASIS FOR THE ITER-FEAT
OUTLINE DESIGN

PROGRESS IN RESOLVING OPEN DESIGN ISSUES
FROM THE OUTLINE DESIGN REPORT

INTERNATIONAL THERMONUCLEAR EXPERIMENTAL REACTOR

**TECHNICAL BASIS
FOR THE
ITER-FEAT
OUTLINE DESIGN**

18th January 2000

OVERALL TABLE OF CONTENTS

- I Overview
 - I.0 Introduction
 - I.1 Plant Design Specification
 - I.2 Main Physics Parameters and Assessment
 - I.3 Design Overview
 - I.4 Cost and Schedule
- II Design Description and Analysis
 - II.1 Magnet System
 - II.2 Vacuum Vessel and In-vessel Components
 - II.3 Cryostat and Thermal Shields
 - II.4 Fuel Cycle
 - II.5 Water Cooling System
 - II.6 Plasma Diagnostic System
 - II.7 Heating and Current Drive System
 - II.8 Site Layout - Buildings - Plant Service Systems
 - II.9 Initial Assembly
 - II.10 Tokamak Maintenance

I OVERVIEW

I.0 Introduction

Six years of joint work under the ITER EDA agreement yielded, by July 1998, a mature design for ITER as presented in the ITER Final Design Report, Cost Review and Safety Analysis (FDR)¹ (the 1998 ITER design), supported by a body of scientific and technological data which both validated that design and established an extensive knowledge base for designs for a next step, reactor-oriented tokamak experiment. The 1998 ITER design fulfilled the overall programmatic objective of ITER - to demonstrate the scientific and technological feasibility of fusion energy for peaceful purposes - and complied with the detailed technical objectives and technical approaches, and cost target adopted by the ITER Parties at the start of the EDA.

When they accepted the FDR report, the ITER Parties, recognising the possibility that they might be unable, for financial reasons, to proceed to the construction of the then foreseen device, established a Special Working Group (SWG)², and charged it with two tasks:

- to *propose technical guidelines for possible changes to the detailed technical objectives and overall technical margins, with a view to establishing option(s) of minimum cost still satisfying the overall programmatic objective of the ITER EDA Agreement, and*
- to *provide information on broader concepts as a basis for its rationale for proposed guidelines, and articulate likely impacts on the development path towards fusion energy.*

In reporting on the first task, the SWG³ proposed revised guidelines for Performance and Testing Requirements, Design Requirements, and Operation Requirements, noting that “*preliminary studies suggest that the direct capital costs of ITER can be reduced significantly by targeting the less demanding performance objectives recommended...*” and expressing the view that “*these less demanding performance objectives will satisfy the overall programmatic objectives of the ITER Agreement even though these performance objectives are necessarily less than those that could be achieved with the present [1998] design.*” Consequently, the ITER Council adopted the recommended revised guidelines and asked the Director “*to continue efforts with high priority toward establishing option(s) of minimum cost aimed at a target of approximately 50% of the direct capital cost of the present design with reduced detailed technical objectives, which would still satisfy the overall programmatic objective of ITER.*”⁴

In addressing the second task, the SWG reviewed and compared two possible strategies for meeting the programmatic objective of demonstrating the scientific and technological feasibility of fusion, based on:

- an ITER-like machine, capable of addressing both scientific and technological issues in an integrated fashion, and
- a number of complementary lower cost experiments each of which would specialise on scientific/technological issues.

With regard to the second strategy, the SWG⁵ found that the complex non-linear interactions between α -particle heating, confinement barriers and pressure and current profile control,

¹ ITER Final Design Report, Cost Review and Safety Analysis, IC-13 ROD Attachment 6

² IC-13 ROD Attachment 10

³ ITER Special Working Group Report to the ITER Council on Task #1 Results, EIC-1 ROD Attachment 1

⁴ EIC-1 ROD 3.1

⁵ SWG report to the ITER Council on Task #2 Result, ITER Meeting 10-3-1999 ROM Attachment 5

and their compatibility with a divertor can be addressed only in an integrated physics/technology experiment such as ITER, capable of providing long burn under conditions in which α -particles are the dominant source of plasma heating. A satisfactory understanding of these physics/plasma/technology interactions is essential to any reactor-oriented fusion development programme. Moreover the SWG expressed the unanimous opinion that the world programme is “*scientifically and technically ready to take the important ITER step.*”

ITER Design Work

Given the instruction to address revised technical guidelines from the SWG Task 1 and against the programmatic background of the SWG Task 2 conclusions, the main features of ITER design activities since July 1998 have therefore been:

- the study of options for cost reductions against the new, reduced, technical objectives by reducing plasma performance and technical margins, using the advances in physics and technology understandings, and tools arising out of the ITER collaboration to date, and
- the studied convergence towards a specific single design, following newly adopted guidelines.

The revised performance specifications adopted by the ITER Council are set out in full in I.1 below. In summary they require:

- to achieve extended burn in inductive operation with $Q \geq 10$, not precluding ignition, with an inductive burn duration between 300 and 500 s, a 14 MeV average neutron wall load $\geq 0.5 \text{ MW/m}^2$, and a neutron fluence $\geq 0.3 \text{ MWa/m}^2$;
- to aim at demonstrating steady-state operation using non-inductive current drive with $Q \geq 5$;
- to use, as far as possible, technical solutions and concepts developed and qualified during the EDA;
- to target about 50% of the direct capital cost of the 1998 ITER design with particular attention devoted to cash flow.

System Studies

As a first approach to identifying designs that might meet the revised objectives, system codes were used which summarise in quantitative form the inter-relationships among the main plasma parameters, physics design constraints and engineering features, and can be combined with costing algorithms.

Such an analysis combines a detailed plasma power balance and boundaries for the plasma operating window, providing the required range of Q for the DT burn, with engineering concepts and limits. Four key parameters — aspect ratio, peak toroidal field, elongation, and burn flux — are intimately linked, allowing options in the systems analysis to be characterised principally by the aspect ratio (A), in addition to the device size, given by the major radius R . Access to the plasma (e.g. for heating systems) and allowable elongation (simultaneously constrained by plasma vertical position and shape control, and by the necessary neutron shield thickness), are functions of aspect ratio.

On this basis the system studies indicated a domain of feasible design space, with aspect ratios in the range 2.5 to 3.5 and a major radius around 6 m, able to meet the reduced

requirements, with a shallow cost minimum across the range. The shallowness of the cost curve and the inevitable approximate nature of the system studies made it clear that no particular choice can be made on the optimal aspect ratio based on estimated costs alone. In addition, there are other important aspects for which the cost or performance impact may not be easily factored into a systems optimization.

Study of Representative Options

In order to provide a basis for rigorous exploration and quantification of the issues and costings, representative options that span an appropriate range of aspect ratio and magnetic field were selected for further elaboration and more comprehensive consideration, as reported to the ITER meeting in Cadarache, March 1999¹.

The development of specific representative options provided a more tangible appreciation of the key issues and a practical framework for the process of convergence was explored and clarified in a joint JCT/Home Team "Concept Improvement Task Force" constituted in April 1999, following the guiding principles:

- to preserve as far as possible physics performance and margins against the revised targets, and the scope for experimental flexibility, within the cost target and relevant engineering constraints;
- to exploit the recent advances in understanding of key physics and engineering issues to be drawn from the results of the ITER voluntary physics programme and the large technology R&D projects;
- to maintain the priority given to safety and environmental characteristics, using the principles, analyses and tools developed through ITER collaboration to date.

The Task Force recommendations, presented to the Programme Directors' Meeting in Grenoble (July 1999)², were instrumental in developing consensus on the criteria and rationale for the selection of major parameters and concepts as the precursor to converging and integrating the various considerations into a single coherent outline design.

Following intensive joint work through an "Integration Task Force", the JCT and Home Teams have been able to converge to a single configuration, referred to as ITER-FEAT, which represents an appropriate balance of the key technical factors and the use of the conservative option for the energy confinement scaling. ITER-FEAT is now the focus for ongoing design development, analysis and optimisation that has evolved to the point of an Outline Design, the technical basis of which is presented in this report.

The report comprises two chapters. The first, "Overview", presents the Plant Design Specifications — the revised technical objectives, the Safety Principles and Environmental Criteria, and the Site Requirements and Site Design Assumptions — which make up the framework of external constraints for the design process. The following sections then outline the key features of the ITER-FEAT design, including main physics parameters and assessment, design overview and preliminary safety assessment, cost and schedule. The second chapter, "Design Description and Analysis" presents in more detail the main components/systems of the ITER-FEAT design. While the proposed designs rely mostly on

¹ Study of options for the Reduced Technical Objectives/Reduced Cost (RTO/RC) ITER, (ROM 1999-03-10 Attachment 8)

² Study of options for the RTO/RC ITER, Director's Progress Report, Grenoble July 1999.

technical solutions qualified for the 1998 ITER design, they require more analysis for adaptation and therefore the level of information provided in this report is commensurate with an outline design.

A valid cost estimate of ITER-FEAT will be obtained only after the engineering details have been worked out to provide specifications for an industrial cost analysis to be undertaken by firms of the Parties in the second half of 2000. Pending such analysis, only a rescaling from the costs of the 1998 ITER design can be done, the result of which slightly exceeds the specified target. However, this simple scaling cannot take into account the expected improvements in the design and in the industrial fabrication process. The latter is now the most important area of activity for reducing costs further towards the target.

With the assistance of the Home Teams, especially through the two Task Forces, the design of ITER-FEAT is now ready to progress, subject to the views of the ITER Council and Parties, into the detailed design process with a view to completing, before the end of the ITER EDA extension, a "Final Design Report" that will provide the technical base for a possible decision by the Parties to commit to the construction and operation of ITER.

I.1 Plant Design Specification

I.1.1	Programmatic Objective	3
I.1.2	Technical Objectives and their Interpretation	3
I.1.2.1	Interpretation	3
I.1.2.2	Scope of the EDA	9
I.1.2.3	Design Principles	10
I.1.3	Safety Principles and Criteria	10
I.1.3.1	Safety Objectives	10
I.1.3.2	Safety Design Principles	11
I.1.3.2.1	Deployment of Fusion's Safety Characteristics	11
I.1.3.2.2	Passive Safety	11
I.1.3.2.3	Defence-in-Depth	11
I.1.3.2.4	Consideration of the Experimental Nature	12
I.1.3.2.5	Review and Assessment	12
I.1.3.3	Safety and Environmental Criteria	13
I.1.3.4	Generic Elements of the Safety Approach	15
I.1.3.4.1	Confinement	15
I.1.3.4.1.1	Confinement of Radioactive and Toxic Materials	16
I.1.3.4.1.2	Protection of the Confinement	16
I.1.3.4.2	Component Classification	17
I.1.3.4.3	Earthquake	17
I.1.3.4.4	Environmental Qualification	19
I.1.3.4.5	Fire	19
I.1.3.4.6	Decommissioning and Waste	19
I.1.3.4.7	Effluents	20
I.1.3.4.8	Radiation Protection	20
I.1.3.4.9	Hazardous Materials	21
I.1.3.4.10	Conventional Hazards	22
I.1.3.4.11	Security and Proliferation	22
I.1.4	Site Requirements & Assumptions	22
	Introduction	22
I	Principles for Site Requirements and Site Design Assumptions	23
II	Site Requirements	24
A.	Land	24
1.	Land Area	24
2.	Geotechnical Characteristics	24
3.	Water Supply	25
4.	Sanitary and Industrial Sewage	25
B.	Heat Sink	25
C.	Energy and Electrical Power	26
D.	Transport and Shipping	26
1.	Maximum Size of Components to be shipped	26
2.	Maximum Weight of Shipments	27
E.	External Hazards and Accident Initiators	27
F.	Infrastructure	28
G.	Regulations and Decommissioning	28
III	Site Design Assumptions	28
A.	Land	28
1.	Land Area	28
2.	Topography	28
3.	Geotechnical Characteristics	29
4.	Hydrological Characteristics	29
5.	Seismic Characteristics	29
6.	Meteorological Characteristics	30
B.	Heat Sink: Water Supply for the Heat Rejection System	30
C.	Energy and Electrical Power	31
1.	Electrical Power Reliability during Operation	31
2.	ITER Plant Pulsed Electrical Supply	31

D.	Transport and Shipping	32
1.	Highway Transport	32
2.	Air Transport	32
3.	Rail and Waterway Transport	32
E.	External Hazards and Accident Initiators	32
1.	External Hazards	32
2.	External (Natural) Accident Initiators	32
F.	Infrastructure	33
1.	Industrial	33
2.	Workforce	34
3.	Socioeconomic Infrastructure	34
G.	Regulations and Decommissioning	35
1.	General Decommissioning	35
2.	ITER Plant "Deactivation" Scope of Work	35
H.	Construction Phase	36
I.1.5.	General Definitions	36
Table I.1.5-1	Remote Handling Classes	36
Table I.1.5-2	Steady-State Power Classes	36
Table I.1.5-3	Loading Conditions for Component Design	37
Table I.1.5-4	Damage Limits in Plant and Component Level	38
Table I.1.5-5	Damage Limits for Loading Conditions	39
Table I.1.5-6	Plant States	39
Table I.1.5-7	General Acronyms	40
I.1.6	ITER Design Documentation	41

I.1.1 Programmatic Objective

According to the ITER EDA Agreement, "the overall programmatic objective of ITER is to demonstrate the scientific and technological feasibility of fusion energy for peaceful purposes."

I.1.2 Technical Objectives and their Interpretation

Following the recommendations of a Special Working Group (SWG) [see verbatim quote from the report in the panel overleaf], the ITER Council asked the Director "to continue efforts with high priority toward establishing, with the assistance of the JCT and Home Teams, option(s) of minimum cost aimed at a target of approximately 50% of the direct capital cost of the [1998 ITER] design with reduced detailed technical objectives, which would still satisfy the overall programmatic objective of ITER. The work should follow the adopted technical guidelines and make the most cost-effective use of existing design solutions and their associated R&D."

I.1.2.1 Interpretation

These technical objectives have been interpreted as follows:

- Maintainability features will be incorporated into the design in such a way as to achieve the mission reliability, operational availability, and scheduled maintenance requirements. In particular, remote handling (RH) features will be designed and qualified that permit timely insertion and removal of in-vessel components, blanket test modules and other test articles.
- The ITER design shall incorporate features that permit testing to:
 - demonstrate the reliability of nuclear components;
 - furnish data for comparing candidate concepts for nuclear components and to provide a basis of extrapolation;
 - demonstrate tritium breeding;
 - provide fusion materials testing data.
- The existing physics database will require:
 - H-mode scaling law as recommended by the Confinement Expert Group;
 - normalized beta, $\beta_N = \beta_a B/I < 2.5$;
 - normalized density, $n/n_{GW} = n\pi a^2/I < 1.0$;
 - safety factor, $q_{95} \sim 3$;
 - $Z_{eff} \leq 2.0$;
 - a well controlled, divertor plasma configuration.

Plasma Performance

The device should:

- *achieve extended burn in inductively driven plasmas with the ratio of fusion power to auxiliary heating power of at least 10 for a range of operating scenarios and with a duration sufficient to achieve stationary conditions on the timescales characteristic of plasma processes.*
- *aim at demonstrating steady-state operation using non-inductive current drive with the ratio of fusion power to input power for current drive of at least 5.*

In addition, the possibility of controlled ignition should not be precluded.

Engineering Performance and Testing

The device should:

- *demonstrate the availability and integration of technologies essential for a fusion reactor (such as superconducting magnets and remote maintenance);*
- *test components for a future reactor (such as systems to exhaust power and particles from the plasma);*
- *Test tritium breeding module concepts that would lead in a future reactor to tritium self-sufficiency, the extraction of high grade heat, and electricity production.*

Design Requirements

- *Engineering choices and design solutions should be adopted which implement the above performance requirements and make maximum appropriate use of existing R&D database (technology and physics) developed for ITER.*
- *The choice of machine parameters should be consistent with margins that give confidence in achieving the required plasma and engineering performance in accordance with physics design rules documented and agreed upon by the ITER Physics Expert Groups.*
- *The design should be capable of supporting advanced modes of plasma operation under investigation in existing experiments, and should permit a wide operating parameter space to allow for optimising plasma performance.*
- *The design should be confirmed by the scientific and technological database available at the end of the EDA.*
- *In order to satisfy the above plasma performance requirements an inductive flat-top capability during burn of 300 to 500 s, under nominal operating conditions, should be provided.*
- *In order to limit the fatigue of components, operation should be limited to a few 10s of thousands of pulses*
- *In view of the goal of demonstrating steady-state operation using non-inductive current drive in reactor-relevant regimes, the machine design should be able to support equilibria with high bootstrap current fraction and plasma heating dominated by alpha particles.*
- *To carry out nuclear and high heat flux component testing relevant to a future fusion reactor, the engineering requirements are*
 Average neutron flux $\geq 0.5 \text{ MW/m}^2$
 Average neutron fluence $\geq 0.3 \text{ MWa/m}^2$
- *The option for later installation of a tritium breeding blanket on the outboard of the device should not be precluded.*
- *The engineering design choices should be made with the objective of achieving the minimum cost device that meets all the stated requirements.*

Operation Requirements

The operation should address the issues of burning plasma, steady-state operation and improved modes of confinement, and testing of blanket modules.

- *Burning plasma experiments will address confinement, stability, exhaust of helium ash, and impurity control in plasmas dominated by alpha particle heating.*
- *Steady-state experiments will address issues of non-inductive current drive and other means for profile and burn control and for achieving improved modes of confinement and stability.*
- *Operating modes should be determined having sufficient reliability for nuclear testing. Provision should be made for low-fluence functional tests of blanket modules to be conducted early in the experimental programme. Higher fluence nuclear tests will be mainly dedicated to DEMO-relevant blanket modules in the above flux and fluence conditions.*
- *In order to execute this program, the device is anticipated to operate over an approximately 20 year period. Planning for operation must provide for an adequate tritium supply. It is assumed that there will be an adequate supply from external sources throughout the operational life.*

- The mechanical design of the device shall withstand the expected temperatures, pressures, electromagnetic fields, chemical environment, and radiation environment under all projected operating conditions and assumed accident conditions.
- Prior to site selection, structural evaluation shall be in accordance with specific codes and standards which are agreed among the three Parties. If no such codes and standards exist, standards or guidelines established by the JCT shall be surrogated. The design must not preclude readily achievable modifications to incorporate alternate codes and standards, which may be required by the Host Party.
- The design shall facilitate decommissioning, and reduce occupational exposures, by:
 - use of modular components for easy dismantling;
 - segregating radioactive systems or components;
 - designing to avoid contamination or to allow easy decontamination;
 - selection of construction materials to reduce activation products in materials subject to irradiation.
- ITER shall have a waste management program that minimises waste. The treatment systems for radioactive wastes generated in ITER shall be designed to minimize dispersion of radioactive materials during all stages of handling. ITER systems shall be designed to package radioactive waste in accordance with the requirements of the Party that will ship, handle and intern the waste, so that no additional handling or exposure is required by re-packaging.
- ITER operation is divided into four phases. Before achieving full DT operation, which itself is split into two phases, ITER is expected to go through two operation phases, a hydrogen phase and a deuterium phase, for commissioning of the entire plant.
- The hydrogen phase is a non-nuclear phase, mainly planned for full commissioning of the tokamak system in a non-nuclear environment where full remote handling is not required.

The discharge scenario of the full DT phase reference operation such as plasma current initiation, current ramp-up, formation of a divertor configuration and current ramp-down can be developed or simulated in this phase. The semi-detached divertor operation in DT plasma can be also checked since the peak heat flux onto the divertor target will be of the same order of magnitude as for the full DT phase.

Characteristics of electromagnetic loads due to disruptions or vertical displacement events, and heat loads due to runaway electrons, will be basically the same as those of the DT phase. Studies of the design-basis physics will significantly reduce the uncertainties of the full DT operation. Mitigation of severe disruptions and VDEs or better control of these events in later phases will become possible, leading to a more efficient DT operational phase.

However, some important technical issues will not be fully tested in this phase because of smaller plasma thermal energy content and lack of neutrons and energetic

alpha-particles. For example, evaporation of the divertor target surface expected at the thermal quench phase of disruption, effects of neutron irradiation of the in-vessel materials, and alpha-particle heating of the plasma, will not be tested.

The following studies can be carried out to prepare for the full DT phase:

- (1) accessibility of the H-mode and other improved confinement modes (confirmation of the adequacy of the heating power);
- (2) verification of operational compatibility with plasma density close to the Greenwald limit, beta limit, $q_{95} \sim 3$, semi-detached divertor, low impurity level, and sufficiently good confinement, which is required in the reference high Q operation in the full DT phase; studies of high β_N operation by stabilising neoclassical modes with ECCD etc., high plasma density operation by optimized fuelling etc., and further improved confinement modes; assessment of the necessity to improve these capabilities;
- (3) steady-state operation with a negative or weak central magnetic shear and an internal transport barrier; improvement of the beta limit by stabilising kink modes and resistive wall modes; assessment of the necessity to improve current drive capabilities and stability control.

If the hydrogen phase is substantial, the initial construction cost of ITER could be significantly reduced by delaying the installation of some of the nuclear-related facilities. The actual length of the hydrogen operation phase will depend on the merit of this phase with regard to its impact on the later full DT operation. Operation in this phase is subject to several uncertainties¹: how high the magnetic field can be without the plasma density exceeding the Greenwald limit, and how high the plasma density needs to be to access the H-mode, avoiding locked modes and beam shine-through, and ensuring adequate divertor operation.

If the H-mode threshold power is higher than expected, it may be necessary to operate with the magnetic field less than the half of the full field and with the safety factor less than 3, i.e., ~ 2.6 , to stretch the Greenwald plasma density limit. Additional installation of the heating system may be needed to solve the problem.

- In the deuterium phase, neutrons will be produced, and tritium will be produced from DD reactions. Part of this tritium will then be burnt in DT reactions. Although the fusion power is low, the activation level inside the vacuum vessel will not allow human access after several deuterium discharges with powerful heating. However, the capacity of the heat transfer system (except for the divertor and heating devices) could be minimal, and demand for the tritium processing system would be very small.

Characteristics of deuterium plasma behaviour are very similar to those of DT plasma except for the amount of alpha heating. Therefore, the reference DT operational scenarios, i.e., high Q , inductive operation and non-inductive steady-state operation, can be simulated in this phase. Since tritium already exists in the plasma, addition of

¹ G A0 RI 1 99-02-12 W0.2, Study of RTO/RC ITER Options, section I.3.2.2.1

a small amount of tritium from an external source will not significantly change the activation level of the machine. Fusion power production at a significant power level for a short period of time without fully implementing cooling and tritium-recycle systems which would be required in the subsequent full DT phase could therefore also be demonstrated. By using limited amounts of tritium in a deuterium plasma, the integrated commissioning of the device is possible. In particular, the shielding performance can be checked. The major achievements in the D phase should be as follows:

- replacement of H by D, clean D plasma;
 - confirmation of L-H threshold power and confinement scalings;
 - establishment of a reference plasma (current, heating power, density, detached/semi-detached divertor, ELMy H-mode, etc.);
 - particle control (fuel/ash/impurity/fuelling/pumping);
 - steady-state operation with full heating power;
 - finalisation of nuclear commissioning with a limited amount of tritium;
 - demonstration of high fusion power comparable to the nominal value for the full DT burn, for a short time.
- Following these two phases the ITER plant will have been almost fully commissioned. Most of the plasma operational and control techniques necessary to achieve the technical goals of the DT phase will have been mastered by then. DT operation can be divided into two phases predominantly oriented towards physics and engineering goals respectively

During the first phase the fusion power and burn pulse length will be gradually increased until the inductive operational goal is reached. Non-inductive, steady-state operation will also be developed. The DEMO-relevant test blanket modules will also be tested whenever significant neutron fluxes are available, and a reference mode of operation for that testing will be established.

The second phase of full DT operation will emphasise improvement of the overall performance and the testing of components and materials with higher neutron fluences. This phase should address the issues of higher availability of operation and further improved modes of plasma operation. Implementation of this phase should be decided following a review of the results from the preceding three operational phases and assessment of the merits and priorities of programmatic proposals.

- A decision on incorporating tritium breeding during the course of the second DT phase will be decided on the basis of the availability of tritium from external sources, the results of breeder blanket testing, and experience with plasma and machine performance. Such a decision will depend on the R&D completed during the first phase indicating the viability of a tritium breeding blanket, almost certainly within the same space envelope as the shielding blanket, able to maintain a low tritium inventory with bakeout at 240°C.
- In all operating phases, ITER shall provide facilities for the receipt, storage, processing /recycling and utilisation of hydrogen isotopes for the tokamak. Apart from the H phase, this will include tritium, and the recycling capability shall include the possibility to recover tritium from plasma-facing materials.

- ITER shall have a duty factor¹ capability of about 25%.
- Comprehensive plasma diagnostic information shall allow attainment and monitoring of reliable modes of operation. In the final part of the twenty year operation, pulse reliability² shall be greater than 90%. In the final part of the twenty year operation, ITER will also be required to operate at very high availability³ for periods lasting 1-2 weeks.
- The following principles shall be adhered to in the design:
 - simplicity;
 - fail-safe and fault-tolerant design;
 - redundancy;
 - diversity;
 - independence;
 - testability.
- ITER will follow a “staged” approach to maximize the opportunities for deferring cost and reducing the peak demand for funding in any single year. This will also allow early experimental results to better quantify the technical requirements of successively installed equipment. In particular, the ability to study steady-state operation will, if necessary, be provided through additional investment.
- Delivery of components, systems and structures will be just in time to fulfil the needs of the experimental programme subject to the following limitations:
 - the initial design and construction must anticipate the requirements for all stages and include those features which are impractical or extremely costly to add at a later time;
 - deferral of a component, system or structure shall not increase the cost of other components, systems or structures greater than the amount of the cost saved by deferral.

¹ the ratio of plasma burn to total pulse length (including both electrical-on and dwell times)

² defined as the probability of:

- the necessary subset of data for achieving the goal of a given pulse being successfully acquired and archived, and
- no failure during the pulse which would preclude the initiation of the next pulse.

³ the ratio of the product of the actual number of pulses and their average duration in an operation plan period in which the device is operational at its acceptable or planned performance level, to the product of the number of pulses and their average duration which could be achieved during that run period in the absence of component failures and software errors.

I.1.2.2 Scope of the EDA

The scope of the EDA is described in the adjacent panel from the ITER EDA Agreement.

The Parties shall conduct the following EDA:

- (a) *to establish the engineering design of ITER including*
 - (i) *a complete description of the tokamak and its auxiliary systems and facilities,*
 - (ii) *detailed designs with specifications, calculations and drawings of the components of ITER with specific regard to their interfaces,*
 - (iii) *a planning schedule for the various stages of supply, construction, assembly, tests and commissioning of ITER together with corresponding plan for human and financial resource requirements,*
 - (iv) *specifications allowing [timely] calls for tender for the supply of items needed for the start-up of the construction of ITER if and when so decided;*
- (b) *to establish the site requirements for ITER, and perform the necessary safety, environmental and economic analyses;*
- (c) *to establish both the proposed program and the cost, manpower and schedule estimates for the operation, exploitation and decommissioning of ITER;*
- (d) *to carry out validating research and development work required for performing the activities described above, including development, manufacturing and testing of scalable models to ensure engineering feasibility;*
- (e) *to develop proposals on approaches to joint implementation for decisions by the Parties on future construction, operation, exploitation and decommissioning of ITER.*

For the EDA extension this is interpreted as in the following.

- (a) (ii) shall apply only for components critical to the construction decision during the EDA. For the remainder, the design should be scoped to ensure that it can be developed in time within the constraints produced by the detailed design of the critical components.
- Site specific activities shall include design adaptations and their cost estimates, and safety analysis and technical support for the preparation of license applications.
- ITER shall maintain a current estimate of the construction costs, as design progresses. The JCT shall be responsible for developing adaptations of the design and cost estimates to candidate sites which the Parties have proposed. A final cost estimate may be developed for the site selected with the assistance of the site host.
- Project schedules shall be developed by the JCT relevant to the ITER Project and siting decisions reached by the Parties.
- A cost estimate and schedule for deferred components, systems or structures shall be developed so that they may be procured, constructed and commissioned prior to the stage in which they are required.
- The JCT shall maintain current estimates of the R&D costs as the design progresses and shall justify deviations from the construction costs given above.

I.1.2.3 Design Principles

Based on all the foregoing, the ITER design philosophy adopted during the EDA is based on the following design principles:

- optimise the design for the objectives of the first phase of active operation and ensure flexibility and capability to accommodate the goals and constraints of following phases;
- within the given resources, maximise the development of the basic tokamak machine and defer that of external systems that can be changed or added later;
- use advanced but proven technologies, but keep the flexibility to introduce new technologies when proven;
- avoid irrevocable choices today if they may be made later when better information is available;
- for systems to be developed and designed later, reserve the maximum space available;
- avoid on-site production and testing as much as possible;
- never compromise safety of the machine operation to improve performance or decrease cost;
- plasma facing components should be excluded from safety functions;
- emphasise passive safety in the design.

I.1.3 Safety Principles and Criteria

This section provides:

- the safety objectives, principles and criteria that are the high level requirements which should be maintained independently from any design,
- generic elements for the implementation of the safety approach so that each Party can describe how the implementation will satisfy national laws and regulations; or possibly so that the ITER Parties can agree on a common safety approach for an international realisation of 'a first of a kind' machine like ITER.

This section deals with the safety and environmental issues from the design point of view. Safety requirements for the operation phase will be developed at a later stage in the project.

In the following, the word 'shall' is used to denote a firm requirement, the word 'should' to denote a desirable option and the word 'may' to denote permission, i.e. neither a requirement nor a desirable option.

I.1.3.1 Safety Objectives

A main goal of ITER is to demonstrate from the viewpoint of safety the attractiveness of fusion and thereby provide a good precedent for the safety of future fusion power reactors. However, it is necessary to account for the experimental nature of the ITER facility, the related design and material choices, and the fact that not all of them are suited for future fusion power reactors. To accomplish this, ITER safety needs to address the full range of hazards and minimise exposure to these, and to permit siting by any Party.

The following safety objectives are taken into account:

- **General safety:** to protect individuals, society and the environment; to ensure in normal operation that exposure to hazards within the premises and due to any release of hazardous material from the premises is controlled and kept below prescribed limits; to prevent accidents with high confidence, to ensure that the consequences of more frequent events, if any, are minor; to ensure that the consequences of accidents are bounded and the likelihood is small.
- **No evacuation:** to demonstrate that the favourable safety characteristics of fusion and appropriate safety approaches limit the hazards from internal accidents such that there is, for some countries, technical justification for not needing evacuation of the public.
- **Waste reduction:** to reduce radioactive waste hazards and volumes.

ITER shall be developed in such a way that it can be sited by any participant in the ITER EDA Agreement with minor design modifications.

I.1.3.2 Safety Design Principles

The following principles shall be considered in the safety approach. These safety principles not only provide direction to guide the design, but also include on-going, independent review and assessment to ensure the design will meet safety objectives.

I.1.3.2.1 Deployment of Fusion's Safety Characteristics

The safety approach shall be driven by a deployment of fusion's favourable safety characteristics to the maximum extent feasible. Relevant characteristics are:

- the fuel inventory in the plasma is always below 1 g so that the fusion energy content is small;
- plasma burn is terminated inherently when fuelling is stopped due to the limited confinement by the plasma of energy and particles;
- plasma burn is self-limiting with regard to power excursions;
- plasma burn is passively terminated by the ingress of impurities under abnormal conditions (e.g. by evaporation or gas release or by coolant leakage);
- the energy and power densities are low;
- the energy inventories are relatively low;
- large heat transfer surfaces and of big masses exist and are available as heat sinks;
- confinement barriers exist and must be leak-tight for operational reasons.

I.1.3.2.2 Passive Safety

Passive safety shall be given special attention. It is based on natural laws, properties of materials, and internally stored energy. Passive features, in particular, help assure ultimate safety margins.

I.1.3.2.3 Defence-in-Depth

The ITER safety approach incorporates 'defence-in-depth', the recognised basis for safety technology: All activities are subject to overlapping levels of safety provisions so that a failure at one level would be compensated by other provisions.

Three sequential levels of defence are established which, in priority order, are 'prevention', 'protection', and 'mitigation'. Defence-in-depth, is repeated at each of the three fundamental levels. All elements of defence-in-depth must be available at all times during normal power operation and appropriate elements must be available when power is off (shutdown, maintenance, repair, decommissioning). The existence of several but not all elements is no justification for start or continuation of power operation.

Prevention

Accident prevention shall be the first priority. Prevention is implemented, for example, by minimisation of hazardous inventories, provision of primary confinement, use of passive safety features, conservative design, quality assurance and surveillance, well established practices ('safety culture'), and qualified staff.

Protection

Protection is implemented, for example, by control of the operation including the detection of faults, response to any indication of failures, and redundant and diverse engineered safety systems.

Mitigation

Mitigation is provided, for example, by adding confinement barriers to the primary one, and protection systems to prevent the evolution of failures and human errors into accidents.

I.1.3.2.4 Consideration of the Experimental Nature

A robust safety envelope shall be provided to enable flexible experimental usage. Since ITER is the first experimental fusion device on a reactor scale, it will be equipped with a number of 'experimental components', in particular inside the vacuum vessel. In view of uncertain plasma physics and lack of operational experience, the experimental components will be designed considering the expected loads from plasma transients so as to reduce the demands on systems which are required for safety. In particular, a safety function will not be assigned to experimental components.

Nevertheless, faults in experimental components that can affect safety will be subject to safety assessments. On this basis, related measures will be incorporated in the design as appropriate.

The experimental programs will be developed in such a way that design modifications will take account of experience from preceding operations and will stay within the safety envelope of the design.

I.1.3.2.5 Review and Assessment

Safety assessments shall be an integral part of the design process and results will be available to assist in the preparation of safety documentation for regulatory approval. These analyses shall comprise normal operation, all categories of accidents, and waste management and disposal.

An assessment shall be made of potential effluents from the ITER site throughout its lifetime. All effluents (airborne and waterborne) shall be identified and their quantity and

characteristics estimated. Effluent assessment shall address normal operation and maintenance (Category I) and shall include, as a minimum, radioactive materials, toxic materials, direct radiation, magnetic fields, and thermal emissions. Releases of radioactive materials shall be assessed as part of a demonstration that such releases are ALARA.

A plant safety assessment shall be made, including a systematic review of the ways in which components might fail and identifying the consequences of such failures. The objective of the plant level sequence analysis is to support the choice of the sequences analysed in the reference accident analysis and in the ultimate safety margins analysis, and to demonstrate, for a comprehensive set of event sequences, that the consequences of each sequence will be below the release limits established for the category to which the sequence belongs. Further, the plant level analysis supports the Safety Importance Classification of the components (see Table I.1.3-3). To approach completeness as far as possible, a comprehensive identification procedure shall be applied: Postulated initiating events (PIEs) should be identified by a systematic 'bottom-up' method like the Failure Modes and Effects Analysis (FMEA) as well as by a 'top-down' approach like Global Event Trees or Master Logic Diagrams.

A combined deterministic and probabilistic approach may be used to develop a set of 'reference accidents' (limited in number) which shall encompass the entire spectrum of events in Category II, III and IV (see Table I.1.3-1). Analysis of reference accidents shall also address loss of power and aggravating failures in safety systems.

Hypothetical sequences should be used to investigate the ultimate safety margins. The intent is to demonstrate the robustness of the safety case with regard to the project's objectives and radiological requirements.

An assessment of waste arising during operations and decommissioning shall be made to provide a detailed characterisation.

I.1.3.3 Safety and Environmental Criteria

Regulatory approval is required before the construction of ITER and preparations for the future application for approval shall be included in the design process. Before site selection, the design will follow international recommendations, in particular technology-independent ones. Limits on doses to the public and staff from radioactivity and related releases shall be met by design, construction, operation and decommissioning. These project limits shall follow the recommendations by the ICRP and the IAEA. Following site selection, Host Country regulations will apply.

An important element of the safety analyses is the assessment of consequences. Doses and releases to the public shall be limited to the guidelines established by the project in Table I.1.3-1. In addition, there should be margins between calculated values and the project guidelines.

Using IAEA recommendations, the no-evacuation objective implies the need to limit doses to the local population to approximately 50 mSv/event early dose.

Table I.1.3-1
Event Classification and Project Guidelines for Doses to the Public

EVENT SEQUENCE CATEGORY	I OPERATIONAL EVENTS	II LIKELY SEQUENCES	III UNLIKELY SEQUENCES	IV EXTREMELY UNLIKELY SEQUENCES
Category Description	Events and plant conditions planned and required for ITER normal operation, including some faults and events which can occur as a result of the ITER experimental nature.	Event sequences not planned but likely to occur one or more times during the life of the plant but not including Category I events.	Event sequences not likely to occur during the life of the plant.	Event sequences not likely to occur during the life of the plant with a very large margin.
Typical Annual Expected Occurrence Rate	List of operational events to be defined explicitly.	$f > \sim 10^{-2}/a$	$10^{-2}/a > f > 10^{-4}/a$	$10^{-4}/a > f > 10^{-6}/a$
ITER Objectives	ALARA.	Avoid releases.	Avoid any potential need for any public counter-measures.	Avoid potential for public evacuation.
Meet appropriate national criteria.				
Dose Guidelines (a)	0.1 mSv/a chronic dose (all pathways); <u>and</u> ALARA.	0.1 mSv/event chronic dose (without ingestion) <u>and</u> 0.1 mSv/a chronic dose integrated over all Category II events; and (b).	5 mSv/event chronic dose (without ingestion).	5-50 mSv /event dose (c).
Release Guideline for HTO (tritiated water) (d) (e)				
Elevated (100 m)	-1 g T/a (f)	1.5 g T/event	80 g T/event	150 g T/event
Ground level	0.1 g/a (f)	0.1 g T/event	5 g T/event	10 g T/event
Release Guideline for Divertor-First Wall Activation Products (AP) (d)				
Elevated (100 m)	10 g metal/a (f)	5 g metal /event	300 g metal/event	2500 g metal/event
Ground level	1 g metal/a (f)	1 g metal/event	50 g metal/event	300 g metal/event
Release Guideline for Activated Corrosion Products (ACP) (d)				
Elevated (100 m)	50 g/a (f)	5 g/event	300 g/event	30 000 g/event
Ground level	5 g/a (f)	1 g/event	50 g/event	2000 g/event
<p>(a) The type of dose is chosen to be an appropriate technical measure corresponding to the ITER objectives for that Category. Where dose criteria are "per year," average annual weather is assumed. Where dose criteria are "per event", 'conservative weather' is used.</p> <p>(b) The summation of Category I and Category II events must be ≤ 0.2 mSv/a.</p> <p>(c) The range for Category IV results from significant variations among how national dose criteria are expressed, e.g., the type of dose. For design purposes, an appropriate dose limit is used to derive release limits that will meet national dose criteria. 10 mSv/event early dose is used for this purpose.</p> <p>(d) Release guidelines have been conservatively set to ensure dose guidelines will not be exceeded with margins to accommodate actual site conditions and host country dose calculation procedures.</p> <p>(e) For tritium in the HT form, use 10 times the values shown here.</p> <p>(f) Category I release guideline have been conservatively set at $\sim 1/10^{\text{th}}$ allowable release to ensure that summation over all exposure pathways and releases will not exceed the Category I dose guideline, and as part of ALARA.</p>				

ITER shall comply with the ICRP recommendations regarding public and occupational exposures (see Table I.1.3-2 for guidelines established by the project). The radiation protection practices shall be consistent with the IAEA and ICRP recommendations and should make use of best practices. In particular, efforts shall be made to design such that exposures during operation, maintenance, modification and decommissioning are ALARA, economic and social factors being taken into account.

Activated materials are considered long-term waste if criteria for unconditional clearance following IAEA recommendations are not met after a decay period of 100 years.

Table I.1.3-2
Limits and Project Guidelines for Doses from Occupational Exposure

Dose Limits	
ICRP recommended limit for annual individual worker doses	50 mSv 20 mSv averaged over 5 years
Project Guidelines	
Project guideline for annual individual worker doses	5 mSv
Project guideline for individual dose per shift	0.5 mSv/shift
Collective annual worker dose target averaged over life time of plant	0.5 man-Sv
ALARA threshold for dose rates	100 μ Sv/h
ALARA threshold for collective worker dose to operate and maintain a system for a year	30 pers-mSv
ALARA threshold for collective worker dose for a task performed less often than annually	30 pers-mSv
(a) An 'ALARA threshold' is a level that triggers a formal ALARA assessment during the ITER design phase. This does not imply that ALARA reviews will not be performed when the design is below the thresholds.	

I.1.3.4 Generic Elements of the Safety Approach

There can be a number of acceptable safety approaches to meet safety objectives. The following sections provide generic elements of a safety approach implementing the ITER safety principles.

The safety approach shall cover both public and occupational safety for both normal operation and accidents. The approach shall use a combination of design features and administrative controls to protect the site staff and the public from hazards and to control releases of radionuclides and hazardous materials from the facility. The level of protection required depends on the level of the hazard present in the facility.

I.1.3.4.1 Confinement

Confinement of radioactive and toxic materials is a fundamental safety requirement. Confinement is defined here as all types of physical and functional barriers which provide protection against the spread and release of radioactive material. Containment is a special type of confinement which can accommodate significant pressurisation. Releases would most significantly occur upon breach of barriers, hence confinement shall be protected by appropriate measures such as heat removal, control of energies and monitoring.

1.1.3.4.1.1 Confinement of Radioactive and Toxic Materials

The barriers shall be of sufficient number, strength and performance (in terms of leak tightness, retention factors, reliability, etc.) so that releases of radioactive and/or toxic materials during normal operation and for accidents do not exceed the project release guidelines listed in Table I.1.3-1.

The design of confinement barriers may be graded. Significant, vulnerable, radioactive and/or toxic inventories will require highly reliable barriers, whereas moderate and small inventories will require less reliable barriers.

The design basis for the confinement barriers shall take into account all events, ranging from the initiating events to consequential accidents, loads and environmental conditions as identified by the safety assessments.

The design of confinement barriers shall implement the principles of redundancy, diversity and independence. Specifically, in the case of multiple barriers, failure of one barrier shall not result in the failure of another barrier.

After pressurisation due to an accident, confinement volumes shall be returned to below atmospheric pressure within a specified period following the accident and a filtered, monitored pathway shall be provided to maintain the pressure inside the volume to below atmospheric pressure.

Consideration should also be given to the mitigation of consequences from confinement degradation by accidents beyond Category I through IV, i.e. by hypothetical sequences.

1.1.3.4.1.2 Protection of the Confinement

Heat removal

To protect the confinement against phenomena, such as breach, evaporation and melting, the design shall provide reliable means to remove the heat generated during normal operation as well as the decay heat of activation products and the heat from potential chemical reactions. Their reliability shall be commensurate with the consequences from losses of decay heat removal and the subsequent impact on the confinement. Passive means for decay heat removal shall be provided as a last resort.

Control of coolant enthalpy

To ensure confinement is not threatened, the design shall provide means to accommodate the accidental release of coolants used, in particular, for in-vessel components, vacuum vessel and superconducting magnets. For the magnets, due consideration shall be given to the fact that cryogenic fluids can absorb large amounts of energy from the ambient so that phenomena such as underpressure and overpressure can be generated.

Control of chemical energy

The design shall be such that chemical energy inventories are controlled to avoid energy and pressurisation threats to confinement. ITER shall be designed, in particular, to minimise hydrogen production during accidents, to avoid explosive mixtures of hydrogen with air/oxygen and to minimise the release of chemical energy as heat. Excessive chemical reactions between beryllium and steam shall be limited by avoiding elevated temperatures.

Control of magnetic energy

The magnet systems shall be designed in such a way that failures in the systems will not damage safety functions by mechanical impact, pressure loads or electric arcs leading to a release of radioactivity exceeding the project guidelines specified in Table I.1.3-1.

Monitoring and control

The design shall provide means for monitoring and controlling radioactive or toxic releases from ITER as well as dose rates to the public around the site and in areas accessible to site staff.

The design shall provide systems for assuring reliable information on all operational events and accidents, and for monitoring the performance of the confinement and its protection during accidents.

I.1.3.4.2 Component Classification

The importance to safety of structures, systems and components (termed ‘components’ in the following) is not uniform. Therefore, graded requirements should be used in the safety design. This is achieved by classifying components according to their importance to safety.

A Safety Importance Classification (SIC) may be used for determining which codes and standards to apply, levels of quality assurance, inspection requirements, etc. Each component is classified according to its importance to safety as in Table I.1.3-3. A design objective is to have no SIC-1 components in ITER.

The quality level required for components should be commensurate with the SIC and the required reliability.

The SIC of components shall be determined by using a plant level analysis (I.1.3.2.4) that establishes for each component the functions to which the component contributes or has an effect, and assesses how the component failure would influence the functions. If a component is associated with more than one function, the procedure shall be applied for each function and the highest SIC obtained for the component shall be assigned.

I.1.3.4.3 Earthquake

Components required to perform a safety function shall be designed such that the capabilities are maintained during or after a design basis earthquake.

Before the ITER site is decided, an assumption for design and safety analysis purposes is to consider three levels (SL-2, SL-1, SL-0) of ground motion. These are specified in I.1.4.III.A.5. SIC-1, -2, and -3 components shall be divided into three seismic classes (2A, 2B, 1) in terms of their importance to safety in the event of an earthquake (see Table I.1.3-4). Components with the most important safety role will be designed with adequate structural margins against the SL-2 earthquake by applying graded performance requirements, whereas the components with a less important safety role will be designed to withstand the more frequent SL-1 earthquake without damage.

The assignment of a component to seismic classes (2A, 2B, 1) shall be based on functional requirements to assure safety. According to their different functions, parts of the same system may belong to different classes. Leak-tightness, degree of damage (crack, tear, etc.), mechanical or electrical functional capability, maximum displacement, degree of permanent distortion and preservation of geometrical dimensions are examples of aspects which shall be considered.

Table I.1.3-3
Safety Importance Classification

Safety Importance Class	Classification Rules
SIC-1	Components are classified in SIC-1 if the following rule applies: Rule 1: The component implements a safety function ^a that is needed in normal operation or after occurrence of Category II (Likely) events and the failure of that safety function under such conditions leads to a release that exceeds the Category IV (Extremely Unlikely) limits.
SIC-2	Components are classified in SIC-2 if the following rule applies: Rule 2: The component implements a safety function ^a that is needed after occurrence of Category III (Unlikely) or Category IV (Extremely Unlikely) events and the failure of that safety function under such conditions leads to a release that exceeds the Category IV (Extremely Unlikely) limits. If the same safety function can be accomplished by another independent system, different from the one the component belongs to, then the component may be declassified to SIC-3.
SIC-3	Components are classified in SIC-3 if any of the following rules apply: Rule 3-1: The component implements a safety function ^a whose failure could lead to a release that exceeds the Category II (Likely) limits but is lower than the Category IV (Extremely Unlikely) limits. Rule 3-2: The component implements a safety function needed to protect the facility personnel from radiological hazards. ^b Rule 3-3: The component is needed for radiological monitoring of accidental releases to the environment when they exceed the Category II limits.
SIC-4	Not safety classified
Notes: ^a Auxiliary services that provide essential support to a SIC component (such as cooling, lubrication, and energy supply) forming part of a system important to safety shall be regarded as part of that component. Their reliability, redundancy, diversity, independence, and provision of features for isolation and for testing of functional capability shall be commensurate with the reliability of the SIC component that is supported. Other non-essential support services shall be designed so that a failure does not degrade the safety function below an acceptable level. ^b The component implements a safety function whose malfunction could lead to an unplanned occupational exposure in excess of the project guideline for exposure per year (I.1.3.3).	

When, as the result of an earthquake, the collapse, falling, dislodgement or any other spatial response of a component is expected to occur and could jeopardise the functioning of components in a higher category:

- such components shall be classified in the same category as the endangered components, or
- for the respective earthquakes, the continued safety function of the lower class components shall be demonstrated, or
- the endangered components shall be suitably protected so they are not jeopardised.

As a conservative measure, it is recommended that Seismic Classes 2A and 2B include those SIC-2 components which are designed to mitigate the consequences of Category III (Unlikely) and Category IV (Extremely Unlikely) events which may be postulated to occur, despite the fact that components were designed to withstand earthquake loads.

Loads from earthquakes shall be combined with loading events as follows:

- for Seismic Class 2A and 2B items, Category I and II loading events should be combined with SL-2 loads;
- for Seismic Class 1, Category I and II loading events should be combined with SL-1 loads.

Table I.1.3-4
Project Guidelines for Seismic Classification

Seismic Class	Seismic Level	Definition and Functional Requirements of Components
2A	SL-2	<ul style="list-style-type: none"> • SIC-2 or SIC-3 components which must satisfy the following illustrative functional requirements in the event of an SL-2 earthquake: <ul style="list-style-type: none"> - leak tightness to the degree assumed in safety analyses; - no through-wall crack; - performance of active safety functions; - displacement must not affect the safety function of another SIC-2 or a group of SIC-3 components.
2B	SL-2	<ul style="list-style-type: none"> • SIC-2 or SIC-3 components which must satisfy the following illustrative functional requirements in the event of an SL-2 earthquake: <ul style="list-style-type: none"> - fluid boundary maintains leak tightness and flow passage, although these functions are somewhat degraded; - a crack should not propagate to cause dimensional instability; - no requirement to perform active safety functions; - support of the components remains functional; - no collapse, falling, or dislodgement of the components that may damage another SIC-2 or a group of SIC-3 components.
1	SL-1	<ul style="list-style-type: none"> • SIC-3 components, not included in Seismic Class 2A or 2B.
Note: Component may be classified from the point of view of investment protection rather than from its safety importance.		

I.1.3.4.4 Environmental Qualification

Components which perform safety functions shall be designed to withstand the environmental conditions created by an accident (such as pressure, temperature, radiation, flooding) under which they are expected to function.

I.1.3.4.5 Fire

ITER shall be designed to assure that the:

- required safety functions are maintained in case of fire, through a combination of fire prevention, fire detection and suppression, and mitigation of adverse effects on components important to safety;
- propagation of fire consequences that may impair safety functions are limited by spatial separation, redundancy, diversity, etc.

I.1.3.4.6 Decommissioning and Waste

The design shall support decommissioning as appropriate for an experimental device by:

- use of modular components to simplify dismantling and reduce waste;
- use of remote handling equipment and procedures developed for normal operation;
- shielding to reduce induced activation of ex-vessel components during operation.

The design shall reduce the quantities of radioactive liquid waste.

The design shall further incorporate means to reduce the volumes and radiotoxicity of materials which may remain as long-term waste after decommissioning by:

- limiting impurities in the materials to allow their clearance as early as practical;
- re-use of components to the extent practical.

I.1.3.4.7 Effluents

The design shall:

- prove that the effluents comply with the project guidelines in Table I.1.3-1;
- reduce radioactivity such that effluents are ALARA;
- monitor the effluents.

I.1.3.4.8 Radiation Protection

ITER shall implement design and administrative measures to protect on-site staff against exposure to radiological hazards.

To assure that the radiological requirements are met, through the entire life cycle of ITER, a radiation protection program (RPP) shall be developed and implemented. The scope of the RPP includes programs and processes required for the safety of staff during normal operation and maintenance work. The objectives of the RPP are to:

- prevent acute over-exposures;
- prevent occupational doses over legal limits;
- maintain staff doses ALARA;
- minimise spread of contamination.

The work to be performed during operation, maintenance, and repair shall be assessed to determine the accessibility and the estimated exposures for activities, against the radiological requirements in Table I.1.3-2 and against recognised limits of exposure to conventional (non-nuclear) hazards.

The design shall provide the means to ensure that the spread of contamination and occupational exposures to radiological hazards are kept ALARA during operation, maintenance and repair. This should include, but not be limited to, access control and zoning, the provision of remote handling, shielding, contamination control, and decontamination equipment as appropriate.

Access Control and Zoning

All areas of the ITER plant shall be zoned depending on the anticipated radiological hazard and conditions during short-term maintenance. During activities/events that cause prohibitive radiation levels (e.g. plasma burn phase, in-vessel transport activities, etc.), areas that are otherwise accessible may be designated as 'Restricted' for the duration of the activity, and

physical access should be prevented. Such locations shall be returned to accessible only after a formal change control.

Table I.1.3-5 lists the Radiation Access Zones, personnel access limitations, and defines the conditions acceptable in these zones. For contamination control, monitoring is required when crossing from a higher to a lower contamination hazard area, and ventilated air flow shall not move from a higher to a lower contamination hazard area.

Table I.1.3-5
Area Classifications and Radiation Access Zones

Access Zone (Area Classification)	Access Limitations	Airborne / Total Dose Rate / Area Contamination Characteristics
Zone A (Non-Supervised Area)	Unlimited Access.	<ul style="list-style-type: none"> No airborne contamination. Dose rate $< 0.5 \mu\text{Sv/h}$; WHITE contamination control zones only: No surface or airborne contamination and no reasonable possibility of cross-contamination.
Zone B (Supervised Area)	Limited Access for NRW. ^(a) Unlimited Access for RW. ^(a)	<ul style="list-style-type: none"> Total dose rate (internal + external) $< 10 \mu\text{Sv/h}$; GREEN contamination control zones acceptable: No loose contamination tolerated. May be subject to temporary surface or airborne cross-contamination, airborne should not exceed 1 DAC.
Zone C (Controlled Area)	Limited Access for all workers. Access requires planning and an appropriate level of approval for the hazards and the class of personnel requiring access.	<ul style="list-style-type: none"> $< 100 \text{ DAC}$ and $< 1 \text{ mSv/h}$; AMBER contamination control zones acceptable: Airborne and loose surface contamination tolerated but must be identified and controlled. Contamination levels shall be maintained ALARA taking into account the risk of exposure, capability of available protective equipment, possibility of contamination spread, and cost. Airborne contamination in AMBER zones should not exceed 100 DAC.
Zone D (Controlled / Restricted Area)	These are restricted access areas, entry occurs only with a high level of approval from both an operational and a radiological safety view. These areas shall have physical barriers to prevent inadvertent personnel entry.	<ul style="list-style-type: none"> Airborne $> 100 \text{ DAC}$ or external dose rate $> 1 \text{ mSv/h}$; RED contamination control zones are only tolerated in Zone D. These areas have permanent or higher than AMBER levels of contamination.
^(a) Personnel performing work requiring exposure to radiological hazards will be designated as Radiation Workers (RW). All other personnel, including non-designated visitors, will be treated as Non-Radiation Workers (NRW). Notes: DAC = Derived Air Concentration: unprotected exposure to 1 DAC = $10 \mu\text{Sv/h}$ $1 \text{ DAC HTO} = 3.1 \times 10^5 \text{ Bq/m}^3 = 8.4 \times 10^{-6} \text{ Ci/m}^3$ For internal dose rate, hazard defined in DAC of airborne contamination For external dose rate, hazard defined as $\mu\text{Sv/h}$		

I.1.3.4.9 Hazardous Materials

Handling, storage and treatment of hazardous materials (such as intermediately stored radioactive waste, and chemically toxic or reactive materials) shall be designed to:

- limit exposure of site staff during all operations;
- limit the spread of contamination during all operations;
- ensure compatibility with other materials and the surrounding environment;
- prevent chemical reactions during normal operation and accidents.

Beryllium

The project guidelines for beryllium concentrations given in Table I.1.3-6 are one tenth of the occupational exposure limits recognised internationally.

**Table I.1.3-6
Project Guidelines for Exposure to Beryllium**

Source	Beryllium Concentration
Airborne (Occupational Exposure Limit)	0.2 $\mu\text{g}/\text{m}^3$
Surface contamination	10 $\mu\text{g}/\text{m}^2$

I.1.3.4.10 Conventional Hazards

Conventional hazards shall be controlled by standard industrial measures. Such hazards include electromagnetic fields, toxic material, asphyxiation, electrocution, cryogenic materials, vacuum, crane loads, and rotating machinery.

Magnetic Field Hazards

The project guidelines for exposure to magnetic fields are listed in Table I.1.3-7.

**Table I.1.3-7
Project Guidelines for Exposure to Magnetic Fields B (T)**

Uncontrolled access	$B < 10 \text{ mT}$
Daily exposure	$B \times \text{time} \leq 60 \text{ mT-h}$
Restricted access	$B > 100 \text{ mT}$

I.1.3.4.11 Security and Proliferation

The design shall provide measures to prevent unauthorised entry to the site and its premises to preclude theft or unauthorised removal of nuclear materials and sabotage.

Design provisions, operational surveillance and administrative measures shall be provided to comply with the international agreements on tritium, lithium-6 and related sensitive technologies with regard to proliferation control.

I.1.4 Site Requirements & Assumptions

This following text is reproduced verbatim from the ITER Site Requirements and ITER Site Design Assumptions (N CL RI 3 99-10-19 W 0.2) updated October 1999.

Introduction

The objective of this document is to define a set of requirements that are compulsory for the ITER site, supplemented by assumptions about the ITER site which are used for design and cost estimates until the actual ITER site is known. Part I of this document contains the principles for the development of the site requirements and site design assumptions. Part II of this document contains the compulsory requirements which are derived from the ITER design and the demands it makes on any site. Part III of this document contains site design

assumptions which are characteristics of the site assumed to exist so that designers can design buildings, structures and equipment that are site sensitive.

Both the Site Requirements and the Site Design Assumptions are organized in the following categories:

- Land
- Heat Sink
- Energy and Electrical Power
- Transport and Shipping
- External Hazards and Accident Initiators
- Infrastructure
- Regulations and Decommissioning

Each of the categories is subdivided into related elements. Some of the categories are broadly defined. For instance, Infrastructure includes personnel, scientific and engineering resources, manufacturing capacity and materials for construction and operation. Requirements and assumptions for the various elements are justified in the **Bases** statements. These statements explain the rationale for their inclusion and provide a perspective in which they may be used.

I Principles for Site Requirements and Site Design Assumptions

1. The compulsory site requirements are based on the ITER site layout and plant design. These requirements are firm in the sense that reasonable reconfiguration of the plant design will not result in a less demanding set of requirements. Some of the requirements are based in part on how the plant and some of its major components, such as the vacuum vessel and the magnet coils, will be fabricated and installed.
2. This document also addresses the assumptions that have been made to carry out the ITER design until a decision on siting is reached. These site design assumptions form some of the bases for the ITER construction cost estimate and schedule. The assumptions are not compulsory site requirements, but are guidelines for designers to follow until the actual site is known.
3. The requirements for public safety and environmental considerations are, by their nature, site sensitive. Also, the regulatory requirements for siting, constructing, operating and decommissioning ITER are likely to be somewhat different for each potential host country. Therefore, the Safety Contact Persons, designated by each potential Host Country, will help the Project Team to consider any particular requirements that siting in their own country would impose. Until that time, the ITER Plant will be designed to a set of safety and environmental assumptions contained in the ITER Plant Specifications [see I.1.3], which are expected to approximate the actual requirements. Site sensitive considerations during operation such as the shipment of radioactive materials including tritium to the site, the temporary storage of wastes on the site, the shipment of wastes from the site and of the effluents from ITER during normal and off-normal operation, are addressed with the design analysis. Accordingly, a Generic Site Safety Report ("Non-Site-Specific Safety Report") will

be available as a firm basis on which the Site Safety Report will later be established to satisfy the licensing authorities of the Host Country.

4. The decommissioning phase of the ITER Plant deserves special attention. In the absence of firm guidance and without prejudice to future negotiations of the Parties, it is assumed that the organization in charge of operating ITER will have a final responsibility to "deactivate" the plant. In this context, "deactivation" is the first phase of decommissioning and includes all actions to shut down the ITER plant and place it in a safe, stable condition. The dismantling phase of decommissioning, which might take place decades after the "deactivation" phase, is assumed to become the responsibility of a new organization within the host country. A technical report on the strategy of deactivation and dismantling will be described inside the design report documentation.
5. In conclusion, the site design assumptions are very important, because without them progress is very limited for the site sensitive designs of buildings, power supplies, site layout and safety/environmental studies. These assumptions were selected so that the design would not be significantly invalidated by actual site deviations from the assumptions. Deviations from the site design assumptions by the actual ITER site may require design and/or construction modifications, but these modifications are expected to be feasible. The modifications may revise the cost estimate and the construction schedule.

II Site Requirements

A. Land

1. Land Area

Requirement The ITER Site shall be up to 40 hectares in area enclosed within a perimeter. All structures and improvements within the perimeter are the responsibility of the ITER project. Land within the perimeter must be committed to ITER use for a period of at least 30 years.

Bases The minimum area for the ITER Site is predicated on sufficient area for the buildings, structures and equipment with allowances for expansion of certain buildings if required for extension of the ITER programme.

The time period is specified to cover the construction (~ 10 years) and operations (~ 20 years) phases. Beyond that, the requirements for any decommissioning will be the responsibility of the Host Country.

2. Geotechnical Characteristics

Requirement The ITER Site shall have foundation soil-bearing capacity adequate for building loads of at least 25 t/m² at locations where buildings are to be built. Nevertheless, it is expected that it will be possible to provide at the specific location of the Tokamak Building means to support the average load of 65 t/m² at a depth of 25 m. The soil (to a depth of 25 m) shall not have

unstable surrounding ground features. The building sites shall not be susceptible to significant subsidence and differential settlement.

Bases The ITER tokamak is composed of large, massive components that must ultimately be supported by the basemat of the structures that house them. Therefore soil-bearing capacity and stability under loads are critical requirements for an acceptable site. The Tokamak Building is composed of three independent halls on separate basemats, but served by the same set of large, overhead bridge cranes. Crane operation would be adversely affected by significant subsidence and differential settlement.

3. *Water Supply*

Requirement The ITER Site host shall provide a continuous fresh water supply of 0.2 m³/minute average and 3 m³/minute peak consumption rates. The average daily consumption is estimated to be about 200 m³. This water supply shall require no treatment or processing for uses such as potable water and water makeup to the plant de-mineralised water system and other systems with low losses.

Bases The ITER plant and its support facilities will require a reliable source of high quality water. The peak rate of 3 m³/minute is specified to deal with conditions such as leakage or fires. This water supply is not used for the cooling towers or other uses which may be satisfied by lower quality, "raw" water.

4. *Sanitary and Industrial Sewage*

Requirement The ITER Site host shall provide sanitary waste capacity for a peak ITER site population of 1000. The host shall also provide industrial sewage capacity for an average of 200 m³/day.

Bases The ITER project will provide sewer lines to the site perimeter for connection to the sewer service provided by the host. The peak industrial sewage rate is expected to be adequate to deal with conditions such as leaks and drainage of industrial sewage stored in tanks until it can be analyzed for release. Rainwater runoff is not included in industrial sewage.

B. *Heat Sink*

Requirement The ITER Site shall have the capability to dissipate, on average, 450 MW (thermal) energy to the environment.

Bases ITER and its associated equipment may develop heat loads as high as 1200 MW (thermal) for pulse periods of the order of 500 s. The capability to dissipate 1200 MW should be possible for steady-state operation which is assumed to be continuous full power for one hour. Duty Cycle requirements for the heat sink at peak loads will not exceed 30%. The average heat load would be no more than 450 MW for periods of 3 to 6 days.

C. Energy and Electrical Power

ITER Plant Steady State Electrical Loads

Requirement The ITER Site shall have the capability to draw from the grid 120 MW of continuous electrical power. Power should not be interrupted because of connection maintenance. At least two connections should be provided from the supply grid to the site.

Bases The ITER Plant has a number of systems which require a steady-state supply of electrical power to operate the plant. It is not acceptable to interrupt this power supply for the maintenance of transmission lines, therefore the offsite transmission lines must be arranged such that scheduled line maintenance will not cause interruption of service. This requirement is based on the operational needs of the ITER Plant.

Maintenance loads are considerably lower than the peak value because heavy loads such as the tokamak heat transfer and heat rejection systems will operate only during preparations for and actual pulsed operation of the tokamak.

D. Transport and Shipping

1. *Maximum Size of Components to be shipped*

Requirement The ITER Site shall be capable of receiving shipments for components having maximum dimensions (not simultaneously) of about:

- Width - 9 m
- Height - 8 m
- Length - 15 m

Bases In order to fabricate the maximum number of components, such as magnet coils and large transformers, off site, the ITER site must have the capability of receiving large shipments. For the reference case, it is assumed that only the Poloidal Field Coils will be manufactured on site, unless the possibility of transporting and shipping these large coils is proven feasible. For the same reason, it is also assumed that the CS will be assembled on site from six modules, unless it proves feasible that the Assembly may be supplied as one large and complete unit. The cryostat will be assembled on site from smaller delivered parts. The width is the most critical maximum dimension and it is set by the Toroidal Field Coils which are about 9 m wide. The height is the next most critical dimension which is set by the 40° Vacuum Vessel Sector. A length of 15 m is required for the TF coils. The following table shows the largest (~ 100 t or more) ITER components to be shipped:

Largest ITER Components to be Shipped

Component	Pkgs	Width (m)	Length (m)	Height (m)	Weight (t) Each Pkg.
TF Coils	18	9	14.3	3.8	280
Vac. Vessel 40° Sector	9	8	12	8	575
CS Modules	6	4.2	4.2	1.9	100
Large HV Transformer	3	4	12	5	250
Crane Trolley Structure*	2	(14)	(18)	(6)	(600)

* Crane dimensions and weight are preliminary estimates.

PF Coils and CS Assembly**

Component	Pkgs	Width (m)	Length (m)	Height (m)	Weight (t) Each Pkg.
PF1	1	9.5	9.5	2.4	200
PF2	1	18.5	18.5	1.9	200
PF3	1	25.5	25.5	1.2	300
PF4	1	26.0	26.0	1.2	450
PF5	1	18.2	18.2	2.4	350
PF6	1	10.8	10.8	2.4	300
CS Assembly	1	4.2	18.8	4.2	850

** Note that transportation and shipping of the PF Coils and of the CS Assembly are not requirements, but could be considered an advantage.

Note, too, that the PF Coils dimensions are for the coil and connection box envelope, and that for each coil there are vertical protrusions of ~ 1.5 – 1.8 m for the terminals.

2. *Maximum Weight of Shipments*

Requirement The ITER Site shall be capable of receiving about a dozen components (packages) having a maximum weight of 600 t and approximately 100 packages with weight between 100 and 600 t each.

Bases In order to fabricate the maximum number of components, including magnet coils, off site, the ITER site must have the capability of receiving very heavy shipments. The single heaviest component (Vacuum Vessel Sector) is not expected to exceed 600 t. All other components are expected to weigh less.

E. External Hazards and Accident Initiators

No Compulsory Requirements.

F. Infrastructure
No Compulsory Requirements

G. Regulations and Decommissioning

Details of the regulatory framework for ITER will depend on the Host Country. At a minimum, the Host's regulatory system must provide a practicable licensing framework to permit ITER to be built and to operate, taking into account, in particular, the following off-site matters:

1. the transport of kilograms of tritium during the course of ITER operations;
2. the acceptance and safe storage of activated material in the order of thousands of tonnes, arising from operation and decommissioning.

The agreement with the Host should provide for the issue of the liability for matters beyond the capacity of the project that may arise from ITER construction, operation and decommissioning.

III Site Design Assumptions

The following assumptions have been made concerning the ITER site. These site design assumptions are uniformly applied to all design work until the actual ITER Site is selected.

A. Land

1. *Land Area*

Assumption During the construction it will be necessary to have temporary use of an additional 30 hectares of land adjacent to or reasonably close to the compulsory land area. It is assumed this land is available for construction laydown, field engineering, pre-assembly, concrete batch plant, excavation spoils and other construction activities.

During operating phases, this land should be available for interim waste storage, heavy equipment storage and activities related to the maintenance or improvement of the ITER Plant.

Bases The assumptions made for the cost and schedule estimates are based on construction experience which uses an additional area of 25 hectares. Only a very limited amount of vehicle parking space (5 hectares) is allocated to the compulsory area, whereas a similar amount will be required to satisfy temporary needs during construction.

2. *Topography*

Assumption The ITER site is assumed to be a topographically "balanced" site. This means that the volumes of soil cuts and fills are approximately equal over the compulsory land area in Requirement A.1. The maximum elevation change for the "balanced" site is less than 10 m about the mean elevation over the land area in the compulsory requirement.

3. *Geotechnical Characteristics*

Assumption The soil surface layer at the ITER Site is thick enough not to require removal of underlying hard rock, if present, for building excavations, except in the area under the Tokamak Building itself, at an excavation of about 25 m.

4. *Hydrological Characteristics*

Assumption Ground water is assumed to be present at 10 m below nominal grade, well above the tokamak building embedment of up to 25 m below nominal grade. This assumption will require engineered ground water control during the construction of the tokamak building pit.

5. *Seismic Characteristics*

Assumption The ITER seismic design specifications for the applicable Safety Importance Class (SIC) are based on an assumed seismic hazard curve. Using the IAEA seismic classification levels of SL-2, SL-1, and SL-0 and the assumed seismic hazard curves, the following seismic specifications are derived:

SIC	IAEA level	Return Period (years)	Peak** Ground Acc.
1*	SL-2S 85% tile	10^4	0.4
2,3	SL-2 50% tile	10^4	0.2
3	SL-1 50% tile	10^2	0.05
4***	SL-0	short	0.05

* No ITER components in this class

** Peak Ground Acceleration is for both horizontal and vertical components in units of the gravitational acceleration, g.

*** SIC 4 components, the seismic specifications are not derived probabilistically - local (uniform) building codes are applied to this class. A peak value of 0.05 g is assumed equal to the SL-1 peak value.

Bases Safety assessments of external accident initiators for facilities, particularly when framed in a probabilistic risk approach, may be dominated by seismic events. Assumed seismic hazard curves are used in a probabilistic approach which is consistent with IAEA recommendations for classification as a function of return period. The selection of the assumed seismic hazard curve is relevant to regions of low to moderate seismic activity. Prior to site selection, specification of the peak horizontal and vertical ground acceleration provide the ITER designers guidelines according to the methodology to be used for seismic analysis, which will rely on a specified Ground Motion Design Response Spectrum and a superposition of modal responses of the structures (according to NRC recommendations). After site selection the actual seismic specifications will be used to adjust the design, in particular by adding seismic isolation, if necessary.

6. *Meteorological Characteristics*

Assumption A general set of meteorological conditions are assumed for design of buildings, civil structures and outdoor equipment, as follows:

- Maximum Steady, Horizontal Wind ≤ 140 km/h (at 10 m elevation)
- Maximum Air Temperature ≤ 35 °C (24 hr average ≤ 30 °C)
- Minimum Air Temperature ≥ -25 °C (24 hr average ≥ -15 °C)
- Maximum Rel. Humidity (24 hr average) $\leq 95\%$ (corresponding vapour pressure ≤ 22 mbar)
- Maximum Rel. Humidity (30 day average) $\leq 90\%$ (corresponding vapour pressure ≤ 18 mbar)
- Barometric Pressure - Sea Level to 500 m
- Maximum Snow Load - 150 kg/m^2
- Maximum Icing - 10 mm
- Maximum 24 hr Rainfall - 20 cm
- Maximum 1 hr Rainfall - 5 cm
- Heavy Air Pollution (Level 3 according to IEC 71-2)

Bases The assumed meteorological data are used as design inputs. These data do not comprise a complete set, but rather the extremes which are likely to define structural or equipment limits. If intermediate meteorological data are required, the designer estimates these data based on the extremes listed above. Steady winds apply a static load on all buildings and outdoor equipment.

B. Heat Sink: Water Supply for the Heat Rejection System

Assumption The JCT has selected forced draft (mechanical) cooling towers as a design solution until the ITER site is selected. At 30% pulse duty cycle (450 MW average heat rejection) the total fresh ("raw") water requirement is about $16 \text{ m}^3/\text{minute}$. This water makes up evaporative losses and provides replacement for blowdown used to reduce the accumulation of dissolved and particulate contaminants in the circulating water system. During periods of no pulsing the water requirement would drop to about $5 \text{ m}^3/\text{minute}$. Each blowdown action will lead to a peak industrial sewage rate of $3000 \text{ m}^3/\text{day}$.

Bases The actual ITER Site could use a number of different methods to provide the heat sink for ITER, but for the purposes of the site non-specific design, the induced draft (mechanical) cooling towers have been assumed. These cooling towers require significant quantities of fresh water ("raw") for their operation. For 450 MW average dissipation, approximately $16 \text{ m}^3/\text{minute}$ of the water is lost by evaporation and drift of water droplets entrained in the air plume, and by blowdown. This water also supplies make up to the storage tanks for the fire protection system after the initial water inventory is depleted. Cooling towers may not be suitable for an ITER site on a seacoast or near a large, cool body of fresh water. Therefore open cycle cooling will be considered as a design option.

C. Energy and Electrical Power

1. *Electrical Power Reliability during Operation*

Assumption The grid supply to the Steady State and to the Pulsed switchyards is assumed to have the following characteristics with respect to reliability:

Single Phase Faults - a few tens/year 80%: $t < 1$ s
 - a few / year 20%: $1 \text{ s} < t < 5 \text{ min}$
 where t = duration of fault

Three Phase Faults - a few/year

Bases ITER power supplies have a direct bearing on equipment availability which is required for tokamak operation. If operation of support systems such as the cryoplant, TF coil supplies and other key equipment are interrupted by frequent or extended power outages, the time required to recover to normal operating conditions is so lengthy that availability goals for the tokamak may not be achieved. Emergency power supplies are based on these power reliability and operational assumptions.

2. *ITER Plant Pulsed Electrical Supply*

Assumption A high voltage line supplies the ITER "pulsed loads". The following table shows the "pulsed load" parameters for the ITER Site:

Characteristic	Values
Peak Active Power* [#]	500 MW
Peak Reactive Power	400 MVar
Power Derivative*	200 MW/s
Power Steps*	60 MW
Fault Level	10-25 GVA
Pulse Repetition time	1800 s
Pulsed Power Duration**	1000 s
[#] from which up to 400 MW is a quasi-steady-state load during the sustained burn phase, while the remaining 80 – 120 MW has essentially pulse character for plasma shape control with a maximum pulse duration of 5 – 10 s and an energy content in the range of 250 – 500 MJ.	
* These power parameters are to be considered both positive and negative. Positive refers to power from the grid, while negative refers to power to the grid. Power variations will remain within the limits given above for the maximum power and for the power derivatives.	
** The capability to increase the pulse power duration to 3600 s is also assumed, in which case the repetition time would increase accordingly to maintain the same duty factor.	

Bases The peak active power, the peak reactive power and the power steps quoted above are evaluated from scenarios under study. Occasional power steps are

present in the power waveform. The supply line for pulsed operation will demand a very "stiff" node on the grid to meet the assumption.

D. Transport and Shipping

Bases Several modes of transport and shipping are assumed for ITER because the diversity of these modes provides protection against disruptions for timely delivery of materials and equipment needed by the project. The assumptions for transport and shipping are based on some general considerations which are common for all modes.

When the assumptions describe the site as having "access" to a mode of transport or shipping, it means that the site is not so far away from the transport that the assumed mode would be impractical. Air transport is a good example, because if the airport is not within reasonable commuting time, the time advantage of this mode would be lost (i.e. it would become impractical).

1. *Highway Transport*

Assumption The ITER Site is accessible by a major highway which connects to major ports of entry and other centers of commerce.

2. *Air Transport*

Assumption The ITER Site is located within reasonable commuting time from an airport with connections to international air service.

3. *Rail and Waterway Transport*

Assumption It is assumed the ITER site will have rail and waterway access. The railway is assumed to connect to major manufacturing centres and ports of entry.

E. External Hazards and Accident Initiators

1. *External Hazards*

Assumption It is assumed the ITER Site is not subject to significant industrial and other man-made hazards.

Bases External hazards, if present at the ITER site, must be recognised in safety, operational and environmental analyses. If these hazards present a significant risk, mitigating actions must be taken to ensure acceptable levels of public safety and financial risk.

2. *External (Natural) Accident Initiators*

Assumption It is assumed the ITER Site is not subject to horizontal winds greater than 140 km/hr (at an elevation of 10 m) or tornadic winds greater than 200 km/hr. The ITER Site is not subject to flooding from streams, rivers, sea water

inundation, or sudden runoff from heavy rainfall or snow/ice melting (flash flood). All other external accident initiators except seismic events are assumed below regulatory consideration.

Bases The wind speeds specified in this requirement are typical of a low to moderate risk site. Tornadoic winds apply dynamic loads of short duration to buildings and outdoor equipment by propelling objects at high speeds creating an impact instead of a steady load. The design engineer uses the tornadoic wind speed in modeling a design basis projectile which is assumed to be propelled by the tornado. This design basis is important for buildings and structures that must contain hazardous or radioactive materials or must protect equipment with a critical safety function.

ITER is an electrically intensive plant, which would complicate recovery from flooded conditions. This assumption does not address heavy rainfall or water accumulation that can be diverted by typical storm water mitigation systems. For the purposes of this assumption, accidents involving fire, flooding and other initiators originating within the ITER plant or its support facilities are not considered external accident initiators.

F. Infrastructure

Bases The ITER Project is sufficiently large and extended in duration that infrastructure will have a significant impact on the outcome. Industrial, workforce and socioeconomic infrastructure assumptions are not quantitatively stated because there are a variety of ways these needs can be met. The assumptions are fulfilled if the actual ITER site and its surrounding region already meets the infrastructure needs for a plant with similar technical, material and schedule needs as ITER requires.

1. *Industrial*

Assumption It is assumed the ITER Site has access to the industrial infrastructure that would typically be required to build and operate a large, complex industrial plant. Industrial infrastructure includes scientific and engineering resources, manufacturing capacity and materials for construction. It is assumed the ITER Site location does not adversely impact the construction cost and time period nor does it slow down operation. The following are examples of the specific infrastructure items assumed to be available in the region of the site:

- Unskilled and skilled construction labour
- Facilities or space for temporary construction labour
- Fire Protection Station to supplement on-site fire brigade
- Medical facilities for emergency and health care
- Contractors for site engineering and scientific services
- Bulk concrete materials (cement, sand, aggregate)
- Bulk steel (rebar, beams, trusses)
- Materials for concrete forms
- Construction heavy equipment
- Off-site hazardous waste storage and disposal facilities
- Industrial solid waste disposal facilities

- Off-site laboratories for non-radioactive sample analysis

Bases Efficiency during construction and operation of a large, complex industrial facility varies significantly depending on the relative accessibility of industrial infrastructure. Accessibility to infrastructure can be demonstrated by comparable plants operating in the general region of the site.

2. *Workforce*

Assumption It is assumed that a competent operating and scientific workforce for the ITER Plant can be recruited from neighbouring communities or the workforce can be recruited elsewhere and relocated to the neighbouring communities.

It is also assumed that ITER has the capability for conducting experiments from remote locations elsewhere in the world. These remote locations would enable "real-time" interaction in the conduct of the experiments, while retaining machine control and safety responsibilities at the ITER Site Control Facility.

Bases The workforce to operate, maintain and support ITER will require several hundred workers. The scientific workforce to conduct the ITER experimental program will also require several hundred scientists and engineers. The assumption that these workers and scientist/engineers come from neighbouring communities is consistent with the site layout plans which have no provisions for on-site dormitories or other housing for plant personnel.

A significant scientific workforce must be located at the ITER Site as indicated in the Assumptions. However, this staff can be greatly augmented and the experimental value of ITER can be significantly enhanced if remote experimental capability is provided. The result of the remote experiment is that scientific staffs around the world could participate in the scientific exploitation of ITER without the necessity of relocation to the ITER Site. Remote experimental capability is judged to be feasible by the time of ITER operation because of advances in the speed and volume of electronic data transfers that are foreseen in the near future.

3. *Socioeconomic Infrastructure*

Assumption The ITER Site is assumed to have neighbouring communities which provide socioeconomic infrastructure. Neighbouring communities are assumed to be not greater than 50 km from the site, or one hour travel. Examples of socioeconomic infrastructure are described in the following list:

- Dwellings (Homes, Apartments, Dormitories)
- International Schools from Kindergarten to Secondary School
- Hospitals and Clinics
- Job Opportunities for Spouses and other Relatives of ITER workers
- Cultural life in a cosmopolitan environment

Bases Over the life of the ITER plant, thousands of workers, scientists, engineers and their families will relocate temporarily or permanently to the communities surrounding the ITER site. These people could comprise all the nationalities represented by the Parties. This "world" community will present special challenges and opportunities to the host site communities.

To attract a competent international workforce, international schools should be provided. Teaching should be partially in the mother tongue following programmes which are compatible with schools in each student's country of origin. All parties should assist with the international schools serving these students.

The list of examples is not intended to be complete but it does illustrate the features considered most important. The assumed 50 km distance should maintain reasonable commuting times less than one hour for workers and their relatives.

G. Regulations and Decommissioning

1. *General Decommissioning*

Assumption During the first phase of decommissioning, the ITER operations organization places the plant in a safe, stable condition. Dismantling may take place decades after the "deactivation" phase. Dismantling of ITER is assumed to be the responsibility of a new organization within the host country. The ITER operations organization will provide the new organization all records, "as-built prints", information and equipment pertinent to decommissioning. Plant characterization will also be provided for dismantling purposes after "deactivation".

Bases Experience and international guidelines (IAEA Safety Series No. 74, 1986, "Safety in Decommissioning of Research Reactors") stress the importance of good record keeping by the operations organization as a key to decommissioning success.

2. *ITER Plant "Deactivation" Scope of Work*

Assumption The ITER operations organization will develop a plan to put the plant in a safe, stable condition while it awaits dismantling.

Residual tritium present at the end of ITER operations will be stabilised or recovered to secure storage and/or shipping containers.

Residual mobile activation products and hazardous materials present at the end of ITER operations will be stabilised or recovered to secure storage and/or shipping containers such that they can be shipped to a repository as soon as practical.

ITER deactivation will include the removal of in-vessel components and their packaging in view of long-term storage. This removal from the vacuum vessel

will be done by personnel and remote handling tools, trained for maintenance during the previous normal operation.

Liquids used in ITER systems may contain activation products, which must be removed before they can be released to the environment or solidified as waste. It is assumed that all liquids will be rendered to a safe, stable form during the "deactivation" phase, and afterwards no more cooling will be necessary

ITER "deactivation" will provide corrosion protection for components which are vulnerable to corrosion during the storage and dismantling period, if such corrosion would lead to spread of contamination or present unacceptable hazards to the public or workers.

Bases It is recommended (IAEA Safety Series No. 74, 1986) that all radioactive materials be rendered into a safe and stable condition as soon as practical after the cessation of operations.

H. Construction Phase

General requirements for the construction phase (except land) are very dependent on local practice. However, water, sewage and power supplies need to be provided at the site for a construction workforce of up to 3000 people.

I.1.5. General Definitions

The following tables define terms used for ITER.

Table I.1.5-1 Remote Handling Classes

Remote Handling Class	Title
RH Class 1	Components that require scheduled remote maintenance or replacement.
RH Class 2	Components that do not require scheduled remote maintenance but are likely to require unscheduled or very infrequent remote maintenance.
RH Class 3	Components not expected to require remote maintenance during the lifetime of ITER.
RH Class 4	Components that do not require remote maintenance.

Table I.1.5-2 Steady-State Power Classes

Class	Title
Class I	Uninterruptible DC
Class II	Uninterruptible AC
Class III	Temporarily interruptible AC
Class IV	Indefinitely interruptible AC

Table I.1.5-3 Loading Conditions for Component Design

Loading Event Category	Frequency of Loading Events
Category I: Operational Loading Events	<ul style="list-style-type: none"> For each representative loading event, assign number of times planned and required for normal operation in the life of component. Should include some faults which need to be considered in the life of the component, which can occur because of experimental nature. Loading events with similar loading histograms should be counted within the number of the representative loading events.
Category II: Likely Loading Events	<ul style="list-style-type: none"> For each representative loading event, assign number of times not planned but required to be considered during the life of the component not including Category I (Operational Loading Events). Loading events with similar loading histograms should be counted within the number of the representative loading events.
Category III: Unlikely Loading Events	<ul style="list-style-type: none"> Select one loading event from the Category II (Likely Loading Events) that represents the most demanding design conditions for the component, and either superimpose other relevant loading events or assume the most conservative operational parameters to provide adequate global structural margins against unforeseen loading conditions. Assume to occur once (one time) in the life of the component. If the loading histograms are very different, additional loading events can be identified assuming each of them to occur once in the life of component.
Category IV: Extremely Unlikely Loading Events	<ul style="list-style-type: none"> Select one design basis loading event, in principle, in the life of the component that needs to be postulated because its consequences would include a potential for the release of significant amounts of radioactive material. Superimpose other relevant loading events, if necessary, to provide adequate conservatism for the design basis loading event that represents the most demanding loading conditions necessary to assure ultimate structural integrity.
Test Loading	<ul style="list-style-type: none"> Assign number of times for tests anticipated in the life of the component.

Table I.1.5-4 Damage Limits in Plant and Component Level

This table gives a guideline for allocation of design margins, such as safety factors specified in structural design codes, to individual loading events.

Damage Limits	Damage Limits to Component Level	Damage Limits in Plant Level and Recovery of the Plant (Plant Operational Condition)
Normal	The component should maintain specified service function.	<ul style="list-style-type: none"> • Within specified operational limit. • No special inspection will be required other than routine maintenance and minor adjustment.
Upset	The component must withstand these loadings without significant damage requiring special inspection or repair.	<ul style="list-style-type: none"> • After minor adjustment, or replacement of the faulty component, the plant can be brought back to normal operation. • No effect on other components that may call for special inspection or repair.
Emergency	<ul style="list-style-type: none"> • Large deformations in areas of structural discontinuity, such as at nozzles, which may necessitate removal of the component from service for inspection or repair. • Insignificant general permanent deformation that may affect safety function of the component concerned. General strains should be within elastic limits. • Active components should be functional at least after transient. 	<ul style="list-style-type: none"> • The plant may require decontamination, major replacement of damaged component or major repair work. • In addition to the damaged component, inspection may reveal localized large deformation in other components, which may call for the repair of the affected components. • Nevertheless, the plant maintains the specified minimum safety function during and after the events.
Faulted	<ul style="list-style-type: none"> • Gross general deformations with some consequent loss of dimensional stability and damage requiring repair, which may require removal of component from service. • Nevertheless deformation should not lead to structural collapse which could damage other components. • The fluid boundary maintains degraded but reasonable leak tightness and flow passage. • Active components may not be functional after transient. 	<ul style="list-style-type: none"> • Gross damage to the affected system or component. No loss of safety function which could lead to doses in excess of the limits established for Category IV Extremely Unlikely Event. • No design consideration will be given for recovery. The recovery of the plant may be judged from the severity of damage. • This level of accident state is not expected to occur, but is postulated because its consequences would include the potential for the release of significant amounts of radioactive material.

Table I.1.5-5 Damage Limits for Loading Conditions

Loading Event Category		Category I: Operational Loading	Category II: Likely Loading	Category III: Unlikely Loading	Category IV: Extremely Unlikely Loading	Test Loading
Plant Level		Normal	Upset	Emergency	Faulted	Normal
Component	SIC-2	Normal	Upset	Emergency	Faulted (note 1)	Normal
Level	SIC-3	Normal	Upset	Emergency	Faulted (note 1)	Normal
	SIC-4	Normal	Upset	(note 2)	(note 2)	Normal

Notes:

1) Faulted for passive components with no deformation limits. Emergency for active components and some passive components in which general deformations should be limited.

2) Events need not be considered from the safety point of view, only for investment protection.

Table I.1.5-6 Plant States

LTM	Construction/long term maintenance
STM	Short term maintenance
TCS	Test and conditioning operation
STS	Short term standby
POS	Plasma operation

Table I.1.5-7 General Acronyms

Acronym	Definition
ALARA	As Low As Reasonably Achievable
CODAC	Command Control and Data Acquisition, Communication
CS	Central Solenoid
DDD	Design Description Document
EC	Electron Cyclotron
FW	First Wall
H&CD	Heating and Current Drive
HRS	Heat Rejection System
HV	High Voltage
HVAC	Heating, Ventilation, and Air Conditioning
ICRP	International Commission on Radiological Protection
IC	Ion Cyclotron
LH	Lower Hybrid
LOCA	Loss of Coolant Accident
LOFA	Loss of Flow Accident
LOPA	Loss of Site Power Accident
LOVA	Loss of Vacuum Accident
NB	Neutral Beam
PF	Poloidal Field
PFC	Plasma-Facing Component
PHTS	Primary Heat Transfer System
RF	Radio Frequency
RH	Remote Handling
TCWS	Tokamak Cooling Water System
TF	Toroidal Field
VDE	Vertical Displacement Event
VV	Vacuum Vessel
WBS	Work Breakdown Structure

I.1.6 ITER Design Documentation

The main features of the ITER documentation are as follows (see Figure I.1-1):

- A top level *Plant Design Specification (PDS)* document, where externally imposed, essentially design-independent requirements at the highest level are defined, including safety principles and criteria.
- Design Requirements and Guidelines Level 1 (DRG1) deals with the requirements and specifications above the system¹ level. This includes not only system-wide requirements but also interfaces or specifications affecting the design of more than one single system. More detailed "Design Background" documents are annexed.
- Design Requirements and Guidelines Level 2 (DRG2) defines in one document the boundaries of each system and deals in more detail with the functions, requirements and specifications at the system level. The system division is identical to that of the DDDs.
- Design Description Documents (DDD) are one per system.
- The Plant Description Document (PDD) is the global plant description. It summarises the design based on the details in the DDDs, gives an overview of major plant processes² which usually involve more than one system, summarises plant level assessments, and overall planning. The latter items are described in more detail in "Plant Assessment" document annexes.

¹ defined here to mean a set of functionally related elements

² defined here to mean the dynamic behaviour of one or more systems

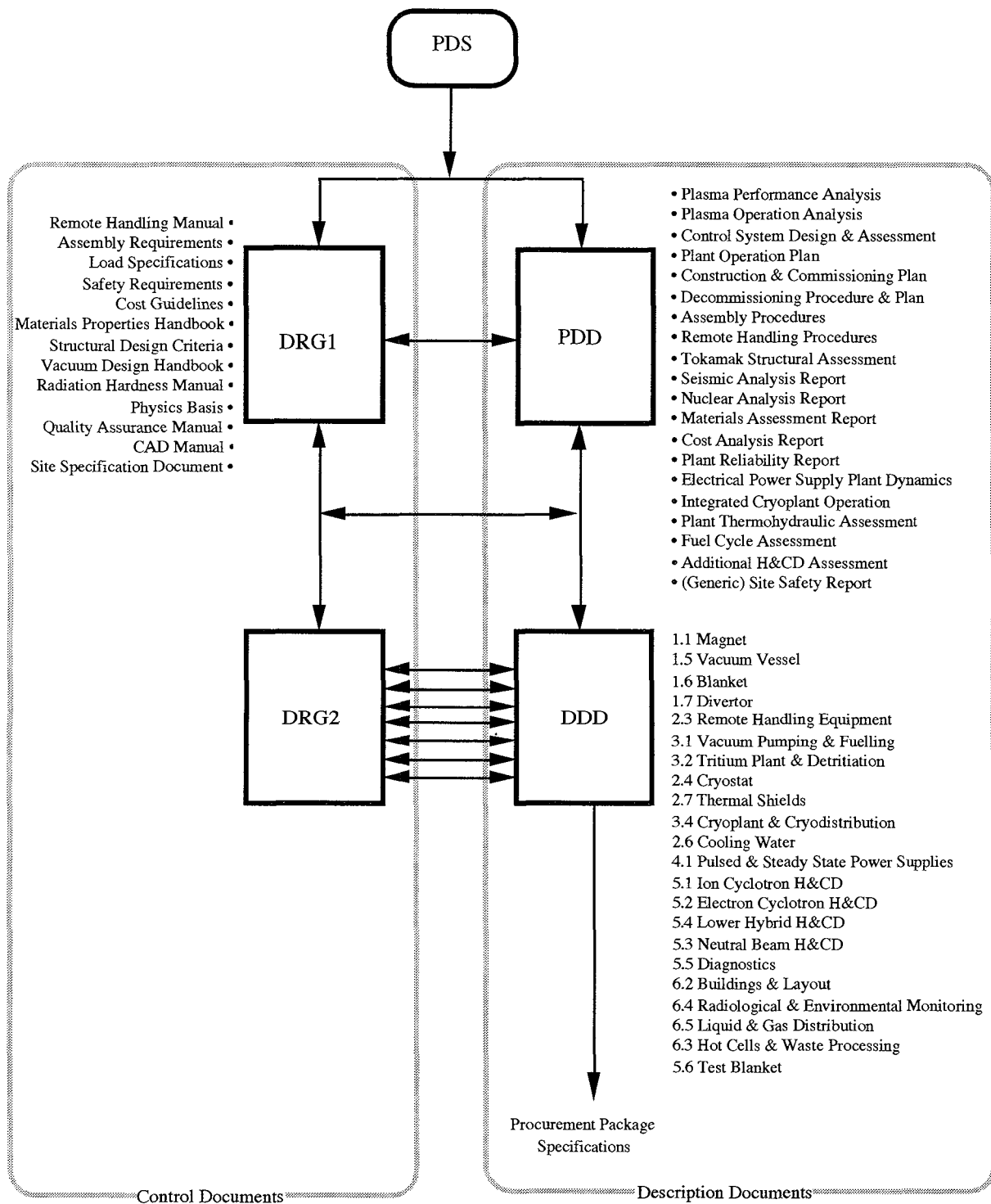


Figure I.1-1 Outline of ITER Documentation

I.2 Main Physics Parameters and Assessment

I.2.1	Introduction	2
I.2.2	Physics Basis and Selection of Plasma Parameters	3
I.2.3	Projection of ITER-FEAT Plasma Performance	9
I.2.3.1	Inductive Operation	9
I.2.3.2	Steady-state and Hybrid Operation	14
I.2.3.2.1	Potential Parameters for Steady-state Operation with Full Minor Radius	15
I.2.3.2.2	Potential Steady-state Operation Space with Reduced Minor Radius at $I = 12$ MA	16
I.2.3.2.3	1.5-D Simulation of Steady-state Operation	17
I.2.3.3	Probabilistic Performance Assessment	20
I.2.3.4	An Alternative Performance Evaluation Methodology based on Dimensional Extrapolation	24
I.2.3.5	Divertor Performance	28
I.2.3.5.1	Introduction	28
I.2.3.5.2	Power Loading Reduction and Helium Exhaust	29
I.2.3.5.3	Operation with Reduced Plasma Current	30
I.2.3.5.4	ELM Control	31
I.2.3.6	Energetic Particle Confinement	32
I.2.4	Plasma Operation and Disruptions	34
I.2.4.1	Operational Limits	35
I.2.4.1.1	Beta Limit	35
I.2.4.1.1.1	Neoclassical Tearing Modes	35
I.2.4.1.1.2	Resistive Wall Modes (RWMs) and their Stabilization	37
I.2.4.2	Recoverable Plasma Disturbances	38
I.2.4.3	Disruptions and Vertical Displacement Events	38
I.2.5	Heating and Current Drive	42
I.2.5.1	Role of Auxiliary Heating and Current Drive Systems	42
I.2.5.2	Bootstrap Current	43
I.2.5.3	Capabilities of Candidate H&CD systems	44
I.2.5.3.1	IC Heating and Current Drive	44
I.2.5.3.2	EC Heating and Current Drive	44
I.2.5.3.3	NB Heating and Current Drive	45
I.2.5.4	Summary of Heating and Current Drive Capability	47
I.2.6	Requirements for Plasma Measurements and Diagnostics	48
I.2.7	Conclusions	50

I.2.1 Introduction

The principal physics goals (see I.1) of ITER-FEAT are:

- (i) to achieve extended burn in inductively-driven plasmas with the ratio of fusion power to auxiliary heating power (Q) of at least 10 for a range of operating scenarios and with a duration sufficient to achieve stationary conditions on the timescales characteristic of plasma processes;
- (ii) to aim at demonstrating steady-state operation using non-inductive current drive with a ratio of fusion power to input power for current drive of at least 5.

In addition, the possibility of higher Q operation will be explored if favourable confinement conditions can be achieved. The reference operating scenario for ITER-FEAT inductive operation is the ELMy H mode, and the rules and methodologies for projection of plasma performance to the ITER scale are those established in the ITER Physics Basis (IPB)¹, which has been developed from broadly-based experimental and modelling activities within the magnetic fusion programmes of the ITER Parties.

The key physics issues relating to plasma performance in the ELMy H-mode regime are the maintenance of H-mode quality confinement at sufficiently high density, the achievement of adequate plasma β to produce the requisite fusion power, and hence Q value, the provision of satisfactory power and particle exhaust to ensure acceptable levels of helium and plasma impurities, and the demonstration of efficient transfer of α -particle power to the thermal plasma (while limiting anomalous α -particle losses via TF ripple or collective instabilities, to prevent damage to the plasma-facing components). At the same time, global magnetohydrodynamic (mhd) stability and plasma control capability must be such that the thermal and electromagnetic loads as well as runaway electron currents, arising from disruptions, are within acceptable bounds.

H-mode operation at high plasma density is favoured by the choice of a high plasma triangularity and the exploitation of high-field-side ('inside') fuel pellet launch, while the overall choice of design parameters allows considerable headroom for $Q = 10$ operation well below the Greenwald density. Plasma performance predictions show that $Q = 10$ operation can be achieved at modest values of β_N (~ 1.5). However, in the event that the β threshold for the onset of neoclassical tearing modes (NTMs) scales unfavourably to ITER-FEAT, stabilization of the modes by localized electron cyclotron current drive (ECCD) is foreseen (see II.7.2.2). The extensive divertor model validation and analysis activities performed so far during the EDA give confidence that the proposed divertor design allows adequate power dissipation to be achieved, with peak power loads below the acceptable level of 10 MWm^{-2} , and that the planned fuelling throughput of $200 \text{ Pam}^3\text{s}^{-1}$ will limit the core helium concentration below 6%. While the detailed evaluation of α -particle loss processes is still in progress, it is expected that the losses via TF ripple can be brought within acceptable limits by reducing the residual TF ripple level via ferromagnetic inserts in the vacuum vessel. In many respects, ITER-FEAT represents a key experimental step in the evaluation of α -particle losses due to collective effects at the reactor scale. Nevertheless, on the basis of studies carried out in support of the 1998 ITER design, it appears unlikely that the excitation of

¹ ITER Physics Expert Groups et al, Nucl. Fusion to be published (1999), ITER Physics Basis

collective mhd instabilities, such as Alfvén eigenmodes, will limit plasma performance in ITER-FEAT inductive scenarios.

The development of plasma operation scenarios that exploit active profile control to access enhanced confinement regimes, which has occurred in the course of the EDA, has allowed greater emphasis to be placed on the use of such scenarios in ITER-FEAT. In particular, these regimes offer the prospect of establishing reactor-relevant, steady-state operation in which a significant fraction of the plasma current is generated via the bootstrap effect. Flexibility in the ITER-FEAT design through plasma shaping, a mixture of heating and current drive systems, and mhd stability control techniques for NTMs and resistive wall modes (RWMs), favours the exploitation of plasma scenarios with either shallow monotonic or negative central shear. Although the precise conditions for the development of internal transport barriers (ITBs) are uncertain, the aim has been to provide ITER-FEAT with the necessary plasma control tools to facilitate access to such modes of operation. Sophisticated diagnostics of key profiles such as q , pressure, and rotation will be required to operate with a high level of reliability from the first phase of plasma experiments, and this has been acknowledged in assigning measurement priorities. The question of α -particle losses via TF ripple losses or collective instabilities, is anticipated to be particularly acute in these regimes, and the design of the ferromagnetic inserts will reflect this consideration. Predictions of steady-state operation in ITER-FEAT, therefore, build upon these recent developments and reflect the expectation that considerable further progress can be achieved in the fusion programme in the future to resolve remaining uncertainties.

1.2.2 Physics Basis and Selection of Plasma Parameters

It can be shown¹ that the linear size and volume of a tokamak designed to achieve a given value of Q can be estimated from a small number of parameters. These parameters arise from simple considerations of energy confinement scaling, mhd stability (essentially current limits), plasma-shaping capability (i.e. the elongation, triangularity, and aspect ratio which are desired and which can be achieved, choice of single versus double null divertor geometry), and desired plasma pulse length, together with basic engineering constraints, such as the maximum stress in the toroidal field coil and the shielding thickness required to ensure that the vacuum vessel can be rewelded in case of repair. However, to realize a specific, self-consistent design, a more detailed analysis is required. Such an analysis combines a detailed plasma power balance and boundaries for the plasma operating window with considerations of such engineering constraints as superconducting coil current and field limits, material stress limits, and access to the plasma (e.g. for heating systems). Not surprisingly, the interaction of these various factors constrains the allowable parameter sets, so that, for example, peak magnetic field at the TF coil, aspect ratio, elongation, and available burn flux (i.e. pulse duration) are not independent.

The reference plasma scenario for inductive $Q = 10$ operation, the ELMy H-mode, is a reproducible and robust mode of tokamak operation with a demonstrated, long-pulse capability. The essential physics which enters into the prediction of plasma performance in ITER-FEAT therefore derives from the two principal ELMy H-mode scalings, i.e. the H-mode power threshold scaling, which defines the lower boundary of the device operating window in terms of fusion power, and the energy confinement time scaling¹. The recommended form for the former scaling is,

¹ ITER Physics Expert Groups et al, Nucl. Fusion to be published (1999), ITER Physics Basis, Chaps. 2, 3, 4

$$P_{\text{LH}} = 2.84 M^{-1} B_T^{0.82} \bar{n}_e^{0.58} R^{1.00} a^{0.81} \quad (\text{rms err. } 0.268) \quad (\text{I.2.2-1})$$

in (MW, AMU, T, 10^{20} m^{-3} , m), with M the effective isotopic mass of the plasma fuel. This scaling expression is based on the latest version of the threshold database (DB3) extended with results from recent, dedicated, H-mode threshold experiments in Alcator C-Mod and in JT-60U¹, the latter using the new ‘W’ shaped divertor. For ITER-like devices, this scaling yields an H-mode power threshold prediction which is approximately a factor of 2 lower than that predicted by an earlier version IPB98(5)² with the 95% (i.e. 2σ) confidence interval of $P_{\text{LH}}(1.7, 0.6)$. There is, however, evidence from JET and JT-60U that the heating power should be 1.3-1.5 times higher than the H-mode threshold to obtain a good H-mode confinement. Therefore, a boundary corresponding to $1.3 \times P_{\text{LH}}$ will also be shown in some of the figures of I.2.3.

Thermal energy confinement in the ELMy H-mode is described by the IPB98(y,2) scaling,

$$\tau_{\text{E,th}}^{\text{IPB98(y,2)}} = 0.0562 I_p^{0.93} B_T^{0.15} P^{-0.69} n_e^{0.41} M^{0.19} R^{1.97} \epsilon^{0.58} \kappa_x^{0.78} \quad (\text{rms err. } 0.145) \quad (\text{I.2.2-2})$$

where the units are (s, MA, T, MW, 10^{19} m^{-3} , AMU, m) and the elongation κ_a is defined as $\kappa_a = S_0/(\pi a^2)$ with S_0 the plasma cross-sectional area. A comparison of the H-mode thermal confinement times with the scaling of eq. (I.2.2-2) for a subset of ELMy data in the ITER H-mode database is shown in Figure I.2.2-1. The 2σ log-linear or the 1σ log non-linear interval for this scaling is approximately $\pm 20\%$. In the IPB report³, five empirical log-linear (power law) scaling expressions for the energy confinement time are presented, which are derived from different subsets of the H-mode global confinement database containing data from 13 tokamak devices. The expressions fall into two distinct groups, of which two expressions, IPB98(y) and IPB98(y,1), include the H-mode data from small tokamaks and predict $\sim 20\%$ higher confinement for an ITER-like machine than three others, IPB98(y,2) to IPB98(y,4), which exclude these data. In the IPB, it is concluded that the available physical and empirical evidence is not strong enough to justify a preferential recommendation amongst these log-linear scalings. IPB98(y,2) has therefore been selected as a conservative option.

Although extensive development of numerical physics-based codes for predicting local transport properties has been undertaken during the EDA, these codes are not yet regarded as accurate enough to provide the principal basis for extrapolation to ITER. For example, the accuracy with which 11 such codes predict the plasma transport in existing tokamak plasmas has been investigated using plasma profiles obtained from a range of experiments⁴. Basing the assessment on several figures of merit (e.g. the ‘incremental’ stored energy above that contained in the H mode edge pedestal), these studies showed that while each model performed well under specific circumstances, the overall rms error was significantly greater

¹ The International H-mode Threshold Database Working Group, presented by J.A. Snipes, to be published in Plasma Phys. Control. Fusion

² ITER Physics Expert Groups et al, Nucl. Fusion to be published (1999), ITER Physics Basis, Chap. 2 Sect. 4.3

³ ITER Physics Expert Groups et al, Nucl. Fusion to be published (1999)), ITER Physics Basis, Chap. 2 Sect. 6.4

⁴ ITER Physics Expert Groups et al, Nucl. Fusion to be published (1999), ITER Physics Basis, Chap. 2 Sect. 8

than that of the ITER confinement database.

Moreover, as an interesting complement to the standard and probabilistic performance assessment outlined in this document, a different methodology¹, which strengthens the confidence in ITER-FEAT to achieve its goals, has been introduced in I.2.3.4. This procedure utilizes the H mode database by means of a similarity approach, where every shot is extrapolated to a machine with the ITER-FEAT performance requirements through the use of the system code.

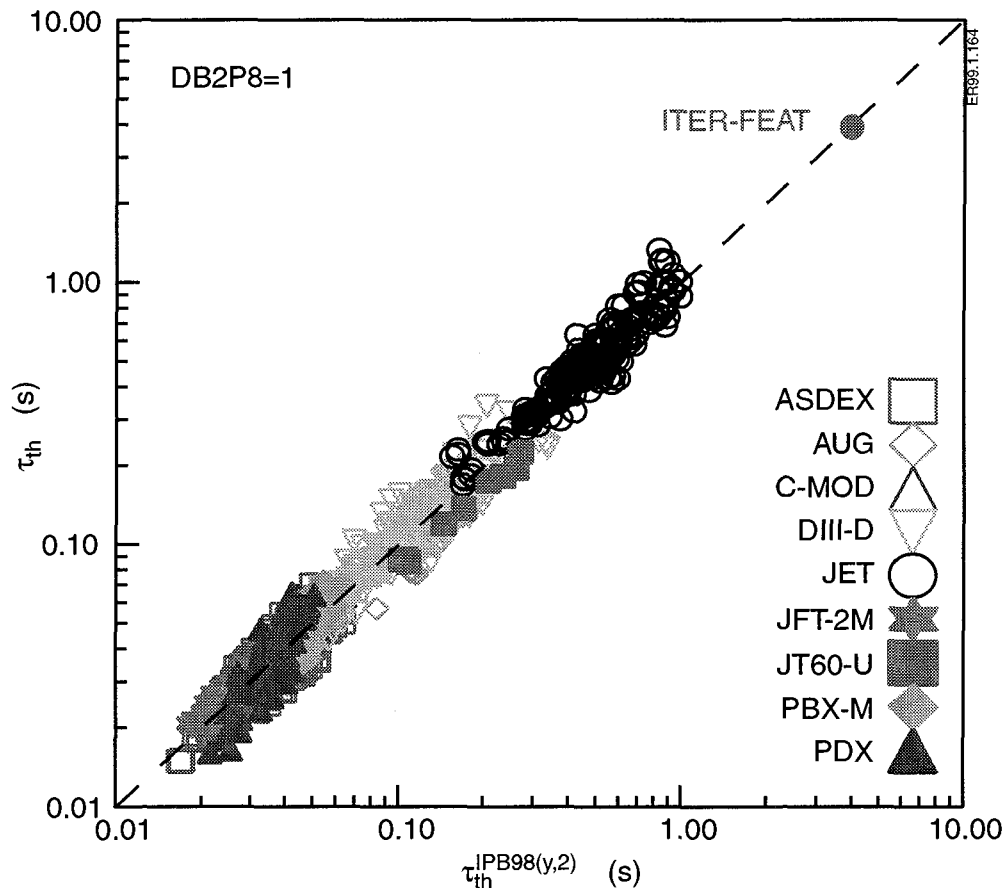


Figure I.2.2-1 Comparison of ELMy H-mode Thermal Energy Confinement Times with the Scaling Expression in Eq. (I.2.2-1). Also shown is the IPE98(y,2) scaling prediction for the energy confinement time in a nominal ITER-FEAT $Q = 10$ discharge

The principal mhd stability constraints which contribute to the definition of the device performance relate to the plasma current, elongation, plasma density, and plasma pressure. There is now an extensive energy confinement database for plasmas with $q_{95} \sim 3$, and proven experience in operation with low disruption frequency. A quantitative analysis of disruption frequency on several tokamaks has shown that ITER's goal of achieving an initial disruption frequency of 10% has been attained in existing devices, with no specific problems² due to the

¹ G 73 MD 25 00-01-12 W0.1 Dimensional scaling approach for ITER sizing with sytem code

² R. Yoshino et al, Fusion Energy Proc. 17th Int. Conf. (Yokohama, 1998) paper IAEA-F1-CN-69/ITERP1/14 to be published (1999)

proximity to $q_{95} = 3$. Although recent experiments¹ found no significant degradation of confinement with decreasing q_{95} over the range $2.3 \leq q_{95} \leq 4$, selection of a lower q_{95} operating point would reduce performance margins (particularly for higher Q operation) and might also impair steady-state capability. Therefore, $q_{95} = 3$ has been retained as an acceptable compromise between good energy confinement and satisfactory mhd stability properties, although flexibility to accommodate discharges with higher currents ($q_{95} \sim 2.7$) at reduced pulse length is under study.

Plasma-shaping capability (elongation and triangularity) derives from a consideration of axisymmetric plasma stability and power required to maintain the plasma vertical position, equilibrium control requirements (particularly if a true single null X-point equilibrium is to be retained) including inner divertor leg length, limits to the acceptable vacuum vessel forces during a vertical displacement event, and the advantages in confinement which may accrue, both from a higher current capability and from direct dependencies of energy confinement on shaping parameters. The range of issues involved in determining the optimum shaping capability has motivated a reassessment of the shaping parameters for ITER-FEAT.

An examination of the H-mode global confinement database confirms that the confinement times from JET and DIII-D are consistent with the IPB98(y,2) scaling up to the highest available values of κ_{95} (~ 1.8 at $q_{95} \leq 3.5$). On the other hand, vertical stability studies in ITER-FEAT-like devices have shown that beyond an elongation of $\kappa_{95} \approx 1.7$, vertical position control cannot be maintained within an acceptable range of PF circuit power and coil voltage if only the passive stabilization of the vacuum vessel and the active stabilization action of external poloidal field coils are employed. As a result, an elongation of $\kappa_{95} = 1.7$ ($\kappa_X \approx 1.84$) has been selected as the reference.

Although there is no explicit dependence of energy confinement time on triangularity, the "high" triangularity of the ITER-FEAT design ($\delta_{95} \approx 0.33$ or $\delta_X \approx 0.45$) reflects several potential advantages. Firstly, the current-carrying capability of the device, and hence confinement capability, is linked to triangularity through q_{95} . In addition, recent results from JET², demonstrate that operation at higher triangularity allows high confinement to be maintained at densities close to the Greenwald value, a result which has been confirmed in ASDEX Upgrade³. Finally, in steady-state scenarios, where the pressure and current profiles are closely linked, it has been predicted⁴ that the β limit should benefit from higher triangularity. One possible disadvantage is that the type I ELM frequency is known to decrease with increasing triangularity (increasing edge shear)⁵ and the resultant increase in the amplitude of heat pulses which may be produced by lower frequency ELMs is likely to lead to increased erosion of the divertor target.

Since, for a given Q value, cost analyses show⁶ that the device cost has a very shallow minimum versus aspect ratio over the range $2.8 \leq R/a \leq 3.5$, selection of the design value

¹ L. D. Horton et al, Nucl. Fusion **39** 993 (1999)

² G. Saibene et al, Nucl. Fusion **39** 1133 (1999)

³ J. Stober et al, Proc. 26th EPS Conf. on Controlled Fusion and Plasma Physics (Maastricht, 1999) to be published

⁴ e.g. A. Bondeson, Controlled Fusion and Plasma Physics Proc. 20th Euro. Conf. (Lisbon, 1993) vol 17C part IV (Geneva: European Physical Society) 1339 (1993)

⁵ JET TEAM, "Effect of divertor configuration on plasma performance in JET", in Fusion Energy 1996 (Proceedings 16th IAEA Conference, Montreal 1996), IAEA Vienna (1997) Vol.1, 371-383

⁶ G A0 RI 1 99-02-12 W0.2 Study of RTO/RC ITER Options Chapter I.2

must be based on additional considerations. A lower aspect ratio design has a lower toroidal field, higher plasma current, and turns out to have a greater margin relative to the H-mode power threshold. A device with higher aspect ratio typically operates at higher magnetic field and lower major radius, therefore plasma density can be higher ($n_{GW} \propto B/R$), that is favourable for semi-detached divertor operation (and hence exhaust power dissipation). In addition, since it can achieve a higher bootstrap current fraction for a given β_N , a higher aspect ratio device has advantages in steady-state operation: for a given Q value, it should be able to operate at lower β_N and H factor (desirable in view of the ITER-FEAT goals). On the other hand, at the ITER-FEAT scale, increasing aspect ratio leads to problems in accessibility, in particular for heating systems (due to the TF coil build), and in maintaining acceptable margins for equilibrium and vertical stability control. The ITER-FEAT design, with an aspect ratio of 3.1, while aiming to increase the potential for steady-state operation via increased aspect ratio, represents a compromise between these conflicting constraints.

As is well recognized, the $\beta^2 B^4$ dependence of fusion power motivates operation at the highest attainable β . However, in recent years, neoclassical tearing modes (NTMs) have been shown to limit the achievable β_N ($= \beta(\%)/[I_p(\text{MA})/a(\text{m})B(\text{T})]$), in ELMy H-mode plasmas, to values below the ideal limit, $\beta_N \sim 3.5$, and this instability might occur in the ITER-FEAT target range of $\beta_N \sim 1.5$ -2.5, leading to a degradation of confinement (or disruptions). A stabilization technique for NTMs based on ECCD is, however, yielding promising results on present experiments¹ and its application is foreseen in ITER-FEAT to allow control of such modes, if necessary. Nevertheless, the assumption $\beta_N \leq 2.5$ has been taken as a pragmatic limit for calculations of the ITER-FEAT operating window.

The maximum density at which high confinement can be sustained is a critical issue, not only for ITER-FEAT, but for tokamak power plants, since optimum use of the plasma pressure for fusion power production implies that densities in the vicinity of (and, in power plants, perhaps beyond) the Greenwald density ($\bar{n}_{GW}(10^{20} \text{ m}^{-3}) = I_p(\text{MA})/\pi a^2(\text{m})$) be attained. Although it has traditionally been difficult to maintain H-mode confinement at densities close to the Greenwald value, experiments at higher triangularity in JET² have obtained H-mode quality confinement at 80% of the Greenwald density. In addition, experiments with inside pellet launch in ASDEX Upgrade³ and recent experiments in DIII-D with pumping at both the inboard and outboard divertor strike points⁴ have sustained H-mode level confinement at densities beyond the Greenwald value. On the basis of these results, the conservative assumption $\bar{n}_e \leq n_{GW}$ is used to limit the density range foreseen for the ITER-FEAT reference regime. In addition, as is shown in I.2.3, ITER-FEAT can achieve its mission of $Q = 10$ at a normalized density of $n/n_{GW} \sim 0.6$, and inside pellet launch will be available to facilitate high density operation.

Several other physics considerations constrain the operating window of the chosen device. In particular, it has been decided to retain a single-null diverted equilibrium, since the scaling of the H-mode threshold power is more favourable in single null, as opposed to double null,

¹ H. Zohm et al, Proc. 26th EPS Conf. on Controlled Fusion and Plasma Physics (Maastricht, 1999) to be published

² G. Saibene et al, 25th EPS Conference on Controlled Fusion and Plasma Physics, Praha (1998)

³ P. T. Lang et al, Phys. Rev. Lett. **79** 1487 (1997)

⁴ T. Osborne et al, "Discharges with High Density and Good Energy Confinement on DIII-D", presented at 10th Workshop of ITER Confinement Database and Modelling Expert Group, unpublished (1999)

plasmas. Moreover, the difficulty of maintaining a double-null equilibrium which is fully up-down symmetric with respect to power handling is likely to impose unrealistic requirements on the accuracy of plasma vertical position control.

Scrape-off layer (SOL) and divertor behaviour influences plasma performance in several ways, but the principal issues for ITER-FEAT performance projections are the peak power to the divertor target, plasma helium fraction, and core plasma impurity content. Assumptions about the latter are derived from the 1998 ITER design basis, which was supported by extensive experimental and modelling studies. The ITER-FEAT plasma is characterized by a beryllium content of 2%, together with a mixture of sputtered carbon and a seeded noble gas, such as argon, to provide SOL/divertor radiation enhancement. There is substantial experimental evidence that helium exhaust rates are determined by the divertor throughput, rather than by helium transport rates in the bulk plasma, and that $\tau_{\text{He}}^* / \tau_E \sim 5$ can be achieved under relevant plasma conditions with the projected throughput of $200 \text{ Pam}^3\text{s}^{-1}$. This would limit helium fractions in ITER-FEAT to acceptable levels, generally below 6%.

Based on the physics constraints outlined above, and with the major dimensionless geometrical parameters determined, it is possible to identify major radius and plasma current on the basis of the requirement that $Q = 10$ be achieved, that acceptable performance margins can be maintained, and that the projected cost of the device falls within the required range. Three machines of differing major radius and plasma current were investigated, spanning the range $R = 5.95\text{--}6.4 \text{ m}$, and $I_p = 13\text{--}17 \text{ MA}$. The smallest device is the most attractive from cost considerations. However, its confinement margin for $Q = 10$ operation is small, it has little likelihood of achieving $Q > 10$ and it offers little flexibility. The largest machine readily achieves $Q = 10$ and has a large operation space for $Q > 10$, but at high cost relative to the cost target. The reference parameter set, having a plasma major radius of 6.2 m and plasma current of 15 MA , was selected as it offers a satisfactory margin for $Q \geq 10$ operation, has adequate flexibility and its cost satisfies the target.

As discussed in detail in I.2.3, performance calculations using the physics guidelines outlined here yield a substantial operating window for $Q \geq 10$ inductive operation for the selected parameter set. Operational flexibility is, nevertheless, desirable to enhance the capability of the ITER-FEAT device, for example to accommodate uncertainties in physics predictions, to allow optimization of the plasma performance, to permit the development of a range of scenarios for fusion power plants, including potential steady-state plasma regimes with internal transport barriers, and to provide for the introduction of more advanced features. Therefore, the design must be capable not only of studying the standard operating regime, but should have the flexibility and extended capability to achieve enhanced performance within the cost constraint. Several aspects of the design address this issue. For example, the inclusion of inside pellet launch opens the route towards operation at high density. Moreover, a variety of active feedback control techniques are provided for the stabilization of mhd instabilities. Active current profile control techniques could also provide an additional tool for the control of mhd activity. To extend the achievable range of Q values (and to counteract any unforeseen degradation of confinement), the possibility of operating the device with plasma currents up to $\sim 17.4 \text{ MA}$ ($q_{95} \sim 2.7$) is being explored, albeit at reduced pulse length ($> 100 \text{ s}$). Finally, the capability of operation at fusion powers up to 40% higher than the reference value (though under the assumption of no increase in total neutron fluence) is included in the design to enhance the possibility of ignited operation and to accommodate the possibility that β values higher than assumed are achieved.

I.2.3 Projection of ITER-FEAT Plasma Performance

I.2.3.1 Inductive Operation

A simple global power balance using the scalings discussed in I.2.2, together with appropriate rules on helium and impurity content and radiation losses, is incorporated in systems codes used to explore the range of design options satisfying the requirement that $Q = 10$ plasmas can be sustained for several hundred seconds. The impurities treated are helium, from fusion reactions, beryllium sputtered from the torus first wall, carbon sputtered from the divertor target, and argon, which is injected to increase radiation so that the peak power flux at the divertor target remains below 10 MWm^{-2} . The combination of impurities used, generally results in a Z_{eff} in the range 1.6-1.9, yielding a DT fuel concentration ranging from 70% to 80% of the electron density.

On this basis, operating domains at specified levels of fusion performance (either Q or fusion power) can be mapped out within the defined operation limits. In addition, more accurate calculations of plasma performance are obtained from the PRETOR¹ and ASTRA² 1.5-D transport codes, which treat effects such as fuel dilution by impurities, radiation losses, and (in PRETOR) divertor plasma behaviour more accurately, and use transport coefficients normalized to yield the predicted global energy confinement.

Parameters of two representative plasmas in ITER-FEAT are listed in Table I.2.3.1-1. The first column shows a reference $Q = 10$ discharge with the nominal plasma current of 15 MA and a fusion power of 400 MW, while the second column tabulates parameters for a regime with higher current, $I_p = 17.4 \text{ MA}$, that has the potential for a higher Q of ~ 25 and higher fusion power of $\sim 600 \text{ MW}$, although with potentially higher risk of plasma disruption³. In these simulations, Ar injection was controlled by a feedback loop used to limit the total power exhausted to the divertor target below 30 MW.

Plasma profiles typical of ITER-FEAT operating conditions are illustrated in Figure I.2.3.1-1 for three values of the auxiliary heating power (i.e. 10, 39 and 80 MW). The temperature profiles would correspond to those expected near the end of a sawtooth period (or persisting during the saturated phase for sawtooth periods which are long compared to the energy confinement time). While the precise shapes of the temperature and density profiles are determined by the form of the transport model in the PRETOR (or ASTRA) code, the electron density profile is virtually flat and therefore has a conservative (though realistic) influence on fusion performance. Moreover, for a given energy confinement time (or β), less peaked temperature profiles would, in fact, be beneficial for fusion performance. The temperature profiles at different heating powers are similar, with the electron temperature in the plasma core typically $\sim 20\%$ higher than the ion temperature,

To illustrate the range of performance which can be achieved in ITER-FEAT, Figures I.2.3.1-2 and I.2.3.1-3 show values of P_{fus} and Q as functions of the auxiliary heating power

¹ D. Boucher, Proc. IAEA Tech. Committee Meeting on Advances in Simulation and Modelling of Thermonuclear Plasmas (Montréal, 1992), Vol. 1 (Vienna: IAEA) p 142 (1992)

² G. Pereverzev, et al., 1997 Report IPP 5/42, Max-Planck-Institut für Plasmaphysik, Garching

³ ITER Physics Expert Groups et al, Nucl. Fusion to be published (1999), ITER Physics Basis, Chap. 3 Sect. 3.4.1.6

Table I .2.3.1-1 Nominal Parameters of ITER-FEAT in Inductive Operation

Parameter	Units	Reference Q = 10	High Q, high P_{fus}	Parameter	Units	Reference Q = 10	High Q, high P_{fus}
R/a	m/m	6.2/2.00	6.2/2.00	P_{aux}	MW	40	23
Volume	m ³	837	837	P_{ohm}	MW	1.3	1.7
Surface	m ²	678	678	P_{tot}	MW	123	144
Sep.length	m	18.4	18.4	P_{brem}	MW	21	29
$S_{cross-sect.}$	m ²	21.9	21.9	P_{syn}	MW	8	10
B_T	T	5.3	5.3	P_{line}	MW	19	20
I_p	MA	15.0	17.4	P_{sad}	MW	48	59
K_x/δ_x		1.86/0.5	1.86/0.5	P_{fus}	MW	410	600
K_{95}/δ_{95}		1.7/0.35	1.7/0.35	P_{sep}/P_{LH}	MW/MW	75/48	84/53
Li(3)		0.86	0.78	Q		10	24
V_{loop}	mV	89	98	τ_E	s	3.7	4.1
q_{95}		3.0	2.7	W_{th}	MJ	325	408
β_N		1.77	1.93	W_{fast}	MJ	25	33
$\langle n_e \rangle$	$10^{19} m^{-3}$	10.14	11.56	$H_{H-IPB95(y,2)}$		1.0	1.0
n/n_{GW}		0.85	0.84	τ_{α}^*/τ_E		5.0	5.0
$\langle T_i \rangle$	keV	8.1	9.1	Z_{eff}		1.65	1.69
$\langle T_e \rangle$	keV	8.9	9.9	$F_{He,axis}$	%	4.1	5.9
$\langle \beta_T \rangle$	%	2.5	3.2	$F_{Be,axis}$	%	2.0	2.0
β_p		0.67	0.62	$f_{C,axis}$	%	0.0	0.0
P_{α}	MW	82	120	$f_{Ar,axis}$	%	0.12	0.11

for discharges with $I_p = 13.1, 15.1$ and 17.4 MA in which an operating point having $H_{H-IPB95(y,2)} = 1$ and $n/n_{GW} = 0.85$ is selected. These results are obtained assuming an impurity content of 2% Be and 1.2% C, with no Ar injection, while the ratio of τ_{He}^*/τ_E is approximately constant at 5 above 40 MW and decreases slightly at lower power. The minimum fusion power at 15.1 and 13.1 MA is limited by the L-H back transition, taken as $1.3 \times P_{LH}$ where P_{LH} is given by eq. (I.2.2-1). Not surprisingly, one can see a strong increase in Q and P_{fus} with the plasma current, and a strong increase in Q with reducing the auxiliary heating power. This emphasizes the fact that the operation space is multidimensional and that plasma parameters can be adjusted to optimize the fusion performance according to whether high Q or high fusion power (e.g. to maximize the neutron wall loading) is required.

As expected, achievable Q values are reduced if plasma dilution and radiative losses associated with plasma impurities increase. Figure 1.2.3.1-4 shows the Q value as a function of the core helium fraction, n_{He}/n_e , for $I = 15.1$ MA and $P_{aux} = 40$ MW. The central He fraction for these conditions ($H_{H[98y,2]} = 1$, $n/n_{GW} = 0.85$, 2% Be, 1.2% C, no particle pinch) is higher than the edge fraction (by an increment of 1.3%). It is clear that a significant increase in the He fraction, from 4% to 6.6%, reduces the Q value from 10 to 8 only.

Similarly, Figure 1.2.3.1-5 shows the Q value as a function of Z_{eff} for these conditions, where the change in Z_{eff} results from a variation of the carbon impurity fraction between 0% and 2.4%.

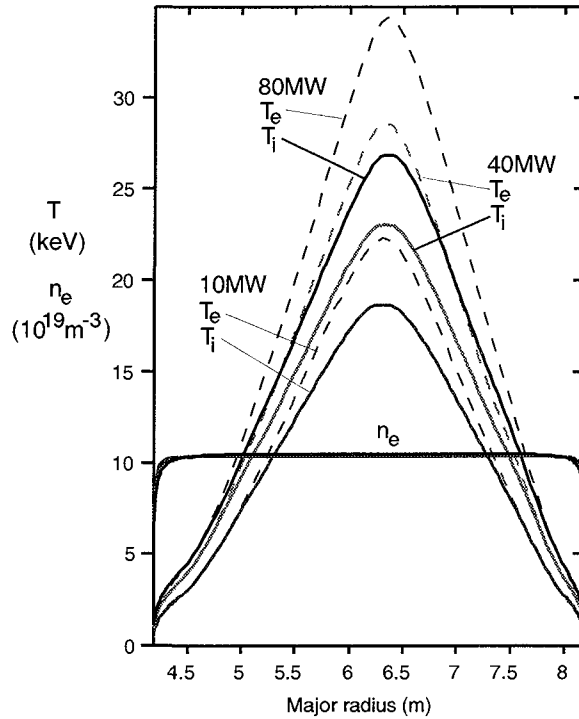


Figure I.2.3.1-1 Temperature and Density Profiles at Nominal Plasma Current $I_p = 15.1$ MA and $P_{\text{aux}} = 10, 40$ and 80 MW

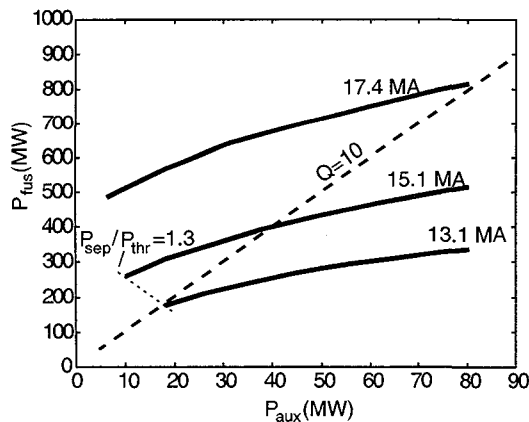


Figure I.2.3.1-2 P_{fus} as a Function of P_{aux} for $I = 13.1, 15.1$ and 17.4 MA at $H_{\text{H-IPB9}(y,2)} = 1$ and $n/n_{\text{GW}} = 0.85$

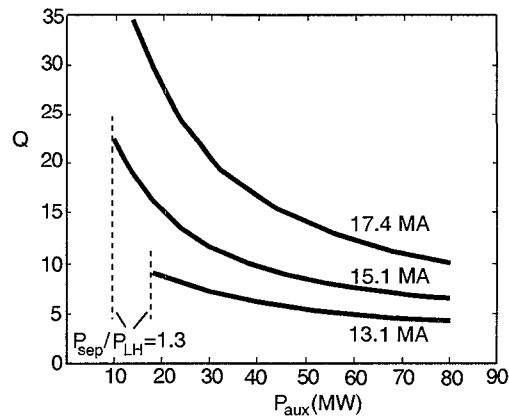


Figure I.2.3.1-3 Q as a Function of P_{aux} for $I = 13.1, 15.1$ and 17.4 MA at $H_{\text{H-IPB9}(y,2)} = 1$ and $n/n_{\text{GW}} = 0.85$

A more complete view of the range of plasma parameters at which $Q = 10$ operation is possible can be gained from an analysis of the operational domain in terms of fusion power and confinement enhancement factor, in which the various operational boundaries

($P_{\text{loss}} = 1.3P_{\text{LH}}$, $n = n_{\text{GW}}$, and $\beta_N = 2.5$) can also be traced, as shown in Figure I.2.3.1-6 and Figure I.2.3.1-7. These figures (as well as the subsequent figures in this section) are calculated using a 0-D code and include impurity contributions from He ($\tau_{\text{He}}^* / \tau_E = 5$), Be (2%) and C (1.2%), with no Ar injection.

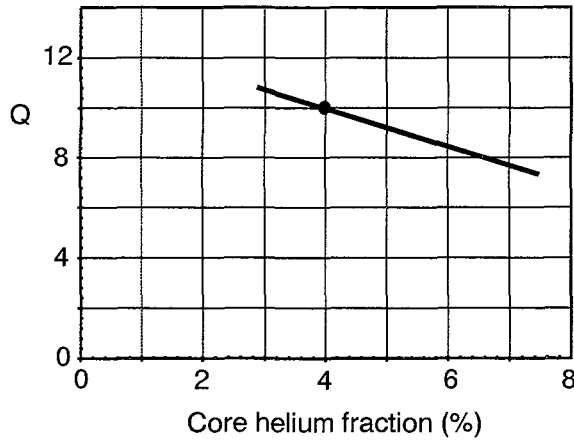


Figure I.2.3.1-4 Q as a Function of Core He fraction for $I_p = 15.1$ MA, $P_{\text{aux}} = 39$ MW at $H_{\text{H}[98y,2]} = 1$ and $n/n_{\text{GW}} = 0.85$

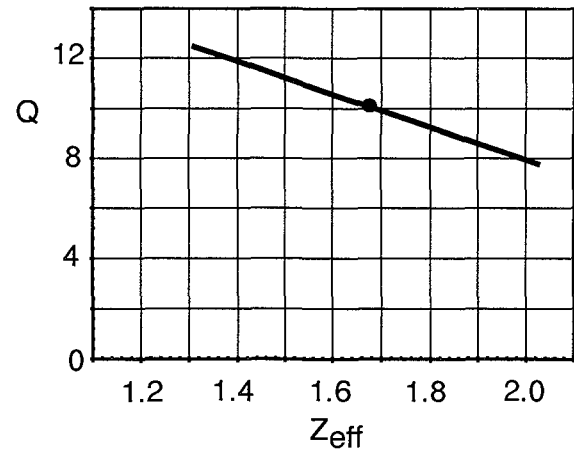


Figure I.2.3.1-5 Q as a Function of Z_{eff} for $I_p = 15.1$ MA, $P_{\text{aux}} = 39$ MW at $H_{\text{H}[98y,2]} = 1$ and $n/n_{\text{GW}} = 0.85$

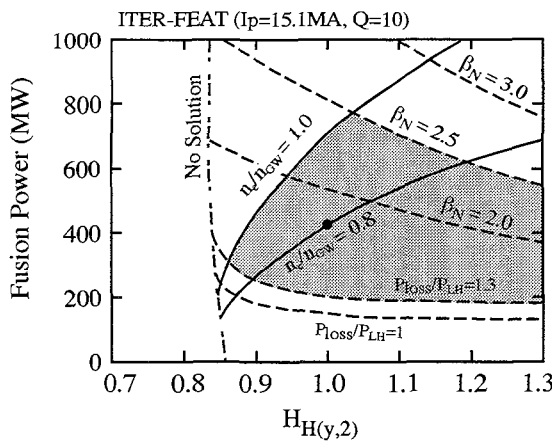


Figure I.2.3.1-6 $Q = 10$ Domain (shaded) for $I_p = 15.1$ MA ($q_{95} = 3.0$)

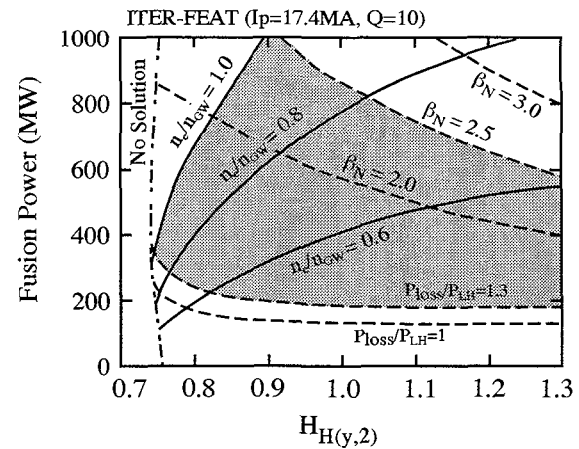


Figure I.2.3.1-7 $Q = 10$ Domain (shaded) for $I_p = 17.4$ MA ($q_{95} = 2.6$)

From the above, the following points are evident.

- For operation at $q_{95} = 3$ the fusion output power from the ITER-FEAT design is in the region of 200-600 MW (at $H_{\text{H}[98y,2]} = 1$), corresponding to a mean separatrix neutron flux ('mean neutron wall loading') of $0.29\text{--}0.86 \text{ MWm}^{-2}$, so that the device retains a significant capability for technology studies, such as tests of tritium breeding blanket modules.
- The margin in H-mode threshold power (at $H_{\text{H}[98y,2]} = 1$) is significantly greater than the predicted uncertainty derived from the scaling of eq. (I.2.2-1).
- The device has a capability for $Q = 10$ operation at $n/n_{\text{GW}} \sim 0.6$ and $\beta_N \sim 1.5$ (when $H_{\text{H}[98y,2]} = 1$). Although operation at higher current ($q_{95} = 2.6$), would entail a shorter burn duration (though still in excess of 100 s), the results illustrate the flexibility of the design, its capacity for responding to factors which may degrade confinement while

maintaining its goal of extended burn $Q = 10$ operation, and, by implication, its ability to explore higher Q operation as long as energy confinement times consistent with the confinement scaling are maintained.

Figures I.2.3.1-8 ($I_p = 15.1$ MA) and I.2.3.1-9 ($I_p = 17.4$ MA) illustrate the window for higher Q operation ($Q = 50$, representative of ‘controlled ignition’) in ITER-FEAT, showing that controlled ignition is not precluded: operation at a range of Q values is possible and values as high as 50 can be attained if $H_{H[98y,2]} \sim 1.2$ is achieved in an improved confinement mode e.g. reversed-shear or shallow-shear mode with internal transport barrier, or high density operation can be extended beyond the Greenwald value, or operation at lower q_{95} (~ 2.6) can be sustained without confinement degradation.

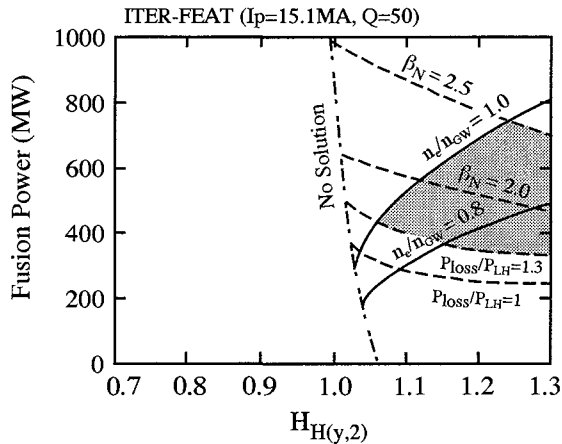


Figure I.2.3.1-8 $Q = 50$ Domain for $I_p = 15.1$ MA ($q_{95} = 3.0$)

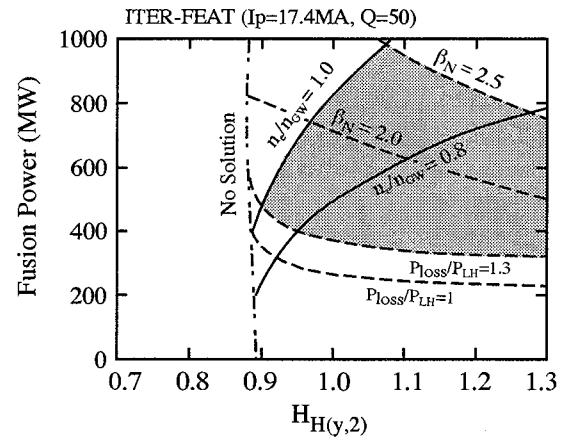


Figure I.2.3.1-9 $Q = 50$ Domain for $I_p = 17.4$ MA ($q_{95} = 2.6$)

The temperature dependence of the fusion cross-section means that plasma fusion performance is sensitive to the form of the temperature profile at fixed β or τ_E . Figures I.2.3.1-10 and I.2.3.1-11 illustrate how this sensitivity affects the operational domain at $Q = 10$ and $Q = 50$ respectively for the 15.1 MA reference scenarios. The 0-D calculations, from which the operational domains discussed here are derived, assume temperature profiles of the form $T(x) = T(0)(1-x^2)^{AT}$, with AT an arbitrary parameter. For the analyses shown in previous figures, $AT = 2$ was assumed (corresponding to a ratio of $T(0)/\langle T \rangle = 3$), while for the analyses in the figures below, $AT = 1.0$. In both figures it can be seen that the Greenwald density represents less of a constraint on the operational domain in the sense that the constant density contours become more vertical, opening a larger confinement margin at high fusion power.

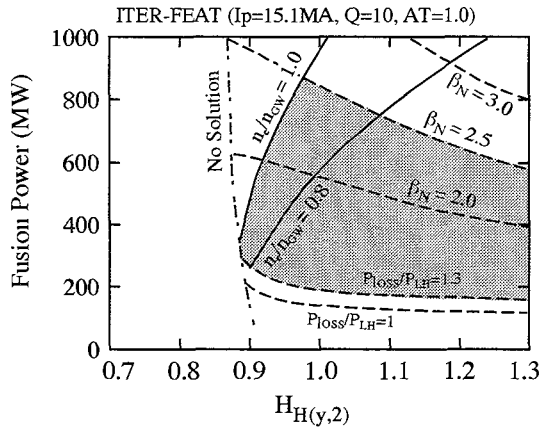


Figure I.2.3.1-10 $Q = 10$ Domain for $I_p = 15.1$ MA ($q_{95} = 3.0$). Here, $T(x) = T(0)(1-x^2)^{AT}$ is assumed, with $AT = 1$

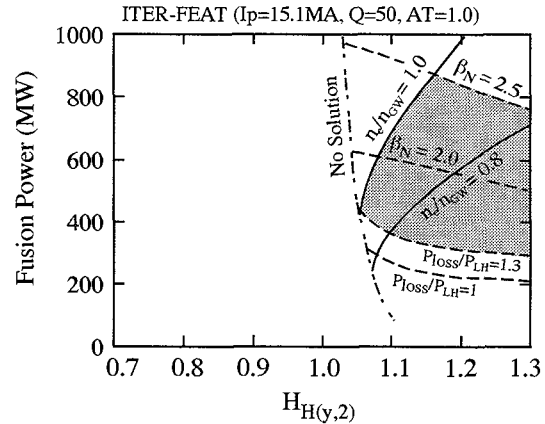


Figure I.2.3.1-11 $Q = 50$ Domain for $I_p = 15.1$ MA ($q_{95} = 3.0$). Here, $T(x) = T(0)(1-x^2)^{AT}$ is assumed, with $AT = 1$

I.2.3.2 Steady-state and Hybrid Operation

A complete scenario for steady-state operation with $Q = 5$ in which energy confinement, plasma profiles, current drive requirements, divertor performance and plasma equilibrium are treated self-consistently and satisfy all relevant constraints, is yet to be developed (and will, in fact, require considerable further analysis). Nevertheless, in ITER it is likely that a variety of candidate steady-state modes of operation will be investigated, and it is therefore essential that the requisite tools for the control of plasma geometry and profiles are available: on-axis and off-axis current drive capabilities to enable plasmas with shallow- or reversed-shear configurations to be sustained, in the latter regime simultaneously maintaining the central safety factor well above unity, while the minimum safety factor is held above two, a poloidal field system capable of controlling the more highly shaped plasmas characteristic of high β_p operation, and methods to allow reliable long pulse operation at high β , including techniques for the stabilization of neoclassical tearing modes and resistive wall modes.

The capability of the ITER-FEAT designs for steady-state operation with $Q = 5$ are being studied numerically within the limitations of current assumptions. Two operational scenarios are under consideration for steady-state operation: high current (12 MA) with monotonic q or shallow shear, and modest current (8 MA) with negative shear. The high current, steady-state operation requires all the current drive power (100 MW) available for ITER-FEAT, but the requirements on confinement ($H_H \sim 1.2$) and beta ($\beta_N \sim 3$) are modest. On the other hand, the low current, steady-state operation requires more challenging values of confinement improvement $H_H \sim 1.5$ and beta ($\beta_N \sim 3.2$ - 3.5). Performance predictions for this mode of operation are much less certain than for inductive operation and high current, steady-state operation. In addition, the potential performance of hybrid modes of operation, in which a substantial fraction of the plasma current is driven by external heating and the bootstrap effect, leading to a substantial extension of the burn duration, is being evaluated as a promising route towards the establishment of true steady-state modes of operation. This form of hybrid operation would be well suited to systems engineering tests.

An operation space, in terms of fusion power versus confinement enhancement factor, and showing the transition from hybrid to true steady-state operation is illustrated in Figure I.2.3.2-1 for $I_p = 12$ MA and $P_{CD} = 100$ MW. Contours of constant n_e/n_{GW} and β_N are indicated, as is the threshold for $Q = 5$ operation. Note that it is assumed that the plasma minor radius is reduced by shifting the magnetic axis outward. For a given value of fusion power (and hence Q), as the confinement enhancement factor, $H_{H[98y,2]}$, increases (simultaneously decreasing plasma density and increasing β_N), the plasma loop voltage falls towards zero. For example, operation with $V_{loop} = 0.02$ V and $I_p = 12$ MA, which corresponds to a flat-top length of 2,500 s, is expected at $H_{H[98y,2]} = 1$, $Q = 5$, $n_e/n_{GW} = 0.7$, and $\beta_N = 2.5$. True steady-state operation at $Q = 5$ can be achieved with $H_{H[98y,2]} = 1.2$ and $\beta_N = 2.8$. This analysis indicates that a long pulse mode of operation is accessible in ITER-FEAT.

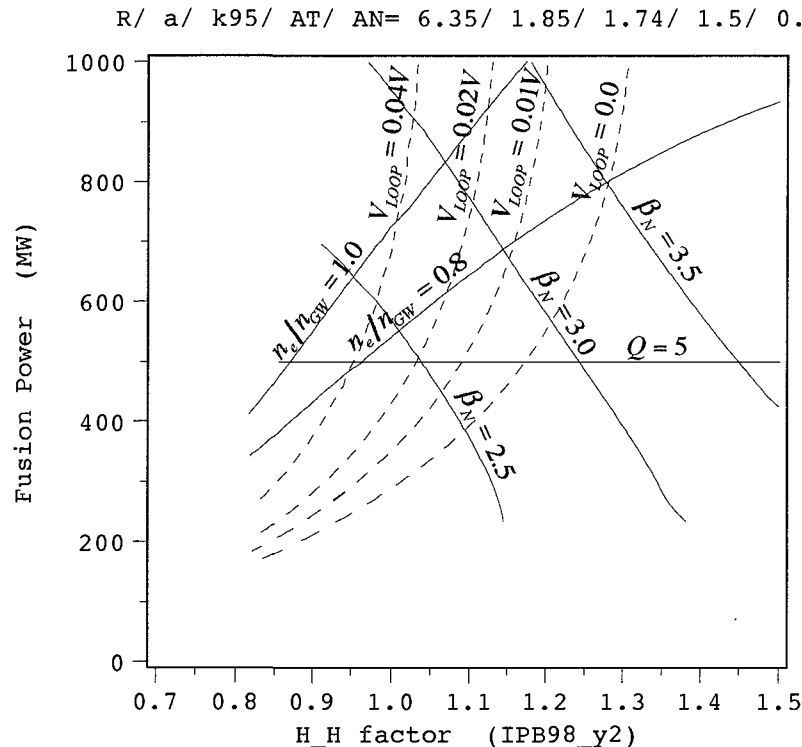


Figure I.2.3.2-1 Operation Space for ITER-FEAT for Hybrid (long pulse) and Steady-state Operation.
Here, $I_p = 12$ MA and $P_{CD} = 100$ MW

I.2.3.2.1 Potential Parameters for Steady-state Operation with Full Minor Radius

The plasma parameters required for steady-state operation in full bore plasmas have been surveyed by using simple 0-D calculations. Figure I.2.3.2-2 shows how confinement enhancement ($H_{H[98y,2]}$), β_N , and current drive power (P_{CD}) can be traded off against one another while satisfying the requirement for steady-state, $Q = 5$ operation (at $n_e/n_{GW} = 0.8$). The current drive power rapidly increases with β_N , while $H_{H[98y,2]}$ decreases with increasing β_N . This allows some selection in parameters, depending on whether enhanced confinement or high β_N operation turns out to be the more difficult to access. From this analysis it can be concluded that if the available current drive power is assumed to be $P_{CD} \leq 100$ MW, the required $H_{H[98y,2]}$ is ~ 1.3 . A further constraint might arise from the product of $\beta_N \times H_{H[98y,2]}$. In current experiments, especially for long pulses, this product is found to be

limited, with $\beta_N H_{H[98y,2]} \leq 4$ when $t \geq 10\tau_E$. With such a restriction, the operation region would be very small (see Figure I.2.3.2-2a). However, this product has been improved to $\beta_N H_{H[98y,2]} \leq 6$ in the most recent experiments and, if this more relaxed constraint is applied, the restriction on the accessible range of $\beta_N H_{H[98y,2]}$ with $P_{CD} \leq 100$ MW can be removed.

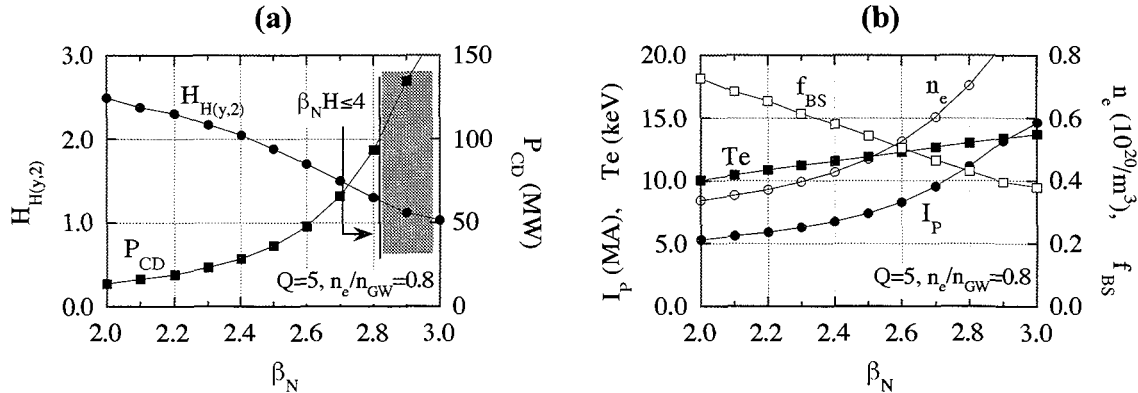


Figure I.2.3.2-2 (a) Possible Steady-state Operation Parameters with Fusion Gain of $Q = 5$ and $n_e/n_{GW} = 0.8$ (b) Electron Density (n_e), Plasma Current (I_P), Electron Temperature (T_e), and Bootstrap Current Fraction (f_{BS}) as a Function of β_N for the Calculated Points Shown in (a)

For completeness, Figure I.2.3.2-3 shows $H_{H[98y,2]}$, current drive power (P_{CD}), electron density (n_e), plasma current (I_P), electron temperature (T_e), and bootstrap current fraction (f_{BS}) as a function of β_N for a fusion gain $Q = 5$ and $n_e/n_{GW} = 0.6$, illustrating how the requirements for steady-state operation change as the normalized plasma density is varied. Similar trends are seen, with the most significant difference being an increased requirement on $\beta_N H_{H[98y,2]}$ at low values of P_{CD} .

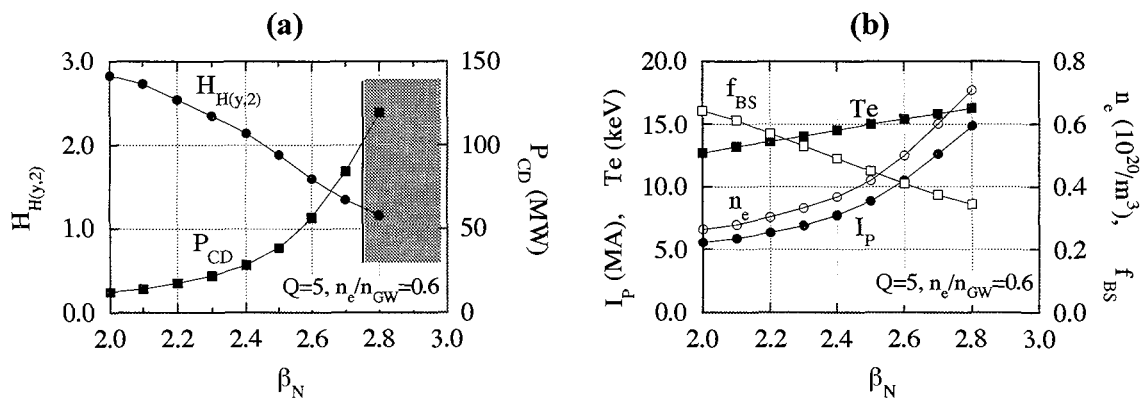


Figure I.2.3.2-3 Possible Steady-state Operation Parameters with Fusion Gain $Q = 5$ and $n_e/n_{GW} = 0.6$

I.2.3.2.2 Potential Steady-state Operation Space with Reduced Minor Radius at $I = 12$ MA

It is expected that plasmas having a higher aspect ratio have better potential, steady-state performance due to the larger bootstrap current contribution. Such plasmas can, in principle,

be established by shifting the plasma magnetic axis outward, and the potential benefits of such an approach are illustrated in Figure I.2.3.2-4. The figure shows the $Q \geq 5$ steady-state operation space with $R = 6.35$ m and $a = 1.85$ m for a plasma current of 12 MA and a slightly increased plasma elongation ($\kappa_{95} = 1.74$). For these calculations the density profile was taken to be flat. Typical values of current drive efficiency obtained are $\gamma_{20} \sim 0.30$ $\text{AW}^{-1}\text{m}^{-2}$ in (a) and ~ 0.36 $\text{AW}^{-1}\text{m}^{-2}$ in (b) (defined as $\gamma_{20} = n_{20} [\times 10^{20} \text{ m}^{-3}] R[\text{m}] I[\text{A}] / P[\text{W}]$).

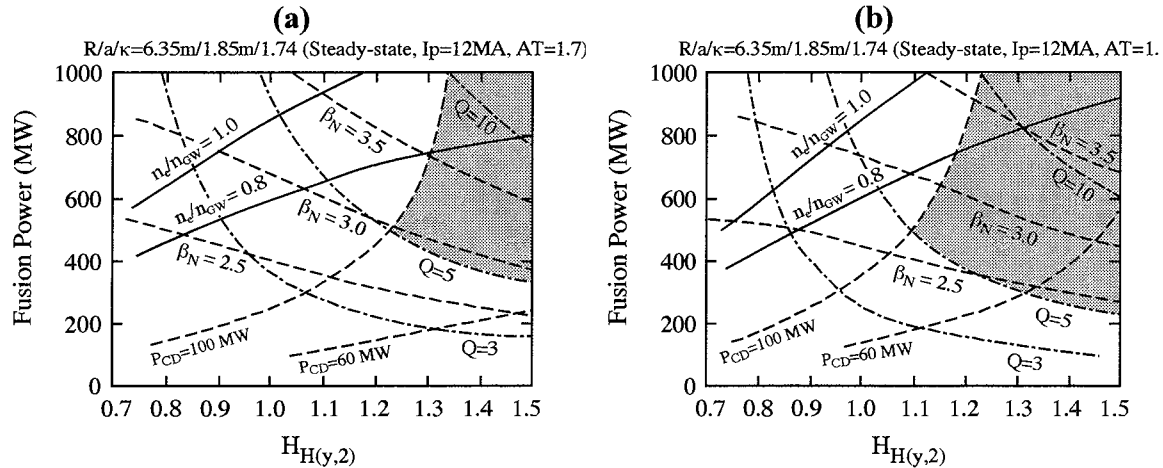


Figure I.2.3.2-4 Steady-state Operation Space for ITER-FEAT with Reduced Minor Radius at $I_p = 12$ MA, $\kappa = 1.74$ and Temperature Profiles of the Form $T(x) = T(0)(1-x^2)^{AT}$: (a) $AT = 1.7$, (b) $AT = 1$.

Here, $f(\text{Be}) = 2\%$, $f(\text{Ar}) = 0.17\%$ and no carbon is assumed. Operation limits defining the shaded area in each plot are given by $Q \geq 5$ and $P_{CD} \leq 100$ MW

Under the assumptions used here, the higher aspect ratio plasma exhibits a larger operation space for $Q \geq 5$ operation than the full bore plasma, with a particularly significant gain for the case with a more peaked temperature. Nevertheless, the minimum requirement for $H_{H[98y,2]}$ is ~ 1.1 , which is the same as for the full bore plasma. The requirement on electron density is, however, larger than that of the full bore plasma, which is favourable for divertor performance. Note that if $H_{H[98y,2]} = 1.3$ can be achieved, steady-state operation would be possible with $P_{CD} = 60$ MW, while $H_{H[98y,2]} = 1.5$ would be required for the full bore plasma.

The conclusions of this initial study are that steady-state operation would be favoured by a broader temperature profile, due to the higher fusion power (and hence gain) achieved for the same plasma energy and higher current drive efficiency which results. A preliminary 1.5-D transport analysis of such cases, however, yielded a profile peaking factor of 2.5 (equivalent to $AT = 1.5$). Considerable further analyses and experimental developments are therefore required to establish self-consistent plasma conditions for steady-state regimes.

I.2.3.2.3 1.5-D Simulation of Steady-state Operation

Since it is probable that steady-state operation will require some form of profile control, and since this will inevitably influence the achievable fusion performance in such regimes, studies of non-inductive operation with 1.5-D transport codes have been initiated. Table I.2.3.2-1 shows parameters for a range of potential $Q = 5$, steady-state scenarios for ITER-FEAT developed in the course of this analysis: cases 1-3 and 5 were studied with ASTRA, while case 4 was analyzed with PRETOR. Cases 1 and 2 have reversed shear with $q_{\min} = 2.5$

and 2.0 respectively, a small minor radius, outward shifted radial position and high elongation. These scenarios are characterized by high β_N (3.17-3.48) and high bootstrap current fractions ($\sim 50\%$). Plasma profiles for case 1 are shown in Figure I.2.3.2-5. The minimum q position is located at $r \sim 0.75$, and inside this radius the ion heat conductivity is reduced to the neoclassical level. However, the density profile is almost flat, except at the plasma edge. Although substantial off-axis heating is required in these cases, if the plasma temperature and density profiles were appropriately controlled, external current drive in the outer region (e.g. $r \geq 0.7$) would not be needed. Case 3 has positive shear with the nominal ITER-FEAT plasma size and shaping, and requiring a more modest β_N of 3.0, while case 4 has shallow shear with higher plasma current (11 MA), for which the required β_N is 2.56.

Table I.2.3.2-1 Potential Scenarios for $Q = 5$ Steady-state Operation

		1	2	3	4	5
		RS	RS	Positive shear	Shallow shear	Weak RS
R/a	(m)/(m)	6.6 / 1.6	6.6/1.6	6.2/2.0	6.2/2.0	6.15/1.85
B	(T)	4.98	4.98	5.3	5.3	5.34
$\kappa_{95} / \delta_{sep}$		2.0 / 0.5	2.0/0.5	1.86/0.5	1.74/0.5	1.74/0.5
I_p	(MA)	7.8	9.0	10.0	11.2	12
$\langle n_e \rangle$	($10^{19}m^{-3}$)	7.8	8.65	6.0	7.2	7.7
n/n_{Gr}		0.83	0.8	0.8	0.8	0.72
$\langle T_i \rangle$	(keV)	10.6	12.1	12.9	11.6	14.1
$\langle T_e \rangle$	(keV)	12.8	14.2	14.5	14.4	14.6
β_N		3.17	3.48	2.98	2.56	3.04
P_{fus}	(MW)	308	457	352	387	503
P_{NB}	(MW)	7	6.5	60	45	100
P_{shth}	(kW)	0.8	0.25	61.8		
P_{EC}	(MW)	0.5	0.5	10	32	0
P_{off} (LH or NB)	(MW)	52	72			
$Q = P_{fus} / P_{aux}$		5.2	5.78	5.0	5.0	5.0
$P_{loss} / P_{thr. L-H}$		2.9	3.87	3.26	3.04	
τ_E	(s)	2.6	2.26	2.44	2.98	1.93
f_α	(%)	3.0	3.5	3.6		3.6
Z_{eff}		1.66	1.67	1.68	1.84	1.8
P_{rad}	(MW)	18.9	24.8	22.4	45	29
I_i (3)		0.49	0.51	1.05	1.0	0.83
I_{CD} / I_p	(%)	46.4	47.5	71.8	73.1	74.8
I_{bs} / I_p	(%)	53.6	52.5	28.2	26.9	25.2
q_{95}		4.1	3.5	4.6	4.3	3.4
$H_{H(y,2)}$		1.49	1.4	1.47	1.5	1.2
τ_α^* / τ_E		5.0	5.0	5.0	4.6	5.0

Cases 1-4 indicate that a substantial improvement over standard H-mode confinement (i.e. $H_{H[98y,2]} = 1.4-1.5$) is required to achieve a steady-state with $Q = 5$. However, case 5 uses high power NB (100 MW) for current drive, which reduces the confinement requirement to $H_{H[98y,2]} \sim 1.2$, illustrating again that the requirement for confinement improvement becomes

more modest with increasing current drive power. On the expectation that comparable current drive efficiencies can be achieved with NB, EC and IC auxiliary power, case 5 is probably feasible with the current drive capability available for ITER-FEAT, i.e. a total of 100 MW current drive power using a combination of NB and RF.

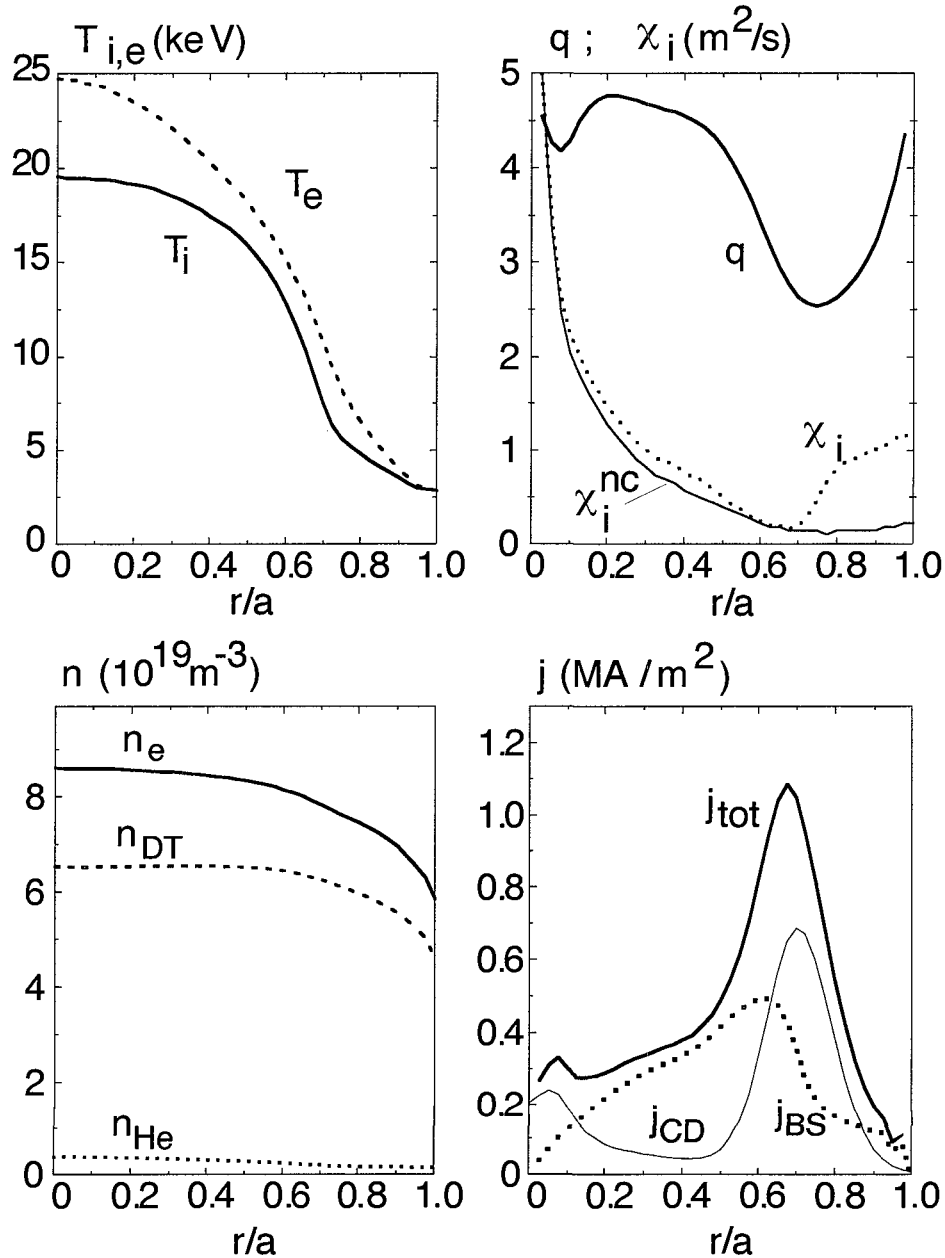


Figure I.2.3.2-5 Radial Profiles for the Potential Reversed Shear ITER-FEAT Steady-state Regime with Strong Off-axis H&CD ($r/a \sim 0.7$)

(NB or LH: CD efficiency $\sim \gamma_{20} = 0.3 \text{ AW}^{-1} \text{ m}^{-2}$): $P(\text{off-axis}) = 52 \text{ MW}$; $P_{NB}(\text{on-axis } \Delta Z = 0.3 \text{ m}) = 7 \text{ MW}$; $P_{ECRF}(\text{on-axis}) = 0.5 \text{ MW}$; $I_p = 7.8 \text{ MA}$; $H_{H(y,2)} = 1.49$; $q_{min} > 2.5$; wide RS region

I.2.3.3 Probabilistic Performance Assessment

A full and rigorous assessment of the probability of an ITER-class device achieving a predetermined level of performance is a complex undertaking. It involves not only an assessment of experimental uncertainties in the ability to extrapolate the interaction of complex physical processes (e.g. transport losses, mhd stability, helium exhaust, impurity production) to the ITER scale, and in particular close to plasma operating limits, but also an analysis of the certainty with which the performance of key engineering systems (ranging from superconducting coils to pellet injection technology) can be predicted. The latter task could probably be attempted using well established engineering reliability analyses, though at considerable expenditure in resources relative to the value that can be placed in the outcome. However, the former implies a deep understanding of the nature of the uncertainties in the experimental measurements available from existing devices. Later, an initial approach to an assessment of the influence of the uncertainties in one key physics parameter, the global energy confinement time, is developed. However, it is perhaps beneficial to consider firstly, a very simple approach to the estimation of the attainable fusion performance in ITER-FEAT.

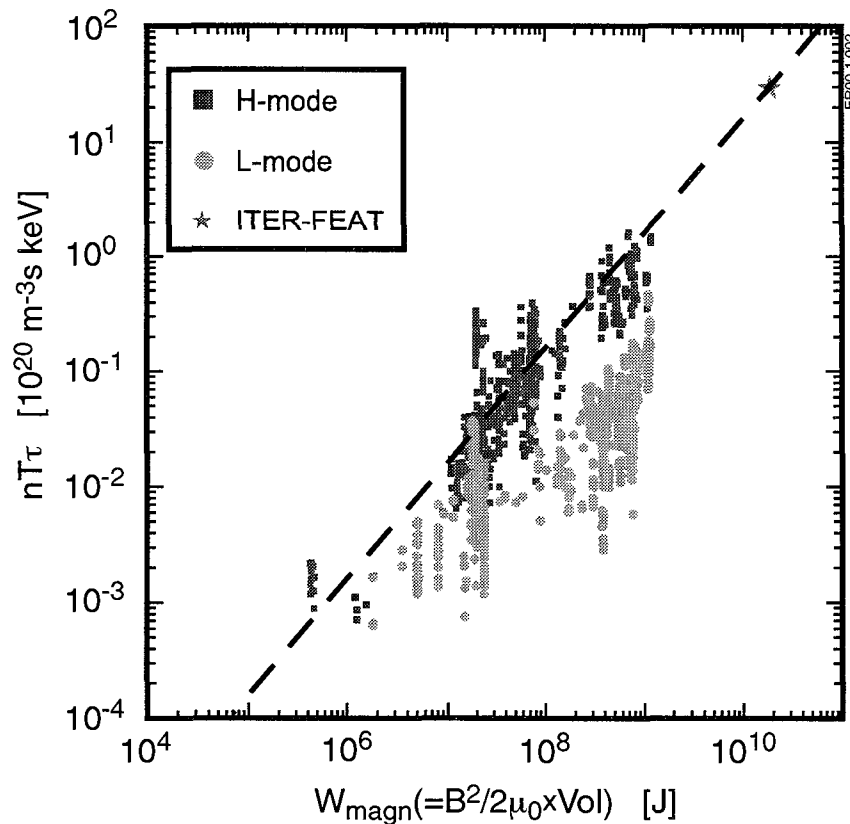


Figure I.2.3.3-1 Plot of the Fusion Triple Product, $nT\tau$, (volume averaged quantities) versus the Toroidal Magnetic Field Energy (within the plasma volume), W_{magn} .¹ The data is taken from the ITER ELMy H-mode and L-mode (excluding ohmic) databases, and the ITER-FEAT point corresponds to the $Q = 10$ operating point in Table I.2.3.1-1. The dashed line, shown to guide the eye, corresponds to a line passing through the ITER-FEAT point and the origin in linear co-ordinates, ie (0, 0)

¹ O.J.W.F. Kardaun, A.Kus and H- and L-mode Database Working Group (1996), in Proceedings of Computational Statistics XII, 313-318 (A. Prat, Ed.) Physica-Verlag, Heidelberg

Figure I.2.3.3-1 shows a plot of the fusion triple product, $nT\tau$, for pulses in the ITER L-mode and ELMy H-mode databases, plotted against a measure of the toroidal magnetic field energy for the devices in question. An estimate for ITER-FEAT has been added based on the performance calculations discussed in I.2.3.1. There are two striking aspects of the figure. Firstly, if one considers the upper envelope of the data, it appears that the device performance can be characterized by an extremely simple (and robust) parameter over many orders of magnitude. Moreover, the projection of the upper range of the data extrapolates comfortably to the $Q = 10$ point in ITER-FEAT, indicating that the device has the correct global dimensions (essentially major radius and magnetic field) to achieve its aims. In other words, there is consistency between the more sophisticated analysis based on plasma transport (with its attendant uncertainties) and a simple characterization of the device performance (which, as illustrated in the figure, is a remarkably good description over an extensive range of device sizes and plasma parameters).

The second aspect is that at each value of the abscissa, there is a large scatter in the data. This reflects several realities of the exploitation of experimental devices.

- i) In the course of experimentation, performance improvements are developed through a better understanding of physics processes (the H mode is the clearest example of this) and through an optimization of plasma properties based on experimentation.
- ii) The devices are not always operated close to the optimum performance: parameters are systematically varied to develop physics understanding, operating limits are investigated, and certain modes of operation are found to degrade plasma performance and are eliminated as experimental scenarios.
- iii) There remain 'hidden parameters', i.e. physical processes (e.g. neutral recycling) the influence of which is not well understood. Nevertheless, as a result of experimentation, tokamak operators can optimize the performance of the plasma in a robust, if empirical, way. The scatter shown does not represent the shot-to-shot or day-to-day variation of plasma performance in well established plasma regimes: these exhibit a high level of reproducibility, with scatter which is close to that due to experimental measurement errors.

The fusion performance capability of any device cannot, therefore, be characterized by a single number. Each device has a substantial range of performance accessible to it, and the development of parameters which lead to the optimum performance is based on an experimental appreciation of the balance between conflicting requirements (e.g. high current and mhd stability) and, in particular, the positioning of the operating point close to operational limits, but still within the region of acceptable confinement. The operating space of the device is, therefore, a multi-dimensional space which is usually projected into two dimensions for the purposes of illustration. The many dimensions (some of which correspond to alternative modes of operation) represent directions in which performance can be optimized to counteract deleterious effects in certain directions: for example, to compensate for confinement degradation in the proximity of the density limit, the current can be increased (again within the bounds of mhd stability and acceptable confinement), as illustrated in Figure I.2.3.1-7; to offset limitations in β_N associated with neoclassical tearing modes, ECCD can be applied for NTM stabilization, or can be used to control the sawtooth period to limit the production of seed islands.

The parameter which lends itself most readily to a probabilistic analysis is the global energy confinement time, since it is derived from an extensive database incorporating results from

many devices and from a wide range of plasma operating conditions. However, it is not a statistical database in the strict sense. In particular, the scatter observed in the measured energy confinement times does not necessarily represent experimental uncertainty, or random irreproducibility, but often represents different ways of operating the devices which are not fully characterized in the database. Moreover, it does not represent a random sample of the parameter space with which it is concerned. Since it is compiled without an explicit focus on extrapolation to the plasma parameters of ITER, the statistical error in the ‘best fit’ confinement time calculated for ITER-FEAT is not necessarily an accurate estimate of the uncertainty in the energy confinement time in the ITER-FEAT operating domain. Finally, the experimental points in the global confinement database may not adequately characterize the behaviour of confinement as operating limits are approached. Therefore, a simple characterization of the uncertainty in the extrapolated confinement time by means of an rms error, or a standard deviation, may not be appropriate over the entire operating domain for a given Q . These caveats must be borne in mind in considering the following analysis.

To provide a preliminary analysis of the probability of achieving a fusion gain of $Q \geq 10$ in ITER-FEAT, a formalism based only on the estimated uncertainty in the form of the confinement scaling has been developed. The analysis makes use of the 0-D operation domains of the type discussed in I.2.3.1. This approach does not provide information on, for example, the probability of achieving a specified neutron fluence, since many other factors influencing the average duty cycle, and the total operational time of the device must be considered.

The starting point for the analysis is the IPB98(y,2) confinement scaling used in the calculation of fusion performance for ITER-FEAT. Based on the log-linear form of the scaling, the estimated value of σ is $\sim 10\%$. An alternative estimation of the uncertainty interval in the projected energy confinement time based on non-log-linear scalings yields a σ estimate of $\sim 20\%$. It is therefore assumed that the energy confinement time (or, in practice, the $H_{H[98y,2]}$ factor) for a given set of plasma parameters can be described by a Gaussian distribution having a standard deviation of either 10% or 20% about the mean (i.e. scaling expression) value. However, for similar discharge conditions the distribution of $H_{H[98y,2]}$ in the database has a smaller spread: for example, with $n_e/n_{GW} \geq 0.65$, $q_{95} \leq 3.5$, $P_{RAD}/P_{HEAT} \leq 0.5$ and $\kappa \geq 1.5$, the spread of $H_{H[98y,2]}$ values in the database is only 5%. This illustrates the point made previously, that only a fraction of the scatter in the experimental data is associated with irreproducibility in discharge conditions.

Figure I.2.3.3-2 shows the operation domains (fusion power vs $H_{H[98y,2]}$) at 15.1 MA for two fixed values of heating power. The probability of achieving $Q \geq Q_0$ (where Q_0 is some given value of fusion gain) is defined by the integral of the distribution function of $H_{H[98y,2]}$ from the minimum value within the shaded area to the maximum. For example, the probability of achieving $Q \geq 11$ when $P_{AUX} = 40$ MW (Figure I.2.3.3-2a) is 50%, since the device parameters are defined so that $P_{fus} = 440$ MW when $H_{H[98y,2]} = 1$ and $P_{AUX} = 40$ MW. The shape of the operation domain for this case is such that the probability of achieving a given value of Q decreases with increasing fusion power (or Q). In contrast, for $P_{AUX} = 15$ MW (Figure I.2.3.3-2b), the probability has a maximum value at a fusion power of 260 MW (i.e. $Q = 17$).

Figure I.2.3.3-3 summarizes the probability of achieving $Q \geq Q_0$ in ELMy H-mode for a range of values of P_{AUX} when $\sigma = 20\%$. For several values of P_{AUX} (= 6, 10, 15 MW), it is

clear that the probability is constant below a certain value of Q_0 , and that the probability lies below 100%. This is associated with the fact that the small value of total loss power ($\sim (1 + Q/5) P_{AUX}$) is insufficient to exceed the H-mode power threshold (the probability of achieving values of Q lower than the corner point of each curve is not, of course, zero, since there is an operation point corresponding to the corner point of the curve, e.g. $Q_0 = 17$ at $P_{AUX} = 15$ MW).

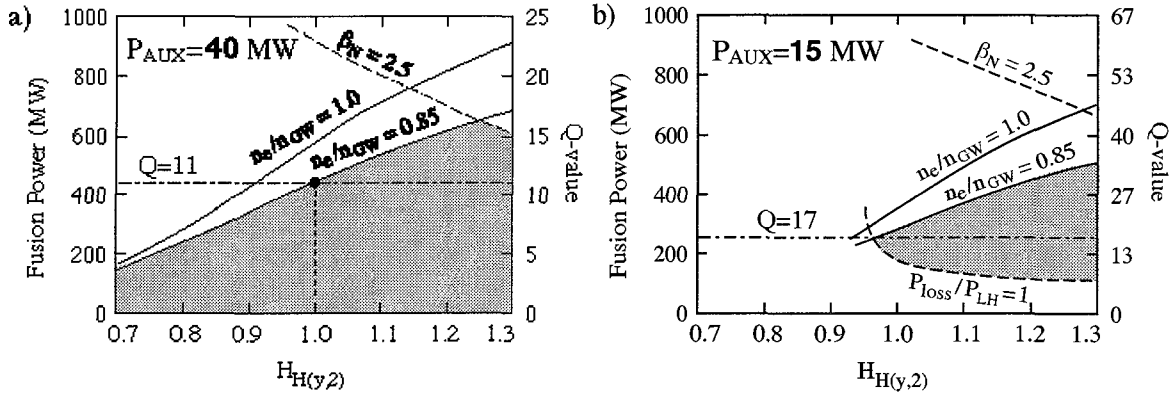


Figure I.2.3.3-2 Operation Domain (shaded) for Fixed Heating Power P_{AUX} : a) $P_{AUX} = 40$ MW, b) $P_{AUX} = 15$ MW, Defined by $n_e/n_{GW} \leq 0.85$, $P_{loss}/P_{LH} \geq 1$ and $\beta_N \leq 2.5$ (conservative assumptions).

In case b). the probability takes the maximum value at $Q = 17 (= Q_{MAX})$

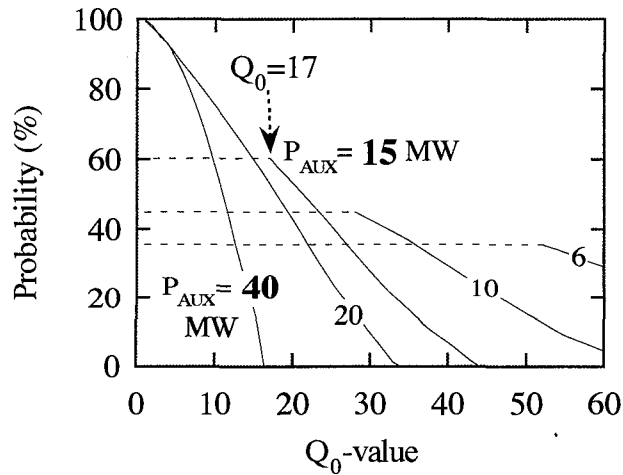


Figure I.2.3.3-3 Probability of Achieving $Q \geq Q_0$ in ELMy H-mode for a Range of Fixed Heating Powers, P_{AUX} , when $\sigma = 20\%$.

Here $n_e/n_{GW} \leq 0.85$ and $\beta_N \leq 2.5$. The flat part of each curve corresponds to $P_{loss} \leq P_{LH}$ (at $P_{AUX} = 6, 10, 15$ MW). In these cases the probability of $Q \geq Q_0$ is equal to that of $Q \geq Q_{MAX}$, where Q_{MAX} is the value which gives the maximum probability

Since we are free to choose P_{AUX} (within the capability of the device), the total probability of achieving a given Q value is given by the envelope of the curves shown in Figure I.2.3.3-3. The results are shown in Figure I.2.3.3-4 for two values of σ . Thus, when $\sigma = 20\%$ the

probability of achieving $Q \geq 10$ is $\sim 75\%$ and that of achieving $Q \geq 50$ is $\sim 35\%$, while for $\sigma = 10\%$ the values are 90% and 24% respectively. In addition, the sensitivity to the precise value of the limiting density and of the H-mode power threshold has been investigated by varying the relevant parameters in the range $n_e/n_{GW} \leq 0.85 \sim 1.0$ and $P_{loss}/P_{LH} \geq 1 \sim 1.5$. This is found to change the probability of achieving $Q \geq 10$ by $\sim 5\%$.

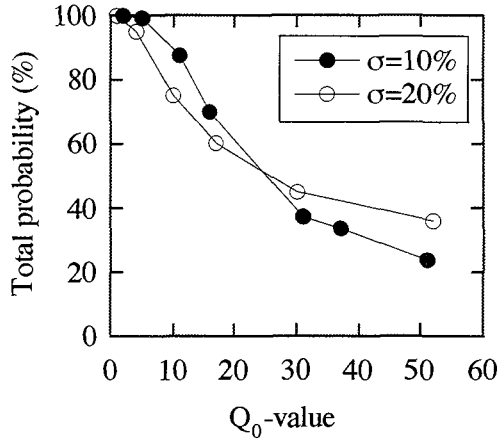


Figure I.2.3.3-4 Probability of Achieving $Q \geq Q_0$ in ELMy H-mode (envelope of Figure I.2.3.3-3) for $\sigma = 10\%$ and 20% with $I_p = 15.1$ MA, $n_e/n_{GW} \leq 0.85$ and $P_{loss} \geq P_{LH}$

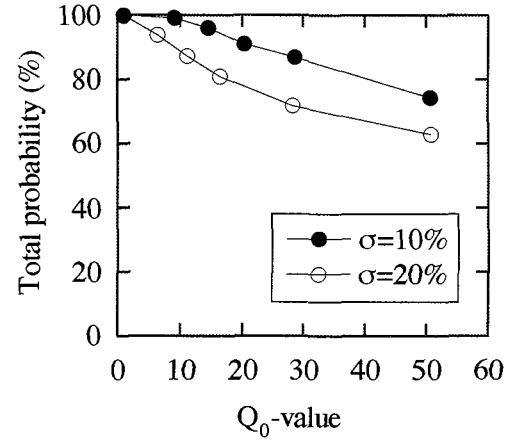


Figure I.2.3.3-5 Probability of Achieving $Q \geq Q_0$ in ELMy H-mode for $\sigma = 10\%$ and 20% with $I_p = 17.4$ MA, $n_e/n_{GW} \leq 0.85$ and $P_{loss} \geq P_{LH}$

On this basis, the probability of achieving $Q \geq 10$ in the ELMy H-mode regime is high. However, if for unexpected reasons $Q \geq 10$ were not achieved under nominal operating conditions, there are, as noted previously, various options for increasing the probability of achieving the required Q . For example, raising the plasma current to 17.4 MA increases the probability of achieving $Q \geq 10$ to $\sim 90\%$ (see Figure I.2.3.3-5). Another is to increase the fuel throughput in the divertor beyond the reference value of $200 \text{ Pam}^3\text{s}^{-1}$ to, say, $400 \text{ Pam}^3\text{s}^{-1}$ (which can be maintained for 200 s), allowing the helium concentration to be reduced by 2% (incremental), which, in fusion performance terms, is equivalent to a 1 MA increase in plasma current. Furthermore, regimes with active profile control could allow enhanced confinement to be accessed in inductive operation.

The probability calculation outlined here is in essentially a ‘model’ calculation, i.e. it represents a numerical result based on simple, well defined assumptions. For the reasons outlined previously, it does not, however, amount to a complete evaluation of the true probability of achieving $Q \geq 10$. In addition, it is a model calculation carried out in only one dimension of the multi-dimensional operating space which describes a burning plasma and it neither fully reflects the complexity of the behaviour close to operating limits, nor the degree to which experimental optimization of plasma parameters can improve plasma performance. In summary, the optimum operating point of a tokamak plasma consists neither of a random selection of parameters, nor a random response to the operating conditions selected, but corresponds, rather, to a well defined and reproducible plasma state resulting from extensive experimental development.

1.2.3.4 An Alternative Performance Evaluation Methodology based on Dimensional Extrapolation

This novel approach tries, amongst other things, to overcome the difficulty associated with the simultaneous choice of non-dimensional parameters ($A = R/a$, κ , δ , q_{95} , β_N , n/n_{GW}) which, when close to their respective limits, may have some significant hidden interactions which affects the energy confinement. As an example, this is observable in the effect of shear (triangularity, q , κ , A) on confinement in high density discharges, or the effect of sawteeth on low edge safety factor discharges at high elongation and triangularity.

In addition, the proposed methodology addresses, in part, the fact that the enhancement factor H_H cannot be treated as a simple scalar because it may hide some additional variables as well as explicitly treated terms (in the energy confinement formula), for example the density or elongation, the influence of which on the energy confinement time may not be mathematically expressed in a simple monomial form within the empirical formula for energy confinement time.

The employed procedure is as follows:

- each shot in the database is evaluated by extracting all of its parameters and sizing by means of the system code (in accordance with the ITER criteria) for a $Q = 10$ machine with the same geometry (k , δ , $A=R/a$), q_{95} , and n/n_{GW} : these parameters are then assumed to come as a “package”;
- the extrapolation in the energy confinement time is performed based on the empirical scaling coefficients applied only on the parameters not kept constant, and by using relative ratios. There is no need for H_H .

The energy confinement time empirical scaling then becomes:

$$\tau_{E,Q10} = \tau_{E,DBSHOT} \left(\frac{I_{Q10}}{I_{DBSHOT}} \right)^{\alpha_I} \left(\frac{P_{Q10}}{P_{DBSHOT}} \right)^{\alpha_P} \left(\frac{B_{Q10}}{B_{DBSHOT}} \right)^{\alpha_B} \left(\frac{R_{Q10}}{R_{DBSHOT}} \right)^{\alpha_R} \left(\frac{M_{Q10}}{M_{DBSHOT}} \right)^{\alpha_M} \left(\frac{n_{Q10}}{n_{DBSHOT}} \right)^{\alpha_n} \quad (I.2.3.4-1)$$

where :

- the subscript “Q10” refers to the $Q = 10$ machine designed from the shot in the H-mode database and indicated with the subscript “DBSHOT”.
- The α_i exponents are the same exponents found in the empirical scaling law for the correspondent parameters.

In addition, considering then the following relationships:

$$q = \frac{BR}{I} * f(\delta, \kappa, A) \quad (I.2.3.4-2)$$

$$n_{GW} = \frac{I}{\pi a^2} \quad (I.2.3.4-3)$$

equation (I.2.3.4-1) further simplifies, because q_{95} , geometry, and normalized density are fixed in the extrapolation, to:

$$\tau_{E,Q10} = \tau_{E,DBSHOT} \left(\frac{P_{Q10}}{P_{DBSHOT}} \right)^{\alpha_P} \cdot \left(\frac{B_{Q10}}{B_{DBSHOT}} \right)^{\alpha_B + \alpha_n + \alpha_I} \cdot \left(\frac{R_{Q10}}{R_{DBSHOT}} \right)^{\alpha_R - \alpha_n + \alpha_I} \cdot \left(\frac{M_{Q10}}{M_{DBSHOT}} \right)^{\alpha_M} \quad (I.2.3.4-4)$$

Considering, for example, the IPB-98y2 empirical scaling law for ELMy H mode:

$$\tau_{E,th}^{IPB98(y,2)} = 0.0562 H_H I^{0.93} B^{0.15} P^{-0.69} n_{19}^{0.41} M^{0.19} R^{1.97} \varepsilon^{0.58} \kappa_a^{0.78} \quad (I.2.3.4-5)$$

then expression (I.2.3.4-4) becomes:

$$\tau_{E,Q10} = \tau_{E,DBSHOT} \left(\frac{P_{Q10}}{P_{DBSHOT}} \right)^{-0.69} \cdot \left(\frac{B_{Q10}}{B_{DBSHOT}} \right)^{1.49} \cdot \left(\frac{R_{Q10}}{R_{DBSHOT}} \right)^{2.49} \cdot \left(\frac{M_{Q10}}{M_{DBSHOT}} \right)^{0.19} \quad (I.2.3.4-6)$$

Of the more than a thousand shots in the ELMy H-mode database, less than half turn out to extrapolate to a $Q = 10$ machine whose major radius is smaller than 8 m, however about 70 extrapolate to a $Q = 10$ machine with $R < 6.2$ m.

Figure I.2.3.4-1 shows the major radius of the extrapolated $Q = 10$ machine versus the edge safety factor q_{95} of the analyzed shots. It is apparent that there are a good number of shots, from DIII-D, JET, and ASDEX-U, which confirm the robustness of the ITER-FEAT design in reaching the $Q = 10$ objective on the basis of the existing experimental results. Of particular interest are those DIII-D shots which are capable of being extrapolated to a competitive $Q = 10$ device, even at a rather large edge safety factor. It is nevertheless clear that the choice of a safety factor of about 3 is sound.

As an even more general simplification to the proposed approach, the use of an empirical scaling formula for the energy confinement time can be completely avoided if the extrapolated device is sized based on a fusion power requirement and not on the amplification factor Q .

In order to do so, the above-mentioned, non-dimensional parameters are chosen to be kept constant, based on the consideration that the most unpredictable, from first principles, turbulent, phenomena taking place in the plasma are mostly influenced by stability and even more so by the geometry of the magnetic field, q and shear profiles.

In addition, in this second methodology, the value of β_N observed in the extrapolated experiment is also fixed. This last hypothesis implies that the magnetic and pressure profiles in the experiment in question and the larger extrapolated device are completely self similar. The pressure scales then as:

$$p \propto B^2 \quad (I.2.3.4-7)$$

And, for a DT experiment, the fusion power then scales approximately as:

$$P_f \approx p^2 \cdot V \propto B^4 R^3 \quad (I.2.3.4-8)$$

However, considering that the total fusion power is not exactly proportional to T^2 , it is in principle necessary, but not too important for the result, to choose an operating density. This

can be taken assuming also in this case the same density normalized to the Greenwald density scaling as:

$$n \propto \frac{I}{a^2} \propto \frac{B}{R} \quad (\text{I.2.3.4-9})$$

Figure I.2.3.4-2 shows the machine major radius versus the safety factor at the edge. Also in this case, a number of shots extrapolate to a 500 MW device with a major radius smaller than the one of ITER-FEAT.

In summary, also in accordance with this alternative design methodology, the ITER-FEAT design seems to be soundly based on the extrapolation of many high performance ELMY H-mode shots from JET, DIII-D, and ASDEX-U.

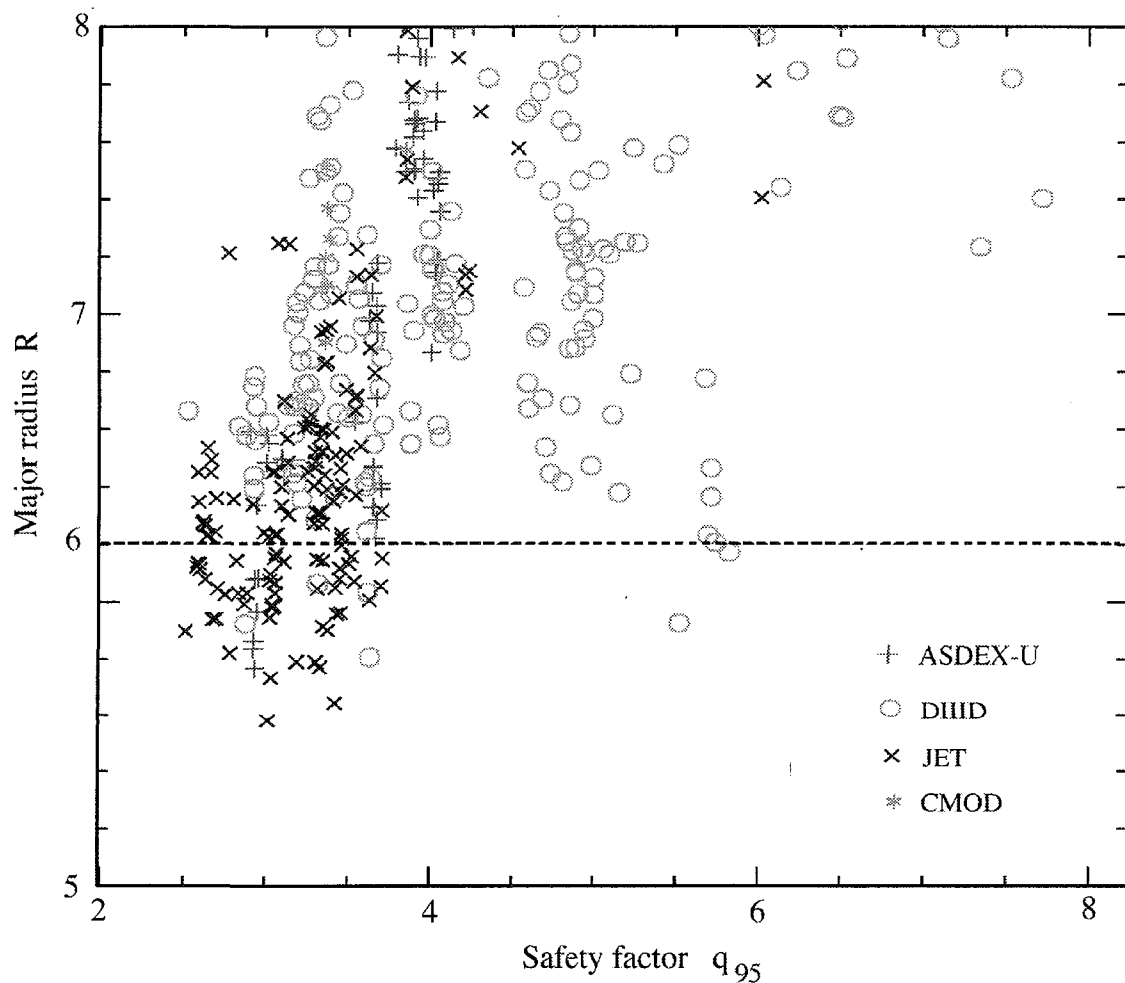


Figure I.2.3.4-1 Major Radius of $Q = 10$ Machine vs. q_{95} Obtained with Dimensional Extrapolation Methodology

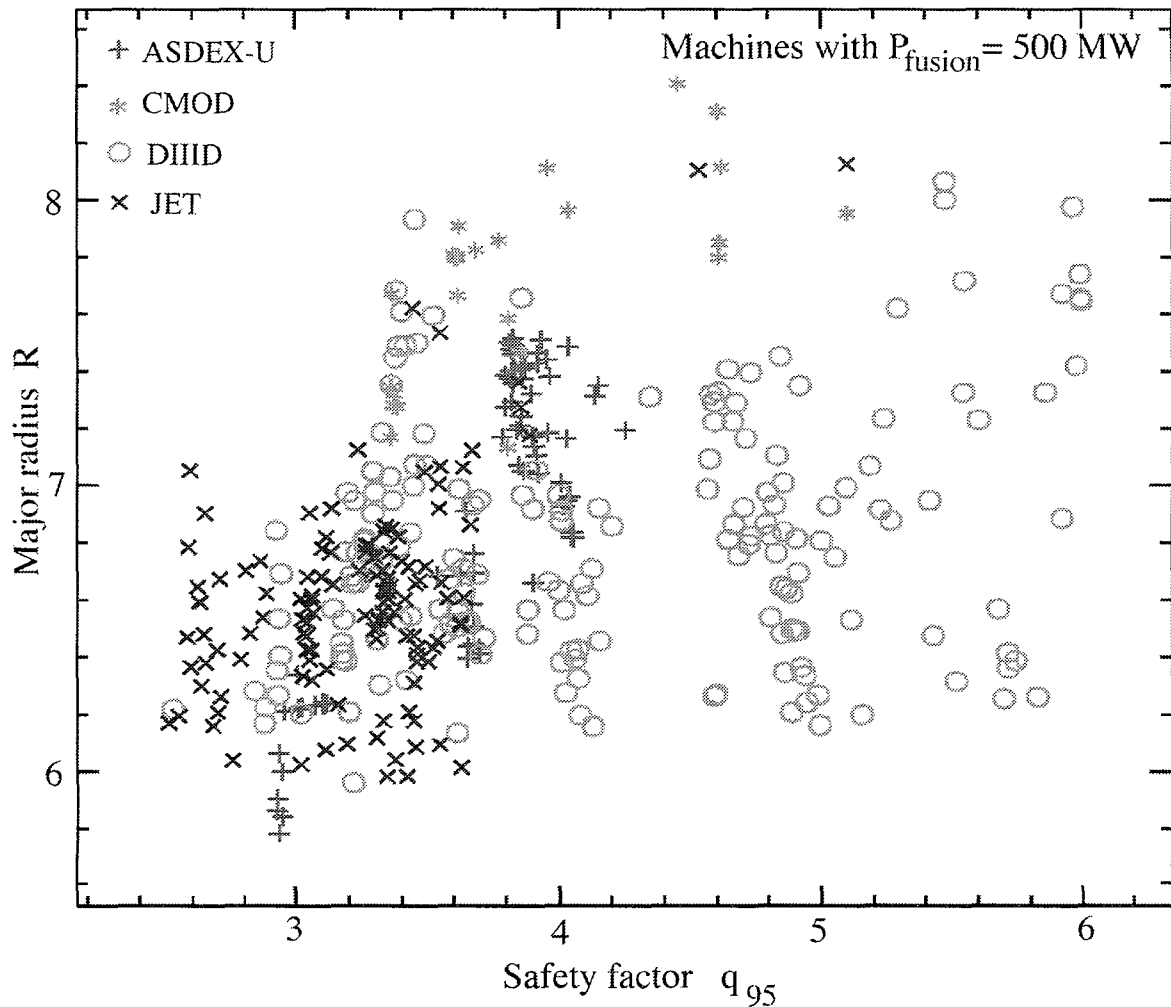


Figure I.2.3.4-2 Major Radius of 500 MW Fusion Power Device versus Safety Factor in the Database under the Assumption of Constant Beta

I.2.3.5 Divertor Performance

I.2.3.5.1 Introduction

The requirement for a long pulse, effectively steady-state, capability in ITER-FEAT implies that the divertor will have the same critical role in controlling power and particle exhaust as in the 1998 ITER design. Essential principles of that divertor design are therefore maintained: a baffled divertor volume with a vertical target is intended to provide an adequate volume for radiation and encourage partially detached operation; in addition, neutrals should be confined in the divertor and efficient pumping of helium ‘ash’ achieved. The overall aim of the power and particle control systems is to limit the peak power loading on the divertor target to less than 10 MWm^{-2} , to provide a helium exhaust capability of $\sim 0.75 \text{ Pam}^3\text{s}^{-1}$ so as to obtain core helium concentrations of less than 6%, to maintain the required density and optimum isotopic fuel mixture, and to limit the core plasma Z_{eff} below 1.8.

The reduced dimensions of the ITER-FEAT design have an impact on the divertor, leading to a reduction in the divertor leg length. Moreover, the use of more triangular plasmas will have a greater impact on the geometry of the inner divertor leg and may produce a second

(upper) X-point inside the first wall, which necessitates a consideration of power sharing between the lower and upper X-point regions and an analysis of the resultant power loading on the first wall in the vicinity of the upper X-point.

I.2.3.5.2 Power Loading Reduction and Helium Exhaust

Detailed modelling of divertor behaviour for ITER-FEAT is in progress, but extensive analysis has been performed for related design variants¹. The quantitative similarity of the predictions for these variants indicates that they can also be taken as representative of ITER-FEAT. These results indicate that the peak power loading of the divertor targets for ITER-FEAT device can remain in the range of 5 to 10 MWm⁻² for a range of upstream (separatrix) plasma densities, 3.3 to 3.8x10¹⁹ m⁻³ (Figure I.2.3.5-1). In such a density range, the upstream helium concentration can be reduced to 3% (Figure I.2.3.5-2).

The peak power loading of the divertor targets and the upstream helium concentration can be lowered by a moderate reduction of the input power. Furthermore, in steady-state operation at Q = 5, with an additional heating power of 75 (100) MW, the estimated power into the edge plasma is about 105 (140) MW, assuming 30% radiation from the core. Shortening the divertor noticeably increases the risk of excessive power loads, particularly at the outer divertor, and further modelling is required to optimise the divertor shape. However, since heat loads at the inner divertor target are significantly lower than at the outer target, there is no concern about the length of the inner leg. Power loading on the first wall region at the top of the plasma should not be a problem as long as the outer separatrix (corresponding to the upper X-point) remains more than 2 cm outside the inner one at the outboard midplane.

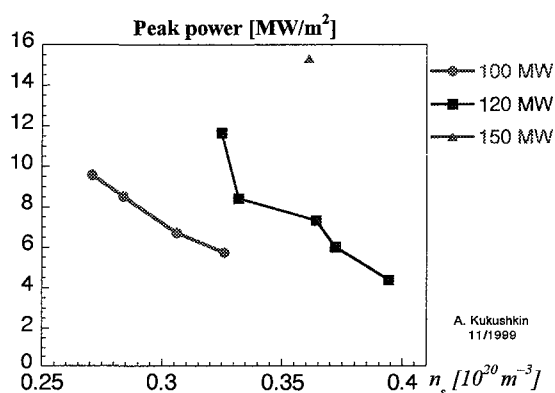


Figure I.2.3.5-1 Peak Power Loading vs. Upstream Density for Different Values of the Estimated Power Flowing to the SOL in a Device Similar to ITER-FEAT. The sharp drop of the peak power from the leftmost point on the 120 MW curve corresponds to the onset of partial detachment in the outer divertor

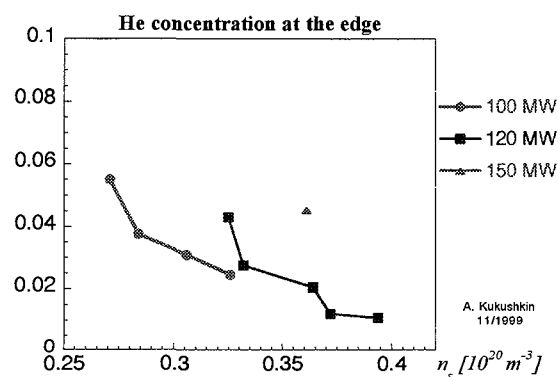


Figure I.2.3.5-2 Helium Concentration at the Plasma Edge vs. Upstream Density in a Device Similar to ITER-FEAT for Different Values of Power Conducted into the SOL.

Fusion power, which determines the helium production rate, was assumed to be 570 MW for the 100 MW and 120 MW cases, and 700 MW for the 150 MW case. Onset of partial detachment in the outer divertor is also seen here

¹ A. S. Kukushkin et al, Proc. 26th EPS Conf. on Controlled Fusion and Plasma Physics (Maastricht, 1999), to be published

Studies in several tokamaks have confirmed that helium can be exhausted from ELMy H-mode plasmas at rates which are consistent with the requirements for ITER-FEAT. In particular, experiments using the ASDEX Upgrade Divertor II and the W-shaped divertor in JT-60U have shown that $\tau_{\text{He}}^* / \tau_E \sim 5$ can be achieved under conditions relevant to ITER-FEAT¹. On the basis of results such as these, modelling projections to ITER-FEAT class devices confirm that the upstream helium concentration depends mainly on the DT throughput in the divertor, as illustrated in Figure I.2.3.5-3. To maintain a capability for limiting n_{He}/n_e below 6%, while maintaining necessary margins, it is therefore intended that the fuelling throughput in ITER-FEAT should be maintained at $200 \text{ Pam}^3\text{s}^{-1}$. This will be supplied by a mixture of gas-puffing and inside pellet launch to provide flexibility for controlling both the divertor plasma conditions and core density, making use of the benefits of inside pellet launch observed in ASDEX Upgrade. Initial calculations comparing helium exhaust with and without baffle indicate little difference in exhaust efficiency. Thus, tight baffling of the divertor may be unnecessary due to the high screening efficiency of the plasma under these conditions, leading to simplification and cost saving for the baffle.

I.2.3.5.3 Operation with Reduced Plasma Current

Certain scenarios involving non-inductive current drive in ITER imply operation with reduced plasma current, corresponding to $q_{95} = 4.4$ (c.f. $q_{95} = 3$ for the inductive reference scenario). To evaluate the possible effects of such operation on divertor performance, a density scan was performed for a device similar to ITER-FEAT with the pitch angle (the ratio $B_{\text{pol}}/B_{\text{tor}}$) reduced by a factor of 0.68. The results are shown in Figure I.2.3.5-4: the reduction in the power loading can be attributed to the longer connection length which facilitates power dissipation via radiation. The performance with respect to helium exhaust is similar for the two cases.

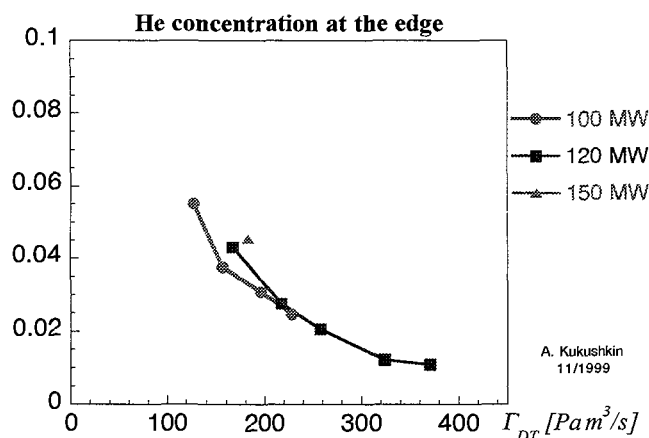


Figure I.2.3.5-3 Helium Concentration at the Plasma Edge vs DT Particle Throughput in a Device Similar to ITER-FEAT

¹ H.-S. Bosch et al, Plasma Phys. Control. Fusion **41** A401 (1999)

A. Sakasai et al, Fusion Energy Proc. 17th Int. Conf. (Yokohama, 1998) paper IAEA-F1-CN-69/EX6/5, to be published (1999)

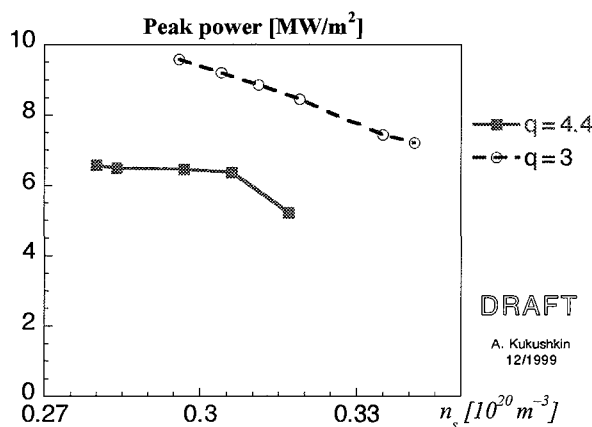


Figure I.2.3.5-4 Comparison of the Divertor Performance (peak power load vs. upstream density) for Higher-q ($q_{95} = 4.4$) and Standard Operation ($q_{95} = 3$) in a Device Similar to ITER-FEAT.

The calculations were performed with 115 MW power conducted into the SOL

I.2.3.5.4 ELM Control

The type I ELMy H-mode is taken to be the reference plasma regime for pulsed operation in ITER-FEAT. This corresponds to the mode of operation in which the highest quasi-steady-state confinement can be achieved in the majority of current experiments. While the processes underlying the confinement improvement in the H mode are not fully understood, there is growing evidence that the improvement in core confinement is associated with high temperatures at the top of the H-mode edge pedestal. Moreover, with increasing density, the pedestal temperature decreases and confinement degradation is generally observed at the highest densities. The density at which this degradation occurs can be raised by increasing the plasma triangularity, as demonstrated in JET, JT-60U and ASDEX Upgrade, or by inside pellet injection, as shown in ASDEX Upgrade. As mentioned in I.2.2, possible disadvantages of increased plasma triangularity are that the ELM frequency is generally observed to decrease, and the ELM energy loss per ELM increases since the ELM energy loss W_{ELM} is directly linked with the pedestal electron stored energy $W_{\text{e,ped}}$, i.e. $W_{\text{ELM}} \approx (0.26-0.36)W_{\text{e,ped}}$, according to the present database. The implications of such a trend for ITER-FEAT are illustrated by the fact that the anticipated value of $Q_{\text{ELM}}/\sqrt{\delta t}$ (proportional to the temperature increase of the divertor plate) is in the range 30-200 $\text{MJ m}^{-2}\text{s}^{-0.5}$ due to a single ELM at 500 MW of fusion power depending on the ELM deposition time $\delta t = 0.1-1$ ms and deposition energy density $Q_{\text{ELM}} = 1-2 \text{ MJm}^{-2}$ evaluated by the database for W_{ELM} . This may exceed the limiting value $Q_{\text{ELM}}/\sqrt{\delta t} \approx 45 \text{ MJ m}^{-2}\text{s}^{-0.5}$ for vaporization of the graphite target plate. High energy deposition during ELMs is associated with high pedestal pressure, which is, in turn, linked to the high energy confinement of the core plasma. Thus, while reduction of ELM amplitude is required to increase the longevity of the target plates, a balance must be struck with any resultant loss of core confinement. The level of energy deposition can be mitigated somewhat by moderate gas puffing, at some small cost in energy confinement, or by pellet injection. Since at low fusion power, e.g. $\leq 250-300$ MW, the ELM amplitude will be less severe and the target temperature rise will be lower, this should provide an opportunity to experiment with ELM mitigation techniques, which will be required to ensure acceptable divertor target lifetimes at higher fusion powers.

In contrast to the present database where W_{ELM} is derived in a relatively low density range (ratio to Greenwald density ≈ 0.4), recent results of DIII-D show that at high density (ratio ≈ 0.7) ELM energy loss reduces significantly (i.e. $W_{\text{ELM}} \approx (0.04-0.1)W_{e,\text{ped}}$) with little or mild expense of the energy confinement in low q_{95} (3.1-3.5), pumped divertor discharges.

Although this result could decrease $Q_{\text{ELM}}/\sqrt{\delta t}$ substantially below the acceptable level even for nominal fusion power, more systematic studies of the ELM energy loss from other machines including the area and in/out asymmetry of ELM energy deposition, as well as the deposition time are urgently needed.

Alternative high confinement modes with small ELM amplitude have been observed in several devices, e.g. grassy ELMs in DIII-D, ‘minute’ ELMs in JT-60U, and the enhanced D_α (EDA) mode in Alcator C-MOD. Although it is not yet verified that these modes all correspond to the same phenomenon, they are all classified here as type II ELMs for convenience. The operating conditions required to achieve such regimes are now being intensively investigated in many experiments. In DIII-D, the operation regime of grassy ELMs is achieved by closing access to “second stability” at the plasma edge, a result demonstrated by increasing the squareness of the plasma cross section. In contrast, the operation regime of minute ELMs in JT-60U is achieved by increasing δ , which opens access to “second stability” at the edge. The edge safety factor, q_{95} , is also an important parameter and the trend is that larger q_{95} requires lower δ to achieve minute ELMs (and vice versa). It is, moreover, observed that q_{95} and δ are important parameters in achieving the EDA mode in Alcator C-MOD. This is more readily achieved at low plasma current ($q_{95} > 3.7 - 4$) with moderate plasma shaping ($0.35 < \delta_x < 0.55$). In the EDA mode, the edge density fluctuations are of relatively large amplitude (compared to an ELM-free H mode) and the particle confinement time is low, while the energy confinement is only $\sim 20\%$ lower than during the ELM-free phase. This characteristic is very similar to that previously observed in the so-called, low particle confinement H mode in JET. These operational regimes, though exhibiting desirable ELM behaviour and acceptable energy confinement, are not yet characterized to the extent required for ITER-FEAT. Further extensive studies in existing experiments are required to demonstrate that one of the modes can meet the requirements of the ITER-FEAT reference scenario, and to determine how its properties can be extrapolated to the ITER scale.

I.2.3.6 Energetic Particle Confinement

ITER-FEAT will allow detailed studies of α -particle confinement and plasma heating and of the interactions of α -particles with mhd instabilities, in particular with Alfvén eigenmodes. In addition, energetic particle populations produced by NB and IC H&CD will co-exist with the α -population. The principal requirements which must be satisfied in ITER-FEAT plasmas, therefore, are that α -particles and other fast particle populations should be well confined and that they should transfer their energy efficiently to the background plasma. Although the confinement margin in the ITER-FEAT reference, inductive scenario allows $Q \geq 10$ to be achieved with α -particle losses of 5-10%, loss rates above 5% could give rise to excessive localized heating of the first wall. Satisfactory confinement and classical slowing down of energetic particle populations has been convincingly demonstrated in many tokamak experiments, where energetic particles produced by auxiliary heating systems do slow down

and transfer their energy to the thermal plasma at the predicted rate¹. Moreover, DT experiments in TFTR² and JET³ confirm that electron heating by α -particles is as expected. The key issues, therefore, are that TF ripple losses should be within acceptable limits and that mhd instabilities, including collective instabilities excited by the energetic particles, should not degrade the energetic particle confinement.

Energetic particle losses due to TF ripple have been studied experimentally in several devices using fast particle populations produced by NB and IC H&CD⁴, as well as fusion-produced α -particles in TFTR⁵. These experiments have tested and validated numerical codes which incorporate the various TF ripple loss mechanisms identified theoretically, with good agreement between experimental observations and code computations.

The essential principle of the location of the outer leg of the TF coil in ITER-FEAT is that the TF ripple, when reduced by ferromagnetic inserts, should limit ripple-induced energetic particle losses within acceptable bounds. Although ripple loss calculations have not yet been completed for the case with ferromagnetic inserts, α -particle loss rates have been calculated for the $Q = 10$ inductive and $Q = 5$ steady-state, reversed-shear (RS) operating scenarios for the TF ripple pattern without inserts using the HYBRID Monte-Carlo numerical code. Results are shown in Table I.2.3.6-1. One can see that in the nominal $Q = 10$ regime, the particle and power loss fractions are low and the peak power load on the first wall produced by escaping α -particles is below 0.1 MWm^{-2} . The reversed-shear scenario suffers a higher α -particle ripple loss since the poloidal magnetic field is lower than in the standard scenarios. In the case analysed, the peak first-wall heat load is $\sim 1 \text{ MWm}^{-2}$ that is higher than the maximum acceptable value of 0.5 MWm^{-2} . Hence a reduction of ripple amplitude by a factor of 2 is required to prevent excessive ripple losses in the reversed-shear scenarios. Available simulation results and design studies show that this reduction is possible with ferromagnetic inserts in the vacuum vessel.

**Table I.2.3.6-1 Ripple Loss of Fusion Alpha-particles
(without ferromagnetic inserts)**

Parameter	Q = 10 inductive regime	Q = 5 steady-state RS regime
Plasma current (MA)	15	10.2
q_{95}	3	4.5
Total particle loss fraction (%)	2.15	20.3
Total power loss fraction (%)	0.66	8.61
Peak FW heat load (MWm^{-2})	< 0.1	~ 1

Analysis of such regimes in a device similar to ITER-FEAT has shown that a reduction by a factor of ~ 2 in the ripple amplitude is required to prevent excessive ripple losses. Available simulation results and design studies show that this reduction is possible with ferromagnetic inserts in the vacuum vessel.

¹ W. W. Heidbrink and G. Sadler, Nucl. Fusion **34** 535 (1994)

² G. Taylor et al, Phys. Rev. Lett. **76** 2722 (1996)

³ P. R. Thomas et al, Phys. Rev. Lett. **80** 5548 (1998)

⁴ e.g. ITER Physics Expert Groups et al, Nucl. Fusion to be published (1999), ITER Physics Basis, Chap. 5

⁵ e.g. R. J. Hawryluk et al, Phys. Plasmas **5** 1577 (1998)

Many of the critical parameters influencing interactions with Alfvén eigenmodes, such as $\beta_\alpha(0)$, v_α/v_A , $RV\beta_\alpha$, differ little ($\sim 10\%$) from those in the 1998 ITER design, and others, such as ρ_α/a , differ by less than a factor of 2. Thus, ITER-FEAT will be able to provide access to this critical aspect of α -particle behaviour and to validate theoretical predictions at the reactor scale. An additional complication which must necessarily be dealt with in the driven burn of ITER-FEAT is the role of fast ions produced by additional heating systems, which may complicate the interpretation of, for example, instability thresholds. Extensive investigations have been performed in existing experiments to validate numerical codes used to calculate Alfvén eigenmode stability and there is now considerable confidence in their accuracy¹. While an extensive body of analysis exists for the 1998 ITER design, indicating that modes with $n > 10$ are likely to be the most problematic, stability calculations for ITER-FEAT inductive and steady-state scenarios are at an early stage. Initial indications are that, unless unstable modes overlap and extend to the wall, nonlinear redistribution of α -particles may merely cause internal profile broadening, without significant loss.

I.2.4 Plasma Operation and Disruptions

Mhd stability plays an defining role in determining the accessible parameter space and thereby setting the limits of fusion performance. To achieve the ITER-FEAT objectives, plasmas must not only satisfy constraints set by global stability limits relating to plasma current, plasma density and plasma pressure (discussed in I.2.2), but must also be resilient to localized mhd modes, such as sawteeth, ELMs, and neoclassical tearing modes, which are potential sources of confinement degradation and disruptions.

Sawtooth activity is an ubiquitous instability of tokamak plasmas which modulates the central plasma parameters, but involves no global loss of plasma energy or particles. At the ITER-FEAT scale, the direct impact on global energy confinement and fusion performance is expected to be small², but sawteeth may be the dominant mechanism producing seed islands which trigger neoclassical tearing modes. A detailed theoretical model of the underlying $m = n = 1$ mhd instability, incorporating non-ideal effects such as resistivity and finite ion Larmor radius and including the stabilizing role played by fast ions and thermal trapped ions, has been developed and applied to the 1998 ITER design³. Although not yet applied to the ITER-FEAT design, the model predictions for the 1998 ITER design suggest that the sawtooth duration in ITER-FEAT could reach several tens of seconds as a result of α -particle stabilization of the $m = 1$ mode. Experience on existing experiments suggests that such long sawtooth periods could lead to sawtooth crashes with large inversion radii⁴ which tend to destabilize further mhd modes, typically with $(m,n) = (3,2)$ or $(2,1)$, which could provide the seed island for the growth of NTMs.

Demonstrated techniques for the control of the sawtooth period include the minority ion current drive scheme developed in JET⁵ and the use of localized ECCD investigated in

¹ e.g. ITER Physics Expert Groups et al, Nucl. Fusion to be published (1999), ITER Physics Basis, Chap. 5

² e.g. "Technical Basis for the Final Design Report, Cost Review and Safety Analysis", 1998 ITER EDA Documentation Series No. 16 (Vienna: IAEA, 1998)

³ F. Porcelli et al, Plasma Phys. Control. Fusion **38** 2163 (1996)

⁴ e.g. D. J. Campbell et al, Phys. Rev. Lett. **60** 2148 (1988)

⁵ V. P. Bhatnagar et al, Nucl. Fusion **34** 1579 (1994)

several experiments¹. On the basis of these results, it seems likely that the most effective form of sawtooth control will be via modification of the current profile in the vicinity of the $q = 1$ surface. The availability of both forms of heating and current drive in ITER-FEAT will allow these control schemes to be applied if necessary. A detailed analysis of the EC radiofrequency scheme is underway to estimate the control power required. Although current tokamak experiments operate routinely at $q_{95} < 3$ and ITER-relevant values of β_N , this control flexibility represents an additional tool for assuring reliable operation at $q_{95} < 3$ in ITER-FEAT, where higher Q operation might be explored.

I.2.4.1 Operational Limits

I.2.4.1.1 Beta Limit

I.2.4.1.1.1 Neoclassical Tearing Modes

ITER-FEAT can achieve its goal of $Q \geq 10$ at β_N as low as 1.5 (see I.2.3.1) and even at fusion power levels of 500 MW, β_N is ~ 2 . Nevertheless, as noted in I.2.2, in present experiments with long-pulse, low collisionality plasmas, NTMs can limit β and degrade energy confinement within the range of β_N foreseen for ITER-FEAT operation² (and well below the ideal mhd stability limit). The predominant modes have $(m,n) = (3,2)$ and $(2,1)$, with the former typically producing a 10-30% degradation in confinement, while the latter can produce major disruptions. Although there is uncertainty over the precise scaling of critical quantities, such as the minimum seed island width, to the ITER scale, it has been found³ in several tokamaks that the minimum β for the onset of NTMs falls with the normalized Larmor radius, varying as $(\rho^*)^\mu$, with $0.5 \leq \mu \leq 1$. Theoretical predictions suggest that the saturated island width normalized to the minor radius, w_{sat}/a , will be of the same order, and therefore produce confinement effects of the same magnitude, as in present experiments. On the other hand, recent analysis of the influence of increased plasma elongation and triangularity on the magnetic well contributions to NTM stability⁴ indicates that this may have a beneficial effect on NTM stability in ITER-FEAT.

The growth time of these modes is determined by the timescale for resistive reconnection in the vicinity of the relevant rational q surface, which is long enough to permit stabilization by ECCD in present experiments⁵ (see Figure I.2.4.1-1), and should lie in the range 10–30 s in ITER-FEAT. It is anticipated, therefore, that an ECCD-based stabilization system for NTMs will be installed to allow for suppression of the $(3,2)$ and $(2,1)$ modes should they occur. Two possibilities have been explored computationally: (i) mode stabilization by ECCD modulated in phase with the island O-point, and (ii) reduction in the width of the saturated

¹ e.g. G. A. Bobrovskii et al, *Fiz. Plazmy* **13** 1155 (1987)

² O. Sauter et al, *Phys. Plasmas* **4** 1654 (1997)

³ e.g. S. Günter et al, *Nucl. Fusion* **38** 325 (1998)

G. Huysmans et al, *Fusion Energy Proc. 17th Int. Conf. (Yokohama, 1998)* paper IAEA-F1-CN-69/EXP3/03, to be published (1999)

⁴ S. V. Konovalov et al, "Calculation of the Magnetic Well Effect on the NTM Stability in IAM", unpublished (1999)

⁵ H. Zohm et al, *Proc. 26th EPS Conf. on Controlled Fusion and Plasma Physics (Maastricht, 1999)*, to be published

island by continuous ECCD. Theoretical calculations show that a modulated ECCD current density

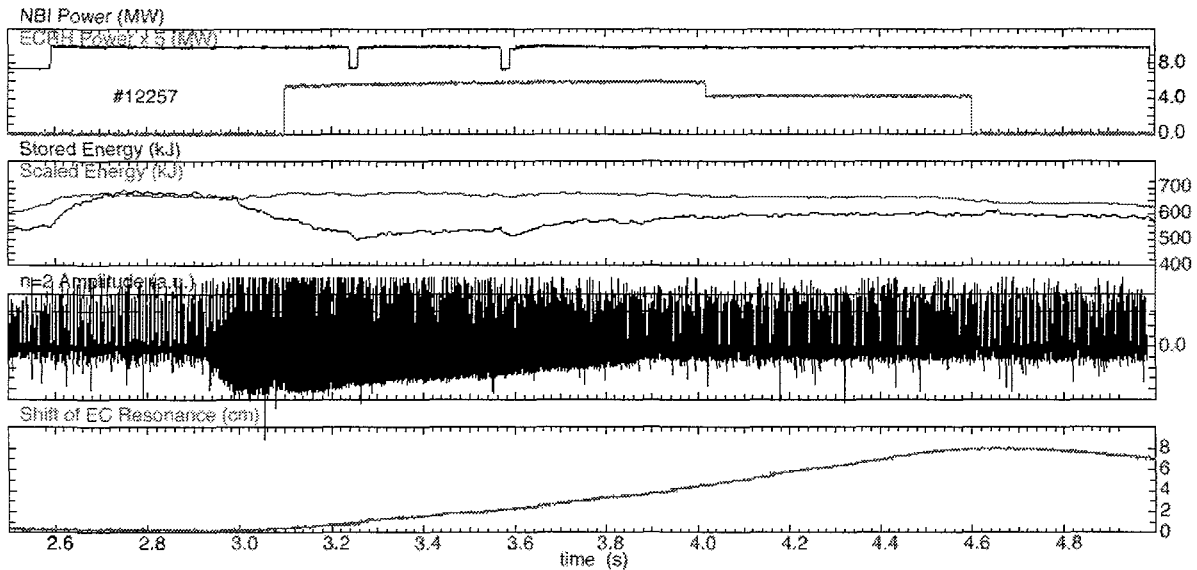


Figure I.2.4.1-1 Complete Stabilization of a (3,2) Neoclassical Tearing Mode in ASDEX Upgrade by Continuous ECCD

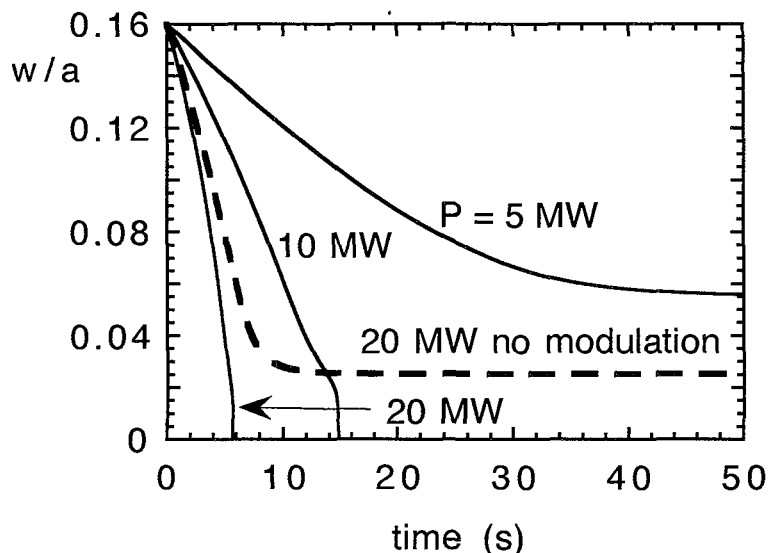


Figure I.2.4.1-2 Predictions of Power Requirements and Timescales for (2,1) Neoclassical Tearing Mode Stabilization by ECCD for Nominal Conditions in a Device with Parameters Similar to ITER-FEAT.

Results are shown in terms of the initial island width, w , normalized to the plasma minor radius, a , at ECCD switch-on. It is assumed that the ECCD power is modulated in phase with the island rotation, except for the dashed curve

exceeding 1.5 times the bootstrap current density in the neighbourhood of the rational surface (driven in the forward direction in the island O-point) will stabilize an arbitrarily small island. Initial analyses of power requirements show that (3,2) and (2,1) NTMs could be stabilized

(individually) in a time of order 10 s by 10-30 MW of modulated ECCD power¹ in devices of the ITER-FEAT class (see Figure I.2.4.1-2). Incorporation of electron temperature effects into the codes could lead to a reduction in the estimated power requirement. Feedback stabilization of the NTMs seems, at present, therefore, to be the most promising route to ensure control of these modes in ITER-FEAT. Direct control of the q profile (for example by attempting to raise q_{\min} above 1.5) might also be feasible, but requires further investigation.

I.2.4.1.1.2 Resistive Wall Modes (RWMs) and their Stabilization

The principal approach to steady-state operation of ITER-FEAT exploits plasmas with low or negative central magnetic shear and a high bootstrap current fraction, allowing good alignment between bootstrap current density and required current density profiles to be achieved. In the absence of a nearby conducting wall, such discharges are known to be unstable to an $n = 1$ external kink mode at values of $\beta_N \leq 3$ (due to the low value of I_i). However, as discussed in I.2.3.2, β_N values of 3 or higher are typically required to achieve $Q = 5$. When a conducting wall is close to the plasma ($a_w/a \leq 1.4$ for ITER-FEAT), the relevant modes are no longer ideally unstable, but can develop into resistive wall modes, which grow on a time scale characteristic of magnetic field penetration through the wall².

Experimental results from DIII-D³ indicate that wall stabilization based on plasma rotation is effective and that discharges can be maintained for a period corresponding to many mhd timescales and to ~ 30 resistive wall decay times. Nevertheless, in all cases analyzed to date, plasma rotation could not be maintained in conditions where kink modes would be unstable in the absence of the conducting wall. The resulting gradual decrease of plasma rotation had the consequence that the growth of modes on resistive wall times could not be avoided. If rotation cannot be maintained in ITER-FEAT in such conditions, then an active $n = 1$ magnetic feedback system will be needed to suppress the growth of the RWMs.

The problem of feedback stabilization of the $n = 1$ RWM is very similar to the control of the $n = 0$ unstable motion (vertical instability), which is slowed by the resistive wall and then stabilized by currents in external coils. For $n = 1$ stabilization, a system of external saddle coils can be used (similar to the error field stabilization coils) producing an $n = 1$ stabilizing magnetic field. To allow modes with arbitrary phases to be stabilized, several sets of such coils may be needed. Preliminary considerations have been made in relation to stabilizing the RWMs in ITER-FEAT. The rather long timescale for penetration of the field through the wall (time constant ~ 0.3 s) allows the mode to be detected with a magnetic loop while the perturbation is still at the level of several Gauss. A set of external saddle coils with a similar configuration to the error field correction coils and operating at a maximum current level of ~ 10 kA can produce adequate field levels (again several Gauss) at the plasma surface to compensate the mode field.

¹ G. Giruzzi et al, Proc. 13th Topical Conf. on Applications of RF Power to Plasmas (Annapolis, 1999), to be published

A. V. Zvonkov "Electron Cyclotron Current Drive Optimization for Control of Neoclassical Tearing Modes in RTO/RC-ITER", unpublished (1999)

² F. Perkins et al, Fusion Energy Proc. 17th Int. Conf. (Yokohama, 1998) paper IAEA-F1-CN-69/ITERP1/11 10, to be published (1999)

³ E. J. Strait et al, Fusion Energy Proc. 17th Int. Conf. (Yokohama, 1998) paper IAEA-F1-CN-69/EXP3/10, to be published (1999)

I.2.4.2 Recoverable Plasma Disturbances

Minor disruptions, sawteeth, and ELMs, are repetitive and recoverable plasma disturbances for which the control system must have an adequate response so as to limit the plasma-wall contact time to ≤ 1 s. These disturbances cause changes in l_i (normalized internal inductance) and β_p , parameters which have the same value for ITER-FEAT plasmas as for the 1998 ITER design. The reference values of changes in these parameters for which the plasma control system is designed are, therefore, derived from the database of experimental values assembled for the 1998 ITER design and are assumed to have the same specifications. Considerations relating to plasma control issues arising from such disturbances are discussed in II.1.1.

I.2.4.3 Disruptions and Vertical Displacement Events

The consequences of disruptions and vertical displacement events (VDEs) impose a significant design constraint on devices at the reactor scale¹. Principal concerns include severe heat loads on the first wall and divertor targets, large electromechanical forces on the vessel structures, and potentially high currents of runaway electrons in the post-disruption plasma. It is an essential aspect of the ITER-FEAT objectives to address these issues, to demonstrate reliable operation in spite of such constraints, and to evaluate potential avoidance and mitigation techniques which can be applied to fusion power plants.

Characterization of disruptions in present devices has yielded considerable progress in the understanding of both the plasma processes which produce disruptions and the phenomena which occur during disruptions², and allows extrapolation of the key timescales and quantities to the ITER-FEAT scale. This has allowed design basis specifications for fast plasma dynamic events and fast shutdown actions to be derived for the ITER-FEAT reference scenario, as listed in Table I.2.4.2-1. The parameters shown are derived under the assumptions that the plasma thermal energy is $W_{th} = 0.35$ GJ, and that the magnetic energy, including the contribution from the poloidal magnetic field between the separatrix and first wall ($\approx 10\%$ increment of magnetic energy), is $W_{mag} = 0.31$ GJ.

Timescales for the energy and current quench phases of disruptions have been derived from experimental databases compiled from disruption measurements in a range of tokamaks during the EDA. From the thermal quench database, the loss of thermal energy is expected to occur in two phases, with an overall quench time of ~ 10 ms. Estimates for the current quench time are derived from the data shown in Figure I.2.4.3-1, where the measured current decay rates (for 60% of the pre-disruption plasma current to decay), dI_p/dt , are plotted against the average pre-disruption current density, $\langle j_{p0} \rangle$. There is considerable scatter in the data, but the maximum current quench rates correspond to a post-disruption plasma temperature of ~ 3 eV, which is understood in terms of plasma cooling as a result of carbon radiation following large impurity influxes caused by the thermal quench. This yields a maximum current quench rate of 400 MA s^{-1} for a 15.1 MA reference plasma, which translates to a minimum current quench time of ~ 25 ms. However, there is considerable scatter in the data, and only a small fraction of the points exhibits the fastest current decay rates. Moreover,

¹ e.g. "Technical Basis for the Final Design Report, Cost Review and Safety Analysis" 1998 ITER EDA Documentation Series No. 16 (Vienna: IAEA, 1998)

² e.g. ITER Physics Expert Groups et al, Nucl. Fusion to be published (1999), ITER Physics Basis, Chap. 3
R. Yoshino et al, Fusion Energy Proc. 17th Int. Conf. (Yokohama, 1998) paper IAEA-F1-CN-69/ITERP1/14, to be published (1999)

since there is no clear correlation with size, it should be expected that current quench rates in ITER-FEAT could exhibit an equally broad range, with a significant proportion of disruptions having a longer current quench.

Table I.2.4.2-1. Key Design Basis Specification for Fast Plasma Dynamic Events

Disturbances	Design basis parameters	Importance/Comments
Major disruptions	$W_{th} = 0.35 \text{ GJ}$, $W_{mag} = 0.31 \text{ GJ}$	10% of full-performance pulses
Major disruptions (during plasma start-up/shut-down and/or full- performance plasma development)	$W_{th} = 0.18 \text{ GJ}$, $W_{mag} = 0.31 \text{ GJ}$	Up to 30% of pulses during commissioning and operations developing phases
VDE	$W_{th} = 35 \text{ MJ}$, $W_{mag} = 0.31 \text{ GJ}$, $I_{halo} \leq 0.4I_{P0}$, $TPF \leq 4$	After each disruption
VDE (loss-of-control)	$W_{th} = 0.35 \text{ GJ}$, $W_{mag} = 0.31 \text{ GJ}$, $I_{halo} \leq 0.4I_{P0}$, $TPF \leq 4$	1% of pulses
Fast shutdown	$\tau_{th}, \tau_{mag} \leq 1 \text{ s}$; by impurity or D injection; D favoured to minimize RA conversion	$\approx 10\%$ of pulses; primary plasma shutdown/in-vessel protection means
Runaway (RA) electron conversion	10 – 15 MeV electrons, I_{RA} to $\approx 90\%$ of I_{P0} . $W_{th} = 60 \text{ MJ}$ for ITER-FEAT, with potentially high poloidal and toroidal localization on the upper FW or outboard lower FW; May occur following disruption, loss-of-control VDE or fast plasma shutdown	Many uncertainties: magnitude of RA current, FW deposition and total RA thermal energy to FW sensitive to mhd fluctuation levels and/or effect of vertical instability; Toroidal localization depends on FW alignment. Shutdown species will influence RA current

Each phase of the disruption will involve the deposition of $\sim 0.35 \text{ GJ}$ of energy onto the plasma-facing components and the localized energy deposition at the divertor targets might reach $\sim 100 \text{ MJm}^{-2}$. Evaporation and localized melting could occur at these levels, but ablation shielding should mitigate the most severe effects. In addition, eddy currents induced by the current quench will contribute to the electromagnetic forces on the vacuum vessel and in-vessel components.

An additional significant component of the electromagnetic forces arises from the VDE which usually follows a disruption in elongated plasmas (or arises from a loss of vertical position control). The vessel forces due to VDEs depend on the magnitude of the halo

current (for scaling purposes this is normalized to the plasma current, $I_{h,max} / I_p$), and the degree of toroidal asymmetry, the toroidal peaking factor (TPF). Although the physics basis of halo currents is understood, the detailed processes determining the magnitude of these two quantities are not, and extrapolation to ITER-FEAT relies on database analysis (see Figure I.2.4.3-2). This has produced a design constraint for ITER of $(I_{h,max} / I_p) \times \text{TPF} = 0.5$ for the 'typical case' and $(I_{h,max} / I_p) \times \text{TPF} = 0.75$ for the 'worst case'¹. There does not appear to be any significant dependence of these parameters on the plasma elongation up to X-point elongations of ~ 2 . There is, in fact, an indication in the database that a favourable size scaling of $I_{h,max} / I_p$ exists, and hence that the bound on maximum halo current fraction in ITER-FEAT may eventually lie below ~ 0.3 , while the toroidal peaking factor may lie within an upper bound of 2. This is illustrated in Figure I.2.4.3-3, which shows recent halo current data from JET and JT-60U.

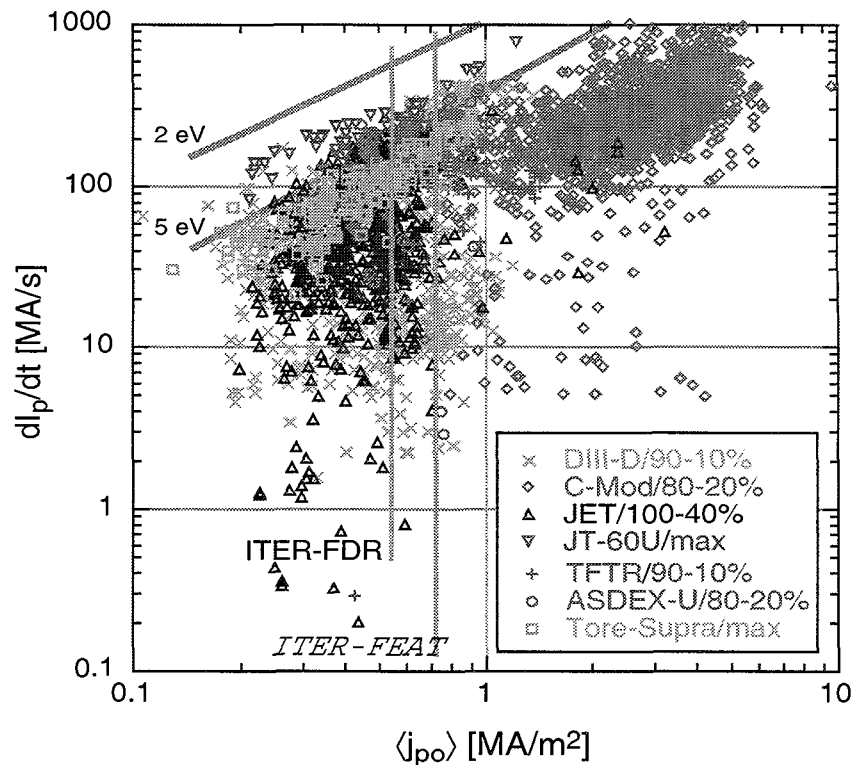


Figure I.2.4.3-1 Database of Current Decay Rates Derived from a Range of Current Tokamak Experiments.

The fastest current decay rate corresponds to a post-disruption plasma temperature of 3 eV, but many disruptions have considerably slower decay rates. Vertical lines correspond to the 1998 ITER design 21 MA and the ITER-FEAT 15.1 MA cases

¹ e.g. ITER Physics Expert Groups et al, Nucl. Fusion to be published (1999), ITER Physics Basis, Chap. 3
R. Yoshino et al, Fusion Energy Proc. 17th Int. Conf. (Yokohama, 1998) paper IAEA-F1-CN-69/ITERP1/14, to be published (1999)

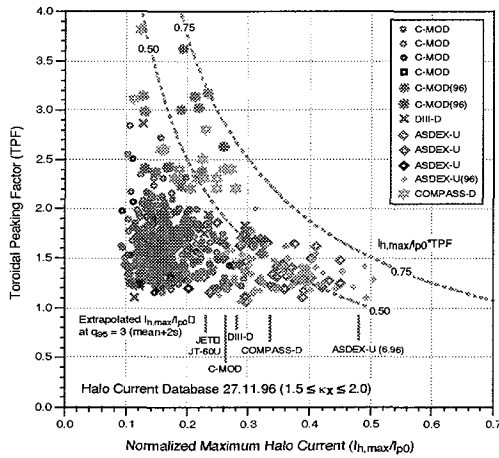


Figure I.2.4.3-2 Halo Current Toroidal Peaking Factor (TPF) Plotted Against the Normalized Maximum Halo Current Fraction, Derived from Data from a Range of Small and Medium-sized Devices in the ITER Disruption Database

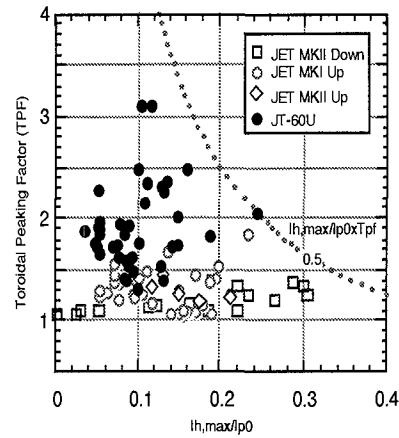


Figure I.2.4.3-3 Halo Current Toroidal Peaking Factor (TPF) Plotted Against the Normalized Maximum Halo Current Fraction, Derived from Recent Data from JET and JT-60U

Runaway electron currents can be generated by an avalanche process in the cold, highly impure plasma produced by disruptions¹. Due to the high current, the number of e-folding times available for amplification of the runaway current in ITER-FEAT disruptions is potentially large, $\gamma_{av}t \approx 2.5I_{p,MA} \approx 38$. The resultant amplification factor of $e^{38} \approx 10^{16}$ is of such a magnitude as to expect that the runaway generation will be only weakly sensitive to the density of seed runaways and the runaway sources. On the other hand, runaway formation might well be sensitive to the loop voltage and, hence, to current quench time.

Numerical simulations of runaway growth during plasma disruptions and VDEs were carried out for a device similar to ITER-FEAT. The modelling was performed using the DINA 1.5-D code, which incorporates an up-to-date configuration of two external conducting 'layers': the vacuum vessel (assumed toroidal resistance $7.25 \mu\Omega$) and a PF system with a segmented central solenoid. Major disruptions were simulated by an instantaneous drop of the plasma temperature (and β) from the initial temperature of the burning plasma (SOB) to a post-thermal quench temperature of 5 eV, 25 eV, or 50 eV. The initial plasma current was 17 MA, plasma internal inductance $l_i = 0.8$, plasma poloidal beta $\beta_p = 0.7$, the central plasma density was maintained at $6 \times 10^{19} \text{ m}^{-3}$, and the plasma density profile was varied to study the sensitivity of the runaway formation to the edge density. The results are summarized in Table I.2.4.2-2.

On the basis of these calculations, ITER-FEAT is susceptible to runaway electron formation. However, significant runaway populations are generated only at fast disruptions with the post-thermal quench temperature less than 25 eV and the current quench time less than 200 ms. The runaway energy probably cannot exceed 60 MJ for a plasma edge density above $2 \times 10^{19} \text{ m}^{-3}$ because runaway electrons are lost at $q \leq 2.5$ in large tokamak experiments such as JT-60U. Note that in these calculations it was found that all VDEs caused by a β drop

¹ M. N. Rosenbluth and S. V. Putvinski, Nucl. Fusion **37** 1355 (1997)

moved in an upward direction, with the plasma-wall contact point in the range $Z = 4 - 5$ m on the inner sector of the first wall.

Interaction of such runaway electrons with the first wall could lead to localized surface damage, and suppression of runaway currents has therefore become a central issue in the development of disruption mitigation and avoidance techniques. A promising development is that magnetic fluctuations associated with disruptions are found to suppress runaway electrons in JT-60U¹. Nevertheless, there is a requirement for a fast plasma shutdown system, such as 'killer pellets', which can mitigate the most severe disruption effects².

Table I.2.4.2-2 Runaway Current and Runaway Energy Deposited on the Wall vs. Post-thermal-quench Plasma Temperature and Edge Plasma Density for a 17 MA Discharge in a Machine Similar to ITER-FEAT

Plasma temperature after thermal quench (eV)	Edge density (10^{20} m^{-3})	Maximum runaway current (MA)	Time when runaway current is formed (ms)	Runaway energy (MJ) deposited on the wall when $q_{\text{edge}} = 2$	Runaway energy (MJ) deposited on the wall when $q_{\text{edge}} = 1$
5	0.6	14.0	40	7.4	68
5	0.2	15.0	38	54	120
5	0.1	14.5	34	120	170
25	0.6	5.5	234	0	0.4
50	0.6	0.7	650	0	4.0

I.2.5 Heating and Current Drive

I.2.5.1 Role of Auxiliary Heating and Current Drive Systems

Auxiliary heating and current drive (H&CD) systems must fulfil several roles in ITER-FEAT operating scenarios.

- Provide sufficient plasma heating power to access H-mode energy confinement in DT plasmas and subsequently to increase plasma temperatures to values where finite-Q driven burn ($Q \geq 10$) will occur. Present estimates are that 50 MW will be sufficient for both requirements.
- Deliver up to 50 MW of continuous (≥ 400 s duration) auxiliary power to supplement α -heating in finite-Q driven burn scenarios. Up to 50 MW of auxiliary heating power must also be available to assist normal plasma shutdown at the end of pulse. The auxiliary H&CD systems must be capable of heating the plasma within a density range $n_e = 0.3 - 1.3 \times 10^{20} \text{ m}^{-3}$ and a temperature range $T = 3 - 40$ keV.

¹ Y. Kawano et al, Fusion Energy Proc. 16th Int. Conf. (Montréal, 1996), Vol. 1 (Vienna: IAEA) p 345 (1997)

² e.g. R. Yoshino et al, Fusion Energy Proc. 17th Int. Conf. (Yokohama, 1998) paper IAEA-F1-CN-69/ITERP1/14, to be published (1999)

- (c) Provide sufficient non-inductive current drive capability to allow for extended-duration ($\sim 3,600$ s) or steady-state operation with $Q \geq 5$ in plasmas with densities in the range of $n_e = 0.4 - 1.0 \times 10^{20} \text{ m}^{-3}$, and plasma currents of $I_p = 8 - 12$ MA. The extended burn and steady-state plasma operational scenarios will require both on-axis and off-axis current drive, at sufficiently high current drive efficiencies to permit plasma performance optimization via local current profile control (profile optimization).
- (d) Allow local control of the plasma current profile for plasma performance optimization by controlling magnetic islands, sawteeth and other forms of mhd activity.
- (e) Provide a plasma start-up capability: an electron cyclotron resonance heating system with 2 MW of input power and a frequency of 120 GHz will be required to facilitate plasma breakdown and impurity burn-through.

In addition, the following ancillary functions are desirable:

- (i) Maintenance of sufficient plasma rotation to avoid locked modes and to stabilize resistive kink instabilities via conducting wall effects.
- (ii) Provision of a wall conditioning capability.

No single form of heating and current drive can fulfil all the above requirements and a combination of auxiliary H&CD systems will be needed to provide flexibility and extend the range of possibilities for optimizing plasma performance. At the present time, neutral beam (NB) injection, ion cyclotron (IC) radiofrequency, electron cyclotron (EC) radiofrequency and lower hybrid (LH) wave heating systems are under consideration, and the ITER-FEAT device is being designed to accommodate a total power of up to about 100 MW.

I.2.5.2 Bootstrap Current

Though not, of course, an auxiliary system, the bootstrap current makes such a significant contribution in extended burn and steady-state scenarios (as noted in I.2.3.2), that several comments are pertinent. For example, with a drive efficiency of $\gamma_{20} = 0.25 \text{ AW}^{-1}\text{m}^{-2}$, a bootstrap current fraction, f_{bs} , of 45% is required to maintain a plasma current of 12 MA. Furthermore, since plasmas with weak or negative central shear are likely to be studied extensively, the bootstrap current profile must be well-aligned with the total current profile to minimize the requirements for current profile control by the auxiliary systems. In particular, due to the lower, off-axis current drive efficiency associated with auxiliary H&CD systems (due to the lower electron temperature and trapped particle effects), it is desirable that a substantial fraction of the plasma current at, say, $r/a \geq 0.5$ be generated by the bootstrap effect. A broad internal transport barrier would help in this respect.

Further significant aspects are:

- (1) since $f_{bs} \propto \beta_p(a/R)^{0.5}$, extended pulse and steady-state operation will exploit plasmas with reduced plasma current to increase β_p ;

- (2) the bootstrap current is dependent on plasma current profile: a hollow profile of plasma current produces larger bootstrap current in the plasma inner region ($r/a \leq 0.5$) due to the weaker poloidal magnetic field in plasma core;
- (3) weak or negative central shear operation with an internal transport barrier enhances the bootstrap current and hence is beneficial for steady-state operation in ITER-FEAT;
- (4) if the plasma temperature and density profiles can be appropriately controlled, external current drive in the outer plasma region (e.g. $r/a \geq 0.5$) would not be needed.

1.2.5.3 Capabilities of Candidate H&CD systems

1.2.5.3.1 IC Heating and Current Drive

The proposed heating scenarios are similar to those of 1998 ITER Design with appropriate frequency changes due to the different toroidal field. The major physics issues are global wave absorption, distribution of power amongst the main plasma species, and current drive efficiency. The ability to heat ions preferentially depends on density, toroidal wave number and scenario. At low density ($2 - 3 \times 10^{20} \text{ m}^{-3}$), an optimized $2\Omega_{cT}$ scenario gives only 20-30% ion heating, while, at the other extreme, the DD-(He³) scenario can provide 70-80% ion heating.

A variety of analyses have been performed¹. For example, dominant ion heating scenarios have been explored with the 2-D version of the full-wave STELION code. Using the $2\Omega_{cT}$ resonance ($f = 52 \text{ MHz}$, $N = 22$) at $r/a \approx 0.25$, it was found possible to deliver 71% of the total radiofrequency power to the tritons, with the power absorption well localized in the plasma core. 16% of the power was absorbed by deuterons and 2% by the helium ash while electrons absorb 11% of the power, with a broad absorption profile. Fast wave (FW) damping on the electrons significantly increases at a frequency of 52 MHz ($N = 22$) when the second harmonic resonance moves to the plasma centre. Electrons absorb 46% of the radiofrequency power, leading to 1.2 MA of FW driven current with an efficiency, $\gamma_{20} = 0.15 \text{ AW}^{-1}\text{m}^{-2}$. Tritons absorb 54% of the radiofrequency power in this scenario.

1.2.5.3.2 EC Heating and Current Drive

Electron cyclotron waves are well suited to localized heating of electrons, to on- and off-axis current drive, and hence to the local control of radial profiles of electron temperature and current. They are also of interest for stabilization of NTMs, as discussed in I.2.4.1.1, and for plasma start-up. The radial deposition of electron cyclotron waves for heating and current drive can readily be changed by varying the toroidal launch angle of the waves. However, the resonance position depends on electron temperature, so that to maintain the resonance position while the plasma is being heated to burn, it will be necessary to vary the toroidal angle of the EC H&CD launcher.

Detailed calculations of current drive efficiency have been performed². A higher frequency offers a higher CD efficiency in the core, though at the expense of reduced flexibility and

¹V.L. Vdovin, ITER Physics Design Group at RRC Kurchatov Institute

²B. Lloyd et al, (UKAEA-EURATOM and Kyoto University)

increased vulnerability to $2\omega_{ce}$ damping. Moreover, the radial location of the driven current can be varied by toroidal steering of the EC radiofrequency beam. At the presently available highest frequency of 170 GHz, ECCD can provide a high CD efficiency of $\gamma_{20} = 0.1 \text{ AW}^{-1}\text{m}^{-2}$ at $r/a = 0.6$ (local $T_e \approx 10 \text{ keV}$) with a toroidal angle of about 45° , and $\gamma_{20} = 0.2 \text{ AW}^{-1}\text{m}^{-2}$ at the plasma centre ($T_{e0} = 20 \text{ keV}$) with a toroidal angle of 30° . As the central electron temperature will be close to 35 keV in the ITER-FEAT plasma, the CD efficiency can be expected to be higher than these values. Results of such calculations for a device similar to ITER-FEAT are summarized in Figure I.2.5.3-1, which shows the current drive efficiency as

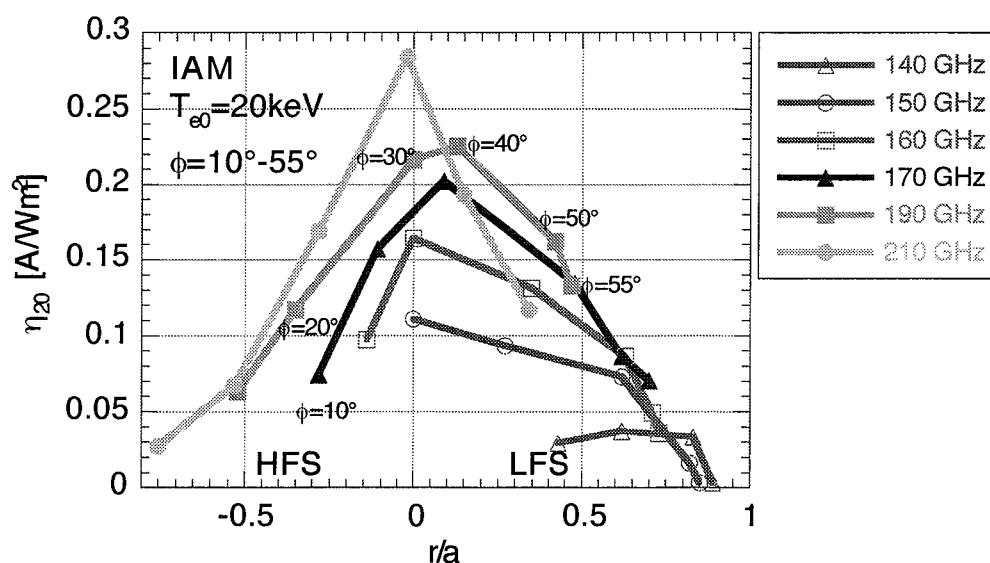


Figure I.2.5.3-1 Current Drive Efficiency versus Radial Position of the Current Peak as the Toroidal Launch Angle is Varied for Frequencies in a Device Similar to ITER-FEAT

a function of the radial position at which power is absorbed. These results are supported by a further study which confirmed that toroidal angles for optimum central current drive at 170 GHz lay in the range $31^\circ - 33^\circ$. For stabilization of NTMs, a launcher with a poloidal steering capability would be desirable to allow the current drive efficiency to be optimized for far off-axis resonance positions (e.g. for stabilizing (2,1) modes). It would, therefore, be advisable in ITER-FEAT to have a second EC H&CD launcher to allow optimization of the NTM stabilization capability (see II.7.2).

I.2.5.3.3 NB Heating and Current Drive

The plasma parameters in ITER-FEAT are such that the 1 MeV negative ion beam technology foreseen for the 1998 ITER design must be retained. The physics of the beam-plasma interaction at conventional energies ($\sim 100 \text{ keV}$) are well established, and recent results from JT-60U¹ have also confirmed this for the higher beam energies characteristic of negative ion beam technology. The major physics issues for NB H&CD are, therefore, that beam shine-through should be within acceptable limits at low plasma densities, that the beam orientation can be optimized for current drive, and that the high energy ions resulting from

¹ S. Ishida et al, Fusion Energy Proc. 17th Int. Conf. (Yokohama, 1998) paper IAEA-F1-CN-69/OV1/1, to be published (1999)

NB injection do not suffer unacceptable TF ripple losses or produce unacceptable amplitudes of mhd instabilities, such as Alfvén eigenmodes (see I.2.3.5 for energetic particle effects).

The evaluation of several of these issues is underway and to date most attention has focussed on the NB current drive capability, particularly in steady-state scenarios, and the beam shine-through losses. Since a vertically shifted beam line can drive an off-axis current efficiently, this will be incorporated into the ITER-FEAT design as far as is consistent with other constraints. In such cases the profile of beam current is broad, with the peak of the beam current almost coincident with that of the beam power. This approach can be exploited, of course, for current profile control in weak or negative shear steady-state scenarios. The resultant global current drive efficiency of such a configuration is shown in Figure I.2.5.3-2. Note that the efficiency increases with increasing R_{tan} , but that engineering constraints set a maximum value of $R_{\text{tan}} \sim 5.3$ m. In addition, hydrogen beam operation provides a higher current drive efficiency (by $\sim 20\%$) than deuterium beam injection due to the greater particle velocity (the current profiles for off-axis current drive are similar in the hydrogen and deuterium cases).

Beam shine-through losses have been studied in a similar device to ITER-FEAT, with the following major results:

- (a) for the typical target plasma for the steady-state operation scenario ($n_{20} \geq 0.6 \text{ m}^{-3}$), both D and H beams with $E_b = 1 \text{ MeV}$ meet the shine-through criterion that losses should be $< 2\%$, when injection lies within the region $4.7 \text{ m} \leq R_{\text{tan}} \leq 5.7 \text{ m}$ and $0 \leq Z_{\text{NB}} \leq 1.5 \text{ m}$;
- (b) with D-beam injection at $R_{\text{tan}} = 5.2 \text{ m}$ and $Z_{\text{NB}} = 1.0 \text{ m}$, the average density can be significantly reduced, to $n_{20} = 0.31 \text{ m}^{-3}$;
- (c) with H-beam injection at $R_{\text{tan}} = 5.2 \text{ m}$ and $Z_{\text{NB}} = 1.0 \text{ m}$, a relatively high density of $n_{20} = 0.51 \text{ m}^{-3}$ is required to meet the shine-through criterion.

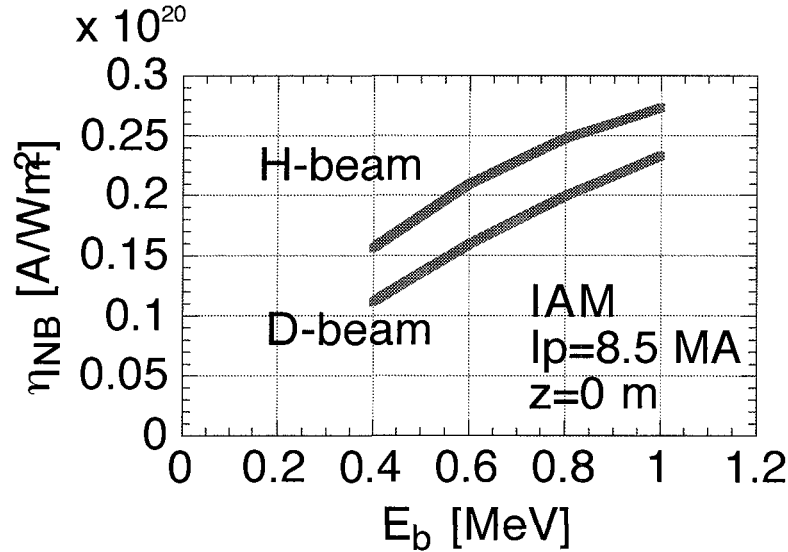


Figure I.2.5.3-2 NB Current Drive Efficiency versus Beam Energy for H and D Beams, where Current Drive Efficiency is Defined by $\eta_{NB} = I_{drive} n_e R / P$.

This calculation was carried out with the following parameters:

$$R = 6.2 \text{ m}, a = 1.9 \text{ m}, \kappa/\delta = 1.8/0.43, R_{tan} = 5.3 \text{ m}, I_p = 8.5 \text{ MA}, B_T = 5.51 \text{ T}, \\ n(0) = 1 \times 10^{20} \text{ m}^{-3}, T(0) = 25 \text{ keV}, p(0)/\langle p \rangle = 2.28, \langle n \rangle = 0.60 \times 10^{20} \text{ m}^{-3}, \beta_p \approx 3.32, \\ q_{95} = 4.92, q_a = 5.45, i_i = 0.62$$

I.2.5.4 Summary of Heating and Current Drive Capability

Several factors influence the selection of the mix of heating and current drive systems, as summarized in I.2.5.1. For example, for driven burn operation, the effect of ion versus electron heating must be considered. A range of cases has been simulated with varying mixtures of ion and electron heating, but only in the pure ion heating case (inapplicable to ITER-FEAT) does the ion temperature exceed the electron temperature.

In terms of on-axis current drive capability, the EC, IC and NB H&CD systems all have satisfactory current drive efficiencies, but LH waves cannot be used as the LH waves do not penetrate to the plasma centre under burn conditions. For EC on-axis current drive, a higher frequency is favourable, while the NB current drive efficiency depends significantly on the beam tangency radius. When used under optimized conditions, the three methods provide on-axis current drive with comparable efficiencies of $\gamma_{20} \geq 0.25 \text{ AW}^{-1} \text{ m}^{-2}$.

The off-axis current drive efficiency is sensitive to the location of the driven current, being mostly proportional to the electron temperature. IC off-axis current drive is not viable in ITER-FEAT because the mode conversion process yields a very low efficiency under the relevant plasma conditions. For EC, as discussed in I.2.5.2, the location of the driven current can be controlled by varying the toroidal launch angle of the radiofrequency beam. NB injection can maintain a high efficiency for off-axis current drive if the beam is optimally oriented. LH current drive, efficient even at low electron temperatures, gives the highest off-axis current drive efficiency, with its maximum current density in the region $0.6 \leq r/a \leq 0.8$.

1.2.6 Requirements for Plasma Measurements and Diagnostics

ITER-FEAT will require the measurement of an extensive range of key plasma and first wall parameters. Some of the measurements will be used in real time to prevent the onset of conditions which could potentially damage the first wall and other in-vessel components (machine protection). Others will be used in real-time feedback control loops to control the value of key parameters at values required for specific plasma performance (plasma control); while yet others will be used to evaluate the plasma performance and to provide information on key phenomena fundamental to ITER performance (physics studies). The measurements of some parameters may contribute to all three roles although the specifications of the measurements (accuracies, resolutions etc.) may be different depending on the role.

Even a relatively short (< 1 s) contact of the plasma with the first wall can result in unacceptable power loads on the wall. Similarly, an uncontrolled rise of the fusion power and/or a full divertor attachment can increase the thermal load onto the divertor plates above the tolerable level. The separatrix/wall gap, first wall temperature, divertor plate surface temperature and fusion power are therefore key machine protection parameters.

Plasma disruptions can deposit high energy loads on the divertor plates during a thermal plasma quench with consequential significant plate erosion. Also, high mechanical stresses can arise in the blanket/shield structure and divertor cassettes due to high halo currents flowing poloidally through these components during a vertical displacement event (VDE). Runaway electrons formed during a disruption can increase the potential for damage to the plasma-facing components. Since disruptions will probably be a major factor defining the life-time of the plasma-facing components, the number of disruptions should be kept small and/or their effects mitigated. Experiments show that locked (non-rotating) modes, especially those induced by the resonant, $m/n = 2/1$ error field component, often lead to disruptions. Additional machine protection parameters are therefore disruption precursors (particularly detection of locked modes), halo currents in key components, and runaway electrons.

The edge localized mode (ELM) is beneficial for impurity and helium expulsion from the plasma edge, but type I ('giant') ELMs can lead to potentially damaging heat loads to the divertor plates. The measurement of ELM type is therefore included as a machine protection parameter. A sudden and strong increase in the emission of a particular impurity, e.g. Be, can be a clear indication of increased plasma-wall interaction. Measurement of specific impurity emission is therefore included as a machine protection parameter. Neutral beam injection in the absence of plasma will produce a localized heat load (typically $35 - 50 \text{ MWm}^{-2}$). A relatively high density plasma, i.e. $\bar{n}_e \geq 0.4 \times 10^{20} \text{ m}^{-3}$ for deuterium beams and $\bar{n}_e \geq 0.5 \times 10^{20} \text{ m}^{-3}$ for hydrogen beams, must be maintained during neutral beam injection to reduce beam shine-through to an acceptable level. Hence, reliable measurement of the line-averaged electron density is also required for machine protection.

The parameters that will be employed for plasma control will include those used for control in the present generation of tokamak plasmas, particularly the plasma shape and position, plasma current and electron density. Operation with a burning DT plasma results in additional plasma control requirements, in particular a simultaneous control of the fusion power, divertor heat load and helium-ash is required. The ITER divertor is designed for a high steady-state peak power load but at full power a substantial fraction ($\sim 75\%$) of the total

power must be radiated to keep the power deposited on the divertor plates to acceptable levels. This operation may require injection of a controlled amount of a specific impurity or a combination of impurities (e.g. Ne, Ar) to the divertor and scrape-off-layer (SOL) plasma, but the bremsstrahlung power loss and plasma dilution in the core must be maintained at levels acceptable for the plasma burn. The kinetic control must also keep the plasma away from the β and density limits and provide sufficient power flow through the separatrix to ensure H-mode plasma operation. It is clear that a sophisticated multi-input, multi-actuator feedback control scheme is required for the successful operation of ITER-FEAT in the basic driven-burn regime. This leads to requirements for a wide range of additional plasma measurements for control, including radiative power loss from the plasma core, SOL, X-point region and from the divertor, plasma density profile, β , n_T/n_D ratio, rotating mhd modes and a degree of divertor detachment, i.e. 'ionization front' position and/or T_e and n_e at the divertor plate.

Further, sustained operation in high confinement modes, for example reverse shear, is a key part of the ITER-FEAT experimental programme. This operation is likely to require control and hence measurement of the spatial profile of key parameters such as q , pressure and rotation. For sustained operation near the β limit, it is expected that suppression of neoclassical tearing modes (NTMs) will be required. Similarly, for steady-state operation at high β levels, stabilization of the resistive wall modes (RWMs) will be required. Measurements of the location and amplitude of these modes are therefore required.

The ITER plasma will be the first in which there is significant α -heating, so the experimental program will have an extensive explorative physics component. Key topics to be investigated include confinement physics, operational limits, high-current plasma disruptions, physics of high power radiative divertor, α -particle effects and steady-state burn. An extensive set of plasma measurements is required to support these programmes. Many of the parameters measured for control purposes can also provide physics data, although the specifications of the measurements (accuracies and resolutions) may have to be enhanced. However, some additional parameters will also be required: for example, confined α -particles, TAE modes, fishbones, n_e and T_e fluctuations, and radial electric field and field fluctuations.

The above requirements imply a need for a large number of measurements. However, resources such as manpower, budget, port space etc are limited and so it is necessary to set priorities. Naturally, the highest priority must be given to measurements for machine protection and basic plasma control. This leads to a convenient classification of the measurements: those that are required for machine protection and basic plasma control (group 1a); those that are required for advanced plasma control (group 1b); and those that are required for evaluation and physics studies (group 2).

The separation of control measurements between basic and advanced is somewhat arbitrary, but it recognizes the fact that some parameters will require real-time control for every ITER pulse, (examples include plasma shape and position, plasma current and line-averaged density), while others will be controlled for specific programmes. Examples of the latter are the plasma rotation and the q profile, which may have to be under real-time control for specific modes of operation but are not necessarily controlled on every ITER pulse.

The setting of priorities according to the control requirements clearly has merits, but it also has some limitations. Measurements of some parameters are essential to evaluate and

optimize the plasma performance, but are presently not envisaged as control parameters: for example, measurements of confined and escaping α -particles will be critical for evaluating the fusion performance, but will probably not be used as control parameters. It would be inappropriate to limit the measurements to only those necessary for machine protection and plasma control.

Taking into account these considerations¹, a list of required measurement parameters has been drawn up. This is arranged according to the priorities for control and is presented in Table I.2.6-1. The principal diagnostic for each parameter is also shown. The implementation of the diagnostics is outlined in II.6.0.

I.2.7 Conclusions

The physics design concept outlined in this chapter demonstrates that ITER-FEAT satisfies its objectives: inductively-driven DT discharge with $Q > 10$ lasting for 300-500 s with reasonable margins in confinement, β and L-H transition power. The nominal operation density is 85% of the Greenwald density, which enables operation with high reliability, particularly with its high triangularity. Improved confinement by a factor of 1.2 or improved confinement up to the Greenwald density will enable studies on plasmas with high $Q \sim 50$, i.e. plasmas which are almost fully self-sustained. These operation domains are significantly expanded with higher current, e.g. 17.4 MA.

Two operational scenarios are under consideration for steady-state operation: high current (12 MA) with monotonic q or shallow shear, and modest current (8 MA) with negative shear. High current, steady-state operation requires all of the current drive power (~ 100 MW) potentially available for ITER-FEAT, but the requirements on confinement ($H_{H(y,2)} \sim 1.2$) and β ($\beta_N \sim 3$) are modest. On the other hand, low current, steady-state operation requires more challenging values of confinement improvement ($H_{H(y,2)} \sim 1.5$) and β ($\beta_N \sim 3.2-3.5$). Although these values have been obtained in recent experiments, further investigation will be required to establish the operation scenarios: pressure and current profile control, stability control and divertor compatibility. Hybrid operation, with combined inductive and non-inductive current drive, will provide long pulses (e.g. $> 1,000$ s) with a more modest requirement on confinement ($H_{H(y,2)} \leq 1.0$). This scenario offers a candidate operation mode for engineering tests.

ITER-FEAT has the capability to exploit NB, EC, IC and/or LH for heating and current drive, which, taking advantage of their different characteristics, offers flexibility and variation in experimental operation. In addition, the diagnostics system is designed to satisfy the profile control needs of enhanced modes of operation.

The advanced features of ITER-FEAT include ECCD for stabilizing neoclassical tearing modes, saddle coils external to the toroidal field coils for stabilizing resistive wall modes and

¹ A.E. Costley, R. Bartiromo, L.de Kock, E. Marmar, et al, "Requirements for ITER Diagnostics", in Diagnostics for Experimental Thermonuclear Fusion Reactors (Proc. of Int. Workshop on Diagnostics for ITER, Varenna, Sept. 1995) Plenum Press, New York, (1996) 23 - 37

V. Mukhovatov, A.E. Costley, R. Bartiromo, D. Boucher et al, "ITER Physics Program and Implications for Plasma Measurements", Rev. of Sci. Instrms, **68** (1997) 1250 - 1255

V. S. Mukhovatov, R. Bartiromo, D. Boucher, A. E. Costley et al, "Role and Requirements for Plasma Measurements on ITER", in Diagnostics for Experimental Thermonuclear Fusion Reactors 2 (Proc. of Int. Workshop on Diagnostics for ITER, Varenna, Sept. 1997) Plenum Press, New York (1998) 25 - 40

Table I.2.6-1 Priorities for Control Measurements

GROUP 1a Mach. Protect.&Basic Control		GROUP 1b Advanced Control		GROUP 2 Evaluation & Physics	
Parameter	Diagnosis	Parameter	Diagnostic	Parameter	Diagnostic
Shape/Position Vertical speed Locked Modes I_p , $q(a)$, $q(95\%)$, β $m = 2$ Mode, I_{halo} , V_{loop}	Magnetics	MHD Activity	Magnetics, ECE, Reflectometry	Fishbones, TAE Modes	Magnetics, Reflectometry, ECE
Impurity and DT influx (main plasma & div.)	Impurity Monitors	Shape/Position (very long pulse)	Reflectometry (plasma posit.)	Confined α -Particles	Collect. Scatt., Knock-on Tail Neut. Spec., NPA
Runaway Electrons	Hard X-Rays, Synchrotron Radiation	Neutron Profile, α -Source Profile	Rad. Neut. Cam., Vert. Neut. Cam	$n_T/n_D/n_H$ (edge)	NPA, H_α Spectr., Laser Induced Fluoresce.(LIF)
Line-averaged Density	Interf./Polarim.	n_{He} Profile	Active CXRS	$n_T/n_D/n_H$ (div.)	H_α Spectrosc.
Div. Detachment (J_{sat} (divertor))	Tile Shuts	Plasma Rotat., T_i Profile. Impurity Profile	Active CXRS, X-Ray Crystal Spectroscopy VUV Spectr.	T_e Profile (edge)	Thomson Scatt. (edge)
Surf. Temp. (divertor plates & FW)	IR Cameras	T_e Prof.(core), n_e Prof.(core)	LIDAR (main), ECE	n_e , T_e Profiles (X-point)	Thomson Scatt. (X-point)
Rad. Power from Core, X-pt and Div.	Bolom. Array (main pl. & div.)	T_i Prof.(core)	Radial Neutron Spectrometer	n_e , T_e (plate)	Langmuir Probes
Fusion Power	Neutron flux monitors	n_e Profile (edge)	Refl.(main)	T_i in Divertor	Imp. Monitor. (div.)
n_T/n_D in Plasma Core	NPA, Fast Wave Reflectometry	q Profile	MSE, Polarim. System	Plasma Flow (div.)	Imp. Monitor. (div.)
Z_{eff} Line-Aver.	Vis. Continuum (single channel)	P_{rad} Profile	Bolom. Arrays (main pl. & div.)	Pellet Ablation	H_α Spectrosc.
H/L Mode Indicator	H_α Spectr. (typ. channel)	Z_{eff} Profile	Visible Cont. Array	T_e Fluctuations	ECE, Soft X-Ray Array
ELMs (typ)	ECE, Refl.(main) H Spectroscopy	n_{He} (divertor)	RGA Imp. Monitor	n_e Fluctuations	Reflectometry, Microw. Scatt.
Gas Pressure (div. & duct)	Pressure Gauges	Heat Depos. Prof. in Div.	IR Camera	Radial E Field and E Fluctuat.	CXRS (plasma rot.)
Gas Composit. (div. & duct)	RGAs	Div. Ionization Front Position	Visib. Spectrom., Bolometry	Edge Turbulen.	Reflectometry
Toroidal Magnetic Field	Current Shunts	Neutral Density (near wall), Particle Source	H_α Spectroscopy (many chann.), Pressure Gauges	MHD Activity in Plasma Core	ECE, Soft X-Ray Array
		n_e , T_e (divertor)	Refl. (div.), ECA (div.), Thoms. Sc. (div.)		
		Impurity & D, T Influxes in Div. with spat. res.	Imp. Monitors, H_α Spectroscopy		
		Alpha Loss	Alpha-Loss Det., IR Camera		
		Neut. Fluence	Neutr. Act. Syst.		
		ELMs	ECE, Refl.(main), Magnetics		
		Sawteeth	ECE, Soft X-Ray Array		
		NTMs	Magnetics, ECE		
		RWMs	Magnetics		
		Erosion (plate)	Imp. Monitors, Reflectometry		

field-side pellet injection, which will expand the operational space and/or improve the stability characteristics of discharges with high β and high density.

To summarize, the physics design concept of ITER-FEAT satisfies the stated mission, embodies all of the state-of-the-art tokamak physics knowledge available to date, and is compatible with the constraints of engineering and cost. ITER-FEAT will allow, for the first time, plasma physics studies on confinement, mhd stability, divertor, and energetic particle confinement under completely integrated, reactor-relevant conditions, and for pulse lengths significantly longer than the characteristic times of plasma processes.

I.3 Design Overview

I.3.1	Plant Overview and System Design Assessments	2
I.3.1.1	Magnet System	6
I.3.1.2	Magnet Coil Power Supplies	10
I.3.1.3	Cryoplant and Cryodistribution System	10
I.3.1.4	Cryostat and Thermal Shields	12
I.3.1.5	Vacuum Vessel	14
I.3.1.6	Blanket	15
I.3.1.7	Divertor	17
I.3.1.8	Water Cooling System	19
I.3.1.9	Fuel Cycle	21
I.3.1.10	Heating and Current Drive	23
I.3.1.11	Diagnostics	25
I.3.1.12	Buildings and Services	27
I.3.1.13	Tokamak Maintenance	32
I.3.1.14	Tokamak Assembly	34
I.3.2	Plant Control & Operation	36
I.3.2.1	Plant Control System	36
I.3.2.2	Plasma Operation Scenarios	40
I.3.2.2.1	Plasma Initiation	40
I.3.2.2.2	Current Ramp-up	40
I.3.2.2.3	Shape and Configuration Control	40
I.3.2.2.4	Heating to Driven Burn	41
I.3.2.2.5	Sustained Burn	41
I.3.2.2.6	Burn Termination	41
I.3.3	Safety and Environment	43
I.3.3.1	Normal Operation	44
I.3.3.1.1	Effluents	44
I.3.3.1.2	Occupational Safety	44
I.3.3.1.3	Radioactive Waste	44
I.3.3.2	Accidents	45
I.3.3.2.1	Loss of Coolant Accidents	47
I.3.3.2.1.1	Ex-vessel Coolant Leak	47
I.3.3.2.1.2	In-vessel Coolant Leak	48
I.3.3.2.2	Decay Heat	49

I.3.1 provides a summary description of the outline design of the ITER-FEAT plant. It lists the systems involved and describes how these various systems (described in more detail in II) are inter-related in operational terms.

In addition to a brief summary of the outline design, there is an assessment of it and a listing of the main open issues and remaining options. The normal work remaining to be done in detailing a design is not regarded as a main outstanding issue and so is not mentioned in this section.

At this level of the development of the design, not all parameters are “frozen”; adjustments will lead to limited modifications. The proposed engineering design relies mainly on technical solutions which have been, or are being, qualified by the on-going R&D, in the Parties’ laboratories and industries. Most of the remaining issues are related to the choice of options which will provide the largest cost saving.

Because of the unwillingness to compromise with physics extrapolation so as to provide enough margins in the physical parameters and physics-related systems e.g. plasma size, fuelling, and heating and current drive, the only remaining possibility is to press mostly on the manufacturing processes (with their feedback on design) to approach as closely as possible the target of 50% saving in direct capital cost from the 1998 ITER design.

The nature of the overall plant operational control is described in I.3.2. Although this report is only the outline design of ITER-FEAT, it has been possible to make initial assessments and draw significant conclusions for the safety of the plant and this is summarised in I.3.3.

I.3.1 Plant Overview and System Design Assessments

The ITER-FEAT plant is made up of the following systems:

- the tokamak itself, consisting of a vacuum vessel (II.2.1) and its internal components; a blanket (II.2.2) and divertor (II.2.3), and superconducting magnets and associated structures (II.1.3);
- a cryoplant and cryodistribution (II.1.4);
- a pulsed electrical power supply (II.1.2);
- a cryostat and its associated thermal shields (II.3);
- a fuelling and exhaust system including an exhaust processing system (II.4);
- a cooling water system (II.5);
- a plasma measurement (diagnostic) system (II.6);
- a heating and current drive system and its electrical power supply (II.7);
- buildings and services (II.8);

The initial assembly of the tokamak (II.9) and its remote maintenance (II.10) are especially important topics at the plant level;

The main parameters for ITER-FEAT are shown in Table I.3.1-1. Figure I.3.1-1 shows an overall schematic of systems important for normal ITER-FEAT operation. A cross-section of the tokamak showing the vacuum vessel, its internal components and its ports, as well as some features of the magnet system and cryostat, is shown in Figure I.3.1-2. A schematic radial build is shown in Figure I.3.1-3.

Table I.3-1 ITER-FEAT Main Parameters

Parameter	Unit	Nominal	Max
Major radius, R	m	6.2	\leq
Minor radius, a	m	2.0	\leq
Plasma current, I_p	MA	15.0	17.4 ¹
Additional heating & CD power ²	MW	73	100
Fusion power	MW	500	700 ³
Toroidal field at major radius, B_0	T	5.3	\leq
Elongation at 95% flux, κ_{95} , κ_X		1.7, 1.85	\leq
Triangularity at 95% flux, δ_{95} , δ_X		0.33, 0.49	\leq
Plasma volume	m ³	837	\leq
Plasma surface	m ²	678	\leq
MHD safety factor at 95% flux, q_{95}		3	
Average neutron wall load at the first wall	MW /m ²	0.57	0.80
Neutron wall load at the outboard equator		0.65	0.91
Total neutron fluence at the outboard equator	MWa/m ²	0.3	0.5 ⁴
Burn duty, %	%	~ 4	25 ⁵

¹ To avoid cost increase, higher current operation would be accessed for a limited number of shots, limited pulse length, limited space of I_i and β_p . 17.4 MA operation is required for machine commissioning during the H Operation Phase.

² In the typical nominal DT operation scenario, the additional heating power is 50 MW. However, the device has the heating power of 73 MW (33 MW for NB and 40 MW for RF) initially. Increase of the heating power at least up to 100 MW (e.g. a third beamline and/or increased RF power) should not be excluded.

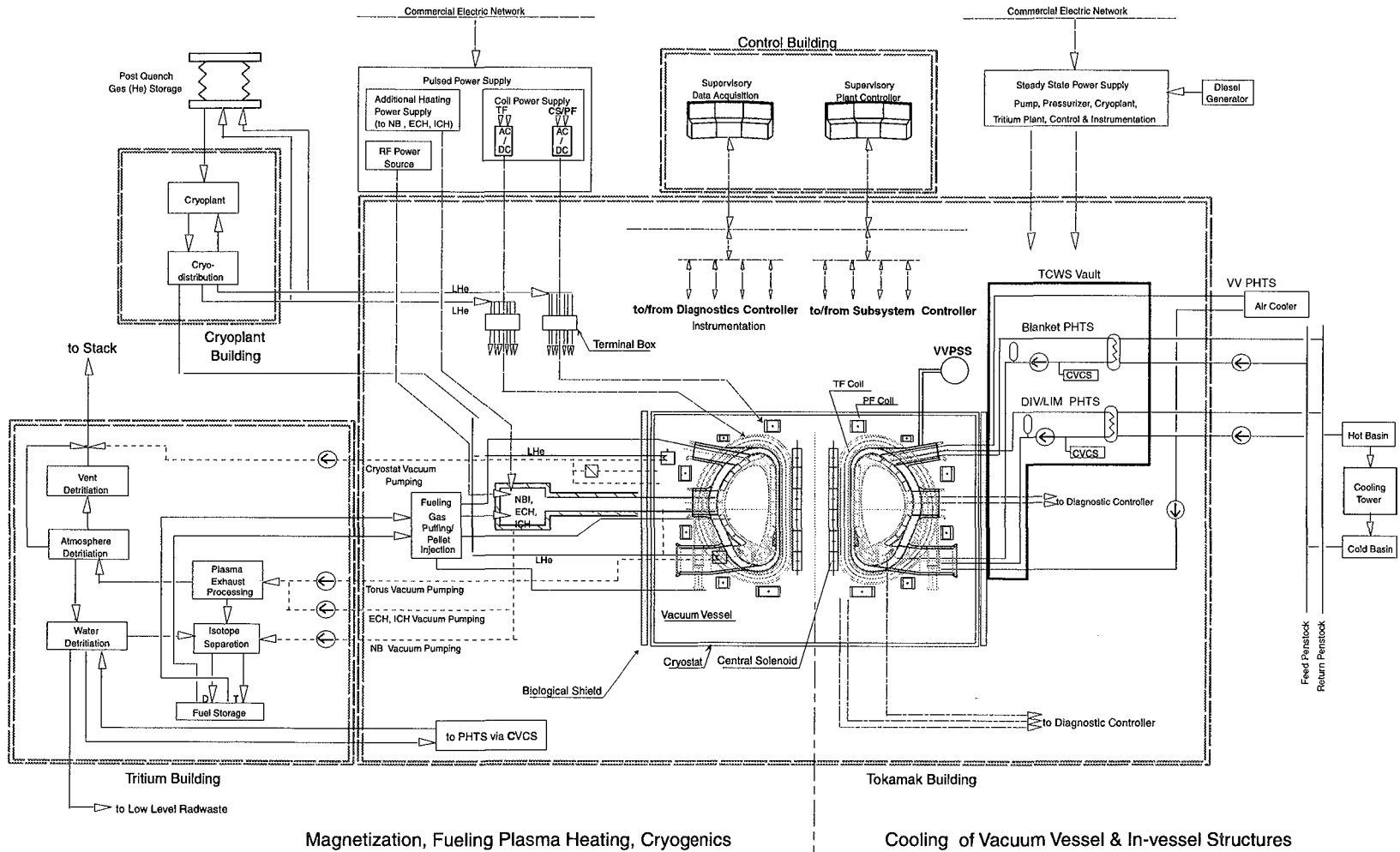
³ High fusion power operation would be accessed by reducing pulse length and duty cycle to avoid capital cost increase.

⁴ Device is designed to be able to accept up to 0.5 MWa/m² without increase in capital cost.

⁵ Nominal burn duty on average throughout DT operation is about 4 %. For demonstration of repeatable pulse operations, the device should be able to operate with burn duty of about 25 % (400 s/1800 s) for a couple of days with reasonable capital cost increase.

Figure I.3.1-1

Plant System Diagram



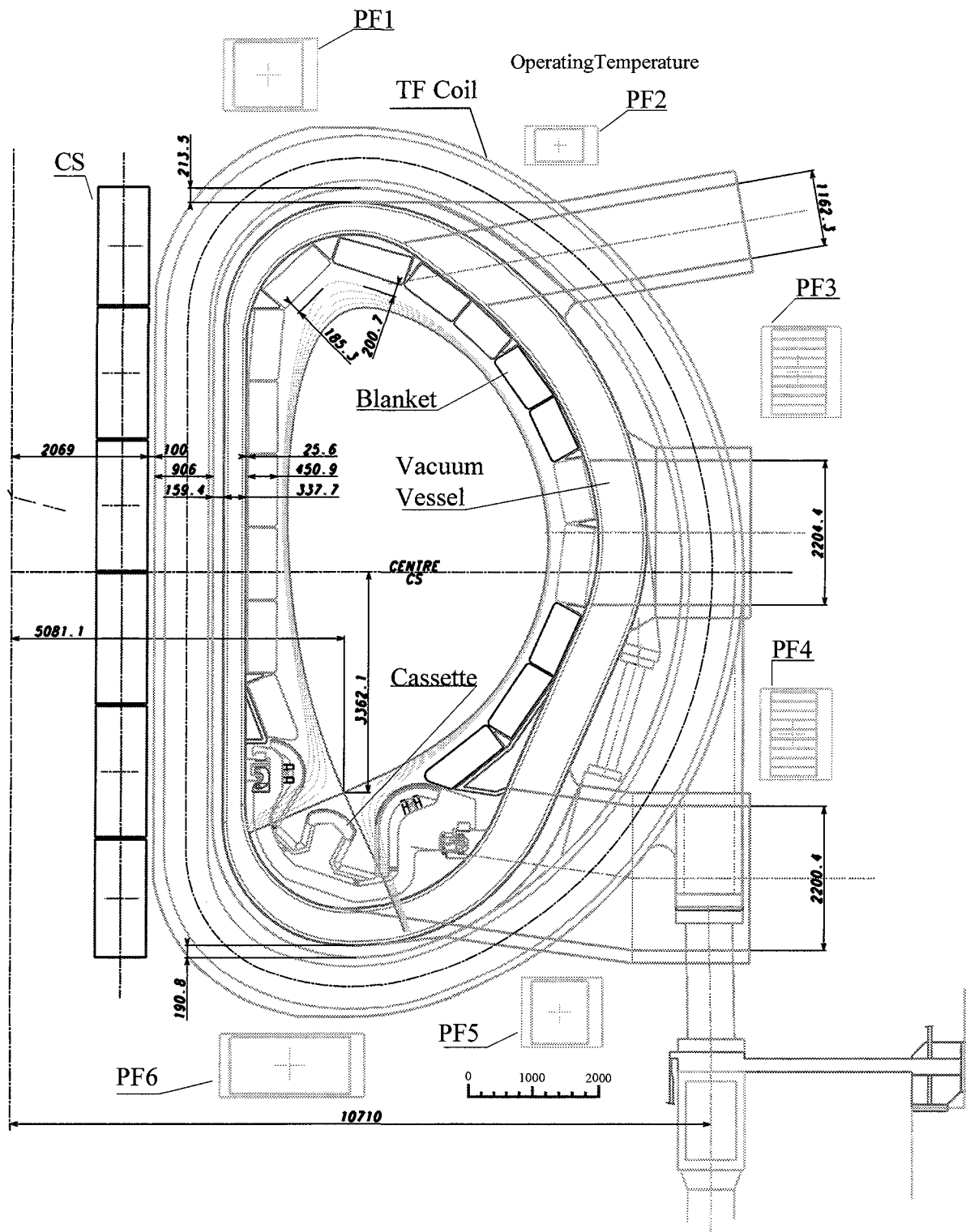


Figure I.3.1-2 Cross-section of Tokamak

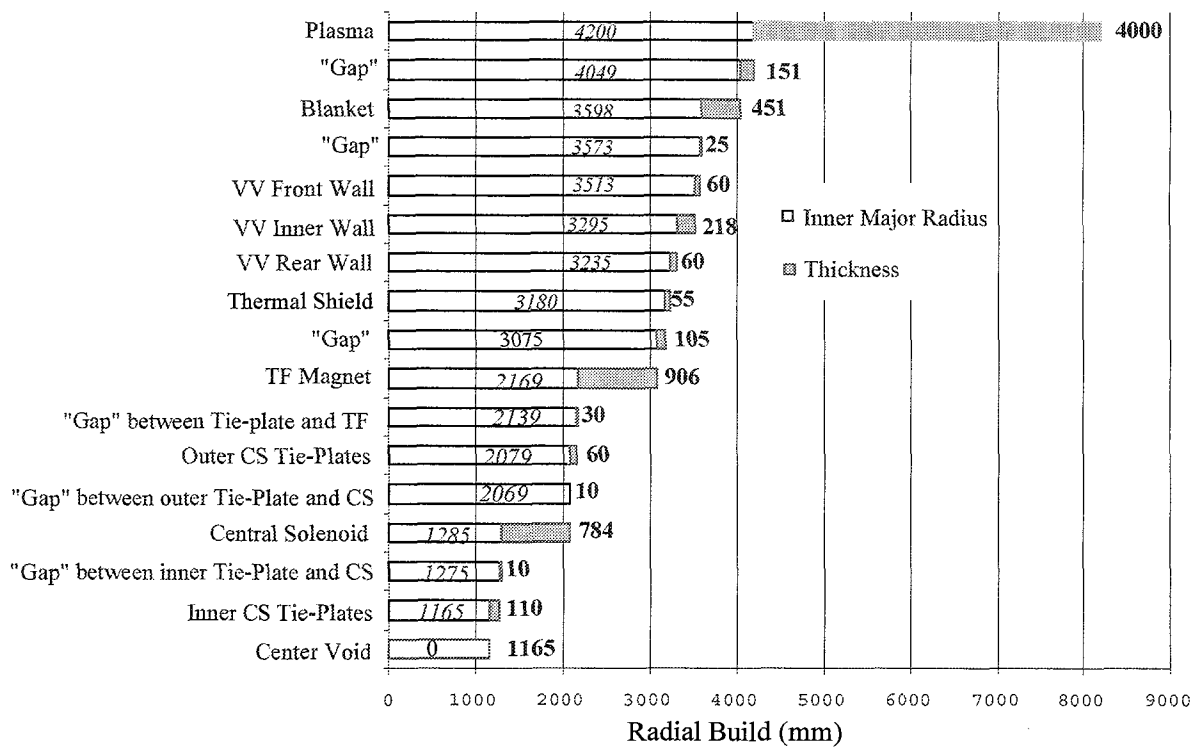


Figure I.3.1-3 Radial Build Schematic

I.3.1.1 Magnet System

The superconducting magnet system confines, shapes and controls the plasma inside a toroidal vacuum vessel. The magnet system is made up of coils which produce the confining/stabilizing toroidal field (the TF coils), the coils which produce a contribution to the positioning and shaping poloidal field (the PF coils), and the coil which provides the main contribution to the induction of current in the plasma (the central solenoid, CS). Correction coils are also required to correct error fields that arise due to imperfections in the actual PF and TF coil configuration and to stabilize the plasma against resistive wall mode instabilities. Correction coils have not been designed yet but will include three coil sets located above, outboard of and below the TF coils. Overall magnet system parameters are shown in Table I.3.1-2.

Table I.3.1-2 Overall Magnet System Parameters

Number of TF coils	18
Number of PF coils	6
Magnetic energy in TF coils (GJ)	~ 41
MAm* in TF coils	5,614
Maximum field in TF coils (T)	11.8
Centering force per TF coil (MN)	404
Vertical force per half TF coil (MN)	202
TF discharge time constant (s)	11
MAm* in CS coil	1,483
CS peak field (T)	13.5
MAm* in PF coils	2,680
Total weight of magnet system (t)	~ 8,700

*Proportional to the overall superconductor length

CS & TF Coils

The CS and TF coils use a conductor with a large number of Nb₃Sn strands (~ 1,000), whereas the remaining PF and correction coils use a similar conductor with NbTi strands. All coils are cooled by supercritical helium at ~ 4.5K. The TF coil case is the main structural component of the magnet system and the machine core. The PF coils and vacuum vessel are linked to the TF coils such that all interaction forces are resisted internally in the system thus eliminating the need for large external load transferring structures and the mechanical moments associated with such structures. The TF coil inboard legs are wedged all along their side walls in operation. At the outboard leg, the out-of-plane support is provided by intercoil structures integrated with the TF coil cases. Views of the TF coil case are shown in Figure I.3.1-4.

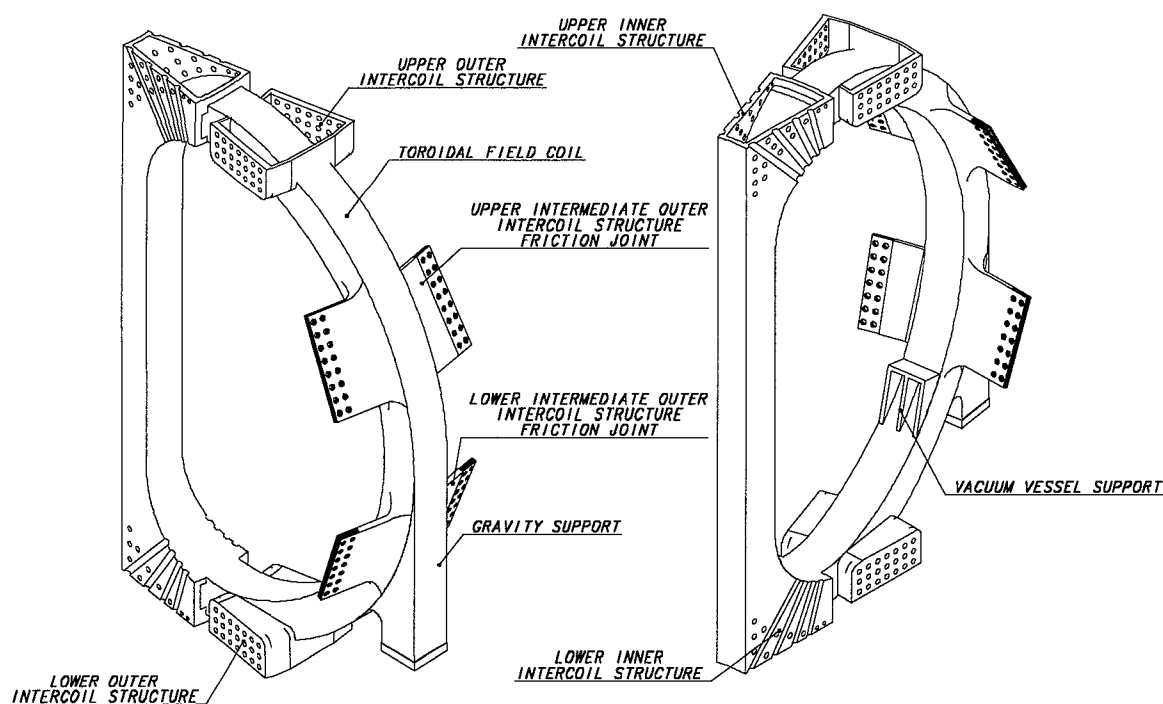


Figure I.3.1-4 3-D Views of the TF Coil Case

Main Outstanding Issues and Remaining Options for the TF Coils and CS

For the TF coils and their intercoil structures a key structural issue is the out-of-plane support of the TF coils at the inboard lower curved region. In this region, out-of-plane loads are severe because of the large poloidal field flux crossing the TF coil in the divertor area. The design of the supporting structures is complicated by the TF coil displacements under their own field, which can result in local de-wedging of the coils. Various design concepts have been analysed but the final design has not yet been established. The solution requires a strengthening of the coil case in the critical region and structures able to resist shear loads between adjacent coils. It is possible that an acceptable design will require a thicker case in the inner leg region, imposing a radial build penalty of a few cm.

Two options are still under investigation for the TF coil winding: one with a circular conductor embedded in radial plates and the other with a square conductor. The radial plate option has advantages in terms of the insulation reliability and fault detection capability, but suffers from cost and radial build penalties.

For the CS winding, there are two options to provide the structural material which is subject to fatigue due to the large number of pulses. The first one uses an Incoloy square jacket with a co-wound strip and the second one uses two, stainless steel, U-channels welded around a thin circular jacket made of Incoloy or titanium. The selection of the option has some limited impact on the CS flux capability, but the choice can be postponed until more R&D results are available.

With a pancake-wound CS, the pancake to pancake joint configuration is unfavourable because of eddy currents which can flow across the joint surface due to radial field changes. Testing of joints in relevant field changes and orientation is not part of the planned R&D programme due to the lack of facilities in the EU or Japan, but is nevertheless required to establish the CS joint design.

Assessment

The conductor and joint designs for the TF coils and CS are based on R&D results available from short length conductor and joint samples, particularly those associated with the Model Coil (MC) programmes. The final verification of the Nb₃Sn conductors in an integrated test will come from the CSMC experimental programme. In this programme, inserts made of the CS and TF type conductors will be tested under external conditions (static and variable field, stress and strain levels, cooling...) simulating those to be met in ITER-FEAT operation.

Conductor manufacture at industrial scale has been achieved for the CS and TF Model Coils. This has established a firm basis for strand production, cabling, jacket manufacture and jacketing. The conductor production and the QA requirements for the full-scale coils can be extrapolated from this basis.

The Model Coil programme has addressed and resolved a number of key issues for the manufacture of the TF coils and the CS. Winding techniques and the Nb₃Sn conductor reaction treatment procedures have been demonstrated at large scale. The “wind, react and transfer” process, where turn insulation is applied after the reaction treatment, has also been demonstrated for both the TF coils and the CS. For the TF coils, specific manufacturing

aspects, related to the use of a circular conductor embedded in radial plates, have also been demonstrated.

Manufacturing feasibility of the TF coil structures is being investigated by R&D programmes for the fabrication of full-scale sections of the TF coil case. This programme includes welding development and the production of large, forged and cast pieces with dimensions relevant to the full-size coil cases and outer intercoil structures. This development has identified manufacturing processes (forgings, castings) which are expected to facilitate manufacture and should result in cost savings. Other areas, which will be the subject of future R&D work, are related to the design, assembly and testing of the insulated shear keys and friction joints of the TF intercoil structures.

In total, this large effort in R&D provides confidence that the remaining issues for the magnet design are not ones of feasibility, but rather, issues which relate to options to reduce the capital cost and to fulfil new requirements for plasma operation (e.g. the segmented CS and wedged TF coils).

PF Coils

The PF coils are designed to control the position and shape of the plasma and to stabilize its displacements caused by changes in internal plasma parameters. The PF configuration analysis has determined the position, size, number of turns, maximum current and magnetic field on the coil as well as the specifications of their power supplies (II.1.1 and 2). The preliminary results of this analysis for the CS and PF coils parameters are shown in Table I.3.1-3.

Table I.3.1-3 PF Coil Position, Size, Number of Turns, Maximum Current and Magnetic Field

Coil	R _c (m)	Z _c (m)	ΔR (m)	ΔZ (m)	Number of turns	I _{max} (MA _t)	B _{max} at IM(T)	B _{max} at EOB
CSU3	1.677	4.974	0.765	1.789	486	21.9	13.5	12.8
CSU2	1.677	3.041	0.765	1.977	538	24.2	13.5	12.8
CSU1	1.677	1.14	0.765	1.977	538	24.2	13.5	12.8
CSL1	1.677	-1.014	0.765	1.977	538	24.2	13.5	12.8
CSL2	1.677	-3.41	0.765	1.977	538	24.2	13.5	12.8
CSL3	1.677	-4.974	0.765	1.789	486	21.9	13.5	12.8
PF1	3.880	7.584	1.027	0.974	270	12.2	6.0	6.0
PF2	8.338	6.509	0.703	0.472	94	4.2	5.0	5.0
PF3	12.014	3.055	0.820	1.262	220	8.7	5.0	5.0
PF4	11.955	-2.465	0.703	1.119	164.5	6.3	5.0	5.0
PF5	8.396	-6.748	0.820	0.945	220	9.9	5.0	5.0
PF6	4.273	-7.559	1.813	0.852	416.5	18.7	6.0	6.0

Main Outstanding Issue for PF Coils

The verification of the performance of the NbTi conductors for the PF coils requires new R&D activities which must include the manufacture of a coil with a full size conductor and

the testing of this coil in pulsed conditions. These new R&D activities have been initiated and the design and test programme for the NbTi coil are under study.

Assessment

Apart from the verification of the superconductor performance, there are no significant issues which would lead to a lack of confidence in the design of the coils.

I.3.1.2 Magnet Coil Power Supplies

A power supply provides the DC coil currents to the different coils from the AC high voltage grid which supplies the ITER-FEAT site. The various coil electrical loads have different characteristics in terms of the currents, power, length of pulse, and so the coil power supply is made up of several subsystems. In addition, because of the possibility of superconducting coils quenching (rapid loss of superconductivity) under certain conditions, protective circuitry is required to discharge the magnetic energy to external resistors (and the helium is discharged to external recovery tanks).

Main Outstanding Issue for the Magnet Coil Power Supplies

The DC switches used for the extraction of the energy stored in the coils required R&D. The results obtained so far have determined the design of the various components in detail, but further limited R&D is foreseen to verify the design margins.

Assessment

For the main components and subsystems, including the AC/DC conversion system, the reference designs are based on existing technology and products available in the world market, or on the progress that is expected to be achieved in the near future.

I.3.1.3 Cryoplant and Cryodistribution System

Liquid helium from a cryoplant is distributed by a cryodistribution system to auxiliary cold boxes feeding the magnet and other loads as well (e.g. cryopumps for the pumping of the vacuum vessel). Circulating pumps force the flow of supercritical helium through the load in each separate circuit, which exchanges heat with a helium bath, whose pressure (and thus temperature) are controlled by a cold compressor in the return path towards the cryoplant (see Figure I.3.1-5). The plant design has to reconcile the pulsed character of the heat deposited in the magnet coils and the cryopumps, with the steady operation of the cryorefrigerator, which handles only the average heat load.

Main Outstanding Issue for the Cryoplant and Cryodistribution System

The key design issue for the cryoplant is to make compatible the pulsed character of the heat deposited in the magnet coils and the cryopumps, and the steady operation of the cryorefrigerator, which handles only the average heat load.

N 34 GR 19 99-11-18 W

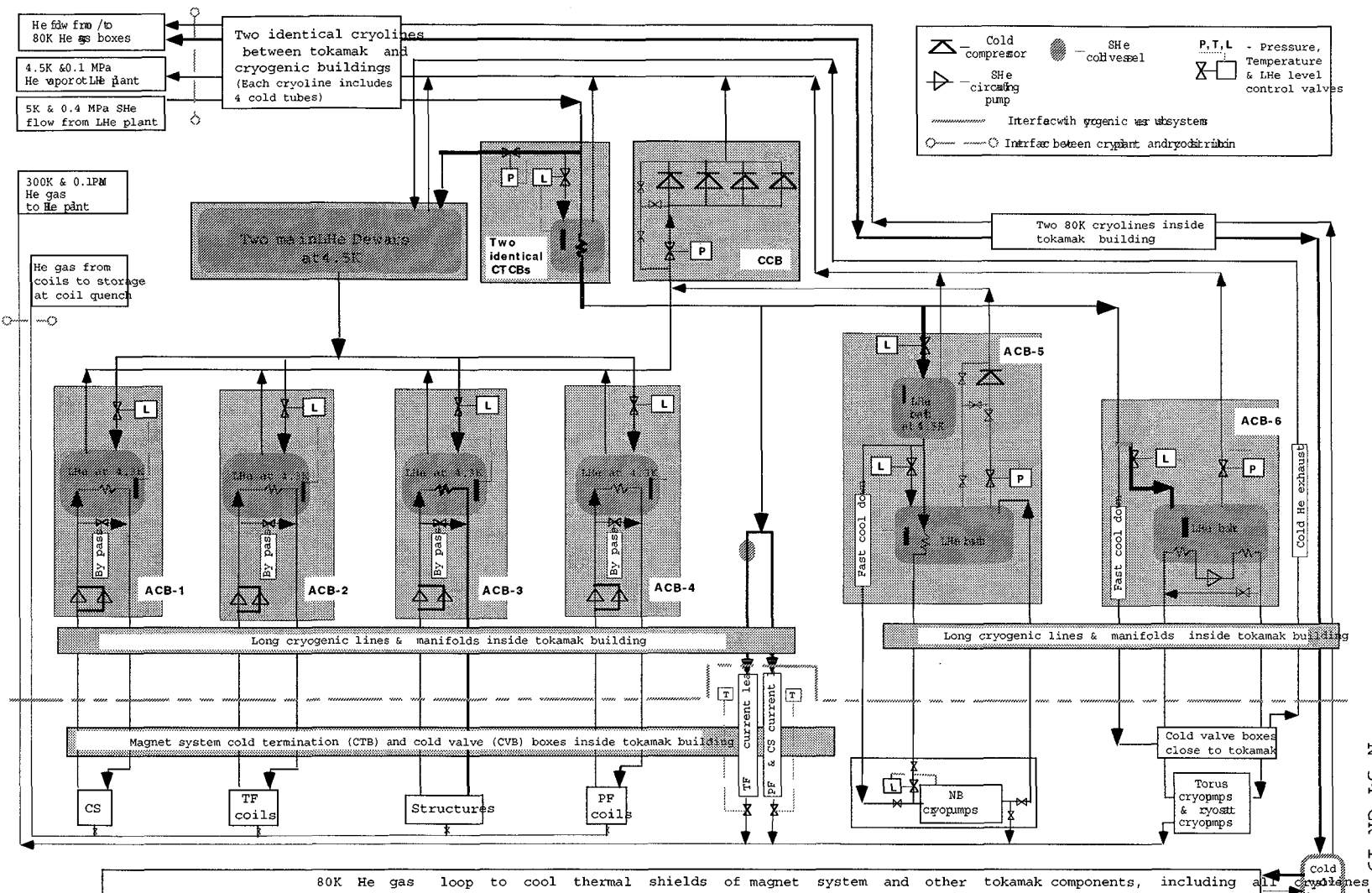


Figure I.3.1-5 Diagram of Cryodistribution System

Assessment

Even if the envisaged cryoplant is a very large and complex facility, the confidence of building such a plant with the required performance is very high. This is based on the facts that the refrigerator unit has already been built for CERN, hot and cold compressors and pump are presently operating, and the nitrogen liquefaction plant is commercially available. The cryodistribution systems for large particle accelerators provide good bases for the ITER-FEAT system design. The cooling capacity of the liquid helium cryoplant is given in Table I.3.1-4.

Table I.3.1-4 Cooling Capacity of the LHe Plant

Liquefaction to cool the current leads	kg/s	0.066
Static heat load	kW	9.3
Averaged pulsed heat load [1]	kW	19
Heat loads of helium circulating pumps	kW	14.1
Heat load of cold compressors	kW	7.5
Torus cryopumps including liquefaction for fast cool down during their regeneration [2]		4 kW + 0.06 kg/s
Small cryogen users	kW	1.0
Total	54.9 kW + 0.126 kg/s	
[1]	Pulsed heat loads are shown for the plasma scenario with a pulse repetition time of 1800 s and 500 s plasma burn phase.	
[2]	Initially 6 cryopumps will be installed. For steady-state operation, 4 additional cryopumps will be added to the 6 cryopumps in order to allow continuous operation in such a way that at any time, 6 cryopumps are pumping and 4 cryopumps are under four different stages of regeneration.	

I.3.1.4 Cryostat and Thermal Shields

The whole tokamak (vacuum vessel, magnet and associated structures) is located within a single-walled cryostat and within the cryostat there are thermal shields at 80K to prevent the cold portions (~ 4K) from receiving heat from the “hotter” parts (see Figure I.3.1-6). Bellows are used to connect the interspace duct wall extensions of the VV ports with the cryostat port to compensate for differential movements.

Main Outstanding Issues for the Cryostat and Thermal Shields

The only outstanding issue is the development of large elastomer bellows suitable for use inside the cryostat. The bellows development is the subject of ongoing R&D.

Issues related to the design of thermal shields include the manufacturing tolerances and application and environmental compatibility of silver coatings to large, non-flat panels. Based on industrial estimates for achievable manufacturing tolerances, space has been allocated for the thermal shields between the VV and the TF coils.

Application of Ag-plating to large panels was carried out for JET and Tore Supra. The long-term emissivity of Ag under neutron irradiation needs to be determined in future irradiation tests.

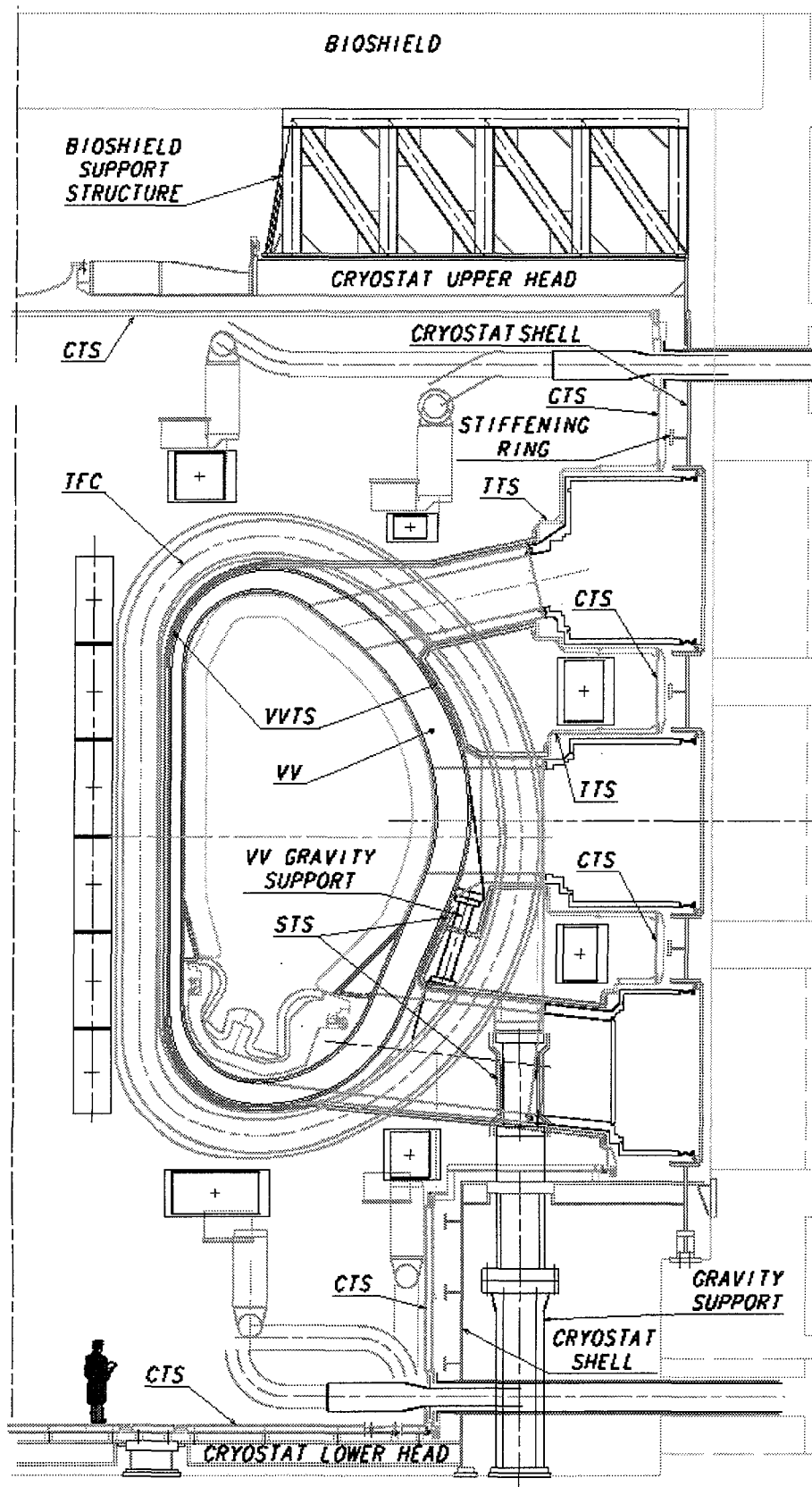


Figure I.3.1-6 Elevation View of Cryostat, Thermal Shields (cryostat (CTS), transition (TTS), vacuum vessel (VVTS) and support (STS)), and Gravity Supports

Assessment

The design and size of the cryostat are within industrial experience, e.g. for large nuclear safety containments. Provided the R&D results confirm the suitability of the intended use of bellows and Ag-plating, there is no reason to doubt that the cryostat and thermal shields can be procured and assembled as intended. In case the R&D results should be negative, alternative, back-up options are available.

I.3.1.5 Vacuum Vessel

The double-walled vacuum vessel is lined by modular removable components, including blanket modules composed of a separate first wall mounted on a shield block, divertor cassettes, and diagnostics sensors, as well as port plugs such as the limiter, heating antennae, and test blanket modules. All these removable components are mechanically attached to the VV wall. These vessel and internal components absorb most of the radiated heat from the plasma and protect the magnet coils from excessive nuclear radiation. This shielding is accomplished by a combination of steel and water, the latter providing the necessary removal of heat from absorbed neutrons. A tight fitting configuration of the VV aids the passive plasma vertical stability, and ferromagnetic material in the VV, localised under the TF coil, reduces the TF ripple. The overall arrangement of one of the 9 vacuum vessel sectors is shown in Figures I.3.1-7 and 8, and the overall parameters of the vacuum vessel are given in Table I.3.1-5.

Integrated functionally with the VV is the vacuum vessel pressure suppression system (VVPSS). This system minimizes the peak pressure inside the vacuum vessel during an in-vessel LOCA, by relieving the pressure (caused by the ingress of a water steam mixture from damaged water-cooled, in-vessel components) through rupture discs via pipework into a steam condenser tank.

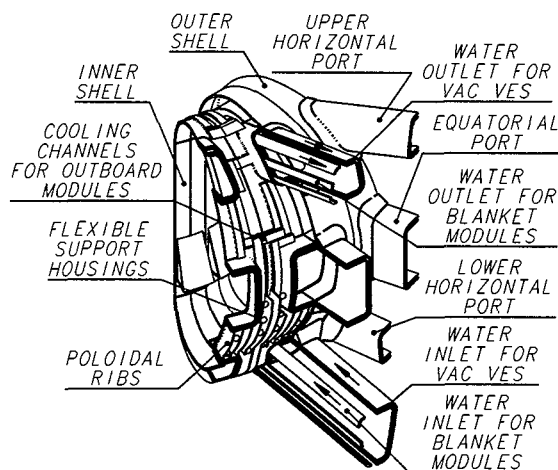


Figure I.3.1-7
Vacuum Vessel Overall Arrangement

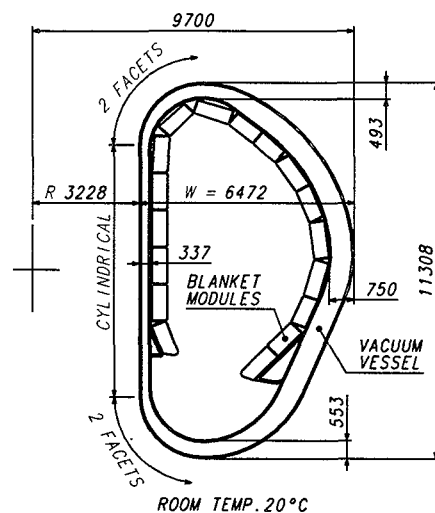


Figure I.3.1-8
Vacuum Vessel Cross-Section

Table I.3.1-5 Main VV Parameters

	Unit	ITER-FEAT
Size		
- Torus OD	m	19.4
- Torus Height	m	11.3
- Double Wall Thickness	m	0.34-0.75
- Toroidal Extent of Sector	°	40
- Number of Sectors		9
- Shell Thickness	mm	60
- Rib Thickness	mm	40
Structure		
- Inboard Straight Region		Cylindrical
- Inboard Top/Bottom (Facets/Sector)		2
- Outboard Region (Facets/Sector)		2
Resistance		
- Toroidal	$\mu\Omega$	8.8
- Poloidal	$\mu\Omega$	3.8
Surface Area / Volume		
- Interior Surface Area	m^2	943
- Interior Volume	m^3	1608
- Structural Volume (cooling channel)	m^3	642
Materials		
- Main Vessel		SS 316L(N)-IG
- Primary Shielding		SS 30467
- Ferromagnetic Insert Shielding		SS 430
Mass (without water)		
- Main Vessel (without shielding)	t	2395
- Shielding	t	2500
- Port Structures	t	1606
- Total	t	6500
Note: Parameters are for the VV with the integrated blanket water cooling channels.		

Main Outstanding Issues and Remaining Options for the Vacuum Vessel

To reduce the VV fabrication cost, forging, powder HIPing and/or casting is being investigated for the large number of housings in the VV for the blanket module support that have a relatively small and simple structure. The preliminary comparison of their fabrication costs with welded structures shows a cost benefit.

As discussed in I.3.1.6, the blanket cooling options have consequences for the design and manufacture of the vacuum vessel, and hence its cost.

Assessment

The manufacture of a full-scale sector of the 1998 ITER design gives a sound basis for the design of the present vessel.

I.3.1.6 Blanket

The initial blanket acts purely as a neutron shield and tritium breeding experiments are confined to the test blanket modules which can be inserted and withdrawn at radial equatorial ports. The shield blanket parameters are shown in Table I.3.1-6 and the blanket system, made up of modules, is shown in Figures I.3.1-9 and 10. The blanket module design consists of a

separate faceted first wall (FW) attached to a shielding block. This minimises radioactive waste and simplifies manufacture.

Table I.3.1-6 Shield Blanket Parameters¹

	Unit	ITER-FEAT
Total blanket thermal power	GW	~ 0.65
Heat flux on FW; nominal, max.	MW/m ²	0.2 , 0.5
Heat flux on limiter; nominal, max.	MW/m ²	~ 3 , ~ 8
Average neutron wall loading; nominal, max.	MW/m ²	0.57 , 0.78
Number of modules; Total, NB injector modules		429, 14
First wall surface area	m ²	682
Weight of modules	t	1813
Weight limit for module	t/mod	4.5
Typical blanket module dimension (Inboard equator)	mm	1415x 1095x450
Coolant inlet pressure during normal operation	MPa	3.0
Coolant temperature; inlet, outlet	°C	100 / 150
(1) Unless stated otherwise, values in this table are based on the nominal fusion power only.		

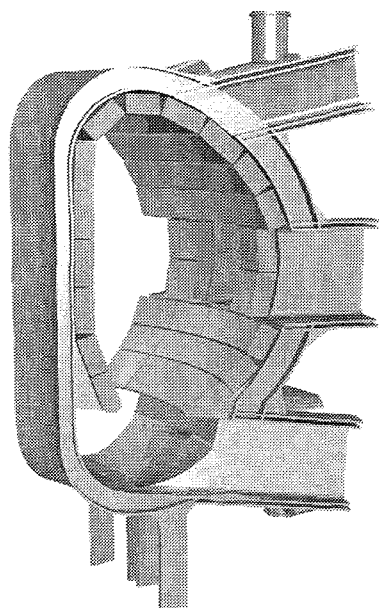


Figure I.3.1-9 Isometric view of blanket system

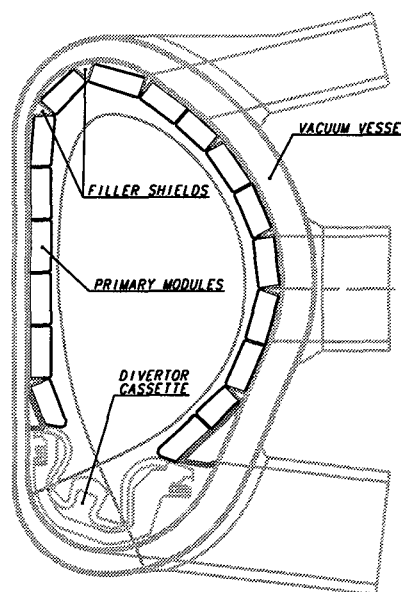


Figure I.3.1-10 Module poloidal segmentation

Main Outstanding Issues and Remaining Options for the Blanket

Two methods are being considered for FW attachment to the shield: a central mechanical attachment, which is bolted to a shield block at its rear side, or a system of bolts (accessed from the first wall) and small shear ribs, to support EM loads and to prevent sliding due to thermal expansion.

Two options are being considered for blanket cooling: one with cooling channels integrated inside the vessel structure between the two walls, the other with channels mounted on the vessel in vacuum. With the former, one concern is contamination (above acceptable levels) of the inside of the VV cooling loop by blanket cooling water. This is unlikely due to the thick plate, multipass welding used on the boundary between the two cooling channels. Continuous leak monitoring is proposed to provide an adequate indication of cracks in the structure. For small leaks, plasma operations could be still maintained with an addition of a water purification system to the VV primary heat transfer system (PHTS). With manifolds mounted on the vessel, fabrication costs will be reduced and the cross-contamination risk is not present. The coolant manifolds could be repaired after the remote removal of blanket modules. The exact layout of cooling pipes has to be optimised to avoid congestion in the port region.

Assessment

The R&D performed for the 1998 ITER blanket design gives a sound basis for the present design. All the blanket materials and joining techniques have been improved and characterised and fulfil all the requirements. Several small and medium scale primary FW mock-ups without Be armour have resisted thermal loads up to 7 MW/m^2 for 1000 cycles. High heat flux testing of limiter mock-ups with brazed Be armour have resisted up to 12 MW/m^2 for 4500 cycles. Large and full scale prototypes of the blanket modules have been successfully manufactured with robust joints and within the required tolerances. Assembly tests have demonstrated the basic feasibility of the blanket installation.

I.3.1.7 Divertor

The divertor exhausts the helium reaction product of the deuterium/tritium fusion reactions and limits the concentration of impurities (non-hydrogen isotopes) in the plasma. It accomplishes this by providing a region in which the magnetic field lines just outside the plasma boundary are “diverted” to meet a target plate at a small angle of incidence. Charged particles escaping from the confined plasma will flow to the target, but on the way will lose a large fraction of their energy by radiation and charge exchange with neutrals, thus limiting the power density on the target plate.

The divertor itself is made up of 54 cassettes. Figure I.3.1-11 is a sketch in a poloidal cross-section of the diverted magnetic field and the divertor showing some features of the construction of a cassette, in particular the targets which are the surfaces subjected to the heat load from the diverted particles (peak heat fluxes are less than 20 MW/m^2).

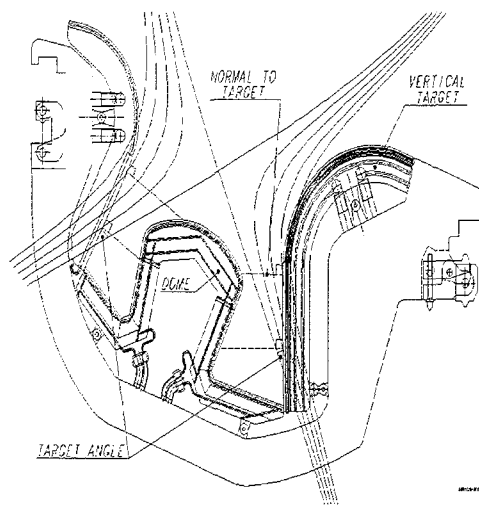


Figure I.3.1-11 Divertor Plasma Facing Components Arrangement

Main Outstanding Issues and Remaining Options for the Divertor

Much of the performance of the ITER-FEAT divertor has been extrapolated from slightly different machine parameters, and this needs verification to confirm the heat loads and performance.

The current design uses carbon at the vertical target strike points. Tungsten is being considered as a backup, and both materials have their advantages and disadvantages. The two options need continuous development so that the best judgement of the relative merits can be made when it comes to procurement. Carbon has the best behaviour to withstand large power density pulses (ELMs, disruptions), but gives rise to tritiated dust. Procedures for the removal of tritium codeposited with carbon and tritiated dust from various components by a number of schemes are under consideration and need further development because some require the provision of hot surfaces and high temperature baking.

The risk and consequences of cascade failure of flat tiles (one of the options) on the vertical target of the divertor are being considered by R&D, as well as the benefits in combination with hypervapotron cooling. The choice of tile curvature (flat or curved) will depend on the result.

Assessment

The development of carbon and tungsten armoured plasma facing components has advanced to a level where it meets the demanding requirements of the ITER-FEAT divertor for the average target heat load. The armour behaviour under large power density pulses could be a limiting factor. A successful R&D campaign has demonstrated that armoured components can routinely operate with heat loads of up to 20 MW/m^2 for carbon and $> 10 \text{ MW/m}^2$ for tungsten, with a promise of also reaching 20 MW/m^2 . A prototypical armoured vertical target compatible with ITER-FEAT divertor requirements has been built and successfully tested. Furthermore, successful operation in tokamaks, with the scrape-off-layer partially attached to the divertor targets, has demonstrated that the average heat flux to the divertor can be reduced to a value where the armour life-time is adequate. This is the basis for the confidence in the design.

I.3.1.8 Water Cooling System

The heat deposited in the vessel-internal components and the vessel is rejected to the environment via the tokamak cooling water system (TCWS) (which is designed to preclude releases of tritium and activated corrosion products to the environment), and the heat rejection system (HRS). The TCWS loops are also used to bake and hence clean the plasma-facing surfaces inside the vessel by releasing impurities. A schematic flow diagram of the water cooling system is shown in Figure I.3.1-12. It shows the TCWS (the primary system) and the HRS (the secondary system) as well as the associated component cooling water system (CCWS), the chilled water system (CHWS) and some auxiliary systems; chemical and volume control systems (CVCs).

In the worst situation, where all active cooling to in-vessel components is lost because of pipe breaks or power failure, natural convection in the vessel is able to exhaust their decay heat and keep components well at a temperature at which there is no significant chemical reaction between steam (air) and Be-dust.

Main Outstanding Issues and Remaining Options for the Water Cooling System

In the event of a guillotine break (in the TCWS vault) of a main pipe of the VV, blanket or divertor loops during vessel baking at 240°C, the TCWS vault would have to accommodate an overpressure of up to ~ 0.37 MPa under a totally closed confinement strategy. As this would lead to unreasonably complex and expensive reinforcement of building slabs etc. increasing the expansion volume is being considered for this highly unlikely event. However, confinement in the vault is retained for a pipe break at a normal operation temperature (150°C).

The normal operation of active components of the TCWS such as the main pumps, small pumps, and motor-operated valves under the operational magnetic field, must be guaranteed. The allowable strength of the magnetic field and the required shielding for each component is under study now.

The occupational radiation exposure, based on the dose rate map, needs to be evaluated to confirm maintenance procedures for the components requiring planned or unplanned access.

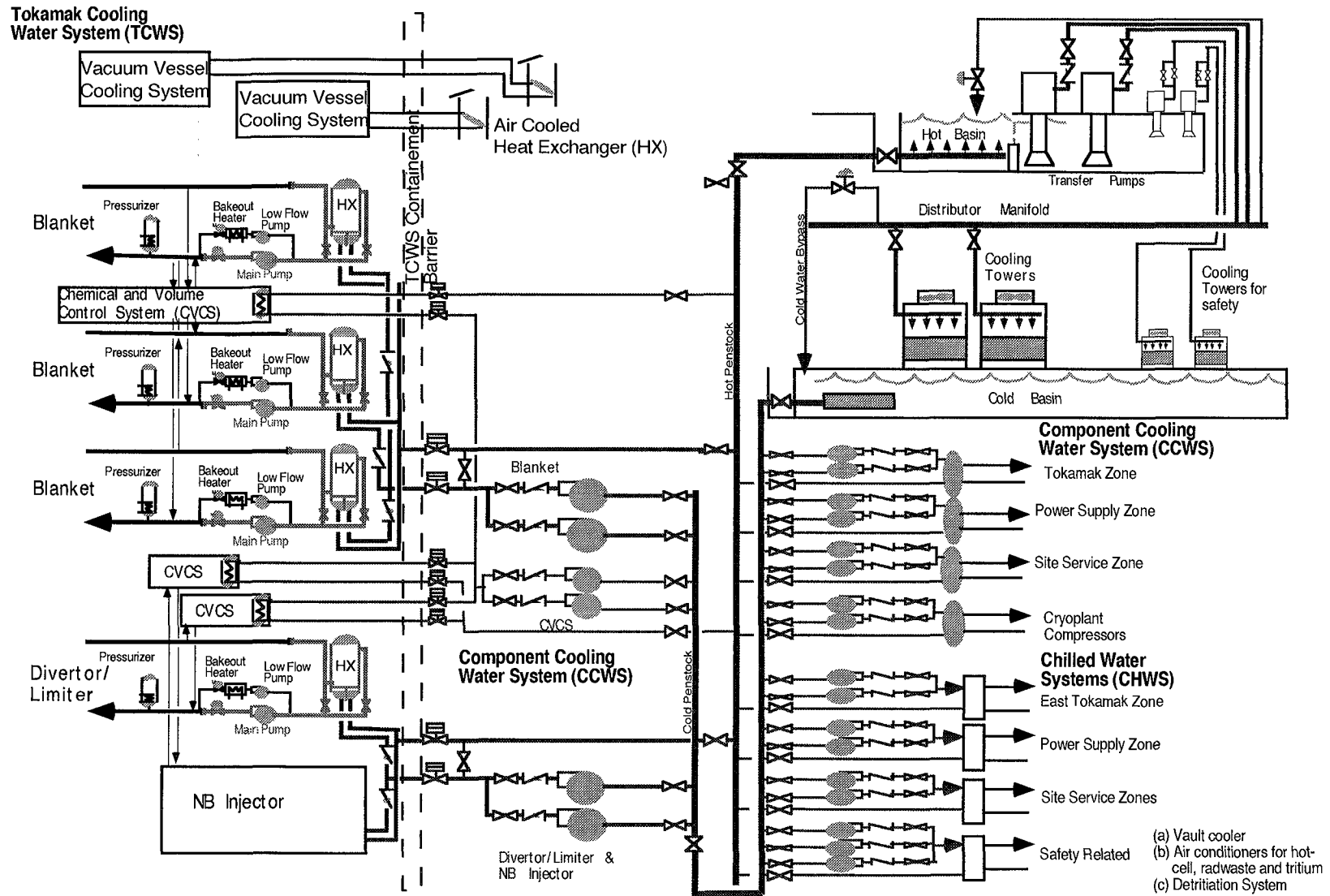
The option of using sea/fresh water instead of forced flow cooling towers as the ultimate heat sink is being considered for a site-specific design. It may be that, in this case, an intermediate cooling water system is required.

The VV cooling system design has not yet been finalized and its design parameters are quite preliminary. Even its power capacity has to be thoroughly analysed. It is expected that heat transfer coefficients in the range of ~ 500 Wm⁻²K⁻¹ can be achieved in the VV using natural circulation. This possibility is being verified.

Assessment

The capacity of the main components in the water cooling system is within industrial experience (or industrial proven technology), therefore no problematic issues on the component design and manufacturing are expected.

Figure I.3.1-12 Schematic Flow Diagram of the Water Cooling System



N 26 GR 386 99-11-19 W 0.2

I.3.1.9 Fuel Cycle

Plasma density control is provided by the fuelling and pumping system. The tokamak fuelling system is capable of gas puffing, and pellet injection from the high field side, into the plasma. These gases are subsequently removed from the plasma together with the helium ash using the torus cryopumps. These pumps are sequentially exhausted to the tritium plant (Figure I.3.1-13) where impurities are removed from the hydrogen stream and the various isotopes of hydrogen are separated and stored. Tritiated impurities are processed to lower their tritium content sufficiently to allow their release. The tritium plant also detritiates water, ventilation air and process fluids and solids.

Main Outstanding Issues and Remaining Options for the Fuel Cycle

Pellet launch is from the high field side of the tokamak to maximise pellet penetration for a given pellet speed, and fuelling efficiency. However, the pellet speeds required are somewhat beyond those currently achieved without pellet disintegration. As a result, R&D is needed to improve the design and geometry of the flight tube.

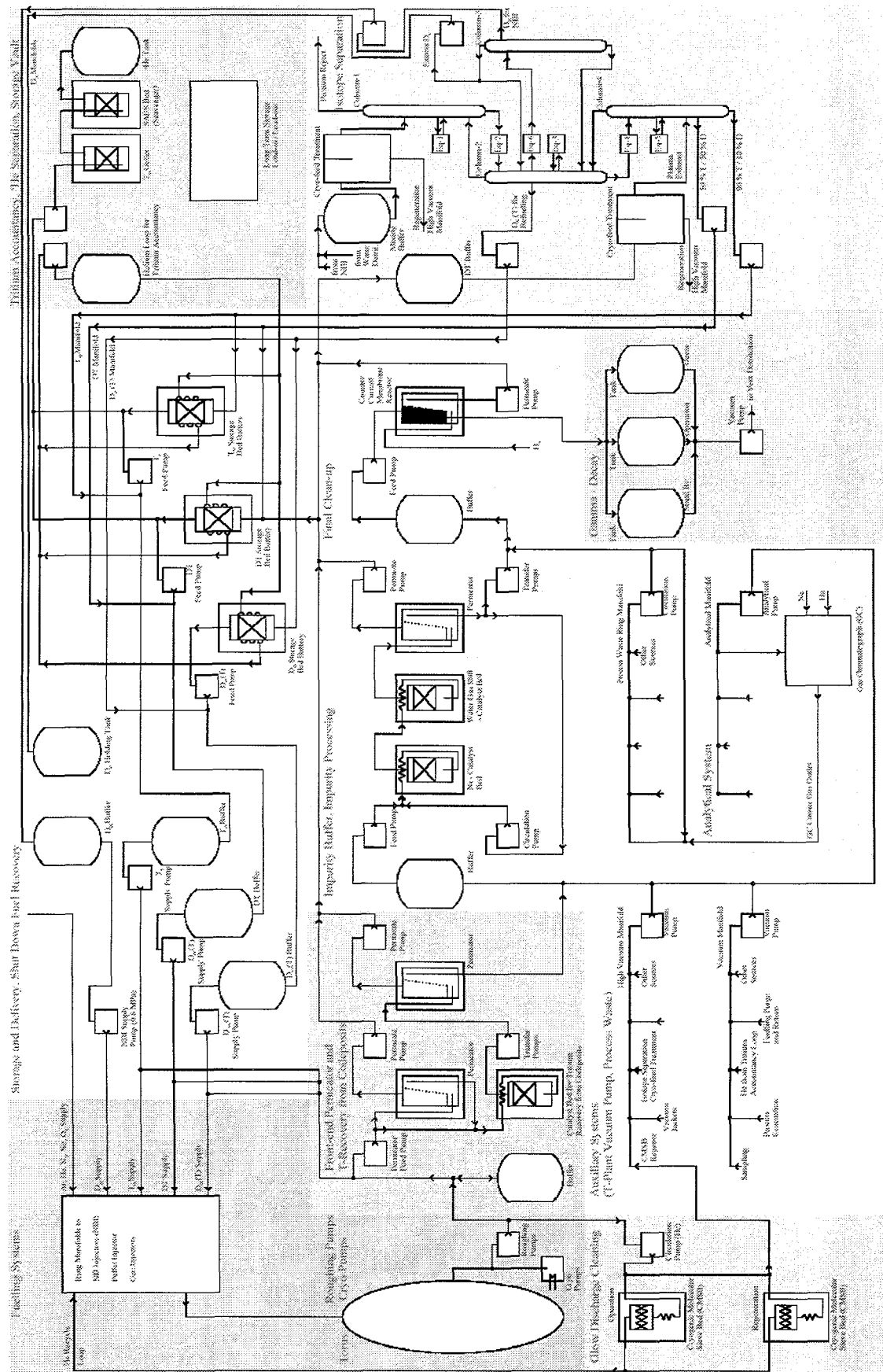
Regarding the tritium plant, nearly all the separation systems have to be present by the start of DD operation since tritium will be generated during this phase of operation. However, systems for water detritiation can be deferred to some extent until full DT operation. The degree of this deferral needs further quantification.

Assessment

Many subsystems in the ITER tritium plant are based on proven, industrial processes at relevant scale. In some instances, the dynamic nature of ITER operation requires additional confirmation and this has been and is being targeted by R&D, e.g. of the isotope separation system and hydrogen storage beds.

The exhaust processing technology is being developed in ongoing R&D. The required detritiation factors have been routinely exceeded. There is no doubt therefore, that given the expected outcome of the R&D, the subsystems can be designed, procured and operated as required.

Following positive R&D results at the component level, a 70% full-scale model of the main torus cryopump is under construction.



N 32 GR 95 99-11-18 W/0.1

Figure I.3.1-13 Fuel Cycle Overall Diagram

1.3.1.10 Heating and Current Drive

The plasma heating systems, neutral beams (NB), electron cyclotron (EC), ion cyclotron (IC), and lower hybrid (LH), must also have the ability to drive current in the plasma (current drive) to extend the tokamak plasma duration beyond the limitations imposed by the inductive current drive provided by the central solenoid. This lengthening of the tokamak pulse is an attempt to reach “steady-state” conditions where the current drive would be entirely non-inductive. The heating and current drive (H&CD) systems under consideration for ITER-FEAT are shown in Table I.3.1-7 and Figure I.3.1-14.

Table I.3.1-7 Heating and Current Drive Systems

	NB	EC (170 GHz)	IC (~ 50 MHz)	LH (5 GHz)
Power (MW) injected per unit equatorial port	16.5	20	20	20
Number of units for the first phase	2	1	1	0
Total power (MW) for the first phase	33	20	20	0
1) Each standard equatorial port can provide 20 MW of RF (EC or IC or LH) 2) The 20 MW of EC module power will be used either i) in 2 upper ports to control neoclassical tearing modes at the $q = 3/2$ and $q = 2$ magnetic surfaces, or ii) in one equatorial port for H&CD mainly in the plasma centre.				

Main Outstanding Issues and Remaining Options for Heating and Current Drive Systems

For the NB, the ceramic insulators (1.8 m ID) used for the bushing between the pressurized high voltage line and the primary vacuum are beyond the common industrial practice. R&D on the fabrication of ITER-relevant prototypes using porcelain insulators with high alumina content is foreseen.

The NB duct shielding needs a careful optimization in order to limit strictly the dose rate two weeks after shutdown inside the cryostat.

For the EC H&CD system, beam injection at different toroidal and poloidal angles is needed to satisfy all heating and current drive functions and to provide neoclassical tearing mode (NTM) stabilization of the plasma. This, however, would require two dimensional (2D) RF beam steering and a large opening at the front end of the EC launcher, which conflicts with the need for efficient neutron shielding. It is planned instead to mount a launcher with toroidal steering in the equatorial port, and one with poloidal steering in the upper port. Due to space limitations, steering mirrors may have to be shared between waveguides. A key issue is the design of the steerable mirror pivot. Remote steering of the beams, if feasible in actual conditions, would provide the most desirable solution, but it requires R&D confirmation.

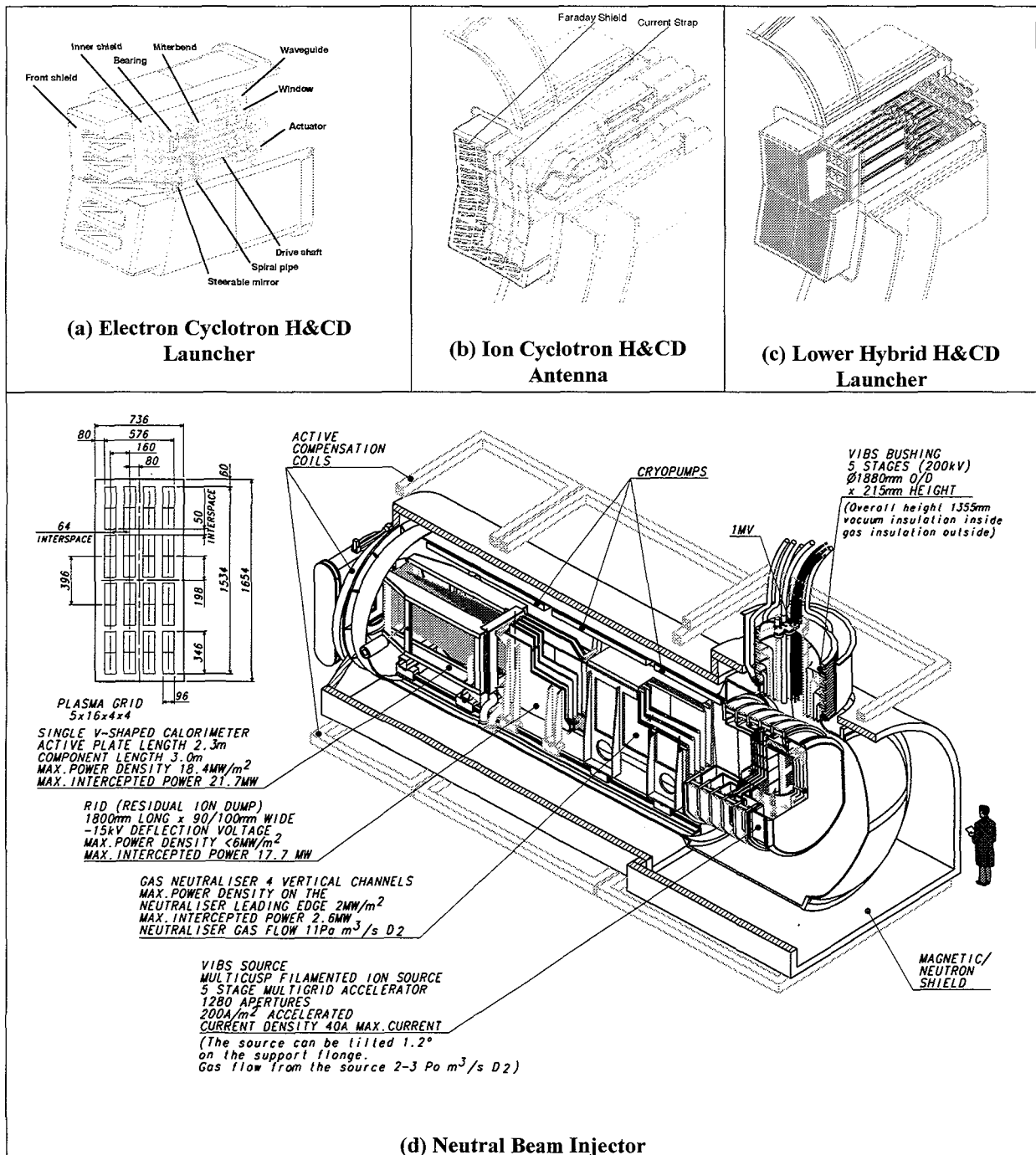


Figure I.3.1-14 Plasma Heating Systems

The IC H&CD system involves several new features in the design of the antenna, in order to increase its array power handling: parallel tuning, balanced feed, strip-line transmission lines are used in order to minimise the space requirements, to decrease the operating voltage and to provide a large radiated power surface density. The estimated performance of the new design concept should be demonstrated by experiment on a module, testing the key features at full scale on an existing tokamak.

Several concepts used in the LH design launcher (the PAM launching structure, hyperguides and mode converters) and the main transmission line have been submitted to only laboratory tests at JET and Tore Supra. A full-scale test of the key features of these components should

be performed on an existing tokamak to demonstrate its overall efficiency and its capability of operation in long pulse conditions.

Assessment

For NB H&CD, the progress in the R&D (on the ion source and on the accelerators) which has been performed so far, gives confidence in the possibility of achieving the accelerated current density (200 A/m^2) at 1 MV, as assumed in the design.

The mechanical design of the beam line components is conventional, but beam lines should not fail during the entire life of ITER (large number of thermal cycles). The R&D of a mock-up of the NB calorimeter will give the necessary data to prove the fatigue limits.

With regard to the NB system power supplies, in comparison with those for the RF systems which are essentially state of the art (apart from the gyrotron tubes), the HV components are without precedent. The R&D performed so far has been very useful, but further progress is essential for design validation.

For RF systems in general, if a reasonable R&D and industrial development is maintained in the above-mentioned areas, during the ITER-FEAT construction phase, a combination of RF systems appears to be capable of providing all requested services with the required availability.

I.3.1.11 Diagnostics

In order to understand the behaviour of the plasma in ITER-FEAT, a large number of special devices (diagnostics) will be applied to the tokamak to measure various properties of the confined plasma, the confining magnetic field and the fusion reaction products. Some of these diagnostics are not only required to evaluate the experiments but are required for machine protection (e.g. to avoid excessive heat loads on vessel-internal surfaces and the consequent damage), and for plasma control (e.g. magnetic field measurements which are required for the control of the plasma shape and position by the PF coils). A preliminary arrangement of diagnostics around the machine in the VV ports at the upper and equatorial levels, is shown in Figure I.3.1-15.

Main Outstanding Issues and Remaining Options for Diagnostics

For magnetic diagnostics, the lifetime of the in-vessel coils and loops are the important issues. The results of the supporting R&D on radiation effects indicate that the necessary lifetime can be achieved. A particularly difficult area is repair and maintenance of the in-vessel components and this is a topic of current activities. Recent tests with a prototype coil and integrator have shown a small radiation induced emf (RIEMF) which would lead to an unacceptable drift during a long pulse ($> 1,000 \text{ s}$). Further tests are planned.

The ability of the neutron cameras to provide the total fusion power and the alpha particle source profile is directly linked to the available access. A wide angle of view is desirable in both the radial and vertical directions. This is difficult to achieve in the vertical direction. A view through the intercoil structure for the vertical camera is being considered but the feasibility has yet to be established.

The optical/infrared (IR) systems view the plasma with a mirror, and a critical issue is the lifetime of this component. A solution for the mirrors is believed to exist for those systems which operate in the visible and IR regions. However, for diagnostics which require a relatively large solid angle of observation, for example, active CXRS (charge exchange recombination spectroscopy) and MSE (motional Stark effect), further work is required. Some systems require the installations of retroreflectors in the vacuum vessel and this is a difficult design issue.

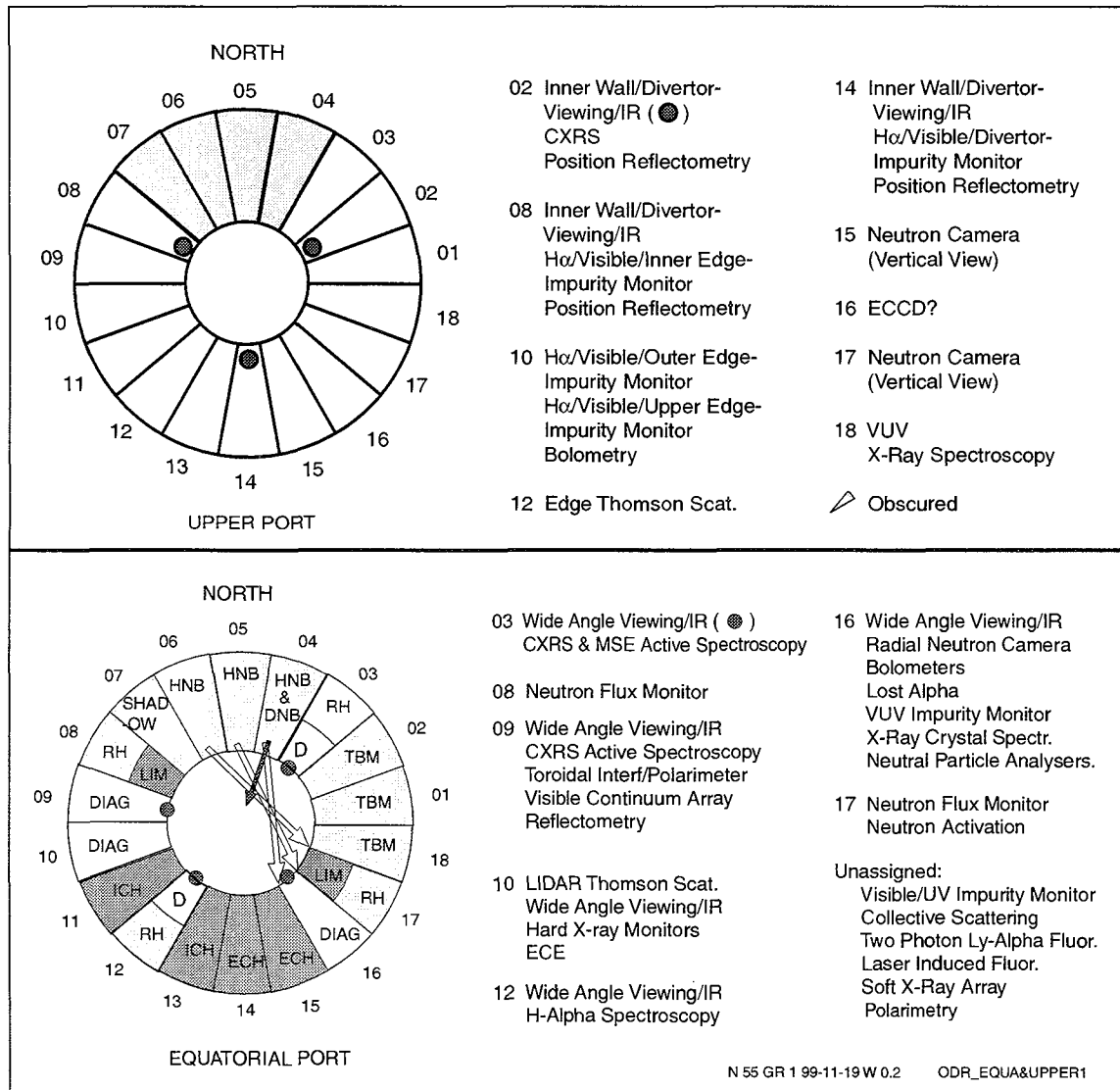


Figure I.3.1-15 Possible Diagnostic Port Allocation

Assessment

Most of the measurements required for the machine protection and basic plasma control can be made using established techniques. It is believed that the issues involved with the technical implementation can be resolved by careful design. In a few cases, however, novel approaches are required. Because of the intense gamma background, the conventional technique for measuring runaway electrons (tangential hard X-ray detection) cannot be applied. A new method, in which the synchrotron emission from the confined runaways is

measured in the infrared, is under development and implementation on ITER appears feasible. Measurement of the surface temperature of the divertor plates using conventional imaging systems is difficult to implement in the restricted divertor space. A novel technique in which the radiation from different locations is multiplexed into one line of sight with a grating and then separated by spectral analysis is under development. For long pulses ($> 1,000$ s), problems may arise with the measurement of plasma shape and position by magnetics particularly due to the small, radiation-induced electromotive force. R&D is in progress to improve the understanding of this phenomenon. A back-up system in which the plasma position and shape are measured by reflectometry with multiple poloidal sightlines is under design and could be implemented if necessary.

For sustained operation in high confinement modes, for example reverse shear, it is anticipated that the profiles of many parameters will have to be brought under active control (I.2.7). Measurements of most of the required profiles can be made but it is not yet clear whether the accuracies and resolutions that can be achieved will be sufficient. A particular difficulty exists with the q profile where there are implementation difficulties with both of the established measurement techniques (MSE and polarimetry). Operation in these modes, and the development of the required measurement techniques and control methods, are active areas of current research.

The goals of the supporting diagnostic R&D programme are driven by the required performance and by the environment of the diagnostic components. These have not changed significantly in the evolution of the design of ITER and so most of the results of the diagnostic R&D work obtained to date are directly applicable to the ITER-FEAT.

I.3.1.12 Buildings and Services

The above systems are housed within buildings and structures along with plant services. Figure I.3.1-16 shows the ITER-FEAT site layout. Table I.3.1-8 lists the buildings and their footprints, and Table I.3.1-9 lists other structures and areas which are required. Considerable effort has been made to make the best use of building space while providing an optimised layout for the required performance of the plant at a minimum cost. The tokamak and its closely associated systems are located mainly in the lower areas of the buildings as shown in Figures I.3.1-17 and 18.

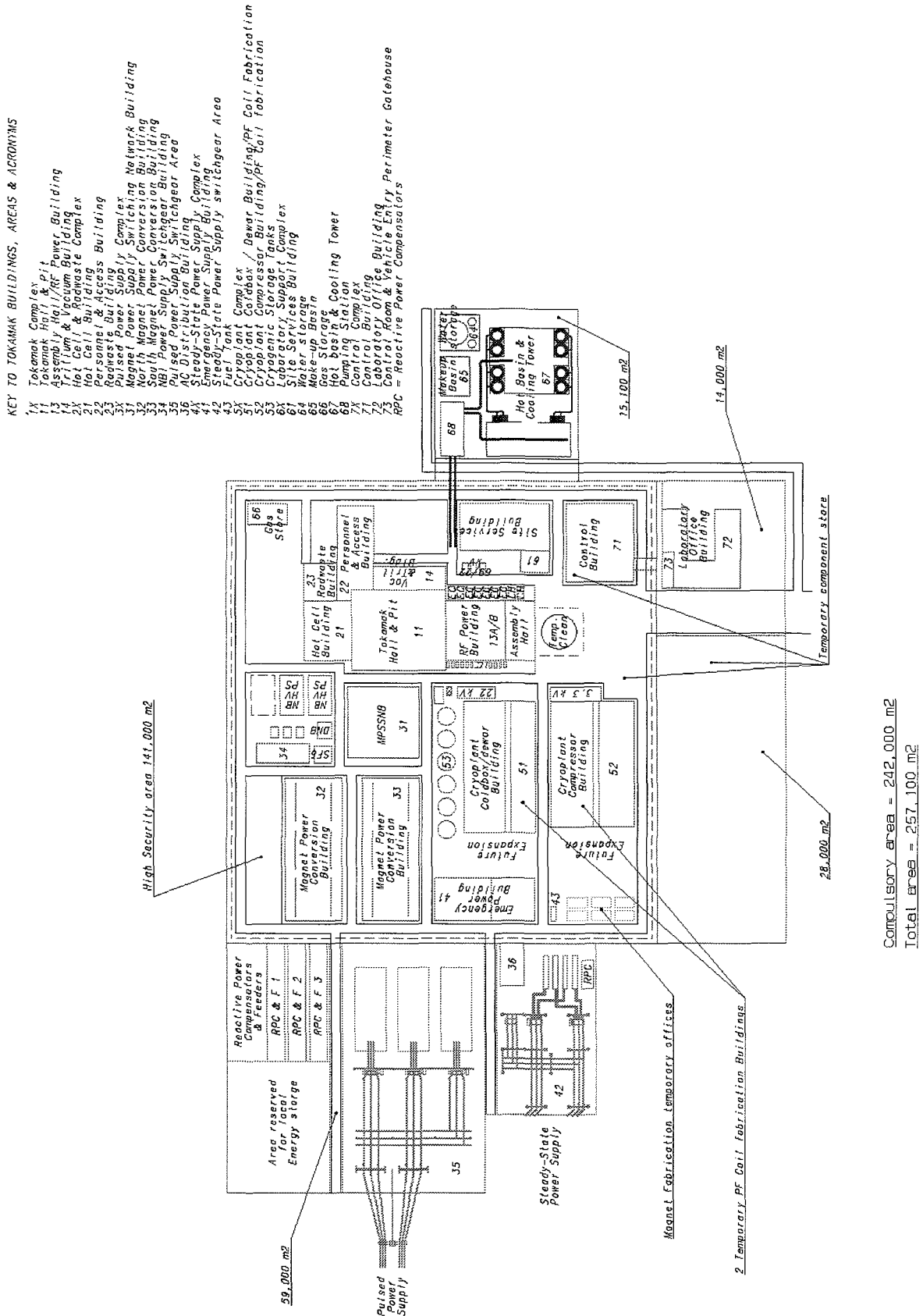


Figure I.3.1-16

Site Layout

Table I.3.1-8 Buildings

Key #	Buildings	Footprint m ²
11	Tokamak Hall	5,482
13	Assembly Hall RF Heating Area in Assembly Hall (2,550 m ²)	3,825
14	Tritium Building	1,210
21	Hot Cell Building	2,040
22	Personnel and Access Control Structure	2,400
23	Radwaste Building	900
31	Magnet Power Network/Switchgear Building	3,600
32	Magnet Power Conversion Building – North	3,600
33	Magnet Power Conversion Building – South	3,600
34	NB Injector Power Conversion Building	720
36	Reactive Power Compensation Building	720
41	Emergency Power Supply Building	3,024
51	Cryopant Cold Box/Dewar Building	6,600
52	Cryopant Compressor Building	7,350
61	Site Services Building	3,432
71	Control Building	3,762
72	Laboratory Office Building	3,367
73	Perimeter Guard/Gatehouse House	300
	Buildings Total	55,932

Table I.3.1-9 Other Structures and Areas

Key #	Other Structures & Areas	Footprint m ²
34	NB Power Supply Area	5,130
35	Pulsed Power Switchyard, Local Energy Storage area, and Reactive Power Compensators and Feeders	42,200
42	Steady-State Switchyard and Switchgear area	11,952
43	Diesel Fuel Storage Tanks	48
53	Cryo-Gas Storage-1	1,060
64	Water Storage	990
65	Makeup Basin	825
66	Gas Storage-2	594
67	Hot Basin & Cooling Tower	8,774
68	Pumping Yard	900
	Sub-Total	72,473
	Outdoor Storage/Expansion Areas	25,050
	Parking Areas	31,410
	Roadways	34,684
	Area Total	91,144
	Building Totals (from Table I.3.1-8)	55,932
	Grand Total	219,549

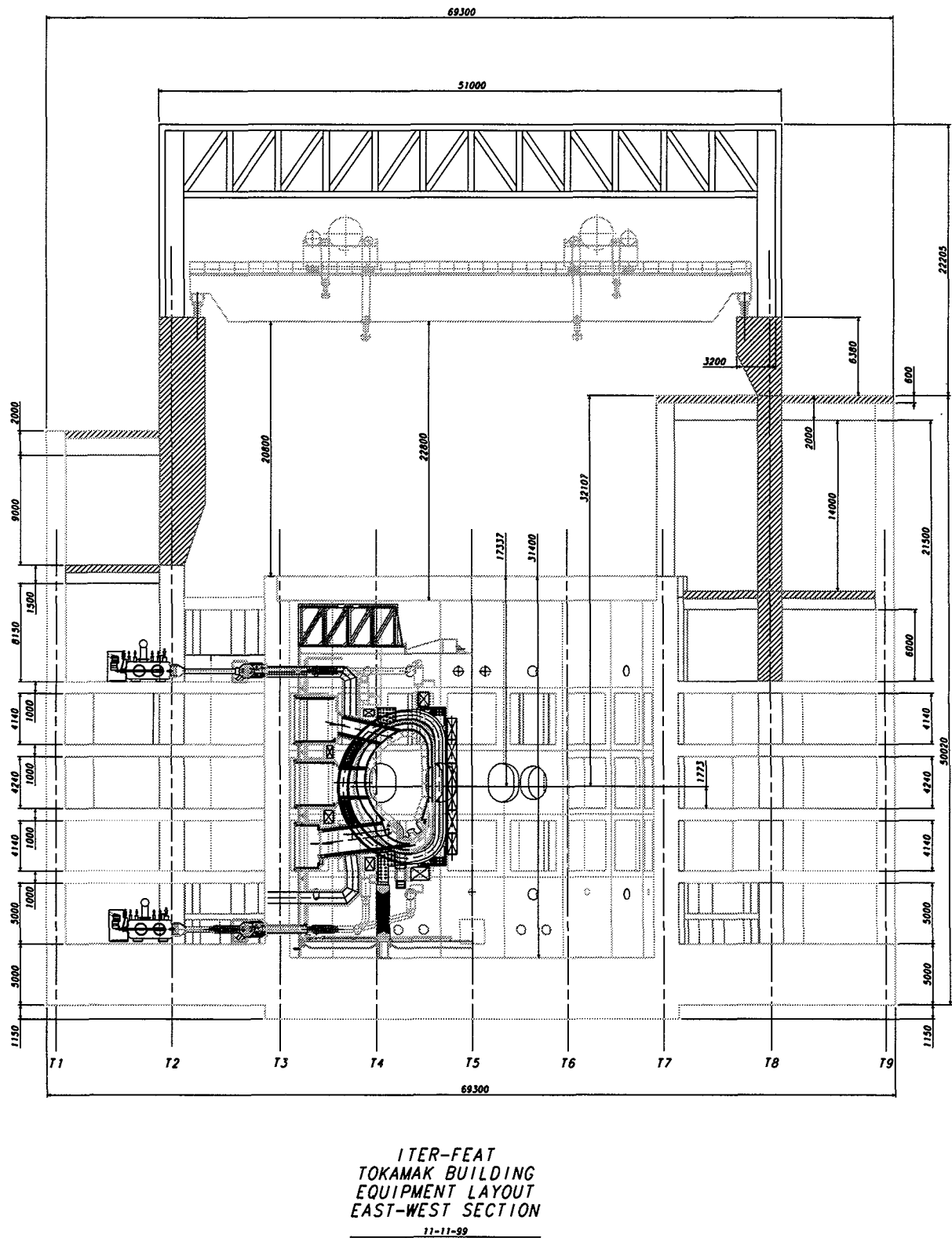


Figure I.3.1-17 Tokamak building east-west section

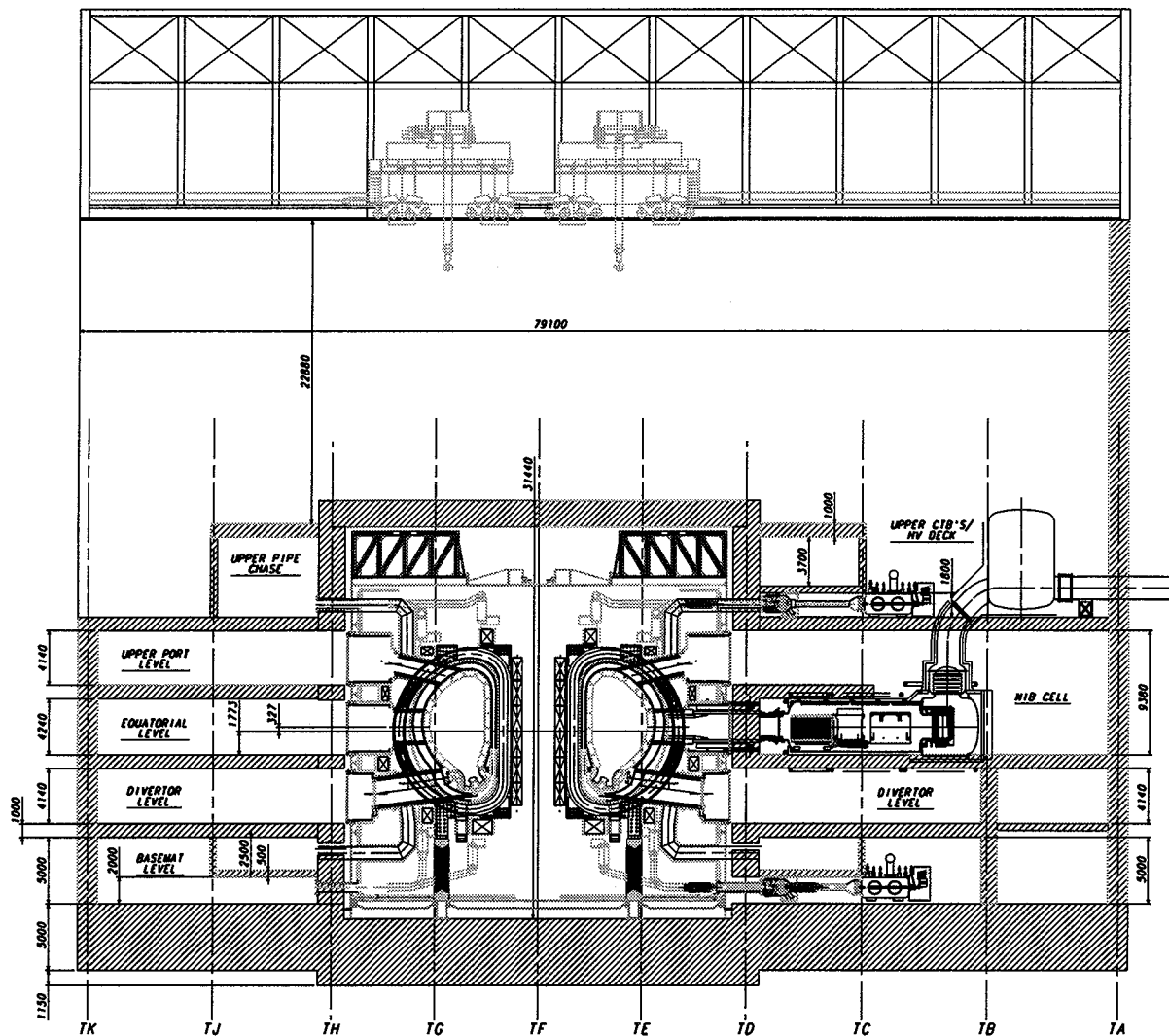


Figure I.3.1-18 Tokamak building north-south section

Main Outstanding Issues in Buildings, Plant Services and Plant Layout

Current information concerning the NB cell power supplies and the bioshield roof does not allow for the "open plan" system above the pit to be all at the same elevation, which would be most convenient. However, attaining this feature is currently under study.

There is not much space available within the tokamak building for the routing of services and essential feeds to the magnet, such as waveguides, cryolines, vacuum lines, power and signal lines, HVAC ducts, cooling and chilled water lines, diagnostic lines, etc. This space limitation is mainly in, but not restricted to, the vertical direction dictated by the VV port orientation. Layout studies are being carried out to ensure that there is adequate space available.

The hot cell building is now planned with a buffer zone of dry air to minimise the processing requirements for tritiated moisture. This design feature needs further exploration.

The provisional allocation of vessel ports for diagnostics makes it logical to study the possibility of providing a dedicated diagnostic hall on the west side of the tokamak building

for the installation of diagnostic systems. This will permit operation of diagnostic systems without long and complicated transmission lines.

Assessment

Although the scale of the buildings and the components is towards the upper end of conventional building and construction experience, there is nothing about the buildings or structures that is outside the realm of current engineering and industrial practice. There are bigger structures, heavier equipment placed, and tighter tolerances used, but not so many all in a single project. Hence, it is an engineering challenge, but well within today's engineering and construction capabilities.

I.3.1.13 Tokamak Maintenance

Because of the production of neutrons in plasmas of deuterium, and of deuterium and tritium, systems near the plasma will become radioactive and will require remote maintenance, with special remote handling equipment. The equipment involves an in-vessel transporter system for the removal and reinstallation of blanket modules (Figure I.3.1-19), multifunction manipulators for divertor cassette removal (Figure I.3.1-20), and specialised manipulators to handle vacuum vessel port plugs. Special casks, which dock horizontally to the access ports of the vacuum vessel, are designed to house such equipment and to transport radioactive items from the tokamak to the hot cell where refurbishment or waste disposal operations can be carried out. Docking of these casks to the vessel and the hot cell flanges is tight, therefore the spreading of contamination is avoided. Hands-on assisted maintenance is used wherever justifiable.

Main Outstanding Issues and Remaining Options for Tokamak Maintenance

For the divertor, the concept of "in-line" maintenance of the plasma-facing components is planned, for which no spare set of divertor cassettes is required. This provides considerable savings. The logistics of the consequent refurbishment is being evaluated.

The design considers the possibility of failures in the pulsed PF coils. This involves providing a larger degree of redundancy in the most severely trapped PF coils near the mid-plane, and providing a moderate redundancy and the possibility of rewinding in situ or locally for the PF coils installed below the vacuum vessel. Though apparently feasible, this aspect requires further consideration.

The CS modules can be removed and repaired or replaced without a major dismantling operation. A fault on a TF coil will, on the contrary, lead to a major disturbance.

Port handling and in-cryostat repair activities are being addressed. The latter still require iteration with the component and, in particular, the shielding design in detail. All in-cryostat equipment is supposed not to require remote maintenance. Human access for repair is contemplated.

Remote replacement of the NB ion sources is a major, complex operation. Studies are therefore underway to explore the possibility of performing RH Class 1 and 2 operations on the NB system without removing the ion source.

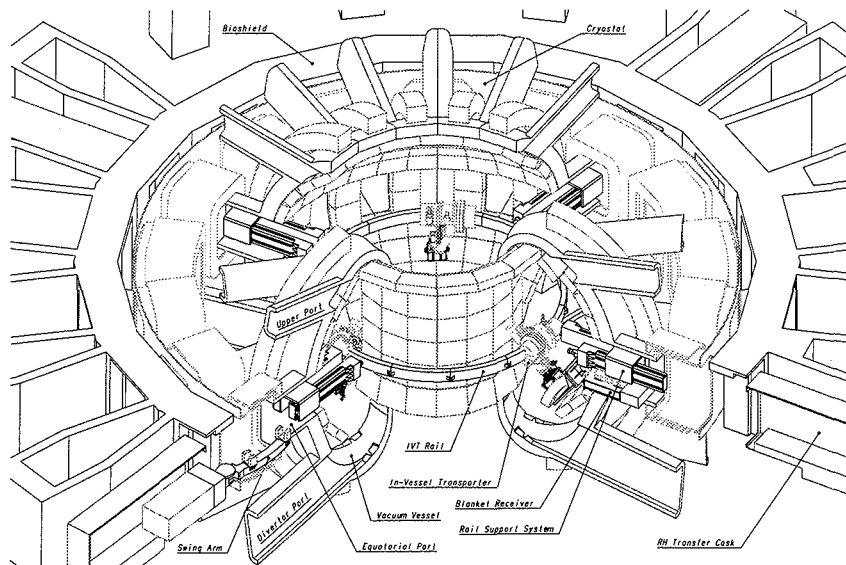


Figure I.3.1-19 In-Vessel Transporter (Rail Mounted Vehicle system)

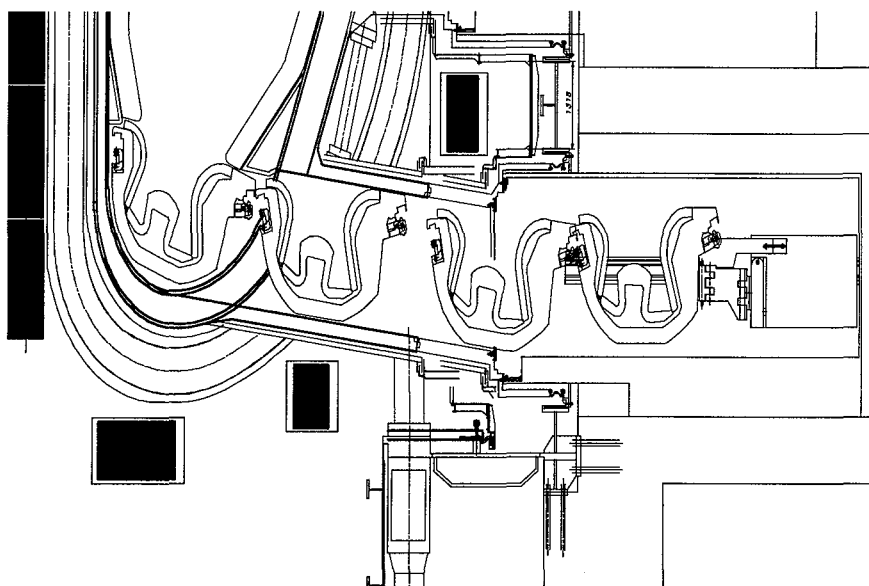


Figure I.3.1-20 Divertor RH port – Cassette Handling

Assessment

A remote handling strategy for ITER has been confirmed by a comprehensive design and R&D programme. Initiated about four years ago, the programme has successfully demonstrated that key maintenance operations like blanket and divertor replacement can be achieved using common, remote handling technology. Several crucial issues like vacuum vessel remote cutting and re-welding, viewing, materials and components radiation hardness have been addressed and demonstrated. The above strategy is directly applicable to ITER-FEAT.

Some maintenance-related items still need to be addressed. In particular, the possibility of adopting a compact hot cell design based on the ability to refurbish divertor cassettes during the maintenance period is being assessed.

Overall, the development programme results so far obtained indicate that the remote maintenance strategy for ITER-FEAT is sound and sufficiently mature to support the ITER programme.

I.3.1.14 Tokamak Assembly

An outline procedure has been developed for the tokamak assembly, as the basis for determining the assembly schedule, manpower and tooling requirements, and the associated cost. A summary of this procedure is shown in Figure I.3.1-21.

The overall sequence is divided into the following six main activities:

- lower cryostat activities: this section covers activities from the initial assembly in this area up to the placement of the first TF/VV/VVTS sector;
- TF/VV/VVTS sub-assembly: each sector includes a pair of TF coils, a 40° segment of the VV and three VVTS parts, an inboard 40° sector and two outboard, opposite hand 20° sectors.
- integrated TF/VV/VVTS assembly: the sequenced assembly of the TF/VV/VVTS sub-assemblies in the cryostat;
- establish the magnetic axis: survey procedures to establish the tokamak magnetic datum;
- ex-vessel activities: these activities occur in parallel with the in-vessel assembly procedures;
- in-vessel activities: further activities up to the preparation for commissioning.

Main Outstanding Issues and Remaining Options for Tokamak Assembly

The machine support system is flexible in the radial direction, thereby allowing relative thermal displacement during a cool-down and warm-up of the cold structures, but extremely stiff in all other directions. One set of 18 flexible supports connects the TF coils to the basemat, and the second set connects the VV to the TF coils.

The high toroidal stiffness of the TF to VV supports makes them unsuitable for use during assembly, prior to the completion of the VV field joint welds, because the weld shrinkage (~ 12 mm, toroidally, per field joint) would subject them to large stresses. Thus, the VV will have to be supported via tooling until the final field joints have been welded, and the VV has been closed toroidally. Following toroidal closure of the VV, with the tooling supporting the weight of the VV, the individual flexible supports may be customised (e.g. shimmed), to guarantee an acceptable sharing of load, prior to being attached to the corresponding TF coil. At this stage the tooling may be used to adjust the position of the completed VV with respect to the magnetic datum, if required.

The TF to VV supports are located in an area which is difficult to access. In fact, access for fastening or adjustment is feasible only through a vertical gap between the intermediate outer intercoil structures (OISs). This gap is closed by an OIS splice plate, which will be welded

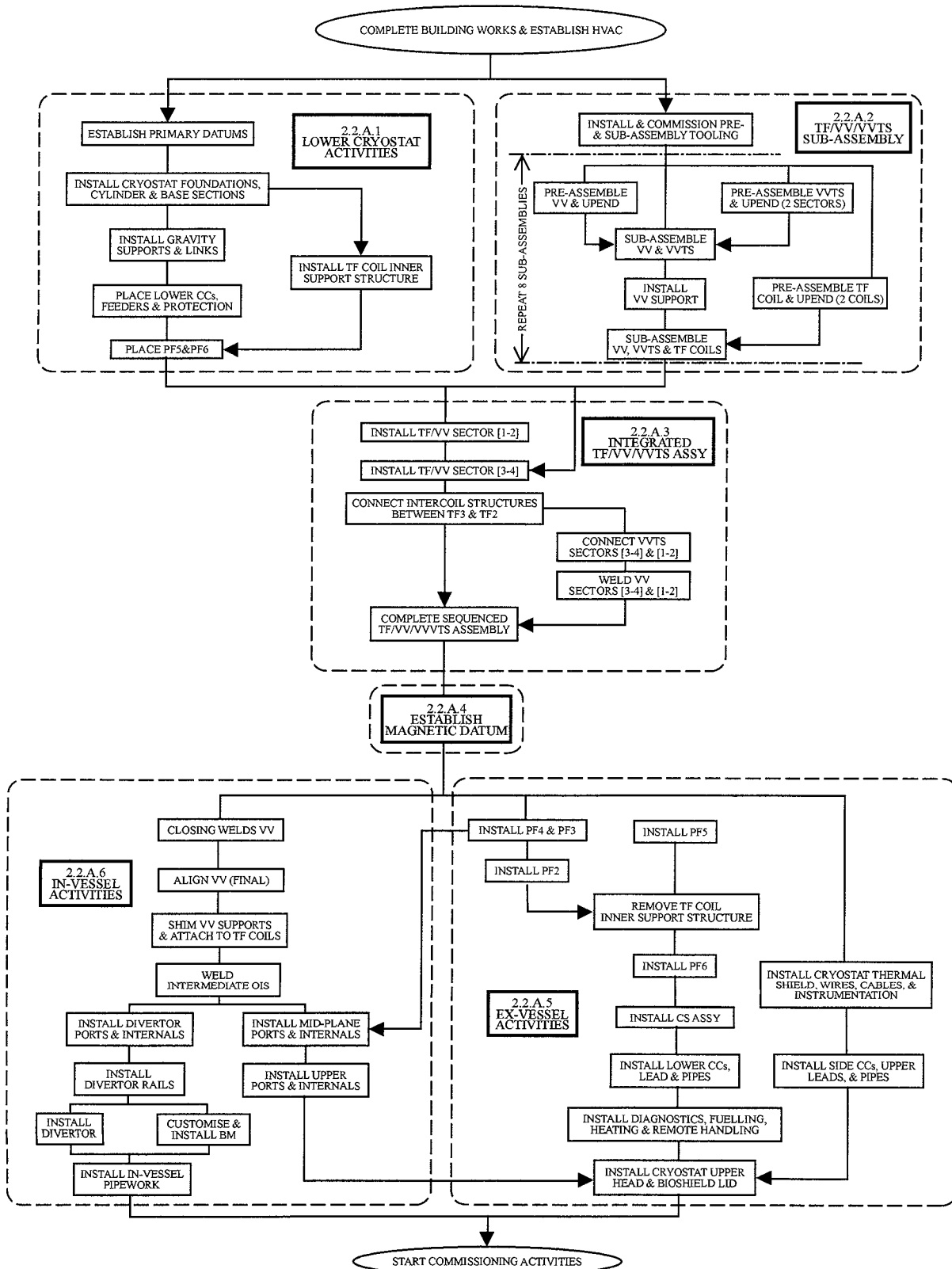


Figure I.3.1-21 Tokamak Assembly Sequence

following completion of the VV assembly and installation of the TF to VV supports. The ability to assemble the machine this way therefore needs further study.

Assessment

While a high level assembly plan has been established, details of many assembly activities remain to be established, e.g. assembly of the TF to VV supports. This will also affect the design of the assembly tooling.

A very accurate fit is required for the mating surfaces between adjacent TF coils. The results of current structural analyses indicate that, in order to maintain acceptable operating stresses, it will be necessary to guarantee near complete contact over the full length of the inboard legs of the coils. This may necessitate lengthy and precise matching operations, e.g. shimming, and a significant impact on the assembly schedule should be anticipated, if the operations are to be carried out on the ITER site. Accordingly, it has been proposed to have pairs of coils pre-assembled and, if required, pre-shimmed at the factory. Concepts and procedures for in situ surveying and shimming have yet to be developed.

I.3.2 Plant Control & Operation

I.3.2.1 Plant Control System

The integrated control and protection of the entire ITER plant will be achieved by the plant and plasma control system, and an independent interlock system.

The operation of the ITER plant is characterised by major plant states, in which many of the plant subsystems wait for commands before changing to another state, or some subsystems are undergoing maintenance or testing, or are in normal operation. The plant control system controls these states and the transitions between them which occur through a sequence of steps.

Five plant operation states have been defined:

- **Construction and Long-Term Maintenance State (LTM)**
Most of the tokamak subsystems which require maintenance will be shut down. This state applies to the construction phase and to any major modifications of the ITER machine after initial construction, as well as to long-term maintenance (> 30 days). Typical activities are large in-vessel and ex-vessel component replacement and maintenance.
- **Short-Term Maintenance State (STM)**
This state is for maintenance activities which typically last for 1 to 30 days. Relatively long time periods between plasma operation may require that the plant be placed in this state with reduced or without toroidal field coil current. Decay heat removal will take place as appropriate. In this state, component maintenance and replacement will be carried out mainly outside of the vessel which remains under high vacuum conditions.

- **Test and Conditioning State (TCS)**
Wall conditioning operations such as baking, glow discharge cleaning and EC discharge cleaning, with or without baking, are major actions while the plant is in this operation state. TF and PF coil excitation tests may be carried out. Additional heating system tests such as NB injector ion source conditioning, RF dummy load tests, and fueling system tests are allowed without any tokamak plasma. During TCS, no in-vessel or major ex-vessel maintenance may be initiated. However, minor ex-vessel component maintenance and trouble-shooting is allowed outside of the pit area.
- **Short-Term Standby State (STS)**
This state implies that the final preparation of each subsystem is completed and that the plant is ready for plasma operation. Limited trouble shooting is allowed. Maintenance activity and conditioning operations are not allowed in this operation state.
- **Plasma Operation State (POS)**
The ITER plant subsystems which directly affect plasma operation receive direct commands from the Supervisory Control System (SCS) during plasma operation.

These plant states and typical transition actions are shown in Figure I.3.2-1. Each box in the figure represents the plant state and representative conditions of plant subsystems are shown. Between the states, there is a well defined sequence of steps to go through. When each step becomes active, a transition to the next step takes place when all the required conditions for the transition are satisfied. In the figure, all these detailed sequences of actions and steps are not shown. Instead, representative actions necessary for the transitions are shown for illustrative purposes.

A schematic diagram of the entire plant control system architecture is shown in Figure I.3.2-2. The control system consists of a centrally-positioned supervisory control system (SCS) and subcontrol systems dedicated to each plant subsystem under the supervision of the SCS. Individual plant and diagnostic subsystems are directly controlled and monitored by their own dedicated intelligent control system. All systems use the same control method of conditional transitions between well-defined sequences of steps to be followed (i.e. SFC - Sequential Functional Control). The SCS controls the transition of the entire ITER plant from one operation state to another, and provides high level commands to plant subsystems, in order to achieve integrated control of the entire plant. The SCS also monitors the operation state of each plant subsystem to ensure it is operating within its proper operational envelope. Some plant subsystems can be brought into operation in parallel, while other subsystems must be sequentially started up.

The interlock system monitors operational events of the plant, and performs preventive and protective actions to maintain the system components in a safe operating condition. The interlock system is also hierarchically structured and has individual interlock subsystems which are dedicated to each plant subsystem under the central supervisory interlock system.

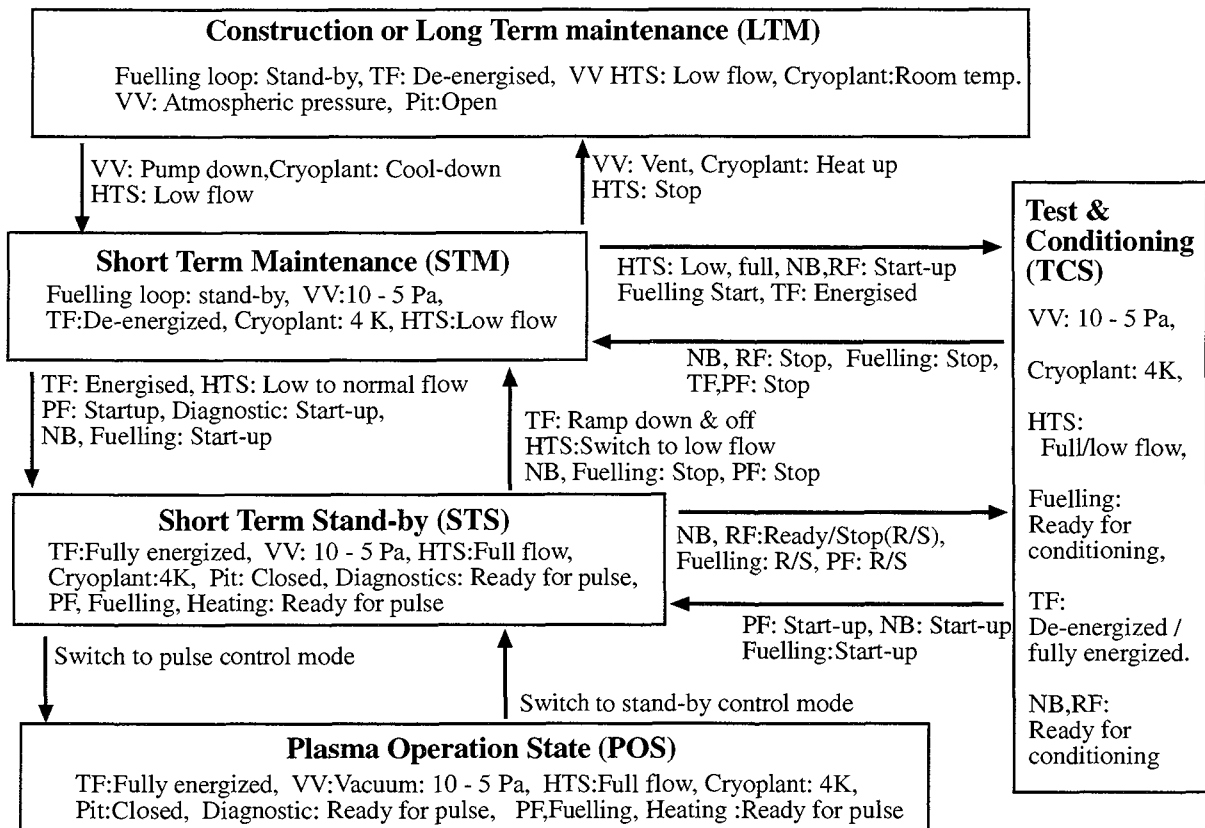


Figure I.3.2-1 Plant States and Transition Actions

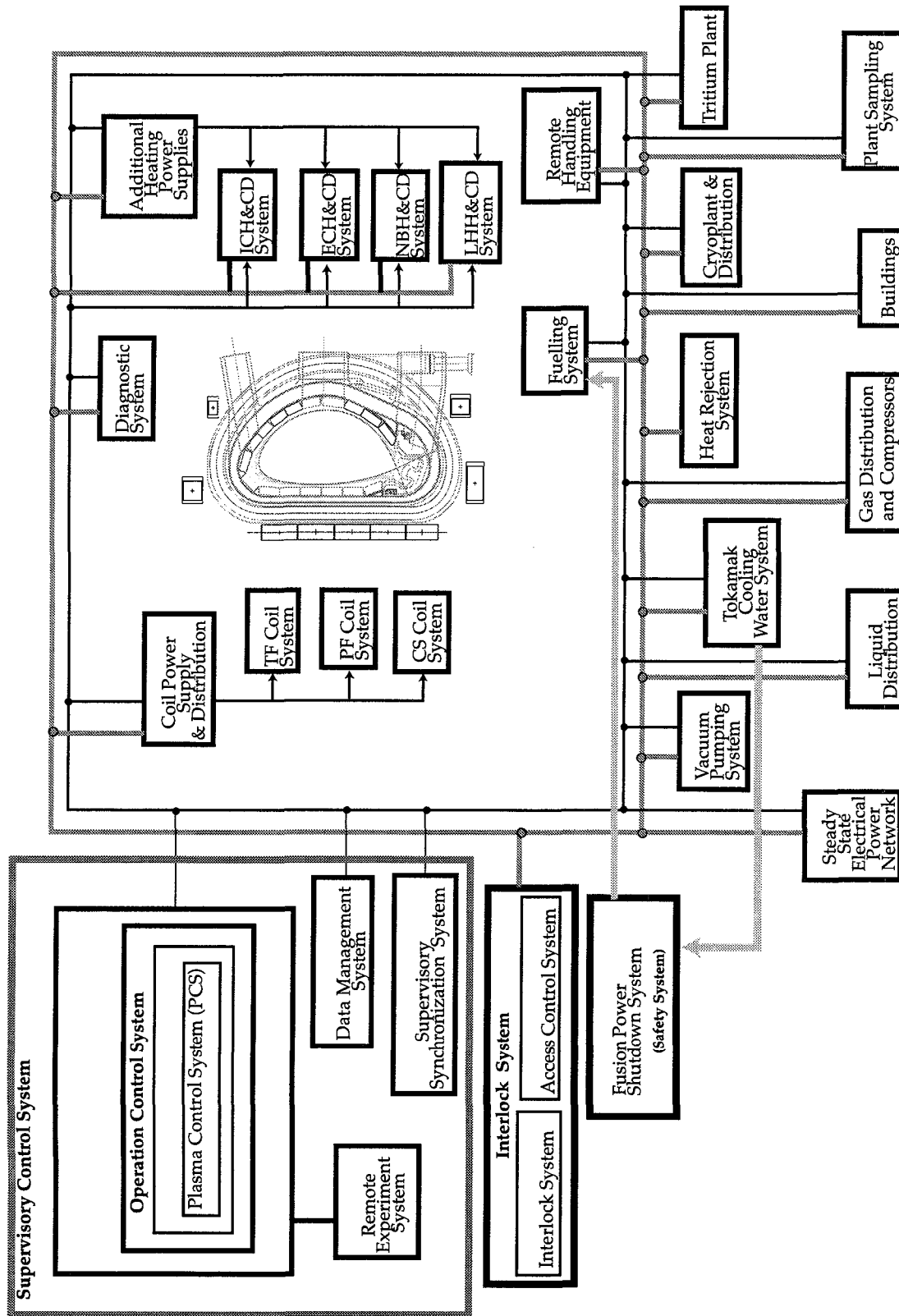


Figure I.3.2-2 ITER-Feat Control System

I.3.2.2 Plasma Operation Scenarios

Figures I.3.2-3 and 4 illustrate the key features of plasma operation scenarios, which show respectively the standard driven-burn and the extended-pulse-duration/steady-state operation. The parameters of the scenario – current, fusion power, auxiliary heating and/or current drive input and burn duration – can vary, but the sequencing requirements and general waveforms remain invariant. Typical main parameters for $Q = 10$ operation are shown in Table I.3.2-1.

I.3.2.2.1 Plasma Initiation

An ITER-FEAT pulse proceeds from pulse initiation with attainment at $t = 0$ of PF coil system pre-magnetisation with a plasma-axis flux linkage of ϕ_{SOP} , as shown in Figure I.3.2-3. This is followed by a 2 s plasma initiation phase that begins with the application of pre-determined voltages to the PF coils. These voltages and the initial PF currents are chosen to produce a dynamic multipole field null with a low poloidal field (< 2 mT within a 0.8 m radius) that is positioned near the port-mounted startup limiters at $t \approx 1$ s. The in-vessel loop voltage is ~ 12 V ($E \approx 0.3$ Vm $^{-1}$) at this time. With a gas fill pressure of about 1.3 mPa, Townsend avalanche breakdown occurs within 50 ms. A 0.5 MA circular plasma with $R \approx 7.5$ m and $a \approx 0.8$ m follows by $t = 2$ s.

During startup, 2 MW of electron cyclotron (EC) power at 120 GHz will be provided for 2 s to facilitate initial breakdown over a range of pre-fill pressures and error-field conditions, and will also provide supplemental heating after breakdown to ensure rapid ionisation (burn-through) of impurities in the initial low-current startup plasma. For the hydrogen operation phase with about half the full value of toroidal field, the application of EC at $2\omega_{ce}$ is expected.

I.3.2.2.2 Current Ramp-up

The balance of plasma initiation for driven-burn operation proceeds with a current ramp-up of average $dI/dt \approx 0.15$ MAs $^{-1}$. This is coordinated with a minor radius expansion and elongation increase to maintain a nearly constant edge safety factor $5 \leq q \leq 6$. The plasma remains limited until $I_{SOD} (\approx 0.5 I_{P0})$ is reached. Attainment of a single null (SN) divertor configuration at I_{SOD} ($q_{95} \approx 4$) follows. Continuation of the current ramp-up results in a I_{P0} current flat-top ($q_{95} \approx 3$) at $t \approx 100$ s.

For extended-pulse-duration/steady-state operation, assuming a WCS/NCS (weak/negative central shear) magnetic configuration for active profile control, the heating of the core plasma from the early phase of startup is needed to hold low plasma current density in the core region and to generate the WCS/NCS configurations at SOF. Based on present experiments, the current ramp-up rate will be ~ 0.15 MAs $^{-1}$, which is the same as that in the driven-burn case. $q_0 > 1$ or $q_{min} > 2$ can be maintained by optimising the ramp-up scenario including additional heating.

I.3.2.2.3 Shape and Configuration Control

Dynamic control of the plasma shape and position is required throughout the scenario. The clearance gap between the first wall and the separatrix is arranged to provide an attractive scenario for ion heating by IC waves and to keep the possibility of having an efficient off-axis current drive by LH waves in the reference configuration. The clearances allowed are

8 cm between the separatrix and the port limiter, and 12 cm between the separatrix and the first wall near the outboard equatorial port area. Away from the outboard equatorial port area, the clearance follows the flux line 4 cm from the separatrix at the outboard equator plus an 8 cm gap.

I.3.2.2.4 Heating to Driven Burn

Following SOF (start-of-flat top), auxiliary heating is applied. This, coordinated with plasma fuelling, results in the attainment of H-mode confinement and sustained fusion burn with ~ 500 MW of fusion power within ~ 50 s. Attainment of the rated fusion power is denoted as the start-of-burn (SOB). The most demanding power requirement in this phase is the L-H threshold power, which depends on plasma density. For example, for a given heating power of ~ 30 MW, the maximum density is $\langle n_e \rangle = 0.4 \times 10^{20} \text{ m}^{-3}$. It is assumed that the required plasma shape and current are achieved at SOF and that plasma heating and β increases are carried out at constant shape and current. Scenarios which modify plasma shape and current during the plasma heating between SOF and SOB can also be considered.

In the extended-pulse-duration/steady-state operation using the WCS/NCS magnetic configuration, the scenario is more complicated. Following SOF, auxiliary power heats the plasma and generates a toroidal current which, together with the bootstrap current, replace the Ohmic current. Generally, the current profile before the addition of auxiliary power is somewhat different from the final profile. The current diffusion time across the whole plasma volume is large, e.g. ~ 200 s for $T_e \approx 5$ keV and ~ 800 s for $T_e \approx 10$ keV. So during the sustained burn, the current profile will evolve to the final state over several 100 s.

I.3.2.2.5 Sustained Burn

Once SOB is attained, an accumulation of thermal helium results in the need to further increase the plasma density to maintain a fixed fusion power: the approach to sustained burn with stationary helium level requires about 200 s. The burn proceeds until the end-of-burn (EOB) inductive flux limit of the PF coil system is reached. For standard plasma confinement and impurity models, the duration from SOB to EOB is about 400 s for the driven-burn.

I.3.2.2.6 Burn Termination

The burn is terminated by reducing the fuelling to ramp-down the fusion power, followed by current and density ramp-down and plasma termination, with measures to avoid disruption.

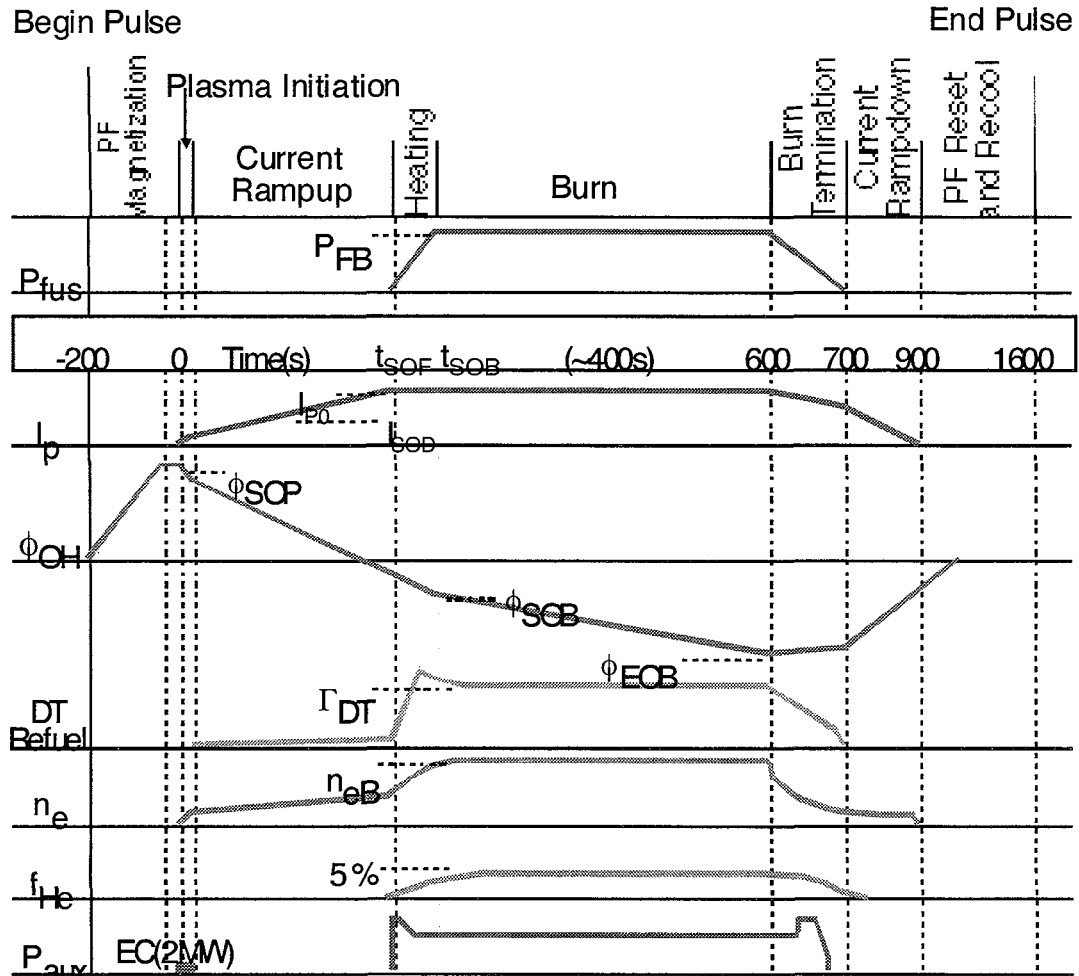


Figure I.3.2-3 Waveforms for Standard Driven-burn Operation Scenario

Table I.3.2-1 Typical Parameters for Driven-burn Operation at $Q = 10$

	ITER-FEAT
P_{FB} [MW]	400/500
P_{aux} [MW]	40/50
I_{P0}/I_{SOD} [MA]	15.0/~ 7.5
t_{SOF}/t_{SOB} [s]	100/150
n_{eB} [$10^{20}/m^3$]	1.0
f_{He} [%]	4.0

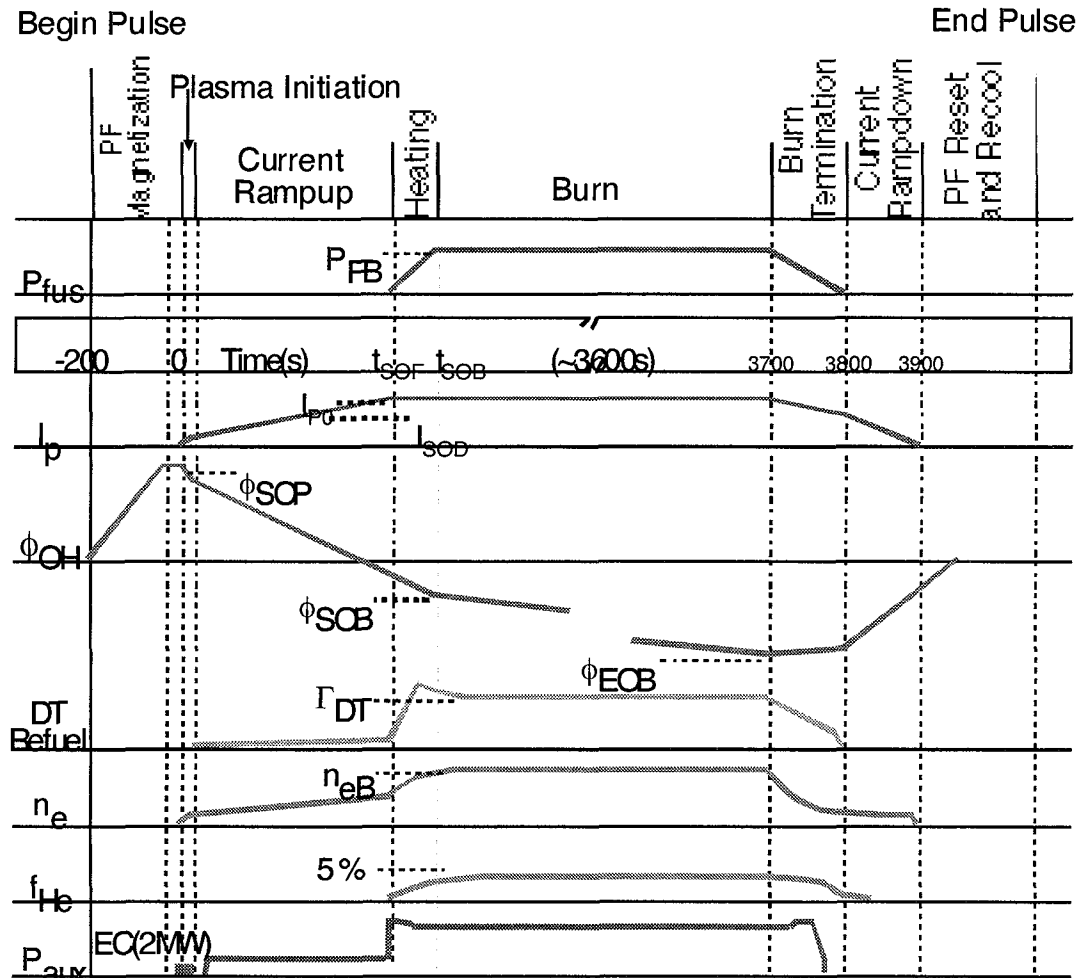


Figure I.3.2-4 Waveforms for Standard Extended-pulse /Steady-state Operation

Table I.3.2-2 Typical Parameters for Extended-pulse/Steady-state Operation

	ITER-FEAT
P_{FB} [MW]	~ 350
P_{aux} [MW]	~ 70
I_{P0}/I_{SOD} [MA]	~ 10 ($q_{95} \approx 5.0$)
t_{SOI}/t_{SOB} [s]	60/110
n_{eB} [$10^{20}/m^3$]	~ 0.6
f_{He} [%]	4.0

I.3.3 Safety and Environment

This section summarises preliminary assessments of the design from the safety and environmental impact perspectives. It is concluded that the design will meet project safety objectives. This conclusion is based on the results of these preliminary assessments combined with a consideration of fusion's favourable safety characteristics and the detailed safety assessment of the 1998 ITER design. While details of the on-going assessments may

change, it is expected that the comprehensive evaluations will continue to demonstrate the safety and environmental attractiveness of the new design.

I.3.3.1 Normal Operation

I.3.3.1.1 Effluents

Operational effluents are expected to be at a level which would cause public doses to the most exposed individual, below 1% of the natural radiation background (postulating a typical 'generic' site).

Most releases are expected during maintenance operations. Presently available assessments¹ suggest that the total tritium releases from the plant are about 0.25 g per year. In terms of doses, the releases of activation products are comparable to those of tritium.

For the design option without a stack, further reductions of effluents are needed to keep public doses below 1% of the natural radiation for a generic ITER site.

I.3.3.1.2 Occupational Safety

Design criteria (I.1) for personnel access, have been established to ensure an acceptable level of occupational safety. Radiological hazards are being estimated by neutron activation analysis of components and structures, associated gamma transport calculations, and activated corrosion product build-up analysis, to assess the design against the design criteria. Non-radiological hazards (EM fields, beryllium, etc) are also being estimated. In addition to meeting the design criteria for access, an iterative assessment process will be applied to operational and maintenance activities to reduce radiation exposure based on the ALARA principle.

I.3.3.1.3 Radioactive Waste

An important objective is to demonstrate the environmental attractiveness of fusion over the entire life cycle of ITER-FEAT, including construction, operation, and decommissioning. In this context it is important to assess the amounts of radioactive solid waste. Activated and contaminated materials arise during the operational phases and remain after final shutdown. Not all these materials would need to go into a waste repository, rather, after some decay time, a significant fraction can be 'cleared', i.e. declared to be no longer radioactive waste. The related processes (e.g. as recommended by IAEA) range from 'unconditional' clearance to clearance 'for recycling'. Of specific importance for ITER-FEAT are the generation of Co-60 and Nb-94, and their clearance levels.

A provisional waste characterisation assessment for the ITER-FEAT has been performed², although a detailed study cannot be done until the design is finalised (or nearly so). The masses of all tokamak components up to the TF coils are scaled from the 1998 ITER design by the change in first wall surface. All components outside the TF coils are scaled by

¹ M. Iseli, "Summary of normal operation tritium effluents for FDR and ITER-FEAT", SEHG Memo, 3 November 1999, ITER Naka JWS (N 83 MD 2 99-11-03 W 0.1)

² J. Raeder, "Radioactive Waste vs Clearance" SEHG Memo, 16 September 1999, ITER Garching JWS (G 80 MD 2 99-09-16 W 0.1)

volume. Using this approach, the amounts of radioactive material are about 50% those of the 1998 ITER design.

As an example, activation calculations have been done to estimate the time for the irradiated material to reach the IAEA-TECDOC-855 clearance levels. The neutronics model was of one-dimensional annulus type, which implies that toroidal and poloidal neutron load peaking, and neutron streaming, could not be taken into account. The structural steel assumed for all components except the cryogenic ones is the ITER reference steel SS 316 L(N)-IG (presently specified 0.01 wt.% of Nb and 0.05 wt.% of Co). The calculations suggest that it is sufficiently stringent with regard to the impact of Nb on clearance to limit the Nb concentration in the structural steels to 0.01 wt %. At lower concentrations, clearance levels would be dominated by Ni-63 and Mo-93 which stem from the alloying elements Ni and Mo in the reference steel.

Overall (without neutron streaming), the assessment shows that the dominant part of the components beyond the inner shell of the vacuum vessel decays to clearance levels in less than 100 years, following an average neutron fluence to the blanket first wall of 0.5 MWa/m^2 . The results from the assessment are summarised in Table I.3.3-1:

Table I.3.3-1 Radioactive Masses [t] for ITER-FEAT

Total radioactive material	39,400
Clearance according to IAEA TECDOC-855:	
Waste (radioactive material) remaining after 100 years of decay	11,900
Waste (radioactive material) remaining after 100 years of decay as a percentage of the total	30 %

About 25 % of the waste (radioactive material remaining after 100 years of decay) stems from the vacuum vessel. Part of this mass could be cleared and a breakdown into a clearable and a non-clearable fraction implies that the vacuum vessel can be disassembled without too much difficulty. Exploitation of the shell structure by design may allow for accomplishing this.

I.3.3.2 Accidents

ITER-FEAT protects personnel and the public using confinement. Multiple physical and functional barriers, depending upon the releasable inventory, protect against spread and release of hazardous materials. The primary confinement barrier is designed to have high reliability to prevent releases. A secondary barrier is provided close to the primary one to limit the spread of contamination and protect personnel from leaks. Exhaust from rooms that can be contaminated is treated by filters and/or detritiation systems, and monitored.

Significant sources of tritium or activated materials reside within the vacuum vessel, in the tokamak cooling water system (TCWS), in the fuel cycle and within the hot cell. The confinement approach for each is illustrated in Figure I.3.3-1 and described below.

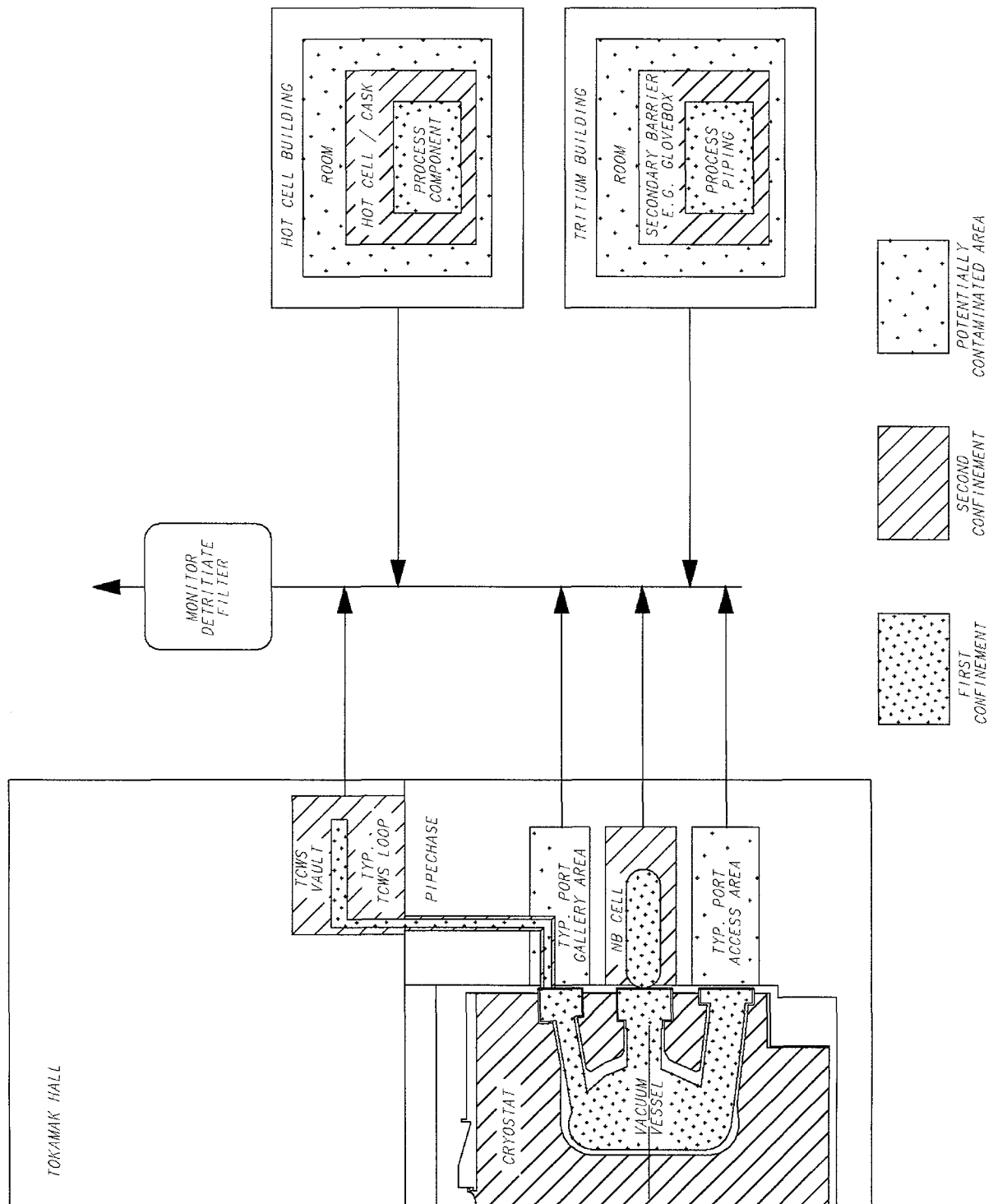


Figure I.3.3-1 Tritium Confinement Concept

The primary confinement for the source term within the vacuum vessel (up to 1.2 kg tritium and up to 100 kg activated dust) is the vacuum vessel and its extensions including the NB injector vessels and windows in the RF heating systems and diagnostics. The TCWS piping forms the primary confinement for tritium and activated corrosion products in these loops. Since experimental components inside the vacuum vessel are not assigned a safety function, the TCWS must also confine the in-vessel source term in some accidents, such as an in-vessel coolant spill.

For the in-vessel and TCWS source terms, the secondary barrier includes the TCWS vault, pipe chases to the vault, the NB cell, and the cryostat and its extensions. The VVPSS minimises peak pressures inside the vacuum vessel during accidents, and the parts of the VVPSS that are external to the cryostat form part of this second barrier. Windows, typically at the cryostat closure plate, in the RF heating systems and diagnostics also form part of this secondary barrier. However, the diagnostics connected to the vacuum vessel or separated only by windows are housed in the NB cell or similar rooms. The TCWS vault and NB cell are designed to be leaktight and withstand pressures following coolant spills. (A variation of the above for the TCWS vault during baking is being studied which would permit a lower design pressure by providing over-pressure relief into an additional volume.) Exhaust from the TCWS vault, NB cell, port access areas and gallery areas that can be potentially contaminated (e.g. due to accidental leakage past confinement barriers or during maintenance) can be treated by filters and detritiation systems and directed to the plant exhaust.

The primary confinement for the fuel cycle source term (~ 1 kg tritium) is the process equipment and pipes of the vacuum pumping system, tritium plant and fuelling system. These are surrounded by secondary barriers such as gloveboxes, cold boxes, vacuum jackets, and other enclosures. Rooms are maintained at a negative pressure with respect to the external atmosphere and the exhaust can be treated by detritiation systems and directed to the plant exhaust.

The hot cell source term includes tritium and activated materials which arise from the refurbishment and the storage of in-vessel components. Hot cells, casks, and process equipment form the primary confinement barrier, and the hot cell building exhaust can be treated by filters and detritiation systems, and is directed to the plant exhaust.

Further detailed analysis and design are needed to clarify the conditions under which the technical need for a 100 m stack for ITER-FEAT can be avoided. One of the conditions is to exclude confinement bypass events by implementing diverse confinement barriers for the penetrations of the vacuum vessel and cryostat as mentioned above. Confinement of large postulated tritium releases within rooms adjacent to large source terms is another necessary condition.

I.3.3.2.1 Loss of Coolant Accidents

I.3.3.2.1.1 Ex-vessel Coolant Leak

Coolant leaks outside the vacuum vessel have been investigated, including two types of breaks: double-ended pipe rupture and a crack of the main pipe located in the TCWS vault. Pressurisation of the vault has been estimated for operating and for baking conditions.

From the safety point of view the preferable option is to keep released steam and water inside the vault ('closed confinement') since this option reduces environmental releases of radioactive materials.

Preliminary assessments assume that the water holdup in one loop of the TCWS for the blanket, is 120 to 140 m³, the internal diameter of the main pipes is 0.5 to 0.6 m, the free

volume of the vault is about 30,000 m³, the water temperatures for normal operation are 100°C/150°C (inlet/outlet), the water temperature during baking is 240 ± 10°C, and a maximum design pressure for the vault is 300 kPa absolute. Several options have been investigated, and the key results are shown in Table I.3.3-2.

**Table I.3.3-2 Tokamak Cooling Water System Vault Pressures [kPa]
from Ex-Vessel Cooling Pipe Breaks**

Loop volume [m ³]	Baking				Normal operation
	Double-ended break			Crack	Double-ended break
	T _w = 250°C	T _w = 240°C	T _w = 230°C	T _w = 250°C	T _w = 100 to 150°C
126	299				
140	316	303	293	180	159

At baking conditions for the cooling loops with a water volume > 126 m³, an additional volume is required where the steam can be expanded to keep the vault pressure below a design limit of 300 kPa.

In the case of a crack-type break (break size = $Dd/4$, where D is the pipe diameter and d is the pipe wall thickness) at baking conditions (water at 250°C, at maximum), the maximum pressure is below 200 kPa.

At normal operating conditions, the maximum pressure in the case of a double-ended break of the main pipe is less than 160 kPa.

An alternative approach to accommodate off-normal pressure, is the release of any overpressure into an additional volume via large blow-down panels. For example, the maximum pressure at a large loss of cooling accident during baking can be kept below 170 kPa absolute if the expansion volume provides 120,000 m³ filled with air at atmospheric pressure.

I.3.3.2.1.2 In-vessel Coolant Leak

A large family of potential accident sequences is grouped around coolant pipe failures resulting in the pressurisation of the vacuum vessel and possible damage to the first confinement barrier. To reduce the in-vessel accidental pressure and the risk of damaging the first barrier, a vacuum vessel pressure suppression system (VVPSS), is foreseen.

It is assumed that the tank of the VVPSS will be located in the upper TCWS vault or elsewhere above the vacuum vessel. This would allow separation of steam and water flows and would reduce the maximum accident pressure inside the vacuum vessel to below 200 kPa absolute. The rupture disks open at a pressure of 150 kPa in the vacuum vessel. Besides the VVPSS tank location, the most important parameters influencing the in-vessel pressure are the water temperature, the breach size, and the total cross-section of the manifolds feeding the water to the damaged blanket modules. These parameters determine the in-vessel water flow and evaporation rates.

A set of MELCOR calculations was done to determine the key parameters of the VVPSS and to estimate the vacuum vessel pressurisation for different types of in-vessel breaks. Detailed analysis assumptions can be found in¹. Key analysis results are shown in Table I.3.3-3.

Table I.3.3-3 Vacuum Vessel Pressures [kPa] from In-Vessel Cooling Pipe Breaks

Water temperature [°C]	Baking, 250°C	Normal operation, 100-150°C					
Type and flow area of the break [m ²]	Double-ended break of 5 cm Tube (one loop) ~ 0.004 m ²	Double-ended break of all FW tubes ~ 0.2 m ²					Double-ended break of some FW tubes ~ 0.03 m ²
Total flow area of the passages [m ²] (dedicated relief passages; gaps refer to passages between blanket modules)	0.1 - 0.6	0.0 no pass. no gaps	0.5 no gaps	0.1 no gaps	0.1 with gaps	0.0 with gaps	0.0 with gaps
Maximum in-vessel pressure [kPa]	150	380	185	217	175	200	165

For a multiple break at normal operating temperatures, the minimum cross-section of the passages connecting the ‘plasma volume’ (i.e. the volume encompassed by the plasma-facing components) with the upper ports, which are equipped with relief pipes, should be about 0.1 m² if the gaps between the blanket modules are taken into account. In this case, the maximum pressure is about 175 kPa (i.e. below the design limit of 200 kPa).

For the design option with the blanket cooling manifold accommodated between the two vacuum vessel shells, cross-contamination between adjacent blanket and vacuum vessel cooling loops has been investigated. Such an event was classified as an unlikely sequence (Category III) because of the thick multi-pass welds between the cooling channels². Radiological consequences have been assessed and were found to be insignificant³.

I.3.3.2.2 Decay Heat

Decay heat densities are very small in ITER-FEAT so that no emergency cooling of the in-vessel components is needed. The vacuum vessel cooling system has the capability to passively remove all decay heat via natural circulation. The maximum temperatures of in-vessel components during accidents are below 330°C with vacuum vessel cooling only. These temperatures are sufficient to radiate the power from the in-vessel components to the vacuum vessel which transports the power to the ultimate heat sink. No significant chemical reactions occur between steam (air) and Be-dust at these temperatures.

1 L. Topilski, “In-vessel LOCA” SEHG Memo 10 May 1999, ITER Garching JWS (G 84 MD 2 99-05-10 W 0.1)

2 N. Taylor, “VV coolant contamination”, UKAEA, Memo for SEHG, ITER Garching JWS, 23 July 1999 (G 71 MD 2 99-07-23 W 0.1)

3 H.-W. Bartels, “Consequences of postulated contamination of VV cooling loop”, ITER Garching JWS, 30 July 1999 (G 71 MD 1 99-12-01 W 0.1)

Venting of the cryostat and air convection at the outer cryostat surface limit the maximum temperatures of the in-vessel components to about 350°C without any cooling of the vacuum vessel.

I.4 Cost and Schedule

I.4.1	Cost	1
I.4.1.1	Introduction	1
I.4.1.2	Cost Estimating Approach	1
I.4.1.3	Construction Cost Estimates Results	2
I.4.1.4	Operation and Decommissioning Cost	6
I.4.1.5	Conclusion	7
I.4.2	Schedule	12
I.4.2.1	Introduction	12
I.4.2.2	Construction Schedule	12
I.4.2.2.1	Initial and Background Conditions	12
I.4.2.2.2	Procurement Strategy	13
I.4.2.2.3	Construction of the Tokamak Building and Assembly	14
I.4.2.2.4	Commissioning for the First Hydrogen Plasma Discharge	14
I.4.2.2.5	Critical path	15
I.4.2.3	Operation Plan	15
I.4.2.3.1	General Considerations	15
I.4.2.3.2	Hydrogen Phase (H phase)	15
I.4.2.3.3	Deuterium Phase with Limited Tritium Use (D phase)	16
I.4.2.3.4	Deuterium-Tritium Plasma Phases	16
I.4.2.3.5	Tritium Supply	16
I.4.2.3.6	Tritium Breeding Blanket Test Program	17
I.4.2.4	ITER Decommissioning Plan	19
I.4.2.4.1	General policy and assumptions	19
I.4.2.4.2	Decommissioning Schedule	20

I.4.1 Cost

I.4.1.1 Introduction

The objective of these cost estimates is to provide for all the machine and plant systems a self-consistent cost re-evaluation based on the approach developed for the 1998 ITER Design¹. All the major cost issues have been addressed, including the capital cost of construction, and the machine operation and decommissioning costs. A valid cost estimate of ITER-FEAT will be obtained only after the engineering details have been worked out to provide specifications for an industrial cost analysis to be undertaken by firms of the Parties in the second half of 2000. Pending such analysis, only a rescaling from the costs of the 1998 ITER design can be done, the result of which slightly exceeds the specified target of 50 %. However, this simple scaling cannot take into account the expected improvements in the design and in the industrial fabrication process. The latter is now the most important area of activity for reducing costs further towards the target.

I.4.1.2 Cost Estimating Approach

The 1998 ITER design cost basis is used as fully as possible. That means that the detailed system cost structures developed for that design by the JCT together with Home Team industry are retained, and cost scaling is done, as far as reasonable, at the component levels. Therefore, all costs are again expressed in the ITER Unit of Account (IUA) defined as \$1000 US in January 1989. The relationship between IUA and the ITER Parties currencies in January 1989 is shown in Table I.4.1-1.

¹ Technical Basis for the ITER Final Design Report, Cost Review and Safety Analysis (FDR), Chapter V

Table I.4.1-1 Currency Parity between ITER Parties in January 1989

IUA	US \$	ECU	¥
1	1000	875.8	127,510

A perspective on the escalated costs to present values in each Party can be obtained by using Consumer Price Indices, Table I.4.1-2.

Table I.4.1-2. Currency Escalation with respect to January 1989 based on Consumer Price Indices¹

US \$	ECU	¥
1.35	1.4	1.14

Many of the ITER-FEAT systems have retained their basic design features from the 1998 ITER design. In such cases their cost is simply scaled down within the same cost structure. For each system the major cost drivers are used to recalculate the component materials costs, the tooling, the fabrication, assembly, testing and shipping costs. The main cost drivers specific for different systems are discussed below.

The amount of materials is typically associated with the number of components and characteristic size or weight. The tooling cost drivers are selected depending on the specific technological procedures used for each system. Often these drivers are used with power scaling factors less than 1, typically 0.7. A similar approach is used for recalculating the labour costs associated with fabrication, assembly, testing and shipping.

Some new design options required the adjustment of the previous cost structure and identification of additional cost drivers. Such changes were applied, e.g. to the multi-sectional central solenoid, and to the vacuum vessel with added back plate functions etc.

Operating costs depend highly on the cost of electricity, the salaries of the professionals and support personnel, the cost of the divertor high heat flux component replacements and general maintenance expenses, and to a lesser extent on the cost of tritium supply and the cost of the disposal of waste, most of which may vary quite substantially amongst the potential host sites for ITER.

The main driver for decommissioning costs included in this estimate is the amount of work necessary to de-activate the machine at the end of the plant operation, remove all in-vessel components and then, after activity decay, finally remove the ex-vessel components and dismantle the vacuum vessel. The required manpower for these operations is scaled according to the size and number of sections of the vacuum vessel. A constant cost is taken for additional equipment envisaged in the 1998 ITER design. The costs of transportation and long term storage of the activated material is not taken into account.

I.4.1.3 Construction Cost Estimates Results

Direct capital cost estimates are given in Tables I.4.1-3 to 6. Cost distribution by systems is

¹ International Financial Statistics Yearbook 1999, International Monetary Fund.

shown in kIUA and percentage comparison with the 1998 ITER design cost. Table I.4.1-3 shows costs of the tokamak basic machine and major systems directly supporting it. Table I.4.1-4 provides the cost summary for buildings and site facilities, hot cell and other balance-of-plant systems. Table I.4.1-5 gives the costs of three heating and current drive systems combined with their supporting power supplies, vacuum pumps etc. Table I.4.1-6 shows costs of diagnostic systems with the expected support (in terms of PPYs) from the Home Teams for their design and construction oversight. The results presented in those tables are commented on system by system in what follows.

Magnets

For all coils the conductor cost is recalculated in proportion to its total length. New design criteria developed as a result of current R&D effort have been used for the design of superconducting cables, and these lead to lower cable unit costs. The major cost drivers for the coil structures are: number of coils, coil perimeters, conductor length per coil, and product of the total coil current and its perimeter (for PF coils). Differences from the 1998 ITER design in the intercoil structure are taken into account, such as: wedged TF coils without support from the central solenoid, no crowns, extra allowance for nose welding and machining. Two options were under investigation for the TF coil winding: one with a circular conductor embedded in radial plates and the other with a square conductor. The cost is presented for the radial plate option, which has been recommended in view of its advantages in terms of insulation reliability and fault detection capability. Nevertheless, the possible savings which might be achieved with the other option for the TF winding, with a square steel conduit conductor may be large, and this calls for a renewed assessment. Anyway, it seems that some margins exist to lower the cost of the preferred option, through a less costly manufacture of the radial plates. A special assessment has been carried out to evaluate the cost impact of the segmented central solenoid (as against the monolithic one in the 1998 ITER design).

The total weight of the magnet system is about 1/3 of the 1998 ITER design while its overall cost is about 1/2 of that (Table I.4.1-3). Thus, a larger fraction of the ITER-FEAT magnets cost is related to labour, and tooling involved in the magnets' fabrication. Therefore, there might be some possibility for cost saving due to further optimizations of the technologies involved.

Vacuum Vessel and In-Vessel Systems

Material cost is scaled down in proportion to the weight of the main vessel and ports. The new design, with the addition of structures to the VV inner shell to support the blanket modules and provide blanket cooling channels, has significantly increased the complexity, welding, machining, and inspection operations, and the corresponding labour costs. However, with the smaller VV size it is found possible to use fewer, wider VV sectors (40° instead of 18°) and thereby save on both fabrication and assembly costs. The VV cost estimate presented in Table I.4.1-3 does not take into account possible savings from switching to the design with separate blanket cooling manifolds, not incorporated into the inter-shell space. Other possible savings can be achieved with the use of casting or forging for the large number of the housings in the VV for the support of blanket modules.

The blanket design and cost structure have been considerably changed, with the attachment of blanket modules directly to the vacuum vessel. The total number of modules has considerably decreased, and the module structure has been divided into two parts: the separable first wall, and the shield block. Expensive HIP technology is envisaged now only for the more sophisticated first wall. The change in geometry of the first wall, replacing 2D curvature by faceted 1D, allows the use of less expensive tooling.

The combined cost of the blanket and vacuum vessel (Table I.4.1-3) is 388 kIUA or 61% of the 1998 ITER design. However, when evaluated per tonne of material, the unit cost is somewhat higher for ITER-FEAT, which means that further investigation should show that some savings may be possible due to design and technology improvements.

The divertor costs are largely driven by the costs of the plasma facing components (PFCs). Savings, as compared with the 1998 ITER design, relate to less toroidal segmentation of PFCs and the elimination of the divertor dump target from the design. Another design change, the incorporation of the baffles in the vertical targets, resulted in a certain cost increase due to larger target lengths. For the cassette bodies, linear scaling with weight is applied for the materials and to the 0.7th power with surface area for fabrication.

Machine Assembly & Tooling

The assembly procedures logic has been completely re-evaluated, with an attempt to simplify the process and to eliminate the need for expensive tools wherever possible. Labour cost savings related to fewer assembled components (namely 9 TF/VV sectors instead of 20, fewer blanket modules, 6 PF coils instead of 9) are taken into account. All this resulted in 64% of the system cost as compared to the 1998 ITER design.

Remote Handling Equipment

The main change, at system level, is the reduction in the size of equipment, of their number due to enhanced standardization, application of a cask docking system to the in-vessel transporter, and standardization of double-seal door and cask structure. The cost estimate presented in Table I.4.1-3 is 67% of the 1998 ITER design cost.

Cryostat, Vacuum Vessel Pressure Suppression System and Thermal Shields

The thermal shields have to cover multiple port structures and supports, and their surface becomes relatively larger in a smaller machine. Therefore the estimated thermal shield cost shows less relative reduction compared with the cryostat, at 74% of the 1998 ITER design cost (Table I.4.1-3).

Vacuum Pumping & Fuelling System

The fuelling and wall conditioning system, having similar requirements, have basically unchanged costs.

The torus cryopumps cost is calculated in proportion to the reduced number of cryopumps (8 for the pulsed operation stage instead of 16 in the 1998 ITER design), and similarly for the

neutral beam injection subsystem. The result is 72% of the 1998 ITER design cost (Table I.4.1-3).

Tritium Plant

The main tritium plant cost driver, the tokamak exhaust flow, did not change from the 1998 ITER design, therefore with similar capacity and system configuration, its cost remains the same. The cost of other subsystems has been scaled down in accordance with lower capacities and elimination of some equipment. In total it gives 65% of the 1998 ITER design cost (Table I.4.1-3).

Cooling Water Systems

The total cost of each cooling subsystem is scaled with the thermal load to the 0.7th power and the number of cooling loops. The number of in-vessel primary cooling loops has been reduced to 5 from the previous 18. The number of heat rejection loops is reduced to four from seven, and the number of cooling towers reduced to two from three due to the decrease in thermal load. The system cost estimate gives 51% of the 1998 ITER design cost (Table I.4.1-3).

Cryoplant and Cryodistribution

Cryoplant cost reduction occurs mainly due to reduction of the number of 4.5K refrigeration units in proportion to the reduction of the cryogenic heat load. Costs for other cryogenic equipment, including He gas purification, gas and liquid storage, control system, design and documentation have been assumed to be identical to that of the 1998 ITER design costs, which results in the total system cost estimate of 65% of the 1998 ITER design cost (Table I.4.1-3).

Power Supply Systems

Costs are re-estimated, component by component, taking into account the decrease in the stored energy, power for plasma control and heating, etc. Also, some additional improvements in the design are considered, such as the integration of the power supplies for the four outer PF coils, PF2 through PF5, in one circuit with one vertical stabilization converter. The resulting cost for the coil power supply system is 55% of the 1998 ITER design cost (Table I.4.1-3).

Cost scaling for different auxiliary heating and current drive power supply systems is done in proportion to the reduced number of the standard units, as in the 1998 ITER design. This reduction is down to 70% for the NB heating and current drive (H&CD) system and less than 50% for the others (Table I.4.1-5).

Buildings and Site Facilities

Buildings nomenclature, use, and layout have been subject to considerable changes compared to the 1998 ITER design. The buildings' costs are re-evaluated in terms of size and volume. The down-scaled costs are then obtained using the previous unit volume costs for each individual type of building. The site area has been re-estimated, and the related costs scaled

down respectively. In total the buildings and site facilities cost is 47% of the 1998 ITER design cost (Table I.4.1-4).

Auxiliary Heating and Current Drive Systems

The costs of the major subsystems for all H&CD systems are generally scaled in proportion to the number of standard units. However, for the ion cyclotron H&CD system the increase of the injected power density per unit port surface by almost a factor 2, as compared with the 1998 ITER design, is taken into account. A system providing 20 MW of RF power to the plasma in one port (instead of 50 MW in the 1998 ITER design for four ports) costs only 27% of the previous one. Together with power supplies and pumping system, the overall ion cyclotron H&CD system cost is 31% of the 1998 ITER design cost, and the unit cost is 1.8 kIUA/MW (Table I.4.1-5).

The cost of the electron cyclotron H&CD system (20 MW of RF power to plasma in one port instead of 50 MW in the 1998 ITER design in two ports) covers two different launchers that can be used alternatively, one in the equatorial port and another, combining two submodules, in two top ports, connected to the same transfer line and gyrotrons. For this reason the launch structure cost is 92% and the pumping system is 100% while the whole system with power supplies is 51% of the 1998 ITER design cost. The unit cost for the system with two launchers is 4.4 kIUA/MW.

For the neutral beam H&CD system, the cost reduction follows the scaling from 3 injectors to 2, but certain subsystems could not be scaled down exactly in proportion to the number of injectors, the overall system cost is 70% of the 1998 ITER design cost, with a unit cost of 4 kIUA/MW.

Diagnostics System

No cost reduction from the 1998 ITER design cost has been envisaged for the diagnostic system (Table I.4.1-6).

I.4.1.4 Operation and Decommissioning Cost

Annual operation costs are considered as an average over 10 years according to the plan for the first 10 years of ITER-FEAT operation (Figure I.4.2-2). The average yearly operation cost for this period is 180 kIUA/year, or 51% of the average of annual operating costs of the 1998 ITER design (Table I.4.1-7).

Project Manpower and Overhead

These costs have been scaled in proportion to the number of professional staff, which is assumed to be 2/3 of the level envisaged in the 1998 ITER design. They result in 1/3 of the total yearly operation cost (Table I.4.1-7). This includes 200 professionals and 400 technicians as permanent staff in charge of plant operations. The scientists in charge of experiments are assumed to be visitors organised in task forces, seconded by the Parties' laboratories. They are not charged to the operation budget.

Electric Power

Base load electricity consumption on cold standby and maintenance is the main driver (~ 90%) for the electricity costs (energy consumption). As for the cost of various general purpose plant systems, it is roughly scaled down to 50% of the 1998 ITER design consumption. The assumed unit cost for grid electricity averaged over times and seasons is 0.05 IUUA/MWh. The energy consumption accounts for 1/7 of the total yearly operation cost (Table I.4.1-7).

Fuel

Taking into account the reduced total fluence objective (1/3 of the 1998 ITER design), smaller first wall surface (0.55 of the 1998 ITER design) and zero tritium breeding, the total fuel consumption for the first 10 years of ITER-FEAT operation is scaled down to 0.18 of that in the 1998 ITER design, assuming the same unit cost of 10 kIUUA/kg. The fuel cost accounts for only 3% of the total yearly operation cost (Table I.4.1-7).

Capital Improvements, Spare Parts, Maintenance

The general allowance to cover capital improvements, spare parts and maintenance costs, is scaled in proportion to the total direct construction capital, except buildings. The cost associated with one refurbishment of the divertor plasma facing components, is included.

Waste Disposal

The cost of waste disposal during the first 10 years of ITER-FEAT operation is negligibly small.

Decommissioning Cost

Decommissioning costs, scaled down as described previously, are presented in Table I.4.1-8. The total is 167 kIUUA or 56% of that in the 1998 ITER design cost. Again, they do not include the cost of transportation and long term storage of activated material.

I.4.1.5 Conclusion

In total, this exercise of rescaling the cost of the 1998 ITER design to ITER-FEAT is a first approximation taking into account mainly the size variation (and some design change). The total cost of 56% of the 1998 ITER design shows that the target of 50% is approximately achieved, but more savings efforts should be pursued, mainly through more efficient manufacturing processes and related design improvements. As stated in I.4.1.1, the estimate for the ITER-FEAT cost will be available only after the engineering details have been worked out and an industrial cost analysis has been undertaken by the Parties in the second half of 2000.

Table I.4.1-3 Cost of Main Tokamak Systems

	ITER-FEAT	
	kIUA	% of 1998
Toroidal Field Coils Fabrication	164	67%
Poloidal Field Coils Fabrication	61	57%
Central Solenoid Fabrication	44	51%
Magnet Structures	240	48%
Conductor	349	42%
Feeders	22	59%
Magnet System	880	49%
Vacuum Vessel	196	96%
Blanket	192	45%
Blanket & VV	388	61%
Divertor	119	54%
Fueling System	24	92%
Machine Assembly & Tooling	84	64%
Remote Handling Equipment	120	67%
Cryostat & Thermal Shields	81	56%
Tokamak Cooling Water System	110	51%
Vacuum Pumping & Leak Detection System	49	72%
Tritium Plant	51	65%
Cryoplant & Cryodistribution	94	65%
Coil Power Supply System	177	55%
Steady-State Power Supply System	47	63%
CODAC	51	100%
Main Tokamak Systems Total	2274	56%

Table I.4.1-4 Cost of Buildings, Site Facilities, and Balance of Plant

	ITER-FEAT	
	kIUA	% of 1998
Tokamak Buildings	153.1	51%
Hot Cell Building	20.3	18%
Tokamak Services Buildings	0.0	0%
Auxiliary Buildings	21.9	52%
Personnel Building	3.7	58%
Radwaste Building	4.2	55%
Laboratory Office Building	10.1	61%
Cryoplant Buildings	24.2	64%
Control Building	7.7	100%
Emergency Power Supply Building	10.2	53%
Site Services Building	5.8	45%
Poloidal Field Coil Fabrication Building	0.0	0%
Utility Tunnels & Site Improvements	53.5	52%
Engineering, management, other	61.5	63%
Buildings and Site Facilities	376.1	47%
Hot Cell Processing and Waste Treatment	45.7	52%
Heat Rejection System	34.0	53%
Liquid Distribution System	31.3	54%
Gas Distribution & Compressors	7.7	54%
Radiological Protection	3.8	60%
Plant Sampling System	4.0	100%
Balance Of Plant	80.8	55%
Total Buildings, Facilities, Balance of Plant	502.6	49%

Table I.4.1-5 Cost of Auxiliary Heating and Current Drive Systems

	ITER-FEAT	
	kIUA	% of 1998
IC Aux. H&CD System for 20 MW (one port)	25.5	27%
Antenna Arrays & Transmission Lines	8.2	31%
Main Transmission Lines	1.4	25%
Matching & Decoupling System	2.5	25%
Power Sources	13.5	25%
System Power Supplies	10.1	49%
Pumping System*	0.3	26%
Total	36.0	31%
EC Aux. H&CD System for 20 MW	72.1	51%
Launch Structure (1 equatorial + 2 upper ports)	19.6	92%
Transmission System	22.0	45%
Gyrotron Sources & Auxiliaries	30.5	42%
System Power Supplies	12.6	48%
Pumping System*	3.5	100%
Total	88.2	51%
NB H&CD System for 33 MW (2 beams)	42.3	66%
Beam Source	12.2	62%
Beam Line Components	6.5	69%
Vessels, Drift Duct, Magnetic Shielding	13.0	73%
Active Correction Compensation Coils	3.0	47%
Engineering Support & Assembly	7.6	69%
System Power Supplies	66.7	70%
Pumping System*	5.9	71%
Special RH Equipment*	4.8	80%
Special Cooling Loops*	8.5	79%
Special Vacuum Vessel Ports*	4.5	86%
Total	132.7	70%

* covered already in Table I.4.1-3

Table I.4.1-6 Cost of Diagnostic Systems

Diagnostic Systems	Industry cost (kIUA)	HT PPY*
Magnetics	3.8	5.1
Neutrons	27.4	31.4
Optical	35.2	46
Bolometry	8.3	6.3
Spectroscopy	31.2	46.4
Microwave	24.8	47.4
Operational	13.3	19.6
DNB	30	0
Generic (Diagnostic blocks, structures, windows etc.)	49.2	0
Credit for some new concept systems not maturing	-8.3	-12.6
Total	215	189

* costs not included in diagnostic system estimate

Table I.4.1-7 ITER-FEAT Yearly Operation Costs (10 year average)

Operation Cost Categories	kIUA/year	% of Total
Project Personnel	60	33%
Electricity	25	14%
Tritium Consumption	5	3%
Capital Improvements, Maintenance, Spare Parts	90	50%
Average Yearly Operation Cost	180	100%
% of FDR	51%	

Table I.4.1-8 ITER-FEAT Decommissioning Cost

Parameters/Items	ITER-FEAT	ITER 1998
Total Manpower, man-years	1023	2500
Unit cost of Manpower, IUA/year	90	90
Cost of Manpower, kIUA	92	225
Cost of Additional Equipment, kIUA	75	75
Total Decommissioning Costs, kIUA	167	300
Percent of ITER 1998 design	56%	100%

I.4.2 Schedule

I.4.2.1 Introduction

The various stages of ITER including procurement and assembly, commissioning, operation and decommissioning have been planned in outline and are described below. The overall project plan is composed of an eight year construction phase including the commissioning necessary for the first hydrogen plasma discharge, followed by approximately 20 years of machine operation (see I.1). For illustrative purposes this operation is divided into four phases: two and half years of hydrogen plasma operation, one and a half years of D operation, 3 years of DT operation at low neutron fluence, and for the remaining time a higher neutron fluence DT operation. There may be a one to two year machine modification phase before starting the second DT phase in which the outboard shield blanket can be replaced with a breeding blanket. A three year de-activation phase follows after twenty years of operation. The ITER organization has the responsibility for the ITER facility up to the end of this phase. The ITER facility is then handed over to an organization inside the Host Party for dismantling and disposal processes.

I.4.2.2 Construction Schedule

I.4.2.2.1 Initial and Background Conditions

It is assumed that:

- an appropriate level of detailed design has been done during the EDA including the extension period;
- the appropriate ITER organization is established when the Construction Agreement is signed;
- the formal regulatory procedure for licensing the construction and operation of ITER is started immediately after the agreement with the new ITER organization; technical understanding on all issues will have been achieved beforehand.

The regulatory approval process largely depends on which Host Party is selected. This will remain speculative until a site is formally selected. The start of the actual construction on the site depends upon when a site license or construction license is issued by the regulatory authority of the Host Party. Therefore, the dates in the construction schedule are measured in months from a start date (" $T = 0$ ") defined as the date at which the actual construction work of excavation for the tokamak building is started, immediately after the site license or construction license is issued. Documents required for the formal regulatory process are prepared by the Host Party to allow the regulatory process to start immediately after the signing of the Construction Agreement.

Furthermore, the following assumptions pertain at $T = 0$:

- preparations of contracts of equipment/material for the longest lead items and critical buildings are complete so as to permit the placing of critical contracts at the appropriate times;
- site preparation has been started earlier by the Host Party, and at $T = 0$ the excavation work on-site can start immediately.

I.4.2.2.2 Procurement Strategy

The lead-times for the different components of ITER vary widely. Therefore, it is assumed that systems/components which are identified to be on the critical path are delivered just in time (but with adequate time reserve) for assembly, and that installation/construction is carried out in accordance with the construction schedule. The policy also includes phased construction as much as possible without affecting the overall schedule, in order to ease the planning and cash flow. Documentation required for specifying the various procurements is assumed to be completed in time for scheduled procurement. A procurement bid cycle typically takes six to twelve months from the initiation of industrial consultations to the placement of the purchase order.

Procurement of Buildings

This is the first critical item to be procured for the project. It is assumed that the contract order will include the detailed construction drawings and process planning for all buildings. The tokamak building and the PF fabrication buildings (the latter will be converted to the two cryopant buildings later) are the most critical for the overall ITER construction.

Procurement of superconductor

One of the most critical items regarding schedule is the production of superconducting strand to meet the TF, CS and PF Coil fabrication schedule. The purchase order for the conductors must be awarded within a couple of months following $T = 0$. About 480 t of Nb_3Sn superconducting strand are required for the TF coils and CS and must be produced by month 42, an average production rate of about approximately 160 t per year for three years. 240 t of NbTi strand for the PF coils have to be produced by month 36, an average production rate of 120 t per year for about two years.

Procurement of TF coils

The procurement of TF coils is also critical. A prototype is manufactured to confirm each step of the fabrication process prior to the fabrication of the 18 TF coils. This prototype will be a reserve for the replacement of any other (i.e. a 19th TF coil). Fabrication of two TF coils in parallel starts at month 30 and takes initially 15 months. In order to meet the TF/VV pre-assembly schedule, the last two TF coils have to be fabricated in 13 months.

PF coil site fabrication

Because of their large size, four of six PF coils are assumed to be manufactured at the site. Two cryopant buildings are used temporarily for the PF coil fabrication. The fabrication of these four PF coils has to be completed by month 48 in order to start the conversion of the buildings for the cryopant facilities no later than a beginning of the fifth year. Therefore, the cryopant buildings have to be constructed immediately starting at $T = 0$ and completed by month 18. Installation and commissioning of winding tools takes place for about six to eight months and actual fabrication is completed in two years. The two lower PF coils are placed at the bottom of the cryostat at the beginning of the tokamak assembly. Another two are stored at the site until they are needed. The two smallest PF coils may be fabricated at the factory and transferred to the site.

I.4.2.2.3 Construction of the Tokamak Building and Assembly

The overall construction schedule that leads to the first hydrogen plasma operation is shown in Figure I.4.2-1. This reference plan, provides the schedule of procurement, construction, assembly and commissioning of ITER, based on the assumptions discussed above. The schedule can be summarized as four years for the building of the Tokamak Building, three years for tokamak assembly and one year for start-up commissioning.

Tokamak Building

The excavation of the tokamak building is started immediately at $T = 0$ and completed within 9 months. The tokamak building must be functional including cranes and the HVAC system by month 45 in order to start the tokamak assembly activities.

Tokamak Assembly

Tokamak assembly (see II.9) starts with the lower cryostat activities to install the lower cryostat lid, lower cryostat cylinder and TF coil supports etc in the pit. At same time, the pre-assembly of the VV sector, TF coils and thermal shield starts in the assembly hall. The first 40° VV/TF/TS sector is installed in the pit at $T = 50$. The other milestones are:

- Complete VV torus: month 73
- Complete ex-vessel assembly and close cryostat lid: month 82
- Complete in-vessel component installation and close VV: month 85.

Leak and pressure tests of each component and pipe are completed before closing the cryostat and vacuum vessel.

I.4.2.2.4 Commissioning for the First Hydrogen Plasma Discharge

About one year of integrated commissioning includes vacuum pumping for a few months and discharge cleaning for a few weeks, before the first plasma discharge. All systems, including in-vessel viewing system and additional heating and current drive system, are tested to the extent possible without plasma. This includes major activities such as:

- (1) vacuum leak and pressure test of VV and cryostat;
- (2) hydraulic and baking test;
- (3) magnet cooldown test with cryogenic system;
- (4) magnet excitation test with coil power supplies;
- (5) discharge cleaning test without plasma;
- (6) fuelling test;
- (7) EC start-up system and additional heating system test.

The integrated commissioning starts at month 86 and is completed at month 96. The first hydrogen plasma discharge is achieved at the end of month 96, 8 years after the start of construction.

Some subsystems may be completed later if they are not needed during H operation and if their installation and/or commissioning can be done in parallel with H operation. For example, the tritium system, water detritiation system, and radioactive material storage, are

not needed during H operation and will be installed in parallel, and the full performance of the cryogenic system and of the water cooling system is not needed. Conditioning for full output power of the heating and current drive system may not be finished. Calibration of the neutron diagnostics will be done later.

I.4.2.2.5 Critical path

The critical path is the longest chain of linked sequential activities, from start to finish, that controls the overall project schedule. The critical path will most probably begin with:

- 1) the setting up of a new organisation after the ITER Construction Agreement is signed;
- 2) the procedure to establish the procurement contract for the first purchase;
- 3) the licensing process.

It is assumed that these three processes will be consistent with the required time scale. Once the tokamak building is available, the critical path always involves the magnet fabrication and assembly and then the installation of the in-vessel components until the start of integrated commissioning.

I.4.2.3 Operation Plan

I.4.2.3.1 General Considerations

As a plasma experimental facility, operation starts from the first plasma with hydrogen. The ITER machine will then be fully commissioned and operated at full plasma current and the full heating power with H plasma discharges. At this time, operating with D plasma discharges with limited tritium, will allow all components and processes to be commissioned ready to work with tritium and with neutron irradiation, before the full deuterium-tritium operation starts to develop high-Q inductive, non-inductive and highly reliable operations suitable for blanket testing.

It is expected to make optimum use of the ITER machine by:

- participation in the experiment by remote sites;
- continuous operation, i.e. 3 shifts - 24 hours/day;
- long operation cycle and a relatively long break, e.g. 10 days of continuous operation and 1 week break;
- a few months break per year for maintenance, further installation and commissioning.

Operation over the first 10 years is illustrated in Figure I.4.2-2.

I.4.2.3.2 Hydrogen Phase (H phase)

In this phase, no fusion reactions occur, and ITER in-vessel components are not activated and are not contaminated by tritium. ITER will be commissioned with tokamak discharges with the same electromagnetic characteristics as for active operation.

By the end of the H phase, the nominal plasma current will have been achieved at the maximum toroidal magnetic field and with about 70 MW of external heating power with a flat top duration of about one hundred seconds. The plasma scenario and its control in normal and off-normal conditions will have been established. The heat flux on the limiter and the peak heat flux on the divertor target will be in the same range of average values as for the

reference operation for the DT phase. Depending on plasma confinement characteristics with hydrogen (achievement of good H-mode at sufficiently large densities), many features of the future operation of DT can be explored. Therefore, the duration of this period may be lengthened if optimistic results are achieved.

I.4.2.3.3 Deuterium Phase with Limited Tritium Use (D phase)

The main purpose of this phase is to assess the mass scalings of performance, by comparison with H operation, and more accurately predict performance with DT, taking any necessary steps to correct or improve plasma control in preparation for full DT operation. By using limited amounts of tritium in a deuterium plasma, the integrated ITER system can be commissioned, especially with regard to shielding performance, including:

- "nuclear commissioning" of the machine with D(T) plasma, including check and calibration of nuclear diagnostics, shielding test and radiation monitoring;
- research confirming operation with D(T) plasma, albeit for short pulses.

Characteristics of D plasma behaviour are expected to be very similar to that of DT even if the alpha heating power is much less than the external heating power. Therefore, the reference plasma operational scenario including L-mode to H-mode transition, very short burn, demonstration of ELMy H-mode for a long period and plasma termination may be confirmed in this phase. The tritium balance can also be studied, and no vacuum vent is planned.

I.4.2.3.4 Deuterium-Tritium Plasma Phases

Initially, physics studies will be done gradually by increasing and optimising the plasma operation space, especially by developing reference scenarios for inductive and non-inductive operations. After developing reliable operation scenarios, series of pulses repeated continuously for a few days are planned mainly for engineering tests particularly relevant to breeding blanket test modules. The neutron fluence at the end of this ~ 6 year phase will be typically ~ 0.1 MWam⁻².

A detailed operational plan for a second DT phase beyond the first ten years of operation has not been developed because it will depend on the plasma performance and operating experience obtained in the first DT phase. However, it is foreseen that there will be more emphasis on the optimization of performances and reliable operation to produce higher neutron fluxes and fluence, using the most promising operational modes developed in the previous phase. It is planned to reach an average neutron fluence on the first wall of at least 0.3 MWam⁻² by the end of the 20 year operation program.

I.4.2.3.5 Tritium Supply

During the first ten years of ITER operation, the equivalent total burn duration at 500 MW is planned to be about 0.15 years or the total equivalent number of pulses is 11,800 at 500 MW. The net consumption of tritium with 500 MW and 400 s burn is about 0.4 g including heating-up and cool-down phases, and the total consumption during the first ten years is about 5 kg. To achieve the reference average neutron fluence on the first wall of 0.3 MWa/m², a total net burn duration of 0.53 years at 500 MW of fusion power is needed, and about an additional 10 kg will be consumed. This tritium can be supplied by external

sources, and would be reduced further if a breeding blanket is installed on the vessel outboard wall.

I.4.2.3.6 Tritium Breeding Blanket Test Program

ITER should (see I.1.2) "test tritium breeding blanket concepts that would lead in a future fusion reactor to tritium self-sufficiency, the extraction of high-grade heat, and electricity generation." To achieve this testing, the ITER Parties will provide specific modules of their own design to be introduced in a few ITER equatorial ports. A common test blanket program will be established with the participation of the ITER Central Team. It is intended to achieve the following main objectives:

- 1) demonstrate tritium breeding performance and verify on-line tritium recovery and control systems;
- 2) demonstrate high-grade heat extraction suitable for electricity generation;
- 3) validate and calibrate the design tools and the database used in the blanket design process including neutronics, electromagnetic, heat transfer, and hydraulics;
- 4) demonstrate the integral performance of blanket systems under different loading conditions;
- 5) observe possible irradiation effects on the performance of the blanket modules.

The test program requires installing the test blanket modules before DT operation. The test plan during the first years of DT operation will be integrated with the aims of the physics programme, with emphasis on test campaigns of repetitive pulses, dedicated to functional blanket tests. Based on these experiments, and after appropriate improvements of the modules or their related auxiliaries, more intensive tests can be done in the second DT phase.

(N 94 GR 1 99-11-26 F1)

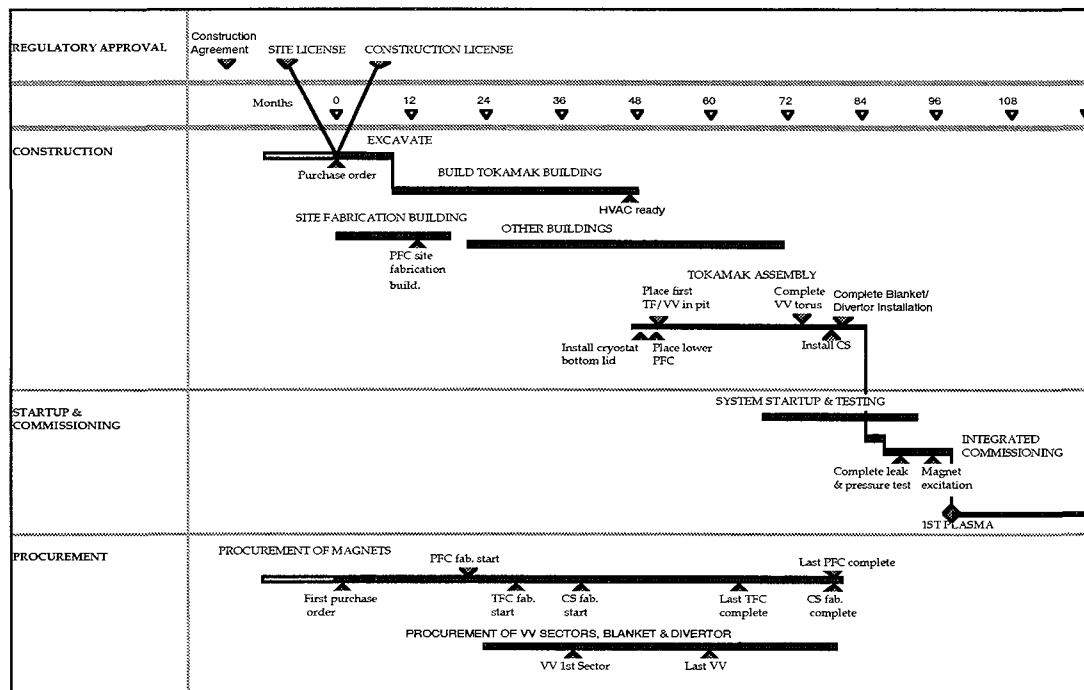
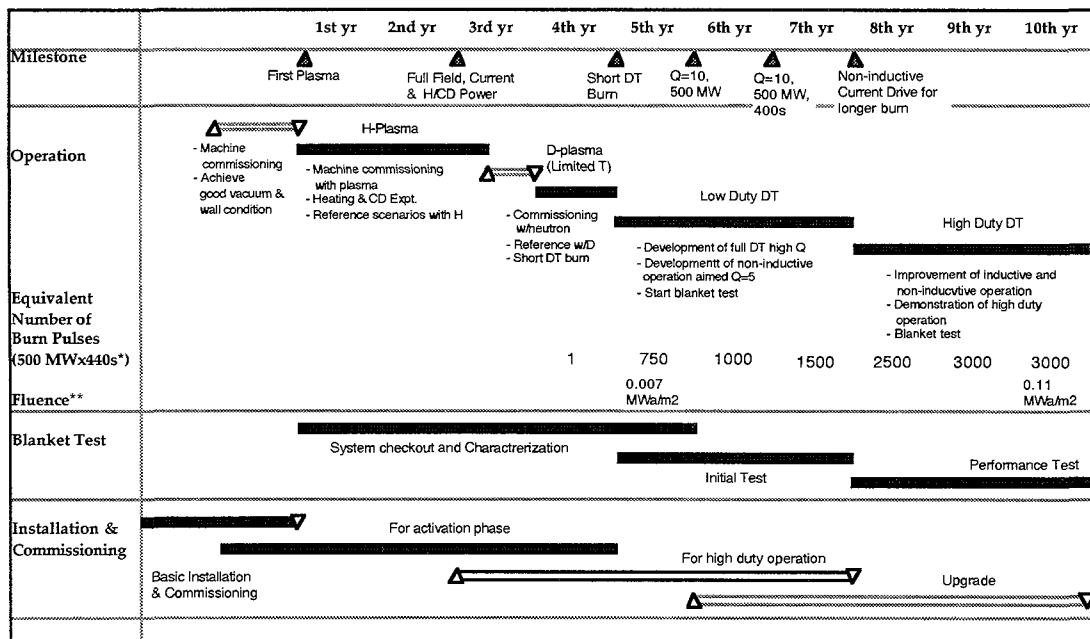


Figure I.4.2-1 ITER-FEAT Construction Schedule



* The burn time of 400 sec includes 400 sec flat top and equivalent time which additional flux is counted during ramp-up and ramp-down.
 ** Fluence at outboard midplane (Neutron wall load is 0.57 MW/m² in average, 0.65 MW/m² at outboard and 0.41 MW/m² at in board.)

Figure I.4.2-2 ITER-FEAT Operation Plan for the First Ten Years

I.4.2.4 ITER Decommissioning Plan

I.4.2.4.1 General policy and assumptions

It is assumed that the ITER organization at the end of operation will be responsible for starting the machine decommissioning through a de-activation period after which the facility will be handed over to a new organization inside the ITER Host Country. It is therefore necessary to provide a feasible and flexible plan for the decommissioning of the ITER machine and associated active components. The plan is based on a logic of resources and equipment usage optimization, and takes into account the statutory Occupational Radiological Exposure (ORE) limits. The plan provides a framework to help the organization decide when and how to implement the ITER facility dismantling, depending on the financial, schedule, resources and/or any other priorities applicable at the time. Flexibility is provided by the use of two separate phases. Each phase duration and activity can be modified (to a certain extent) to accommodate the organization requirements and constraints.

During the first phase, the machine will, immediately after shutdown, be de-activated and cleaned by removing tritium from the in-vessel components and any removable dust. Also, any liquid used in the ITER machine systems will be removed (assuming that no component cooling will be further required) and processed to remove activation products prior to their disposal. De-activation will include the removal and safe disposal of all the in-vessel components and, possibly, the ex-vessel components. ITER de-activation will also provide corrosion protection for components, which are vulnerable to corrosion during the storage and dismantling period, if such corrosion would lead to a spread of contamination, or present unacceptable hazards to the public or workers. These activities, part of phase 1 of the decommissioning schedule, will be carried out by the ITER organization using the remote handling facilities and staff existing at the end of the project. At the end of phase 1, the ITER facility will be handed over to the organization inside the Host Country that will be responsible for the subsequent phase of decommissioning, after a dormant period for radioactive decay.

The proposed decommissioning plan takes into account the impact of essential drivers like the availability of equipment, facilities, staff, etc., and basic constraints like activation decay time. The proposed plan:

- 1 allows the maximization of the use of existing facilities and equipment while taking advantage of the experience and knowledge of the site personnel and equipment availability at the end of ITER operation;
- 2 reduces capital investment required for new equipment and facilities procurement required in the later stages of the decommissioning;
- 3 allows to choose between two decommissioning strategies by offering the following options for dismantling of most ex-vessel components:
 - Option 1 = early dismantling of most ex-vessel components during the de-activation phase;

- Option 2 = postpone until after the decay period the expenditure required for the dismantling of ex-vessel components.

The plan does not include the dismantling of the buildings and of the non-active components (except, when applicable, for the ex-vessel components), or the disposal of wastes from decommissioning.

I.4.2.4.2 Decommissioning Schedule

The proposed decommissioning scenario is broken down into its two main phases as follows:

PHASE	ACTIVITY	DESCRIPTION	DURATION
1	De-activation	a) Removal of mobilizable tritium and dust from the machine using available techniques and equipment Removal and de-activation of coolants. b) Classification and packaging of active, contaminated and toxic material. c) Removal of all the in-vessel components. OPTION 1: removal of ex-vessel components (if not done in phase 2).	3 years
The ITER facility is handed over to an organization inside the host country			
Radioactivity decay period		a) The vacuum vessel radioactivity is left to decay to a level which allows extraction of vessel sectors into the tokamak building (during phase 2) for size reduction and disposal. b) No site activities are required except security and monitoring.	As required
PHASE	ACTIVITY	DESCRIPTION	DURATION
2	Final Dismantling & Disposal	a) Removal of vacuum vessel sectors and their size reduction by remote/semi-remote operations. OPTION 2: removal of ex-vessel components (if not done in phase 1) b) Classification and packaging of active, contaminated and toxic material	~ 6 years

Table I.4.2-1 Summary of the ITER decommissioning plan

II DESIGN DESCRIPTION AND ANALYSIS

II.1 Magnet System

II.1.1	PF Magnetic Configuration, Scenario and Plasma Current, Position and Shape Control	2
II.1.1.1	Introduction	2
II.1.1.2	PF Magnetic Configuration and Scenario	2
II.1.1.2.1	Nominal Magnetic Configuration	2
II.1.1.2.2	Plasma Current Ramp-up in the Nominal Scenario	3
II.1.1.2.3	Scenario with High Plasma Current	4
II.1.1.2.4	Magnetic Configuration with Reversed Shear	4
II.1.1.2.5	Toroidal Field Ripple	5
II.1.1.3	Plasma Current, Position and Shape Control	5
II.1.1.3.1	Passive Stabilization	5
II.1.1.3.2	Active Stabilization and Feedback Control	6
II.1.1.4	Conclusions	8
II.1.2	Coil Power Supply and Distribution System	15
II.1.3	Magnets and Structures	16
II.1.3.1	Main Parameters and General Description	16
II.1.3.2	Design Description of the TF Coils and Structures and Gravity Supports	19
II.1.3.2.1	TF Coil Cases	19
II.1.3.2.2	Structures	20
II.1.3.2.3	TF Winding Pack	21
II.1.3.2.4	Gravity Supports	24
II.1.3.3	Design Description of the Central Solenoid	24
II.1.3.3.1	General Design	24
II.1.3.3.2	Flux Optimization and Peak Field	25
II.1.3.3.3	Conductor Jacket Options	25
II.1.3.3.4	Winding design	26
II.1.3.4	Design Description of the PF Coils	27
II.1.3.4.1	General Design	27
II.1.3.4.2	Redundancy and Maintenance Philosophy	27
II.1.3.5	Conductor Design	28
II.1.3.5.1	TF Conductor	28
II.1.3.5.2	CS Conductor	30
II.1.3.5.3	PF Conductors	31
II.1.3.6	Joint Design	33
II.1.3.7	Structural Design and Analysis	34
II.1.3.7.1	Structural Design Criteria	34
II.1.3.7.2	Inboard Leg	35
II.1.3.7.3	Inboard Curved Regions	36
II.1.3.7.4	Outer Intercoil Structures (OIS)	37
II.1.3.8	Design Assessment and Conclusions	37
II.1.4	Cryoplant and Cryodistribution	39
II.1.4.1	Refrigeration and Liquefaction Requirements for the LHe Plant	39
II.1.4.2	Design of the LHe Plant	40
II.1.4.3	Design of the He Gas Cooling Loop of the 80K Thermal Shields and LN ₂ Subsystem	40
II.1.4.4	Cryodistribution Design	41
II.1.4.5	Assessment	41

II.1.1 PF Magnetic Configuration, Scenario and Plasma Current, Position and Shape Control

II.1.1.1 Introduction

High plasma elongation and triangularity exert a considerable influence on vertical stabilization. The magnetic configuration and the electrically conducting structures (vacuum vessel) need to be considered simultaneously to assess all electromagnetic aspects. An extensive parametric study has been done in which the use of external coils or of internal coils was considered for active control¹. The degree of symmetry of the configuration has been clarified and the importance of toroidally continuous rings, supporting the blanket modules near the divertor, has been established².

Further work has been carried out with increasing elongation. It was concluded that a machine using external coils for active control could be feasible with $\kappa_{95} = 1.70$.

II.1.1.2 PF Magnetic Configuration and Scenario

II.1.1.2.1 Nominal Magnetic Configuration

The nominal inductive scenario of ITER-FEAT is characterized, during flat-top, by the following parameters: $I_p = 15$ MA, $B_{tor} = 5.3$ T, $R = 6.2$ m, $a = 2$ m, $\kappa_{95} = 1.70$, $\delta_{95} = 0.33$, $q_{95} = 3.0$. To achieve such performance the magnetic configuration requires a segmented central solenoid (CS) and six poloidal field (PF) coils, as shown in Figure II.1.1-1a. The main parameters of the CS and PF coils are given in Table II.1.1-1.

The following key points of the scenario were studied: the initial magnetization (IM) of the PF system, the start-of-flat-top state (SOF), the start-of-burn (SOB) and the end-of-burn (EOB). Three values of I_i are considered in the study of the plasma equilibria at SOF, SOB and EOB: 0.7, 0.85 (reference value), 1.0. The value of β_p is considered 0.1 at SOF and 0.85 at SOB, EOB (which corresponds to a β_N of about 2.3).

The CS has six modules³. All CS modules and PF coils have independent power supplies, except the two central CS modules (CSL1 and CSL2) which are connected in series. The CS is designed to have a maximum value of the magnetic field (13.5 T) at IM. The maximum value of the current in the CS modules (shown in Table II.1.1-1) can be achieved at a magnetic field not higher than 12.8 T. The separation force between the CS modules is designed not to exceed 75 MN. The magnetic field on the PF coils is designed not to exceed 6 T on PF1 and PF6 and 5 T on the other PF coils. The maximum currents in the PF coils have been identified considering all the equilibria mentioned above.

The breakdown region is defined as a circle with minor radius 0.8 m, the centre of which is located at $R = 7.48$ m and $Z = 0.33$ m. The magnetic flux in the centre of the breakdown

¹ A. Portone, "Effects of Plasma Elongation on Vertical Stabilization Parameters," JCT Internal Report N 47 RI 29 99-05-14 F 1, 14 May 1999

² Report of the "Concept Improvement Task Force": Section IV.4

³ G A0 RI 1 99-02-12 W0.2, Study of Options for the Reduced Technical Objectives/Reduced Cost (RTO/RC) ITER, Section II.1.1

region is maximized at IM, keeping the value of magnetic field on the CS modules not higher than 13.5 T and the stray magnetic field in the breakdown region not higher than 2 mT. The maximum value of the flux (119 Wb) is achieved with uniform distribution of current along the height of the CS. The stray fields, in the plasma region, are within the specified limits.

The following limitations are applied to the separatrices in the I_i operational range:

- the deviation of all separatrices from the reference separatrix should be not larger than ± 60 mm in the divertor region and not larger than ± 30 mm near the limiter;
- the distance between the inner and outer separatrix (Δ_{sep}), at the equatorial plane, on the outboard side, should not be smaller than 40 mm;
- clearance between the flux surface 4 cm from the separatrix at the outboard plasma equator and the first wall should not be smaller than 8 cm.

The following assumptions on the flux losses are used to define the SOF and SOB flux states: the flux loss at breakdown is 10 Wb, the Ejima coefficient at SOF is 0.45, the resistive flux consumption, during the heating phase (SOF \Rightarrow SOB), is 10 Wb. The EOB state is defined as the state when the currents in the CS modules reach their maximum values specified in Table II.1.1-1, and/or the magnetic field on the CS modules reaches 12.8 T.

The main plasma parameters calculated for the operational I_i range are summarized in Table II.1.1-2. The separatrices overlay is shown in Figure II.1.1-1b. The reference separatrix (SOB at $I_i = 0.85$) has elongation 1.85 and triangularity 0.49. The deviation of all separatrices relative to the reference separatrix is within the specified limits. The distance between the inner and outer separatrix in all equilibria, except of EOB high I_i , is larger than 40 mm. About 30 Wb of flux are available for the driven burn of the reference plasma. All PF coil currents, magnetic fields on the coils and forces are within the specified limits.

A magnetic configuration with the CS capable of operating at a magnetic field of 14 T at the IM and at 13.3 T at the EOB has also been studied following the same approach and allowing the same plasma shaping capability as described above. The 14 T configuration provides more magnetic flux for the driven burn: 35.4 Wb for $I_i = 0.7$, 33.8 Wb for $I_i = 0.85$ and 19.4 Wb for $I_i = 1.0$.

II.1.1.2.2 Plasma Current Ramp-up in the Nominal Scenario

The plasma current ramp-up of the nominal scenario has been studied as a sequence of equilibrium snapshots. The current ramp-up phase starts from about 0.4 MA. By the end of this phase (at SOF) a full-size diverted plasma with the nominal 15 MA current is obtained.

Up to 7.5 MA (50% of the nominal current), the plasma touches the central part of the limiter ($R = 8.28$ m, $Z \approx 0.33$ m). During this limiter phase the PF system provides the expansion of the plasma cross-section to keep the edge safety factor roughly constant ($q_a \approx 4.8$). The plasma elongation and triangularity rise approximately linearly with the current rise. At 7.5 MA, the transition from a limited to a diverted configuration takes place. The plasma current continues to rise in the divertor configuration with minor increases of elongation and of triangularity.

The values of I_i and β_p during the current ramp-up phase are assumed to be constant and equal to 0.85 and 0.1. The plasma resistive flux loss is determined by the Ejima coefficient 0.45.

The evolution of the plasma boundary is shown in Figure II.1.1-2, whereas Figure II.1.1-3 shows the waveforms of the plasma current and of the currents in the PF coils. The plasma current ramp-rate is progressively reduced during the ramp-up, which takes about 100 s.

II.1.1.2.3 Scenario with High Plasma Current

The magnetic configuration described in II.1.1.2.1 and in Table II.1.1-1 can sustain higher plasma current (17.4 MA), corresponding to $q_{95} = 2.6$. The IM state is the same as the nominal scenario, whereas new SOF, SOB and EOB equilibria are obtained having 17.4 MA current flat-top, with $I_i = 0.8$ and with $\beta_p = 0.75$ ($\beta_N \approx 2.33$). During the sustained burn, the flux available is only about 7 Wb.

The high plasma current scenario is more demanding than the nominal scenario. The current in PF6 is in saturation (18.7 MA) in all three states (SOF, SOB and EOB). Currents in the centre CS modules (CS1U and CS1L) are also in saturation at SOF and SOB (24.2 MA), and drop only by 0.1 MA at EOB, when the magnetic field on these modules rises to its maximum level (12.8 T). The separation forces acting on the end CS modules (CS3) reach their limit (75 MN) in all three states.

II.1.1.2.4 Magnetic Configuration with Reversed Shear

The magnetic configuration described in II.1.1.2.1 and in Table II.1.1-1 can sustain, for example, the following reversed shear (RS) scenario. The separatrix, in this case, has to match the reference separatrix only in the divertor region and near IC H&CD antennae and has the following parameters during the quasi-stationary phase: $\kappa_{95} \approx 2$, $\delta_{95} \approx 0.5$, $q_0 \approx 4.5$, $q_{\min} \approx 3.5$ (at $r/a \approx 0.7$), $q_{95} \approx 4.5$, $\beta_N \approx 3.7$, $p_0/\langle p \rangle \approx 2.5$.

The RS scenario comprises the following phases:

- 1 inductive plasma current ramp-up to 5 MA, full aperture, low β plasma;
- 2 transition to high β ($\beta_N \approx 2$) with constant plasma current and with monotonic q -profile, (heating is required);
- 3 transition to high β_p with constant plasma current but with reversed shear (current drive is required);
- 4 transition to high β_p ($\beta_N \approx 3.7$) non-inductive 10 MA plasma current with reversed shear (heating and current drive are required);
- 5 quasi-stationary phase (current drive is required);
- 6 plasma ramp-down.

The following plasma equilibria, corresponding to the key states of the scenario were studied: A - end of the phase 1, B - end of the phase 2, C - end of the phase 3, D - end of the phase 4 (beginning of the quasi-stationary phase).

The main plasma parameters characterizing these four equilibria (A – D) are summarized in Table II.1.1-3. The corresponding separatrices are shown in Figure II.1.1-1c. For comparison, the figure shows also the reference separatrix of the nominal scenario. In the divertor region and near the IC H&CD antennae the difference between the RS separatrices and the reference separatrix is hardly visible.

The distance between the inner and outer separatrix is 40 mm in all equilibria, except for A. About 11 Wb of flux are available for inductive current drive during the quasi-stationary phase (if required). All PF coil currents, magnetic fields on the coils and forces are within the specified limits.

II.1.1.2.5 Toroidal Field Ripple

A detailed study of the toroidal field ripple and of its reduction with ferromagnetic inserts in the vacuum vessel (between the inner and the outer shell) has been carried out in similar geometry to ITER-FEAT¹. The ferromagnetic inserts are located in the “shadow” of the TF coils, in the outer vessel region, from the top to a point between the equatorial and the divertor port ($Z \sim -2.5$ m). The inserts are made of SS430 and their maximum filling factor is 0.8.

The NB ducts reduce the space available for the ferromagnetic inserts near the equatorial plane, and cut-outs are necessary. To avoid error fields and ripple of low “n” modes, the same cut-outs are used near all equatorial ports. Moreover, the blanket cooling channels are taken into account in the analysis. Under these assumptions the maximum value of the ripple on the plasma separatrix is reduced at nominal toroidal field from 1.4% to 0.9% at the separatrix on the outboard equator.

II.1.1.3 Plasma Current, Position and Shape Control

II.1.1.3.1 Passive Stabilization

The vacuum vessel, shown in Figure II.1.1-1, provides the main electrically conducting structure required for plasma passive stabilization. The vessel consists of two shells (inner and outer) in stainless steel ($\rho = 0.85 \mu\Omega \text{ m}$ at 160°C), and each shell is 60 mm thick. Two brackets are attached to the inner shell, as shown in Figure II.1.1-1, to support the blanket modules near the divertor region. Two toroidally continuous rings (SS, 50 mm thick), at the inboard and outboard side, are attached to these brackets. These rings improve the up/down symmetry of the passive structures and reduce the amplitude of the plasma initial displacement and velocity after a plasma disturbance (e.g. minor disruption). Moreover, the rings increase the stability margin.

A 2D model of the vacuum vessel (without ports) has been considered in the PET code: the model has 60 axisymmetric elements. The PET code evaluates the evolution of a free boundary plasma equilibrium in the presence of eddy currents and of currents of the CS and PF coils. Linear non-rigid body plasma models were derived with the PET code and used in the following analyses.

The main indices describing the passive stabilization features of the ITER-FEAT plasmas during the current flat-top of the nominal scenario are reported in Table II.1.1-4. The corresponding plasma equilibrium parameters are listed in Table II.1.1-2. The definitions of the stability margin (m) and participation factors (ξ) are given in ². I_{imb} is the current in the

¹ V. Amoskov et al., “Calculation of the TF Ripple in the ITER/IAM2 Facility”, Efremov Research Institute, November 1999.

² A. Portone, “Stability Margin of Plasma Vertical Instabilities”, JCT Internal Report, Issue 1: 24 March 1999.

VS (vertical stabilisation) converter called the imbalance current (the sum of the currents in PF2-5 coils).

Table II.1.1-4 shows that the minimum stability margin (m) and instability growth time (τ_g) occur, on average, at the SOF state and, in absolute terms, for the SOF, high I_i equilibrium. Such low m and τ_g are due to the increase in the destabilizing force from the equilibrium field necessary to keep approximately the same separatrix elongation despite the peaking of the current density around the magnetic axis. This is evident from the value of the vertical magnetic field decay index N .

The initial plasma current centre vertical displacement and speed after a minor disruption event (see Z_{p0} and dZ_{p0}/dt in Table II.1.1-4) decrease with increasing I_i . This fact helps the control system since it reduces the maximum plasma boundary offsets.

Apart from the SOF, high I_i case, in all the other equilibria analyzed it is possible to achieve $m > 0.5$ and $\tau_g > 100$ ms, which confirms the good stabilization features of the ITER-FEAT vacuum vessel. The SOF, high I_i case is considered too demanding as the basis for the design of the vertical stabilization system. To avoid such a configuration it would be possible to heat the plasma, after X-point formation, during the final phase of the current ramp-up. Alternatively, the SOF, high I_i case could be obtained with smaller elongation.

The effects of the vacuum vessel ports and ports stubs on the plasma vertical instability growth time and stability margin have been studied with a non-rigid plasma model and a 3D model of the vacuum vessel. The preliminary results obtained for the SOF plasma, with $I_i = 0.85$ show a reduction of the instability growth time by 8% and a reduction of the stability margin by 2%.

Other 3D effects are caused by the blanket modules, the TF coil structures, and the inserts (ferromagnetic and non-) between the vacuum vessel shells. No analysis has been done so far for ITER-FEAT. Preliminary estimates gave negligible influence of the blanket modules, of the TF coil outer intercoil structures (OIS) and of the ferromagnetic inserts on the plasma current, position and shape control.

II.1.1.3.2 Active Stabilization and Feedback Control

A feedback controller for the current, position and shape of X-point plasmas has been designed on the basis of the linear, non-rigid body plasma model used in the PET code for the SOF, $I_i = 0.85$ equilibrium (see Table II.1.1-2). The same controller has then been tested on 8 other linear models (also derived with the PET code) which describe the other flat-top equilibria given in Table II.1.1-2.

The controller design aims to:

- stabilize the plasma by derivative control of the plasma current centre vertical offset;
- control the distance between the plasma separatrix and the wall, a distance called in the following “gap”, at the usual six reference points (see Figure II.1.1-4);
- control the plasma current (I_p);
- minimize the steady-state control current demand in the VS converter, shown in Figure II.1.1-5, and in the PF coil circuits.

To achieve the above goals, a two-loop design approach has been followed that relies on the time scale separation between vertical stability (0.5-1s) and shape control (5-10s). The control scheme is shown in Figure II.1.1-5. Its key parameters are as follows:

- the VS converter response to controller command signals is approximated by the transfer function shown in Figure II.1.1-6; the on-load voltage limit of the VS converter is 6 kV;
- the other power supply converters (main converters) respond with the transfer function shown in Figure II.1.1-6; their on-load voltage limit is set at 1.5 kV except for the one driving the CS1U and CS1L coils connected in series, which is set at 3 kV;
- the magnetic diagnostic system is able to provide a continuous time signal (analog) of the plasma current centre vertical speed with the transfer function shown in Figure II.1.1-6 (time constant of 1 ms); the noise affecting the signal has been neglected so far;
- the variations from the equilibrium (pre-programmed values) of the plasma current and of the gaps are assumed to be provided by the magnetic reconstruction with the transfer function shown in Figure II.1.1-6 (time constant of 150 ms); if this is not the case the controller bandwidth is limited by a similar time constant (filtering action in the shape controller).

The selected derivative gain (K_{FAST} in Figure II.1.1-6) is 11.3 kVs/m (voltage/plasma velocity) since such gain maximizes the phase margin at the gain crossover frequency¹. As a consequence this derivative gain has been used in all the simulations.

All these simulations refer to the response to disturbances. In particular, the following cases have been analyzed:

- minor disruption (MD) events at SOF ($\delta I_i = -0.1$), SOB and EOB ($\delta I_i = -0.1$, $\delta \beta_p = -0.2$);
- minor vertical displacement events (minor VDE) at SOF, normalized to 20 mm displacement of the current centre at the moment when feedback is turned on;
- β_p -drop event at SOB and EOB ($\delta \beta_p = -0.2$).

The results are shown in Table II.1.1-5 and Figure II.1.1-7.

As anticipated, by looking at the passive stabilization data, the SOF, $I_i = 1.0$ case can not be included in the range of controllable plasmas since the low phase margin results in a high oscillatory closed-loop response, clearly indicating lack of robust stability.

Good plasma control is achievable for the whole range of flat-top plasmas considered here by using the out-of-vessel PF coils and with no need of copper cladding on the inner vessel shell. Control should still be possible reducing the VS converter on-load voltage from 9 kV² to 6 kV. Moreover, the coils PF2, PF3, PF4 and PF5 should maintain the insulation design for operation of the VS converter up to 9 kV on load³.

Shape control has been studied with both a faster (~ 5 s settling time) and a slower (~ 10 s settling time) controller; only the results with the faster shape controller are reported here.

¹ A. Portone, M. Cavinato "Feedback Control in ITER-FEAT", N 47 RI 34 99-11-10 R 0.1, 10 November 1999

² Report on the "Concept Improvement Task Force": Section IV.3

³ Report of the "Concept Improvement Task Force": Section IV.4

Figure II.1.1-7 shows that about 100 MW are required for the plasma shape control with settling times of about 5 s, whereas about 80 MW are required for vertical stabilization. The voltage and current requirements on all converters are also shown: the maximum variation of the CS and PF coil currents, after all disturbances listed in Table II.1.1-5, are in the range 3 - 13 %. It is not possible to exclude an impact on the coil size (MA_t) at this early phase of the analysis, but this would be for reasons of plasma shape control rather than for reasons of vertical stabilization. The corresponding amplitudes of the gaps deviation¹ are within about ± 100 mm: in particular, gap 3 (located near the limiter) decreases by less than 30 mm and gap 6 (innermost gap) decreases by less than 60 mm. A 200 mm reduction of gap 5 (uppermost gap) corresponds to a 20 mm VDE at SOF with $I_i = 1.0$ which is not part of the operational space.

The total power derivative exceeds the limit of 200 MW/s reported in the site design assumptions (see I.1.4 III C), when the settling time is about 5 s (faster controller). A longer settling time can mitigate this problem. All these aspects will be taken into account in the future when a trade-off in the design of the overall control system is to be done. Power derivatives are likely to be improved, for example, by using voltage rate limiters.

The VS converter imbalance current must avoid large power steps (> 60 MW). With a 6 kV limit in the VS converter, such current should be not larger than 10 kA. This is not strictly true here and, for high β_p , high I_i plasmas $P_{\text{step}} \approx 80$ MW. These steps could be reduced, in principle, either by reducing the imbalance current or by decreasing further the VS maximum voltage. Further work on this subject will clarify if the relevant site assumption has to be increased and by how much.

A parametric study has been carried out² to assess the influence of the time constant in the transfer function of the diagnostic system on plasma vertical stabilization. The plasma state SOF, $I_i = 0.85$ has been considered. The reference controller gain (i.e. 11.3 kVs/m) was used while the diagnostic time constant was varied in the range 1-25 ms. The results show that an increase of the diagnostic time constant up to 5 ms alters the closed loop response in an almost unnoticeable way. At 10 ms some poorly damped oscillations start to be clearly visible, and at 25 ms the closed-loop system corresponding to the SOF equilibrium becomes marginally stable. A direct signal from the flux loops should allow the identification of the plasma vertical velocity without any delay, therefore our assumption of 1 ms time constant³ seems reasonable.

II.1.1.4 Conclusions

About 30 Wb flux are available for the driven burn of the reference plasma (15 MA), but only 7 Wb only are available for driven burn at 17.4 MA current.

¹ A. Portone, M. Cavinato "Feedback Control in ITER-FEAT", N 47 RI 34 99-11-10 R 0.1, 10 November 1999

² A. Portone, "Effect of diagnostic filtering on plasma vertical stabilization in ITER-FEAT", N 47 RI 36 99-11-19 W 0.1, JCT Internal Report, 19 November 1999

³ Study of Options for the Reduced Technical Objectives / Reduced Cost (RTO/RC) ITER, 12 February 1999: Section II. 1.1.

Apart from the SOF, high I_i case, in all the other equilibria analyzed it is possible to achieve $m > 0.5$ and $\tau_g > 100$ ms, which confirms the good (passive) stabilization features of the ITER-FEAT vacuum vessel.

Good plasma control is achievable for the whole range of flat-top plasmas considered here by using the out-of-vessel PF coils and without copper cladding on the inner vessel shell. Control is achieved limiting the VS converter on-load voltage to 6 kV.

Power steps due to the imbalance current of the VS converters are larger than the specified limit (60 MW) even if the VS converter voltage is reduced from 9 kV to 6 kV on load. Further work is needed to confirm this reduction, but it is prudent to design the relevant PF coils for an on-load voltage of the VS converter of 9 kV. It might be necessary to increase the site assumption on the permissible power steps.

Table II.1.1-1 PF Coil Position, Size, Number of Turns, Maximum Current and Magnetic Field

Coil	R_c (m)	Z_c (m)	ΔR (m)	ΔZ (m)	Number of turns	I_{max} (MA)	B_{max} at IM(T)	B_{max} at EOB
CSU3	1.677	4.974	0.765	1.789	486	21.9	13.5	12.8
CSU2	1.677	3.041	0.765	1.977	538	24.2	13.5	12.8
CSU1	1.677	1.014	0.765	1.977	538	24.2	13.5	12.8
CSL1	1.677	-1.014	0.765	1.977	538	24.2	13.5	12.8
CSL2	1.677	-3.041	0.765	1.977	538	24.2	13.5	12.8
CSL3	1.677	-4.974	0.765	1.789	486	21.9	13.5	12.8
PF1	3.880	7.584	1.027	0.974	270	12.2	6.0	6.0
PF2	8.338	6.509	0.703	0.472	94	4.2	5.0	5.0
PF3	12.014	3.055	0.820	1.262	220	8.7	5.0	5.0
PF4	11.955	-2.465	0.703	1.119	164.5	6.3	5.0	5.0
PF5	8.396	-6.748	0.820	0.945	220	9.9	5.0	5.0
PF6	4.273	-7.559	1.813	0.852	416.5	18.7	6.0	6.0

Table II.1.1-2 Plasma Parameters in the Nominal Scenario

State	IM	SOF	SOF	SOF	SOB	SOB	SOB	EOB	EOB	EOB
I_p (MA)		15.00	15.00	15.00	15.00	15.00	15.00	15.00	15.00	15.00
I_i		0.70	0.85	1.00	0.70	0.85	1.00	0.70	0.85	1.00
β_p		0.10	0.10	0.10	0.85	0.85	0.85	0.85	0.85	0.85
q_{axis}		1.50	1.01	1.01	1.40	1.01	0.98	1.40	1.02	0.84
q_{95}		3.00	2.92	2.90	3.04	3.01	3.00	3.04	3.00	2.89
K_{95}		1.75	1.71	1.68	1.73	1.70	1.67	1.72	1.70	1.67
K_{sep}		1.86	1.86	1.85	1.84	1.85	1.84	1.85	1.85	1.83
δ_{95}		0.36	0.33	0.30	0.34	0.33	0.30	0.35	0.32	0.28
δ_{sep}		0.47	0.48	0.48	0.48	0.49	0.48	0.49	0.48	0.47
Δ_{sep} (mm)		92.8	57.1	42.5	74.7	45.4	49.1	52.8	45.4	40.0
ψ_{ext} (Wb)	119.25	-110.6	-110.6	-122.1	-129.8	-129.8	-141.0	-164.0	-159.6	-160.0
$\Delta\psi_{burn}$ (Wb)								34.2	29.8	19.0

Table II.1.1-3 Plasma Parameters in the Scenario with Reversed Shear

State	A	B	C	D (quasi-stationary phase)
$I_p(\text{MA})$	5.000	5.000	5.000	10.156
R/a	3.1	3.1	3.39	3.51
I_i	0.688	0.626	0.363	0.373
β_p	0.100	2.219	2.245	2.077
β_N	0.090	2.000	2.000	3.750
q_{axis}	4.003	3.826	10.084	4.500
q_{min}	4.003	3.826	7.680	3.500
q_{95}	8.713	9.992	9.730	4.500
K_{95}	1.731	1.737	1.899	1.954
δ_{95}	0.354	0.366	0.500	0.500
$\Delta_{\text{sep}}(\text{mm})$	89	40	40	40
$\psi_{\text{ext}}(\text{Wb})$	-55.0	-75.0	-95.0	-115.0

Table II.1.1-4 Passive Stabilization Indices of the ITER FEAT Current Flat-top Equilibria

State	SOF	SOF	SOF	SOB	SOB	SOB	EOB	EOB	EOB
$I_p(\text{MA})$	15.00	15.00	15.00	15.00	15.00	15.00	15.00	15.00	15.00
β_p	0.10	0.10	0.10	0.85	0.85	0.85	0.85	0.85	0.85
I_i	0.70	0.85	1.00	0.70	0.85	1.00	0.70	0.85	1.00
$I_{\text{imb}}(\text{kA})$	2.65	5.78	5.61	11.17	11.76	14.60	7.09	10.61	13.50
N	-1.04	-1.17	-1.29	-0.78	-0.90	-1.01	-0.78	-0.91	-1.01
m	0.63	0.52	0.42	0.92	0.74	0.62	0.90	0.72	0.62
$\tau_g(\text{ms})$	136	105	78	218	159	123	212	154	124
$Z_{p0}(\text{mm})$	-53	-19	-11	-29	-4	-2	-28	-4	-2
$dZ_{p0}/dt(\text{m/s})$	-1.29	-0.77	-0.51	-0.22	-0.29	-0.11	-0.23	-0.26	-0.18
$\xi_{\text{PF}}(\%)$	8	6	4	13	9	6	13	9	7
$\xi_{\text{OR}}(\%)$	7	9	11	7	9	11	7	9	10
$\xi_{\text{IR}}(\%)$	2	2	2	1	1	2	1	1	2
$\xi_{\text{VVi}}(\%)$	54	56	57	50	53	54	50	53	54
$\xi_{\text{VVo}}(\%)$	29	28	26	28	28	27	28	28	27

Table II.1.1-5 Disturbance Analysis Performed and Relative Numbering in Fig. II.1.1-7

Case #	Flux State	Disturbance	l_i	β_p	δl_i	$\delta \beta_p$	$\delta Z_0(m)$
1	SOF	Minor disruption	0.70	0.10	-0.10	0.00	
2	SOF	Minor disruption	0.85	0.10	-0.10	0.00	
3	SOF	Minor disruption	1.00	0.10	-0.10	0.00	
4	SOB	Minor disruption	0.70	0.85	-0.10	-0.20	
5	SOB	Minor disruption	0.85	0.85	-0.10	-0.20	
6	SOB	Minor disruption	1.00	0.85	-0.10	-0.20	
7	EOB	Minor disruption	0.70	0.85	-0.10	-0.20	
8	EOB	Minor disruption	0.85	0.85	-0.10	-0.20	
9	EOB	Minor disruption	1.00	0.85	-0.10	-0.20	
10	SOF	Vertical Displacement	0.70	0.10	0.00	0.00	0.020
11	SOF	Vertical Displacement	0.85	0.10	0.00	0.00	0.020
12	SOF	Vertical Displacement	1.00	0.10	0.00	0.00	0.020
13	SOB	β_p -drop	0.70	0.85	0.00	-0.20	
14	SOB	β_p -drop	0.85	0.85	0.00	-0.20	
15	SOB	β_p -drop	1.00	0.85	0.00	-0.20	
16	EOB	β_p -drop	0.70	0.85	0.00	-0.20	
17	EOB	β_p -drop	0.85	0.85	0.00	-0.20	
18	EOB	β_p -drop	1.00	0.85	0.00	-0.20	

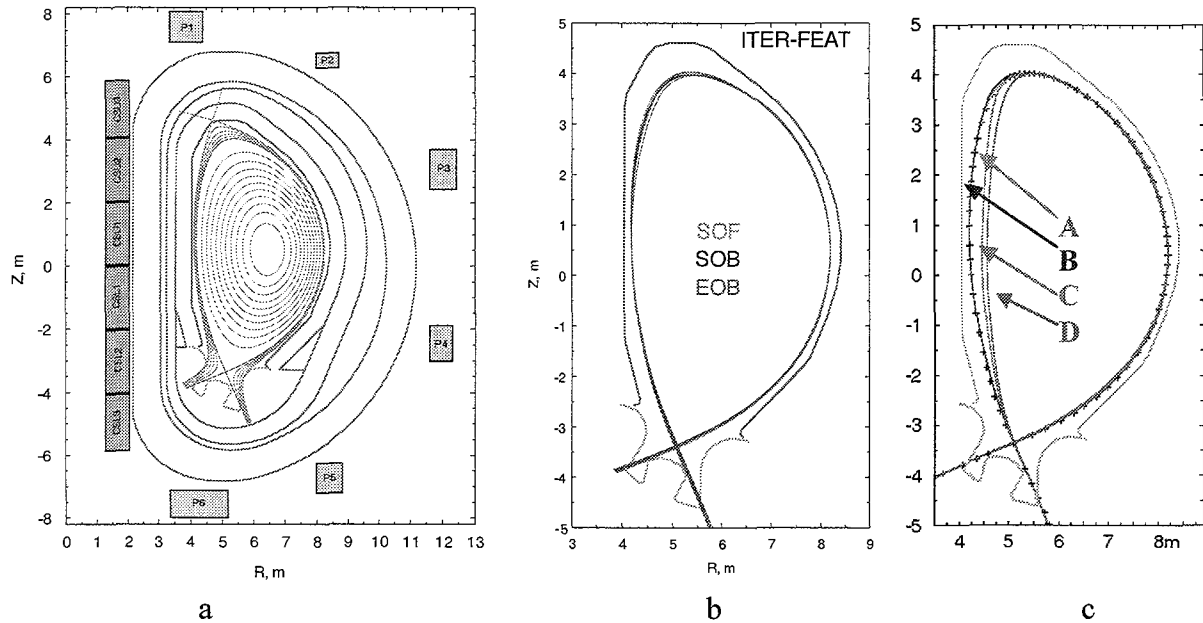
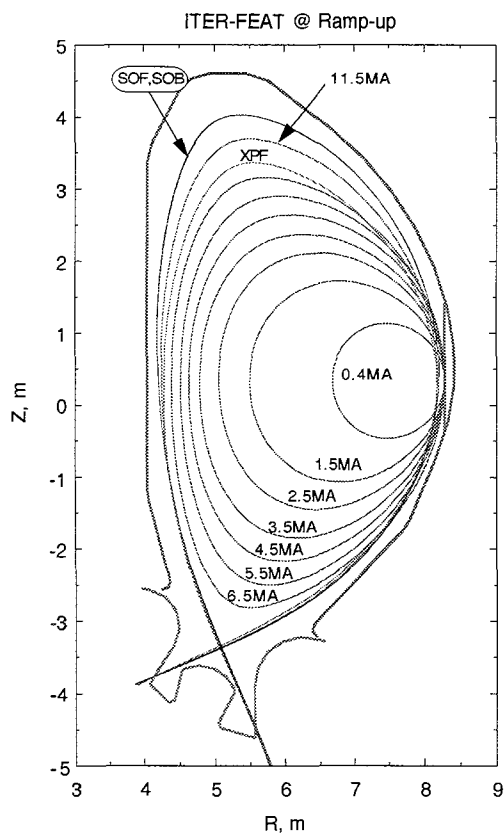
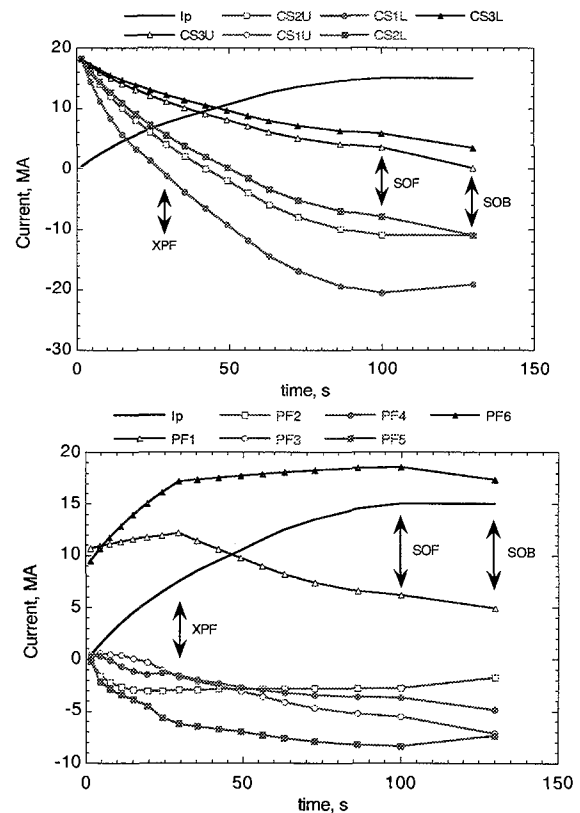


Figure II.1.1-1 a – ITER-FEAT Magnetic Configuration; b – 9 separatrices of the nominal scenario presented in Table II.1.1-2; c – 4 separatrices of the reversed shear scenario presented in Table II.1.1-3 (solid lines) and the reference separatrix of the nominal scenario (crosses)



N 47 GR 4 99-11-18 F 1

Figure II.1.1-2 Evolution of the Plasma Boundary During the Current Ramp-up and Heating Phases



N 47 GR 5 99-11-18 F 1

Figure II.1.1-3 Waveforms of the Plasma and PF Coil Currents During the Current Ramp-up and Heating Phases

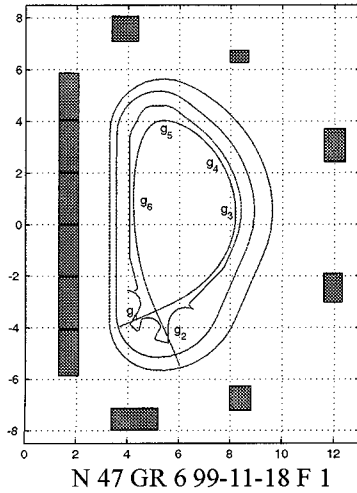


Figure II.1.1-4 Location and Numbering of the Plasma-wall Gaps, which are Controlled

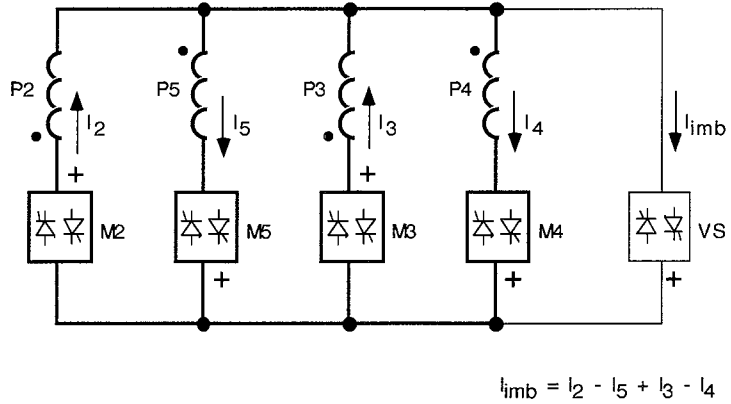


Figure II.1.1-5 Vertical Stabilization circuit

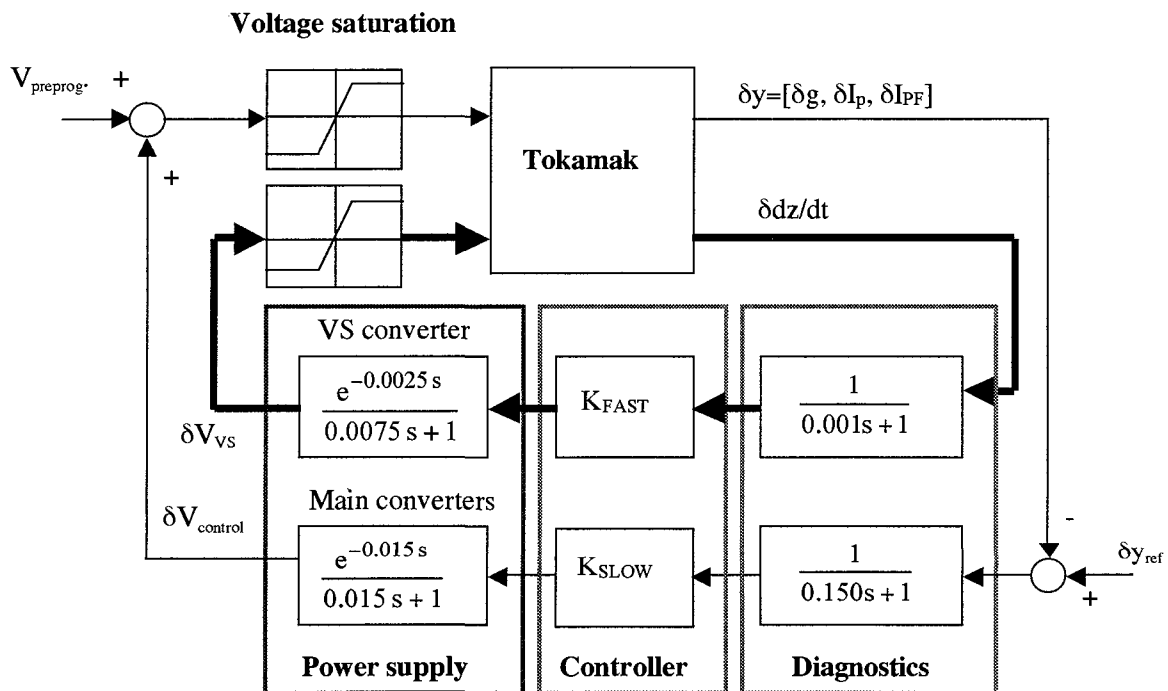
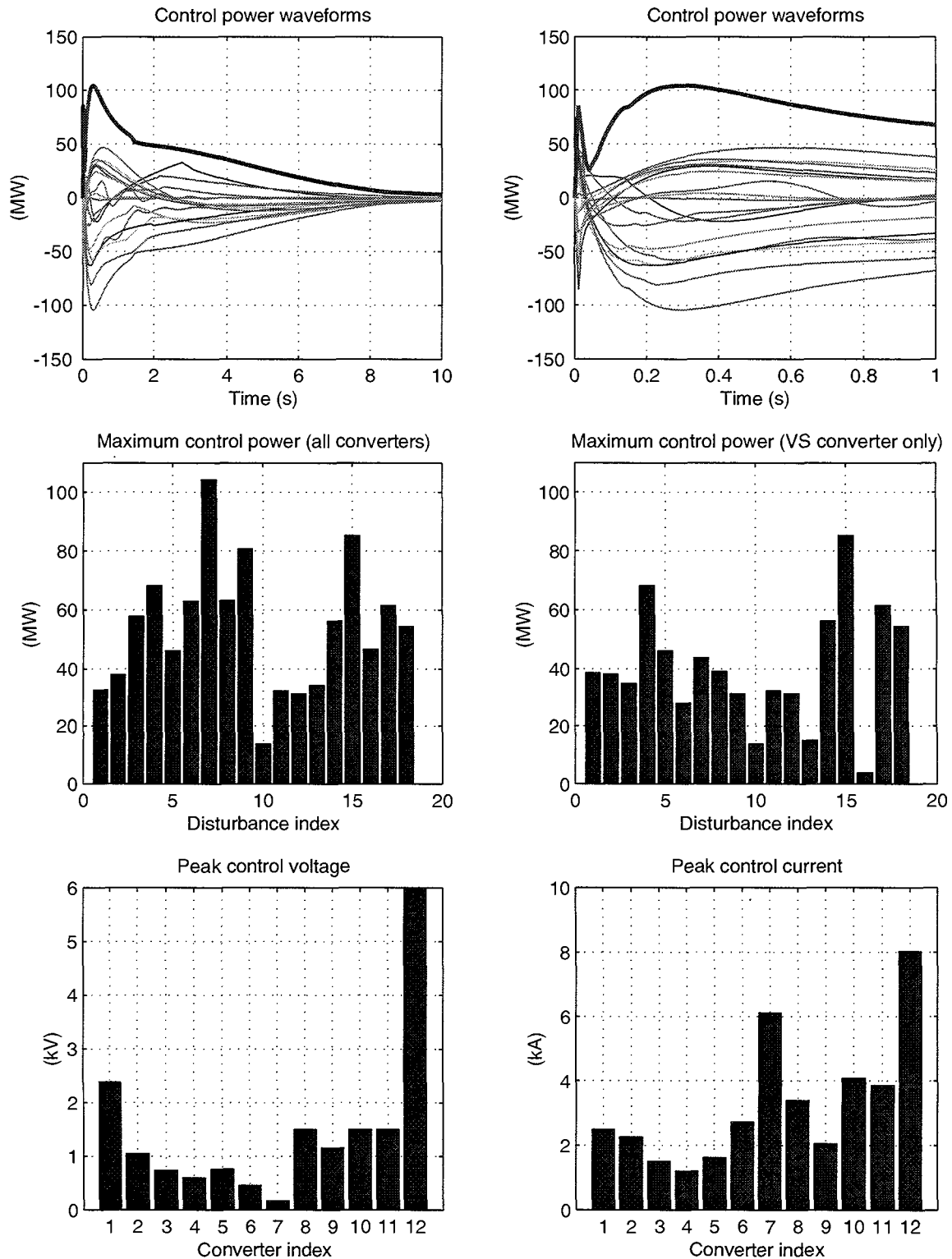


Figure II.1.1-6 Two Loop Control Scheme Adopted (fast loop for vertical stabilization in bold arrows)



N 47 GR 9 99-11-18 F 1

Figure II.1.1-7 Control Power Waveforms (top) and Peaks (centre) Relative to the Disturbances Listed in Table II.1.1-5. The bottom frames show the peak control voltage (left) and current (right) on the main converters (1 through 11) and on the VS converter (index 12). The main converters are identified as follows: index 1 refers to the series CS1U&L, 2 to CS2U, 3 to CS2L, 4 to CS3U and 5 to CS3L. Indices 6 through 11 refer to PF1 through PF6 respectively

II.1.2 Coil Power Supply and Distribution System

The coil power supply and distribution system (CPSDS) consists of a high voltage (HV) substation, AC power distribution system and individual subsystems supplying power to the TF, CS and PF coils, and the correction coils (CCs). The major functions of these subsystems are to provide controlled DC current in the coils and to protect the coils by fast discharge in case of quench.

The basic concepts and design features of the CPSDS¹ are as follows:

- the HV grid available at the ITER site is capable of supplying the pulsed power required by the operating scenario, the plasma current, position and shape control and the heating and current drive systems;
- all TF coils are connected in series and are supplied by a common DC power source; the CS, PF and correction coils are normally supplied by separate power circuits;
- the power needed to charge and stabilize the current in the TF coils and to establish and control the currents in the CS, PF coils and CC during all phases of the plasma pulse is provided by thyristor AC/DC converters;
- resistors, normally bridged by circuit breakers (called together fast discharge units, FDU), are included in series with the coils to dissipate their stored energy, if a quench occurs, and, hence, to protect the coils against over heating; two circuit breakers, connected in series, are included in each of the FDUs: the first, called the current commutation unit (CCU), is designed for multiple operation and will open when a quench is detected; in case of failure in one CCU, the second circuit-breaker (pyrobreaker), not suitable for repetitive operation but very reliable, will interrupt the current;
- the CS and PF power supply systems (PSS) include either switching network units (SNU) or booster AC/DC converters to provide the loop voltage required for breakdown and plasma initiation; similar to the FDU operation, the discharge resistors used in the SNU are inserted in series with the coils upon opening of the CCU, to extract the energy stored in the coils during the premagnetization phase; make switches are added to reduce the resistance and, hence, the voltage at predetermined time steps;
- soft grounding via high impedance resistors is provided for all the coils and power supply components; the typical value of the grounding resistors is 1 k Ω , which is sufficient to limit the ground fault current and the related arc energy; the leakage current to ground will be measured and used for ground fault detection.

In ITER-FEAT the four outer PF coils, PF2 through PF5, are integrated in one circuit, shown in Figure II.1.1-5, and utilize one common AC/DC converter for the vertical stabilization of the plasma².

The total required active power is about 500 MW. 100 to 130 MW (depending on the plasma current derivative) are needed to implement the PF scenario and to compensate the resistive power losses, up to 210 MW (300 MW after extension) are needed for the H&CD system, and 80–120 MW are required for the plasma control. The latter load has substantially a pulsed character and can be, in principle, supplied by a local energy storage (LES). If the

¹ N 41 DDD 7 98-06-12 W0.3, DDD 4.1, 12 June 1998

² N 41 RI 23 99-12-02 F 1, A Roshal. "Coil Power Supply and Distribution System: Preliminary Design for ITER FEAT", Issue 1, 30 November 1999

LES is made up of fly-wheel generators, an additional 40 MW from the grid will be needed to recharge the fly-wheels during the plasma pulse and to compensate their friction losses.

II.1.3 Magnets and Structures

II.1.3.1 Main Parameters and General Description

The ITER-FEAT magnet system consists of 18 toroidal field (TF) coils, a central solenoid (CS), six poloidal field (PF) coils and correction coils (CCs).

The TF coil case, which encloses the winding pack, is the main structural component of the magnet system. The TF coil inboard legs are wedged all along their side walls in operation. In the curved regions, the coils are connected by inner intercoil structures (IIS). At the outboard leg, the out-of-plane support is provided by outer intercoil structures (OIS) integrated with the TF coil cases. These are welded structures acting as shear panels, which are connected to each other to form four toroidal belts. There is electrical insulation between TF coils at the inboard leg wedged region and at the IIS and OIS.

The CS assembly consists of a stack of six independent modules and is hung from the top of the TF coils through its pre-load structure. This structure, which consists of a set of tie-plates located outside and inside the coil stack, provides axial pressure on the stack. The number of CS modules is chosen to suit the plasma equilibrium requirements (see II.1.1).

The six PF coils (PF1 to PF6) are attached to the cases through flexible plates to allow radial expansion. The position and size of these coils are chosen to suit the plasma equilibrium and control requirements (see II.1.1).

Both CS and TF coils operate at high field and use Nb₃Sn-type superconductor. The PF and CC coils use NbTi superconductor. All coils are cooled at 4.5K. Correction coils have not been designed yet but will include three coil sets located above, outboard of and below the TF coils.

The whole magnet system is supported by flexible columns and pedestals, one under each TF coil. Each TF coil is electrically insulated from its support. The TF coil case also supports the vacuum vessel weight and operational loads. All TF coils, the CS and the upper and outer PF coils are designed for removal from the machine in the event of a major fault. The cryostat is designed so that the lower (trapped) PF coils can be rewound in situ under the machine. In addition, the PF coils have accessible joints (located at the outer diameter), so that individual double pancakes can be disconnected in-situ in the event of a fault.

Tables II.1.3-1 to II.1.3-3 give the main magnet parameters and Figure II.1.3-1 shows an elevation of the magnet system.

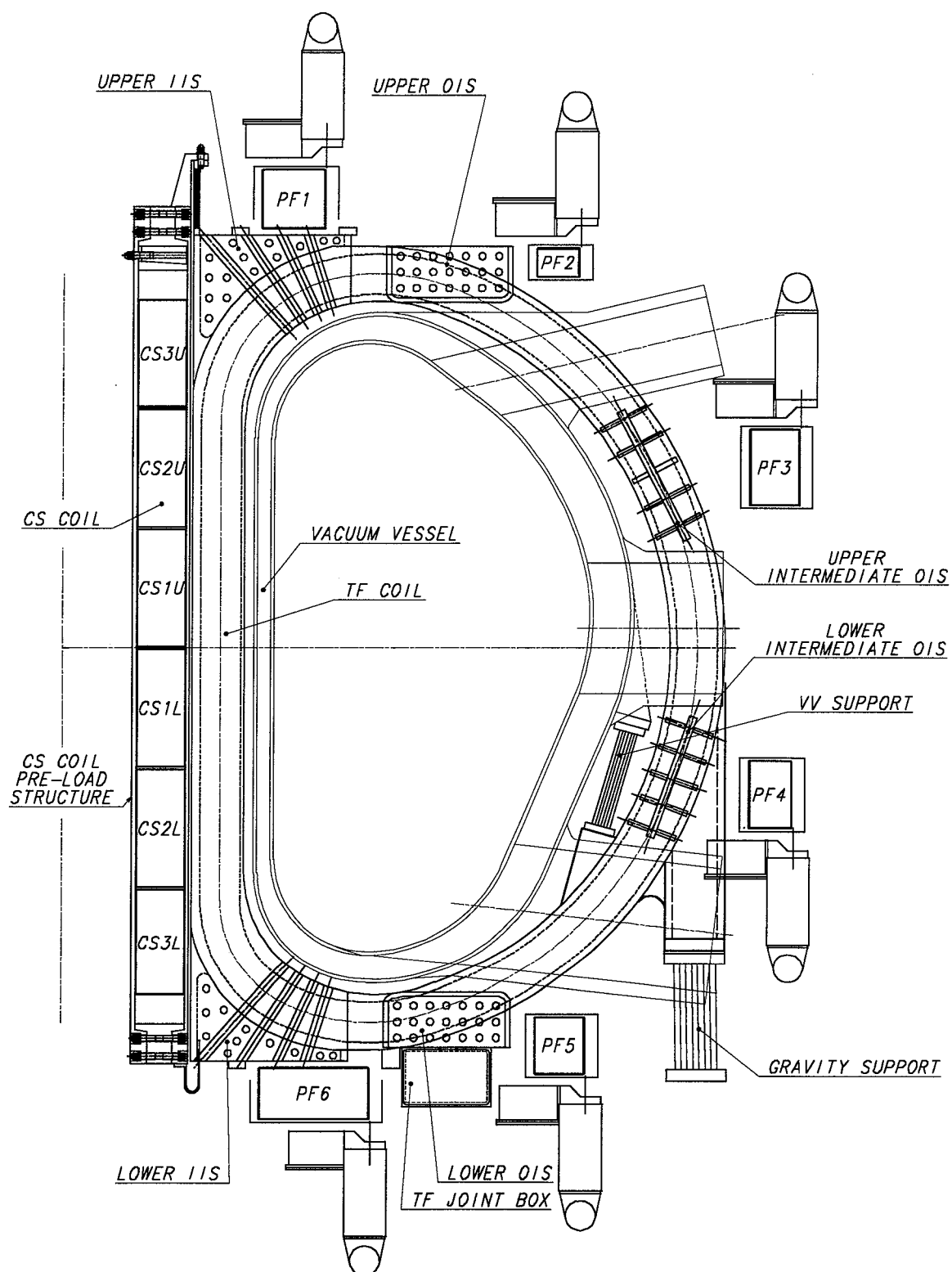


Figure II.1.3-1 Magnet Elevation View

Table II.1.3-1 Overall Magnet System Parameters

Number of TF coils	18
Magnetic energy in TF coils (GJ)	~ 41
MAm* in TF coils	5,614
Maximum field in TF coils (T)	11.8
Centering force per TF coil (MN)	404
Vertical force per half TF coil (MN)	202
TF discharge time constant (s)	11
MAm* in CS coil	1,483
CS peak field (T)	13.5
MAm* in PF coils	2,680
Total weight of magnet system (t)	~ 8,700

*Proportional to the overall superconductor length

Table II.1.3-2 Parameters for TF Coils and CS

	TF Coil	CS	
		Central modules	End modules
Overall weight (including structures) (t)	290 x 18	840	
Coil current (MA)	9.13	24.2	21.9
Number of turns per TF coil / CS module:			
Radial	12	13	13
Toroidal / Vertical	14	42	38
Total	144	538	486
Conductor unit length (m)	820.8	821.7 (for six pancakes)	
Turn voltage (V)	34.7	18.6	20.5
Ground/Terminal voltage (kV) in normal operation	5 / 5 (two coils in series)	5 / 10	
Number of current lead pairs	9	6	

Table II.1.3-3 Parameters for PF coils

	PF1	PF2	PF3	PF4	PF5	PF6
Weight (including structures)	215	159	482	403	379	340
Coil current (MA)	12.2	4.2	8.7	6.3	9.9	18.7
Number of turns per coil:						
Radial	17	12	14	12	14	30
Vertical	16	8	16	14	16	14
Total	270	94	220	165	220	417
Conductor unit length (m) (double pancake, two-in-hand)	414.4	628.7	1056.8	901.4	738.6	805.4
Turn voltage (V)*	625	1750	875	1000	875	714
Ground/Terminal voltage (kV)*	5/10	7/14	7/14	7/14	7/14	5/10

*for PF2 to PF5, a VS converter voltage of 9 kV (on-load voltage) is assumed.

Voltages are for a two-in hand winding configuration.

II.1.3.2 Design Description of the TF Coils and Structures and Gravity Supports

II.1.3.2.1 TF Coil Cases

The TF coil case is shown in Figure II.1.3-2. The centring force on each TF coil is reacted by toroidal hoop pressure in the central vault formed by the straight inboard legs of the coils. The front part or “nose” of each coil case is thickened to take part of the load. In operation, the coil cases are wedged over their full thickness and about half of the centring force is reacted through the winding pack part of the coil, while the other half is reacted by the case. The wedging surfaces must be accurately matched to achieve the required magnetic alignment and reduce stress peaks under the large wedging pressure. Precision machining of the wedging surfaces will be required as well as accurate surveying techniques to measure deviations from the required shape. Flatness tolerances are not expected to be a problem as machining should ensure that deviations from flatness involve only long wave lengths and do not result in localized peak stress. Systematic errors, in particular on the wedge angle, could instead result in significant stress intensification and must be kept within tolerable limits, if necessary by using shims. Some analysis has already been carried out and a comprehensive investigation is planned to specify the acceptable range of tolerances. A low voltage insulating barrier or coating must be applied to these surfaces.

N 11 GR 540 99-11-22 F 1

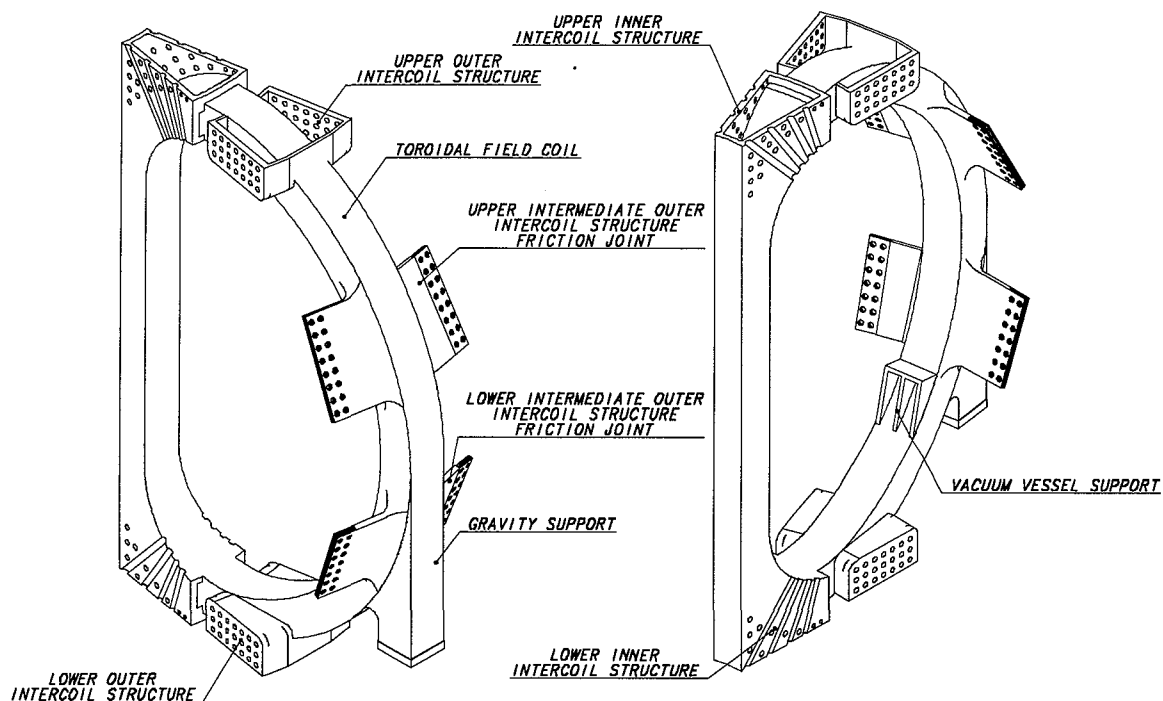


Figure II.1.3-2 3-D views of the TF coil case

The R&D programme on full size fabrication of case sections has clarified a number of issues on the case design and fabrication. The case can be made up of 6 or 7 poloidal sections. These sections are joined by butt welds around the perimeter but the welds can be placed outside the peak stress regions. The high stress sections of the case (the inboard leg and upper and lower inboard curved regions) can be made from high strength forged 316LN (modified)

steel. On the outer part of the coil, cast 316LN sections have lower stress limits but greatly reduce the amount of welding and appear the most attractive design solution. Development for the case closure welds is underway.

II.1.3.2.2 Structures

The out-of-plane loads acting on the TF coils are reacted partly by the central vault formed by the inboard legs, the IIS and partly by the OIS. The IIS design is not fully established yet but will include insulated shear keys running across the full thickness of the coils (Figure II.1.3-2). There are four OIS structures. The upper and lower OIS are located respectively above the upper ports and below the divertor ports of the vacuum vessel (VV). The upper and lower intermediate OIS are located respectively above and below the equatorial ports.

There are two types of OIS. The first one uses box structures consisting of two main shear panels linked by insulated adjustable shear keys, which are oriented in the toroidal direction. These keys are conical to ensure a tight fit and have to withstand simultaneously toroidal tension and shear loads. The second type of OIS uses single shear panels, with a thickness of about 130 mm, protruding from the side walls of the case. Multiple-finger friction joints are then welded to the two adjacent shear panels after survey at assembly. The joints are pre-loaded by two rows of 7 insulated M100 bolts acting on 6 fingers separated by insulated washers. With the multiple-finger arrangement, the friction surfaces and the shear capability of each bolt is multiplied by 7. The arrangement of a typical friction joint is shown in Figure II.1.3-3.

N 11 GR 541 99-11-22 F 1

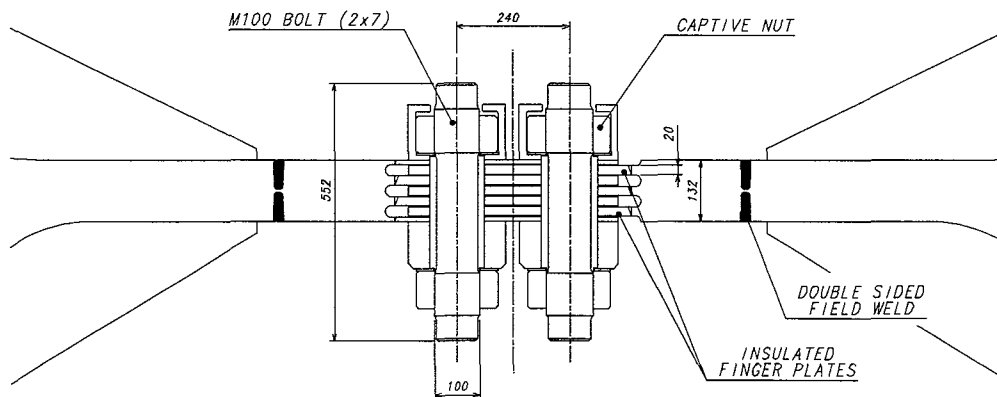


Figure II.1.3-3 Cross-section of a Friction Joint

The present design uses box structures for the upper and lower OIS. These boxes provide a high rigidity to the whole TF magnet during assembly and when the coils are not energized. Friction joints are used in the intermediate OIS where the shear loads are highest.

II.1.3.2.3 TF Winding Pack

Two options for the TF winding pack layout are being considered: (1) circular conductors embedded in radial plates, or (2) conventional winding using square conductors. The various factors to be considered for the selection of one option are as follows.

Radial Plates

The radial plate design option is based on the R&D programme of the TF model coil (TFMC) and the experience gained during the manufacture of the TFMC.

- (i) The conductor can follow the same insulating procedure as used in the TFMC. After heat treatment, the conductor is wrapped with insulation and installed in the groove of the plate with a cover welded onto the plate. An insulating layer is then built up around each radial plate and the conductor and plate insulation is filled with epoxy resin in a single impregnation step. The plates are bonded together to form a winding pack with ground insulation in a second impregnation step.
- (ii) Each radial plate is connected (through a resistor) to the conductor cross-over. The turn insulation voltage is therefore 425 V for a coil terminal voltage of 5 kV. The voltage between pancakes is 850 V.
- (iii) Insulation reliability
 - a) On a conduit with a circular outer cross section, the insulation is uniform and robust since it can contain a high density of glass and dielectric film such as kapton and it is not subject to the stress concentration effects which are present at corners of square conductors.
 - b) The conductor insulation and ground insulation are independent and physically separated by the radial plate. It is therefore impossible for a single insulation fault to affect both conductor and ground insulations.
 - c) A single conductor insulation fault can be detected (before it induces further damage) by monitoring the resistance between conductor and radial plate. This condition, together with the special design of the TF coil terminals and busbars, means that TF coil shorts are avoided by design.
- (iv) It is now foreseen that the conductor will be wound in double pancakes using a single unit length of conductor. However, the TFMC was wound in single pancakes with joints on the inner surface of the coil. The transfer of double pancakes into radial plates requires verification.
- (v) The fabrication route of the full size radial plates must be optimized for minimum cost, as the TFMC programme did not address the fabrication of a large plate from forged or extruded subsections welded together.
- (vi) In the event of a fast discharge of the TF system, eddy currents in the plates cause a quench of the superconductor after about 12 s. The plate temperature rises to about 60K and the conductor temperature to $\sim 40 - 60$ K. During such an event, the helium in the TF coils is expelled and is collected in a cold (LN2 temperature) pressure vessel (volume of about 1800 m³ and pressure of 1.8 MPa).
- (vii) The machining of the grooves in the radial plate and the cover plate welding restrict the minimum thickness of the separation between conductor channels. With a radial plate, this requires a larger winding pack than with square conductors. The case nose is thinner and the winding pack supports about 50% of the toroidal hoop compression.
- (viii) The use of Incoloy or titanium for the conductor jacket gives only a minor advantage in strand j_c and T_c properties, when the peak field is under 12 T. However, the

differential contraction with the radial plate results in tensile stress normal to the interplate insulation and, potentially, in insulation debonding. This effect is avoided with a stainless steel jacket. In the event of a quench, the internal helium pressure also results in insulation tension. Analysis shows that with a steel jacket the insulation tension is below the level where debonding would be expected. In conclusion, stainless steel is preferable to avoid insulation debonding.

Square Conductors

- (i) The conductor can follow the same insulating procedure as used in the CS model coil (CSMC), with an insulation and curing step after heat treatment to allow inspection of the insulation. This step is optional but, if applied, gives a good guarantee of the turn insulation quality. The turns are then bonded into double pancakes by vacuum impregnation. The double pancakes are bonded into the winding and the ground insulation is built up in a final vacuum impregnation step.
- (ii) For a coil terminal voltage of 5 kV, the turn insulation voltage in each pancake is about 35 V and the pancake-to-pancake voltage reaches a maximum of about 850 V.
- (iii) The square conductors show local tension regions in the insulation, which will cause local debonding at the corners extending in the worst case to about 20% of the jacket surface. This debonding exists on all surfaces of the conductors but is most severe on the surfaces in the toroidal direction at the higher field layers. Debonding is suppressed by the radial and wedging pressures nearer the nose of the coil.
- (iv) The winding pack is more compact than with radial plates, thus allowing a thicker case nose to the coil. The winding carries less toroidal hoop compression ($\sim 30\%$).
- (v) The jacket material must match the thermal expansion of the case (i.e. it must be steel), otherwise unacceptable thermal stresses are generated in the case.
- (vi) The jacket material must undergo the Nb₃Sn heat treatment. A suitable stainless steel has been identified in the TFMC development.
- (vii) The design with square conductors requires careful consideration of the manufacturing tolerances, in particular due to the twisting and keystoneing of the conductors during unspooling, straightening and winding of the D-shaped turns. Experience from the CS model coil manufacture shows that such heavy conductors can be affected by a twisting of the order of ± 0.5 mm, plus the deviations from the bending radius in the curved portions. For this reason, a fairly thick turn insulation (1.5 mm) is provided and a clearance of 0.5 mm has been added between turns at the inboard straight leg to compensate for tolerances, together with an overall clearance of 8 mm between winding pack and case for insertion. These allowances can be increased in the curved regions where the space limitations are less stringent. Further work is required to evaluate the manufacturing issues related with these conductors and to minimize the tolerances.

Figures II.1.3-4 and II.1.3-5 show typical cross sections of the TF coil winding pack with radial plates and square conductors.

N 11 GR 542 99-11-22 F 1

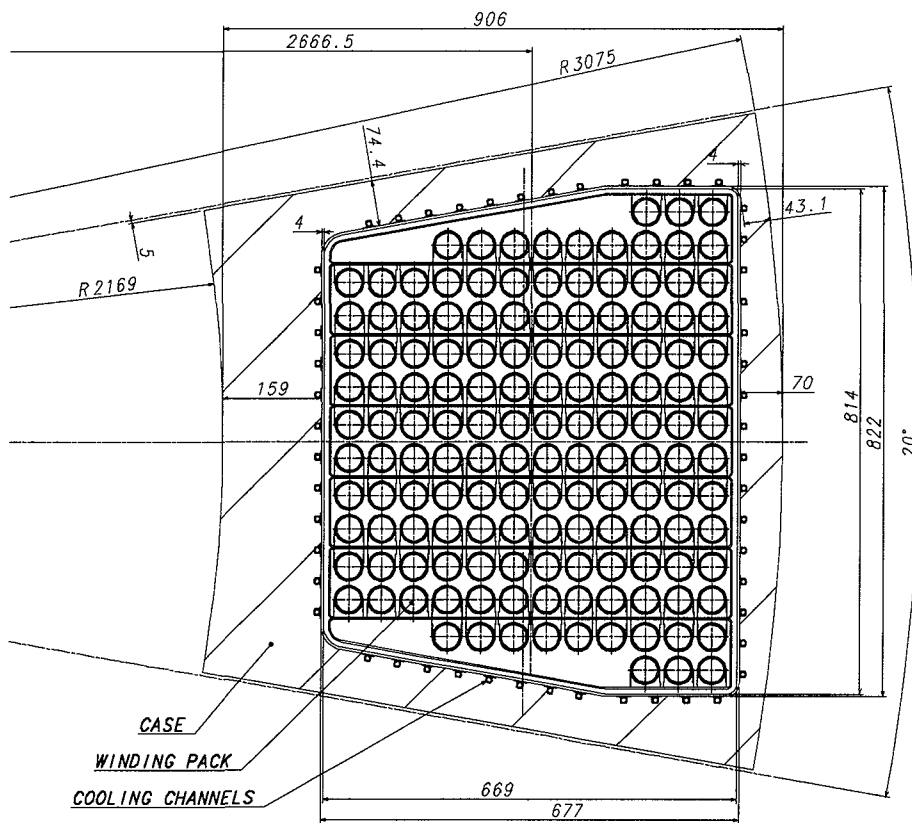


Figure II.1.3-4 Equatorial TF Coil Cross-section with Radial Plates

N 11 GR 544 99-11-22 F 1

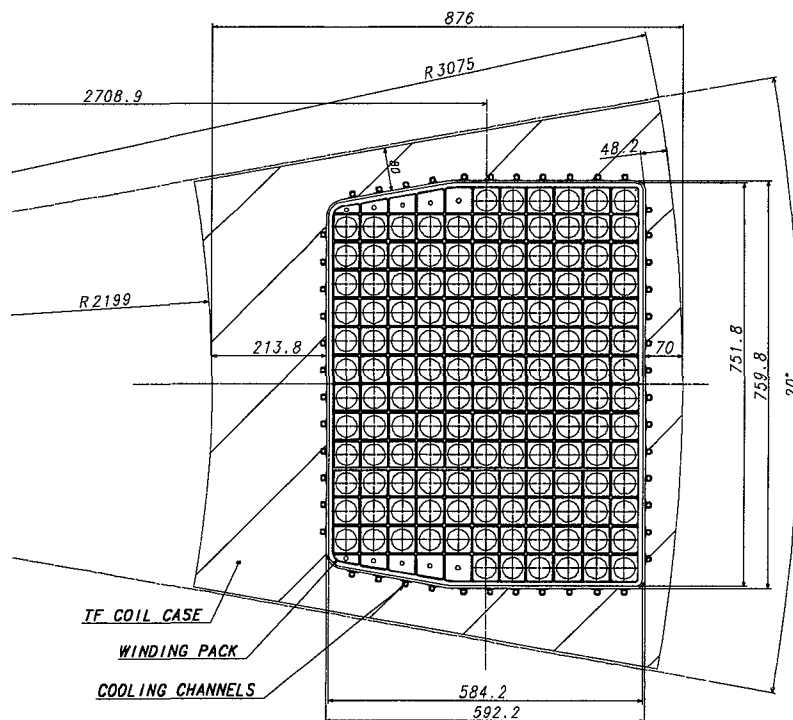


Figure II.1.3-5 Equatorial TF Coil Cross-section with Square Conductors

Cost of Winding Pack Design Options

The cost difference between the radial plate and square conductor design options has been estimated using the 1998 ITER design unit costs. Assuming that the radial plate design must be associated with the choice of a thin stainless steel jacket (rather than Incoloy or titanium) to eliminate insulation debonding issues, then the total TF coil cost with radial plates is about 8% more expensive than with square conductors when there is an identical radial build¹. The stress analysis of the TF coil inboard leg (II.1.3.7.2) indicates that at similar stress levels in the case and radial plate (or square conductor jacket), the radial plate design requires a radial build which is 30 – 50 mm thicker than with square conductors.

Conclusions on the Winding Pack Design Options

The considerations on insulation reliability are given a high, overriding priority and are the basis for a recommendation to use radial plates. There are, however, significant manufacturing cost and radial build penalties associated with this choice.

II.1.3.2.4 Gravity Supports

The gravity supports for the machine are placed under the outer curved region of each TF coil between PF4 and PF5. There is electrical insulation between each TF coil and its support. The machine gravity supports are equipped with flexible plates, so that they flex in the radial direction to allow thermal expansion of the magnet system, but they are rigid to out-of-plane bending caused by TF coil torsion or seismic motion. They are sufficiently robust to transmit out-of-plane moments to a lower supporting ring, which is an integral part of the cryostat structure (II.3). The lower supporting ring transmits the horizontal seismic loads to the building.

The VV supports are attached to the TF coils at the same poloidal location. This arrangement has been selected to minimize the tangential displacements of VV ports during operation. Figure II.1.3-1 shows the support location. The VV supports are designed to resist gravity loads and also the vertical loads during vertical displacement events (VDEs). Similar to the machine gravity supports, they are provided with flexible plates to allow differential expansion with respect to the TF coils and resist horizontal loads due to seismic motion or non-axisymmetric VDEs. Since the VV supports are trapped between the TF coils and the VV outer wall, assembly and the interfaces to the thermal shield, plus access and maintenance to the supports, are issues which need further investigation.

II.1.3.3 Design Description of the Central Solenoid

II.1.3.3.1 General Design

The solenoid is free standing and supports the magnetic loads through structural material within the winding. The main load is the magnetic hoop force, which creates tension in the structural material.

¹ G A0 RI 1 99-02-12 W0.2, Study of RTO/RC ITER Options, Chapter II.1

The CS consists of a stack of six electrically independent modules. The field curvature at the ends of the CS creates vertical forces on the modules. At IM (initial magnetization) and EOB (end-of-burn), these forces are towards the centre of the stack, whereas at some intermediate equilibrium configurations the end modules carry opposite currents to the central ones and are repelled. This means that a vertical support structure is required. This structure applies axial pre-compression to the coil stack so that the modules remain in contact during all operating conditions. To obtain uniform compression, tie plates running axially along the CS are provided at both inside and outside diameters and connect to pressure plates at top and bottom. This structure is designed so that it can restrain the maximum vertical separating load of 75 MN acting on the end modules of the stack. The required axial tension in the structure is achieved partly by pretensioning at room temperature and partly by differential contraction during cool-down. This requires a jacket material of the CS conductor with a lower contraction coefficient than the tie plates which use stainless steel.

II.1.3.3.2 Flux Optimization and Peak Field

Because of its central position in the machine, the CS has a major role in driving the radial build while itself forming a fairly minor fraction of the total magnet cost (about 12%). Global optimisation studies have shown that in order to minimize the total cost of the machine, it is preferable to adopt the most compact, high field design option, even if it is not the lowest cost choice for the CS itself.

Optimisation studies of the CS show that the field at which the maximum flux occurs is dependent on the allowable operating stress, which in turn depends on the allowable fatigue life. Incoloy, as used in the CSMC, is one of the options for the jacket material. It offers a high fatigue strength in the base metal and contracts less than the tie plates during cool-down, maintaining the vertical pretension. Other strengthened austenitic steels can be considered for the jacket material. JK2, a Japanese high strength cryogenic steel, has a somewhat lower fatigue life but a thermal contraction coefficient similar to Incoloy. JK2 is not able to resist the Nb₃Sn heat treatment. Either of these materials would reach a maximum flux capability in the solenoid at peak fields between 14 and 15 T (maintaining the same engineering margins on stress and superconductor performance as at 13 T and noting that the strand database is estimated up to 15 T). A modified AISI 316LN can resist the Nb₃Sn heat treatment, but offers a much lower fatigue life. Table II.1.3-4 shows the plasma burn time achievable as a function of the maximum field in the case of an Incoloy-jacketed conductor. The advantage in selecting high field values is clear.

Table II.1.3-4 Plasma Burn Time ($I_i = 0.85$) vs. peak field (Incoloy jacket conductor)

Peak field in CS (T)	13.5	14
Flux for plasma burn (Wb)	29.8*	33.8

*see Table II.1.1-2

The reference design uses a peak field of 13.5 T, thus leaving, in principle, some design margin to cover a range of possible jacket materials.

II.1.3.3.3 Conductor Jacket Options

The use of the 316LN steel results in a loss of CS performance due to both the strain degradation of the Nb₃Sn (which is minor) and the high fatigue crack growth rate (which is

the most severe limit).

This leaves two design options :

(i) The use of Incoloy 908.

This design option is based on the R&D programme carried out for the CSMC and the experience gained during the manufacture of the CSMC. The jacket material is provided as square sections (as for the CSMC) and a co-wound strip. The co-wound strip is necessary as the structural material section required is too large for the jacket to be provided as a single square section. This option requires some R&D to verify that a new weld wire can avoid the hot cracking issue found in the CSMC with multiple pass welds. Details of co-winding the reinforcing strip and especially welding it to the adjacent conductor, while avoiding SAGBO, have also to be addressed.

(ii) A double armour option.

This option involves the use of an inner titanium or Incoloy or 316LN-type steel circular jacket about 1.5 mm thick, reinforced by two outer U-channels which are applied after the heat treatment of the conductor. This type of construction, albeit for a smaller conductor, has been used and tested for the Japanese DPC-TJ coil programme. An industrial design study has also confirmed the general feasibility of the full size CS with this double armour technology. As indicated above in II.1.3.3.2, JK2 is a possible candidate for the U-channel material. For the inner jacket, Incoloy or titanium are candidate materials and would allow better performance of the Nb₃Sn, although, in the case of titanium, the structural contribution will be negligible. Both materials require some R&D to demonstrate the successful production of a Nb₃Sn conductor in a thin circular jacket. The use of 316LN-type steel for the inner jacket is not expected to be possible due to its lower fatigue performance (JK2 is not an option for the inner jacket as it becomes brittle during heat treatment). Details of the assembly process of the U-channels after heat treatment of the inner conductor have still to be addressed.

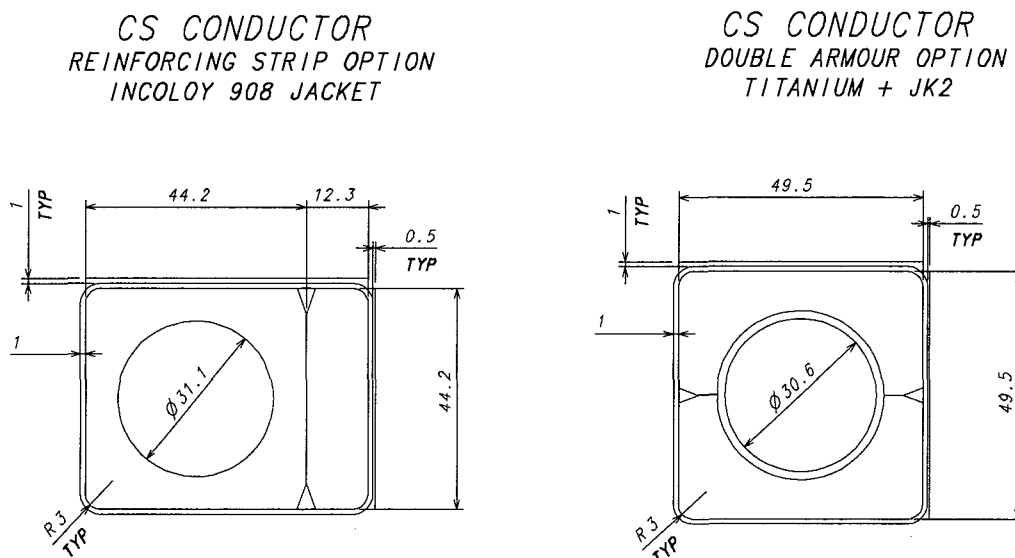
Cross sectional views of these two conductor options are shown in Figure II.1.3-6. Both the Incoloy and the double jacket options are considered feasible but require additional development and cost comparison before a final choice can be made. In terms of performance, the Incoloy option is superior due to the better fatigue behaviour of Incoloy (allowable cyclic stress of 490 MPa for Incoloy versus 440 MPa for JK2 for 30,000 tokamak pulses). The difference in the flux available for plasma burn should be about 4 Wb. At this stage of the design, the decision can be postponed until more information becomes available.

II.1.3.3.4 Winding design

The CS is pancake wound. In the current design, a single conductor length of 820 m is adequate for six pancakes. This “hexa-pancake” winding arrangement minimizes the number of joints at the outer diameter, and therefore, it reduces the complication associated with the joint configuration which includes the joint itself with its mechanical clamps, the helium pipes and the tie plates which carry the mechanical hoop tension. These components must fit in a narrow space between the CS and TF coils. On the other hand, this configuration requires more complicated manufacturing processes and tools, in particular for the winding of a conductor when the winding starts from the outer diameter. A preliminary study on the CS manufacture has been performed by industry and indicated a possible process to make hexa-pancakes with some conceptual design of tooling. A more conventional double pancake

winding is of course possible and is being considered as a backup option, but it requires three times as many joints.

Helium is supplied through a jacket penetration on the inside cross-over between the pancakes and flows outwards to outlets at the outer diameter. The high field regions are cooled with the coldest helium and the joints at the conductor ends are placed only in the low field region at the outer diameter. This configuration also locates the joints far away from the high field region, thus providing a long cable length for current redistribution to occur between joints and the high field area.



N 11 GR 543 99-11-22 F 1

Figure II.1.3-6 Central Solenoid Conductor Design Options

II.1.3.4 Design Description of the PF Coils

II.1.3.4.1 General Design

The PF coils are pancake wound with NbTi superconductors in square jackets. Because of the operational reliability requirements, especially for the electrical insulation, and the difficulty in replacing a coil, the conductor is provided with double turn insulation to ensure that an incipient short can be detected before significant damage occurs. For PF1, PF2, PF5 and PF6, the winding pack consists of a stack of double pancakes enclosed in a common ground insulation wrap. PF3 and PF4 have double pancakes with individual ground insulation for the reasons explained in the next section.

II.1.3.4.2 Redundancy and Maintenance Philosophy

All PF coils use double turn insulation consisting of two insulation layers with a thin metal screen in between. Double pancakes are wound two-in-hand. This arrangement allows detection of an incipient short before it develops into a full short resulting in significant damage to the coil and, as a consequence, the need for a major coil repair or replacement. In

the event of the detection of an incipient short in a double pancake, the faulty double pancake must be disconnected and by-passed using busbar links. This work is to be carried out hands-on and requires access to the joint regions at the outer diameter of the coils. Following the by-pass of a double pancake, plasma operation can continue at full performance by using the remaining double pancakes at higher current. This mode of operation is referred to as “backup” mode in II.1.3.5.3 and Table II.1.3-10. For PF2, PF3, PF4 and PF5, the conductor is designed to allow the backup mode without any need to decrease the conductor operating temperature. In the case of PF1 and PF6 which are operated at higher field, sub-cooling at inlet temperatures below 4.2K would be required.

The use of double turn insulation and the ability to continue operation with a by-passed double pancake should make a major coil repair or replacement unnecessary throughout the life of ITER-FEAT. Should, however, such major repair be required, the following strategy could be followed:

- PF1 and PF2 can be relatively easily removed from the cryostat. For them, major repair work, or rewinding, should be carried out outside the cryostat.
- For PF5 and PF6, major repair work, including rewinding, should be carried out under the machine inside the cryostat.
- PF3 and PF4 are trapped by VV ports and are the most difficult to repair. For this reason, their design includes sufficient inherent insulation redundancy to make such major repair unnecessary. PF3 and PF4 include:
 - double turn insulation;
 - double pancakes with individual ground insulation and metal plate separators between double pancakes to limit damage propagation in the event of a fault.

II.1.3.5 Conductor Design

II.1.3.5.1 TF Conductor

In this section, the conductor is described for the radial plate design option. The TF conductor will use the existing TF Model Coil conductor concept.

The conductor features a circular Nb₃Sn cable-in-conduit with a central cooling channel, cooled by 4.5K supercritical helium, as shown in Table II.1.3-6. The cable design criteria (1K temperature margin, 1000 W/m²K heat transfer coefficient in the Stekly criterion, 150K hot spot temperature) and the reference strand parameters have been established from the Model Coil programme (Table II.1.3-5). The size of the central channel will depend on the nuclear heat loads, but with the present level of shielding, a channel similar to that used for the Model Coils will be required (8 mm). For a cooling flow rate of 12 g/s/channel the pressure drop will be about 0.15 MPa. The distribution of the nuclear heat load in the TF coils is shown in Table II.1.3-7. AC losses are shown in Table II.1.3-11.

The conductor is jacketed with a circular stainless steel tube to match the radial plate material and avoid the insulation delamination that occurs above the cover plate of the conductor groove if a jacket with a different thermal contraction coefficient is used. The technology for a steel jacketed conductor has been developed for the TFMC production. The extra strand cost implied by the selection of steel rather than Incoloy or titanium is small, about 7%, and the decrease in cable space current density is about 3%.

The cooling inlets to each pancake are located at the inner surface of the coil. The cold helium then quickly reaches the high field region and, after passing through the pancake, exits on the outer surface of the coil on the outside. The conductor design point of maximum field and maximum temperature occurs towards the end of the TF coil inboard leg, where the helium in the first turn reaches the maximum temperature due to the nuclear heat at the inboard leg (where the shielding is thinnest).

With the reference strand and cable configurations (the cable coupling time constant is assumed to be 50 ms), AC losses during plasma operation are low compared to the nuclear heating and do not represent a design constraint, as shown in Table II.1.3-11.

Table II.1.3-5 Reference Strand Properties for TF Coils and CS ($\epsilon = -0.25\%$)

J_c non copper at 12 T @4.2 K	650 A/mm ²
B_{com}	28 T
T_{com}	18 K
T_c at 12 T	11.7 K
Hysteresis loss (+/- 3 T cycle)	400 mJ/cm ³ of non copper

Table II.1.3-6 TF and CS Conductor Designs

	TF	CS
Jacket type	Circular	Square
Jacket material	Steel	Incoloy
Operating current (kA) IM / EOB	63.4	40.5 / 45.0
Nominal peak field (T) IM / EOB	11.8	13.5 / 12.8
Operating temperature (K)	5.0	4.5
Strain (%)	-0.5	-0.05
Discharge time constant for hot spot (s)	11 + 2 (delay)	7.5 + 2 (delay)
I_{op} / I_c IM	0.77	0.75
T_{cs} (K) IM	6.02	5.80
Cable diameter (mm)	38.9	31.1
Central spiral OD x ID (mm)	8 x 6	8 x 6
Conductor OD (mm)	Ø42.1	44.2 x 44.2
sc strand diameter (mm)	0.70	0.74
sc strand cu : non-cu	1.25	1.50
cabling pattern	((3x3+1)x4+1) x5+1)x6	((3x3x3+1) x4+1)x6
sc strand number	1080	648
sc strand weight/m of conductor (kg)	3.894	2.611
$J_{cable\ space}$ (A/mm ²) IM/EOB	53.33	53.31 / 59.24
Conductor cost (IUA/m)	2.20	2.19

Table II.1.3-7 Nuclear Heat Loads in TF coils (kW)

Heat in case	8.08
Heat in first conductor row	1.79
Heat in winding pack	5.61

The discharge time constant of the TF coils has a significant impact on the conductor current density. The electrical discharge time constant is limited to 11 s, as faster values create unacceptable stresses on the vacuum vessel due to eddy currents. The quench detection time for the TF coils is estimated to be a minimum of 2 s, giving an equivalent thermal discharge time constant of 15 s.

A critical design issue is the case heating after a disruption. The case temperature rises by about 15K due to the eddy currents. This heat conducts slowly to the conductor and may cause quench on a timescale of 50 – 100 s after the disruption. Analysis has shown that, in the case of a pancake inside the winding pack, adequate cooling can be provided to both conductors and coil case to avoid a quench. Similar analysis remains to be carried out to ensure that the conductor lengths of the side pancakes have adequate cooling.

II.1.3.5.2 CS Conductor

The superconductor for the CS will be a Nb₃Sn cable-in-conduit type as used for the CS Model Coil. Design details are given in Table II.1.3-6. Due to the short channel length (about 150 m), the central cooling channel can be reduced in size or eliminated as the helium pressure drop is so low. For the 6 mm channel given in the table, a mass flow rate of 8 g/s/channel requires a pressure drop of 0.04 MPa. The usual conductor design criteria are applied (1K, 1000 W/m²K, 150K).

The partition of the CS into modules allows a high discharge voltage, while still remaining within the capabilities of the insulation. Combined with the low CS energy, the electrical discharge time constant can be well under 10 s. The detection time for a quench then is an important factor, relative to the actual electrical discharge time. A time of 2 s is expected to be the minimum achievable with a primary (voltage based) system, while about 4 s can be achieved with a backup pressure system. Choosing an electrical discharge time of 7.5 s then gives an equivalent thermal discharge time constant of 11.5 s. In the case of the backup pressure based detection system, the discharge time would increase to 15.5 s. The temperature rise would then be well above 150K (the design criteria) but below the temperature where permanent insulation degradation would be expected. Further reductions in electrical discharge time increase the sensitivity of the maximum temperature to the detection time and seem undesirable given the uncertainty on the quench detectability.

The CS operates in pulse mode and the time-varying currents and fields generate AC losses in the cable. The conductor layout, with high field cooling by the cold helium at inlet, can tolerate very high cycle AC losses as the temperature margin increases as the field drops along the conductor. AC losses are shown in Table II.1.3-11. The losses are about 60% hysteretic and 40% coupling and could be reduced by the use of a lower loss strand.

II.1.3.5.3 PF Conductors

The PF coils will use NbTi superconductor, cooled by supercritical helium at an inlet temperature of 4.5K. This gives a substantial cost saving compared to Nb₃Sn and the elimination of a reaction heat treatment greatly simplifies the insulation of such large diameter coils.

The cable configuration is similar to that used with Nb₃Sn with 6 sub-cables arranged around a central cooling space. For the longest channel length (500 m) a mass flow rate of 12 g/s/channel requires a pressure drop of about 0.075 MPa.

Non-uniform current distribution can be a more sensitive issue with NbTi cables than with Nb₃Sn cables because of the lower value of T_c . To ensure a uniform current distribution in each sub-cable, a low resistance solder coating is used on the strands. AC losses (shown in Table II.1.3-11) are controlled by the Inconel wrap on each sub-cable to limit the coupling time constant (τ) to 50 ms and the joint layout must aim to provide a uniform contact to each of these sub-cables. The losses in the coils are at a maximum about 25% due to coupling, so if necessary a significantly higher coupling time constant could be tolerated. These conductor optimization issues are planned to be addressed in a NbTi conductor R&D programme, currently under discussion, which will include, as an essential part, the manufacture of a NbTi coil and its testing in pulsed conditions.

The conductor design criteria (1.5K, 600 W/m²K and 150K) are slightly different to Nb₃Sn (the temperature margin is higher) because of the lower critical temperature of NbTi. The reference strand parameters are given in Table II.1.3-8 and the conductor configuration in Table II.1.3-10. Four different designs are selected to accommodate the various combinations of operating current and field in both normal and backup modes as shown in Table II.1.3-9. This selection of four designs requires confirmation by cost optimization studies. The selected operating temperatures include a 0.5K temperature increase (due mainly to AC losses) within the coil.

Table II.1.3-8 NbTi Strand Parameters

J_c non copper at 5 T, 4.2 K	2900 A/mm ²
T_c at 5 T	7.17 K
Filament diameter	5 μ m
Strand layout	no CuNi internal barriers, solder surface coating

Table II.1.3-9 Four Types of PF Conductor

	Design Current (kA), Peak Field (T), Operating Temp. (K)	
	I_{op} @ B_{op} @ T_{op}	
	Normal mode	Backup mode
PF1 & PF6	45.0 kA @6.0 T @5.0K	52.0 kA @6.4 T @4.7K
PF2	45.0 kA @4.0 T @5.0K	60.0 kA @4.0 T @5.0K
PF3 & PF4	39.4 kA @4.0 T @5.0K	45.0 kA @4.0 T @5.0K
PF5	45.0 kA @5.0 T @5.0K	51.0 kA @5.0 T @5.0K

Table II.1.3-10 PF conductors

	PF1&6	PF3&4	PF2	PF5
Jacket type	heavy circle in square	heavy circle in square	heavy circle in square	heavy circle in square
Jacket material	steel	steel	steel	steel
Operating current (kA) normal / backup	45 / 52	39.4 / 45	45 / 60	45 / 51
Nominal peak field (T) normal / backup	6.0 / 6.4	4.0	4.0	5.0
Operating temperature (K) normal / backup	5.0 / 4.7	5.0	5.0	5.0
Equiv. discharge time Constant (s) for hot spot	18	18	18	18
I_{op}/I_c normal / backup	0.127 / 0.144	0.364 / 0.415	0.312 / 0.416	0.271 / 0.307
T_{cs} (K) normal / backup	6.5 / 6.27	6.66 / 6.52	6.79 / 6.52	6.58 / 6.50
Cable diameter (mm)	38.2	32.5	36.6	35.0
Central spiral OD x ID (mm)	12 x 10	12 x 10	12 x 10	12 x 10
Jacket area (mm ²)	1740	1860	1640	1730
Conductor OD (mm)	53.8 x 53.8	51.9 x 51.9	51.9 x 51.9	51.9 x 51.9
sc strand diam (mm)	0.73	0.70	0.70	0.71
sc strand cu : non-cu	1.6	6.75	6.75	4.4
cabling pattern	3x4x4x5x6	((3x3x3+1) x5+1)x6	((3x3x4+1) x5+1)x6	((3x3x4+1) x5+1)x6
sc strand number	1440	810	1080	1080
sc strand weight/m of conductor (kg)	4.885	2.527	3.369	3.466
$J_{cable\ space}$ (A/mm ²) normal / backup	39.26 / 45.37	47.49 / 54.24	42.77 / 57.03	46.77 / 53.00
Conductor cost (IUA/m)	1.26	0.91	1.01	1.04

Table II.1.3-11 Conductor AC Losses Integrated over 1800 s of Operating Pulse

Coil Coupling time const. $\tau = 50$ ms	AC losses (kJ)				Total
	scenario			control**	
	hysteresis	coupling	total*		
CS	2184.1	1367.8	3662.3	150.1	3812.4
TF (Conductor & radial plates)	1290.8	53.3	1365.6	50.0	1415.6
PF1	127.9	58.4	192.1	26.7	218.8
PF2	12.0	13.8	27.2	36.7	63.9
PF3	25.5	14.2	41.1	49.6	90.7
PF4	18.1	6.2	24.8	7.3	32.1
PF5	45.5	32.8	81.6	12.8	94.4
PF6	198.0	53.1	256.7	10.5	267.2
PF Total	427.0	178.5	623.5	143.6	767.1
TOTAL	3901.9	1599.6	5651.4	343.7	5995.1

* The total value includes eddy current losses in conductor jacket or radial plates. Such losses are not shown in the table explicitly, for they are relatively small.

** Control losses assume (per pulse) 3 minor disruptions, 10 compound ELMS and ELMS (1 Hz).

II.1.3.6 Joint Design

The TF coils can use the lap-type joints which have been developed and tested for the TFMC. On the basis of test results obtained with short samples (at the SULTAN facility), these joints function well above the specification, with resistance under 1 n Ω .

For the CS, the joint configuration is constrained by the joint location at the outer diameter of the CS. The joints must occupy a minimal radial space and their toroidal extent must also be limited as they have to be placed around the coil circumference between the vertical tie plates, busbars and cooling pipes which are located in the space between CS and TF coils. This implies that the joints are designed to be 'embedded' in the winding pack, with no access for repair or disconnection.

Two generic types of joint configuration have been established during the model coil fabrication, the 'lap' and the 'butt'. Lap joints from the EU and US completed successful testing in the SULTAN facility (the US joints were also tested in the PTF facility at MIT). The test results of the original JA full size butt joint were not fully satisfactory. A modified version went through a limited test procedure in a domestic facility. Either of these could be used in the CS, although only a lap joint is suitable for the busbar connections.

The most convenient joint configuration for the inter-pancake lap joint is with the contact surface in the plane of the pancake. However, this configuration is the least favourable for the joint eddy current pattern, as current flow can occur across the joint contact surface due to the changing radial field component. There is little data available for the EU/US lap joint behaviour under these field conditions as they did not exist previously. Applying estimates of

the relevant time constants for CSMC-type lap joints suggests that in a plasma disruption the maximum energy input could be 650 J/joint, giving a temperature rise of 4 – 5K, which would be acceptable. The heating during plasma initiation is less, causing a temperature rise of about 1K.

There is eddy current data available for the butt joint but the stability to pulsed conditions is unknown and may (as with the original design) be a limiting factor. The CSMC should provide some information for the butt joint under relevant field conditions (but not for the lap joint because of the orientation of the contact surfaces).

A design choice for the CS will not be possible unless an adequate pulsed joint test can be performed. The MIT PTF facility would be able to test the existing conductor samples under appropriate pulsed field conditions but the funding of such tests is an issue.

No detailed design or R&D is available for the PF joint. However, any of the lap joints developed in the model coil programme could be applied to NbTi and the butt joint sintering technique may also be applicable. The joint losses/stability need to be assessed, and the final joint will be qualified in the manufacture and test of a NbTi insert coil.

II.1.3.7 Structural Design and Analysis

II.1.3.7.1 Structural Design Criteria

Two structural criteria are applicable at this stage of the case design, the static stress limit and the fatigue limit. Only base metal is considered, assuming that welds can either be placed outside the peak stress regions or can achieve comparable properties.

The static stress limit is dependent on the material and the static stress system it has to support. Following the ITER criteria for materials at cryogenic temperatures, operation up to 2/3 of the yield stress is allowed for primary membrane stress systems and up to 30% above this for primary membrane plus bending stresses. The material is assumed to be one of the family of strengthened austenitic steels defined in the ITER materials specifications that have been developed for cryogenic applications. The minimum yield stress of these materials is 1000 MPa.

The fatigue stress limit is determined from an assumption of an initial defect size by integration of the crack growth rate following the Paris Law. The procedure is defined in detail in the ITER design criteria, with an overall safety factor of 2 applied to the number of cycles. As an example, a 250 mm thick section of the material would be assumed to have an initial surface crack depth (a) of 4.775 mm and a length (2c) of 47 mm. The allowable peak stress for 30,000 plasma pulses depends on the material considered and the R ratio which is the minimum stress divided by the maximum stress. The allowable peak stress for a 316LN type of steel and a high strength cryogenic steel (such as the Japanese JJ1) is shown in Table II.1.3-12.

Table II.1.3-12 Allowable Peak Stress in MPa (30,000 pulses, wall thickness: 250 mm)

R ratio	0.1	0.5	0.7
316LN	370	460	560
JJ1	420	640	820

II.1.3.7.2 Inboard Leg

Stress analysis of the inboard TF leg subjected to in-plane loads (centring force and poloidal tensile force) has been carried out for both designs with radial plates and square conductors. In these analyses, a radial build of 876 mm and 906 mm has been used for the square conductor design and the radial plate design, respectively. The larger radial build for the radial plate design was found necessary to reduce the level of stress and was achieved by reducing the CS outer diameter (thus reducing the flux available for burn).

Table II.1.3-13 shows how the poloidal tensile and toroidal compressive forces are shared between the case and the winding pack. For the square conductor design, the table shows that all stresses are within allowables with some margin to cover for non-uniform wedging pressure, which is expected due to the flatness and angular tolerances of the wedging surfaces. Preliminary analysis using "axisymmetric" tolerance gaps (i.e. where each coil has the same pattern) suggest that to avoid stress increases over 10% (about 60 MPa) the metal surfaces should be within about ± 0.2 mm of their design location. However, more realistic random variations of tolerance will be much less severe and should allow larger variations. For the radial plate design, stresses are somewhat larger thus leaving smaller margins. Some local stresses in the radial plate webs are above allowable limits but this can be easily corrected by a small increase in the web thickness for a few turns at the nose, and a concomitant reduction of the case thickness. Further analyses including the out-of-plane behaviour of the coil may also show that some increase of the radial build (~ 2 cm) is required to reduce the stresses in the case.

Table II.1.3-13 Force and Stress at TF Inboard Leg

		Radial Plate Design Option	Square Cond. Design Option	
Radial build (mm)		906	876	
Vertical force:	(MN)			
- Winding pack		46	34	
- Case		54	66	
Toroidal force:	(MN/m)			
- Winding pack		-68	-49	
- Case		-88	-106	
<i>Maximum stresses in</i>	<i>Stress Type</i>	<i>Stress Value (MPa)</i>	<i>Stress Value (MPa)</i>	<i>Allowables (MPa)</i>
Case nose	SINT	712	653	
	SY	653	559	
	Pm	575	556	
	Pm+Pb	712	662	
Stainless steel jacket	SINT	732	754	
	Pm		560	
	Pm+Pb		720	
Radial plates	SINT	891	NA	
	Pm	680	NA	
	Pm+Pb	785		
Insulation	SXY	35	60	68*

SINT: Tresca stress; SY: toroidal stress; Pm: primary membrane stress; Pb: bending stress; SXY: shear stress;

*: shear stress allowable with ~ 50 MPa compression.

II.1.3.7.3 Inboard Curved Regions

Structural analysis has been made using a global finite element model of the TF coils and structures. This model incorporates both in-plane and out-of-plane loads and the load cases considered include, typically, TF magnet cool-down, TF magnet energized, initial CS magnetization, and end-of-burn. Results of this global analysis are reported in this section and II.1.3.7.4.

At each end of the inboard straight leg, the coils separate and curve round to the horizontal, while over the same region the out-of-plane force peaks and reverses direction (due to the presence of PF1 and PF6). This curved region of the coil case is the most critical to design, with stress peaks located at the side plates at the end of the straight leg and on one side of the coil on the inner surface in the curved region. The location where the maximum occurs depends on which out-of-plane support is used.

Many possible design options to support the out-of-plane forces have been investigated for this inboard curved region. The most promising options include the following:

- (i) Shear keys normal to the coil centreline (the so-called “poloidal keys”) and running across the full case thickness as shown in Figure II.1.3-2. With this design, the stresses in the case are close to the allowable. Detailed analyses of this design option are underway.
- (ii) Pre-compression rings located in the region between the CS outer surface and the PF6 (or PF1) inner diameter. These rings are used to pull the curved parts radially inward thus providing some wedging pressure. The friction forces in this extended, wedged region can react some of the out-of-plane loads. Preliminary results show acceptable stresses in the TF case (450 – 470 MPa). This design option has also a significant impact on the in-plane behaviour of the coil (reduction of OIS toroidal loads). The design of the pre-compression rings has not been started yet.
- (iii) Strengthening of the coil case in the curved region (i.e. thickening the case walls as space becomes available as they leave the inboard leg region).

Based on the structural analyses performed so far, the following can be concluded. A solution to providing the out-of-plane support in the curved region must include:

- (a) Strengthening of the coil case:
Strengthening of only the sides or the nose of the case is inadequate as the coil deforms by a combination of torsion, plus in-plane and out-of-plane bending. It is necessary in the curved region to reinforce the inner case wall (on the plasma side) from the inboard leg case section to a thickness comparable to the outer wall, about 20-25 cm, while the side walls have a thickness of not less than about 10 cm (in the inboard leg it can be as low as 7 cm). This increase in thickness should be applied in a smooth way to avoid abrupt changes in the mechanical properties of the cross section such as the moment of inertia.
- (b) Structures able to resist shear loads between adjacent coils:
These structures should include shear keys or compression rings as described in (i) and (ii) above or, more likely, a combination of these structural options.

II.1.3.7.4 Outer Intercoil Structures (OIS)

Global model structural analyses of the TF system have been made using the two configurations of the OIS, box structures and friction joints, for the two intermediate OIS. Based on these preliminary structural analyses, the following can be concluded:

- i) The shear loads due to the twisting motion of the whole TF magnet assembly are essentially resisted by the intermediate OIS. Shear loads on the upper and lower OIS are moderate. Table II.1.3-14 shows the shear loads on the OIS.
- ii) If the TF coil inboard legs are wedged at assembly (no assembly gap), large toroidal hoop tensile loads develop at the OIS when the coils are energized.
- iii) The toroidal tensile load in the OIS is sensitive to the assembly gaps between inboard legs and the use of precompression rings. The shear loads, instead, are not affected by assembly gaps. Table II.1.3-15 shows the toroidal tensile loads on the OIS for different toroidal assembly gaps. In these analyses the use of poloidal shear keys between coils is considered for the IIS.
- iv) The combination of shear and toroidal tensile loads at the intermediate OIS results in excessive stress on the conical shear keys of the box structures. Friction joints OIS can resist much higher toroidal tensile loads than box structures and are therefore selected for the intermediate OIS. However, the friction joints are less rigid than box structures and out-of-plane displacements reach a maximum of 27 mm (compared with 20 mm with the more rigid box structures).
- v) At the upper and lower OIS, the box structures with conical shear keys can be maintained and are preferred because they provide a rigid mechanical reference during assembly.

Table II.1.3-14 Shear Loads (MN) on OIS

	Radial direction	Vertical direction
Upper OIS segment	1.7	2.4
Upper intermediate OIS segment	8.8	20.2
Lower intermediate OIS segment	8.7	19.8
Lower OIS segment	1.7	3.0

Table II.1.3-15 Toroidal Tensile (MN) Loads on OIS for Different Assembly Gaps

Assembly gaps	0 mm along straight leg; 0 mm at keys.	2 mm along straight leg; 0 mm at keys.	Pre-compr. rings with 0 mm gap
Upper OIS	19.1	9.8	5.1
Upper intermediate OIS	22.7	25.3	1.7
Lower intermediate OIS	22.4	23.8	1.7
Lower OIS	22.3	10.5	6.6

II.1.3.8 Design Assessment and Conclusions

Conductors and Joints

The conductors for the TF coils, CS and PF coils have been designed according to the design criteria that have been defined during the periods of the EDA and EDA extension. For the TF coils and CS, the designs are based on R&D results available from component testing,

particularly that associated with the Model Coil programmes. The final verification of the Nb₃Sn conductors in an integrated test will come from the CSMC experimental programme.

Two aspects are at present missing from the planned testing:

- i) the testing of lap joints in an orientation that is relevant to the CS: such testing is not part of the planned R&D programme due to the lack of facilities in the EU or Japan but is nevertheless required to establish the CS joint design;
- ii) an integrated test of a NbTi based coil: the verification of the performance of the NbTi conductors for the PF coils is necessary to support the design. New R&D activities have been initiated in this area which must include, as the essential part, the manufacture of a coil with a full size conductor and conductor length of the order of 100 m. This coil should be tested in pulsed conditions. The design and test programme for the NbTi coil are under study.

Winding

There are two options to provide the structural material within the CS winding. The first one is based on the CSMC development and uses an Incoloy square jacket with a co-wound strip. The second one uses two U-channels welded around a thin circular jacket. The selection of the option has some limited impact on the CS flux capability but the choice can be postponed until more R&D data is available. The Incoloy option requires some R&D to demonstrate consistent butt weld quality without hot cracking. For the double jacket option, details of the assembly process of the U-channels after heat treatment of the inner conductor have still to be addressed.

Two options of the TF coil winding are still under investigation: one with a circular conductor embedded in radial plates and the other with a square conductor. The radial plate option is based on the TFMC development and is preferred in view of its advantages in terms of the insulation reliability and fault detection capability. However, this option suffers from cost and radial build penalties. The difference in inboard leg radial build is 30-50 mm and this has an influence on the radial build of the whole machine. The selection of the radial plate option requires the initiation of R&D on the fabrication procedure for full-size plates to minimize cost.

Structures

The key structural issue remains the out-of-plane supports of the TF coils at the inboard curved region in the vicinity of the divertor. Various design concepts have been analysed but the final design has not yet been established. The solution will require a strengthening of the coil case in the critical region and structures able to resist shear loads between adjacent coils. It is possible that an acceptable design will require a thicker case in the inner leg region, imposing a radial build penalty of a few cm. The main issue is a proper analysis of the final coil design to demonstrate that the support design is effective and sufficiently insensitive to manufacturing and assembly tolerances. This is expected to take several months from the time that the coil geometry is finalised, without including design iterations.

Manufacturing feasibility of the TF coil structures is being investigated by R&D programs for the fabrication of full scale sections of the coil case. This development has identified manufacturing processes (forgings, castings, welding) which are expected to result in cost savings. Other areas, which will be the subject of future R&D work, are related to the design,

assembly and testing of mock-ups of the insulated shear keys and friction joints of the TF intercoil structures.

II.1.4 Cryoplant and Cryodistribution

The cryogenic system provides cooling for the following components: the superconducting magnet system, the thermal shields, the torus, NB and cryostat cryopumps, as well as small users including pellet fuelling, gyrotrons and diagnostics. The main load by far is the magnet system.

The cryogenic system includes two types of equipment: the cryoplant and the cryodistribution system. The cryoplant consists of a conventional LHe production plant and subsystems that contain a He gas loop together with LN₂ refrigerators for cooling the thermal shields by 80K forced-flow helium.

The cryodistribution system comprises the auxiliary cold boxes (ACBs) with cold helium circulating pumps, cold compressor boxes (CCBs) and a system of cryogenic transfer lines that distribute liquid helium at 4K and 80K helium to the different components of the tokamak.

Pulsed heat loads are deposited in the magnet system due to electromagnetic variations and nuclear heating. The operating temperature of the LHe plant is kept at 4.3K in order to allow the active smoothing of the pulsed heat loads and ensure that the helium temperature at the inlet of the magnet system does not exceed 4.5K. Cold helium compressors are incorporated in the cryodistribution system for operating at 4.3K and the work of these compressors is an additional heat load.

Another key requirement for the design of the cryodistribution system is the necessity to provide forced-flow cooling for the magnet system by cold circulating pumps. This requirement leads also to an additional heat load on the LHe plant. A further significant factor for the LHe plant design is the requirement for fast cooldown of the cryopumps as required after regeneration.

II.1.4.1 Refrigeration and Liquefaction Requirements for the LHe Plant

The LHe plant is operated in a combined refrigeration/liquefaction cryogenic cycle. Liquefaction capacity is required to cool the current leads of the magnet system and to provide cooldown of the cryopumps (see Table II.1.4-1). The requirement to operate in the liquefaction cycle has a strong impact on the design of the LHe plant because thermodynamic efficiency of the liquefaction cycle is significantly lower than the efficiency of the refrigeration cycle.

The refrigeration heat loads (see Table II.1.4-1) are subdivided in three different categories from the point of view of their impact on the LHe plant operational controllability. The first category includes static/permanent heat loads as a result of thermal radiation and conduction through the 80K thermal shields and gravity supports. The second category covers pulsed heat loads due to electromagnetic variations and nuclear heating and the third category comprises the variable heat loads of the cold circulation pumps and compressors.

Table II.1.4-1 Cooling Capacity of the LHe Plant

Liquefaction to cool the current leads	kg/s	0.066
Static heat load	kW	9.3
Averaged pulsed heat load [1]	kW	19
Heat loads of helium circulating pumps	kW	14.1
Heat load of cold compressors	kW	7.5
Torus cryopumps including liquefaction for fast cooldown during their regeneration [2]		4 kW + 0.06 kg/s
Small cryogen users	kW	1.0
Total	54.9 kW + 0.126 kg/s	

[1] Pulsed heat loads are shown for the plasma scenario with a pulse repetition time of 1800 s and 500 s plasma burn phase.

[2] Initially 6 cryopumps will be installed. For steady state operation, 4 additional cryopumps will be added to the 6 cryopumps in order to allow continuous operation in such a way that at any time, 6 cryopumps are pumping and 4 cryopumps are under four different stages of regeneration.

II.1.4.2 Design of the LHe Plant

The design of the cryoplant is based on proven technology. There already exists a design of 18 kW refrigerators for CERN to supply the superconducting ring of the Large Hadron Collider. A modification selected for ITER is the use of LN₂ precooling as the reference for the LHe plant, because this option allows more flexibility for the gradual cooldown of the magnet system as well as the possibility of using LN₂ from the LHe plant to cope with the increased heat load on the thermal shields during VV baking. With this arrangement the total cooling capacity of the LN₂ subsystem is a minimum. The LHe plant of ITER-FEAT has four 18 kW CERN-type modules. The heat load from the LHe plant on the LN₂ refrigerators is 200 kW.

II.1.4.3 Design of the He Gas Cooling Loop of the 80K Thermal Shields and LN₂ Subsystem

The 80K compressed helium gas flow is used for active cooling of the 80K thermal shields. The helium gas is cooled down to 80K by boiling LN₂. The heat loads on the 80K helium cooling loop and LN₂ refrigerators for normal operation (VV at 140°C) is approximately 660 kW. This not only covers the thermal shields inside the cryostat as well as those for the VV, cryopumps, cryolines, etc. When baking of the VV is required, its temperature will be increased giving a higher heat input to the surrounding thermal shield. However, during this time there is no plasma operation, resulting in a much reduced load on the cryoplant, so that the additional load to the thermal shields is compensated for by the increased LN₂ supply available from the cryoplant.

The 80K helium loop together with the LN₂ refrigerators are subdivided into two identical cooling groups. This cooling scheme provides redundancy for maintaining the thermal shields at 80K (as well as the magnet system at 4.5K) in case any of the 80K cold boxes or 80K cryogenic transfer lines of one cooling group is unavailable due to a vacuum leak or malfunction.

II.1.4.4 Cryodistribution Design

The cryodistribution system consists of six separate ACBs plus one CCB for operating at 4.3K (see Figure II.1.4-1). Two identical cryoplant termination cold boxes (CTCBs) are incorporated in the cryodistribution system in order to allow for nominal operation in case one CTCB is unavailable.

Each ACB contains two identical helium circulating pumps for redundancy against pump failure and a helium heat exchanger that is immersed in a bath with boiling liquid helium. Cold control and bypass valves are installed in each ACB of the magnet system in order to smooth heat loads on the LHe plant by bypassing the helium heat exchanger.

The CCB for operation at 4.3K contains four helium cold compressors connected in parallel to provide redundancy against compressor failure and flexibility to operate at reduced cooling capacity.

Cryogenic transfer lines are incorporated in the cryodistribution to connect the CCBs/ACBs with the many coil termination boxes (CTBs) and cold valve boxes (CVBs) of the different components. Each cryogenic line is terminated with a half (or quarter) circumferential ring manifold which has many tee-sections in order to connect with the CTBs or CVBs. The cryodistribution system includes 2 parallel cryolines connecting the ACBs/CCBs to the main cryoplant cold boxes, which are located in the cryoplant buildings. The total length all of the cryolines and manifolds is about 1 km.

II.1.4.5 Assessment

The LHe plant includes four refrigerator modules, similar to those of CERN, to operate at the nominal plasma repetition time of 1800 s and plasma burn time of 500 s. There appear to be no principle problems for detailed design work. However, the arrangement and layout of the ACBs, CCBs and cryogenic transfer lines require detailed studies to allow integration in the tokamak building and provide the necessary access for installation and maintenance of the cryodistribution system.

For the magnet system, attention will continue to be focused on analyses related to smoothing the large pulsed heat loads so as to facilitate efficient operation of the LHe plant as a quasi-steady-state device.

Heat load data for steady state operation have not yet been estimated. Until a detailed evaluation is undertaken, it is assumed that while for long pulse operation the accumulated nuclear heat load and control losses are proportional with pulse length, the scenario losses would be proportionally less, and hence the two might overall cancel out. If this is confirmed, then steady-state operation would have little or no impact on the cryoplant¹.

¹ N 10 MD 6 99-09-22 W 0.1 Initial considerations on Impact of Steady State Operation of RTO/RC ITER on Tritium Plant, Cooling Water System and Cryoplant.

224

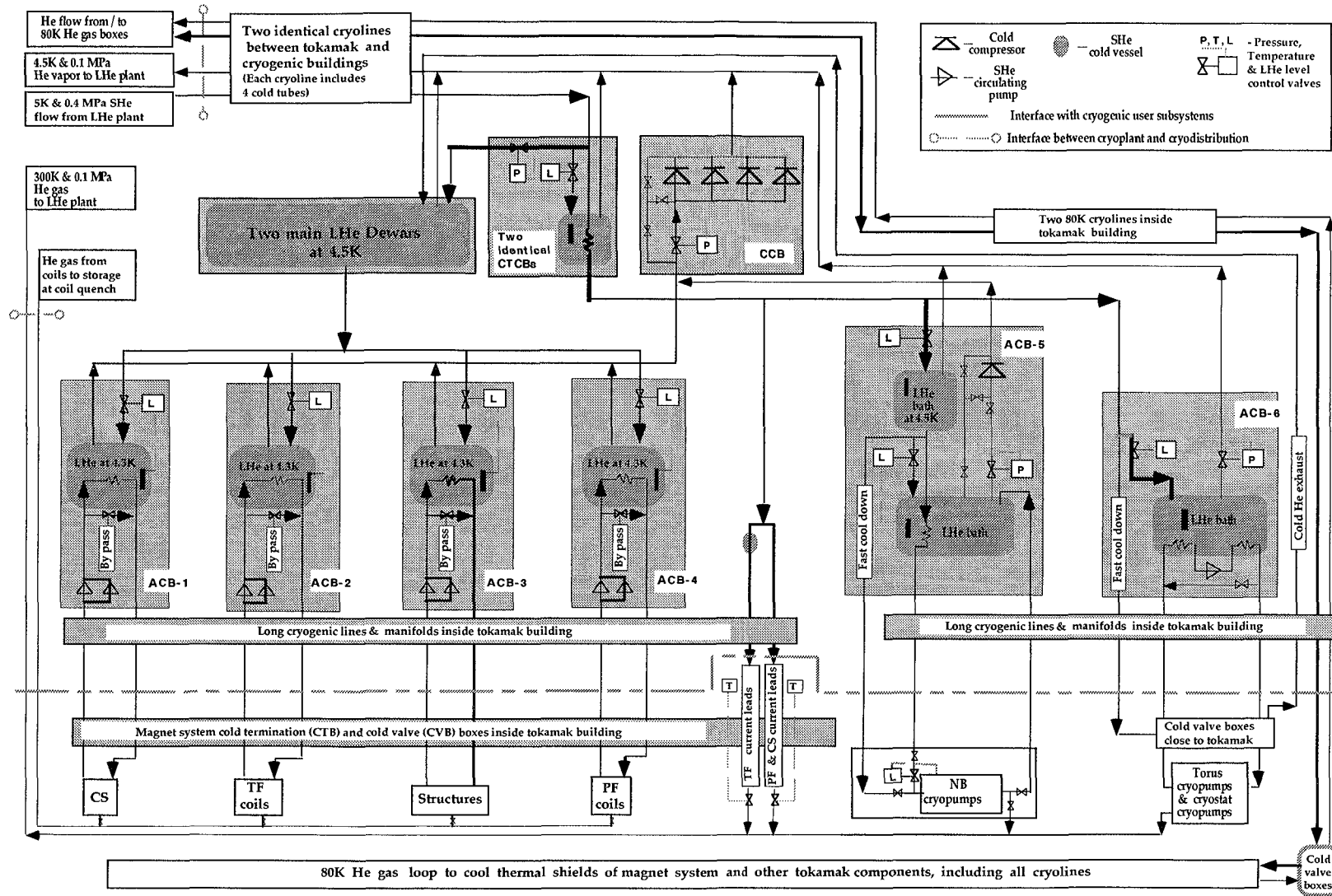


Figure II.1.4-1 Principal schematic of the cryodistribution system

N 34 GR 19 99-11-18 W 0.1

G A0 R12 00-01-18 R1.0

II.2 Vacuum Vessel and In-vessel Components

II.2.1 Vacuum Vessel

II.2.1.1	Vacuum Vessel Function and Main Components	1
II.2.1.2	Vacuum Vessel Design	1
II.2.1.2.1	Overall arrangement	1
II.2.1.2.2	Main vessel structure	3
II.2.1.2.3	Shielding structures	4
II.2.1.2.4	Port arrangement	4
II.2.1.3	VV Cooling and Baking	6
II.2.1.4	Vacuum Vessel Fabrication	6
II.2.1.5	Vacuum Vessel Assembly	7
II.2.1.6	Loads and Analysis	8
II.2.1.7	Vacuum Vessel Pressure Suppression System (VVPSS)	10
II.2.1.8	Conclusions	10

II.2.1.1 Vacuum Vessel Function and Main Components

The primary functions of the vacuum vessel (VV) are to provide a high quality vacuum for the plasma, as well as the first confinement barrier of radioactive materials and a second barrier (after the cryostat) for the separation of air from potential sources of in-vessel hydrogen generation. The VV decay heat can be removed by the water in the VV cooling system, even when all the in-vessel cooling loops are not functioning. The vessel supports the blanket and divertor components against electromagnetic loads during plasma disruptions and vertical displacement events. In addition, a tight fitting configuration of the VV aids the plasma vertical stability, and the ferromagnetic material in the VV reduces the toroidal field ripple. Along with other in-vessel components, the VV provides radiation shielding in particular for the magnets.

The main components that make up the VV are the main vessel, port assemblies, and mechanical support structures for in-vessel components.

Integrated functionally with the VV is the vacuum vessel pressure suppression system (VVPSS). This system minimizes the peak pressure inside the vacuum vessel during an in-vessel LOCA by relieving the pressure, caused by the ingress of a water steam mixture from damaged, water-cooled, in-vessel components, through rupture discs via pipework into a steam condenser tank.

II.2.1.2 Vacuum Vessel Design

II.2.1.2.1 Overall arrangement

The VV is a torus-shaped, double-wall structure with shielding and cooling water between the shells. The VV is located inside the cryostat and supported by flexible supports from the toroidal field (TF) coil case (see II.1.3.2.4).

The blanket and divertor are mounted on the vessel interior and all loads are transferred through the vessel to the vessel supports. The blanket modules are supported directly by the VV and the blanket cooling channels are either part of the VV double wall or are routed over its plasma-side surface (see II.2.2). The basic configuration and poloidal cross-section of the

VV (with the integrated blanket cooling channels) are shown in Figures II.2.1-1 and 2, respectively. Detailed parameters are shown in Table II.2.1-1.

G 15 GR 65 99-12-06 W0.1

G 15 GR 66 99-12-06 W0.1

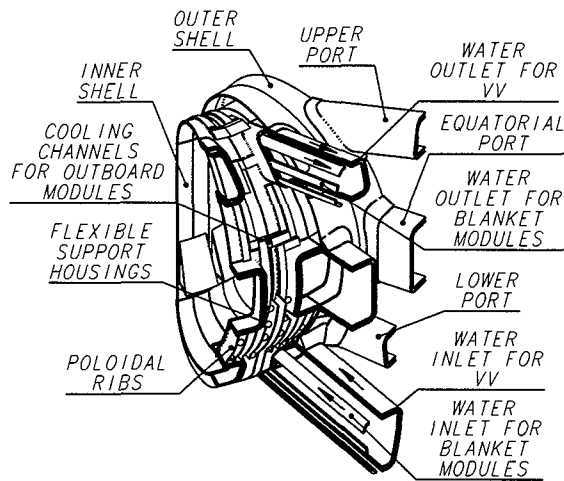


Figure II.2.1-1

Vacuum Vessel Overall Arrangement

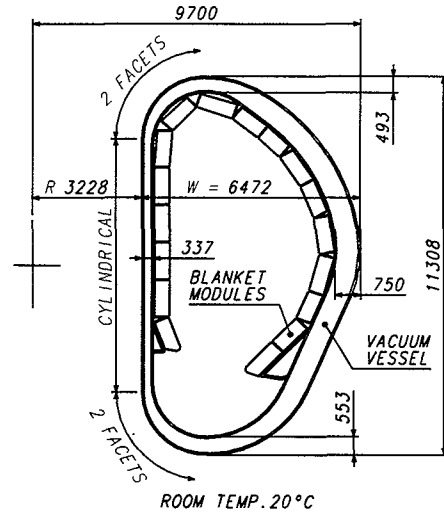


Figure II.2.1-2

Vacuum Vessel Cross-Section

Table II.2.1-1 Main VV Parameters

	ITER-FEAT
Size	
- Torus OD	19.4 m
- Torus Height	11.3 m
- Double-Wall Thickness	0.34-0.75 m
- Toroidal Extent of Sector	40°
- Number of Sectors	9
- Shell Thickness	60 mm
- Rib Thickness	40 mm
Structure	
- Inboard Straight Region	Cylindrical
- Inboard Top/Bottom (Facets/Sector)	2
- Outboard Region (Facets/Sector)	2
Resistance	
- Toroidal	8.8 $\mu\Omega$
- Poloidal	3.8 $\mu\Omega$
Surface Area / Volume	
- Interior Surface Area	943 m ²
- Interior Volume	1608 m ³
- Structural Volume (cooling channel)	642 m ³
Materials	
- Main Vessel	SS 316L(N)-IG
- Primary Shielding	SS 30467
- Ferromagnetic Insert Shielding	SS 430
Mass (without water)	
- Main Vessel (without shielding)	2395 t
- Shielding	2500 t
- Port Structures	1606 t
- Total	6501 t

Note) Parameters are for the VV with the integrated blanket water cooling channels.

II.2.1.2.2 Main vessel structure

The double-wall structure is made from SS 316L(N)-IG (ITER Grade), with stiffening ribs between the shells to give the required mechanical strength. The inner and outer shells are both 60 mm plates and the stiffening ribs 40 mm plate. The space between the shells will be filled with plates made of SS 304 containing 2% boron (SS 30467), and the ferromagnetic SS 430 (see II.2.1.2.3). With integrated blanket cooling channels in the vessel inter-wall volume there is less space for shielding plates. However, shielding fill factors of ~ 60 % in the spaces around the module support housings and the blanket cooling channels appear to be adequate for the expected neutron load.

Because of the direct attachment of the blanket modules to the VV inner shell, a "tight fitting" configuration is beneficial. The tight fitting vessel, together with the toroidally continuous structure of the triangular support frame for the bottom blanket modules (see II.2.1.6), also aids the plasma vertical stability. If further improvement is required in the plasma vertical stability, copper cladding¹ could be added partially to the vessel inner shell.

Each blanket module is attached directly to the VV (or the triangular support frame) by a set of four radial flexible supports located symmetrically with respect to its centre (see Figure II.2.1-3). The supports are mounted in housings that are recessed into the vessel inter-wall volume (see II.2.2.5.) The inclusion of the support housings into the VV double wall complicates the VV structure and significantly increases the amount of welding and machining required during fabrication. In addition, stresses in the VV due to loads on the blanket modules are localized. Furthermore, the higher neutron load on the VV due to the reduced shielding thickness of the blanket system and the direct neutron streaming through the gaps between modules, causes increased nuclear heating of the VV². However, this can be accommodated by increasing the VV coolant velocity (see II.2.1.3) with small impact on the VV cooling loop cost. The benefits of having the modules mounted directly on the VV is that without an intermediate structure (such as a back plate) between the module and the VV, the maximum temperature of the modules during a LOCA will be lower, the total thickness of the VV and blanket (radial build) is reduced, and the VV/blanket assembly time is reduced.

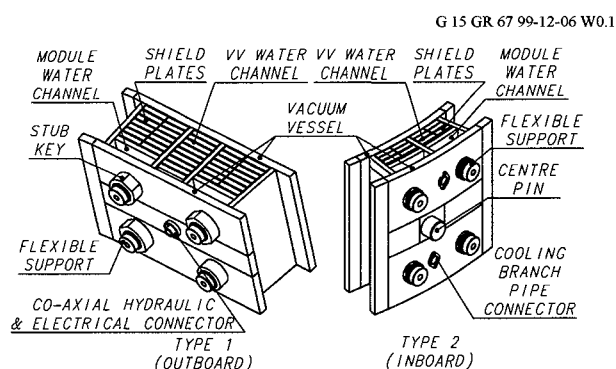


Figure II.2.1-3
Module Attachment to Vacuum Vessel

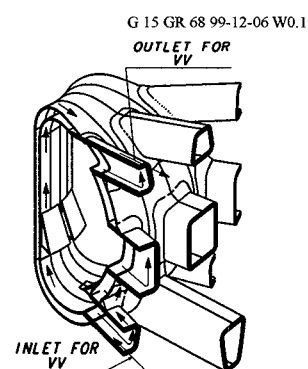


Figure II.2.1-4
VV Water Routing

¹ "Report on investigation of copper cladding VV design" - JAHT report, INT-9006 Rev. 1 - June 9, 1999.

² G 15 MD 168 99-11-17 W 0.1, "Preliminary assessment of required cooling condition for vacuum vessel of ITER-FEAT," and G 15 MD 167 99-11-17 W 0.1, "Preliminary estimation of heat load for VV PHTS of ITER-FEAT."

The cooling water for the VV is routed to a manifold structure at the bottom of the sector and from here flows up both sides of the sector to the top and out as shown in Figure II.2.1-4. Two independent water loops are used in each of the 9 sectors, feeding all sectors (see II.5) in parallel. This configuration was selected to provide a system with maximum natural convection cooling to remove decay heat during a loss of power or pump failure.

For the solution with blanket cooling channels integrated into the VV double-wall structure, each VV 40° sector contains six independent blanket cooling circuits, two inboard and four outboard. Cooling water is supplied to the toroidally centred divertor port of each sector and is then routed upward. The cooling water exits the toroidally centred upper radial port stub of each sector (see Figure II.2.1-1). The blanket cooling channels within the vessel are located on the back of the inner walls of the VV, while those in the port extensions are routed within the double-wall structure. The possible concern of cross-contamination of blanket and vessel coolant loops with this design solution is discussed in II.2.2.7.

The ITER-FEAT configuration is viewed as feasible with no major issues from a design standpoint.

II.2.1.2.3 Shielding structures

To provide an adequate neutron shielding, the space between the shells is filled up to 60% with plates made of SS 304 with 2% boron (UNS designation SS 30467). The ferromagnetic SS 430 is used as the shielding material under the TF coils in the outboard volume area instead of SS 30467. These plates fill up to 80% of the volume between the shells to reduce toroidal field ripple.

The integration of the module support structures within the VV double wall makes the arrangement of the shielding plates complex. Each plate must now be individually cut and positioned around these obstructions (see Figure II.2.1-5). This added complexity is not a feasibility issue but will have some cost impact.

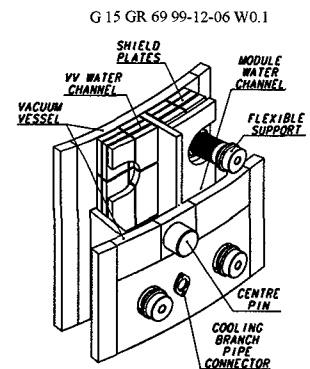


**Figure II.2.1-5
VV Shield Structures**

II.2.1.2.4 Port arrangement

The vacuum vessel has upper, equatorial, and lower port structures used for equipment installation, utility feedthroughs, vacuum pumping, and access inside the vessel for maintenance. The basic port arrangement is shown in Figure II.2.1-1. A preliminary summary of the port allocation and the port inside dimensions is given in Table II.2.1-2.

The upper ports have a trapezoidal cross-section and are inclined upwards. The upper ports will be used for diagnostics, EC neoclassical tearing mode stabilisation, connections with the VV pressure suppression system, and blanket/VV water outlet piping. The openings for the upper ports are designed to provide the access required for the diagnostics, etc. and neutron shielding.

For the diagnostic ports, a diagnostic plug with the diagnostic equipment/feedthroughs is located inside the port and attached to the port with a flange joint. The vacuum/pressure seal

is made with a lip joint which is incorporated into the bolting flange. Special components to withstand the loads acting on the plugs may be also incorporated into the flange joints (e.g. the wedges to withstand the torsional loads).

For the piping ports, the pipes for the VV and the blanket cooling are attached to the port outer surface¹. These pipes may be enclosed with thin-wall guard pipes. A shielding plug will also be placed inside the port and some equipment may be integrated into this plug.

The equatorial ports include regular ports and neutral beam (NB) ports. For the regular ports, the in-port components are integrated into one sub-assembly (the port plug). These ports have a rectangular cross-section and the port plug is attached to the port with the flange joint and supported as a cantilever. Similar to the upper port, the vacuum/pressure seal is made with a lip joint and the wedges are incorporated into the flange joint to withstand radial torque (torsional) loads.

The NB ports are located in adjacent sectors of the machine. The port structure is rather long and extends to the interface points with the cryostat and the NB system. To enhance local shielding, a massive shield plug is integrated into the port structure. The port components and the liner may consist of several parts which would be assembled on-site.

The lower ports have a trapezoidal cross-section and are inclined downwards. Based on a preliminary port allocation, these ports include three ports with large openings that will be used for divertor cassette maintenance and diagnostics. The remaining ports have smaller openings and are used for vacuum pumping and diagnostics and to provide the connection points for blanket/VV water inlet piping. The blanket/VV layout is in general analogous to that at the upper port level. In addition to the blanket/VV pipes, the divertor pipe feedthroughs penetrate through every lower port.

The general design of all port structures includes a port stub, a port extension and a port plug/closure plate. All port components are of double-wall construction with stiffening ribs between the walls. The total thickness of the port stubs/extensions is normally 200 mm. The NB port components generally require a thicker wall to enhance the port shielding properties. Steel plates may be incorporated between the walls of some ports to enhance local shielding.

Table II.2.1-2 Summary of Port Arrangement

Port Type	Number of Ports	Inside Dimensions (m)
Upper		
- Diagnostics, EC, Pressure Suppression System, piping for Blanket/VV cooling	18	0.6 to 1.2 (width) x 1.2 (height)
Equatorial		
- Regular (RH/Port Limiter, Heating Systems, Diagnostics, Test Blanket Modules)	15-16	1.8 (width) x 2.2 (height)
- Neutral Beam	3-2	0.6 (width) x 1.2 (min. height)
Lower		
- RH & Diagnostics	3	0.4 to 1.4 (width) x 2.2 (height)
- Diagnostics, Cryopump & Piping	15	0.4 to 1.3 (width) x 1.9 (height)

Note) Preliminary port arrangement and dimensions

¹ G 15 MD 165-99-10-06 W0.1, "Proposed Layout of the VV and Blanket Pipes for IAM."

II.2.1.3 VV Cooling and Baking

The water flow velocity and flow rate for normal operation needs to cope with the nuclear heating rate in the VV mentioned above, in such a way that will keep thermal stresses in the VV structure at acceptable levels. Table II.2.1-3 summarizes the VV cooling and baking conditions for the VV. The required water flow condition for normal operation is forced turbulent flow. Irrespective of the choice of integrated or separate cooling channels, it is preferable for the VV and blanket cooling water temperatures to be similar for normal and baking operations to minimize thermal stresses in the VV structure. For normal operation in the integrated case, since the water temperature for the modules is between 100°C (inlet temperature) and ~ 150°C (outlet temperature), the inlet temperature for the VV water was set at 120°C. For baking operation, the VV and module water temperatures are both 240°C.

The inlet pressure for the VV cooling system for both normal and baking conditions is 1.8 MPa and 5.2 MPa, respectively. Natural convection cooling is required to remove the decay heat of both the VV and blanket during off-normal events, such as a VV LOFA (e.g. a multiple cooling pump trip).

Table II.2.1-3 Cooling/Baking Conditions of the Vacuum Vessel

Parameters	Unit	Value*
Maximum Total Heat Removal	MW	14
Water Parameters		
- Normal Operation		
- Inlet / Outlet Temperatures	°C	120 / ~ 124
- Inlet Pressure	MPa	~ 1.8
- Flow Velocity	m/s	0.04
- Total Flow Rate for Parallel Cooling System	kg/s	~ 950
- Baking Operation		
- Inlet Temperature	°C	240
- Inlet Pressure	MPa	~ 5.2

*: Preliminary values for the VV with the integrated blanket water cooling channels.

II.2.1.4 Vacuum Vessel Fabrication

The VV is to be fabricated in the factory as 9 sectors each spanning 40°. Each sector includes a full set of ports at the toroidal centre of the sector and a set of half ports (split on the port centre) on each side. The port stubs on the lateral sides of the sector are not installed in the factory. This allows the TF coils to be installed in the assembly area (discussed in II.2.1.5).

Two concepts have been considered for the sector fabrication scheme. One is to complete the inner shell first because the inner shell forms the first confinement boundary. Butt weld joints can be fully applied to the inner shell and inspection can be easily performed. Another concept is to utilize poloidal segments of a double-wall structure, which are fabricated first then welded together to form a sector. This scheme was employed for the full-scale vessel sector fabrication in the L-3 R&D project.

Due to the addition of the blanket supports and (possibly) the blanket cooling channels into the VV double-wall structure, the total amount of welding and machining is high. The

consequence of this additional welding during the fabrication of the sector is a high fabrication cost and possibly increased weld distortions. For the weld distortion, however, careful welding design, procedure and control can make the target tolerances (sector fabrication tolerance: ± 10 mm) achievable. For the VV with the separate blanket cooling manifolds, the VV fabrication cost will be somewhat less.

To reduce the VV fabrication cost, a forged and/or cast structure has been investigated¹. The bottom of the VV is a highly-stressed region, requiring numerous reinforcements. Instead of an all-welded shell structure, a forged structure would reduce the fabrication cost and improve the fabrication tolerances there. In addition, a large number of the housings in the VV for the blanket module supports that have a relatively small and simple structure can be manufactured by precision casting or forging for cost saving. A preliminary comparison of the fabrication costs between the forged/precision cast structures and the welded structures shows a cost benefit for the forged/precision cast structure. Powder HIPing is also being considered for further cost reduction.

The most important VV R&D performed so far during the EDA was associated with the fabrication of a sector. The Full Scale Sector Model, fabricated and tested as a part of the L-3 project, provided critical information related to fabrication technology required to produce a high quality sector, and the magnitude of welding distortions and achievable tolerances. Since the basic design of the ITER-FEAT VV is the same as the fabricated sector model (i.e. the material, the basic torus shape, and the double-wall structure with shielding and cooling water between the shells), this R&D also validated the fundamental feasibility of the ITER-FEAT double-wall design. Additional R&D, such as the fabrication of a partial VV sector model, may be required to confirm the improved fabrication technology and associated tolerances.

II.2.1.5 Vacuum Vessel Assembly

At the ITER site, each 40° sector is mated to two TF coils (and thermal shield) and assembled. Sector /coil mating involves moving a TF coil over each end of the sector. The port stubs are then welded in place. The sector and TF coils assembly is lowered into the pit. After the sectors and coils are positioned in the pit, 9 field joints (located on the centre of the ports) can be TIG-welded using splice plates to compensate for the size differences of the sectors. The final machine assembly sequence involves a sequential attachment of adjacent sectors until the resulting 160° and 200° segments are finally joined.

If disassembly of a sector is required after ITER operation has begun, the plan is for the replaced unit to be the same size as the one initially installed (i.e. a 40° sector).

The advantages of the proposed VV sector geometry versus one relying on one shop-manufactured sector per TF coil result from the reduction in operations and associated requirements. The three most important benefits to assembling this larger sector are (1) the reduction of assembly cost by reducing the number of field joints; (2) improved dimensional stability due to the reduction in field joint welding; and (3) the reduction of pre-assembly and assembly time. In addition, the proposed VV sector geometry provides simple water routings

¹ "Improvement of VV fabrication method for RC-ITER" - JAHT report, INT-9022 - June 11, 1999 and "EU contribution to the task force report, Section VI.5 Improvement of manufacturing processes for cost reduction," EUHT report, June 14, 1999.

for the VV and blanket modules in the VV structure, and full port structures at the toroidal centre of the sector.

II.2.1.6 Loads and Analysis

The VV must withstand many individual and combined loading conditions during both normal and off-normal operation. For normal operating conditions (category I and II events), the most severe loads are caused by the coolant pressure, VV and in-vessel component weights, seismic events, plasma disruptions and VDEs, and the TF coil fast discharge (TFCFD). The loads that will most likely drive the design are due to a centred disruption, VDE, and a TFCFD. An initial estimate of VV loads is shown in Table II.2.1-4. The component masses and the coolant pressure loads are defined in II.2.1.2.1 and II.2.1.3 respectively.

Table II.2.1-4 VV Load Summary¹

	ITER Load Category (see I.1.5)	Loads
Plasma current quench		
- EM pressure on inboard/outboard VV wall due to induced currents (MPa)	II	1.2/0.6
Centered disruption		
- Maximum radial moment on a module at the inboard wall (MNm)	II	-0.62
- Maximum poloidal moment on a module at the inboard wall (MNm)	II	0.95
VDE followed by a fast current quench (Fast VDE)		
- Maximum radial moment on a module at the inboard wall (MNm)	II	-0.87
- Maximum poloidal moment on a module at the inboard wall (MNm)	II	1.13
VDE followed by a slow current quench (Slow VDE)		
- Maximum EM pressure on the VV wall due to halo current (MPa)	III	3.96
- Poloidal force on a module (MN)	III	0.9
- Radial force on a module (MN)	III	1.0
- Maximum total net vertical force on VV and blanket for downward/ upward slow VDE (MN)	III	-70/ 40
- Maximum total net horizontal force on the VV and blanket (plasma tilting and shifting) (MN)	III	25
TF coil fast discharge		
- EM pressure on the VV inboard wall due to the poloidal induced current (MPa) [Current quench time (s)]	I	1.7 [11]

A 20° section computer model of the VV has been generated to make preliminary estimates of the induced EM loads for the cases of a centred plasma disruption, VDEs and TFCFD². In this analysis it was assumed that copper cladding layers were located on the VV inner shell at the inboard and outboard regions. For example, in the case of a centred disruption, a plasma current of 13.3 MA was assumed to linearly decrease to zero in the 25 ms of the disruption time. A peak EM pressure value of 2.1 MPa is found near the equatorial port corner at the outboard region.

¹ G 15 MD 174 99-12-08 W 0.1, "EM loads on vacuum vessel and modules for ITER-FEAT."

² "RFHT Report on Initial electromagnetic analysis of vacuum vessel and blanket for IAM," October, 1999.

An assessment of the elastic buckling¹ and inelastic buckling² has shown the lowest buckling load of 6.6 MPa for the VV in the case of a TFCFD with an inboard wall thickness of 388 mm (6.5 MPa for the current VV geometry with the inboard wall thickness of 337 mm). Following the RCC-MR code (load factor = 2.5), the maximum allowable EM pressure to prevent buckling will be 2.6 MPa.

Special attention has been given to the analysis of the VV inboard wall and the stress caused by the direct attachment of the blanket modules to the VV³. The design of this region is driven by the TFCFD loads and the plasma VDEs which are assumed to occur at the same time. In this case with a downward VDE, large stresses have been found in the lower region of the straight part of the VV inboard wall where the halo current loads are also greatest. To prevent the structural buckling of the VV inboard wall and to keep the primary stresses below the allowable values, the support frame for the modules in the inboard bottom region needs to be a toroidally continuous structure⁴. In case the TF coil fast discharge event is not combined with a plasma disruption or a VDE, the primary stress in the VV is below the allowable even without this structural reinforcement⁵. Table II.2.1-5 summarizes the preliminary results of the primary membrane stress intensities in the VV inboard region with and without the toroidally continuous structure of the triangular support frame for the modules.

Table II.2.1-5 Preliminary Results of the Primary Membrane Stress Intensities at the VV Inboard Region

Case	EM Pressure (MPa)		Primary Membrane Stress Intensities at the Inboard Region (MPa) [Safety Margin*]		ITER Load Category	Allowable Stresses** (MPa)
	TFCFD	VDE	Without Toroidal Connection***	With Toroidal Connection***		
TFCFD	1.7	-	66 [2.1]	66 [2.1]	I	137
TFCFD + VDE I ⁺	1.7	2.2	131 [1.0]	121 [1.1]	II	137
TFCFD + VDE II ⁺⁺	1.7	2.7	147 [1.1]	137 [1.2]	III	164

* The stress safety margin is the ratio between the allowable stress and the calculated stress intensity.

** Allowable stresses are at 200°C.

*** With or without the toroidally continuous structure of the triangular support frame for the modules in the inboard-bottom region.

+ $I_{\text{halo}}/I_{\text{plasma}} \times \text{TPF}$ (toroidal peaking factor) = 0.348 (60% of the VDE III).

++ $I_{\text{halo}}/I_{\text{plasma}} \times \text{TPF}$ = 0.435 (75% of the VDE III).

¹ G 15 MD 144 99-04-27 W0.1, "Elastic buckling of the RTO-RC ITER VV inboard wall due to TFC fast current discharge"

² G 15 MD 149 99-06-15 W0.1, "Inelastic buckling of the RTO/RC ITER VV inboard wall due to TFC fast current discharge"

³ G 15 MD 135 98-11-13 W0.1, "Primary Stress in the VV Inboard Wall due to the Module Direct Attachment (RC-ITER IAM Configuration - Short Flexible)"

⁴ G 15 MD 150 99-06-18 W0.1, "Structural analysis of the VV IAM inboard wall in case of TFC fast discharge + slow VDE"

⁵ G 15 MD 153 99-06-25 W0.1, "TFC fast current discharge : Stress in the VV inboard wall"

A study has been performed¹ to assess the effect of the vertical support location on the VV structure. Support locations considered include the bottom of the VV and the region between the equatorial ports and the top of the VV. The results did not show a considerable difference in the stress values. Some localized high stresses are found, but they can be alleviated by local reinforcements.

Temperature gradients in the VV structure due to differences between the blanket coolant inlet and outlet temperature (50°C), differences between VV and blanket coolant temperatures, and the nuclear heating of the VV shells, result in thermal stresses in the VV. The maximum thermal stress occurs in the inner shell at the outboard wall. The thermal stresses (from start-up to normal operating steady-state conditions, at locations far from local structural discontinuities) in the outboard and inboard walls are 242 MPa and 215 MPa, respectively, which are in a range of $2S_m$ ².

Based on the analyses performed to date, the VV appears structurally capable of withstanding the loads to which it can be expected to be subjected.

II.2.1.7 Vacuum Vessel Pressure Suppression System (VVPSS)

Analysis³ shows that the combination of an upper quench tank with lower drain tanks would result in the lowest peak pressure during an in-vessel LOCA. Moreover, using a relief point at a high level inside the VV, the ejected medium is in the form of steam, and qualified codes may be used to compute the time pressure history. Using a duct cross-sectional area no smaller than 1 m² between vessel and quench tank (0.1 m² through the blanket), the peak pressure can be kept below 0.2 MPa. This limits the design pressure of the VV to around 0.2 MPa, which is important, especially for the design of its many port flanges and penetrations. Based on the postulated ingress of water and steam from the in-vessel coolant loops, the VVPSS quench tank capacity requirement is approximately 1100 m³. This tank will be installed inside the cryodistribution hall, at the west side of the tokamak hall.

The pressure relief pipe inside the cryostat is in stainless steel, but the external pipework and the quench tank are, for cost reasons, fabricated in carbon steel.

II.2.1.8 Conclusions

The VV design is still in an early phase of development but the basic design approach and concept appears feasible. The blanket modules are supported directly by the VV and the blanket cooling channels may be structurally part of the VV double wall. From an overall system standpoint, these changes have several important advantages such as the total thickness of the VV and blanket (radial build) is reduced, and the VV/ blanket assembly time is reduced. These advantages make this the correct choice for the ITER-FEAT machine. However, this change imposes additional requirements on the VV which makes the design more complex.

¹ G 15 MD 162 99-10-04 W0.1, "Stress in the RTO/RC ITER VV for different vertical support locations"

² G 15 MD 134 98-10-30 W0.1, "Thermal Stress in Steady State Condition in the VV Inboard Wall (RC-ITER LAM Configuration - Short Flexible)" and G 15 MD 138 98-12-18 W0.1, "Thermal stress in LAM and IAM VV in normal operation cycle"

³ S 84 MD 28 98-12-09 W 0.1, "Pressurization transients"

The attachment of the blanket modules directly to the VV results in an increase of the EM loads on the VV. These loads, although substantial, will be accommodated by structural reinforcements to the VV double wall.

Further detailed optimization and analyses of the VV structure are required.

In addition, detailed thermodynamic and structural analysis of the VVPSS will be required, followed by detailed design.

II.2.2 Blanket

II.2.2.1	Blanket Function and Main Components	1
II.2.2.2	Shielding Blanket Module Arrangement	2
II.2.2.3	Plasma-Facing and Heat Sink Materials	3
II.2.2.4	Blanket Module Design	3
II.2.2.5	Blanket Attachment Scheme	4
II.2.2.6	Port Limiters	6
II.2.2.7	Blanket Cooling and Baking	7
II.2.2.8	Blanket Fabrication	10
II.2.2.9	Blanket Assembly	12
II.2.2.10	Loads and Analysis	12
II.2.2.10.1	EM Loads	12
II.2.2.10.2	Structural Analysis	13
II.2.2.10.3	Nuclear Analyses of Torus Components	14
II.2.2.11	Conclusions	16

II.2.2.1 Blanket Function and Main Components

The basic function of the blanket system is to provide the main thermal and nuclear shielding to the vessel and external machine components. The blanket system is also designed to make possible the planned partial conversion (outboard area only) of the shielding blanket to the breeding blanket in a later stage of operation (if justifiable).

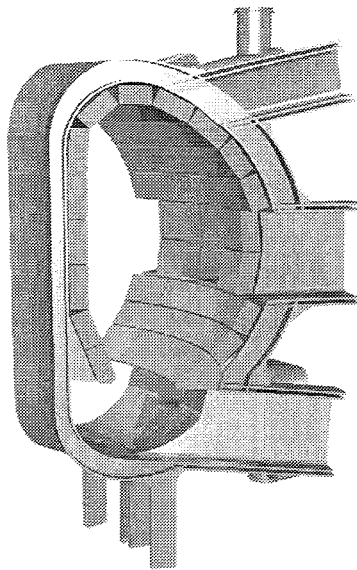
The basic component of the blanket is a module with a mechanical attachment system. The blanket modules (BM) are attached directly to the vacuum vessel. Manifolds that supply cooling water to the modules are integrated in the vacuum vessel. A summary of the component design is given below:

- (i) The blanket module thickness is 450 mm. On the one hand, a thick module is required to accommodate the thermal stress limits of the VV inner shell and to provide adequate neutron shielding for the VV. On the other hand, a 4.5 t RH payload and the layout of mechanical attachments limit the thickness of the module.
- (ii) The blanket shielding modules are proposed to contain a separable first wall, reducing the fabrication cost and the future volume of radioactive waste. They have a straight poloidal profile that eliminates double curvature of the first wall, apart from the modules adjacent to the divertor.
- (iii) The modules will be attached mechanically to the vacuum vessel utilizing flexible supports. The flexible support design has no active cooling.
- (iv) The inlet temperature and pressure of the cooling are 100°C and 3.0 MPa, respectively. From a materials point of view, the embrittlement of Cu under irradiation is acceptable (see II.2.2.3).

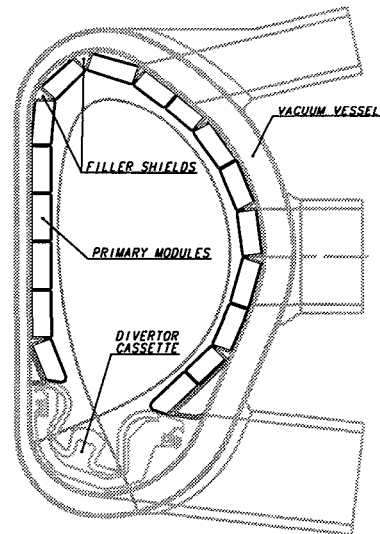
Table II.2.2-1 Shield Blanket Parameters

Total blanket thermal power ⁽¹⁾	GW	~ 0.65
Heat flux on first wall (FW), average/max.	MW/m ²	0.2 / 0.5
Heat flux on limiter, average/max.	MW/m ²	~ 3 / ~ 8
Neutron wall loading, average/max.	MW/m ²	0.57 / 0.78
Number of modules, total/NB injector modules		429 / 14
First wall surface area	m ²	682
Weight of modules	t	1813
Weight limit for module	t/mod.	4.5
Typical blanket module dimension (Inboard equator)	mm	1415x 1095x450
Coolant inlet pressure during normal operation	MPa	3.0
Coolant temperature, inlet/outlet	°C	100 / 150

(1) Unless stated otherwise, values in this table are based on the nominal fusion power only.



G 16 GR 11 99-12-07 W0.1

Figure II.2.2-1 Isometric View of Blanket System for ITER-FEAT

G 16 GR 12 99-12-07 W0.1

Figure II.2.2-2 Module Poloidal Segmentation for ITER-FEAT

II.2.2.2 Shielding Blanket Module Arrangement

The segmentation of the shield modules is established by taking into account the weight limit of 4.5 t per module imposed by the remote maintenance equipment, and the desire to minimize the number of modules for cost reduction. The module toroidal length varies from 1.1 to 1.9 m relative to 0.86 to 1.14 m for the poloidal length. The first wall (FW)/shield modules have a toroidal segmentation of 20° (18 modules) on the inboard, 10° (36 modules) on the outboard and 13.3° (27 modules) on the top. This segmentation may be adjusted following more detailed design of the blanket system including the cooling manifold and module attachment. The arrangements of shielding blanket modules is shown in Figures II.2.2-1 and -2.

II.2.2.3 Plasma-Facing and Heat Sink Materials

The armour, heat sink and structural materials are Be, Cu alloys and SS, respectively. Results of the EDA R&D lead to the conclusion that there are no major negative effects in operating with an inlet water temperature of 100°C.¹ In particular:

- although the work-hardening capability of irradiated Cu alloys decreases with temperature, the difference in uniform elongation in the range 140°-100°C is small both for the CuAl25-IG and CuCrZr-IG alloy selected as primary options for the blanket FW and divertor heat sink components;
- lower temperature operation increases the strength, fracture toughness and corrosion resistance of the structural materials;
- there is no significant impact on the performance of plasma-facing materials and joints in this temperature range.

II.2.2.4 Blanket Module Design

The ITER-FEAT blanket module is designed to reduce

- (a) module unit manufacturing cost,
- (b) nuclear waste associated with module replacement,
- (c) EM loads on blanket modules due to disruptions/VDEs.

The module configuration consists of a shield body to which a separable first wall (FW) is mounted. The separable first wall has a facet geometry consisting of multiple flat panels, where 3-D machining will not be required. This produces a simple unit design with low associated machining costs. Several FW panels can be produced in each hot isostatic pressing (HIP) cycle. The use of small separate FW panels eases the Be tile HIP joint and will minimise the scrap rate. The separation of the FW from the shield body allows manufacturing process costs to be minimised, and solid HIP will be used only for the FW panel fabrication. The use of multiple panels also makes possible the replacement of individual damaged units, reducing nuclear waste volume, and it simplifies the repair and replacement methods in the hot cell. A configuration with deep slits minimises the induced eddy currents and EM loads.

The blanket module consists of four or six separable FW panels. Two attachment methods are being considered: one is based on a central mechanical attachment, which is bolted to a shield block at its rear side², and the other is based on M12 or M16 bolts and small shear ribs to support EM loads and to prevent sliding due to thermal expansion³. Blanket module concepts with separable FW panels are shown in Figures II.2.2-3 and 4. The FW panel will be manufactured using solid HIP, the shield block is made from flat forged blocks and the coolant channels are produced simply by drilling and plugging. Powder HIP can also be used for the shield block or FW panel fabrication, and also the casting fabrication method for the shield block.

¹ G 73 MD 7 99-04-27 F1 – Assessment effect of inlet water temperature decreasing on materials behavior

² G 16 MD 228 99-04-21 Rev.1 – RTO/RC ITER primary wall blanket module design with separable mechanical attached first wall

³ G 16 MD 258 99-11-24 – Bolted first wall panel, and

EU contribution to the task force report, Section VI.5.2, EUHT proposal for a separated first wall/shield concept, EFET report KWU NDM1/99/E088, June 8, 1999

G 16 GR 13 99-12-07 W0.1

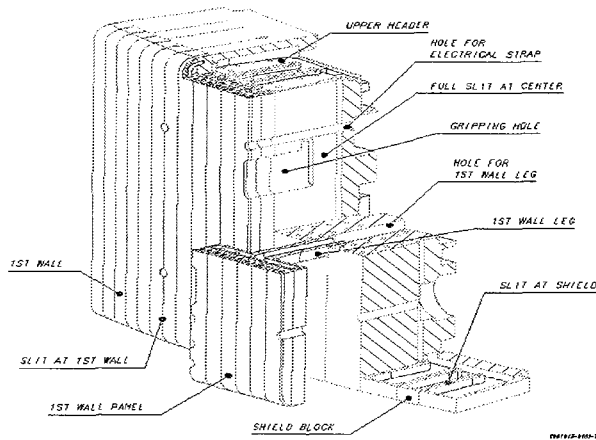


Figure II.2.2-3 FW Panel/Shield Block Bolted at the Rear Side using FW Leg

G 16 GR 14 99-12-07 W0.1

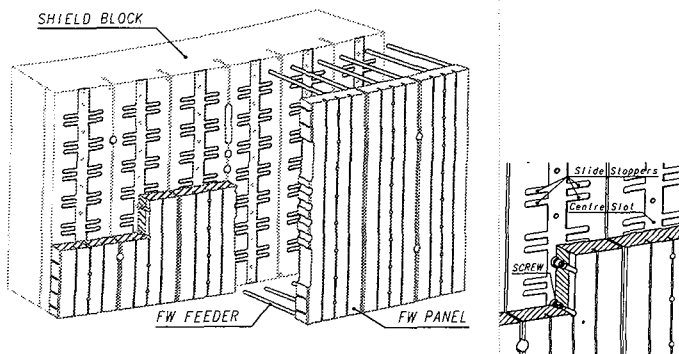


Figure II.2.2-4 FW Panel/Shield Block Bolted at the Front Side of Shield Block

The breeding blanket module is designed to make possible the planned partial conversion (outboard area only) of the shielding blanket modules, with the same dimensional, installation, support, coolant and maintenance constraints as the shielding blanket. Lithium zirconate is used as the ceramic breeder, with lithium titanate and silicate as alternatives. Beryllium pebbles are used for neutron multiplication, and water for heat removal. 316L(N)-IG stainless steel is used as structural material and Be armour is attached to the steel without using a copper heat sink.

II.2.2.5 Blanket Attachment Scheme

The blanket module attachment has functional requirements, such as positioning accuracy, movement allowances and load capability. The hydraulic, electrical and mechanical attachment system for the blanket modules to the VV are designed to transfer normal loads in the module to the VV while allowing small relative movements due to the different structural rigidities and thermal responses of the modules and the VV.

Flexible supports (see Figure II.2.2-5)

The depth of the vessel inter-wall volume is larger than the height of the supports, so the supports can be located behind the blanket module in a shielded position. The flexible cartridge does not need to be actively cooled. Under these conditions it is better to install the supports in the vessel rather than on the module. The tolerances of the vacuum vessel are compensated by adapting, i.e. custom machining, the large thread on the flange of the

cartridge¹. The attachment of the module involves driving the bolt from the tip, rather than from the head.

The flexible cartridges are made from Ti-alloy (Ti-6Al-4V) due to its high strength and low Young's modulus. The supports are connected to the VV support housings via M150x4 threads and to the modules with Inconel 718 (ASTM B637) bolts. The bolt preload (650 kN) is maintained under nuclear heating, and the stress cycle is within the fatigue limits. Radial adjustments of the flexible attachments allow accurate radial positioning of the first wall against the tolerances of the VV.

Some prototypes of the titanium flexible cartridges were successfully produced in earlier EDA R&D, and are being tested for loading, fatigue and buckling.

Keys and pin

Considering the reaction scheme of the radial torque and the toroidal and poloidal forces, two module attachment concepts are used:

- Type 1 (see Figure II.2.2-6) – The “stub key” with flat contact pads is integrated into the flexible support housing. A single unit with a co-axial interface for hydraulic connections and electrical straps is located in the centre of the module.
- Type 2 (see Figure II.2.2-7) – The attachment design utilizes a centre pin, two branch pipes, two electrical straps, and a key between the modules.

G 16 GR 3 99-12-07 W0.1

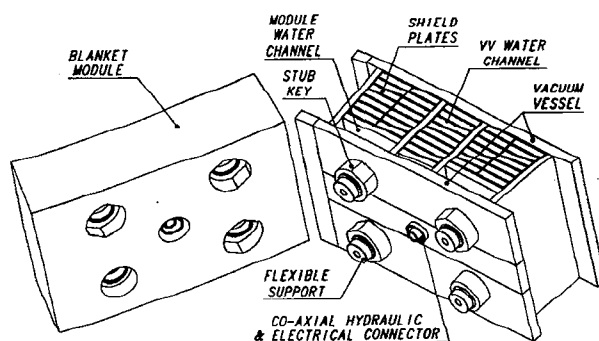


Figure II.2.2-6 Blanket Module Attachment by Stub Keys (Type 1)

The Type 2 attachment is used in the VV inboard region where the electromagnetic forces are large. The Type 1 attachment will be used in the outboard and top regions of the blanket. The centre pin, the stub keys and the flexible supports include an electrical insulating break, and the key way is electrically insulated from the remainder of the module so that adjacent modules are insulated, avoiding toroidal currents. A trial assembly of the module mock-up on a dummy structure with Type 2 attachment has been fabricated, and has been tested to verify the module assembly. The feasibility of blanket assembly under nominal conditions (no

¹ RF contribution to the design integration task force, The improvement of module/flexible attachment/vacuum vessel system integration, RFHT draft report, October 1999

misalignments) and with the required tolerances and clearances has been demonstrated, and a demonstration of assembly with misalignments is planned.

G 16 GR 4 99-12-07 W0.1

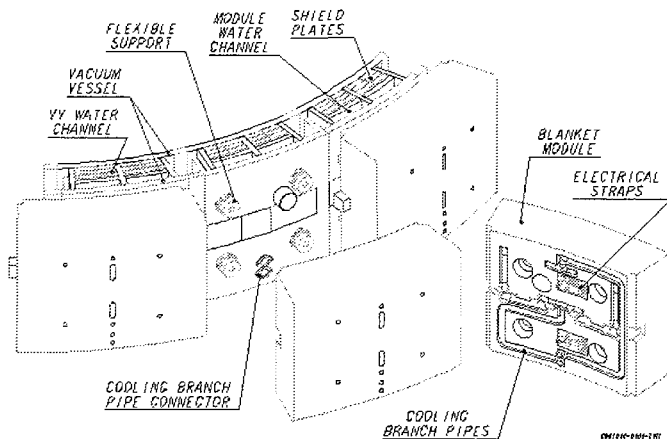


Figure II.2.2-7 Blanket Module Attachment by Inter-modular Key (Type 2)

Hydraulic and Electric Connections

In the Type 2 attachment concept, long, flexible, branch pipes provide the connection between the cooling circuits in the modules and those in the VV while upper and lower centrally located straps provide a poloidal electrical path for halo currents. The branch pipe's end fittings will be constructed from 316L(N)-IG stainless steel and the pipe section from Inconel 625. The electrical strap will be fabricated from CuCrZr alloy because of its low electrical resistance and relatively high strength at high temperatures. Although also low, CuCrZr alloy has a higher ductility than DSCu at high temperature.

For the Type 1 attachment (see Figure II.2.2-8), a design concept using a coaxial hydraulic and electrical connector has been developed for the blanket modules to minimise the number of seal welds inside the vessel. The strap is assembled from four high strength copper alloy sheets, formed by bending without any weld¹.

G 16 GR 16 99-12-08 W0.1

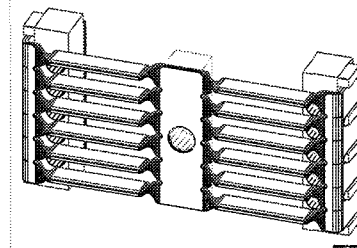


Figure II.2.2-8 Electrical connection for Type 1 attachment

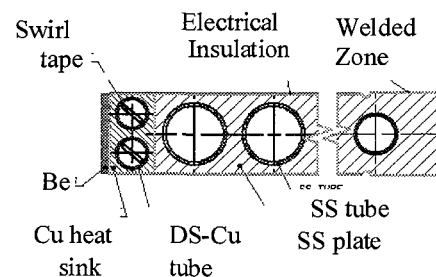
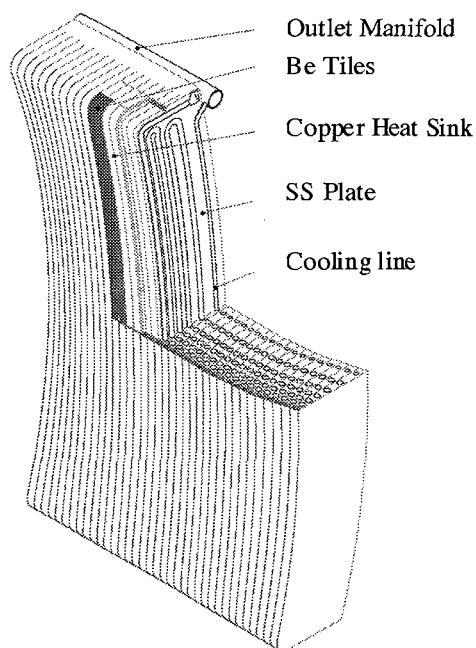
II.2.2.6 Port Limiters

The port limiter, which is located in the equatorial port for ease of maintenance, is attached to its shield plug by an adjustable attachment. As shown in Figures II.2.2-9 and 10, the limiter is an assembly of ~ 40 mm thick vertical plates welded together at the rear section. Each limiter plate is formed by one-step solid HIPing of two stainless steel plates which include a serpentine cooling tube and the FW copper heat sink with its two cooling tubes (1030°C, 150 MPa, 2.5 h). The ~ 4 mm thick Be tiles are brazed to the Cu-alloy part using an

¹ G 16 MD 240 99-08-09 W0.1 - Bent sheet electrical strap for the module attachment, and EU contribution to the design integration task force, Conceptual design of an integrated hydraulic and electrical connection for the next step blanket modules, EUHT/EFET draft report, October 1999

amorphous braze material. The electron beam (EB) welded rear section forms a strong continuous backing and the ~ 1 mm gap between plates is insulated with alumina to prevent arcing. The vertical slots significantly reduce the EM loads due to plasma disruptions. The ability of the plates to independently expand also keeps the thermal stresses low. The limiter cooling is in common with that of the divertor system. Small mock-ups of the limiter module show the basic feasibility of the limiter design. Tests on Be armoured samples attached with a CuInSnNi fast amorphous brazing technology (800°C for a few minutes) have withstood 12 MW/m² for 4500 cycles.

G 16 GR 5 99-12-07 W0.1



G 16 GR 6 99-12-07 W0.1

Figure II.2.2-10 Detail of Limiter Plate

Figure II.2.2.-9 Limiter Module

The maximum heat flux to the limiter FW is limited to 8 MW/m², which will allow a total maximum plasma power of 20 MW at start-up and shut-down. The distance between the limiter module and the port frame is 50 mm, resulting from a 30 mm dogleg and 20 mm gap. The toroidal and poloidal dimensions of the module are 1704 mm and 2104 mm, respectively.

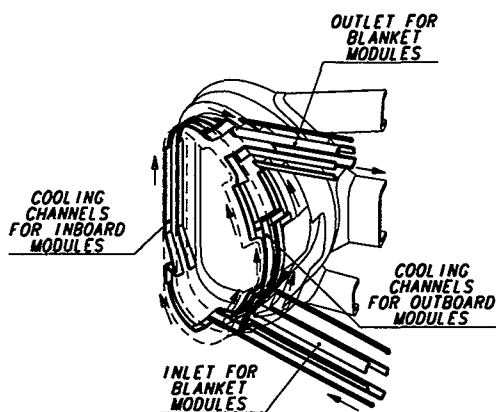
II.2.2.7 Blanket Cooling and Baking

The performance parameter variances between the VV and blanket require the utilization of separate cooling circuits (parameters for the VV water are shown in II.2.1.3). Two options are being considered for blanket cooling: one with cooling channels integrated inside the vessel structure between the two walls, the other with channels on the vessel in vacuum.

The former, with the integrated cooling manifold inside the VV, would maintain a simple overall in-vessel configuration compatible with blanket module attachment, magnetic probes, helium purge gas lines and other in-vessel components, and be structurally robust. There is a possible concern about contamination (above acceptable levels) of the inside of the VV

cooling loop by blanket cooling water. This contamination is very unlikely due to the thick plate multipass welding used on the boundary between the two cooling channels. Leak monitoring of the cooling channels is expected to provide an adequate indication of cracks in the structure. An option under consideration is to add a tracer to the blanket cooling loops and then to take samples from the VV cooling loops¹. In case of small leaks, plasma operation could be continued with the addition of a water purification system to the VV PHTS.

Six independent circuits, two inboard and four outboard, are positioned in each VV 40° sector. The number of circuits is designed to help minimize the effect of a LOCA and to facilitate draining/drying and leak testing operations. Cooling/baking water is supplied to the toroidally centred divertor port of each VV sector and is then routed upward. The water is then supplied to each blanket module through either a coaxial hydraulic connector or two flexible branch pipes. The water exits the toroidally centred upper radial port stub of each sector (see Figure II.2.2-11). The blanket cooling channels within the vessel, are located on the back of the inner walls of the VV and are aligned with the poloidal centrelines of the modules (see Figures II.2.2-6 and 7). The cooling channels in the port extensions are routed within the double-wall structure thus leaving the port openings unobstructed. Since the blanket cooling lines are routed within a 40° sector, there is no interference with the VV field joints.

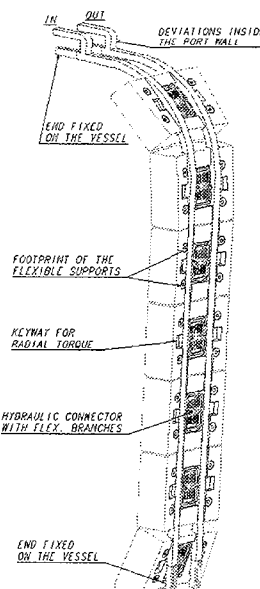


G 16 GR 7 99-12-07 W0.1

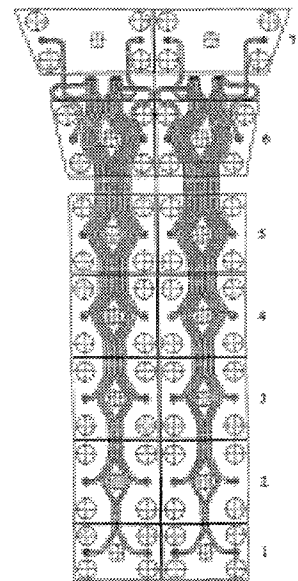
Figure II.2.2-11 Integrated Cooling Manifold Design

G 16 GR 8 99-12-07 W0.1

G 16 GR 17 99-12-08 W0.1



(a) Straight manifold concept



(b) Serpentine pipe concept

Figure II.2.2-12 Separate Cooling Manifold Concepts Designed for the Inboard Area

¹ G 16 MD 261 99-12-06 W 0.1 - Study of Water-to-Water Leak Detection between the VV and Blanket Cooling Channels, and Leak detection method sensitivity of VV/back plate issues, (i) Investigation of the sensitivity of the leak detection - JAHT report, INT-9004-Rev. 1 - June 9, 1999

A second concept, with separate manifolds, has also been developed for the blanket cooling system¹. Cooling manifolds are fixed on the plasma-side surface of the VV and will not generate large thermal stresses in the VV. This concept would avoid possible cross contamination between the blanket and VV cooling systems. The coolant manifolds could be repaired after removal of blanket modules if the repair location is accessible and its repair can be done with remote handling equipment. When its repair is not possible, the vessel sector would need to be replaced. Some additional space may need to be cut out from the modules to accommodate the channels.

One possibility with the separate manifold concept is to adopt large manifolds feeding modules in a poloidal row (see Figure II.2.2-12 (a)). The manifolds in a vertical plane are anchored on the vessel at both ends. Their small cross-section allows the restraint of the axial thermal expansion with a reasonable reaction force. This concept has complexity in the outboard region and in the port stub field joint region. Another possibility is to use single manifolds for each module in a serpentine configuration (see Figure II.2.2-12 (b)). These are clamped on the vessel and the differential thermal expansions will be accommodated. In this approach, the space available on the vessel inner surface is very limited at the top. Further work will be necessary to establish the relative feasibility of the concepts.

Table II.2.2-2 Preliminary Estimate of Cooling/Baking Conditions of the Blanket

Parameters	Unit	Value*
Required Total Removal Heat	MW	~ 650**
Water Parameters		
- Normal Operation		
- Inlet / Outlet Temperature	°C	100 / ~ 150
- Inlet Pressure	MPa	3.0
- Total Flow Rate	kg/s	3130
- Baking Operation		
- Inlet / Outlet Temperature	°C	240
- Inlet Pressure	MPa	5.7

* Preliminary values.

** ~ 650 MW is the value for the basic DT operation case with the fusion power of 500 MW + the additional heating power of 50 MW. For the design condition of the blanket cooling water system, ~ 690 MW is used assuming the fusion power of 500 MW + the additional heating power of 100 MW.

The blanket cooling conditions are summarized in Table II.2.2-2². (see II.5.2.1). A preliminary estimate yields a total in-vessel pressure drop of ~ 0.7 MPa. However, it is dependent on the choice of module cooling design configuration; for example, if serpentine

¹ G 16 MD 253 99-11-12 W0.1- External cooling manifolds for the blanket, EU contribution to the task force report, Section VI.2.5, A separate manifold system for primary wall modules and its integration with a coaxial hydraulic connector, EUHT report N/X/0823/7/A, June 10, 1999
EU contribution to the design integration task force, External manifold blanket cooling – IAM3 machine, EUHT/EFET draft report, November 1999

² G 16 MD 254 99-11-18 W 0.1 – Preliminary estimation of heat load for blanket PHTS of ITER-FEAT, G 16 MD 256 99-11-17 W 0.1 – Preliminary assessment of required cooling condition for the blanket of ITER-FEAT, and G 16 MD 257 99-11-18 W 0.1 - Preliminary assessment of required removal heat for port-limiter of ITER-FEAT

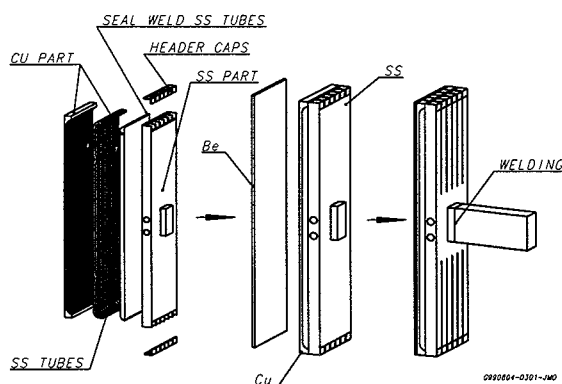
tubes with several passes in series are adopted as the design choice for FW cooling, this pressure drop could be increased.

The flow rate of the blanket cooling system can be reduced significantly in the hydrogen operation phase. In such an initial operation stage, the required number of blanket cooling loops will be one instead of the three required for DT operation.

II.2.2.8 Blanket Fabrication

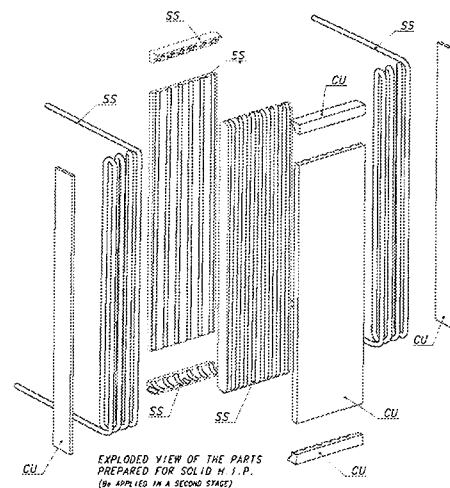
The FW panels will be fabricated by solid HIPing or by powder HIPing, depending upon the results of the on-going R&D and costing. A possible fabrication method for the option with central mechanical attachment is shown schematically in Figure II.2.2-13. In this procedure, Cu-alloy and SS plates are machined to produce (a) a foot for attaching the supporting beam in the SS panel, (b) semi-circular grooves for inserting SS cooling tubes in the Cu-alloy plate, and (c) coolant headers. The FW assembled parts are joined by one-step solid HIP ($T = 980-1050^{\circ}\text{C}$, $p = \sim 150 \text{ MPa}$, $t = \sim 2 \text{ h}$). The feasibility and the robustness of one-step solid HIP for joining both Cu-alloy/SS and SS/SS has been demonstrated by manufacturing and testing several small and medium scale mock-ups and finally two prototypes. The joints have resisted thermal loads up to $5-7 \text{ MW/m}^2$ for 1000 cycles.

The cooling channels for the SS plate, the intermediate collectors and the supporting beam are made by drilling. Based on R&D results, HIP of large tiles (e.g. $50 \times 100 \text{ mm}$) using a Ti interlayer is a prime candidate technology for joining the Be armour of the primary wall to the Cu-alloy heat sink (e.g. $800-850^{\circ}\text{C}$, 2 h , 120 MPa). In thermo-mechanical tests a mock up has resisted 2.5 MW/m^2 for 1000 cycles without damage. The supporting beam and the header closure caps are attached by welding.



G 16 GR 99-12-07 W0.1

Figure II.2.2-13 FW Panel Fabrication Method for the Option with Central Mechanical Attachment



G 16 GR 10 99-12-07 W0.1

Figure II.2.2-14 FW Panel Fabrication Method for the Option with Bolts and Small Shear Ribs

A possible fabrication method for the option with bolts and small shear ribs is shown in Figure II.2.2-14. In this method, serpentine tubes are joined to SS and Cu-alloy grooved plates by one-step solid HIPing or are imbedded in SS and Cu alloy powder and joined by

two-step powder HIPing. The feasibility of powder HIPing for the fabrication of the FW panels, in particular regarding the tight dimensional tolerances required, still needs to be demonstrated by R&D.

The shield can be made by drilling and milling. The manufacturing steps will be:

- (i) produce four separate forged blocks,
- (ii) drill the cooling channels inside the blocks and produce the front access penetrations and the intermediate toroidal collectors,
- (iii) EB weld the four blocks together,
- (iv) mill cut-outs for the keys and machine the flexible holes,
- (v) mill main groove for branch pipes and make the hole for the centre pin,
- (vi) cut the additional poloidal slots in the shield block,
- (vii) mill upper and lower headers,
- (viii) weld closure plates,
- (ix) assemble the first wall panels on the shield and weld the hydraulic connections to the respective inlet/outlet headers.

The feasibility of obtaining the drilled forged shield blocks within the required tolerances and with welding closure plates has been demonstrated in a module prototype.

The shield can be fabricated also by powder HIPing. For the option with radial cooling, it consists of concentric cylinders of appropriate diameters and lengths to accommodate the space needed at the rear side of the shield for all the required recesses. This assembly is then inserted into a properly designed can to give the fully-dense end-product in the required shape. The can is filled with SS powder and then HIPed at 1100°C and 120 MPa for 4 hours. The feasibility of this technique for the shield fabrication has been demonstrated by manufacturing a prototype. The first row of cooling passages closer to the FW showed a pitch error of ± 1 mm. For the last rows this error is increased up to 7 mm. A new prototype is being manufactured and this error is expected to be reduced significantly.

Preliminary cost estimates have been performed by the Home Teams, and the estimated reduction in the unit blanket module cost comparing with the 1998 ITER design is approximately 30-40%.¹ An additional substantial cost reduction for the FW could be obtained by the selection of CuCrZr instead of DS-Cu. The use of alternative Be/Cu-alloy joining techniques such as brazing or diffusion bonding could also result in cost saving, if the feasibility of these techniques is demonstrated by an appropriate R&D programme. Another cost reduction approach is to use larger contact surface roughness for solid HIPing of the FW panel.

The fabrication method will be selected based on design and R&D results, and finally on a fabrication cost comparison.

¹ EU contribution to the task force report, Section VI.5.2, Primary wall modules cost estimates, EFET report NVMI DC 991543/SLB rev.B, June 1999

II.2.2.9 Blanket Assembly

The assembly procedure will be as follows:

1. Pre-assembly stage:
 - (i) The majority of diagnostics and helium purge lines are mounted on the plasma-facing wall of the VV. All the interior cabling and pipelines are routed to the vessel exterior and checked for continuity and leakage.
 - (ii) The module flexible supports are pre-installed in their housings in the VV.
2. The vacuum vessel is aligned to the machine magnetic centreline, all global adjustments made and the vessel supports fixed. The measurement data will be utilized to provide a best-fit determination of the mounting profile information necessary to customize the module attachments.
3. Installation of toroidal loops and waveguides of diagnostics on the plasma-facing wall of the VV and the loops connected to the interior cabling. This loop crosses the field joints. A waveguide is installed on a field joint.
4. Measurement of the VV module attachment profile.
5. Customization of the module attachments.
6. Mounting of module attachments.
7. Pre-mounting of blanket modules by temporary supporting bolts.
8. Fixing of blanket shielding modules. The module flexible supports have to pretension the bolting using heat.
9. Blanket commissioning test: global leak and pressure test; global flow and pressure drop tests, and global/local thermal transient response tests.

II.2.2.10 Loads and Analysis

II.2.2.10.1 EM Loads

Centred Disruption and Fast VDE

The plasma disruption database shows that the high plasma current density leads to a fast current quench, resulting in a short quench time of 27 ms. This leads to high electromagnetic (EM) loads, unless deep slits are used. These are effective in reducing the EM loads on blanket modules, as shown in Table II.2.2-3

Slow VDE

The FW-normal halo current density is assumed to be 0.18 MA/m^2 under the worst case halo current event, as specified the $I_{\text{halo}}/I_{\text{plasma}}$ multiplied by the toroidal peaking factor, $\text{TPF} = 0.58$. The design loads on modules are shown in Table II.2.2-3. The maximum halo current is $\sim 0.26 \text{ MA/module}$, and the shearing and pushing force is $\sim 0.9 \text{ MN/module}$ and 1.0 MN/module , respectively.

Table II.2.2-3 EM Loads on the Inboard Module

		Shield block	FW
1) Centred disruption		($t_p = 27$ ms)	($t_p = 27$ ms)
Torque M_r due to I_{rad}	MNm	-0.62	-0.007
Torque M_p due to I_{pol}	MNm	0.95	0.0034
2) Fast VDE		($t_p = 19$ ms)	($t_p = 19$ ms)
Torque M_r due to I_{rad}	MNm	-0.87	-0.011
Torque M_p due to I_{pol}	MNm	1.13	0.0048
3) Slow VDE			
I_{halo} / module (FW)	MA	0.26	0.065
B_{tor} in inboard-bottom module	T	7.94	7.94
EM force F_p on module (FW)	MN	0.9	0.2
EM force F_r on module (FW)	MN	1.0	± 0.06

Remarks: The equivalent quench time during fast VDE is assumed to be 1.4 times faster than the centred disruption (CD), considering the additional magnetic field change due to plasma movement under the same current quench time as a CD.

II.2.2.10.2 Structural Analysis

The structural integrity of the separable first wall panel under thermal and EM loads is investigated below¹. Detailed stress analyses for the flexible supports and keys were performed in the 1998 ITER design².

Thermal stress

Taking advantage of symmetry, only a quarter sector of the first wall panel was modelled using a FE model. The temperature ranges and maximum stresses at steady state due to the above thermal conditions are summarized in Table II.2.2-4. Stresses due to the normal operating loads are below the $3S_m$ limit. Thermal deflection relative to the FW panel centre is 1.7 mm in the poloidal and 0.5 mm in the toroidal direction and these are small enough from a gap control viewpoint.

¹ G 16 MD 229 98-12-18 – Thermomechanical Analysis of the Separable Mechanically Attached First Wall, G 16 MD 252 99-11-11 - Updated Thermal and Mechanical Analysis for ITER-FEAT Separable First Wall

² G 15 MD 89 97-06-06 W0.1 – The titanium flexible supports of the modules, G 16 MD 145 97-10-21 W0.1 3D stress analysis of the titanium flexibles, G 15 MD 82 97-08-06 W0.1 3D buckling analysis of the titanium flexibles, G 16 MD 196 98-03-02 W0.1 Beyond design performance of the bolt connection, G 15 MD 90 97-07-18 W0.1 Stress analysis of the key between modules, and G 16 MD 201 98-03-19 W0.1 The stub keys for the modules between the ports

Table II.2.2-4 Temperature and Thermal Stress in First Wall Panel

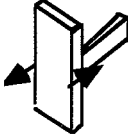
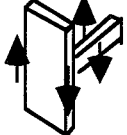
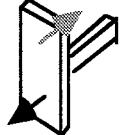
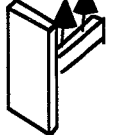
	Temp. range min. - max. (°C)	Max. stress (MPa)	Temp. at max. stress point (°C)	3S _m (MPa)
Cu	162 - 224	~ 124 *	224	294
SS tube	143 - 200	~ 200 **	144	444
SS region	115 - 225	~ 293 ***	185	465

* Be interface, ** wetted part, *** wetted part of cooling channel

Mechanical stress under EM loads

The first wall panel is attached to the shield block by its leg. Structural analyses of the separable first wall panel under EM loads have been performed to assess the stresses in the panel and the leg. Table II.2.2-5 summarizes the input loads and the maximum stresses. The stresses are below allowables. These results indicate that it is feasible to support the first wall panel by its leg for EM loads.

Table II.2.2-5 Mechanical Stress in First Wall Panel

EM loads	M _p due to ΔB _r  Moment around poloidal axis = 4.8 kNm	M _r due to ΔB _p  Moment around radial axis = 10.5 kNm	M _t /F _r due to I _{halo}  Moment around toroidal axis = 19.3 kNm Radial force = 58 kN	F _p due to I _{halo}  Poloidal force = 200 kN
Max. stress	σ = 31 MPa (leg)	τ = 45 MPa (leg)	σ = 79 MPa (leg) σ = 26 MPa (FW) σ = 185 MPa (bolt)	σ = 112 MPa (leg)

II.2.2.10.3 Nuclear Analyses of Torus Components

Nuclear responses of torus components were estimated with a scaling from earlier 1D and 3D calculations ¹. The integrated cooling manifold design is assumed for the blanket module in the following description.

Nuclear Heating

The nuclear heat distribution among in-vessel components is summarised in Table II.2.2-6 for a reference fusion power of 500 MW. The resulting neutron energy multiplication is 1.41 = 563/400.

¹ G 73 RI 108 99-07-21 F1 - Nuclear response analysis in TFC and VV for RC/RTO-ITER

Table II.2.2-6 Nuclear Heat Deposition in the In-vessel Components

Component	Nuclear heating (MW)
Blanket including fillers and port plugs, excluding P/L and P/L plug	497
VV including port walls and NB injector duct liners	13
Divertor	45
Port limiter (P/L) and P/L plug	8
Total	563

Table II.2.2-7 shows the expected nuclear heating in the TF coils, which is scaled from the earlier detailed 3-D calculation. The shield thickness is ~ 79 cm for the inboard and 120 cm for the outboard wall. A maximum TF coil nuclear heating of ~ 19 kW is expected at the maximum fusion power of 700 MW.

Table II.2.2-7 Nuclear Heating in the TF Coils (kW)

	Inboard Leg	Behind Divertor	Around Ports	N-16 in Coolant	Total
Coil Case	5.4	0.75	0.4	1.6	8.1
Winding Pack	5.3	0.3	-	-	5.6
Total	10.7	1.1	0.4	1.6	13.7

Radiation Damage to Superconductors and He production in the VV

The epoxy insulator dose and the fast neutron fluence in the superconductors are estimated as shown in Table II.2.2-8. They are (by about a factor of ~ 3) smaller than the design limits.

Table II.2.2-8 Insulator Dose and Fluence (normalised to 0.5 MWa/m² at the first wall)

Nuclear Responses (Units)	Design Limits	ITER-FEAT Values
Epoxy insulator dose (Gy)	1×10^7	2.9×10^6
Fast neutron fluence in winding pack (n/cm ²)	1×10^{18}	3.5×10^{17}

The He production rates are estimated to be ~ 0.8 appm in the front layer of the vacuum vessel and 0.5 – 1.5 at the cooling branch pipes in the blanket modules. They are lower than the design limits (1 appm for vacuum vessel thick plate welding and 3 appm for branch pipe thin plate welding¹).

Activation of the Torus Components (clearance level & decay heat)

The in-vessel components including the vacuum vessel will be highly activated so that their activity can not be below the clearance level even after long periods of cooling (> 100 years).

¹ S. Kawano et al., Simulation of helium bubble behavior in neutron-irradiated stainless steel during welding, Journal of Nuclear Materials 258-263 (1998) 2008-2012

The activity of TF coil cases will be below the clearance level after 100 years but that of the winding pack will be still higher than the clearance level 100 years after reactor shutdown because of the high Nb content. The decay heat at the end of life (0.5 MWa/m^2) is estimated to be $10.5 - 0.3 \text{ MW}$ depending on the cooling time after shutdown ($1 \text{ s} - 5 \times 10^5 \text{ s}$).

II.2.2.11 Conclusions

The basic concept of the blanket system uses mechanically attached modules. The installation of a breeding blanket at a later date has not been precluded, but would be limited to the outboard area only, with a tritium breeding ratio of ~ 0.6 as a target.

The modules are arranged to minimize their number and reduce cost, and the segmentation of the shield modules is consistent with shielding and installation layout requirements as well as the weight limit of 4.5 t per module imposed by the remote maintenance equipment.

The inlet temperature of the blanket cooling is 100°C . From a materials point of view, there are no negative effects in operating with this temperature.

The blanket module design has been developed to minimise the fabrication cost, volume of radioactive waste and the EM loads. The configuration consists of a shield body to which a separable first wall is mounted. The separable first wall has a facet geometry consisting of multiple flat panels. The resulting configuration allows for simple design and manufacturing of the main components thus minimising the associated costs.

The blanket module attachment can be located in a shielded position behind the blanket module, since the depth of the vessel inter-wall volume is larger than the height of the supports. The flexible cartridge can be passively cooled. Under these conditions it is better to install the supports in the vessel rather than on the blanket module.

II.2.3 Divertor

II.2.3.1	Introduction	1
II.2.3.2	Requirements and Design Drivers	1
II.2.3.3	Design Layout	2
II.2.3.4	Heat Flux to the Plasma-Facing Components	4
II.2.3.5	Plasma-Facing Components	5
II.2.3.5.1	Armour Selection	5
II.2.3.5.2	Vertical Target	6
II.2.3.5.3	Private Flux Region PFC	6
II.2.3.5.4	Coolant Parameters	7
II.2.3.6	Cassette Design	8
II.2.3.7	PFC to Cassette Attachments	8
II.2.3.8	Integration of Diagnostics	9
II.2.3.9	Costing	9
II.2.3.10	Steady-State and High Power Operation	10
II.2.3.11	Conclusions and Future Work	10

II.2.3.1 Introduction

Replaceable cassettes are installed in the vessel to form the ITER-FEAT divertor. The layout of the divertor is arranged to maximise the length of the divertor channels. Code evaluations indicate that the normal operating mode of a partially detached plasma can be expected at the envisaged operating density and scrape-off layer (SOL) power, leading to a steady-state heat flux $\leq 10 \text{ MWm}^{-2}$ on the divertor targets. In the case of off-normal events, in particular when the full power conducted into the SOL transiently lands on the vertical target (loss of partial detachment), the predicted peak heat flux is $\sim 20 \text{ MWm}^{-2}$ (see II.2.3.4). During a plasma transient such as an ELM or disruption, a pulsed energy flux between 10 and 100 MJm^{-2} can be deposited in less than 1 ms. On the basis of the conceptual design, a cost evaluation has been carried out by scaling from the industrial costing provided by the Home Teams for the 1998 ITER design. This shows that a divertor for ITER-FEAT can be expected to be $\sim 60\%$ of previous costs. As a result of on-going R&D, a series of potential design simplifications have been identified that promise to make the cost goal of 50% of the 1998 ITER design achievable, and in addition, are likely to provide a more robust design.

II.2.3.2 Requirements and Design Drivers

The design developed for the ITER-FEAT has to meet the following requirements:

- (i) the divertor plasma-facing component (PFC) geometry needs to ensure that the majority of the neutral recycling fluxes are beneath the dome in order to achieve partial detachment in a reasonable SOL density window which in turn yields acceptable target power loads and sufficient He exhaust;
- (ii) the targets need to be configured such that, during transients when the full SOL power reaches the target, the peak heat flux $< 20 \text{ MWm}^{-2}$;
- (iii) the conductance through the divertor has to be compatible with a throughput of $200 \text{ Pam}^3\text{s}^{-1}$;
- (iv) the divertor needs to be capable of being remotely exchanged during a shutdown;
- (v) the total nuclear heat input to the toroidal field coil must be limited and, in particular, the goal is to limit to 75 W the nuclear heating to the first turn caused by radiation through the divertor.

In addition to the requirements above, there is a goal for the cost of the ITER-FEAT divertor to be 50% of the 1998 ITER design value. Finally, for cost reductions in the heat transfer system, there is a desire to minimise the number of coolant loops. In order that the divertor can be supplied by one coolant loop, the total divertor coolant flow needs to be $< 1000 \text{ kgs}^{-1}$.

II.2.3.3 Design Layout

The divertor is segmented into 54 cassettes, 3 per sector. This is based on the maximum size of cassette that can be handled via the maintenance ports and still have an integer number of cassettes per sector. Of the 18 divertor level ports, 3 equally spaced ports are allocated to divertor remote maintenance (see II.10.2) and diagnostics, 10 ports contain cryopumps, and a number of ports can accommodate diagnostic equipment (including the in-vessel viewing system). For a preliminary port allocation see drawing 10.73.1 in II.8. Each cassette supports 3 PFCs: an outboard vertical target, a private region PFC combining dome and liners, and an inboard vertical target.

Figure II.2.3-1 shows an elevation view of the divertor. The divertor level ports are 2 m high, which is large enough to allow the cassettes to pass through them during installation. The ports are inclined so as not to interfere with the inter-coil structure (see II.1.3.2) or with the building slab between the equatorial and divertor level ports.

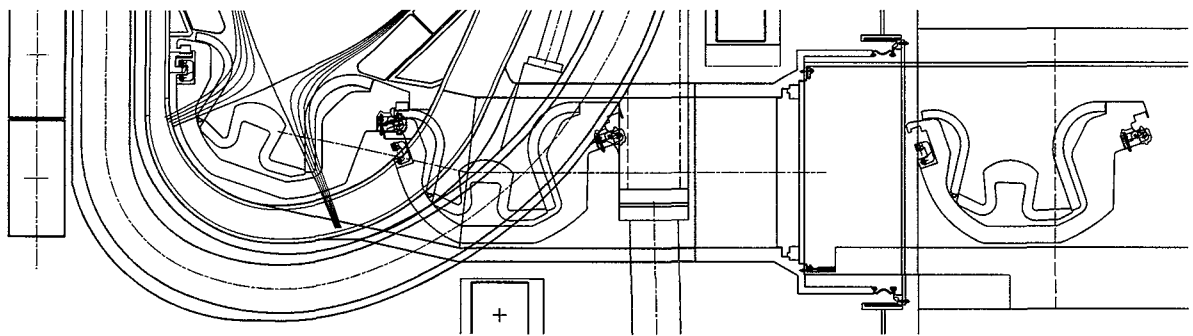
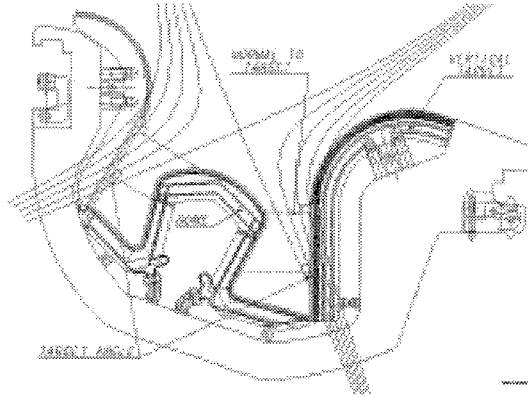


Figure II.2.3-1 Elevation View of Divertor & Divertor Level RH Port

For the divertor itself, the space allocated below the X-point, and hence available to the high heat flux region of the divertor, has been defined by applying the design guidelines given below. With the proposed use of high triangularity plasmas, the space for the inboard channel is particularly restricted. The guidelines are as follows:

- (i) the angle of the vertical target is such that the maximum heat flux during transient off-normal events does not exceed 20 MWm^{-2} ;
- (ii) the line drawn perpendicular to the surface of the outboard vertical target where the target intercepts the flux line 3 decay lengths from the separatrix (Figure II.2.3-2), should not intercept the private flux region PFCs higher than the dome; 2 decay lengths is used at the inboard where plasma detachment is more readily achieved;
- (iii) the dome profile should follow the magnetic surface in the private flux region with a $\Delta\psi$ (change of magnetic flux) from the separatrix corresponding to the same $\Delta\psi$ over 1 cm at the outboard equator;
- (iv) the dome should extend to provide sufficient baffling of neutrals (factor 10 reduction in flux) and to protect the liner from being intercepted by the SOL.



G17 GR 20 99-12-03 W0.1

Figure II.2.3-2 Sketch Illustrating Divertor PFC Design Guidelines

These guidelines ensure that the target power loads do not exceed 20 MWm^{-2} (see II.2.3.4) and that the majority of the recycling fluxes are located below the dome. They also define the divertor channel length and thus the amount of space needed between the X-point and the vacuum vessel for a functioning divertor.

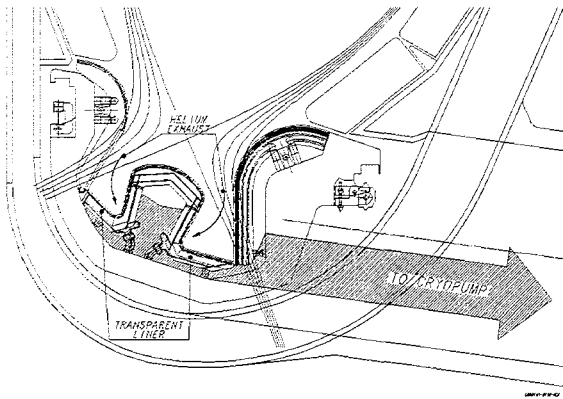
In the divertor the vertical targets extend upwards to form baffles. In this way, apart from the limiters, all the components required to sustain surface heat loads $> 1 \text{ MWm}^{-2}$ are integrated into the divertor cassettes. This division of PFCs allows a uniform design of blanket modules and is expected to minimise overall in-vessel costs. Furthermore, incorporating the baffles in this way will localise configuration changes to the divertor cassette alone.

In order to maximise the divertor channel lengths and in so doing minimise the peak heat flux on the vertical targets, it has been necessary 1) to have the lower face of the cassette body closely follow the internal profile of the vessel, especially in the regions immediately beneath the targets, 2) to position the toroidal support rails in the upper region of the cassette such that the cassette is hung from the rails, 3) to employ a remote handling (RH) concept that does not require access beneath the cassettes, 4) to locate the pumping channel to use the volume between the cassette body and the PFCs, and 5) to restrict the thickness of the cassette body to the minimum governed by the electromagnetic forces and shielding requirements.

A gap of 70 mm between the bottom of the cassette body and the vessel is maintained to accommodate build tolerances, differential movement of the vessel and divertor under thermal or electromagnetically induced loads, and to leave space for diagnostic cable runs as well as for pellet injector guide tubes. The flattening of the cassette body profile beneath the dome creates a region that is provisionally reserved for dust removal. This space is not used for the toroidal handling of the cassettes, as it is too small and in any case is inboard of the centre of gravity of the cassettes.

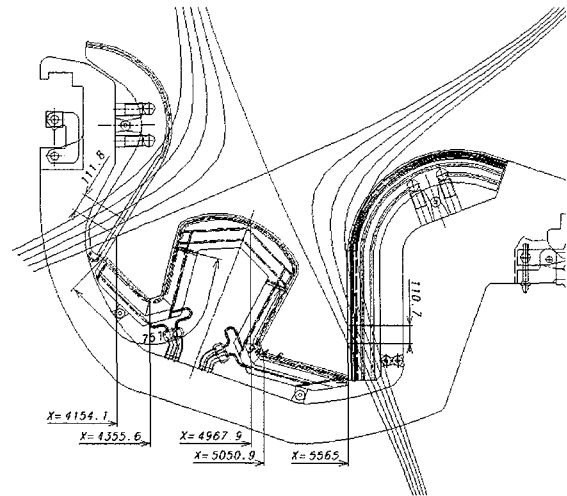
Gas is exhausted via the private flux region of the divertor. The flow path is through the semi-transparent liners located beneath the dome (see Figure II.2.3-3), then radially outwards beneath the outboard PFCs and through a pumping slot (500 mm high by 100 mm wide) formed by matching cut-outs in adjacent cassette bodies. This slot is behind the outer vertical target where the neutron streaming is low. There will be re-circulation of neutrals from the

inboard to the outboard private region and re-ionisation in the outer divertor plasma (lower pressures in the outer channel are assumed).



G17 GR 22 99-12-03 W0.1

Figure II.2.3-3
Pumping Slot



G17 GR 21 99-12-03 W0.1

Figure II.2.3-4
Divertor Target Geometry

II.2.3.4 Heat Flux to the Plasma-Facing Components

The power intercepted by the divertor targets during high power transients (no partial detachment) is determined according to the following rules. The total heating power to the plasma is taken as 20% of the total fusion power + all the auxiliary heating. From this total plasma heating 75% is assumed to reach the divertor.

$$P_{cond} = (1-f)(P_{\alpha} + P_{aux})$$

where P_{cond} is the total power conducted to the divertor, P_{α} is the power carried by the alpha particles (20% of the 500 MW of fusion power), P_{aux} is the additional heating (50 MW), and f is the fraction of power radiated from the plasma and SOL (0.25). This gives ~ 112.5 MW conducted to the divertor via the SOL. In order to take account of uncertainties in the distribution of power to the divertor, the inboard channel is assumed to receive up to half the total and the outboard up to two thirds (naturally not simultaneously). The peak heat flux is equivalent to P_{cond} divided by the target area within the first decay length, and Table II.2.3-1 shows this to be $< 20 \text{ MWm}^{-2}$ for both inner and outer targets. The area is taken from the geometry developed using the guidelines and shown in Figure II.2.3-4.

Table II.2.3-1 Power and Peak Heat Flux in ITER-FEAT Divertor

Total power conducted to divertor	MW	112.5	
		Inboard	Outboard
Fraction of total power to target		0.5	0.67
Maximum power to target	MW	56.3	75
Target area within first decay length	m ²	2.92	3.87
Peak heat flux	MWm ⁻²	19.3	19.4

Based on B2-EIRENE code evaluations for machine configurations similar to ITER-FEAT with divertor geometry developed using the same design guidelines, a partially detached

plasma (the normal operation mode) is likely at the envisaged operating density and SOL power¹ resulting in a continuous heat flux $\leq 10 \text{ MWm}^{-2}$ on the vertical targets.

II.2.3.5 Plasma-Facing Components

II.2.3.5.1 Armour Selection

Carbon-fibre Composite (CFC) is the reference armour for the strike point regions of the targets, and tungsten for the baffle regions of the target and the surface of the dome². The lifetime of this armour combination is expected to meet the goal of sustaining 3,000 full-power discharges of 400 s duration, with one in ten discharges ending in a disruption and with a frequency of one high power transient per ten discharges, that occur when the SOL is fully attached to the target. During DT operation the co-deposition of tritium with carbon has the potential to trap the entire allowable tritium inventory for ITER in a few hundred pulses (1 – 5 g tritium/pulse). Even taking into account recent R&D results of 1) the impact that flux dependence could have in reducing the co-deposition rate and 2) the potential mitigating effect of the hot liner in allowing tritium to be pumped (see II.2.3.5.3), there will still need to be machine outages during which tritium is removed from the machine. The most promising method of achieving the removal remains the baking of the co-deposited regions to $\sim 350^\circ\text{C}$ in the presence of oxygen at low pressure, followed by a period of wall re-conditioning. Heating using gas baking via the divertor PHTS (and possibly the vessel/blanket PHTS) or using radio-frequency heating, is also under consideration.

One way of avoiding this problem completely is to eliminate carbon from the machine, and in response tungsten armour technology has been developed to a level where the feasibility of building reliable targets capable of handling 20 MWm^{-2} has been demonstrated³. Results of plasma performance while operating with high-Z, armoured PFCs are promising⁴. However, concerns still remain over what will happen to the melt layer of the tungsten target (up to 100 μm deep during a disruption) and what effect that will have on operations and target lifetime. Hence, tungsten is only likely to be used for the strike point regions of the target, when precise control of discharges can be assured, and a much wider experience of operating tokamaks with a tungsten first wall has been gained. In the meantime, carbon remains the choice for the lower vertical target where its ablative property makes it a very forgiving material against disruptions and target misalignments that can result in very high heat flux on leading edges ($\sim 100 \text{ MWm}^{-2}$).

¹ A. S. Kukushkin, et al; "Divertor Performance in RTO/RC- ITER"; EPS Maastricht 1999

² G. Federici, et al., Issues arising from plasma wall interactions in reactor-class tokamaks, to appear in Nuclear Fusion.

³ M. Merola, et al., Manufacturing and Testing of a Prototypical Divertor Vertical Target for ITER, 9th Int. Conf. on Fusion Reactor Materials, October 10-15, 1999, Colorado Springs, to appear in J. Nucl. Materials..

G. Vieider, et al., European Development of Prototypes for ITER High Heat Flux Components, ISFNT-5, Rome, 1999.

A. Makhankov, et al., Development and Optimization of Tungsten Armour Geometry for ITER Divertor. Proceed. of 20 Symposium on Fusion Technology, Marseille, September 1998, p.267-270

R.E.Nygren, et al., "Heat sinks armoured with tungsten rods" ISFNT-5 Rome, Sept. 1999

⁴ Greenwald, M., H Mode confinement in Alcator C-MOD, Nuclear Fusion, 37 (1997) 793

Krieger, K., Maier, H., Neu, R., and the ASDEX Upgrade Team, J. Nucl. Mater. 266-269 (1999) 207

II.2.3.5.2 Vertical Target

The EDA has seen impressive progress made in the development of CFC to Cu and tungsten to Cu joints, that are not reliant on the use of silver, an element which transmutes under neutron bombardment to the element cadmium which is unacceptable from the ultra high vacuum point of view. The reference geometry for the lower part of the vertical targets in the region of the SOL strike point is a CFC monoblock, incorporating a twisted tape turbulence enhancer inside a 10 mm bore and 12 mm OD CuCrZr alloy tube. The monoblock has been shown to be a robust design for the CFC armour, and in tests EU HT¹ built mock-ups have survived > 1000 cycles at 20 MWm⁻². It is preferred over the less expensive flat tile design, because of concerns over the observed tendency for flat tiles to suddenly and totally detach. Loss of a single tile might be tolerated, but what is not acceptable is a possible cascade failure, whereby the loss of a tile causes the heat load to the tile downstream in the SOL to be doubled causing it to detach, and so on. An alternative design uses annular flow which adopts a hairpin return at the lower end of the vertical target. This promises to provide a more robust design by eliminating many of the vulnerable coolant connections. The JA HT² have demonstrated the feasibility of using monoblocks on tubes up to 20 mm OD for a heat flux of 20 MWm⁻² and the EU HT showed that the thermo-hydraulic performance of annular flow can have sufficient margin on the critical heat flux (CHF) ³.

With regard to the low cycle fatigue (LCF) life-time of the heat sink for the reference monoblock design and the coolant parameters described in II.2.3.4, initial analysis indicates⁴ a life-time of 8×10^4 cycles at 5 MWm⁻². Based on this result and extrapolating previous work⁵, for a 10 MWm⁻² heat flux, the heat sink should satisfy the ISDC⁶ criteria for a LCF > 3000 cycles. The RF HT is assessing the LCF for 10 and 20 MWm⁻².

For the upper target/baffle and dome, where there is tungsten armour, a flat tile is preferred. A tungsten brush-like armour design is employed that overcomes the disparity in the thermal expansion coefficients of tungsten and copper. The armour-Cu joining process, the choice of heat sink geometry and the performance under high heat flux of these reference options are discussed in detail elsewhere⁷.

II.2.3.5.3 Private Flux Region PFC

The high heat flux (HHF) components in the private flux region receive a heat flux which is at least an order of magnitude lower than that on the vertical target. The high neutral pressures found in the private flux region, both in experiment and in modelling with B2-EIRENE, means that helium and hydrogen isotopes are exhausted through a transparent tungsten liner in the private flux region below the dome. This liner has two main functions,

1 G. Vieider, et al; European Development of Prototypes for ITER High Heat Flux Components, ISFNT-5, Rome, 1999.

2. S. Suzuki, et al; "Thermal Fatigue Damage of the Divertor Plate", ISFNT-5, Rome, Sept. 1999.

3 I. Smid, J Schlosser, et al; "Comparison between Various, Thermal-hydraulic Tube Concepts for the ITER Divertor"; Proc. 19th SOFT, Lisbon, Sept 1996

4 Private communication M. Korolkov, Efremov Institute, St Petersburg.

5 Summary of Structural Analyses of the PFCs, IDoMS No. G 17 MD 108 97-11-27 W 0.1

6 "ITER Structural Design Criteria for In-Vessel Components," IDoMS: S 74 MA 1

7 S. Chiocchio et al; "The Divertor for the Reduced Technical Objective/Reduced Cost ITER" SOFE, Albuquerque, Oct. 1999.

R. Tivey et al, "ITER Divertor, Design Issues and R&D", Fus. Eng. & Des. 46(1999) 207-220

firstly to protect the cold ($\sim 100^\circ\text{C}$) stainless steel cassette body from the power that is radiated from the divertor channel and vertical target, and secondly to minimise the co-deposition of tritium with carbon, which is eroded from the vertical targets. Therefore, besides the presence of He and DT gas in the private flux region, there will be significant quantities of carbon and hydrocarbons that have been chemically and physically eroded from the vertical target. It has been shown in laboratory and tokamak experiments¹ that the nature of these hydrocarbons i.e. the volatile and active species, is such that they can form thick, hydrogenated coatings on cool surfaces ($< 300^\circ\text{C}$). Thus, the present design philosophy for the liner is to operate at a high temperature (800 to 1000°C) and to provide sufficient area for surface collisions to recombine the active components, such as H^0 and C_xH_y radicals, into volatile compounds that can be pumped safely away, or to deposit de-hydrogenated carbon layers (at temperatures $> 350^\circ\text{C}$). This will prevent soft hydrogenated carbon deposition being formed on the liner and cold surfaces behind the liner. Thus, with the correct design and operation of the liner, the tritium inventory in the divertor might be kept below the safe operating limits (1 kg tritium inventory inside the VV) without frequent cleanup.

To reach the operating temperatures needed, it is proposed to use the radiated power from the divertor channel to heat 2.5 mm thick, radiatively cooled, tungsten tiles². These tiles are shaped in such a way as to prevent line of sight to the cassette body and to give a channel of sufficient length and width so as to provide the required number of surface collisions to ensure recombination. However, recent laboratory results³, show that some hydrocarbon radicals (e.g. CH_3) have a low sticking probability and this brings into question the effectiveness of the liner in mitigating the co-deposition. At present all the parties within ITER are investigating the physics of hydrocarbon radicals to decide whether the above design assumptions can result in acceptably low T deposition rates or if CFC has to be avoided altogether in a long pulse machine operating with T.

II.2.3.5.4 Coolant Parameters

The main driver for the cooling layout is the need to maintain an adequate margin to the CHF, and not, as may at first be thought, the total input power to the divertor.

Data on the mechanical properties of irradiated CuCrZr ⁴, indicate that operating with inlet temperatures as low as 100°C could be beneficial rather than detrimental to the component life-time. This (100 - 140°C) allows the coolant to be fed in series through the PFCs of the divertor⁵. Employing the reference monoblock design and by flowing the coolant in series through the outer vertical target, then the inner vertical target and finally through the private flux region PFCs, coolant parameters that are compatible with the adoption of a single heat transfer loop for the entire divertor are achieved. A higher coolant velocity is employed in the downstream inner vertical target in order to compensate for its lower sub-cooling and to

¹ G. Federici, et al., Issues arising from plasma wall interactions in reactor-class tokamaks, to appear in Nuclear Fusion.

² A. Makhankov, et. al; "Design of a Radiative Semi-transparent Liner for the ITER Divertor Cassette", ISFNT-5 Rome 1999

³ A. von Keudel, C. Hopf, T. Schwarz-Selinger, W. Jakob ; "Surface loss probabilities of hydrocarbon radicals on amorphous hydrogenated carbon film surfaces", Nuclear Fusion, 37 (1999) 1451

⁴ "Materials Assessment Report (MAR)"; IDoMS No.G A1 DDD 1 98-05-28 W 0.3

⁵ "ITER FEAT Divertor coolant layout " IDoMS: G 17 MD 131 99-11-26 W 0.1

achieve the same margin on CHF as the outer vertical target. The coolant parameters and margins on CHF for each PFC are given in Table II.2.3-2.

Table II.2.3-2 Coolant parameters and margins on CHF for each PFC

Inlet pressure	4.3 MPa
Inlet temperature	100 °C
Flow rate	709 kgs ⁻¹
Total pressure drop	1.0 MPa
Total temperature increase	40 °C
Axial velocity in the swirl section of the outer target	9.0 ms ⁻¹
Axial velocity in the swirl section of the inner target	10.7 ms ⁻¹
Coolant flow rates in the liner (outer / inner)	373 / 336 kgs ⁻¹
Minimum margin to CHF in the outer vertical target (based on 20 MWm ⁻²)	1.7
Minimum margin to CHF in the inner vertical target (based on 20 MWm ⁻²)	1.56
Minimum margin to CHF in the liner (based on 2 MWm ⁻²)	4.7
Minimum margin to CHF in the dome (based on 5 MWm ⁻²)	1.84

II.2.3.6 Cassette Design

The cassette to vacuum vessel attachments employ a pinned location at the outermost end of the cassette, which allows rotation, and a link element at the innermost end, which allows rotation and the differential radial movement between cassette and vessel.

The cassette thickness is determined by the bending stress in the section during the rare, worst-case disruption loads and by the need to provide adequate shielding for the vacuum vessel and coils. Pending design specific simulations of the halo current sharing between vessel and cassette, present calculations pessimistically assume that the vessel carries none of the halo current, and a peaking factor of 1.5 is assumed for an individual cassette. For a cassette thickness of 250 mm a peak bending stress of 130 MPa is computed for the worst case loading condition, which is assumed to occur once in the components life-time. This value is well below the allowable of 240 MPa for such an event.

More precise evaluations are needed using results from disruption simulation codes (e.g. TSC¹ or MAXFEA²) and taking into account pressure and thermal loads, and to check the eddy current generated loads, which may now cause the worst loads for the cassette body.

With a 200 mm thick cassette (20% water, 80% steel), the total heat to the first turn of the TF conductor from neutrons passing through the divertor is estimated at < 60 W, which is within the limit specified in II.2.3.2.

II.2.3.7 PFC to Cassette Attachments

All three PFCs are supported from the cassette body using two pairs of remotely maintainable

¹ S.C. Jardin, N. Pomphrey, and J. DeLucia, "Dynamic Modeling of Transport and Positional Control of Tokamaks," J. Comp. Physics 66, 481 (1986)

² P. Barabaschi, Fus.Eng.& Des.30 (1995) 1149

attachments (Figure II.2.3-5)¹. One pair of attachments, the upper ones in the case of the vertical targets, accommodate both rotation and translation. In this design a series of links engage at one end in slots in the PFC and at the other in slots in the cassette body. The holes in the links are aligned at one end with holes in the cassette body and at the other with holes in the PFC. Thick, aluminium-bronze tubes (~ 30 mm outer diameter and ~ 20 mm bore) are then inserted into each of the holes of the inter-linked components (clearance of 0.5 mm) and one at a time the pins are expanded by drawing a mandrel through them. The second attachment uses only one expanded pin and is capable of rotation only. In this case no links are needed, and instead a series of tongues (part of the cassette body) are inserted into slots in the PFC. The attachments are removed by simply drilling out the pins using the central hole as a guide.

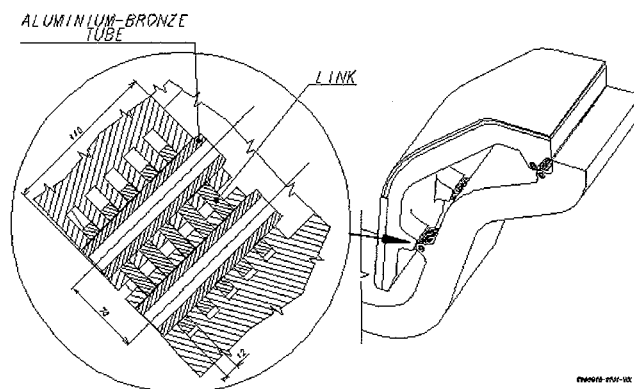


Figure II.2.3-5 PFC to Cassette Attachments

II.2.3.8 Integration of Diagnostics

At the divertor level, diagnostics are integrated into the 6 ports dedicated to diagnostics and the 3 maintenance ports. Optics or waveguides will view the plasma either via the slots between cassettes (side plates will be mounted on the cassette body) or through the pumping slots and mirrors mounted behind the liner. Thermocouples, Langmuir probes etc. will be built into side plates which are then attached to the second cassettes.

Neutron analyses indicate that slot widths up to 150 mm can be accommodated in the outboard region of the cassette body and in the outer part of the vertical target away from the strike point (baffle region). The strength of the cassette in this region is not an issue and the heat flux to the cassette body remains below 0.15 MWm^{-2} even in the region immediately below the opening in the target. To avoid the need for vertical ports in the vacuum vessel, the in-vessel viewing (IVV) system (see also II.10.5) is located in some of the divertor level ports. The IVV system is installed in each of the 6 ports dedicated to diagnostics and is enough to give $\sim 95\%$ visual coverage of the divertor and blanket first wall.

II.2.3.9 Costing

Based purely on scaling from industrial cost estimates, ITER-FEAT is likely to achieve a $\sim 40\%$ cost reduction with respect to the 1998 ITER divertor design. Any additional savings must come through simplifications of the design and the manufacturing process. Previously

¹ S. Chiochio, A. Turner, et al; "The Attachment System of the ITER Divertor Plasma Facing Components", Proc. 20th SOFT, Marseille, Sept.1998

the PFCs accounted for 70% of the total cost, and the cassette bodies, support shoes, diagnostic blocks and assembly of the cassettes (excluding RH and installation costs) accounted for the remaining 30%. Hence, savings in the PFC costs are more significant than savings in the remainder.

The PFCs are built by assembling armoured slices and the number of slices is a strong driver for their cost. R&D and design effort have focused on reducing the number of parts by using wider PFC slices and fewer PFCs per cassette, as well as simplifying the manufacturing process. These efforts promise to yield the additional savings to achieve the 50% cost goal¹. What also needs to be taken into account is the combined effect on the cost of blanket and divertor of incorporating the baffle into the divertor.

II.2.3.10 Steady-State and High Power Operation

For the ITER-FEAT divertor under steady-state conditions, it is predicted that the fusion power will be 500 MW and the auxiliary heating 100 MW ($Q = 5$)². Hence, the conducted power to the divertor is ~ 150 MW (195 MW including neutron heat load), an increase of $\sim 25\%$ on the value for the reference plasma (see II.2.3.5). For the transiently attached plasma this would reduce the margin on CHF to 1.05. However, a margin of 1.4 can be maintained by increasing the coolant sub-cooling, and this can be achieved either by reducing the coolant inlet temperature, say to 70°C (nominal is 100°C), and/or by increasing the inlet pressure, to say ~ 6.5 MPa (nominal is 4.4 MPa, see Table II.5-2). It is assumed that discharges of relatively short duration will be used to learn how to maintain a semi-detached, radiating divertor that is free from the occurrence of high power transients. In any case, operation without semi-detachment will result in insufficient helium being pumped, and hence the fusion power output will be curtailed. Following this learning phase, the nominal 100°C, 4.4 MPa coolant inlet parameters can be re-instated. Since operation with modified coolant parameters will be for a limited total integrated time, the effects of Cu embrittlement and reduced fatigue life-time should be tolerable.

For the assumed extreme parameters of fusion power (700 MW) and additional heating (50 MW), similar discharge length and helium pumping restrictions as for steady-state operation can be taken into consideration. In this case, extrapolation from normal operation gives a power conducted to the divertor of 143 MW (206 MW including neutron heat load). These values are roughly comparable with the steady-state demands on the divertor, and similar modifications can be applied to the coolant parameters.

II.2.3.11 Conclusions and Future Work

The outline design of ITER-FEAT indicates that a working divertor in this configuration is feasible. However, more work is needed to arrive at a fully consistent design that meets the requirements associated with fitting the divertor into the allotted space and in operating with one divertor coolant loop. Further analysis is required to justify the PFC heat sink designs. In order to meet the full 50% cost reduction goal, a series of R&D and design studies have been launched to develop the options outlined in II.2.3.5. R&D tasks have also been launched 1) to study and test the cascade failure of flat tiles, 2) to study the possibility of using the

¹ Divertor Cost Scaling for ITER-FEAT IDoMS No G 17 MD 130 99-11-26 W 0.1

² P. Barabaschi, T. Mizoguchi, M. Shimada; "Reference Parameters of IAM4 (ITER FEAT) IDoMS No. G73MD21 99-10-29 W0.1

hypervapotron in conjunction with flat tiles as a means of lowering the maximum heat sink surface temperature, and 3) to study HIP and fast brazing techniques that maintain good CuCrZr mechanical properties.

II.3 Cryostat and Thermal Shields

II.3.1	Cryostat System	1
II.3.1.1	Cryostat Vessel Details	2
II.3.1.2	Bellows and Penetrations	2
II.3.1.3	Assembly and Installation of the Cryostat	3
II.3.2	Design of Thermal Shields	3
II.3.2.1	Robustness of Design and Minimization of Space Envelope	4
II.3.2.2	Minimization of Thermal Load to 4K Components and Optimization of Thermal Load to Cryoplant	4
II.3.2.3	Access for Inspection and Repair	5
II.3.2.4	Cost	5
II.3.3	Assessment and Future Work	5

The cryostat provides the vacuum environment for conductive and convective thermal insulation of the superconducting magnets and cold structures, and forms the secondary confinement barrier for the radioactive inventory inside the vacuum vessel (VV).

The thermal shield system minimizes heat loads transferred by thermal radiation from warm components to the components and structure that operate at 4.5K. Reduction of these heat loads by over two orders of magnitude facilitates the removal of the residual heat load by the cryoplant with reasonable capacity.

II.3.1 Cryostat System

An elevation view of the cryostat is shown in Figure II.3-1. Its diameter, 28 m internal, is determined by the dimension of the largest component located inside, the poloidal field coils PF3 and PF4, with an additional small radial clearance of approximately 1 m for access space for in-situ repair. Its height, 24 m internal, is determined by the size of components inside as well as the vertical space needed to make the interconnections with external systems.

In principle, several different cryostat design configurations could be possible. These were considered¹ and for cost reasons as well as industrial experience, the present design, which is basically a reduced-size version of a cryostat design extensively analyzed previously², was selected. It is a single-wall, cylindrical configuration with flat top and bottom heads, providing an optimized compactness in layout.

The cryostat is supported on the basemat of the building and surrounded by a concrete bioshield keeping a radial clearance of approximately 0.5 m. The bioshield extends above the cryostat and includes a 2 m thick slab above the cryostat that is supported by a truss structure connected to the upper head of the cryostat. The diameter of the cryostat cylinder below the VV is reduced in one step to 18 m. The horizontal, annular section, which interconnects between the main and reduced diameter cylinders, is connected at its inner bore with the gravity support of the tokamak and at its outer circumference it is firmly connected with the bioshield at a position where an external floor slab provides additional lateral stiffness. This layout provides a very strong radial support, minimizing lateral deflections of the machine support under horizontal seismic loads. A further feature of this design is that it

¹ N24 MD 4 99-05-27 W 0.1 "Rationale for selection of the cryostat design for RTO/RC ITER" T.Kuribayashi, R.Haange

² N24 DDD 5 97-11-17 W 0.3 DDD 2.4 Appendix G "Cryostat Structural Analysis"

improves the accessibility, through ports in the lower cylindrical part, into the cryostat for eventual repair or inspection access.

The cryostat is a fully-welded, stainless steel vessel with a large number of horizontal ports for access to VV ports at three levels, further horizontal penetrations for coolant pipework at upper and lower levels, and cryofeedlines to magnets at upper and lower levels. Furthermore, access ports for manned or remote access for repair or inspection are included in the lower cryostat cylinder for horizontal entry, and in the upper cryostat head for vertical entry. In the very unlikely case that large components located inside the cryostat need to be replaced, the upper bioshield slab can be removed, and the cryostat head with the support structure can be cut from the cryostat cylinder and also removed.

The total weight of the bioshield slab is approximately 3500 t, which exceeds the capacity of the main crane (approx. 1400 t). The bioshield slab is therefore designed to be installed and removed in several parts. The weight of the cryostat head, including truss work is below 1000 t and can therefore be removed with the main crane without subdividing.

II.3.1.1 Cryostat Vessel Details

The upper head is a circular flat plate with radial stiffening ribs spaced every 10 degrees and integrated with the bioshield support which consists of a steel truss structure. The head, through which VVPSS steam pipes as well as a neutron diagnostic penetrate, is connected via welding to the vertical cylindrical shell. The lower head is reinforced similarly to the upper head and also connected to the cylindrical shell by welding.

The wall thickness of the cylindrical shell is generally 50 mm. Its upper, middle and lower regions need reinforcement for the large divertor and equatorial ports openings. All of these shell portions are stiffened for external pressure by equally-spaced, circumferential and vertical stiffening rings. The minimum required thickness and distance between stiffening rings have been studied for external pressure in accordance with ASME Code Section VIII, Division 2, Article D-3. Because of its minimum intrusion into the inner space of the cryostat, a T-section reinforcement profile with adequate margin has been selected.

II.3.1.2 Bellows and Penetrations

Initially, circular metallic bellows were considered to connect the interspace duct wall extensions of the VV ports with the cryostat port. Bellows are required to compensate for differential movements. However, due to the relatively large port sizes, these bellows would become so large that there would be insufficient space left between them for accessing (for repair operations) the region between the equatorial and divertor ports inside the cryostat.

Two alternative designs have been proposed involving either metallic, circular bellows that are attached outside the interspace, or rectangular bellows made of reinforced elastomer materials. The latter leave maximum space for interventions inside the cryostat near the equatorial and divertor port regions and have the least impact on the building and component layout. The use of rectangular, elastomer bellows is therefore the present reference configuration. Development of suitable bellows is the subject of the present R&D programme.

II.3.1.3 Assembly and Installation of the Cryostat

Pre-formed plate sections fabricated in the factory will be shipped to the ITER site and assembled inside a temporary building into three main sections: (i) an approximately 6 m high section comprising the lower head and reduced-diameter cylindrical section, including cryofedline and coolant penetrations with horizontal annular plateau, connected to a short cylindrical section having the diameter of the main cylinder; (ii) an approximately 18 m high sector consisting of the main cylinder with port penetrations at three levels and upper penetrations for coolant pipework and cryofedlines; (iii) an approximately 4 m high section comprising the upper head with vertical port penetrations for access into the cryostat, and the support structure of the bioshield.

After fabrication of a main sector, it is loaded onto a large, heavy duty transporter using a construction crane, and brought to a staging area for final cleaning. After transfer into the assembly hall, it can be outfitted with a cryostat thermal shield to the maximum extent permitted considering further in-pit assembly activities, and installed inside the tokamak pit, starting with the lowest section. All three sections weigh below the capacity of the main crane and can therefore be lowered into the pit using the main crane. Circumferential welding of the three sections will be done, as far as possible, with automatic equipment from both the inside and outside of the cryostat. The supports of the lower cryostat section are fastened by bolting into the building structures.

At a time commensurate with the overall assembly sequence, VV port extensions and interspace ducts are installed and interconnected to the cryostat shell by the elastomer bellows. In parallel, the other penetrations are installed. After completion of the in-cryostat operations, the upper head can be installed and welded to the shell. This is followed by connecting the external part of the relief pipe to the head, and final testing.

II.3.2 Design of Thermal Shields

The thermal shields comprise the vacuum vessel thermal shield (VVTs), which interposes between the VV and the cold structures, the cryostat thermal shield (CTS), which is mounted alongside the walls of the cryostat (bottom, cylinder and upper head), thereby preventing direct line of sight of the room temperature walls to the cold structures, the transition thermal shields (TTSs) that enwrap the port extensions and service lines that are routed between the cryostat walls and the VV, and the support thermal shields (STSs) that enwrap the VV gravity supports and machine gravity supports. The STSs include thermal anchors to limit the heat load to cold structures due to conductance through the support structures.

An elevation view of the thermal shields is shown in Figure II.3-1. The VVTs is of self-standing design supported on the toroidal field coils by inboard and outboard supports. Inboard supports are slender stainless steel rods allowing radial and toroidal movements, whereas on the outboard side, supports are used to fix the radial and toroidal position of the VVTs. All other thermal shields are modular, and fixed on the warm components via low-conductivity supports.

In all cases the thermal shields consist of stainless steel panels that are cooled by helium gas with 80K inlet temperature. The cooling lines remove the heat load intercepted from the warm

surfaces. The cold structures, operating around 4K face the TS surfaces. The conductive heat loads from all thermal shields are limited to small losses through their supports.

The main criteria used in the development of the design of the thermal shields are:

- robustness of design and minimization of space envelope;
- minimization of thermal load to 4K components;
- optimization of thermal load to cryoplant;
- access for inspection or repair;
- cost.

II.3.2.1 Robustness of Design and Minimization of Space Envelope

The TS must withstand loads in normal and off-normal operation regimes. Therefore, robustness of the design is of extreme importance, especially for the vacuum vessel thermal shield (VVTs) which forms a permanent part of the machine, its inboard part and large areas of the outboard portion being inaccessible after machine installation. Repair of damage would involve disassembly of the relevant VV sector and is therefore to be avoided. Furthermore, loss of cooling of the thermal shields, especially the VVTs would lead to heating up of the cold structures. Recovery times may be very long. Therefore, the cooling lines connected to the thermal shield panels are designed to be fully redundant. This not only applies to the in-cryostat cryolines, but also to their valve boxes, the cryolines between the valve boxes and the cryoplant, as well as relevant cryoplant components.

To enhance mechanical robustness, it has been decided not to employ multilayer insulation (MLI) on the thermal shields as this can be easily damaged. Moreover, it is very difficult to outgas once it has been contaminated by moisture etc. On the VVTs, with the virtual impossibility of having access for repair and high values of induced electro-magnetic loads, no multi-foil stacks will be employed for the same reason. Also, for the CTS, simple panels are foreseen in the reference design. Further enhancements against failure are obtained by having electrical breaks incorporated in panel joints, reducing the electro-mechanical loads on the VVTs and the probability of arcing between components, and by having bumpers, in the form of leaf springs, mounted on both the inside and external side of the VVTs, thereby avoiding or mitigating impulse loads during major seismic or off-normal load events.

The space envelope is particularly critical for the VVTs. The clearance between the VV and the TF coils, in which the VVTs resides, needs to be kept as small as practical. A considerable effort has therefore been expended on keeping the design of the VVTs as slim as possible. Additional clearance has to be available for VV assembly and disassembly operations. The requested clearance (35 mm) is not fully available in the present design and additional design effort will therefore be needed in the near future. The base design of the thermal shield consists of a single or double stainless steel panel onto which are mounted two independent helium cooling lines. The panels fully interpose between the warm and cold surfaces. Helium flow is controlled by valves located in a valve box external to the bioshield.

II.3.2.2 Minimization of Thermal Load to 4K Components and Optimization of Thermal Load to Cryoplant

Within the constraints of the required robustness of design and minimization of the space envelope, heat load reduction is obtained by using low emissivity coatings. The thermal

shields will therefore be coated on both the warm and the cold facing surface by a thin layer of silver. To keep the heat load to the VVTS within reasonable limits, it is proposed to lower the emissivity of the VV surface facing the VVTS by a burnishing procedure. Reduction of the heat load to the VVTS and to structures operating at 4K would also be possible by adding stacks of reflecting foils onto the warm and cold sides of the panels, but these stacks are judged too vulnerable considering that manned entry for inspection or repair inside the cryostat may be required, (see II.3.2.3). The reference CTS design therefore is based on simple, Ag-plated stainless steel panels that sandwich a thin (~ 0.5 mm thick) copper sheet for increased temperature conduction, thereby allowing larger distances between the meandering coolant tubes.

II.3.2.3 Access for Inspection and Repair

The difficulty of accessing the VVTS has already been mentioned before. There are, in principle, two possibilities for the position of the CTS: close to the cold structures to protect the 4K surfaces, or to connect the CTS to the cryostat wall, i.e. as far as possible away from the cold surfaces. The latter option has been selected for two reasons: (i) it allows good access to the outer perimeter of the PF and TF coils as well as to breaker boxes, clamps etc, and (ii) the overall contour of the CTS is basically following the cryostat shell and therefore much simpler than following the complex shape of the cold structures.

II.3.2.4 Cost

Cost is mainly driven by the complexity of design and the total surface area. Simplicity in design is achieved by keeping the basic panels of the CTS, TTSs and STSs flat and of rectangular shape for most areas. However, the VVTS has to closely follow the shape of the VV, for space reasons and is therefore of a segmented, toroidal design. Its complexity, apart from the overall shape, lies in the fact that sector joints, some of which are electrically insulated, have to be made suitable for remote operations and even the initial hands-on installation is made more difficult as it is partly made through narrow openings in the VV.

II.3.3 Assessment and Future Work

The cryostat and thermal shields conceptual designs are relatively well-developed based on previous work. The following issues need particular attention:

- (i) development of reinforced elastomer bellows;
- (ii) detailed mechanical design including penetrations, ports, and bellows;
- (iii) detailed procedure of assembly and installation;
- (iv) detailed analyses and design of thermal shields including the study of fabrication and installation, particularly provision of increased clearance for VV disassembly operations;
- (v) study of the application of Ag coating, and possibly R&D to provide data on long-term behaviour of Ag emissivity properties.

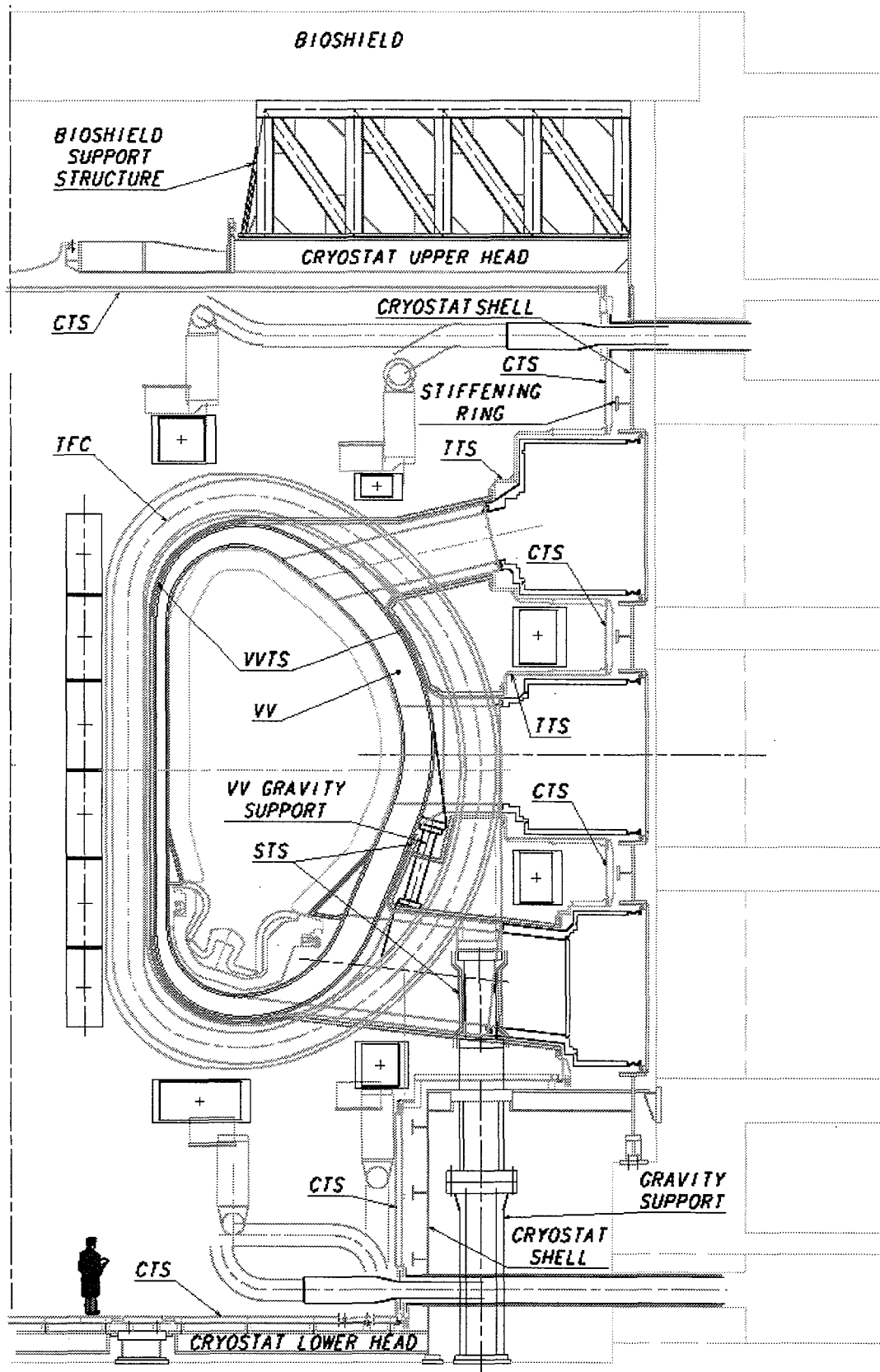


Figure II.3-1 Elevation View of Cryostat, Thermal Shields (cryostat (CTS), transition (TTS), vacuum vessel (VVTS) and support (STS)), and Gravity Supports

II.4 Fuel Cycle

II.4.1	Fuelling and Wall Conditioning Systems	1
II.4.2	Vacuum Pumping Systems	2
II.4.3	Tritium Plant	4
II.4.4	Staged Installation	6
II.4.5	Cost Reduction	6
II.4.6	Conclusions	7

The fuelling rate, specified as $200 \text{ Pam}^3\text{s}^{-1}$, the flat-top burn of 400 s, and the repetition rate of two pulses per hour are the parameters which have the greatest influence on the design of the fuel cycle. This section presents the outline design of the fuel cycle to satisfy these parameters and the impact of extending the pulse length to 3,600 s.

Staged installation as a means of deferring capital cost has been investigated and the preliminary findings are summarized later in this section. It has been established that the production of tritium during DD operation is significant¹ and well above the maximum allowable chronic release rate. As a result, tritium contamination of fuel cycle components and the processing of the tritiated exhaust must be actively considered in the planning of any potential staged installations.

II.4.1 Fuelling and Wall Conditioning Systems

The fuelling during plasma operation is provided by a combination of both gas puffing and pellet fuelling up to a combined average fuelling rate of up to $200 \text{ Pam}^3\text{s}^{-1}$. Both systems are suitable for long pulse operation without modification or the need for additional equipment. During the DT phase of operation the available DT fuelling rate will be $200 \text{ Pam}^3\text{s}^{-1}$, whereas the T_2 fuelling rate will be limited to $50 \text{ Pam}^3\text{s}^{-1}$ for either gas puffing or pellet fuelling, or any combination of each.

The gas injection system (GIS) comprises a total of 8 valve boxes, with 4 boxes uniformly distributed at each of two poloidal locations, the upper and divertor port levels. All valve boxes are located outside the bioshield and are connected to the gas supply manifold which delivers fuelling gases from the tritium plant. A single gas injection line is routed from each valve box through the adjacent port and, in the case of the upper port, terminates behind the blanket from where the gas distributes through the gaps between the blanket modules. At the divertor level the gas injection line is routed through the port under the divertor cassette to terminate in the private flux region of the divertor. The GIS is designed to provide a nominal flow of $200 \text{ Pam}^3\text{s}^{-1}$ over the length of the pulse with a fuelling rate of up to $500 \text{ Pam}^3\text{s}^{-1}$ being available for up to 10 s several times during the pulse. The GIS is design to deliver up to 6 gases (with 9 gases being available for delivery at any one time from the tritium plant) during plasma operations suitable for fuelling, physics investigations and radiative cooling of the divertor. The GIS also supplies the gases needed for wall conditioning and the fusion power shutdown system to initiate a slow plasma termination. The response time of the GIS will be $< 1 \text{ s}$ and set point control will be better than 5%.

¹ G 17 MD 129 99-11-26 W 0.1 Analysis of T production during DD operation phase

The pellet injector system (PIS) is designed for steady-state fuelling, for pulses of any length, and for the injection of impurity pellets for physics and transport studies. The delivery flight tube is configured for inside launch to maximize both pellet penetration and fuelling efficiency. The pellet fuelling rate will be up to $100 \text{ Pam}^3\text{s}^{-1}$ for all gases except T_2 , which will be limited to $50 \text{ Pam}^3\text{s}^{-1}$. Injection rates for impurities will be limited to $10 \text{ Pam}^3\text{s}^{-1}$. A combination of pellet size and injection frequency will be used to limit density perturbations to $< 10\%$. To satisfy the fuelling requirement, pellet sizes in the range of 3 - 6 mm will be available with injection frequencies up to 50 Hz provided for the smaller pellet size.

The need for a fast plasma termination system has been recognized, but the requirements for this system remain to be defined.

A common gas delivery manifold, routed from the tritium plant to the machine, is provided to supply the various gases needed not only for GIS and PIS operation but also for the neutral beams (NB) used for heating and current drive and the diagnostic neutral beam (DNB). Up to 6 gases can be supplied to the GIS and PIS, at flow rates needed to satisfy the fuelling requirements of these systems at a delivery pressure of 0.1 MPa. Gas supplies available for NB and DNB operation are H_2 and D_2 delivered at 0.6 MPa. The common supply manifold, which is secondarily confined, is routed around the bioshield to the individual delivery points required for the various systems and components.

Baking, in conjunction with glow discharge cleaning (GDC), will be conducted following the initial closing of the vessel and subsequently following a vessel opening. Baking will be conducted at a temperature of 240°C for a period of 5 - 10 days. GDC will employ a total of 6 electrodes deployed from the divertor level ports and use conditioning gases of H_2 , D_2 and He at an operating pressure of $\sim 0.1 \text{ Pa}$. A combination of baking and GDC will also be undertaken prior to vessel opening following the start of DD operations.

ECR-DC can be used for conditioning between discharges, where less efficient impurity/hydrogen removal will be required, employing about 1 MW of power which will be provided by two start-up systems (90 to 140 GHz) and one heating and current drive system (170 GHz) of the ECH&CD system. H_2 , D_2 and He will be employed operating at a pressure of $\sim 0.1 \text{ Pa}$.

In addition to the above wall conditioning methods, the capability for reactive cleaning (etching) will also be provided for the removal of co-deposited layers. The GIS will be used to deliver O_2 to the chamber which will be continuously evacuated by the torus roughing pumping system, throttled to maintain a chamber pressure of $\sim 1.5 \text{ kPa}$ at a nominal throughput of $\sim 5 \text{ Pam}^3\text{s}^{-1}$. Divertor temperatures up to 350°C may also be required to ensure that reactive cleaning can be conducted within a reasonable time period. This activity is also planned to be undertaken prior to vessel opening following the start of DD operations.

II.4.2 Vacuum Pumping Systems

The torus high vacuum pumping system is used during plasma operation to pump the torus exhaust consisting primarily of hydrogen isotopes together with helium and other impurity gases. It also provides high vacuum pumping during all other phases of machine operation including evacuation during the dwell period between plasma discharges, wall conditioning, bake-out, and leak testing. These pumps are independently controlled to allow individual

pumps to be regenerated, to shut down in the event of failure, or to regulate the pumping speed at the torus. During plasma operations, the pumping system will be required to exhaust up to $200 \text{ Pam}^3\text{s}^{-1}$ of DT at a divertor neutral pressure of $\sim 3 - 4 \text{ Pa}$, together with the helium ash which will be generated with other impurities. These pumping requirements are satisfied by a number of helium-cooled cryopumps, with the number required being dictated by the pulse length.

During the initial phase of operation, the torus cryopumps will be operated in a pulsed mode, with regeneration after an accumulated burn time of 450 s. For longer pulse operation, regeneration during the pulse will be needed and additional pumps installed to satisfy this requirement. However, this long pulse capability will not be required until the later phases of operation and the installation of these extra pumps can be deferred. This two phase strategy allows not only a reduction in the initial complement of pumps needed but also reduces the initial capacity of the cryoplant by reducing the fast cooldown requirement needed for long pulse operation. The size and number of pumps needed to perform the plasma exhaust function is primarily dictated by considerations of throughput, deflagration and incremental cycle time. Consideration of these factors results in the selection of a pump with an internal diameter 1.40 m operating on an incremental cycle time of 75 s. In order to provide pulsed operation up to the maximum pulse length of 450 s, 6 pumps will be needed. For pulse length $> 450 \text{ s}$, the number of pumps will need to be increased to 10. Each one of the pumps will be installed in one of the vacuum vessel divertor ports, and will be located behind the divertor cassettes. The pumps will be evenly distributed toroidally to the maximum extent possible to ensure uniformity of pumping. Since the plasma exhaust will be routed through the divertor, the design of the flow passages (II.2.3) ensures that the pumping conductance of the divertor does not compromise the overall pumping speed of the system. In fact, the design of the divertor results in an essentially balanced design (divertor conductance \approx pumping speed) without compromising the neutron streaming and shielding functions of the divertor.

During regeneration, the pumps undergo sequential warm-up from 4.5K to 80K, pump out of the desorbed gases, primarily hydrogen species and helium, and subsequent re-cooling to 4.5K. To minimize cryogen consumption, the cool-down time is maximized, within the time available, to satisfy the pulse repetition of two pulses per hour. This cool-down time is the major time variable in the system since the pump-out time needed to satisfy long pulse operation is fixed at 75 s (using the same rough pumping system). This offers the opportunity to increase the cool-down to 183 s from the 75 s needed for long pulse operation while still meeting the specified repetition frequency.

For long pulsed operation ($> 450 \text{ s}$) a 4-stage regeneration strategy is adopted, in which 6 pumps are in pumping mode and 4 pumps are in various stages of regeneration. The pumps are taken off-line (inlet valve closed, no pumping) sequentially and returned to the pumping mode following regeneration. As each pump is taken off-line it is replaced by a pump returning to the pumping mode and thereby a constant system throughput is retained. In the first 2 stages of the regeneration sequence the inlet valve is closed and the temperature of the sorbent panel increased from 4.5K to 80K during the 150 s available. In the third stage, the exhaust valve of the pump is opened and the pump evacuated using the torus roughing systems from $\sim 1 \text{ kPa}$, the pressure within the pump at full inventory, to $< 10 \text{ Pa}$ in 75 s. In the final stage of regeneration the pump is cooled to 4.5K in 75 s before being returned to the pumping mode. No other changes are required to accommodate pulse lengths of 3,600 s or longer.

In either pulsed or long pulse operation, using the above strategy, the maximum inventory of each individual pump is limited, at a 50/50 DT fuelling rate of $200 \text{ Pam}^3\text{s}^{-1}$, to 33.0 g DT (19.8 g T_2). At this fuelling rate the maximum inventory of the system will be 198.0 g DT (118.9 g T_2) for pulsed operation, and 181.7 g DT (109.0 g T_2) for long pulse operation. Of this inventory the maximum amount at risk at any time (at the start of the pump-out cycle), and outside the vacuum vessel boundary, is that of one pump.

The pumps are operated at three nominal temperature levels: 4.5K for the cryopanel surfaces, 80K for the radiation shields and inlet baffle, and 300K to maintain the cryopump housing and inlet valve below the vacuum vessel port temperature. The 80K radiation shield and inlet baffle provide an optically-tight, thermal radiation shield to limit heat transfer to the 4.5K panel. The 80K inlet baffle also serves to cool the incoming gas before it reaches the 4.5K cryopanel surfaces, thereby reducing the heat load to the 4.5K surfaces. Cooling of the housing and valve with 300K gaseous helium is necessary to reduce the heat transfer to the 80K surfaces which would occur if directly exposed to the port which is at 380K during plasma operations and 475K during bake-out. The cryopanel will be coated on both sides with charcoal sorbent material in order to pump helium. The cryopanel will normally be cooled using supercritical helium with an inlet temperature and pressure of 4.5K and 400 kPa respectively. The surface temperature of the charcoal will be 5.3K during DT operations which provides adequate pumping speed, capacity and base pressure for cryosorption pumping of helium and protium and cryocondensation pumping of the other hydrogen isotopes. A valve, mounted on the inlet to the pump, is provided to allow regulation of pumping speed and also allow total regeneration of the pump.

In addition to the torus high vacuum system described above, ITER-FEAT will require the following additional vacuum systems to be developed during the detailed design phase:

- torus vacuum pumping system,
- cryostat vacuum pumping system,
- NB injector auxiliary external pumping system,
- IC H&CD vacuum pumping system,
- EC H&CD vacuum pumping system,
- guard vacuum pumping system,
- service vacuum pumping system,
- diagnostic vacuum pumping system and
- leak detection systems

II.4.3 Tritium Plant

The ITER tritium plant is composed of four large subsystems:

- fuel cycle systems,
- long-term tritium storage system,
- atmosphere detritiation systems,
- water detritiation system.

The fuel cycle systems contain a variety of process systems such as:

- front-end permeator - to separate hydrogen isotopes from all impurities;
- isotope separation (ISS) - to remove protium from the tokamak exhaust, and change the DT composition to match fuelling requirements;

- fuel storage and delivery and shut-down fuel recovery - to provide proper fuel mixtures at delivery speeds to match fuelling requirements, storage for excess D₂ gas, and to provide rapid tritium accountancy during non-plasma operation periods with in-bed calorimetry;
- impurity detritiation - to recover tritium from tritiated impurities in the tokamak exhaust, which will allow detritiated impurity release to the atmosphere;
- ³He recovery – to recover the decay product ³He from fuel storage beds;
- activated gas decay tanks – to reduce activation of gases exhausted from the tokamak before rejection to the environment;
- co-deposited tritium recovery - to recover tritium from the tokamak during in-situ recovery campaigns.

A preliminary, overall process fuel cycle has been developed as shown in Figure II.4-1. The long-term tritium storage system comprises a robust vault for the storage of tritium shipping containers, a tritium accountancy system, and tritium loading/unloading system. The atmosphere detritiation systems include a glovebox atmosphere detritiation system (GDS), a normal vent gas detritiation system (Normal-VDS), a room air detritiation system (Standby ADS), a tokamak maintenance detritiation system (MDS), and a tokamak vessel emergency vent detritiation system (EDS). The water detritiation system is based on a combined electrolysis and catalytic exchange (CECE) process. By increasing the number of electrolysis units, overall capacity of this system can be increased without changing the capacity of the CECE process and the hydrogen isotope separation system.

Long pulse operation up to 3,600 s requires some upgrade of the exhaust processing system and of the fuel storage. The exhaust processing system needs to be increased by about 50% to cope on line with the exhaust rate during burn. The need for an upgrade of the storage system stems from the fact that the Isotope Separation System (ISS) processing capacity is about 30% of the fuelling rate. As a result, the excess exhaust gas has to be temporarily stored until it can be processed during the next dwell period. The extra temporary storage required an additional ~ 10 storage beds.

The confinement philosophy of the tritium plant is based on the ALARA principle and multiple barrier approach, i.e. tritium process equipment and pipes are the first barrier, and secondary enclosures such as gloveboxes, cold boxes and vacuum jackets form the secondary barriers. Building rooms backed up with the Normal-VDS, and isolation valves on the heating ventilation air conditioning (HVAC) system, are the final barrier against release into the environment. For the Category IV event of tritium release (tritium releases into an area in the tritium building and/or in the tokamak pit), HVAC isolation valves are closed by signals provided by area tritium monitors. To maintain the room pressure negative with respect to the external atmosphere, room air is partially extracted by the Normal-VDS which operates independently from the HVAC during normal operations. For the Category IV tokamak vessel event (in-vessel coolant leakage, in-vessel air ingress), the tokamak vessel EDS pumps the vessel gas/steam to the Normal-VDS via the roughing pump lines and an EDS condenser/cooler to maintain the vessel internal pressure slightly below atmospheric pressure. Emergency power (II.8) and safety-related component cooling and chilled water system (II.5) are provided for operation of the Normal-VDS and EDS and the HVAC isolation valves. The concept of overall tritium confinement logic is shown in Figure II.4-2.

A preliminary layout of the overall tritium plant within the tritium building is shown in Drawings 62.334.1 and 62.334.2 (see II.8). This layout will be further developed as the design of the various tritium plant systems evolve during the detailed design phase. The building comprises four floors, i.e. the first floor will be occupied by the tokamak vacuum pumping systems and leak detection support systems, the remaining three floors are allocated to all tritium fuel cycle processing systems, storage vault, atmosphere detritiation systems, water detritiation system and tritium building HVAC equipment. Careful attention will be given to the room height and HVAC duct layout for the hydrogen isotope separation system and hydrogen gas holding tanks to prevent the local accumulation of explosive mixtures. Some processing areas for the front-end permeator system, impurity processing, and activated gas decay tanks require gamma ray shielding. The complete tritium building including the stairs and lifts are designated as a "green zone". In areas where no contamination is expected under normal conditions, negative room air pressure (~ -20 mm H₂O) is maintained and room air tritium concentration is kept below 3.1×10^4 Bq/m³ (~ 0.1 DAC HTO). To minimize emergency isolation valves and to standardize HVAC equipment and radiation monitoring systems, the tritium building is divided into two green zones, each with its dedicated HVAC system. One zone is for the water detritiation system (WDS), which occupies a large vertical space at one end of the building, and the other for the remaining floors of the building. Each floor is connected to a supply and return from that dedicated HVAC system.

II.4.4 Staged Installation

No areas have been identified where staged installation of the fuelling and wall conditioning systems can be used to defer the capital costs of these systems.

The torus pumping system has been identified as a potential candidate for staged installation. The initial installation of 6 cryopumps will allow pulsed operations < 450 s to be undertaken. During the later phases of operation, where longer pulses will be required, a further 4 cryopumps will be installed to allow online regeneration to be conducted during the pulse. It is unlikely that staged installation will be a viable option for any other subsystem of the vacuum pumping system.

By taking into account a lead time for installation and commissioning, it was found that the full capacity of the fuel cycle systems, including the fuel storage and atmosphere detritiation systems, have to be ready by the time DD operations commence. However, the installation of the water detritiation system can be deferred until it is needed. Initial tokamak operation with DT and initial hot cell operations will provide a good indication of the amounts of tritiated water that will be generated and should therefore allow extrapolation to the required capacity when a detritiation system is required. Early installation of the electrolysis units may be necessary to limit the accumulation of high level tritiated water, which will be generated from various sources such as the atmosphere detritiation systems, the tokamak maintenance system, etc.

II.4.5 Cost Reduction

A number of areas within the fuel cycle provide the opportunity for cost reduction when compared with the 1998 ITER design. These reductions are, in the main, due to changes in the size of the machine and the design parameters for these systems. The anticipated cost

reductions together with the associated rationale relative to the 1998 ITER design are summarized below.

The design parameters for the fuelling and wall conditioning systems have remained essentially unchanged, which has limited potential savings on these systems to $\sim 5\%$. This saving is primarily due to a reduction in the number of gas injection valve boxes from 10 to 8.

A significant improvement in the net pumping speed of the plasma exhaust has been achieved with a new design of divertor which has allowed the number of cryopumps to be reduced from 16 to 10 (long pulse operation) while maintaining the required system throughput. The number of ports on the machine is also reduced allowing a corresponding reduction in the number of port secondary pumping systems which need to be installed leading to a slight cost reduction in this area. Other minor savings are also projected due to a reduction in the overall size of the machine. With these above changes an overall cost savings of $\sim 20\%$ is projected for the vacuum pumping system.

The adoption of a nominal duty cycle of 25% has allowed a reduction in the time-averaged capacity of the tokamak exhaust processing and hydrogen isotope separation systems to satisfy the nominal pulse length. However, for long pulse operation up to 3,600 s, an increase in the capacity of the exhaust processing system and additional DT storage beds will be needed. The additional cost associated with this increase in exhaust processing capacity and storage will be equivalent to and/or larger than the savings in the hydrogen isotope separation system obtained by the reduction in the nominal pulse length and duty cycle. A decrease in the free volume of the tokamak, when compared to the 1998 ITER design, has allowed a substantial reduction in the throughput of the MDS to be made which has led to a large cost savings in this area. Implementation of reactive cleaning (etching) for the removal of co-deposited layers may result in some increase in the capacity of the tokamak exhaust processing and storage systems, but these increases will be small and have a minimal impact on the overall cost of these systems. Instituting the changes outlined above will result in an overall cost reduction of the order of 10 % in the cost of the tritium plant.

The overall impact of these changes in the design of the ITER-FEAT fuel cycle are incorporated in the costing data presented in I.4.

II.4.6 Conclusions

No obstacles have been identified that will prevent the design of the fuelling and wall conditioning systems from meeting the requirements that have been established for ITER-FEAT. The implications of long pulse operation up to 3,600 s has been assessed and it has been determined that this additional requirement has no impact on the design of these systems. However, these systems do not offer any opportunity for staged installation, and cost reductions will be limited to $\sim 5\%$.

The design of the vacuum pumping system presented will satisfy the requirements that have been established. The only opportunity available for staged installation is by limiting the initial complement of torus cryopumps to 6, but this will constrain the operational pulse length to < 450 s. The later installation of an additional 4 pumps will provide the capability

for long pulse operation up to 3,600 s, and no further modifications will be required. Cost reductions of the order of 20% for the whole vacuum pumping system are projected.

The outline design of the tritium plant plasma exhaust processing system and the hydrogen isotope separation system have been developed to satisfy pulsed operations up to 450 s at a repetition rate of 2 pulses per hour (nominally 25% duty cycle). This has resulted in a substantial reduction in the throughput capacity of the DT separating column in the hydrogen isotope separation system to that required to satisfy steady-state operation. To satisfy long pulse operation up to 3,600 s at the nominal duty cycle specified, the capacity of the plasma exhaust processing system will need to be increased by ~ 50% and the number of DT storage beds increased by ~ 10. With these additional beds providing temporary storage of the hydrogen stream of the plasma exhaust before ISS processing¹, the effect of pulse duration on other systems within the tritium plant will be minimal. Overall costs savings for the tritium plant are projected to be ~ 10%.

¹ N 10 MD 6 99-09-22 W 0.1
Initial considerations on Impact of Steady State Operation of RTO/RC ITER on Tritium Plant, Cooling Water System, and Cryoplant
N32 MD 11 99-11-16 W0.1
Fuelling and Exhaust Processing for Nominal DT pulses and Steady State Burn

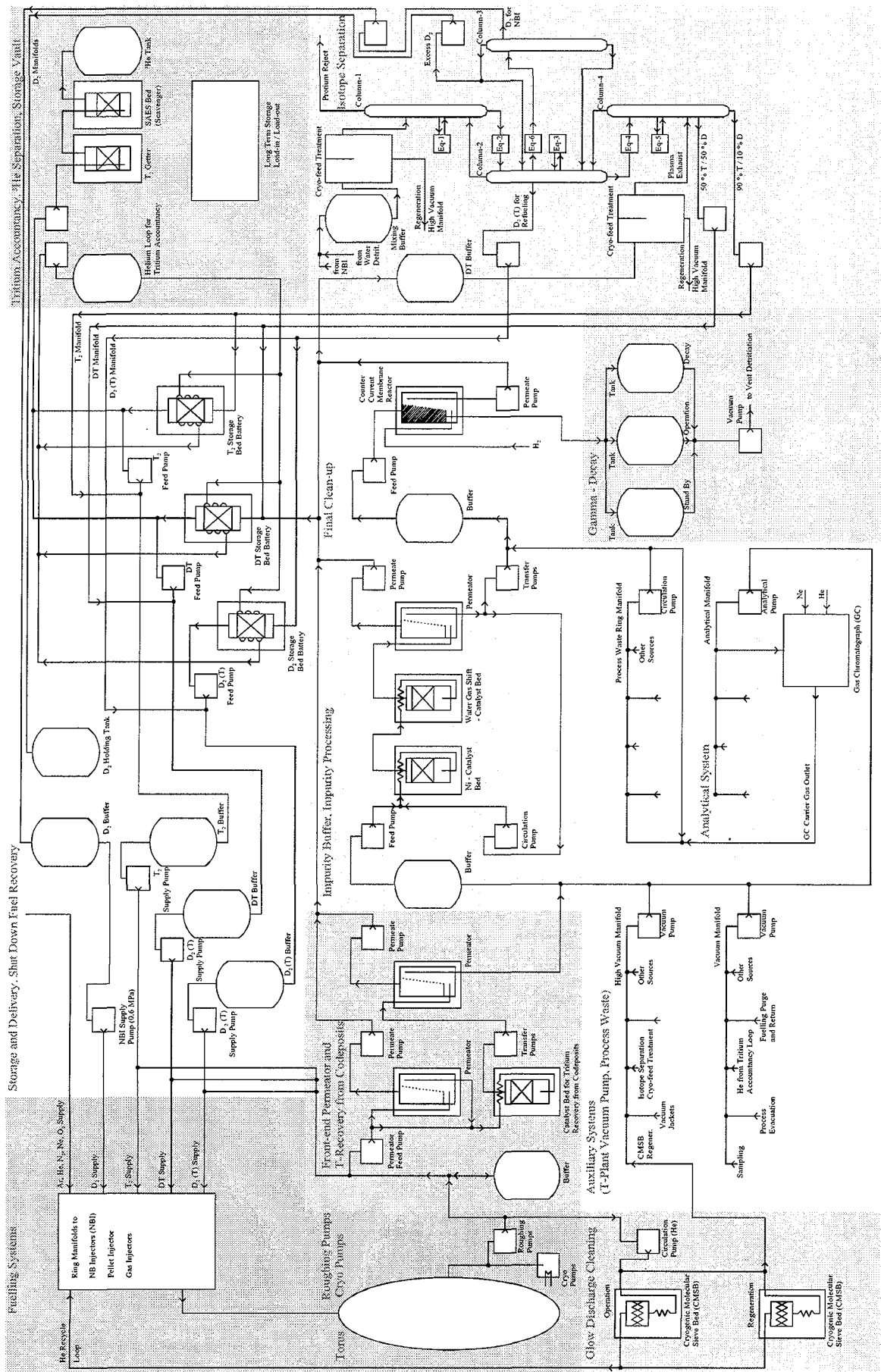
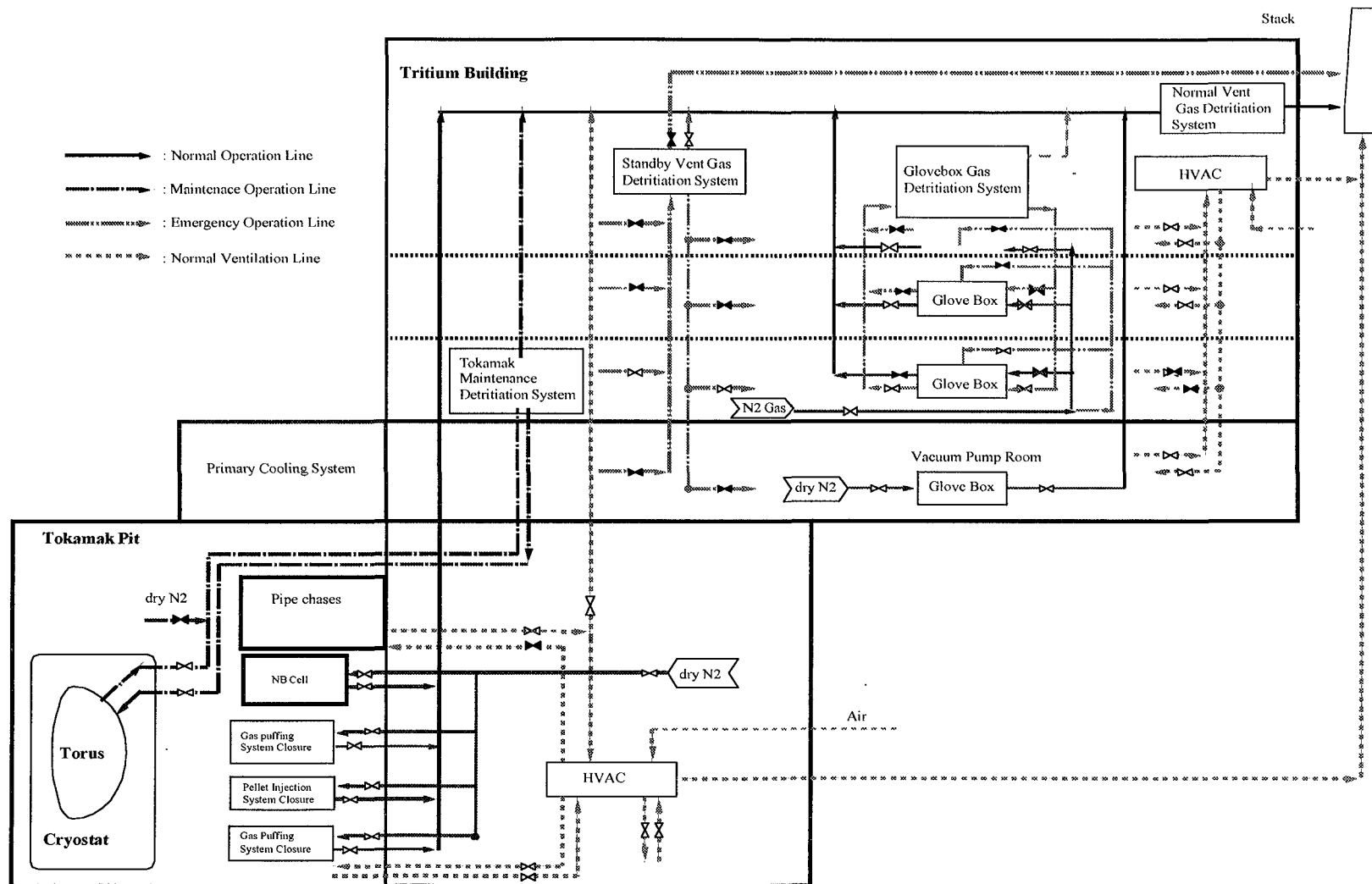


Figure II.4-1 ITER-FeAT Fuel Cycle Overall Flow Diagram

N 32 GR 95 99-11-18 W0.1



N 32 GR 94 99-12-08 W0.1

Figure II.4-2 ITER FEAT Tritium Confinement Concept

II.5 Water Cooling System

II.5.1	Design Philosophy and Constraints	1
II.5.2	Design Status	3
II.5.2.1	Tokamak Cooling Water System (TCWS)	3
II.5.2.2	Heat Rejection System (HRS)	5
II.5.2.3	Component Cooling Water and Chilled Water Systems (CWS and CHWS)	6
II.5.2.4	Auxiliary Systems	6
II.5.2.5	Layout	7
II.5.3	System Performance	7
II.5.3.1	Decay Heat Removal	7
II.5.3.2	Confinement Approach	8
II.5.3.3	Operation Duration under Higher Fusion Power	8
II.5.4	Staged Installation	9
II.5.5	Conclusions and Issues	9

The ITER water cooling system comprises the tokamak cooling water system (TCWS), the heat rejection system (HRS), the component cooling water system (CCWS) and the chilled water system (CHWS). The main function of the water cooling system is to remove heat from various heat sources under controlled flow rate, temperature and pressure conditions, and to release the transferred heat into the environment. An additional function of the TCWS loops is to heat up the vessel and in-vessel components to achieve accelerated outgassing for surface conditioning. For ITER-FEAT, the number of water cooling loops has been reduced to the lowest practical number to minimize investment cost.

The work undertaken has focused on generating design details for the reference design for ITER-FEAT, including a study of issues. This section summarizes the reference design of the water cooling system.

II.5.1 Design Philosophy and Constraints

The design philosophy applied to the water cooling system of ITER-FEAT is to adopt proven technology, to minimize cost, and to base the control of temperature, flow rate, and pressure, on schemes that have already been analyzed in detail previously. This philosophy results in a system configuration based on pressurized loops with heat exchangers (HXs) in the TCWS, closed loops with HXs in the CCWS, closed loops with chiller units in the CHWS, and an open loop with cooling towers in the HRS.

Environmental annual conditions (see I.1) include ambient air temperatures from -25°C to 35°C (for one hour) and -15°C to 30°C (for 24 hours). These conditions are naturally dependent on the actual site conditions and some design adaptations are expected when the design is updated for a specific ITER site.

The number of loops is minimized for cost saving reasons, but is constrained by component size (considering component manufacturability), by coolant water inventory per loop, and by design limitations including coolant velocity. The last has been limited to ~ 6.0 m/s and ~ 4.0 m/s, for stainless steel pipe and carbon steel pipe respectively, to avoid excessive corrosion, and to ~ 2.0 m/s for HX tubes to avoid large pressure losses in the HXs.

Heat loads to the water cooling system for the illustrative, "nominal operational" case (~ 500 MW of fusion power and ~ 70 MW of additional heating power capacity from an initially installed H&CD power of 33 MW for NB, 20 MW for EC, and 20 MW for IC), and for a "maximum operational" case (500 MW of nominal fusion power and ~ 110 MW of additional heating power capacity assuming a H&CD power of 50 MW for NB, and 60 MW for the RF systems, or a H&CD power of 33 MW for NB, and 80 MW for the RF systems) are summarized in Table II.5-1. The reason for the significant heat load in the VV is due to limitations in nuclear shielding provided by the shield blanket including some streaming through relatively large gaps between the blanket modules.

Table II.5-1 Heat Load List for Water Cooling Systems in ITER-FEAT

Heat Source	FEAT (nom.)	FEAT (max.)
Total heat dissipated from plasma to in-vessel components (TCWS & HRS)	~ 750 MW	~ 800 MW
Blanket Modules	(~ 650 MW)	(~ 690 MW)
Divertor and Limiters	(~ 170 MW)	(~ 210 MW)
Vacuum Vessel (not to HRS)	(~ 14 MW)	(~ 14 MW)
NB injectors	72 MW	72** - 100*** MW
Low Voltage (TCWS & HRS)	(72 MW)	(72 - 100 MW)
High Voltage (TCWS & via chiller to HRS)	(incl. East. Tokamak* Chiller)	(incl. East. Tokamak* Chiller)
NB Injector CVCS+	(incl. CVCS+)	(incl. CVCS+)
Component cooling water system (CCWS & HRS)	~ 75 MW	~ 105*** - ~130** MW
East Tokamak Zone*	(45 MW)	(75 - 100 MW)
West Tokamak Zone*	(incl. above)	(incl. above)
Power Supply Zone*	(29 MW)	(29 MW)
Site Service Zone*	(1.0 MW)	(1.0 MW)
Chilled water system (CHWS & HRS)	~ 39 MW	~ 44 MW
East Tokamak * Chiller	(20.5 MW)	(23.5 MW)
West Tokamak * Chiller	(incl. above)	(incl. above)
Power Supply Chiller	(3.1 MW)	(3.1 MW)
Hot Cell Chiller	(incl. Safety-related chiller)	(incl. Safety-related chiller)
Site Service Chiller	(7.0 MW)	(7.0 MW)
Safety-Related Chiller	(7.8 MW)	(7.8 MW)
Miscellaneous (CCWS & HRS)	~ 29 MW	~ 29 MW
Cryoplant Compressor	(25 MW)	(25 MW)
CVCS+	(3.7 MW)	(3.7 MW)
Total	~ 970 MW	~ 1080 MW

+ Chemical and Volume Control System

* Denotes location of client systems

** For case of 50 MW for NB, and 60 MW for the RF systems

*** For case of 33 MW for NB, and 80 MW for the RF systems

The strategy is to design the systems for the nominal case and to explore ways to operate under special circumstances at the maximum load, without (or minimizing) additional investment cost. However, the full investment in piping, that matches the maximum flow

rate, has to be accepted during initial installation because later modification of the pipework is practically impossible.

The effect of deferring installed capacity of the HXs and pumps for the TCWS loop of the NB injector has been investigated¹, and the results indicate that deferring installed capacity of HXs and pumps requires additional space. This is not feasible unless the TCWS vault, where the main loop components are installed, is enlarged. Therefore, the maximum heat load case is considered for the layout of all components in the buildings and on the site. However, staged installation is foreseen whereby components are installed only when required for ITER operation.

II.5.2 Design Status

One of the main features of the water cooling system is the location of the main TCWS loop components inside a common TCWS vault including the NB injectors loop. The water cooling system must provide confinement, and deal not only with normal operational thermal loads but also with those in specific fault conditions. In particular, the VV loop must provide decay heat removal from the vessel and in-vessel systems. The overall flow diagram for the water cooling systems is shown in Figure II.5-1. Sizing of the main components and their layout has been carried out. The detailed design of the water cooling systems for the ITER-FEAT is given in a design summary report¹.

II.5.2.1 Tokamak Cooling Water System (TCWS)

Two concepts of the feed and return of the blanket cooling are under investigation. One option has the feed and return pipes to and from blanket modules inside the VV shell (the integrated coolant channel) and the other has separate pipes located between the blanket modules and the VV (the external manifold). The integrated coolant channel concept is considered for the current TCWS design because its design is further advanced. In this option, the inlet temperature of the VV coolant loops has been set to the average between inlet and outlet temperatures of the blanket to minimize thermal stress in the VV shell. The baking temperature is tentatively fixed at 240°C for the in-vessel components and the VV, to minimize the heat loss between the blanket channel and the VV shell.

The main parameters of the TCWS are summarized in Table II.5-2. The flow rate for each in-vessel component is dominated by the limitations of the temperature rise inside the blanket modules to accommodate the thermal stress, and in the divertor cassettes to maintain the thermal margin with respect to the departure from nucleate boiling (DNB), and the requirement for a relatively high heat transfer coefficient in the VV shell to limit thermal stresses. The temperature rise (temperature difference between inlet and outlet) is set to ~ 50°C for the blanket and the divertor, and the flow rate in the VV loops to ~ 950 kg/s. The investigation of the heat transfer characteristics along the VV shell, considering heat transfer by natural convection, is underway, aiming at a flow rate reduction in the VV loops for cost and layout reasons. If it can be concluded that the heat transfer by natural convection results in sufficiently high heat transfer coefficients ($> 500 \text{ W/m}^2\text{K}$), it would result in the reduction of the flow rate and hence pipe diameters and pump capacities.

¹ N 26 MD 32 99-11-17 W 0.1, "Design Basis on Neutral Beam Injector PHTS for ITER-FEAT"

¹ N 26 MD 19 99-11-26 W 0.3, "Summary of water cooling system design for ITER-FEAT"

Table II.5-2 Thermal Hydraulic Requirements for TCWS Loops

ITEM	ITER-FEAT
Fusion power (MW)	500
Blanket	
• Pulse	
Thermal load (MW)	~ 690
Flow rate (kg/s)	3130 ¹⁾ (+/- 5%) ²⁾
Inlet temperature (°C)	100 (+5/- 10)
Inlet pressure (MPa)	3.0 (+/- 0.2) ³⁾
• Baking	
Inlet temperature (°C)	240 (+/- 10)
Inlet pressure (MPa)	5.7 (+/- 0.2) ³⁾
Divertor & Limiter	
• Pulse	
Thermal load (MW)	210
Flow rate (kg/s)	1040 ¹⁾ (+/- 5%)
Inlet temperature (°C)	100 (+5/-10)
Inlet pressure (MPa)	4.2 (+/- 0.2)
• Baking	
Inlet temperature (°C)	240 (+/- 10)
Inlet pressure (MPa)	4.4 (+/- 0.2)
NB Injectors	
• Low voltage	
Thermal load (MW)	100
Flow rate (kg/s)	828 (+/- 10%)
Inlet temperature (°C)	≤ 80
• High voltage	
Thermal load (MW)	12
Flow rate (kg/s)	72 (+10/-0%)
Inlet temperature (°C)	30 (+/- 5)
Vacuum Vessel	
• Pulse	
Thermal load (MW)	14 ⁴⁾
Flow rate (kg/s)	~ 950 (+/- 6%)
Inlet temperature (°C)	120 (+/- 10)
Inlet pressure (MPa)	~ 1.8 (+/- 0.2)
• Baking	
Inlet temperature (°C)	240 (+/- 10)
Inlet pressure (MPa)	~ 5.2 (+/- 0.2)
• Decay heat removal	
Heat load to VV (MW)	0.8 (peak)

1) ~ 50°C temperature rise in the blanket, the port limiter, and the divertor.

2) Control bands considered.

3) Higher pressure than that for the VV cooling loop (~ 0.5 MPa including pressure fluctuation in each loop) is considered for leak detection inside the integrated cooling channel.

4) Maximum value from preliminary evaluation, re-evaluation is underway.

The number of TCWS loops based on the heat loads shown in Table II.5-1 are; three for the blanket cooling including the in-port component cooling (the blanket primary heat transfer system (PHTS)), one for the divertor and the port limiter cooling (the divertor and limiter PHTS), one for high and low voltage components combined in the NB injectors (NB injectors PHTS), and two for the VV cooling (VV PHTS). The in-vessel component cooling systems have been designed for the full capacity during pulsed plasma operation. There is no limitation on pulse length.

The VV coolant loops must be capable of the passive removal of decay heat (i.e. by means of natural convection). To meet the requirement, two independent, pressurized loops with naturally-drafted, air-cooled HXs are selected as the present reference design. The HXs of one loop are located on top of the TCWS vault, east of the tokamak hall, whereas the HXs of the other loop are located on top of the cryodistribution hall, west of the tokamak hall. The high level location provides natural convection enhancement and the separation in two locations provides enhanced protection of the redundancy given by the two loops. Due to the very large thermal mass of the VV PHTS including the VV structure, and the pulsed operation, the transfer of the instantaneous heat load received during the burn period can be averaged over the whole pulse period (burn and dwell). Therefore, for an instantaneous heat load per loop of 7 MW, the number of HX units per loop can be limited to providing a capacity of 2 MW as a time-averaged load during pulse and dwell.

In the external manifold case, the thermal hydraulic requirements for the VV PHTS would be less demanding because the cooling channels for the blanket and the VV are decoupled thermally and no significant thermal stress is therefore expected. The operation temperature for plasma operation and for baking, as well as the flow rate and the operating pressure in the VV PHTS and in the blanket PHTS during baking, may be lowered significantly.

II.5.2.2 Heat Rejection System (HRS)

The total heat to be removed is estimated as approximately 1.1 GW during a nominal plasma pulse, including heat from auxiliary component cooling systems, site utilities, etc. The final heat release to the environment via cooling towers is used as the reference heat rejection scheme. For site specific designs, sea or fresh water cooling can also be considered.

The number of loops of the HRS is three loops for the TCWS, four loops for the component cooling water and four loops for the chilled water. Water is circulated from a cold penstock, through pumps located in a pump yard. The design of the cooling tower system including the basins is based on a cost optimum between the cooling tower heat rejection capacity and the temperature-levelling capacity in the hot basin. The number of cooling tower units is two for the pulse cycle (500 s of burn and 1300 s of dwell). In case of extended burn periods, e.g. 3600 s, the temperature levelling effect of the hot basin disappears because the complete volume is replaced with the coolant at the return temperature from the CWS. In this case, additional cooling tower capacity and/or hot basin capacity has to be installed to match the full heat load in Table II.5-1. Dedicated cooling towers with a safety function are under consideration in order to remove the heat load from safety-related components for a long confinement period. The operation period and condition of the safety-related systems affects the design and capacity of the safety-dedicated cooling towers. Ideally, the heat accumulation in the basins would be adequate. The detailed requirements, including the operation period for the off-normal condition are still under discussion.

The impact of sea or fresh water cooling rather than cooling tower cooling has been tentatively investigated. Sea or fresh water cooling may require additional intermediate cooling loops between the TCWS and the sea or fresh water heat sink. The immediate impact of the intermediate cooling loop is the enlargement of the primary HX, due to the higher temperature ($\sim 50^{\circ}\text{C}$) at the HX inlet at the intermediate side necessary to give the required temperature difference for the additional secondary HX between the intermediate loops and the final heat sink. Despite this, only a small cost difference between cooling towers and sea or fresh water heat rejection is expected. Firm data can be established when carrying out site specific design work. This is planned for the immediate future.

II.5.2.3 Component Cooling Water and Chilled Water Systems (CCWS and CHWS)

The division of loops for the CCWS and CHWS, shown in Table II.5-1, corresponds to their client location. There are two pumps per loop each providing 50% capacity resulting in partial redundancy, except for the safety-related CHWS system, which has three pumps of 50% capacity each, providing full redundancy.

The heat load for the CHWS is not final because firm data can be established only after the detailed design activity for the HVAC (see II.8.2.2.1.7) and the high voltage component in the NB injectors PHTS are complete. If the heat load from the high voltage components of the NB injector to the CHWS can be reduced significantly, the heat load to the east tokamak chiller would also be significantly reduced.

The HXs for the CCWS and the chiller units for the CHWS with associated circulation pumps will be installed in the buildings corresponding to each zone.

II.5.2.4 Auxiliary Systems

The TCWS includes various auxiliary systems such as the chemical and volume control systems (CVCs), the draining and refilling systems and the drying system. The drying system, the function of which is to reduce the humidity in the in-vessel component cooling paths for leak detection, is closely coupled to the draining and the leak detection methods that will be employed for the in-vessel components. Since the discussion of these methods is still ongoing, the start of the detailed design of the drying system is correspondingly deferred.

In case of an in-vessel LOCA, a decrease of the peak steam pressure inside the vessel is achieved by steam release to the quench tank of the vacuum vessel pressure suppression system (VVPSS) (see II.2.1), which is located above the tokamak, and simultaneously by the quick drainage of residual water in the VV into drain tanks located at basement level¹. For drainage to be effective in reducing the peak in-vessel pressure, it is required that the water pool formed in the VV during an in-vessel LOCA be in communication with the drain pipes. The assigned drain tanks are connected with the divertor ports via rupture disks ($\sim 0.41 \text{ m}^2$ in total), and evacuated during normal operation to be ready for drainage acceptance. The drain tanks are intended also to be used through isolation valves for normal drainage during maintenance.

¹ S 84 MD 28 98-12-09 W 0.1, "Pressurization transients"

II.5.2.5 Layout

The TCWS pipework layout comprises feeder manifolds for the divertor, blanket and VV loops contained inside a lower, circumferential pipe chase, just outside the bioshield. Coolant is routed to and from the TCWS vault to the lower pipe chase via vertical service shafts that penetrate the pit levels in between the access pathways to the cryostat and VV ports. The NB cell is connected via vertical service shafts to the TCWS vault. This not only provides some additional expansion volume, but also allows the elimination of isolation valves in the NB PHTS loops. An upper pipe chase, similar to the lower one, is partly integrated with the TCWS vault and located circumferentially around the upper part of the bioshield. The upper pipe chase contains the collector manifolds for the divertor, distributor and collector manifolds for the blanket, and collector manifolds for the VV loops. The even numbered upper horizontal ports and divertor ports are assigned for the cooling water pipe connection, and the odd numbered ports are connected with pipework for pressure relief and drainage. The tokamak building design includes a large crane which is supported on structural pillars that penetrate the TCWS vault. (c.f. II.8.2.2). The present pipe configurations inside both pipe chases are shown in Drawings. 26.74.2 and 26.83.2.

The layout of the loop components in the vault aims at achieving a high degree of standardization and large block assembly (modularization) in the factory to reduce the overall cost. The structural pillars inside the vault do have a slight negative effect on the modularization. Furthermore, the blocks are designed such that a limited but acceptable maintenance area around the main components is preserved. Drawings 26.69.1 and 26.71.1 show the TCWS component layout inside the TCWS vault. This layout as well as the minimized number of loops will contribute to a reduction in the occupational radiation exposure (ORE). A wider TCWS vault and/or no structural pillars in the TCWS vault might lead to a further reduction in ORE. The present layout is not complete in as far as additional pipework for a drying system, if needed, is not included, nor have the many different support structures and cable trays. Should the integration of these lead to a requirement for more space in the pipe chases and vault, this could have a direct knock-on effect on the width and possibly also on the overall height of the building.

II.5.3 System Performance

Several key performance parameters of the water cooling system have been analyzed, and the results are summarized here. The detailed results are described in a design summary report¹.

II.5.3.1 Decay Heat Removal

Only the natural convection capability in the VV loops is a safety-related feature. The peak thermal load during an off-normal event² is ~ 0.8 MW. The decay heat removal by natural convection in the VV loops has been analyzed, and a parametric evaluation of natural convection and decay heat removal capability for the pressurized VV loops with water-air HXs has been performed. The results indicate that a steady, natural convection flow of more than 20 kg/s is established within 1 h after an off-normal event initiation, contributing to a continuous temperature decrease in the VV structure and VV coolant. The natural convection flow rate and the rate of temperature decrease depend on the pipe size and the HX capacity.

¹ N 26 MD 19 99-11-26 W 0.3, "Summary of water cooling system design for ITER-FEAT"

² S81 RI 28 98-10-08 W 0.1, "Preliminary Assessment of Decay Heat in RC-ITER"

These are, however, designed for nominal capacity, which corresponds at present to 950 kg/s flow rate, but this could in future be decreased to ~ 100 kg/s, requiring smaller diameter pipework and hence a considerable increase in friction for natural convection flow. However, the analysis showed that even under these worst case conditions for natural convection, the maximum temperature of the VV structure in the analyzed range stays below 150°C .

II.5.3.2 Confinement Approach

One approach to confinement under an ex-vessel LOCA in the TCWS vault is to provide "closed containment". The free volume of the containment space, the TCWS vault, the NB cell, the pipe chases and the vertical shafts, is approximately $29,000\text{ m}^3$. The coolant inventory of each blanket loop is $\sim 140\text{ m}^3$, of the divertor/limiter loop $\sim 170\text{ m}^3$, and of each VV loop $\sim 190\text{ m}^3$. The TCWS vault pressure-bearing capability under an ex-vessel LOCA during baking operation would be $\sim 0.32\text{ MPa}$ for a blanket loop, and $\sim 0.37\text{ MPa}$ for a VV loop for the closed containment strategy. These pressure-bearing capacities require very massive, complex and expensive steel structures for the building and the vault wall.

An alternative logic, to maintain closed containment under the most probable LOCAs and to relieve pressure if the vault pressure increases above $\sim 0.2\text{ MPa}$ under the largest LOCA, is being studied aiming at reducing the maximum pressure for the TCWS vault. One of the alternatives is to have over-pressure relief from the vault into an additional expansion volume. Results from a collaborative study done by the JA Home Team shows that pressure relief, of the excessive pressure buildup in the vault during an ex-vessel LOCA of one PHTS loop under baking conditions into the general pit volume, satisfies the containment logic. In this case, the maximum pressure-bearing capacity of the vault can be decreased to 0.18 MPa , commensurate with the peak pressure occurring during an ex-vessel LOCA of one TCWS loop during normal plasma operation. This is a much more acceptable pressure for the building structures.

II.5.3.3 Operation Duration under Higher Fusion Power

The allowable duration of operation of the heat removal systems under a possible higher fusion power ($\sim 700\text{ MW}$) has been studied for the blanket cooling system, without considering the performance of in-vessel components under the increased power condition.

The coolant temperature in the blanket modules increases due to heat load increase, with a certain time delay, and this higher coolant temperature moves through the cooling loop with near flow velocity. The heat transfer capacity in the HX increases corresponding to the primary coolant temperature increase, and the temperature in the cold leg depends on this HX capacity. The allowable duration with 40% higher fusion power is $\sim 60\text{ s}$ if it is necessary to limit the blanket inlet temperature to keep sufficient margin from DNB inside the blanket modules. This is the only reason to limit the duration of higher fusion power operation in the TCWS. Other items related to the higher temperature condition do not pose immediate limitations for the water cooling system.

A countermeasure to permit lengthening of the allowable duration is to set a lower inlet temperature in advance of the expected higher fusion power and to set a lower HRS temperature for the HX to keep the same heat transfer capacity in the HX. In this case, the cold leg temperature during the first pass will be lower than the upper limit of the blanket modules and longer operation will be possible. The allowable duration with 90°C blanket

inlet temperature and 25°C at the HX inlet on the HRS side is ~ 160 s. Moreover, during winter periods with 85°C blanket inlet temperature and 20°C HX inlet on the HRS side, ~ 260 s of operation duration is expected to be achievable.

II.5.4 Staged Installation

The heat load to be rejected to the environment during the initial hydrogen and deuterium plasma operation phases is a small fraction compared to the heat load during DT operation. At the same time, the NB and divertor loops may experience nearly the same thermal duty as in the DT phase. These two loops must therefore be available and commissioned prior to the start of plasma operations, but the other loops, and associated HRS components, can be partly deferred to the DT phase.

The proposal is to initially install, for the hydrogen and deuterium operation phases, only one of the three blanket loops. However, some subcomponents of the two deferred loops must be installed already for hydrogen and deuterium operation, i.e. the heaters, to allow surface conditioning for plasma operation, and all the pipework, valves, etc. in the pipe chases and service shafts, as retrofitting is virtually impossible. The piping from one loop to all blanket modules can be accommodated by some temporary interconnections of the loop manifolds inside the pipe chases. Removal of these interconnections will be needed for DT operations that require the full operation of all loops. It is assumed that the draining and refilling systems as well as the drying system are required from the start of operations, but that the CVCSs will be needed only in proportion to the loops of the PHTSs which are installed.

The VV cooling will not be required before DT operation, but only for the baking function and keeping the VV shell at an appropriate temperature level for thermal stress reasons. The components, except the main piping in the VV loops, may be largely deferred until the DT phase by temporarily connecting the VV main loop with the blanket loop. Additionally, the containment function of the vault would not be required until the start of DT operations. Therefore large openings may be left for installation of the deferred components prior to the DT phase. Overall, this aggressive approach would lead to a deferral of ~ 1/4 of the total ITER-FEAT TCWS cost.

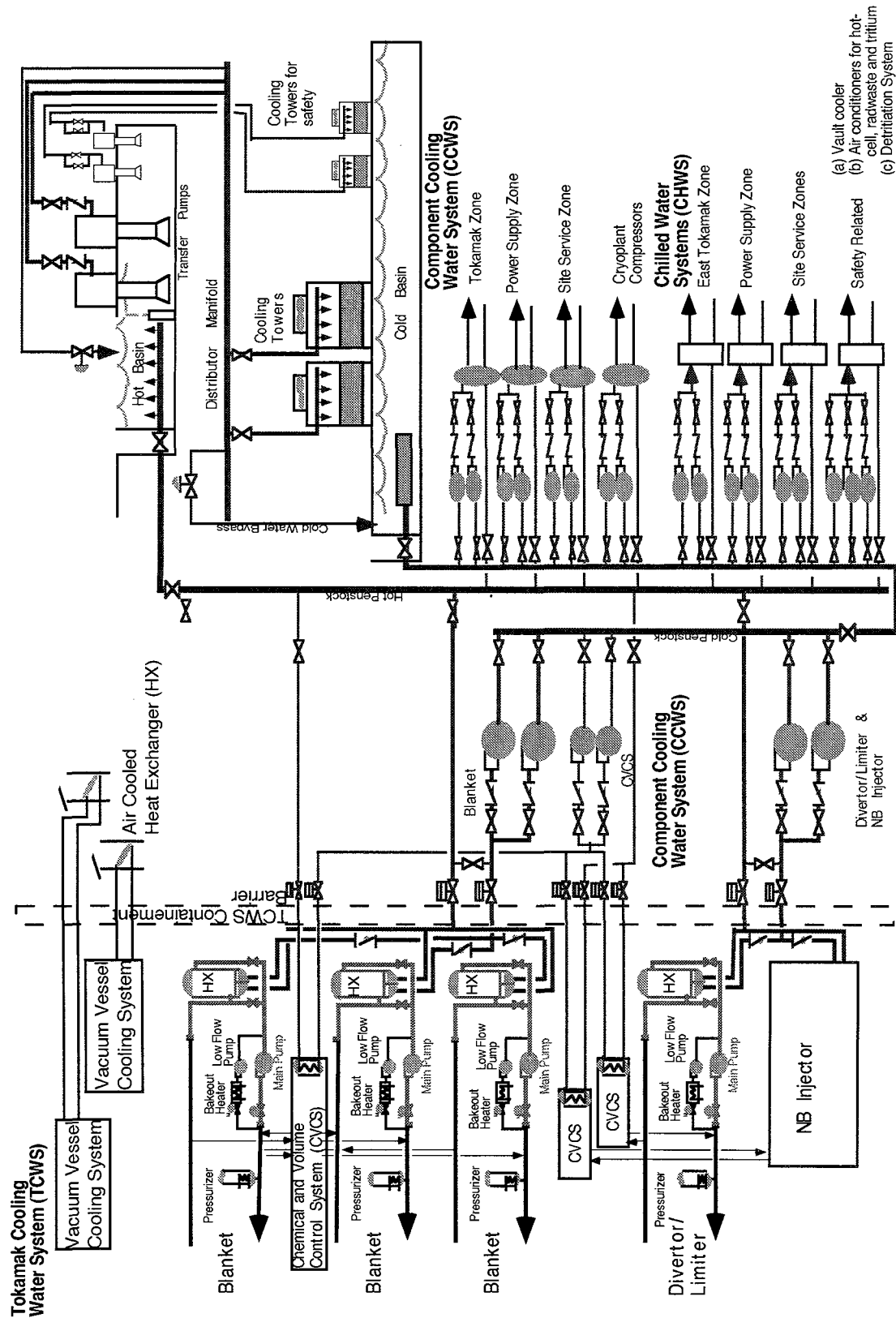
For the other systems, one loop in three of the CCWS for the PHTSs will suffice for hydrogen operation. Moreover, one of the two cooling towers for the reference case and associated transfer pumps can also be deferred. The safety-dedicated cooling towers are also not needed in this phase. However, additional cooling towers to match the full heat load have to be considered for extended burn operation (~ 3,600 s).

II.5.5 Conclusions and Issues

The concept of the water cooling system for ITER-FEAT has been established based on a proven technology basis, and preliminary component sizing and layout have been performed. The following activities need to be carried out for the detailed design:

- derive, in a concerted effort with safety experts, in-vessel component and building designers, a consensus on the detailed TCWS vault containment approach;
- optimize the thermal hydraulic conditions including the temperature increase in components and the baking temperature, as well as the possible reduction in mass flow rate in the VV loops;
- carry out site-specific design and layout with associated supports and cables;

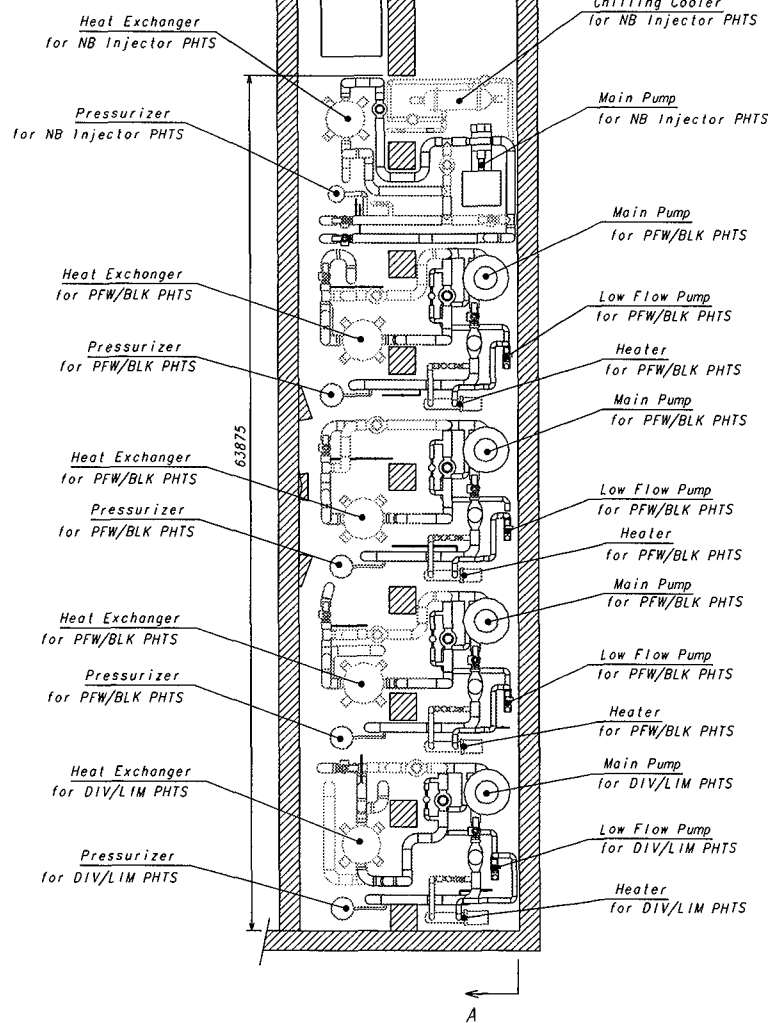
- re-evaluate the ORE for the TCWS;
- confirm the allowable magnetic field for TCWS components and, if necessary, design local magnetic shielding for components.



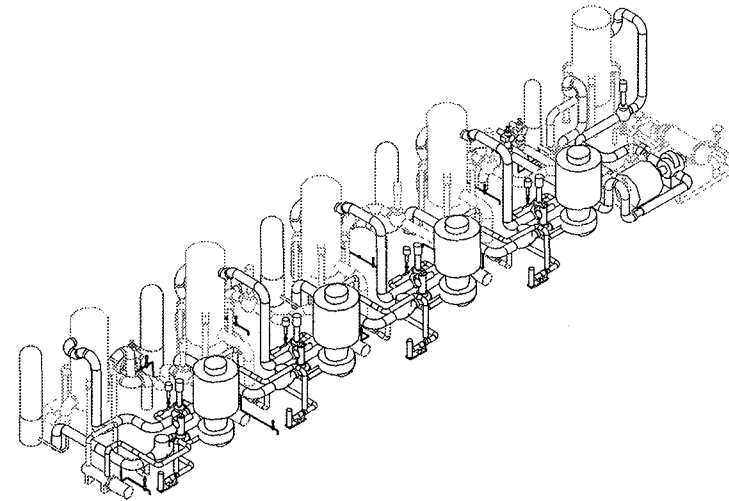
N 26 GR 386 99-11-19 W 0.2

Figure II.5-1 Schematic Flow Diagram of Water Cooling System for ITER-FEAT

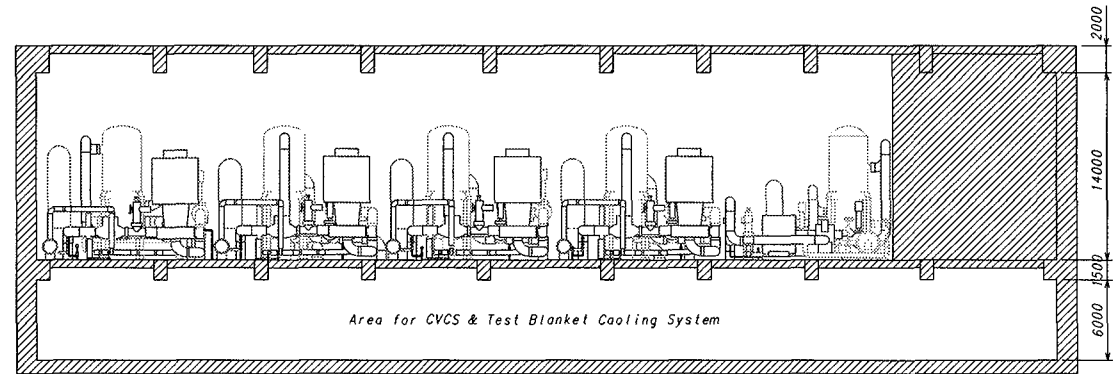
DIMENSIONS RELATE TO ROOM TEMPERATURE (293K)



Plan View of PHTS Loops in TCWS Vault



Isometric View of PHTS Loops in TCWS Vault

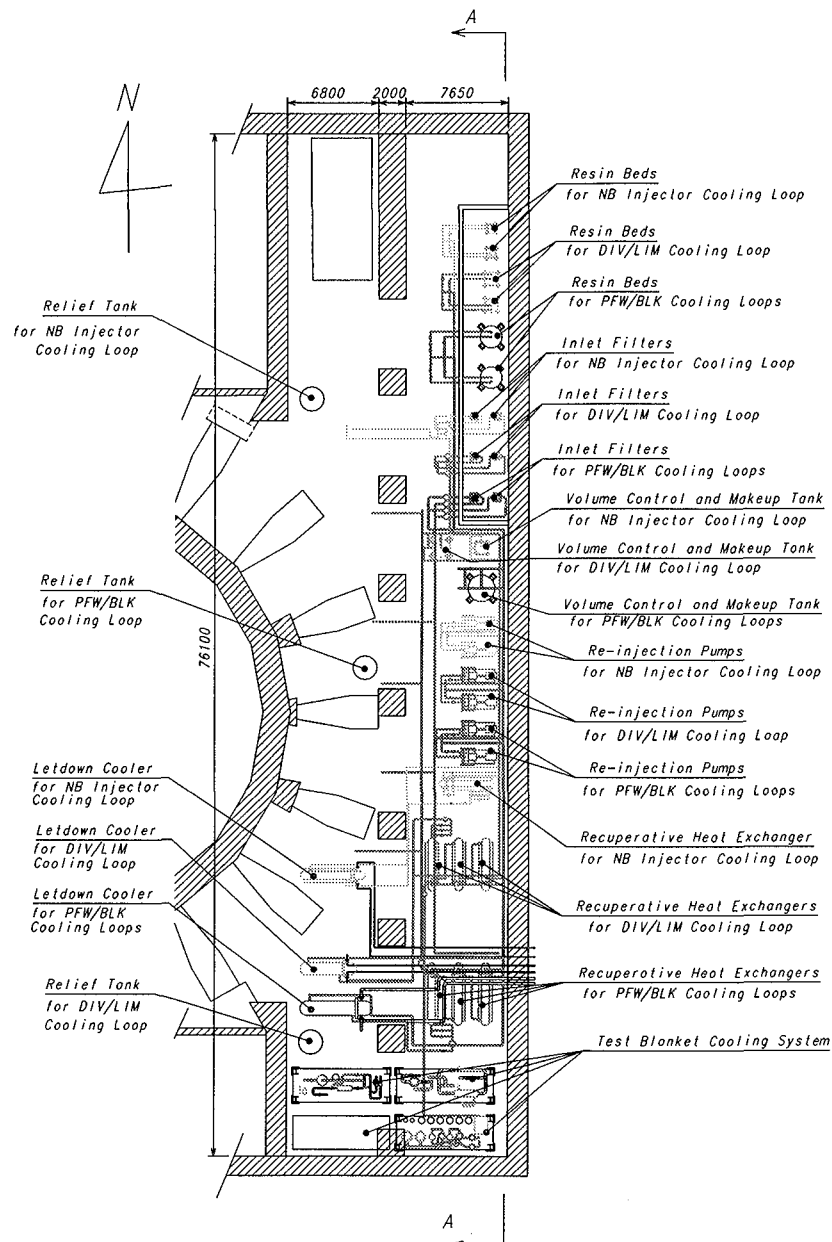


View A-A

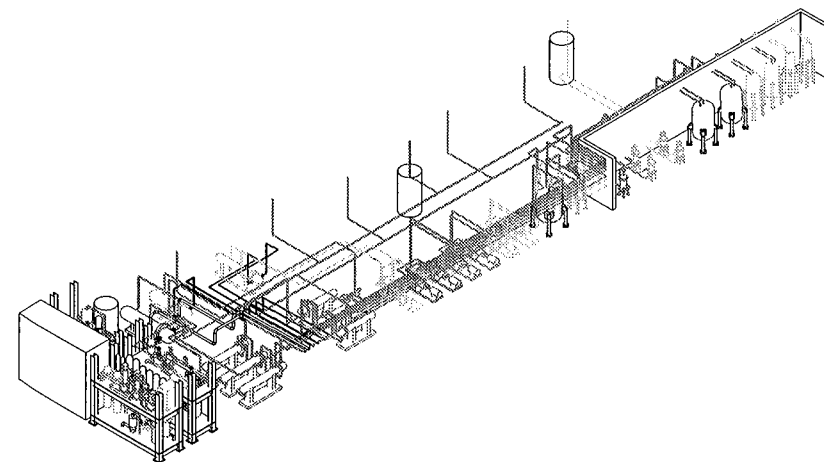
TITLE PFW/BLK DIV/LIM & NB INJECTOR PHTS IN TCWS VAULT		DRG FRAME SIZE 840 x 584 DRAWN D.O. CHK'D D.O.M. Y.Y.A. G.D.C. G.D.C.		ITER-EDA NOT FOR PUBLICATION The information on this drawing is confidential under the terms of the ITER EDA agreement. This information shall not be transmitted to anyone who is not authorized to receive it.			
DATE 18-NOV-99	WORK BREAKDOWN STRUCTURE 2.6		RESP. ENGR JWS			CHK'D JWS	RESP. OFFR YKI
W.B.S. TITLE Tokamak Cooling Water System		NAME OF ORGANISATION NAKA JWS				PROJECT TYPE FORMAL REV. WORKING REV. STATUS	
DO NOT TAKE MEASUREMENTS USE ONLY DIMENSIONS GIVEN		THIRD ANGLE PROJECTION	BASELINE VERSION 1.A.M.	DRAWING NUMBER 2.610.0.6.910.0.0.1	2.00.0.0.1.W.		

291

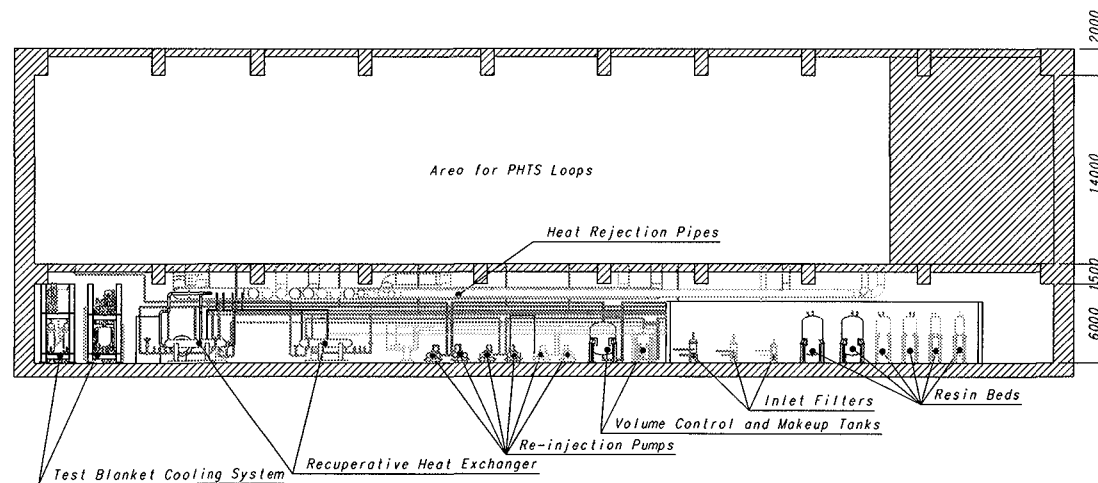
DIMENSIONS RELATE TO ROOM TEMPERATURE (293K)



Plan View of CVCS in TCWS Vault



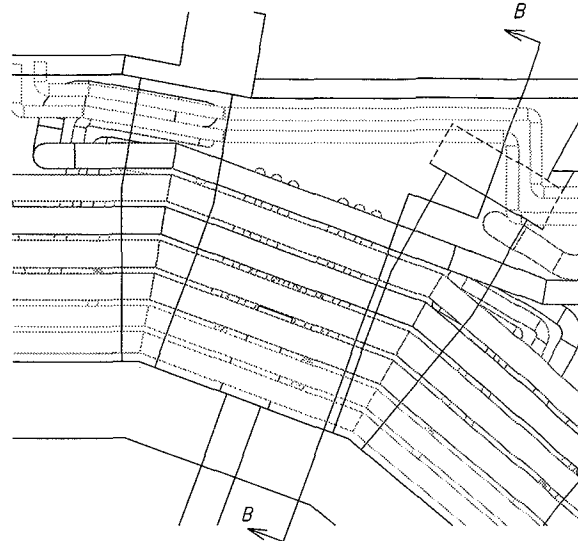
Isometric View of CVCS in TCWS Vault



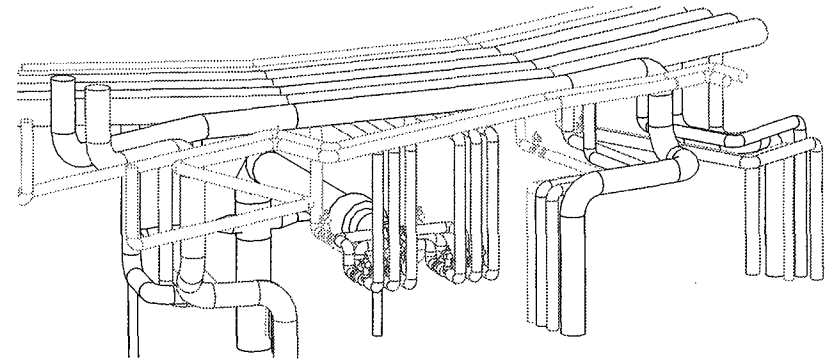
View A-A

TITLE CVCS IN TCWS VAULT		DRG FRAME SIZE 840 x 594		ITER-EDA NOT FOR PUBLICATION The information on this drawing is confidential under the terms of the ITER EDA agreement. This information shall not be transmitted to anyone who is not authorized to receive it.	
DATE 18-NOV-99	WORK BREAKDOWN STRUCTURE 2.6.L	DRAWN D.D. CHK'D D.D.M.	YTA GDC GDC		
W.B.S. TITLE Chemical Volume Control Systems (Cv)	NAME OF ORGANISATION NAKA JWS	RESP. ENGR JWS CHK'D RASP OFFR	YKA --- YKI		
DO NOT TAKE MEASUREMENTS USE ONLY DIMENSIONS GIVEN	THIRD ANGLE PROJECTION	BASELINE VERSION I.A.M.-	DRAWING NUMBER 2.610.0.7.110.0.0.1		
		PROJECT TOP 12.0.0.0.1W			

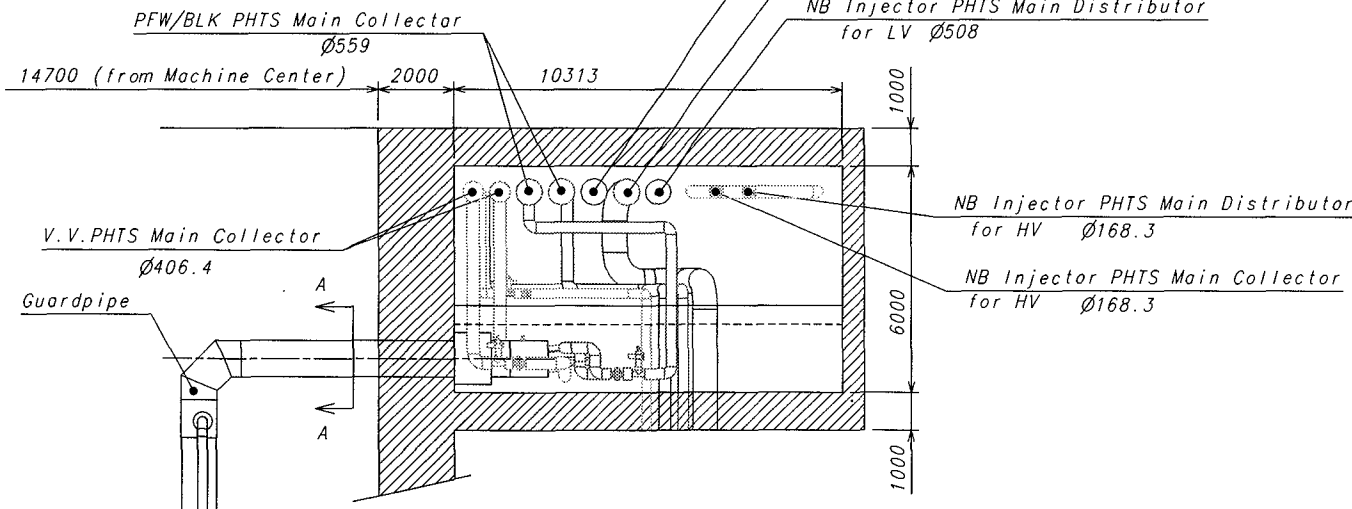
DIMENSIONS RELATE TO ROOM TEMPERATURE (293K)



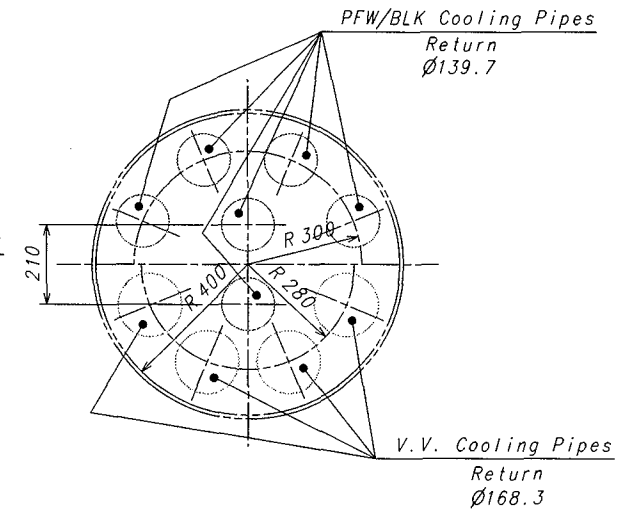
Plan View of Port-04



Isometric View of Port-04



Elevation View of Port-04
Section B-B



Section A-A

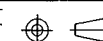
TITLE DETAIL VIEWS OF PIPING ARRANGEMENT
IN UPPER PIPE CHASE

DATE 18-NOV-99 WORK BREAKDOWN STRUCTURE 2.6

W.B.S. TITLE
Tokamak Cooling Water System

DO NOT TAKE MEASUREMENTS
USE ONLY DIMENSIONS GIVEN

THIRD ANGLE
PROJECTION



BASELINE VERSION

1.A.M.-

DRG FRAME SIZE 594 x 420

DRAWN D.O. CHK'D D.O.M.

YYA GDC GDC

RESP. ENGR JWS CHK'D RESP. OFFR

YKA --- YKI

NAME OF ORGANISATION

NAKA JWS

DRAWING NUMBER

2.610.0740.00.2

ITER-EDA

NOT FOR PUBLICATION

The information on this drawing is confidential
under the terms of the ITER EDA agreement.
This information shall not be transmitted to anyone
who is not authorised to receive it



OBJECT TYP

2.D

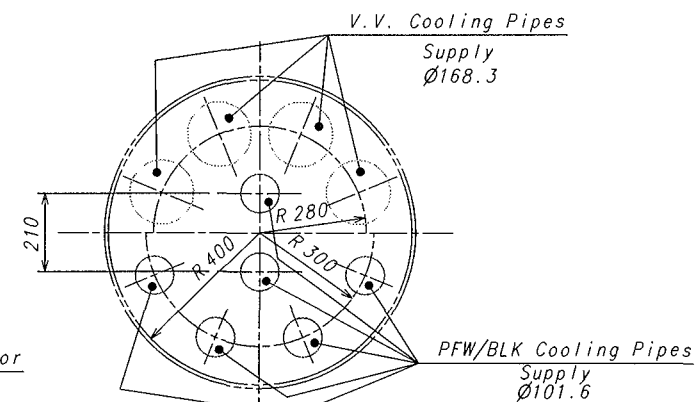
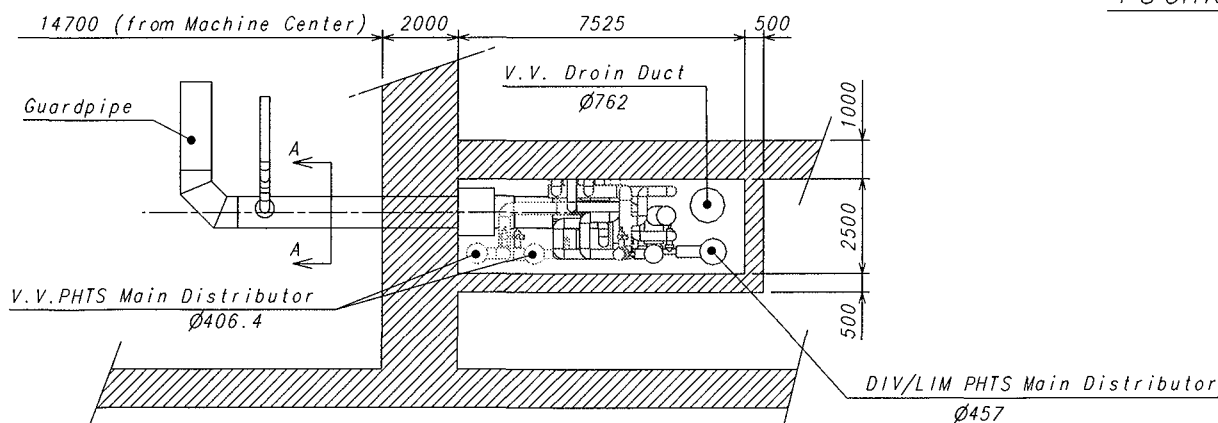
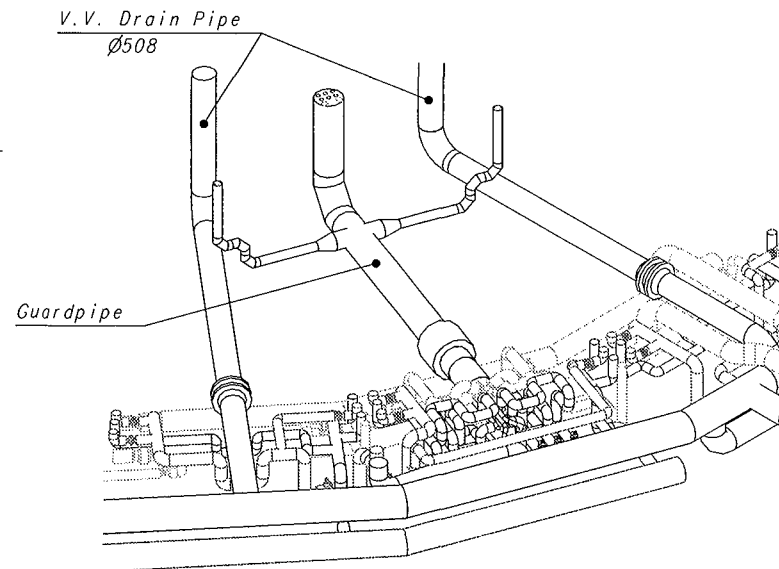
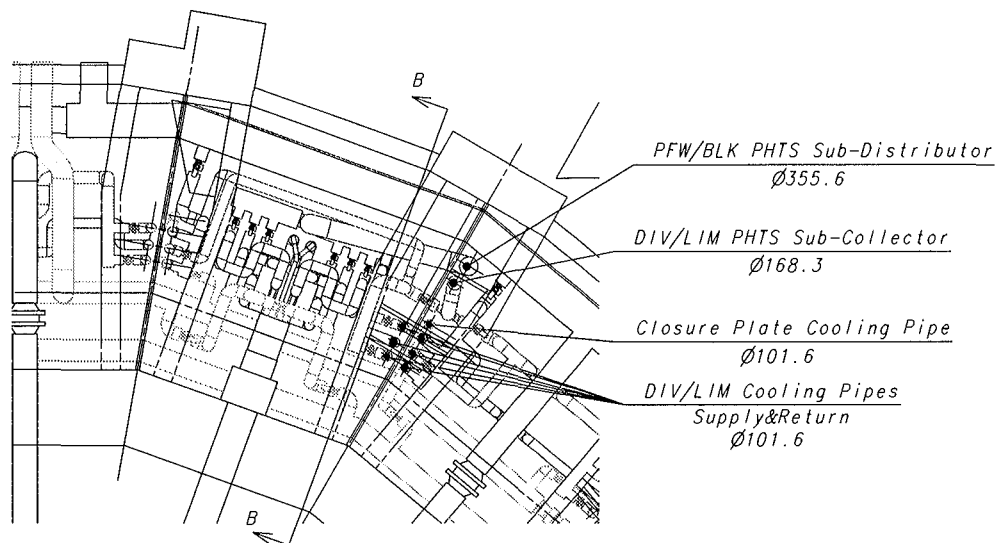
FORMAL REV

0.00.1

WORKING REV

STATUS

DIMENSIONS RELATE TO ROOM TEMPERATURE (293K)



TITLE <i>DETAIL VIEWS OF PIPING ARRANGEMENT IN LOWER PIPE CHASE</i>		DRG FRAME SIZE 594 x 420		ITER-EDA NOT FOR PUBLICATION <small>The information on this drawing is confidential under the terms of the ITER EDA agreement. This information shall not be transmitted to anyone who is not authorised to receive it</small>			
DRAWN YYA	D.O. CHK'D GDC	D.O. M. GDC	NAME OF ORGANISATION NAKA JWS				
DATE 18-NOV-99	WORK BREAKDOWN STRUCTURE 2.6		DRAWING NUMBER 2.610.0.8.30.0.0.2				
W.B.S. TITLE Tokamak Cooling Water System	RESP. ENGR YKA	JWS CHK'D ---	RESP. OFFR YK1				
DO NOT TAKE MEASUREMENTS USE ONLY DIMENSIONS GIVEN		THIRD ANGLE PROJECTION	BASELINE VERSION 1.A.M.-	OBJECT TYPE 2.D	FORMAL REV 0.0	WORKING REV 0.1	STATUS W

II.6 Plasma Diagnostic System

II.6	Plasma Diagnostic System	1
II.6.1	Selected Diagnostic Systems and Startup Set	1
II.6.2	Diagnostic Specific Issues	3
II.6.2.1	Magnetics	3
II.6.2.2	Neutron Systems	4
II.6.2.3	Optical / Infrared Systems	5
II.6.2.4	Bolometry	6
II.6.2.5	Spectroscopic and Neutral Particle Analyzer Systems	6
II.6.2.6	Microwave Systems	7
II.6.2.7	Plasma Facing and Operational Diagnostics	8
II.6.2.8	Diagnostic Neutral Beam	9
II.6.3	Diagnostic Integration and Maintenance	9
II.6.4	Conclusions – System Performance Assessment and Key Issues	11

To meet the requirements for plasma and first wall measurements outlined in I.2.6, an extensive diagnostic set of about 40 individual measurement systems is required. The details of the performance of the individual systems – i.e. spatial and temporal resolution and accuracy - derive from the expected role of the measurements in the operation and evaluation of the tokamak. In general, very high levels of reliability are necessary, particularly for systems providing measurements for protecting the in-vessel machine components from abnormal events, and/or used in real-time control. Most systems are based on the experience of similar ones on current machines, but in order to fulfil some measurement requirements it has been necessary to use techniques still under development. All the systems satisfy the ITER general design requirements relating to vacuum integrity, tritium containment, neutron shielding and capability for remote maintenance.

II.6.1 Selected Diagnostic Systems and Startup Set

It is neither necessary nor desirable to build all diagnostics during the machine construction phase: some will not be required until later in the operational programme and a phased installation will permit the most advanced techniques and technologies to be used. However, it will be necessary to assess the interface, space and service requirements of all diagnostics that will eventually be used, and make any necessary provisions during machine construction to avoid expensive modification costs later. The subset of diagnostics for initial machine operation is called the ‘Startup Set’. A provisional selection of the Startup Set has been made and is included in the list of diagnostic systems and their planned readiness (see Table II.6-1). For some systems only a limited measurement capability will be available for first plasma. Novel diagnostics still under development are marked with ‘N/C’ (new concept). Some systems require a dedicated diagnostic neutral beam (DNB), which is also shown in the table.

Table II.6-1 Status of Diagnostic Systems at Startup of H Phase and DT Phase

Diagnostic	Status at Startup (H phase)	Status at start of DT Phase
Magnetic Diagnostics		
Vessel Wall Sensors, Divertor Magnetics, Continuous Rogowski Coils, Diamagnetic Loop	Complete	
Neutron Diagnostics		
Radial Neutron Camera, Vertical Neutron Camera	Interfaces complete	Complete
Micro-fission Chambers (In-Vessel) (N/C)	In-vessel components and interfaces complete	Complete
Neutron Flux Monitors (Ex-Vessel)	Interfaces complete	Complete
Gamma-Ray Spectrometer		Complete
Activation System (In-Vessel), Lost Alpha Detectors	In-vessel components and interfaces complete	Complete
Knock-on Tail Neutron Spectrometer (N/C)		Complete
Optical/IR (infra-red) Systems		
Core Thomson Scattering	Complete except for two lasers and one power supply system	Complete except for spare laser
Edge Thomson Scattering , X-Point Thomson Scattering	Complete	
Divertor Thomson Scattering	One chord complete	Complete
Toroidal Interferometer/ Polarimeter, Polarimeter (Poloidal Field Measurement)	Complete	
Collective Scattering System (N/C)	Penetrations, in-vessel optics and interfaces complete	Complete
Bolometric Systems		
Arrays For Main Plasma, Arrays For Divertor	Complete	
Spectroscopic and Neutral Particle Analyzer Systems		
Charge eXchange Recombination Spectroscopy (CXRS) based on DNB	Penetrations, in-vessel optics, windows; partially ready to operate in passive mode	
Motional Stark Effect (MSE): based on heating beam, H Alpha Spectroscopy, Main Plasma & Divertor Impurity Monitors, X-Ray Crystal Spectrometers, Visible Continuum Array, Soft X-ray Array	Complete	
Neutral Particle Analyzers (NPA)	Penetrations, interfaces; one channel ready to work in passive mode	Complete
Two Photon Lyman-Alpha Fluorescence (N/C), Laser Induced Fluorescence (N/C)	Penetrations, in-vessel optics and interfaces complete	Complete

Microwave Diagnostics		
Electron Cyclotron Emission (ECE)	Complete except for one spectrometer	Complete
Main Plasma Reflectometer	One LFS (low field side) X-mode and one LFS O-mode complete	Complete
Plasma Position Reflectometer, Divertor Reflectometer, Divertor EC absorption (ECA), Main Plasma Microwave Scattering, Fast Wave Reflectometry (N/C)	In-vessel components, interfaces	Complete
Plasma-Facing Components and Operational Diagnostics		
IR/Visible Cameras, Thermocouples, Pressure Gauges, Residual Gas Analyzers, Hard X-Ray Monitor, IR Thermography (Divertor), Langmuir Probes	Complete	
Diagnostic Neutral Beam		
Diagnostic Neutral Beam (DNB)	Interfaces complete	Complete

II.6.2 Diagnostic Specific Issues

The systems form the seven generic groups shown in Table II.6-1 (the DNB is not a diagnostic group, but a tool used by other diagnostics). It is convenient to discuss the implementation issues for these groups separately. Integration issues follow in II.6.3.

II.6.2.1 Magnetism

Magnetic diagnostics will measure the plasma shape and position, plasma current, loop voltage, plasma energy and the magnitude of the 'halo' currents in some key support structures. The system consists of several individual subsystems:

- sets of pick-up coils, saddle loops and voltage loops mounted on the inner wall of the vacuum vessel for equilibrium and high frequency (HF) measurements;
- continuous poloidal (Rogowski) loops mounted on the outside of the vacuum vessel and poloidal diamagnetic loops mounted inside the vessel;
- sets of coils mounted in the divertor diagnostic cassettes;
- Rogowski coils mounted around earth straps of the blanket/shield modules for measuring the 'halo' currents.

The equilibrium pick-up coils are made of mineral insulated (MI) cable wound on a stainless steel former with a protective cover. They are cooled by conduction. The voltage loops are also MI cables with a bridge at every sector joint. They are repairable if it is necessary to exchange a sector. The coils, the MI cable and other ceramics (e.g. those used in the HF coils) are sufficiently shielded by the presence of the blanket modules that their lifetime is comparable or longer than the lifetime of ITER. The arrangement of the coils and loops is shown schematically in Figure II.6-1.

The information on which to base the choice of materials for magnetism, and for the other diagnostic systems, has come from an extensive 4-Party R&D programme on irradiation effects that has been underway since the beginning of the EDA. A wide range of materials have been investigated and their mechanical, electrical and optical properties have been

documented¹. The work has established a substantial database, which is used in material selection for diagnostic components.

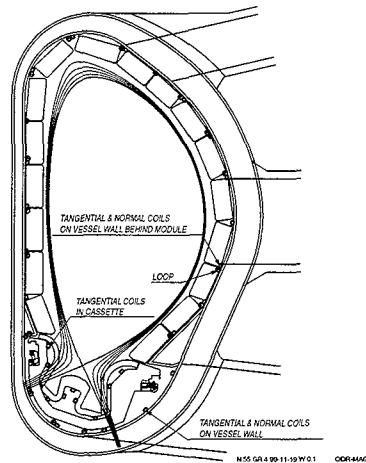


Figure II.6-1 Preliminary Distribution of Magnetic Sensors, Folded Into One Poloidal Plane

II.6.2.2 Neutron Systems

The principal neutron systems are a radial neutron camera, a vertical neutron camera, neutron spectrometers, neutron flux monitors, and a neutron activation system.

The radial neutron camera consists of a fan-shaped array of flight tubes, viewing the ITER plasma through slots in the blanket/shield, intersecting at a common aperture defined by a specialized shielding plug in an equatorial port, and penetrating the vacuum vessel, cryostat, and biological shield through thin stainless steel "windows" (Figure II.6-2). The detectors for each tube are housed in an auxiliary shielded enclosure outside the biological shield. Additional shielding along and between flight tubes provides collimation. All electronics are outside the biological shield. The vertical neutron camera has a different configuration. Each sight-line views through gaps between the blanket modules and long narrow holes in the intercoil structure. The first collimator tube has a ~ 30 mm diameter and 2 mm stainless steel "window" in the vacuum vessel. The second collimator is surrounded by the shield on the upper cryostat and is followed by the detector housing and beam dump. There is no flight tube between the collimators. Six or seven sight-lines are distributed over two upper ports. The cameras provide the measurement of the total neutron flux and emission profile from which the fusion power, power density, and alpha particle source profile are derived.

Several types of neutron detectors and spectrometers are considered for ion temperature and, possibly, n_T/n_D ratio measurement. These range from compact natural diamond detectors to several kinds of proton recoil detectors and time of flight spectrometers. The radial camera

¹ Radiation Problems and Testing of ITER Diagnostic Components' E R Hodgson in "Diagnostics for Experimental Thermonuclear Fusion Reactors 2" (Proc. of Int. Workshop on Diagnostics for ITER, Varenna, Sept 1997) Plenum Press, New York (1998) 261 - 268.

Irradiation Tests on ITER Diagnostic Components' S Yamamoto, L deKock, V Belyakov, D Orlinski et al in the proceedings referenced above, 269 - 278.

ITER Physics Basis. Chapter 7: Measurement of Plasma Parameters' ITER Physics Expert Group on Diagnostics and ITER Physics Basis Editors, to be published in Nuclear Fusion.

design is sufficiently flexible to accommodate many possible instruments of this type, and this is the preferred arrangement.

The neutron flux is measured by fission chambers containing ^{235}U or other isotopes, situated around the tokamak inside the vacuum vessel and biological shield. These measure the global neutron source strength from which the total fusion power is obtained. The neutron activation system uses pneumatic transfer to place a sample of material close to the plasma for irradiation. The system will provide a robust relative measure of fusion power and allows absolute calibration of fusion power.

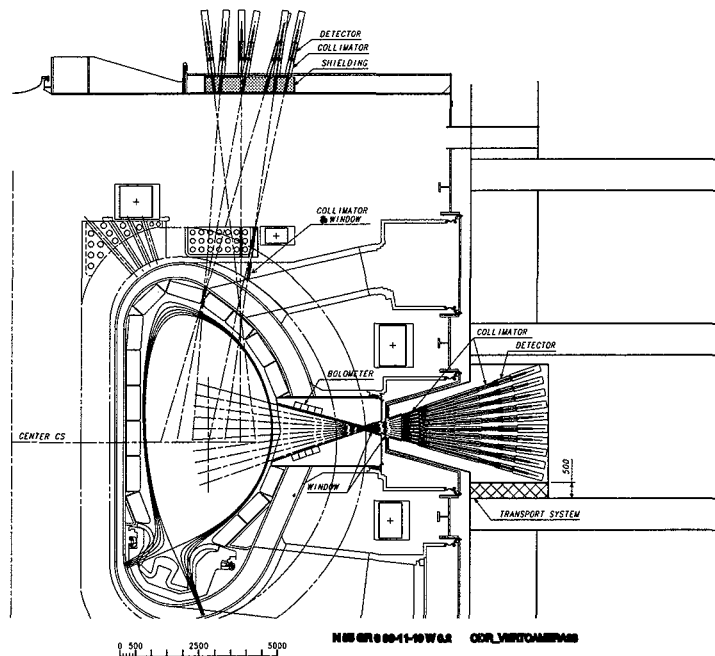


Figure II.6.2 Schematic of Radial and Vertical Neutron Cameras.
The sight-lines for the vertical camera will be distributed at
2 or 3 different toroidal locations.

II.6.2.3 Optical / Infrared Systems

The principal optical systems are two multi-pulse Thomson scattering (TS) systems (core and edge), an equatorial plane interferometer, and a poloidal interferometer/polarimeter.

The core TS system operates on the time-of-flight (LIDAR) principle. Light from a high power laser is transmitted to the plasma using a folded mirror arrangement inside a shielded labyrinth at an equatorial port. The plasma facing mirror is metallic and actively cooled. Scattered radiation returns along the same labyrinth to remote spectrometers. A LIDAR type system will not provide the spatial resolution necessary for measurements in the high-gradient edge region. Hence, the design of the edge system is being based on a conventional Thomson scattering arrangement (Figure II.6-3).

A vibration-compensated interferometer employing Faraday rotation techniques will be used to measure line-integrated density for use in feedback control. The equatorial probing beams use wavelengths of $10.6\ \mu\text{m}$ and $3.39\ \mu\text{m}$. Radiation will be transmitted to and from the plasma through shielding labyrinths in an equatorial port, and small retroreflectors viewing

the beams through the horizontal gaps between blanket modules and positioned at several toroidal locations will return the radiation. The lasers and detectors will be sited remotely.

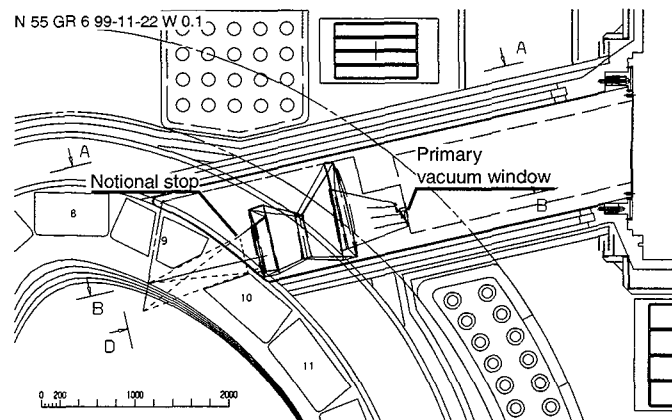


Figure II.6-3 Schematic of the Thomson Scattering System Installed in an Upper Port (only notional blanket gaps are shown)

Multi-chord polarimetry in the poloidal plane will be used to provide measurements of the q profile and / or to anchor reconstructions of the magnetic equilibrium. As for the interferometer, in-vessel retroreflectors will be used, mounted in the vertical gaps between blanket modules at several poloidal locations.

Additional planned optical systems under investigation are Thomson scattering systems for the X-point and divertor regions and a collective scattering system to provide measurements of the confined alpha particle population.

The most critical design issue is the survivability of the first mirrors: these must maintain a good optical quality in the presence of the nuclear heating, plasma radiation and neutral particle bombardment. For the Thomson scattering systems, the mirrors also have to handle the high level of laser power. The mirrors will be actively cooled, metallic, and possibly protected with shutters. Key tests on candidate mirror materials are being pursued in the diagnostic R&D programme.

II.6.2.4 Bolometry

The bolometric systems aim to provide the spatial distribution of the radiated power in the main plasma and in the divertor region with spatial resolutions of 20 cm and 5 cm, respectively. The proposed method, used on many tokamaks, is sparse-data tomography. Bolometer arrays will be installed in the equatorial and upper ports, in selected locations on the vacuum vessel (viewing through the gaps between adjacent blanket/shield modules) and on the specially instrumented divertor cassettes (viewing through the gap between cassettes). From each of these locations, the plasma is viewed along several arrays of lines of sight; the total number is ~ 200 . Designs of potentially suitable bolometers exist but further development is required to ensure and validate that they are radiation hard.

II.6.2.5 Spectroscopic and Neutral Particle Analyzer Systems

An extensive array of spectroscopic instrumentation will be installed covering the visible to X-ray wavelength range. Both passive and active measurement techniques will be employed.

The four main regions of the plasma - the core, the radiation mantle, the scrape-off layer (SOL), and the divertor - will be probed.

For the X-ray region, there will be two systems: a medium resolution survey instrument providing full coverage in the wavelength range 0.1 – 10 nm and a high resolution, multi-channel instrument, with narrow spectral coverage in the range between about 0.1 - 0.2 nm and multiple radial sight-lines. The spectrometers will have to be directly coupled to the tokamak vacuum because it is not possible to use windows. However, mirrors can be used at low angles of reflection so it is possible to shield the detectors from neutron and gamma radiation

Passive spectral measurements in the visible wavelength range are of limited value for probing the core because of the high temperatures. However, active measurements employing charge exchange recombination spectroscopy (CXRS) with beams of energetic neutrals are a rich source of information. For several of the important measurements, the optimum beam energy is ~ 100 keV/amu, well below the energy of the heating beams (1 MeV). This generates a requirement for a dedicated diagnostic neutral beam. The beams are viewed through labyrinths imbedded in shielding blocks by separate optical systems for the motional Stark effect (MSE) and CXRS.

Measurements in the divertor region will be made through slots in divertor “diagnostic” cassettes. The gaps (~ 20 mm) between divertor cassettes are also used. The wavelength range is limited to wavelengths > 200 nm due to absorption in the windows. The light will be transported with mirrors, lenses and optical fibres to spectrometers sited outside the biological shield. Consideration is also being given to making vacuum ultraviolet (VUV) measurements, by viewing the plasma through the cassette gaps, using spectrometers mounted within the divertor port.

The spectroscopic diagnostics will be supplemented by two neutral particle analyzers (NPA) viewing radially through an equatorial port along the same line of sight. One will be used for monitoring the n_T/n_D ratio and preliminary calculations have shown that it should be possible to make measurements into $r/a \sim 0.5$. The second NPA will measure the fast alpha particle and the hydrogenic ion distribution functions in the energy range 0.5 to 4 MeV.

II.6.2.6 Microwave Systems

The principal microwave diagnostics will be a system to measure the electron cyclotron emission (ECE) from the main plasma, and three reflectometry systems for probing the main plasma, the divertor plasma, and for measuring the plasma position. Additional systems under study are an electron cyclotron absorption (ECA) system for use in the divertor region, a fast wave reflectometry system and a microwave scattering system.

The ECE system consists of an antenna array, a transmission line set, and spectrometers for analyzing the emission. The antennas are mounted in an equatorial port plug. The transmission system carries the radiation through the vacuum vessel, cryostat and shield and on to the spectrometers in the diagnostic hall. Calibration of the system is an important process and special equipment is employed. The spatial resolution of the measurement is limited by the intrinsic localisation of the emission, shown in Figure II.6-4.

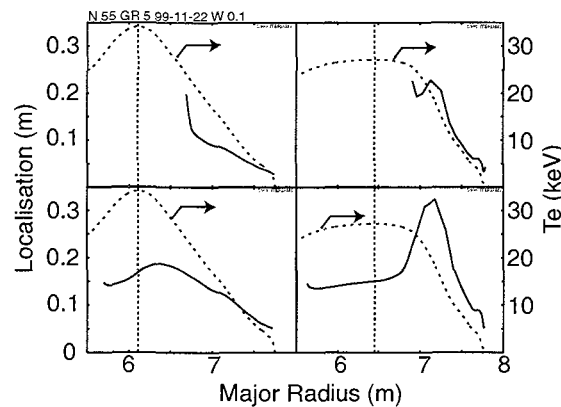


Figure II.6-4 Plot of the Effective Localisation (solid line) for the Second Harmonic Extraordinary Mode (upper) and First Harmonic Ordinary Mode (lower) for an ELMy H-mode (left) and a Reverse Shear Scenario (right). The dotted lines represent the temperature profile used for the analysis; the location of the plasma axis is also shown.

The reflectometer for the main plasma has three subsystems (i) a system using the upper cutoff (extraordinary mode) from the low-field side (LFS) of the plasma to provide measurements of the density profile in the scrape-off, (ii) a system using the plasma frequency cutoff (ordinary mode) from the low-field and high-field sides of the plasma to give the inboard and outboard density profile in the gradient region, and (iii) a system using the lower cutoff (extraordinary mode) from the high-field side (HFS) of the plasma to provide the core profile. The plasma position reflectometer provides the location of density layers near the separatrix. This system is intended as a stand-by reference to the plasma position and shape control system for very long pulses (> 3000 s). The divertor reflectometer is intended to provide density profiles across the divertor legs. Multiple sight-lines are employed for each leg, and profile information is synthesized from several bands due to the extremely wide density range.

For all systems, dog-leg structures in the transmission lines reduce neutron streaming outside the vacuum vessel and bioshield. Distinct vacuum windows of fused quartz directly bonded to metal structures provide pressure boundaries. The windows are inclined at the Brewster angle for the appropriate polarization wherever possible.

II.6.2.7 Plasma Facing and Operational Diagnostics

A range of diagnostics will be installed to aid the protection and operation of the tokamak. Several diagnostics will be dedicated to monitoring the condition of the high heat flux components in the main chamber and the divertor; other systems include Langmuir probes, pressure gauges, residual gas analyzers, and runaway monitors (hard X-ray detectors and tangential view IR systems).

The principal high heat flux protection system will be a wide-angle camera system which will give views of the in-vessel components (including parts of the divertor) in the IR and visible wavelength ranges. Combining several cameras can achieve high coverage ($\sim 80\%$) of the area of the first wall. The first element of the system is a metal mirror and the image is transmitted through a rigid labyrinth to a flattening array immediately before the vacuum

window. From here the image is transmitted by lenses to cameras mounted on the shielded side of the biological shield.

Dedicated divertor diagnostics include an IR thermography system for the power deposition profile on target plates, Langmuir probes for local measurements of plasma parameters and attachment/detachment indicator, and fast pressure gauges, all to be installed in diagnostic divertor cassettes. These have special provisions for diagnostic sensors and provide access for optical and microwave transmission lines. IR thermography provides surface temperature measurements of both divertor target plates in a poloidal plane with good spatial and temporal resolution. Novel collection optics merge the thermal radiation collected at different wavelengths from different points on the target plates into a single beam. This is achieved using a shielded low-frequency grating close to the front mirror. Using this “inverse spectrometer” set-up, the number of optical elements inside the vacuum vessel is drastically reduced and only a small diameter optical window is needed.

II.6.2.8 Diagnostic Neutral Beam

The optimum beam energy for the diagnostic neutral beam is ~ 100 keV/amu. This is considerably below the energy of the heating beams (1 MeV), so a dedicated beam is required. To minimize the cost with high reliability, a conservative approach is proposed, i.e. to use 4-channel geometry and the same negative ion source as the reference source as in the main ITER injectors without changing the arrangement of segments and apertures in the source grids. The beam would have a beam current of 15 A (H^0 atoms), a footprint of 30×30 cm and pulse duration 1 – 3 s every 10 – 20 s. The beam can be modulated at 5 Hz. The performance of the CXRS diagnostic needs to be re-evaluated using this beam.

II.6.3 Diagnostic Integration and Maintenance

Individual diagnostic systems have to be installed on the tokamak in a manner that makes the best possible use of limited space. Several factors have to be taken into account: measurement requirements, shielding, activation and tritium containment requirements; total system path length and complexity, and maintenance requirements. Unavoidably, priorities have to be set and within diagnostics this is done according to the expected role of the associated measurements. Systems which provide measurements for machine protection and basic plasma control are given the highest priority, followed by those which provide measurements for control of high performance modes (groups 1a and 1b respectively, in Table I.2.6-1).

Diagnostic components are installed in four locations – within the vacuum vessel (VV), in divertor ports, and in equatorial and upper ports. The principal diagnostic components mounted in the VV are sensors for the magnetic diagnostics, bolometers, soft X-ray detectors, and waveguides for reflectometry. A number of the systems involved are fundamental for tokamak operation and due to their nature must be permanently or semi-permanently installed. Therefore, the components have to survive the full ITER life and must tolerate the possible removal of a torus sector (requiring redundancy and reparability). In the integration of these systems three principal guidelines are applied a) all systems are mounted on the VV wall, b) with the exception of the various magnetics diagnostic loops and reflectometer antennas, all sensors are mounted in small replaceable diagnostic sockets integrated into the vacuum vessel, and c) the plasma is viewed through the gaps between blanket modules. The

diagnostic sockets can be removed remotely (sometimes after removing two blanket modules). All sensors are subject to high levels of neutron and gamma radiation, and some VUV/X-radiation. For high reliability at low cost, they are cooled by conduction and radiation and operate at elevated temperatures.

In the divertor, diagnostic components are concentrated in the three remote handling ports and on the divertor cassettes within these. At each location there are two instrumented cassettes (Langmuir probes, bolometers, pressure gauges, etc.) on either side of a central cassette. The latter is modified to incorporate optical and microwave diagnostics. In the space between the VV closure plate and the divertor cassette, a diagnostic block is installed which carries waveguides and optical equipment. In addition to the three divertor remote handling ports there are six potential diagnostic ports where small diagnostic carriers for optical access and modified cassettes can be placed. These ports will have to be shared with the in-vessel viewing system. Presently, not all of these ports have diagnostic systems allocated. Remote maintenance inside the machine is performed for the diagnostic cassettes in the same way as for standard cassettes. Special integrated assemblies are mounted on the

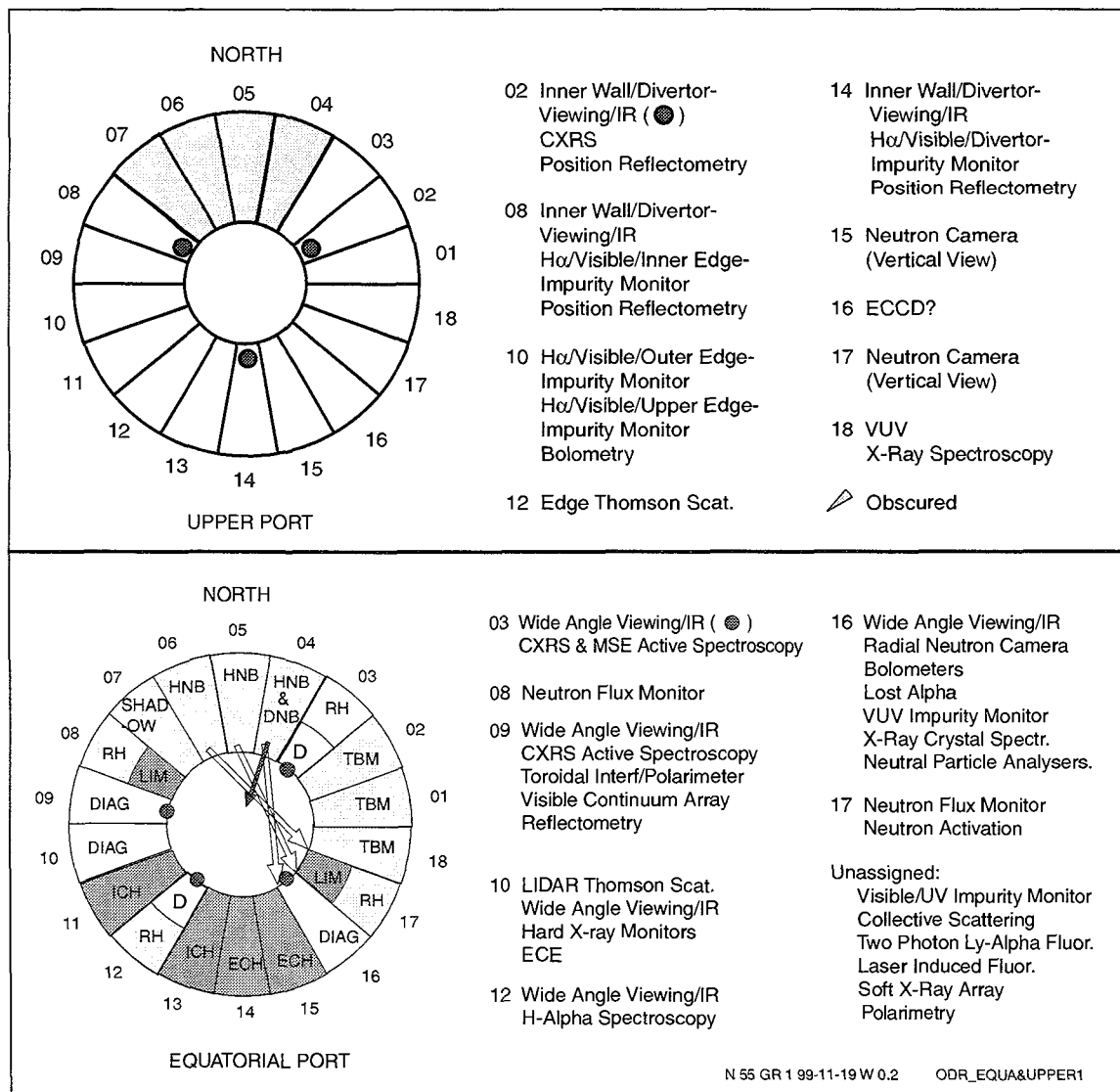


Figure II.6-5 Proposed Diagnostic Port Allocation at the Upper and Equatorial Levels

diagnostic cassettes (e.g. side plates incorporating various sensors) to allow simple replacement of diagnostic components inside the hot cell. Parts of the fixed services, such as cable looms coming from components mounted on the VV wall, are routed through the cryo-pumping ports into the pit.

Equatorial ports are the preferred access for diagnostics. Three regular ports are dedicated to them. Two more ports, allocated to remote handling are foreseen to have diagnostics that can be removed easily. Different factors are taken into account in optimising the distribution: for example, large aperture systems are placed at port centres and tangential viewing systems at the sides of ports, whereas systems which need to view one of the beams, need to use specific ports. The provisional port allocation is shown in Figure II.6-5.

In most cases, equipment in equatorial ports is mounted in a single port plug assembly within the primary vacuum (incorporating a first wall blanket part, a VV port plug for shielding and a VV closure plate), and in an interspace diagnostic block (incorporating the cryostat closure plate and all equipment needed between VV and cryostat closure plate). This modularity allows a single concept for remote maintenance of all the port plugs and a standardised approach for hot cell maintenance. In some ports there is a relatively simple optical connection between the VV and the cryostat closure plate, whereas in others there may be substantial connections of diagnostic transmission lines, such as waveguides, or vacuum extensions. The installation of the VUV, X-ray crystal spectrometry and the NPA systems requires the use of vacuum extension(s) and this will be contained in dedicated shielding/containment enclosure(s).

Diagnostic equipment in the port plug takes account of all boundary conditions arising from maintenance and shielding requirements. In order to simplify and to standardise the maintenance of these plugs, modular subassemblies are used. Services and cooling connections, mechanical attachments for larger plug subassemblies as well as positioning and alignment of these subassemblies are simplified to use standard tooling. Before and after maintenance of the port, the plugs are placed in a dummy port for testing. Tests prior to repairs are foreseen to define a repair plan, and after repairs to ensure full functionality as well as leak tightness. While in the dummy port, the windows and other feed-throughs on the vacuum vessel flange can be replaced hands-on, simplifying the hot cell equipment.

Diagnostics installed in the upper ports should be able to utilize the concepts and approach developed for the equatorial ports. However, some diagnostic equipment in these ports will have permanent features such as wiring and waveguides with as few connections as practical. The neutron camera will have a special arrangement outside these ports (II.6.2.2). The detailed implementation has yet to be worked out.

II.6.4 Conclusions – System Performance Assessment and Key Issues

The ability of the diagnostic systems to meet their individual measurement requirements depends on factors which are in general different for each generic group of diagnostics.

For the magnetic diagnostics, it is expected that the chosen configuration of coils and loops will meet the measurement requirements. However, a key issue is the lifetime of the in-vessel coils and loops. By using materials examined in the supporting radiation effects R&D programme, it is believed that necessary lifetimes can be achieved. A particularly difficult

area is repair and maintenance of the in-vessel diagnostic components and this is a topic of current activities. Recent tests with a prototype coil and integrator have shown a small radiation induced electromotive force which would lead to an unacceptable drift during a long pulse (< 1000 s). Further tests are planned.

No insurmountable difficulties are expected for the implementation of the neutron flux monitors and activation systems. However, the ability of the neutron cameras to provide the measurements for which they are intended, for example the total fusion power and the alpha particle source profile, is directly linked to the available access. A wide angle of view is necessary in both the radial and vertical directions. This is difficult to achieve in the vertical direction due to the limited port height. The view through the intercoil structure for the vertical camera is a new concept and its feasibility has yet to be established.

All optical/IR, spectroscopic and microwave systems require apertures through the blanket shield plugs which are mounted in the diagnostic ports. Promising design concepts for these modules have been developed and it is expected that the required apertures can be achieved. The optical/IR systems view the plasma with a mirror and a critical issue is the lifetime of this component. It is believed that the solutions for the first mirrors exist for those systems which operate in the visible and IR regions and do not require a large angle of observation, for example interferometry and Thomson scattering systems. However, for diagnostics which require a relatively large solid angle of observation, for example, Active CXRS and MSE, further work is required. Some systems, for example, multichord polarimetry for the poloidal field measurement, require the installation of retroreflectors in the vacuum vessel. Promising concepts for the design and installation of retroreflectors on the vacuum vessel in the gaps between blanket modules have been developed but the engineering details have yet to be worked out. The problem of damage to mirrors is especially pronounced for mirrors installed in the divertor region where substantial erosion may occur during disruptions. Baffles can be used to alleviate this problem and these are included in the system designs. Alternative views from the equatorial and upper ports are also under consideration.

For Bolometry, the cylindrical inserts installed at different poloidal locations on the vacuum vessel in the gaps between blanket modules are used for installing the detectors. These enable bolometric measurements along many different lines of sight as required. A bolometer which is believed to be sufficiently radiation hard for use during the initial DT operation exists but a device with enhanced radiation hardness may be required for the anticipated end-of-life fluence level of the machine. Potentially suitable devices are being investigated in a supporting R&D programme. Dedicated development is likely to be necessary.

Concepts for the implementation of the spectroscopic systems which require direct coupling (X-ray crystal and VUV spectrometers and NPA systems) have been developed for measurements on the main plasma and it is believed that good performance will be achieved. VUV measurements in the divertor are difficult but a design concept in which the spectrometer and detector are installed in the divertor port is under development.

For the microwave measurements (ECE and reflectometry) which are made from the low-field side, no insurmountable problems are foreseen. However, for the reflectometry measurements on the high-field side, and at various locations in the poloidal cross-section for the plasma position reflectometer, the installation of the antennas and waveguides is a key

design issue. Promising design concepts exist but the engineering details have yet to be worked out. The installation of waveguides through the divertor ports and in the divertor cassettes appears feasible but the development of the associated diagnostics (electron cyclotron absorption (ECA) and divertor reflectometry) is still in an early stage and so the information that can be reliably obtained from these measurements is not certain.

A promising design has been developed for the wide angle visible/IR viewing diagnostic and it is expected that it will meet its measurements specifications. A key issue is the extent of the surface coverage that is necessary, and this is a topic of current investigation. Measurement of the surface temperature of the divertor plates is an important operational measurement and conventional imaging systems are difficult to implement in the restricted divertor space. A novel technique in which the radiation from different locations is multiplexed into one line of sight with a grating and then separated by spectral analysis is under development. No insurmountable difficulties are foreseen with the basic operational diagnostics such as pressure gauges and gas analyzers.

Substantial progress has been made with the integration of the diagnostic neutral beam onto the tokamak but only minor progress with the design of the injector has been possible, although an injector suitable for the application appears to be feasible. Neutronic calculations performed on typical diagnostics ports accommodating several diagnostic systems have confirmed that it will be possible to achieve the necessary shielding.

In terms of the overall measurement capability, it is expected that all the measurements necessary for the machine protection and basic plasma control can be made although the detailed performance has yet to be determined. There are difficulties with some of the measurements necessary for advanced control, for example the q profile measurement, but it is too early in the design process to determine what limits, if any, there will ultimately be to the operation of the tokamak. Some of the measurements which are intended solely for physics purposes also have implementation difficulties. Current design and R&D work is focussed in these areas.

Further details of the diagnostic systems and their integration into the tokamak can be found in references¹. A discussion of the key issues in diagnostics has also been published². Considerable further design work is required to permit the implementation of specific diagnostics on ITER-FEAT. This work requires special skills and knowledge. These are, in particular, available in the fusion laboratories of the Home Teams, and it is expected that they will take the lead in developing individual diagnostics for ITER.

¹ 'Overview Of The ITER Diagnostic System' A E Costley, K Ebisawa, P Edmonds, G Janeschitz, et al in "Diagnostics for Experimental Thermonuclear Fusion Reactors 2" (Proc. of Int. Workshop on Diagnostics for ITER, Varenna, Sept 1997) Plenum Press, New York (1998) 41 - 56.

'ITER Physics Basis. Chapter 7: Measurement of Plasma Parameters' ITER Physics Expert Group on Diagnostics and ITER Physics Basis Editors, to be published in Nuclear Fusion.

'Integration of Diagnostics into the ITER Machine' G A Janeschitz, C Walker, A Costley, L deKock et al, paper IAEA-F1-CN-69/ITERP1/15 in Proc. of 17th IAEA Fusion Energy Conference, Yokhama, Japan, 1998.

² 'Key issues in ITER Diagnostics: Problems and Solutions' A E Costley and Members of the ITER Joint Central Team and Home Teams, Rev Sci Instrum, 70 No 1 (1999) 391 - 396.

II.7 Heating and Current Drive (H&CD)

II.7.1	Neutral Beam Heating and Current Drive (NB H&CD) System	1
II.7.1.1	System Parameters	1
II.7.1.2	System Layout and Integration	2
II.7.1.3	System Design	3
II.7.1.4	Component Design	4
II.7.2	Radio Frequency Heating and Current Drive (RF H&CD) Systems	6
II.7.2.1	General Features	6
II.7.2.1.1	Modularity	6
II.7.2.1.2	General Mechanical Layout	6
II.7.2.1.3	Maintenance	7
II.7.2.1.4	Nuclear Shielding	7
II.7.2.1.5	Auxiliaries and Services	7
II.7.2.2	Electron Cyclotron System	8
II.7.2.2.1	Design Issues	8
II.7.2.2.2	Launcher Design	8
II.7.2.3	Ion Cyclotron System	10
II.7.2.3.1	Operating Scenarios	10
II.7.2.3.2	Design	11
II.7.2.4	Lower Hybrid System	12
II.7.2.4.1	Design	12
II.7.3	Heating and Current Drive Power Supplies	13

In ITER-FEAT operation, heating and current drive (H&CD) systems provide essential functions, ranging from pre-ionization and assisted current startup, to access to the H-mode, bulk central heating, and on- and off-axis current drive.

In particular for high plasma performance operation, several kinetic control functions (such as stabilization of MHD modes, sawtooth suppression and neo-classical tearing mode (NTM) control are required to maintain confinement parameters within the prescribed range. Furthermore, the core energy confinement can be significantly improved by modifying the plasma current profile, and transport can be reduced to its neoclassical value in the centre of the plasma within internal transport barriers (ITB), obtained by the control of the local shear.

An ancillary but important service, also assigned to the heating system, is wall conditioning, performed (possibly continuously) during the inter-pulse period.

To achieve these different functions, a combination of auxiliary heating and current drive techniques appear to be necessary. Accordingly, a (negative ion) neutral beam (NB) injection system and three radio frequency (RF) heating systems are being planned for ITER-FEAT.

In the first phase of the operation, 30 MW of auxiliary power are planned from NB H&CD and 20 MW from IC H&CD and EC H&CD systems. The level of power would be subsequently increased to a total of 100 MW.

II.7.1 Neutral Beam Heating and Current Drive (NB H&CD) System

II.7.1.1 System Parameters

The NB H&CD system consists of two injectors. Each injector will deliver a deuterium beam of 16.7 MW at 1 MeV (total 33 MW), and will be able to operate for long pulses (up to

3600 s). The layout allows for a third injector to reach a total NB H&CD power up to 50 MW. The basic concept and most of the engineering details are described elsewhere¹.

The design assumes 200 A/m² as a limit for negative ion accelerated current density (a small extrapolation from the relevant R&D results). This limit, together with the size of the ion source, defines the maximum current that can be accelerated as about 40 A. The acceleration voltage remains the only free variable. Higher voltages are desirable to increase the power and the current drive efficiency. On the other hand higher voltages imply larger insulation distances (both in gas and vacuum) and higher beam shinethrough. Considering ITER-FEAT dimensions, 1 MV is considered as a good compromise. Plasma rotation is also provided by the NB injection. If necessary, the system can be adapted, with minor modifications, to inject a hydrogen beam to the plasma.

II.7.1.2 System Layout and Integration

Figure II.7.1-1 shows the NB layout: the two injectors are located on the north side/equatorial level of the tokamak building, where tangential injection is achieved using the equatorial ports #4 (sharing the port with the diagnostic neutral beam injector) and #5. Space has been allocated for a third injector which could be mounted on port #6.

The injector's vessel is an extension of the primary vacuum boundary and is part of the primary safety barrier for contamination confinement. The common enclosure for all the injectors, the NB cell, forms the secondary confinement barrier.

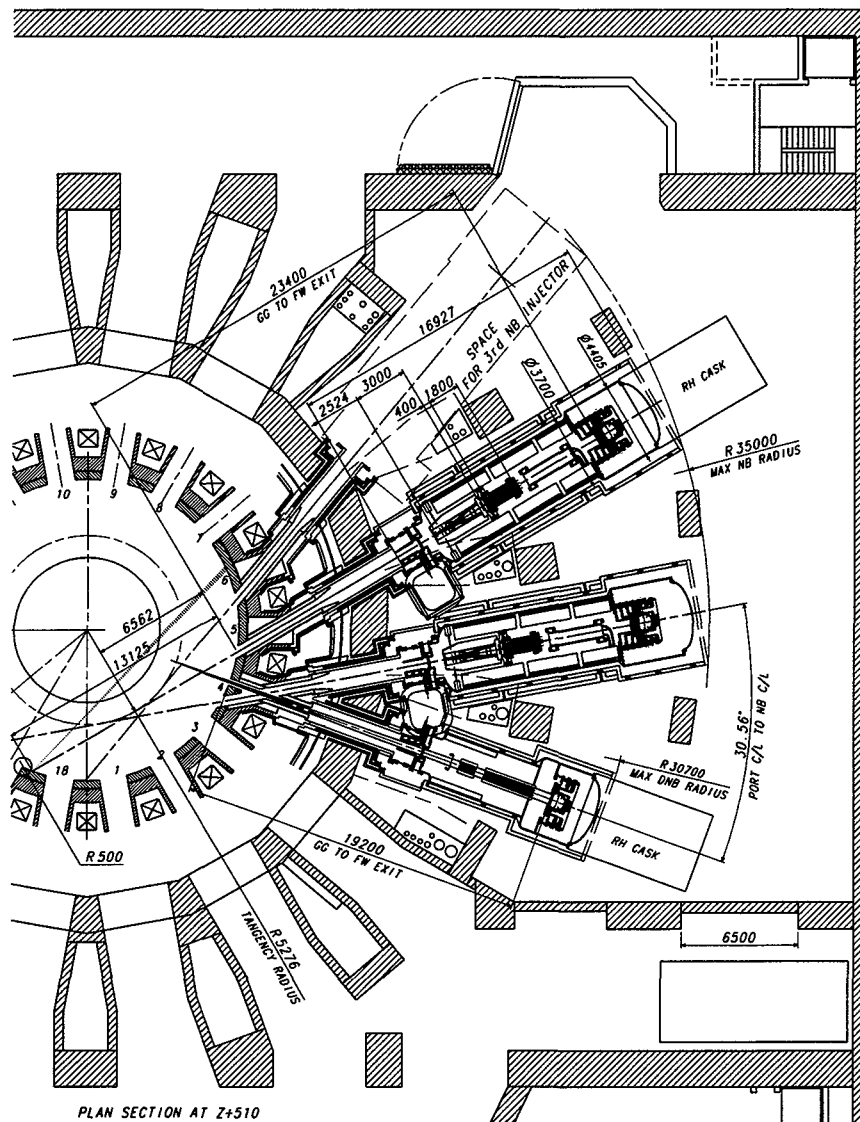
The horizontal angle of injection is defined by the NB duct size (including beam envelope, vacuum confinement, neutron shielding, tolerances and clearances) and the space between toroidal field coils for duct passage. The nuclear heating, due to neutron streaming through the NB duct, in the nearby toroidal field coils is evaluated to be < 100 W. Two weeks after shutdown, the dose rate inside the cryostat in the vicinity of the NB port, is ~ 150 µSv/h. This is somewhat above the design aim of 100 µSv/h.

Within the NB duct height, the beam can be aimed at two extreme (on-axis and off-axis) positions by tilting the beam source (1.2°) on its support flange. To cover a range of vertical distances from the plasma equatorial plane (at the tangency point) suitable both for on- and off-axis CD, the beam axis can be tilted vertically by 2°. This tilted beam layout enables the NB duct to be compatible with the standard equatorial port, the toroidal field coils, intercoil structures, poloidal field coils and thermal shields, and the building design. The main layout parameters are listed in Table II.7.1-1.

Table II.7.1-1 System Layout Main Parameters

Beam tangency radius (m)	Beam axis vertical position from the plasma equatorial plane (at tangency radius) (mm)		Duct width on First Wall (mm)	Duct height on first wall (mm)	Distance from grounded grid to first wall (m)
	Highest	Lowest			
5.28	-277	-900	584	1263	23.4

¹ N 53 DDD 15 98-06-12 W0.2, NB H&CD DDD5.3 (1998).



N 53 GR 385 99-12-06 W 0.1

Figure II.7.1-1 ITER-FEAT NB System Layout Plan View

The tangency radius is 5.28 m if the strike area on the far wall of the vacuum vessel is constrained not to include a port. If this constraint were removed the tangency radius would be 5.54 m.

II.7.1.3 System Design

Since the early stages of the EDA, the injector has been designed to reduce its axial length, and hence to limit the cost impact on the tokamak building. The concept¹ is to subdivide the neutralizer, and, consequently, the residual ion dump (RID) to form four vertical channels. The design of the channels is a compromise between gas flow and beam transmission

¹ "Study of Options for the Reduced Technical Objectives/Reduced Cost (RTO/RC) ITER" (section II.7.1)

requirements. In spite of the narrow channels, a NB injection efficiency of $\geq 40\%$ is achieved with a D^- beam of ≤ 7 mrad (85 % in core) + 15 mrad (15 % halo) divergence.

The stray magnetic field in the volume occupied by the beamline is in the range 10 – 50 mT. By adapting a combination of passive shielding (~ 0.15 m thick) and active coils (~ 200 kA/coil), the field in the beam path can be reduced to an acceptable value ($\leq 4 \times 10^{-4}$ Tm from the beam source to the exit of the neutralizer). Figure II.7.1-2 shows the NB system design.

II.7.1.4 Component Design

Beam Source: A D^- ion beam of 1 MeV, 40 A is produced by a single large beam source mounted on each injector. The negative ions are extracted from a multi-cusp, filamented, ion source where caesium is seeded to enhance the negative ion current density. The electrostatic accelerator consists of five stages, each stage consisting of 5 grid segments for beam aiming. Post insulators separate the five stages. The beam source is in the primary vacuum. The reasons for vacuum insulation of the beam source are given in ¹. The use of a vacuum insulated beam source (VIBS) gives an additional advantage: lateral pumping, through the post insulators, keeps the stripping loss of the ions in the accelerator to 25 %. The primary vacuum is sealed by a 1 MV, five stage, bushing where 1.8 m diameter porcelain insulators are used.

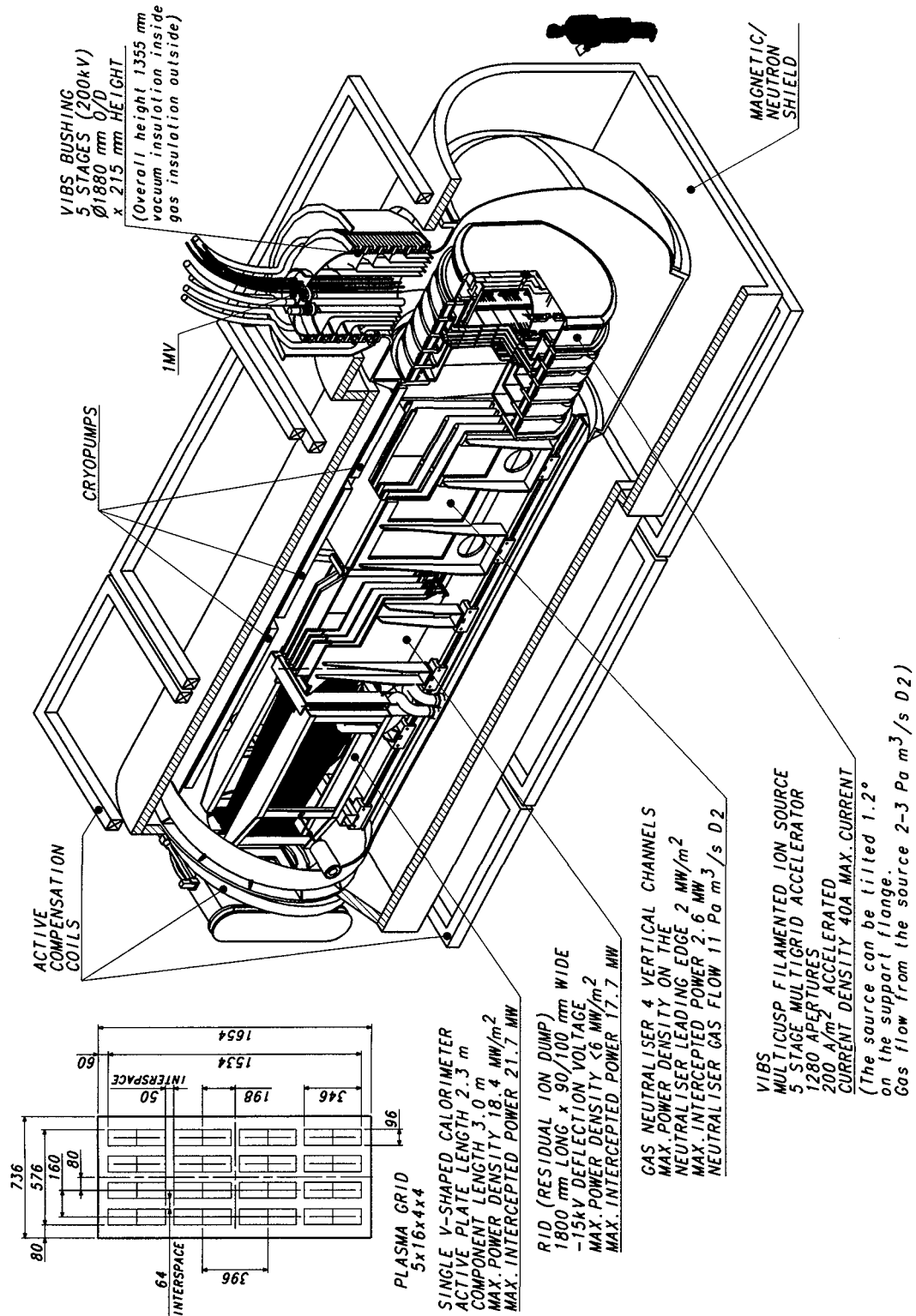
Neutralizer: The neutralizer is a conventional gas neutralizer which provides $\sim 60\%$ neutralization efficiency for the 1 MeV D^- ions. The beam aiming reduces the power to 2.6 MW on the neutraliser and the power density on the neutraliser leading edge to ≤ 2 MW/m². The beam exiting from the neutralizer consists of neutrals and residual ions (D^- and D^+ , each $\sim 20\%$).

RID: The ions are deflected and dumped on the five plates of the residual ion dump (RID) by an electrostatic field obtained by biasing the RID plates as follows: the odd plates (the two external and the central) at zero potential, the even plates at - 15 kV. The peak power density is ≤ 6 MW/m².

Calorimeter: The neutral beam impinges on a movable calorimeter in commissioning and conditioning phases. A single, V-shaped calorimeter is used. The use of a pivoting movement (5.5° rotation) produced by magnetically coupled drives allows long stroke bellows to be avoided. The calorimeter plates consist of an array of swirl tube elements, parallel to the beam direction. A limited deflection of the swirl tubes array (about 20 mm) can be allowed and secondary stresses (due to the peak power density of 17.5 MW/m²) can be reduced to less than 200 MPa.

The design of the RID and calorimeter guarantees an acceptable thermal fatigue of the components throughout the ITER-FEAT operative life.

¹ Mondino, PL., et al., "ITER Neutral Beam system" to be published in IAEA Nuclear Fusion Yokohama Special Issue (1999).



N 53 GR 386 99-12-06 W 0.1

Figure II.7.1-2 ITER-FEAT NB Injector Isometric View

II.7.2 Radio Frequency Heating and Current Drive (RF H&CD) Systems

Three RF heating and current drive systems are designed for possible use in ITER-FEAT: the electron cyclotron (EC), the ion cyclotron (IC) and the lower hybrid (LH) systems. A total of 40 MW of RF power (20 MW EC and 20 MW IC) are planned in the first phase of operation. A further 40 MW (20 MW EC and 20 MW LH) is possible in a second phase. A modular approach is adopted in RF system design, to facilitate their progressive installation, to provide flexibility in utilization and to reduce the number and cost of components.

II.7.2.1 General Features

II.7.2.1.1 Modularity

The RF launcher assemblies are designed as interchangeable plugs, inserted in the vacuum vessel equatorial ports, featuring:

- the same nominal installed power per port (20 MW/port),
- the same neutron shielding/ activation performance,
- the same confinement boundaries and interfaces with the VV port,
- the same remote maintenance requirements, interfaces and procedures.

The ITER-FEAT equatorial ports have a cross section of 1818 (toroidal) x 2204 (poloidal) mm² and a radial depth of ~ 2800 mm. Constraints related to the design of the port closure plate further reduce the usable cross section to ~ 1300 x 1700 mm². Each RF plug can operate at a maximum power density of 9.3 MW/m² and deliver to the plasma a maximum power of 20 MW.

II.7.2.1.2 General Mechanical Layout

The launcher assembly is supported by a mechanical structure, cantilevered at the port closure plate and otherwise disconnected from the other port components.

All RF plugs use the same support structure (Figure II.7.2.1-1), which includes the port closure plate and all mechanical interfaces with vacuum vessel and blanket. The support structure is also used as a coolant manifold, distributing the cooling water from two standard inlet/outlets to all RF components.

At the plasma end, the RF plugs are flush with the blanket first wall and therefore shielded from conduction heat loads. A gap of 20 mm is allowed from the port walls all around the plug and a dogleg of 30 mm is present at the plasma end, to avoid direct neutron streaming. A nominal gap of 120 mm is allowed between the plasma separatrix and the first wall.

For all systems, the primary confinement boundary is located at the vacuum vessel closure plate. The secondary boundary is at the cryostat closure plate. Single-disk, water-cooled ceramic windows are used in each waveguide or coaxial line. The dielectric window materials are different in different systems: BeO is used for IC and LH and polycrystalline diamond for EC.

II.7.2.1.3 Maintenance

The RF systems are designed to make maintenance operations simple, both in situ and in the hot cell. The use of a single support structure makes remote maintenance equipment and procedures identical for all systems.

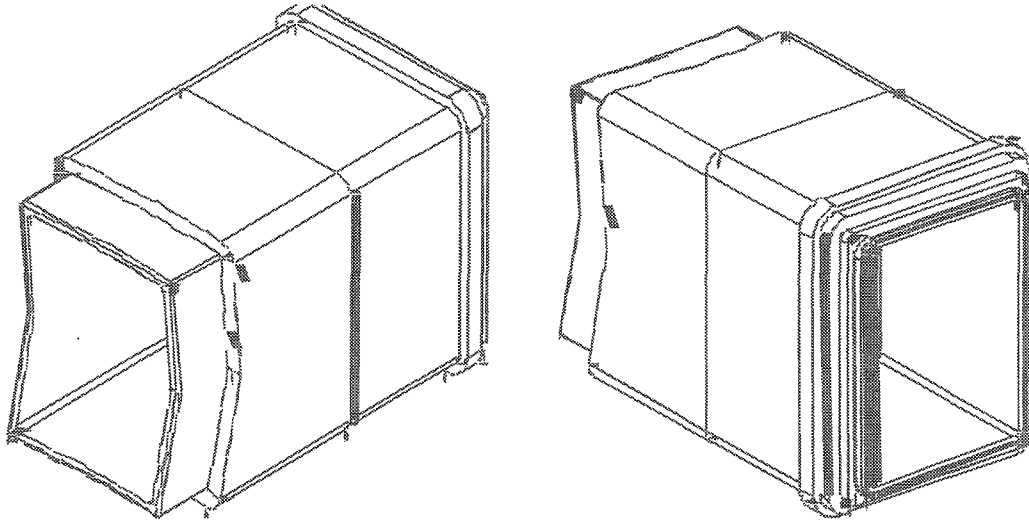


Figure II.7.2.1-1 Standard Support and Interface Structure used by all RF Systems

The port plug includes all components within the vacuum vessel. The RF launcher assemblies are initially delivered leak tested, fully operational and commissioned to full performance. Their integration in the port requires installation and welding of the closure plate lip seal only.

The waveguide/transmission lines block is located outside the primary vacuum boundary, between the VV port closure plate and cryostat. It houses different types of transmission systems (coax transmission (IC), rectangular waveguide (LH) and circular, corrugated waveguide (EC)) bounded in equal volumes. Assembly /disassembly operations of the block will probably be performed hands on. A secondary vacuum window is located in each transmission line/waveguide at the cryostat closure plate.

II.7.2.1.4 Nuclear Shielding

In all RF systems, nuclear shielding limits the average activation level outside the primary closure plate to a level below 100 μ Sv/hour, 2 weeks after shutdown, adequate for hands-on maintenance at that port closure plate location.

II.7.2.1.5 Auxiliaries and Services

The transmission systems and power source layouts have been designed to minimize costs. The different RF systems use, whenever practical, the same auxiliaries and services, control and data acquisition loops and interfaces with the central control, monitoring and protection system. In view of a staged use, the HV DC supplies should be modular and re-configurable.

II.7.2.2 Electron Cyclotron System

II.7.2.2.1 Design Issues

- Beam injection at different toroidal and poloidal angles is needed to satisfy all EC H&CD functions and to provide neoclassical tearing mode (NTM) stabilization. This, however, would require two dimensional (2D) RF beam steering, and a large opening at the front end of the EC launcher, which conflicts with the need for an efficient neutron shielding to be provided by the RF plug.
- Material and reliability issues are raised by the need of adjustable beam steering components operating in the intense neutron field at the front end of the launcher and exposed to the intense plasma heat load. To allow for beam steering in one dimension only, the EC functions are shared among two types of launchers. Toroidal steering is used in the equatorial plane for H&CD (Type A) and poloidal steering is proposed for NTM stabilization with launch from an upper port (Type B), as summarized in Table II.7.2.2-1.
- The amount of RF power injected by Type A launcher is 20 MW. The available space in a port, however, is not enough to install one pair of mirrors per waveguide as in the FDR design. The use of a steerable mirror for more than one waveguide is being investigated in order to maximise the injected power, still maintaining a large angular span for the beam deflection.

Table II.7.2.2-1 Summary of Design Requirements of EC System

Type	A	B
Functions	1. Plasma heating and access to H-mode. 2. On- & off-axis CD for steady-state operation. 3. Initial discharge for plasma startup. 4. Discharge cleaning.	Off-axis CD mainly for NTM stabilisation.
Port for RF injection	Equatorial port	Upper port
RF injection power	20 MW/port	10 MW/port
Frequency	170 GHz	170 GHz
RF beam steering	Toroidal steering (beam steering angle: $\Delta\phi = 25^\circ$)	Poloidal steering (beam steering angle: $\Delta\theta = 30^\circ$)

II.7.2.2.2 Launcher Design

The requirements for the RF beam power and injection angles are shown in Tables II.7.2.2-2 and II.7.2.2-3.

A type A launcher (Figure II.7.2.2-1) consists of an array of many waveguides, (of which several are dedicated to pre-ionization and wall conditioning), injecting the mm-wave beam using a number of mirrors which can be toroidally steered.

Three bends are introduced in the waveguide paths in order to reduce the neutron flux at the RF windows, which are located at the port closure plate.

Table II.7.2.2-2 RF Beam Parameters for H&CD System where the Beam Launching Position is $R = 8.9$ m and $Z = 0.5$ m for Launching at an Equatorial Port

Function	Frequency (GHz)	Injection angle (deg.)		CD efficiency ($T_{eo} = 20$ keV)	Power (MW)
		toroidal (ϕ)	poloidal (θ)		
On-axis CD	170	30 ~ 33	0	0.2	40
Off-axis CD (at $r/a=0.6$)	170	45	0	0.1	40
On-axis H	170	20 ~ 30	0	—	40

Table II.7.2.2-3 RF Beam Parameters for NTM Stabilisation where the Beam Launching Position is $R = 6.77$ m and $Z = 4.05$ m for Launching at an Upper Port

Option	Frequency	Power (MW)		Injection angle (degrees)				Total
	(GHz)	q = 2/1	q = 3/2	q = 2/1		q = 3/2		Power
				ϕ	θ	ϕ	θ	(MW)
Equatorial port	170	10	13	12	33.1	11.5	29.5	23
Upper port	170	12	20	17	-50	17	-58	32

A type B launcher is an array of five pairs of waveguides illuminating a number of poloidally steerable mirrors and is designed to be located in an upper port (Figure II.7.2.2-2).

A system of waveguide switches allows the gyrotron power sources to be shared between both launching structures.

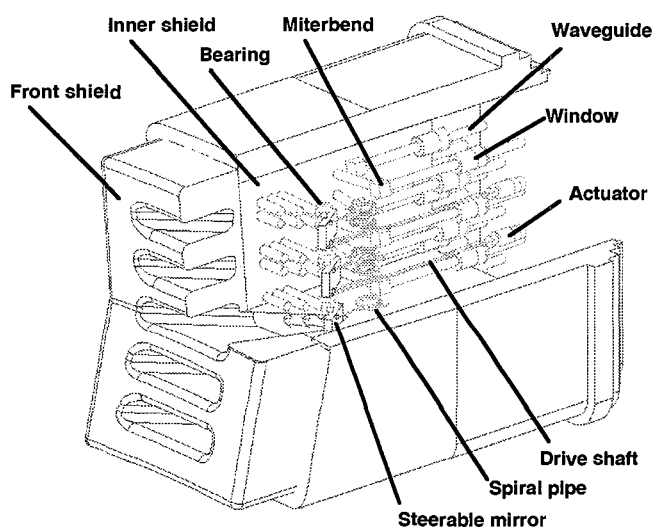


Figure II.7.2.2-1 Equatorial Port EC Launcher, with Radiation Shield Partially Removed to Show the Inner Components

Spiral pipes of 1 mm thickness, 12 mm outer diameter, and 150 mm spiral diameter are used to provide a flexible connection of the cooling channels to the steerable mirrors. They are all (with the exception of the mirror surface) as far as possible shielded from direct plasma radiation.

The actuator of the mirror rotation is a flexible driving shaft, connected to the mirror support plate by a pivot and driven at the other end by a hydraulic actuator. No cams, links or wheels are used to rotate the mirror.

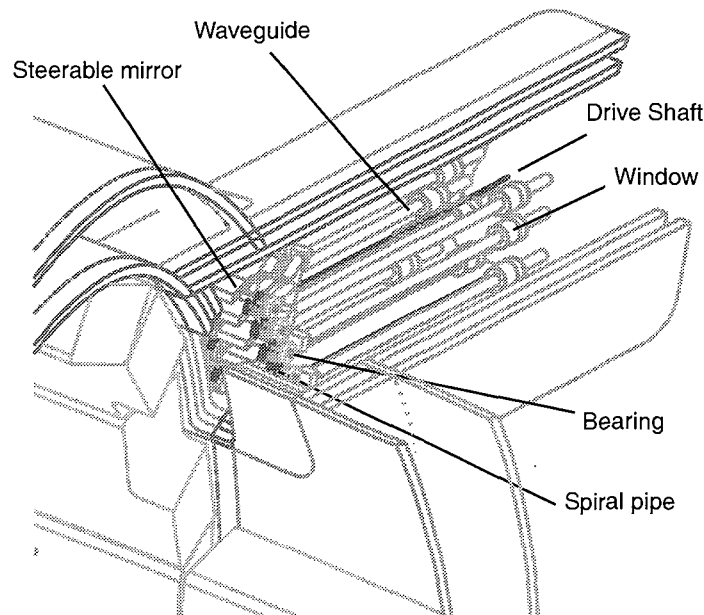


Figure II.7.2.2-2 Upper Port EC launcher, with Radiation Shield Partially Removed to show the Inner Components

The head of the shaft is cooled by water from the mirror. The distortion of the shaft due to its transverse displacement is negligible.

II.7.2.3 Ion Cyclotron System

II.7.2.3.1 Operating Scenarios

The heating scenarios of the ion cyclotron H&CD system in ITER-FEAT are second tritium harmonic ($2\Omega_T$) in a DT mixture and ^3He minority heating in H and/or DT mixture ($\Omega_{^3\text{He}}$). The latter scheme enhances ion heating. At $B_T = 5.3$ T, the resonant frequency is $f_H \sim 53$ MHz. An operating range $\Delta f = 35 - 60$ MHz allows operation at (60%) reduced toroidal field and could encompass the D minority heating (40 MHz) scheme. The nominal half wavelength in vacuum ($\lambda/2$) varies from 2.5 to 4.2 m, which can be accommodated in the port. A summary of IC resonances usable in the frequency range is summarized in Table II.7.2.3-1.

On-axis current drive can be performed at $f_{CD} \sim 56$ MHz, with an expected CD efficiency $\eta_{CD} \sim 0.2 \times 10^{20} \text{ m}^2 \text{ A/W}$.

Plasma heating in H majority plasma is possible by using minority heating at the ^3He and D fundamental frequencies. In these cases, the wave confluence cut-off is on the low-field side of the resonant layer and low minority fractions are required for an efficient tunnelling. A large experimental database is available for D majority at the ^3He fundamental in the "reversed" minority schemes.

Table II.7.2.3-1 Ion Cyclotron Resonance for ITER-FEAT

Resonance	Frequency (MHz)	Comments
$2\Omega_T = \Omega_{He}$	53	Second harmonic and minority heating
Ω_D	40	Minority heating
FWCD	56	On-axis current drive

II.7.2.3.2 Design

The IC H&CD system has been designed to upgrade its power handling at constant RF voltage. The IC array consists of an array of 4x2 elements fed by 8 coaxial transmission lines each carrying a nominal RF power of 2.5 MW.

The most important design features are:

- the design uses a variation of the resonant double loop antenna concept, with parallel tuning and balanced feed; short straps are used in order to decrease the operating voltage at the plasma interface and to improve its structural resistance (Figure II.7.2.3-1);

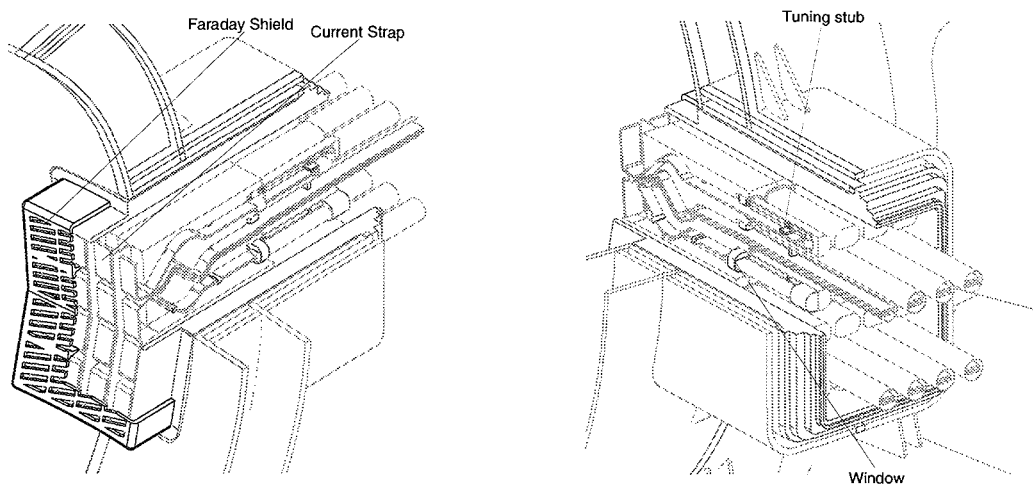


Figure II.7.2.3-1 IC Launcher, with Radiation Shield Partially Removed to Show Inner Components

- impedance matching is performed by reactances in parallel to the current straps; the tuning elements are rectangular cross-section, short-circuited strip-line sections of variable length, supported by stub-like dielectric spacers; they run in the port in radial direction and are possibly folded to minimize neutron streaming; the variable short circuits are accommodated in straight sections, which can be individually maintained without disassembling the plug from the port;
- the high voltage regions are located ~ 1 m away from the plasma interface; the electric field at the plasma end is reduced to $\sim 3.5 \text{ kVmm}^{-1}$ at a power density of 9.2 MWm^{-2} ;
- a detachable Faraday shield is used;
- the antenna is tolerant to large load variations (such as ELMs, etc.), thus providing intrinsic broad band operation.

The main features of the IC system are summarized in Table II.7.2.3-2.

Table II.7.2.3-2 ITER-FEAT Ion Cyclotron System Features and Target Performance

No. of IC arrays (ports)		Power per IC array (MW)	
No. of elements per array	8	Power density at launcher (MW/m ²)	9.2
No. of transmission lines per array	8	Max. strap voltage (kV)	35
No. of power sources	16	Max. Strap current (kA)	1.2
Power per strap (MW)	2.5		

II.7.2.4 Lower Hybrid System

The design of the lower hybrid (LH) system focuses on the optimization of current drive, for current profile control during the burn phase, and plasma kinetic control functions (such as sawtooth control). Its unique feature, among the other CD systems, of maintaining a high current drive efficiency at low electron temperature, makes it particularly suitable for profile control during the ramp-up phase and for off-axis current drive.

The system operates at 5 GHz, which is selected mainly to avoid absorption by alpha particles. The power deposition on electrons is mostly off-axis, for $n_e T_e < 1.5 \times 10^{21} \text{ keV m}^{-3}$. The predicted current drive efficiency is above $0.3 \times 10^{20} \text{ m}^{-2} \text{ A W}^{-1}$.

II.7.2.4.1 Design

The system is designed to deliver a total power of 20 MW from one launcher installed in an equatorial port. Each plug is connected to 8 main transmission lines (MTL) fed by 8 LH clusters of 3 klystrons (1 MW CW output power). The total installed power is 24 MW, with losses in the MTL and the launcher plug of the order of 0.7 dB.

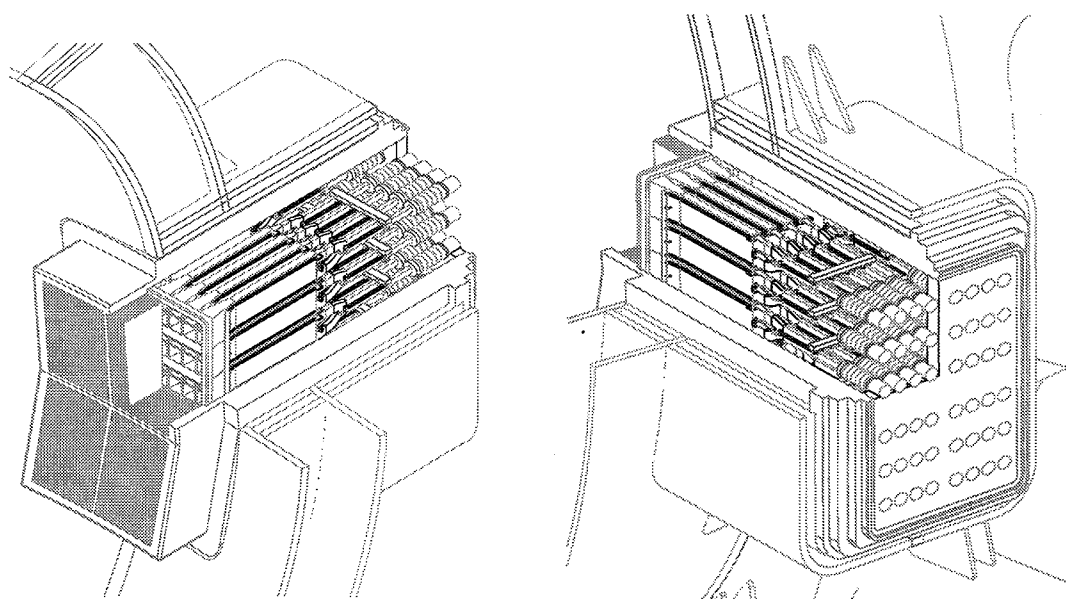
The launcher design is based on the passive/active multijunction (PAM) concept. Four PAM waveguide arrays are integrated in the launcher and connected, by means of a "hyper guide" power division section and mode converters to a bank of standard rectangular waveguides which house the ceramic vacuum widows (Figure II.7.2.4-1). The new parameters are summarized in Table II.7.2.4-1.

Good power coupling to the plasma is achieved if the density at the launcher mouth is greater than 1.5 to 2 times the cut-off density n_c ($n_c = 3.1 \times 10^{17} \text{ m}^{-3}$). As the front of the launcher is submitted to radiation thermal loads only, Be can be used for all plasma facing components.

The plasma pumps the waveguide volume of the launcher out through the mouth of the launcher.

Table II.7.2.4-1: LH Launcher Plug Specifications

Number of launchers	1
Power per launcher (MW)	20
Power density (active waveguide) (MW/m ²)	20
Working electric field (kV/cm)	< 2.3
Overall section (m ²)	1.3 x 1.7
Total weight (t)	32
N _{//} and directivity	N _{//} = 2, D ~ 70%
Number of PAM (per launcher)	4
Number of active/passive waveguide	28/29
Phasing between adjacent active waveguide	270°

**Figure II.7.2.4-1 LH launcher, with Radiation Shield Partially Removed to Show Internal Components**

II.7.3 Heating and Current Drive Power Supplies

The heating and current drive power supplies (H&CD PS)¹ receive power from the AC power distribution system and convert it into DC power needed to feed the four H&CD systems: IC, EC, LH and NB.

The power foreseen for the first phase of operation and the main parameters of the H&CD power supplies are listed in Table II.7.3-1.

¹ I Benfatto, "Heating and Current Drive Power Supplies: preliminary design for the ITER FEAT", Issue 1: 30 November 1999/ IDoMS N 42 RI 2 99-12-03 W 0.1

Table II.7.3-1 H&CD Power Supply Parameters

	IC	EC	LH	NB
Total power to the plasma (MW)	20	20	-	33
Total power from the AC supply (MW)	33	60	-	115
Number of power supply units	8	3	-	2
Number of generators/sources supplied by each power supply unit	1	10	12	1
Output voltage of the main supply (kV)	5-26	45-55	80	1000
Output current of one power supply unit (A)	150	450	300	59

The IC power supply basic unit is based on pulse step modulator (PSM) technology. The PSM uses 52 separate voltage steps, which can be electronically switched in and out of the circuit. In this way the output voltage can be rapidly varied to meet the voltage requirements of the tetrode. Load protection is accomplished by rapidly ($< 10 \mu\text{s}$) switching off all voltage steps. The PSM is commercially available.

The EC and LH power supply basic units are based on conventional thyristor and diode rectifiers connected in series with an IGBT (insulated gate bipolar transistor) switch. This switch, which provides load protection, has already been developed and tested for JT-60U, therefore, no further development is required. The EC and LH H&CD power supplies will use large basic units (31 MVA/each), which have the advantage of lower cost/MVA.

The design of the NB power supply basic unit is based on AC/DC/AC frequency and voltage conversion, oil insulated step-up transformers, and an SF₆ gas-insulated DC rectification system. The resultant output power is then transmitted to the NB injector source via a multi-conductor, gas-insulated, HV transmission line. The HV auxiliary NB injector power supplies consist of controllers and 1 MV insulation transformers, located in the NB HV area, and transformers and diode rectifier, located in a high voltage deck attached to the transmission line near the NB injector source. These HV components are without precedent, requiring further R&D.

II.8 Site Layout – Buildings – Plant Service Systems

II.8.1	ITER-FEAT Site Layout	3
II.8.1.1	Site Layout Strategy	3
II.8.1.2	Features of Radiologically Controlled Buildings	5
II.8.1.2.1	General	5
II.8.1.2.2	Confinement	5
II.8.1.2.3	Temperature / Humidity / Contamination Control	6
II.8.1.2.4	Radiation and Magnetic Fields	6
II.8.1.3	Dual Uses of Buildings	6
II.8.1.4	Site Description	7
II.8.2	Buildings	8
II.8.2.1	Design Strategy	8
II.8.2.2	Tokamak Building	8
II.8.2.2.1	Design Considerations	8
II.8.2.2.1.1	General Approach	8
II.8.2.2.1.2	NB Cell Configuration	9
II.8.2.2.1.3	Crane over the Gallery	10
II.8.2.2.1.4	Building Height Minimisation	10
II.8.2.2.1.5	Remote Handling, Shielding, and Access	11
II.8.2.2.1.6	Seismic Isolation and Restraints	11
II.8.2.2.1.7	Air Handling for Tokamak Building Complex	13
II.8.2.2.1.8	Cooling System Configuration	13
II.8.2.2.1.9	Magnet Feeds	14
II.8.2.2.1.10	Vacuum Vessel Pressure Suppression	14
II.8.2.2.1.11	Diagnostic Hall	14
II.8.2.2.2	Tokamak Building Design Description	15
II.8.2.2.3	Vacuum Vessel Port Allocation	17
II.8.2.3	Adjacent Buildings	17
II.8.2.3.1	Assembly Hall	17
II.8.2.3.2	Tritium Building	18
II.8.2.3.3	Low Level Radwaste Building	18
II.8.2.3.4	Personnel Access Building(s)	19
II.8.2.4	Power Related Structures	19
II.8.2.4.1	Pulsed Power Supply	20
II.8.2.4.2	Emergency Power and Diesel Storage	20
II.8.2.4.3	Steady-state Power	20
II.8.2.5	Cryoplant Buildings	20
II.8.2.6	Other Buildings	21
II.8.2.6.1	Control Building	21
II.8.2.6.2	Laboratory / Office / Reception Building	21
II.8.2.6.3	Site Services Building	21
II.8.2.7	Other Site Required Facilities	21
II.8.2.7.1	Analytical Chemistry Laboratories	21
II.8.2.7.2	Perimeter Security	22
II.8.2.7.3	Construction Services Facilities	22
II.8.2.7.3.1	Metrology Laboratory	22
II.8.2.7.3.2	Metallurgy Laboratory	22
II.8.2.7.3.3	Beryllium Analysis Laboratory	22
II.8.2.7.3.4	Safety and Health Physics Laboratory	22
II.8.3	Plant Services	23
II.8.3.1	Introduction	23
II.8.3.2	Service Water Systems	23
II.8.3.2.1	Potable and Fire Water	23
II.8.3.2.2	Steam, Condensate, and Demineralized Water	24
II.8.3.2.3	Sanitary and Industrial Sewage	24
II.8.3.3	Gaseous Systems	25
II.8.3.3.1	Compressed Air	25
II.8.3.3.2	Breathing Air	26
II.8.3.3.3	Nitrogen, Helium, and Special Gases	26
II.8.3.4	Tunnels and Bridges	27

II.8.3.5	Steady-state Electrical Power Network	27
II.8.4	Conclusions	29
II.8.4.1	Space Utilisation	29
II.8.4.2	Future Work	29

II.8.1 ITER-FEAT Site Layout

II.8.1.1 Site Layout Strategy

The overall strategy is to create appropriate system layouts, and building designs and arrangements for a generic site at minimum investment cost. This generic design will have to be modified to meet actual conditions on the selected site to adapt for service entrance locations, topology, geology, hydrology, and seismicity. However, the generic site plan follows some key design strategies which affect the building layout, including:

- a general layout policy to avoid the crossing of different service types such as electrical power, cooling water, and waste handling - clearly, the extent to which services can be segregated decreases as they get closer to the tokamak;
- separation of services: with the tokamak building located in the centre, the site is arranged so that electrical services enter from the west, cooling systems are located on the east, personnel-related functions are concentrated on the south, and waste management functions are located on the north (these directions are for identification purposes only);
- staged construction and expandability: to the maximum extent possible, the design of systems, buildings, and the site will be such that future additions in system capacity are not precluded.

Construction of the tokamak itself is primarily through access from the south, but construction access for the site is available from other points as well. Outside the tokamak building, systems which require a protected environment are located in dedicated structures. The overall site layout has been developed to minimise the connection distances and the complexity of system interfaces.

The site layout provides physical space for the buildings and the structures shown in Table II.8-1 and for the other areas listed in Table II.8-2. The key number refers to the building designator shown in the site layout diagram, Drawing 61.2.1.

In addition to the space required for buildings, structures and areas, the site layout allows for access, roadways, separation, and similar requirements. Space must be allowed for the passage of services such as electrical power, cooling water, and movement of personnel and materials. Access must be available for all phases of the project, including construction, operation, maintenance, and decommissioning.

Table II.8-1 ITER-FEAT Buildings

Key #	Buildings	Footprint m ²
11	Tokamak Hall	5,482
13	Assembly Hall RF Heating Area in Assembly Hall (2,550 m ²)	3,825
14	Tritium Building	1,210
21	Hot Cell Building	2,040
22	Personnel and Access Control Structure	2,400
23	Radwaste Building	900
31	Magnet Power Network/Switchgear Building	3,600
32	Magnet Power Conversion Building – North	3,600
33	Magnet Power Conversion Building – South	3,600
34	NBI Power Conversion Building	720
36	Reactive Power Compensation Building	720
41	Emergency Power Supply Building	3,024
51	Cryoplant Cold Box/Dewar Building	6,600
52	Cryoplant Compressor Building	7,350
61	Site Services Building	3,432
71	Control Building	3,762
72	Laboratory Office Building	3,367
73	Perimeter Guard/Gatehouse House	300
	Buildings Total	55,932

Table II.8-2 Other ITER-FEAT Structures and Areas

Key #	Other Structures & Areas	Footprint m ²
34	NB Power Supply Area	5,130
35	Pulsed Power Switchyard, Local Energy Storage area, and Reactive Power compensators and Feeders	42,200
42	Steady State Switchyard and Switchgear area	11,952
43	Diesel Fuel Storage Tanks	48
53	Cryo-Gas Storage-1	1,060
64	Water Storage	990
65	Makeup Basin	825
66	Gas Storage-2	594
67	Hot Basin & Cooling Tower	8,774
68	Pumping Yard	900
	Sub-Total	72,473
	Outdoor Storage /Expansion Areas	25,050
	Parking Areas	31,410
	Roadways	34,684
	Area Total	91,144
	Buildings Total (from Table II-8-1)	55,932
	Grand Total	219,549

II.8.1.2 Features of Radiologically Controlled Buildings

II.8.1.2.1 General

The radiologically controlled buildings include the tokamak building, tritium building, hot cell building (see II.10.8), low level radwaste building, and personnel building. These buildings have been designed to provide appropriate radiation shielding, ventilation, drainage, and access control. They are generally seismic class 2B, and designed to resist SL-2 earthquake criteria. Other buildings are expected to be free of radioactive contamination, and access control will exist primarily for purposes of accountability and industrial safety. Floor drainage from radiologically controlled areas is collected in tanks where it can be monitored and, if necessary, treated before it is released to the environment. Ventilation from the potentially contaminated radiologically controlled spaces in these buildings is routed to the plant gaseous exhaust, discharging from the roof of the tritium building.

Health physics offices and amenities are located in the personnel building. This building provides a wing for personnel access control which contains shower and change facilities, and provides the pathway for personnel entering the hot cell or radwaste buildings. The personnel access control is contiguous with the tokamak building and provides for personnel access to the tritium building, the hot cells, and the tokamak building. It also houses the radiological sample laboratory and the chemical laboratory.

When plasma facing components are removed through the tokamak ports, they are handled in casks which move on floor-supported air-bearing vehicles. To limit the weight of the casks, no radiation shielding is included in the casks themselves. The shielding function is performed instead by the buildings and structures through which the casks pass. The destination for most radioactive components and materials is either the hot cell building or the low level radwaste building. Objects will exit the tokamak pit via a lift shaft located in the gallery space and be delivered to the hot cell complex.

II.8.1.2.2 Confinement

All the ITER buildings in which tritium or tritium-bearing components and materials are used, are designed to control radiation and radioactive contamination. The ITER plasma will produce energetic neutrons which will interact with materials and coolant to create some activated material. Buildings where activated material is handled are also designed appropriately for confinement requirements.

In particular, the ITER plant is being designed to limit releases of radioactive material to the environment, and radioactive exposure to workers and the public. Confinement for ITER is achieved by establishing barriers around the various radionuclide sources. In some cases, the buildings provide a confinement barrier. Further, building atmosphere pressures are arranged to ensure that the pressure gradient is always in the direction which is toward areas of higher contamination, and discharge flow is always directed to the plant exhaust.

II.8.1.2.3 Temperature / Humidity / Contamination Control

For tokamak assembly it is necessary to maintain the temperature within $\pm 1^\circ\text{C}$ at a comfortable working temperature in the range $20^\circ\text{C} - 25^\circ\text{C}$, up to an elevation of approximately 5 m above the top of the bioshield wall, and relative humidity $< 70\%$. A dust loading goal of $< 10^5$ particles m^{-3} (0.3 micron) has been set in order to assure quality in the assembly process. When tokamak assembly is complete and the cryostat and tokamak systems are closed, temperature and air quality maintenance is less restrictive.

The heating, ventilation, and air conditioning (HVAC) systems are designed to provide suitable air change rates and to remove heat rejected to air in the building. The HVAC systems also play an important role in maintaining acceptable levels of airborne radioactive contamination. The design of HVAC systems ensures appropriate pressure and flow gradients within the building so that air flows from regions of lowest probability of contamination towards areas of higher probability of contamination. Potentially contaminated air is treated by filters, detritiation systems, and directed to the plant exhaust. The air space between the cryostat and the bioshield is also treated with a dryer to remove moisture from this region and minimise the radiolytic formation of corrosive acids. The HVAC system is also designed to respond to potential accident events. HVAC for building spaces which are potential locations for a loss of vacuum accident (LOVA) or loss of coolant accidents (LOCAs) are equipped with high-efficiency particulate filters. Areas where the release of elemental tritium or tritiated water is possible are equipped so that the exhaust flow can be passed through a vent detritiation system (VDS).

II.8.1.2.4 Radiation and Magnetic Fields

During tokamak operations, magnetic and radiation fields are generated. These fields will be sufficiently large to require human access to the tokamak pit and gallery region to be excluded. In addition, it is expected that there will be no need for personnel access in the below ground portions of the tokamak hall, or tritium building. Magnetic fields are also expected to be high enough to warrant exclusion of personnel from the top of the tokamak bioshield during operation.

The radiation fields which will exist during DT pulsing have been estimated, and detailed calculations of radiation levels throughout the tokamak building are continuing. These fields will be important due to their effect on materials and electronics in the tokamak pit and will prevent human access to some areas. The gamma ray fields from activated materials will be present at all times after DT operations have begun. These fields are the composite of emissions from a few isotopes. The field strength decreases rapidly as short-lived isotopes decay, then remains fairly constant as longer-lived isotopes dominate. To minimise operator exposure, entry into the tokamak pit for extended periods will not normally be permitted without supervision within 24 hours of a DT pulse.

The radiation fields experienced by operators performing maintenance or experimental work in the tokamak pit will vary with the location in the pit and the design of the radiation shielding.

II.8.1.3 Dual Uses of Buildings

The proposed site layout and construction schedule (see I.4.2) have been examined to determine which opportunities were available to provide dual use of buildings. For those buildings for

which the schedule indicates such a potential opportunity, the building sizes and service requirements were also examined, and any potential logistical problems identified.

There are several candidates of buildings that could be considered for dual use. The buildings that were originally identified as being used during the assembly of ITER and then have no further use include:

- (1) PF coil fabrication building (PFCFB)
- (2) tokamak assembly hall (TAH)
- (3) temporary staging facility for remote handling equipment

There are several facilities that are not needed until later in the schedule:

- (4) cryoplant coldbox/dewar building (CCDB) and cryoplant compressor building (CCB)
- (5) RF heating building (RFHB)
- (6) hot cell building

An examination of the schedule requirements indicates that a pairing of (1) with (4), (2) with (5), and (3) with (6) would be possible.

For the “coupling” of the PFCFB and the CCDB/CCB, a detailed examination of the schedule indicates that the PFCFB construction starts very early, in month 1, and takes 18 months to complete. Then, the PF coil outfitting takes until month 24, fabrication starts and takes about 24 months to complete, by month 48. The PF coils would be moved to an appropriate temporary storage area until they are incorporated into the machine assembly sequence. Once the PF coils are completed, the conversion of the PFCFB to the CCDB+CCB could be started at about month 50 for completion as early as month 74 (as the foundations and the building will be already prepared). Commissioning in 9 months, by month 83, leaves 8 months for the final connections to the tokamak building and the start of magnet cooling, scheduled for month 91. Should this “marriage” not be feasible due to schedule conflicts, and should the PF coil fabrication be done on site, it is suggested that temporary buildings be purchased, located on the eventual parking lot area, and serve as both PF coil fabrication buildings and as pipe and small component assembly facilities later in the construction.

The tokamak building will be ready for machine assembly by month 42, and the assembly will take about 36 months (to month 78). However, as the workload in the assembly hall diminishes towards month 72, the conversion of the TAH to the RFHB can begin in time for completion and commissioning by month 96. In order to make this viable, a temporary screen would have to be installed between the RFHB installation area and the still active assembly area.

Finally, the hot cells will be built early in the schedule, and will be available for the temporary storage of RH equipment used for in-vessel assembly, as well as storage and assembly of some of the in-vessel assembly components.

II.8.1.4 Site Description

The ITER-FEAT proposed site is divided into several areas, shown in Drawing 61.2.1:

- in the centre is the main area, called the “High Security Area” (just under 15 ha), which houses the tokamak building complex (tokamak building proper which is close to the centre of the site, tokamak assembly hall, tokamak laydown hall, tritium building, hot cells, low level liquid radwaste building, and the personnel building), as well as the

- support buildings for power supply and emergency power, cryoplant, site services, and main control, and distribution of site services;
- on the west is the power supply complex (5.9 ha), which includes the steady-state power supply, the pulsed power supply, the reactive power compensators and feeders, and the energy storage devices;
- on the east is the heat sink (1.5 ha), consisting of the cooling towers, complete with hot and cold basins, a makeup basin, some additional water storage for emergencies, and the cooling water pumping station;
- on the south side is the laboratory and office building (1.4 ha including parking), which also serves as the main access point during operations;
- also on the south side is a “buffer” area (about 2.8 ha), to allow for other construction activities, future expansion, temporary parking, etc.

The total site “compulsory” area, without regard for an exclusion boundary set by the host country, is 24.2 ha, which excludes the area of the heat sink. Not shown on the drawing is the estimated 45 ha for construction, designated to be on the south side of the site.

II.8.2 Buildings

In this section, the auxiliaries and support systems are described, as are the tokamak layout and the building design. Considerable work has been undertaken to develop the design of the tokamak complex of buildings and the layout of systems which must be directly connected to the tokamak via penetrations in the cryostat

II.8.2.1 Design Strategy

The tokamak building design strategy is to provide a building that provides the following key parameters:

- assembly and maintenance: the tokamak building is designed for assembly of the machine from the top; the surrounding buildings and systems are organised to permit approach to the tokamak from both north and south; the tokamak buildings and site arrangement would allow future construction for tokamak repair or decommissioning to be achieved at a minimum cost;
- operation: all aspects of tokamak experimental operation are accommodated, providing a convenient and a safe operating environment in the minimum size and cost of facilities;
- access and exposure control: radiologically controlled areas will be developed so that they are enclosed in a contiguous boundary, to facilitate maintenance, remote handling, HVAC maintenance, access control, and personnel exposure management.

II.8.2.2 Tokamak Building

II.8.2.2.1 Design Considerations

II.8.2.2.1.1 General Approach

The building arrangement is designed to accommodate a tokamak machine of 18 sectors with radial ports at three vertical levels and vacuum vessel pressure relief from the upper part of the vacuum vessel. It houses a cryostat diameter of approximately 27.6 m. The development of floor levels and radial wall or pillar positions is directly related to port access and the remote

handling cask docking/transport system. A number of issues arise in the layout of the tokamak buildings:

- embedment and plan shape: the maximum embedment depth that could be considered for the tokamak building is approximately 30 m, the extent of the concrete structure, which is insufficient to reach a satisfactory soil bearing stratum without the provision of structural piles; consideration of the optimum length of piles for the generic site, combined with the embedment depth, indicated that the selection of the equatorial level as a datum for grade level would be cost beneficial; this choice is favourable for access and, with the tokamak building less deeply embedded, it is not necessary to make embedded parts circular; further development of the plan shape produced a rectilinear layout, where spaces are available which better suit the location of plant components, escape routes, and other services not directly connected to bioshield penetrations; in addition, access from other buildings into the tokamak building is made through the side of the building, rather than only in the top; as a result, there is more available space for such penetrations and connections. However, as vertical space is limited in spite of this approach, further investigation into the allowable allocations of penetrations is required;
- routes for electrical and cooling systems: cost efficiency is achieved by reducing the overall length of piping, busbars, and other service conductors due to the tokamak cooling water systems and magnet feed systems being collected on each side of the tokamak building; this strategy also tends to balance the equipment density in the tokamak hall, and allows the incorporation of a single TCWS vault;
- vertical service shafts: the tokamak building suffers from constraints in the vertical buildup of spaces and slab positions, which lead to a requirement for inclination of the upper radial port extensions and divertor level port extensions; the size and position of the port extensions limits the available locations for slab elements which provide access to the divertor level ports, equatorial level ports, and upper radial ports; because the building designs must accommodate clear spans on the order of 10 m and maintenance loads on the order of 100 t, it is not practicable to make slab elements generally less than about 1 m thick; unless specifically designed composite structures are incorporated; the residual clearance between the bottom of the slabs and the top of the remote handling casks is on the order of 0.5 m, and insufficient for the routing of services such as EC and IC H&CD waveguides, which must connect to the ports; in order to connect services to the ports without crossing the gallery and thereby blocking the movement of remote handling vehicles, it is proposed to route them between the ports in vertical service shafts; a removable section of the service shaft will be provided in order to access test blanket modules (TBMs) or RF antenna modules located in equatorial ports.

II.8.2.2.1.2 NB Cell Configuration

The plasma heating systems comprise RF heating systems (EC, LH and IC) and two NB injectors (NBIs). The building layout incorporates a cell for the NBIs, which accommodates space for a diagnostic neutral beam (DNB) injector together with a third NBI, thereby making provision for future expansion. Several configurations of layout were considered to optimise the arrangement of the NB cell within the building. The option selected has the least impact on the functionality of the equatorial and upper port levels of the building. The NBIs require a clear space about 6.4 m high, more than the space between the equatorial level floor and ceiling slabs. Consequently, the upper horizontal ports above the NBI locations are limited in size and access. Piping services and perhaps some diagnostics at these upper horizontal port positions may be accommodated and therefore some access to these port locations is provided on a mezzanine

floor. The NB cell includes a corridor on the north side that provides a route for the maintenance casks to exit to the main equipment lift on the east side. This corridor also provides an alternative access route for the remote handling casks if the gallery is obstructed by a temporarily disabled transport vehicle. The corridor is connected to the gallery by an airtight door.

The horizontal alignment of the NBIs has an impact on the floor structure of the NB cell. The amount of interference is dependent upon the NBI alignment with the plasma and this aspect is the subject of further study. Structural proposals under consideration to mitigate the impact include the reduction in thickness of the NB cell floor by a steel and concrete composite slab.

II.8.2.2.1.3 Crane over the Gallery

Strategies to reduce the embedment, to make the building rectangular, and to locate the heat transfer equipment into a single asymmetric vault produced some options for placement of the crane support structures. Several options were considered for the structural support wall for the crane rail. On the west side of the building, the crane support wall could be located either on the bioshield, or over the gallery wall. Based on input from the assembly process, to maximise the utility of the assembly hall and to offer full crane cover over the tokamak pit, the gallery wall was selected as the optimum location. On the east side of the building, the crane support wall interacts with the TCWS vault. To create an optimal size for the TCWS vault, the crane wall should be located over the bioshield, but this solution is structurally unfavourable and produces layout difficulties at the lower levels when accommodating service routes around the support columns. Locating the crane wall over the gallery resolved the column difficulties for services but produced a central dividing wall within the vault. Structural investigation demonstrated that adequate penetrations could be formed in the dividing wall to accommodate the TCWS equipment after some re-arrangement to the piping layout. Since the crane beam required an overhang to access the bioshield, the actual crane span is not increased and therefore there is no cost penalty with the wall located over the gallery. This results in a distance between the crane rails of approximately 45 m. This span places the maximum useful service area including all of the area inside the bioshield within the operating scope of the crane.

II.8.2.2.1.4 Building Height Minimisation

The building height is determined by two factors: the height of the pit below the bioshield top is dependent upon the machine port arrangement and the equipment on each floor, which sets the construction height of the floor slabs, and the height of the hall above the bioshield is dependent upon the maximum crane lift for the largest machine component in the assembly process.

The pit height has been minimised following careful studies of the connection terminal box (CTB) and pipe chase requirements at both the basement level and the upper pipe chase level, together with the cask and service constraints at the divertor, equator and upper port levels. In addition, the structural design has been optimised to reduce the floor slab thickness to 1 m generally, for economic use of reinforced concrete. It is proposed to study the use of composite steel and concrete floors to further reduce the thickness, where this proves practicable and cost effective, but it depends on detailed design and shielding requirements. The bioshield roof design comprises a 2 m thick concrete shield with steel lattice girder supports, with the dual purpose of providing reinforcement to the cryostat head. Efforts to reduce the overall height of the building and to make a proper procedure for the removal of inner cryostat equipment, prompted a review of this concept and a revised proposal, separating the dual functions and combining the steel

structure with radiation shielding, thereby providing a height saving. Further design work is required to develop this proposal.

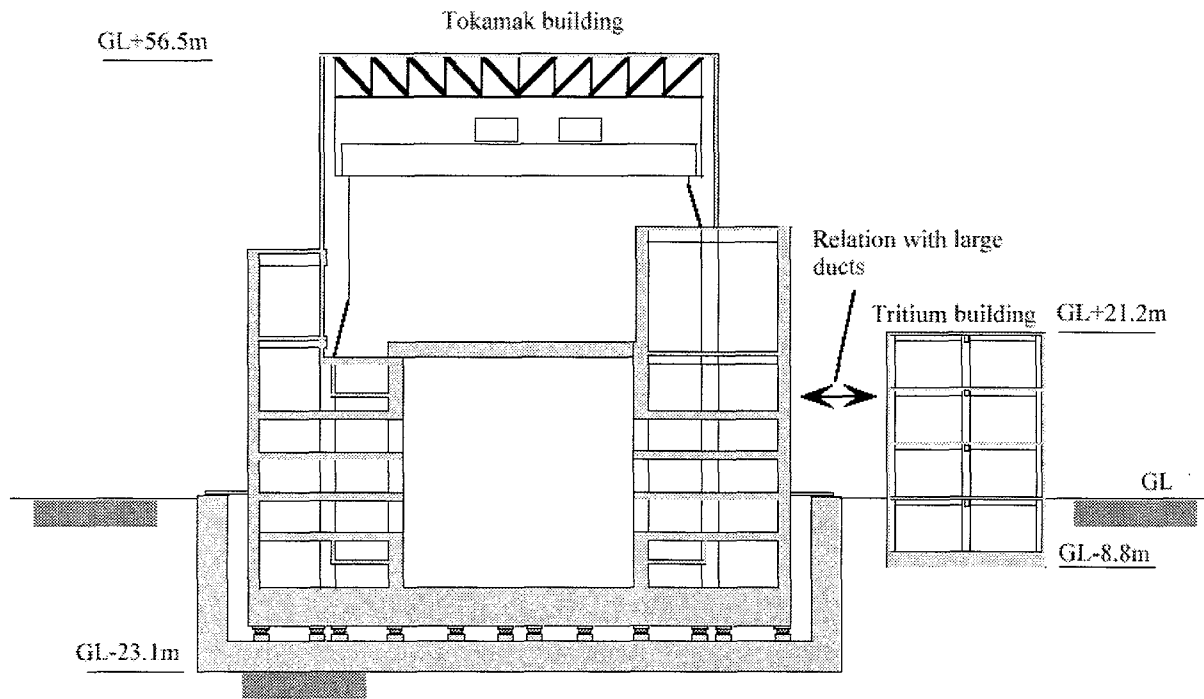
The tokamak hall height is related to the tallest component lift. The height of the central solenoid is approximately 18.5 m, the specific lifting tool is 1 m deep and the manoeuvre requires a 0.5 m ground clearance. Hence, the overall height is approximately 20 m and the lifting beam arrangement for the crane requires a further 3 m. In order to mitigate the impact of this lift requirement on the height of the building, it is proposed to incorporate a removable section in the bioshield wall. This feature will save 2 m from the crane clearance height and should be available both for the initial assembly and any subsequent maintenance activity requiring CS removal. In addition, it is anticipated that the crane lifting beam could be designed to allow the lift to rise between the 2 cranes, saving a further 1 m in building height. However, input from a crane manufacturer is required before this concept can be developed.

II.8.2.2.1.5 Remote Handling, Shielding, and Access

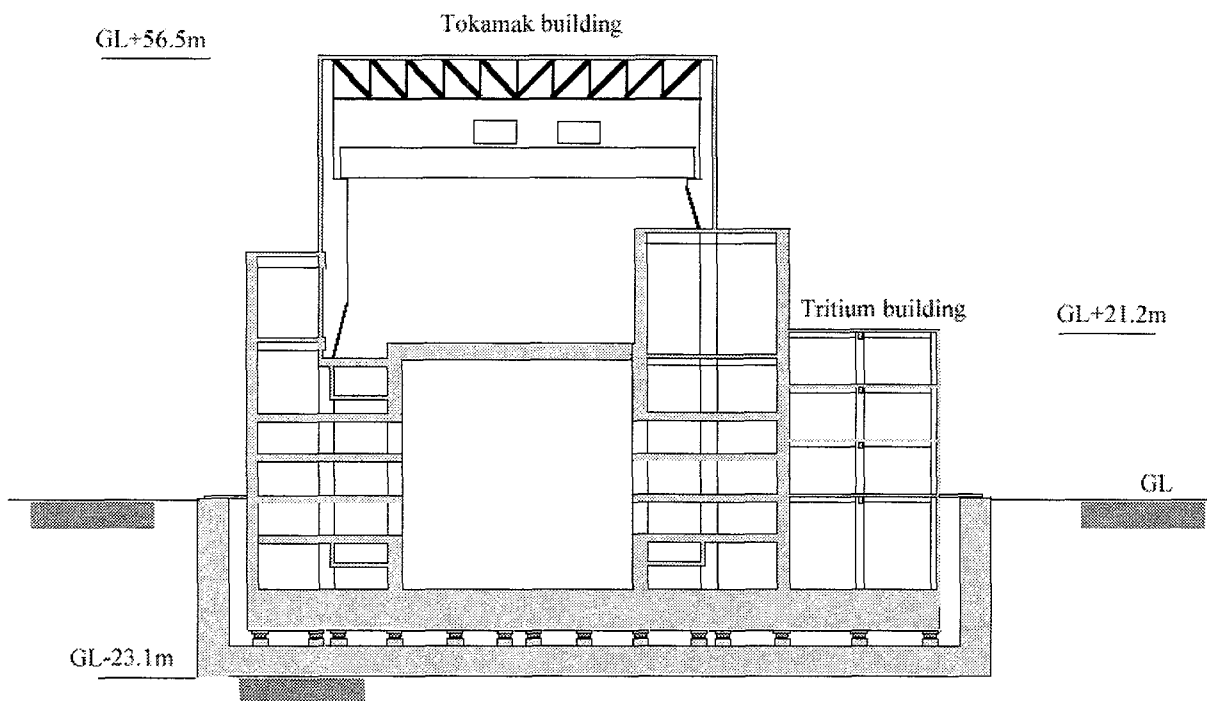
Remote handling cask envelope dimensions are specified by the port size and design of on-board tooling. The width of galleries and ultimately the position of several exterior walls are determined by the space needed by the remote handling casks to negotiate access to various ports. Other constraints are related to the space needed for busbars, cryogenic piping, and coil terminal boxes at the basemat level. Preliminary dynamic analyses of remote handling vehicle motion have been performed to set wall and column positions so that all available ports are accessible. These same studies have been used to select a location for the remote handling lift in the north east corner of the building, against the face of the east crane wall. All ports allocated for remote handling can be accessed by casks which are able to manoeuvre via the galleries to the main equipment lift. Provision has also been made for cask rescue, in the event of breakdown, by an alternative route to the lift on both the equatorial and divertor levels of the building. This feature is not possible on the upper port level due to the additional height requirement of the NB cell.

II.8.2.2.1.6 Seismic Isolation and Restraints

If it proves necessary to protect ITER-FEAT from large seismic forces, it will be necessary to place part of the plant on seismic isolation bearings. As a result of seismic isolation, there may be an unavoidable large horizontal relative displacement between the seismically isolated building and the adjacent non-isolated building, up to 50 cm. Crossing this “seismic” gap requires extra lengths and bends of pipes and some special designs for non-pipe components. Therefore, the optimum boundary of seismic isolation has a small number of pipes and ducts that cross the seismic gap. In this respect, it is better to have a combined structure of tokamak building and tritium building because of the large number of pipes and ducts that run between them. The tritium building has a significant tritium inventory as does the tokamak building; therefore this concept of combining the two buildings makes engineering of the complex much simpler. Also, as seismic isolation requires space for devices and footings, a secondary basemat, and an extra wall to withstand the pressures from the soil and groundwater, would increase cost. Almost 6 m deeper excavation and additional bearing capacity, almost 10 tm^{-2} , would be necessary. Figure II.8-1 shows the conceptual approach to combining the two buildings onto a common basemat with seismic restraint.



CASE 1: Tokamak Building - Seismic Isolated
Tritium Building - Non-isolated



CASE 2: Seismic Isolated Building Complex

N 62 GR 1 99-11-17 W 0.2

**Figure II.8-1 Conceptual View of Tokamak Building and Tritium Building
with Seismic Isolation**

Since the hot cell and the assembly hall structures and, in the reference design, the tritium building, have no seismic isolation system, the relation between the tokamak building and those buildings has to be considered carefully, especially when considering radiation shielding and confinement and avoiding impact of the structures under earthquake conditions. Of special concern is the confinement design for the route for transferring a cask through the buildings. Crane rails would have to cross the seismic gap, and to follow small relative motions by small earthquakes it is proposed that the rails at the building boundaries are equipped with mechanical links designed to allow small relative displacement, but which would break surely and safely before breaking buildings.

II.8.2.2.1.7 Air Handling for Tokamak Building Complex

The heating, ventilation, and air conditioning (HVAC) systems are designed to provide suitable air change rates to remove heat rejected to air in the building and also to play an important role in maintaining acceptable levels of airborne radioactive contamination. The design of the HVAC systems ensures appropriate pressure and flow gradients within the building so that air flows from regions of lowest probability of contamination towards areas of higher probability of contamination. Potentially contaminated air is treated by filters, detritiation systems, and directed to the plant stack. Dryers are included in the HVAC systems for areas such as the TCWS vault to capture water that may be tritiated due to chronic small leaks in the systems. The air space between the cryostat and the bioshield is treated with a dryer to remove moisture from this region and minimise the radiolytic formation of corrosive acids. The HVAC system will be designed to respond to potential accident events. HVAC for building spaces that are potential locations for LOCAs are equipped with high-efficiency particulate filters. Areas where the release of elemental tritium or tritiated water is possible are equipped so that the exhaust flow can be passed through a ventilation detritiation system (VDS). However, under normal operation, there is no open connection between the HVAC system and the VDS. The interface of these detritiation systems with the tritium plant is described in II.4.3.

The building is divided into a series of confinement zones based on their potential contamination (see Table I.1.3-5) ranging from "white" (uncontaminated) through "green" and "amber" to "red" (with different degrees of airborne and surface contamination). Gallery spaces will be designated as green, and provided with recirculation HVAC with about 30% fresh makeup. Exhaust from gallery spaces and all others within the radiologically controlled areas will be collected and discharged via the common stack. Corner spaces in the tokamak building will also be designated as green, however these areas will be separately ventilated to assure that they contain breathable air under all potential escape situations. Areas which may be designated as amber zones include the NB cell and the remote handling tool workshop spaces in the hot cell building. It is anticipated that the only red zones will be the interior of the tokamak and interior of storage and processing hot cells.

The air extraction systems from the tokamak complex, hot cell, radwaste and personnel access buildings will be routed to a plenum located in the tritium building and exhausted through the common stack.

II.8.2.2.1.8 Cooling System Configuration

The volume available for relief pressure resulting from ex-vessel LOCAs consists of the TCWS vault, the vertical shafts, pipe chases, and NB cell. In this case, as the relative pressure is

approximately 2 bar, thick slabs and walls are required. Slab thickness is a critical issue, as the overall floor heights are critical in the current design, and are dictated by the configuration of the tokamak VV. This is especially true in the case of the floor slab under the NB cell. A special structure that consists of plates at upper and lower surface and ribs has to be adopted. In this case, the influence on magnetic field and structural integrity cannot be ignored. To avoid such a situation, using the whole tokamak building as a pressure relief volume is being considered. The proposed design solution for this problem is to design the vault as a pressure confinement to a structurally practicable level to cover the most probable LOCAs, and to provide bursting panels to an additional expansion volume for the largest LOCA, when the LOCA pressure exceeds the vault structure design capability.

The proposed cooling system is arranged to be consistent with the layout strategy of locating most heat transfer equipment above grade on the east side of the tokamak building. However, cooling water must be provided to the blanket modules, divertor cassettes, and vacuum vessel at every sector. To interconnect the tokamak with the heat transfer equipment, the building layout provides a space for annular upper and lower ring headers, interconnecting with the vertical pipe shafts, and service connections to each tokamak sector. These piping spaces also enclose coolant pipes inside a shielding boundary, and inside a confinement boundary, connected to the TCWS vault. At this stage of the design, the piping layout is shown only in the detail sufficient to show the feasibility of the routing. Allowances are made for such components as hangers, snubbers, expansion, etc., but are not shown in detail at this time. The main cooling systems contain so much water that the TCWS vault would be able to resist the pressure from a VV loop if it expanded into the vault during baking at 240°C, only if a very complex design with a very large amount of special reinforcement structures were developed.

II.8.2.2.1.9 Magnet Feeds

The TF CTBs and those for the lower PF coils and lower half of the CS sectors are located in the basement level below the divertor access area. The lower piping ring header is also located here and the CTBs must be moved radially outward from the bioshield to eliminate a conflict with the lower pipe chase. The upper PF coils, the upper half of CS coil modules, and upper correction coils are served by CTBs located above the upper horizontal port access region, either above the NB cell or on the west side of the tokamak hall. To permit magnet feeds and other services to enter the cryostat sidewall, space is made available between the vertical shafts and beneath the upper horizontal ring header.

II.8.2.2.1.10 Vacuum Vessel Pressure Suppression

Preliminary studies have indicated that the peak calculated pressure following an in-vessel LOCA can be reduced if the vacuum vessel can be vented at the top. These same studies also indicate a benefit in creating a connection between the bottom of the vessel and the evacuated drain tanks. Current building and layout developments are based on this. The top vents are connected to a vacuum vessel pressure suppression tank, located on the west side of the tokamak building, above the upper magnet feed equipment.

II.8.2.2.1.11 Diagnostic Hall

Details of the requirements for ITER-FEAT diagnostics have recently been identified, as well as of the logic for the layout of the area of the plant to house these systems. It appears as if the

logical location for the diagnostic systems is on the west side of the tokamak building, at grade level, to avoid interference between diagnostic lines and wave guides within the building.

II.8.2.2.2 Tokamak Building Design Description

The east-west section view of the tokamak building is shown in Drawing 21.29.2. The building is set so that the equatorial port access slab is set at grade. Preliminary member sizing gives a basemat thickness of 5 m, and intermediate floor slab thickness of 1.0 m. The vertical space between slabs at the basemat level is 5.0 m, and at the divertor level it is 4.14 m, so the top of the basemat is less than 11 m below grade. The vertical height in the equator port access area is 4.24 m, with 4.14 m required at the upper horizontal port level. As a result, the main floor in the crane hall is at elevation 10.38 m. The maximum elevation of the upper pipe chase is 17.38 m. Based on the maximum lift requirements, the crane and crane support walls are designed to lift loads with a clearance height of 20.8 m above the pipe chase. Allowing about 15.8 m for the combined height of the crane (including the bridge beams, trolley, and clearance) and for the depth of the roof trusses, the elevation of the top of the tokamak building roof would be at about 56 m.

This east-west section also shows the horizontal buildup of the structure with the tokamak centreline located on the building centreline, and the bioshield walls symmetrical about the centre. The port access areas and gallery spaces are also completely symmetrical, primarily because the crane walls are located over the gallery walls on both the east and west. Above the upper port level, the structure becomes asymmetrical. The upper pipe chase fills the space between the bioshield and the west crane wall, but can be deleted on the east side where pipes enter the TCWS vault. The TCWS vault extends from 10.38 m elevation to 33.88 m elevation, and is 16.2 m wide internally. A mezzanine floor and supporting columns exist inside the TCWS vault. It is planned to lay equipment out in the vault so that piping, chemical and volume control systems (CVCs), and other cooling support systems such as dryout equipment are located below the mezzanine floor. Primary pumps, heat exchangers, and pressurisers will be located above the mezzanine. The interior of the vault will be served by a hoist to facilitate component maintenance. Around the exterior of the bioshield, structural spaces accommodate the upper CTBs and on the west side, the vacuum vessel pressure suppression tank, and TF coil electrical apparatus such as counterpulse capacitors and fast dump resistors. The overall external width of the building is 69.3 m. The tokamak hall roof system extends over the ends of the crane walls, giving a reduced width of 51 m for this volume.

Drawing 21.29.1 shows the north-south section view of the building and the distinctive feature here is the NB cell at the north end. The clear height inside the NB cell is 9.38 m, which is the combined height of both the equatorial and upper port level floors. The NB cell extends northwards beyond the divertor level gallery to allow NB maintenance casks to access the injector source modules. The additional space below the NB cell extension, on the divertor and basemat levels, provides a suitable location for the drain tanks and the vacuum vessel cooling system components. This north-south section also shows both the upper and lower pipe chases. The overall external length of the building is 79.1 m.

Drawing 21.29.8 shows a plan view of the tokamak building at the basemat level. The bioshield, vault wall support columns, service shaft columns, gallery walls and crane support columns are shown. Their positions are chosen to provide appropriate equipment and service spaces without exceeding clear spans of about 10 m. The lift shaft is shown as a rectangle, 4.5 m by 10.5 m in

the north-east corner of the building. The footprint dimensions of the building are 69.3 m by 79.1 m.

Drawing 21.29.7 shows a plan view of the tokamak building at the divertor port access level. This view includes details of the vertical service shafts configured radially around the bioshield. The walls enclosing the service shafts have been made nominally 50 cm thick and will serve as part of shield boundaries and part of the TCWS confinement boundary. The shaft walls are not considered as structural reinforcements and hence the bioshield wall has been made 2 m thick to mitigate loss of structural strength due to the large penetrations in the wall. The space beneath the NB Cell will house the VV cooling and a partial floor slab at the level of the divertor port access slab will be provided to support equipment.

Drawing 21.29.6 shows the layout plan view at the equatorial port access level. The service gallery at this level is interrupted by the NB cell, which is connected to the service shaft walls. Columns are required within the NB cell to prevent exceeding the maximum allowable unsupported span in the cell roof. Access to the building lift from the NB cell must be made through a penetration equipped with a confinement and shield door. A similar door is provided in the west wall of the NB cell to allow the passage of RH casks in a rescue scenario. The floor of the NB cell matches the floor level in the laydown hall, and direct access for initial assembly or major maintenance could be provided.

Drawing 21.29.5 shows a plan view of the tokamak building at the upper radial port access level. As previously described, the ports above the NB system cannot be accessed at this level by a standard remote handling cask due to the height of the NB cell. However, it is proposed to provide cooling system connections at these ports and there may be a requirement to be able to insert pipe cutting or maintenance tools. To facilitate this possibility, a mezzanine floor has been incorporated into the NB cell at this port level, which may be accessed via a confinement door connecting to the gallery.

Drawing 21.29.4 shows the layout plan view at the level of the TCWS and upper pipe chase at 10.38 m above grade. In this view, the rectangular shape of the TCWS vault on the east side with the dividing crane wall is visible. The main equipment lift could be designed to service the vault; however, it would be necessary to surround the lift with a shielding wall, which functions as a pressure tight confinement boundary wall incorporating an air tight door.

The roof slab over the NB cell is utilised for the CTBs and high voltage decks connected to the NB systems. If the design of this equipment permits, an additional roof could be included to provide a useful laydown area. In this case, a vertical plug in this slab could be provided to enable crane access to the NB cell. The region to the south of the bioshield at the same floor level will also accommodate CTBs. To the west of the west crane support wall, the building superstructure is divided into rooms and cells by intermediate slabs and walls. A clear height of about 8 m will be provided at the 10.38 m level for further CTBs and auxiliary cold boxes. Cryogenic feeds from CTBs on this level will penetrate the crane wall and pass below the upper pipe chase and between the vertical service shafts, through the bioshield to enter the side wall of the cryostat. On the west side, the intermediate slab above this level provides additional space with approximately 9 m height to accommodate the vacuum vessel pressure suppression tank (see Drawing 21.29.3).

As the floor-to-floor height is restricted due to port position on the VV, space for services, such as electricity, HVAC, and drainage, may be insufficient. If this is the case, a corridor around the present building to house those services might be considered.

The current design of the building is asymmetrical both horizontally and vertically about the east and west crane rails. There exists scope to resolve the vertical build on the west side and provide space for an additional level to accommodate the TF coil support systems such as counterpulse capacitors and secondary switchgear. The ventilation fans for the TF fast dump resistors could be located on the roof above. These elements are subject to further design development.

II.8.2.2.3 Vacuum Vessel Port Allocation

The design of the tokamak building is strongly influenced by the tokamak vacuum vessel, its ports, the port orientation, and the port allocation. The layout provided is both cost effective and operationally convenient, and attempts to maximise utility while maintaining these goals. The following drawings show the port allocations:

- at the divertor level, Drawing 10.73.1;
- at the equatorial level, Drawing 10.72.1;
- at the upper port level, Drawing 10.74.1.

An example of the strong influence of the port allocation on the building design is the consideration required for accounting for the impact of the NB cells on the structure. Because of this impact, the ports beneath these components are required to be small ports, as shown. Also, as seen by the cross-sectional views of the building (Drawings 21.29.1 and 2), the room height at these levels is dictated by the port orientation.

II.8.2.3 Adjacent Buildings

II.8.2.3.1 Assembly Hall

The tokamak hall above the pit is integrated with an assembly hall on the south end, which combines both laydown and assembly functions. There is no dividing wall, the main cranes serve both areas equally and the total volume is treated as one in terms of air handling. The width of the assembly hall is determined by the crane span in the tokamak hall. The length of approximately 75 m is set by the needs of the assembly and laydown processes for layout and staging of tokamak sector assembly.

To facilitate the assembly process, it is desirable that the main floor level in the tokamak building matches the floor level in the assembly hall. However, it is essential that the assembly hall has a grade level entry zone for large components and hence a loading bay at grade will be provided at the main entrance door in the south elevation.

The initial design solution is to provide an internal platform in the assembly hall to raise the working surface for the assembly process, which also provides useful floor space to accommodate diagnostic and other laboratory areas that may link to the tokamak pit at the upper port level. However, this caused considerable constraint in the area immediately adjacent to the tokamak building, as placement of large components there would restrict the size of equipment that could be lifted overhead, travelling from the tokamak hall to the laydown area at the far south end of the assembly hall (and also for travelling in the opposite direction). One solution

was to lower the assembly hall into the ground to make this raised surface come to grade level. If this were done for the diagnostic connections, this would mean lowering the entire tokamak hall by the same amount. After examining the specific needs for diagnostic analysis, the location of the ports allocated to diagnostics, and the impact of the RF heating equipment and waveguides, it became clear that the diagnostic analysis area is best suited to be located on the west wall of the tokamak building, at grade. This solution will be examined in detail.

The assembly hall will be a reinforced concrete wall and column structure up to the crane rail with a steel-clad roof. The basemat slab at grade will require piles to establish a suitable soil-bearing foundation.

Following the completion of vacuum vessel sector assembly, about two years prior to tokamak operation, it is proposed that the assembly hall be converted for use as a plasma heating equipment hall. The size and shape of the building appear well suited for a layout in which the power supply transformers can be located outdoors, and switchgear and generating equipment can be installed inside the crane hall space.

II.8.2.3.2 Tritium Building

The functions of the tritium building are described in II.4.3. The building is a 4-story building with a footprint of 60.5 m x 20 m, located on the east side of the tokamak building. The reference design provides a building separate from, but adjacent to the tokamak building. This building layout is shown in Drawing 62.334.1 and 2, with functions allocated to each section of the building. Of special interest is the approach to air handling within the tritium building, and the collection of potentially tritium-bearing air from other buildings for treatment prior to release (see also II.8.2.2.1.7). Instead of having several separated areas on each floor, the floors are kept as individual green zones, with air supply and return common to each floor. This minimises the emergency air supply controls and sensing systems considerably. Several high-tritium-containing lines pass between the tokamak and the tritium buildings, and the difficulty of providing security to these lines during an earthquake suggests that these two buildings should be combined into one common building on the same seismically qualified foundation (see Figure II.8-1)

II.8.2.3.3 Low Level Radwaste Building

The low-level radwaste building provides space for systems which process mildly contaminated water. Floor drainage from radiologically controlled buildings, active laboratories, primary heat transfer systems equipment drains, and shower and laundry drains, are treated here. Paper, plastic, and other dry solid material are collected and stored for appropriate packaging. The low-level radwaste building is configured to facilitate the handling of loaded filter and demineralizer beds. Filters and demineralizers are designed so that the beds can be sealed in a disposable liner and handled as wet solid waste. A de-watering step may be necessary before these materials can be transferred for disposal, and a connection to the hot cells provides for a common exit for this transfer. Materials are sealed in containers for off-site disposal by the host country. It is intended that the radwaste facility will be able to package materials so that they do not require any further processing prior to disposal by the host. The low-level radwaste building will be constructed using cast-in-place reinforced concrete.

Primary coolant will be continuously cleaned by the CVCSs to remove particulate and ionic material, some of which may have become activated. When the CVCSs filters and demineralizer

beds reach their end-of-service life, the filter medium or demineralizer resin bed will be replaced. The spent filters and demineralizer beds may be treated as wet solid radioactive waste and packaged for disposal. Alternatively, ITER may have features which would allow backwashing of filters or regeneration of CVCSs demineralizer beds thereby reducing the waste volume.

When primary coolant is intentionally removed from the system, it will be collected in drain tanks. Normally, primary coolant systems will be refilled from these tanks to resume operation. Occasionally, it will be necessary to remove primary coolant to the waste systems. Primary coolant, water which is spilled onto the floor and collected in drains within the radiologically controlled areas, fluid from active laboratory drains, and decontamination fluid, will be collected in tanks in the radwaste building and treated in a dedicated waste process stream. Fluid will be sampled before and after processing. This process stream will include oil separators, filters, and demineralizers. If the product water meets the specifications for primary coolant, but exceeds the allowable tritium content for release to the environment it will be sent to a water detritiation system where tritium will be extracted and detritiated water can be discharged. If the water does not meet primary coolant specifications, it must be recycled until additional particulate and ionic activity have been removed. The filter beds and demineralizer resins from this stream will also be treated as waste and handled in a manner similar to the primary coolant CVCS filters and demineralizers.

II.8.2.3.4 Personnel Access Building(s)

The personnel access control building will be used to provide controlled access to the potentially contaminated regions in the tokamak hall and pit, hot cell and radwaste buildings. Health physics for ITER will be based in the personnel building, which will also provide space for analytical chemical laboratories, the beryllium analytical facility, first aid, change rooms, showers, laundry facilities, electrical power distribution equipment, and eating facilities. The personnel building will be of steel frame construction on a slab at ground level.

II.8.2.4 Power Related Structures

The equipment and systems used to provide power to the tokamak magnets and plasma heating systems are located in the four buildings in this group, all of which are constructed using steel framing on concrete slabs at ground level. The two structurally identical power conversion buildings are used to house the magnet power rectifier systems. These systems consist of a number of power conversion modules, each consisting of a transformer, phase-controllable rectifier modules, and related power conditioning equipment. Power conversion modules are connected in series and parallel to generate the current and voltage waveforms needed to operate the tokamak magnets. The space required for the power conversion modules, and the selection of outdoor locations of the transformers, result in long narrow buildings. The power modules are located along each side of these buildings. Overhead AC power is fed to the transformers, and output DC power flows in busbars running the length of the buildings at an upper level.

Busbars from the power conversion building carry DC power to the magnet power supply switching network building (MPSSNB). This building is sized to house magnet-related switchgear, capacitors, dump resistors, and related electrical apparatus. No special constraints on this building are anticipated, and it is of conventional industrial construction. Handling of equipment busbar segments, and other heavy objects will generally be performed using floor

supported portable lifting equipment (e.g. forklift trucks). The size of the building is 60 m by 74 m, by 20 m high.

The neutral beam power supplies will consist of mainly outdoor equipment, located on support foundations north of the magnet power conversion buildings. There is space to accommodate three beamline power supplies, each consisting of five 200 kV modules connected in series.

The ion cyclotron (IC) system is located in the assembly hall. A separate area of the building is dedicated to the high frequency power generators used to provide power for the electron cyclotron (EC) plasma heating and current drive systems. Generally, the power supply equipment for these systems consists of transformers, switchgear, rectifier units and control apparatus. The system is arranged with transformers and switchgear at the ground level and high frequency generators on a second level, with appropriate space between generators and structural members. The output from the IC high frequency generators is carried in co-axial conductors about 300 mm in diameter. The output from the EC system is carried in 60 mm diameter evacuated waveguides.

II.8.2.4.1 Pulsed Power Supply

There is an area of 210 m x 120 m set aside for the pulsed power supply and switchyard.

II.8.2.4.2 Emergency Power and Diesel Storage

The emergency power building is 84 m x 36 m, and houses the emergency power generators and emergency control system. A diesel storage tank of 12 m x 4 m is located nearby in the same area, but underground for protection.

II.8.2.4.3 Steady-state Power

There is an area of 144 m x 83 m set aside for the steady-state power switchyard and switchgear.

II.8.2.5 Cryoplant Buildings

The cryoplant is housed in two separate buildings. The compressors are noisy and do not require clean conditions. Their maintenance requirements are also relatively modest, therefore one building is dedicated to them. The cryoplant compressor building is 105 m x 70 m and about 16 m high. The building is divided into two bays and each bay is equipped with a lightweight overhead bridge crane for maintenance of the compressors and drivers. Piping is routed to the space between the bays.

The cold box portion of the cryoplant is housed in the other cryoplant building. The cryoplant cold box/dewar building is 110 m x 60 m. Elevations for the building vary from grade to + 33 m.

Both of the buildings are industrial grade buildings and of structural steel. The floor slabs are thick concrete and supported by an adequate foundation. As indicated in the section on dual use of buildings, these buildings will be used for fabrication of the PF coils prior to being outfitted for cryoplant service. In this case, there are additional requirements for crane and access over and above those of the cryoplant.

II.8.2.6 Other Buildings

II.8.2.6.1 Control Building

The ITER control building will be used to house the online supervisory control system (SCS) computers and work stations used by plant operators and experimenters. The control building is located inside the high security area, but close to the laboratory office building, to ease access. The control building will be constructed of cast-in-place reinforced concrete, and will be designed to resist external hazards so that plant operators will be able to maintain their interface with the SCS system under all conditions. Space will be provided for an incident response facility (if required by the host country), an electronic archive system, and a visitors' gallery. A tunnel will connect the control building with the basement of the assembly hall, which can be used to route instrumentation links, and for pedestrian access during inclement weather. The building is estimated to be 66 m x 57 m.

II.8.2.6.2 Laboratory / Office / Reception Building

The laboratory/office building is located outside the high security area. It will provide office space for 750 scientists, engineers, and administrative staff. It will also house an off-line data processing centre, library, and meeting rooms. This structure will be built using conventional steel frame office construction. Final dimensions will be established at a later date.

II.8.2.6.3 Site Services Building

The site services building (a steel framed building on a concrete slab at ground level.) provides space for many of the site services and their operating support. It will house boilers for process steam and building heating, demineralized water systems, potable and hot water treatment systems, compressed and breathing air systems, miscellaneous gas distribution, and some electrical power distribution. A machine shop is also provided in this building. It will also provide space for waste handling (both normal garbage and toxic, non-radioactive waste), and provide limited space for warehousing of spare parts and machine shops. An area of 40 m x 75 m with an annex of 24 m x 18 m has been provided.

II.8.2.7 Other Site Required Facilities

II.8.2.7.1 Analytical Chemistry Laboratories

The plant sampling laboratory is divided into two separate laboratory analysis subsystems, one dedicated to radio-chemical analysis of radioactive materials and the other for non-radioactive materials. The first subsystem, hot laboratory analysis, will be capable of handling radioactive samples in solid, liquid or gaseous form. It contains alpha, beta and gamma counters and spectrographic instrumentation as well as wet-chemistry facilities for separation and preparation of measurement samples. The second subsystem, cold laboratory analysis, will handle non-radioactive samples including potentially hazardous chemicals in solid, liquid or gaseous form. It contains analytic chemistry, water chemistry and some metallographic facilities for analysis of material samples from throughout the site. Both facilities operate on a sample basis. There are no direct process connections. The combination of both sub-systems allows characterisation of radioactive and/or hazardous waste prior to shipment off-site.

Both subsystems are designed to be available on demand such that no maintenance or operations activity will be delayed beyond the minimum practical sample processing time. Routine samples that may be safely contracted to outside laboratories will be routed to the off-site laboratories only if such action is cost effective and does not interfere with priority samples. All samples will be discarded to either radwaste or hazardous waste systems unless they qualify for unrestricted release.

II.8.2.7.2 Perimeter Security

A high security fence is provided around the perimeter of the buildings, structures and areas that are required to have controlled access. In addition to this high security area, the power supply areas are also maintained as high security for safety reasons, and accessed through locked gates and/or through the secured area.

II.8.2.7.3 Construction Services Facilities

II.8.2.7.3.1 Metrology Laboratory

This provides dimensional control of individual components, via conventional metrology instruments, and of the overall build of the tokamak using advanced 3D optical metrology systems (OMS). It is used to provide a stabilised environment for calibrating the OMS, which provides dimensional control during tokamak assembly as well as to prepare protocols and to secure data storage. It is required from the start of assembly (or earlier).

II.8.2.7.3.2 Metallurgy Laboratory

This is needed primarily to support welding operations, and to qualify procedures and operators. It also undertakes production testing of mechanical, chemical, metallographic, fractographic, and non-destructive examination, and prepares protocols and secures data storage. It is required from the start of assembly (or earlier).

II.8.2.7.3.3 Beryllium Analysis Laboratory

This is required to support the sampling and analysis of air and swab samples, and is required to be fully operational from the date of delivery of the first Be components.

II.8.2.7.3.4 Safety and Health Physics Laboratory

This is required primarily to support the non-destructive testing (radiography) of site welds. Site personnel safety training (industrial safety) may be required, depending on local regulations. It is required from the start of assembly (or earlier).

The required estimated footprints for each of these facilities are shown in the following table.

Table II.8-3 Construction Service Facilities

Title	Est. Area (m²)
Metrology Laboratory	300
Metallurgy Laboratory ¹	1000
Beryllium Analysis Laboratory	60
Safety and Health Physics Laboratory	125

1. Area includes 200 m² for NDE facilities

II.8.3 Plant Services

II.8.3.1 Introduction

Plant services includes essential steady-state electric power, cooling water, potable and fire water, sewage, gases, steam and demineralized water, analytical laboratories and others. Steady-state electrical services are described in II.8.3.5.

II.8.3.2 Service Water Systems

II.8.3.2.1 Potable and Fire Water

The potable water system supplies and distributes water for human needs (e.g. kitchens, lavatories, drinking fountains, etc.) throughout the ITER site. The system is sized to supply the needs of 1,000 people, or $\sim 300 \text{ m}^3\text{d}^{-1}$. Water is supplied from an off-site utility system, and the water quality meets biological standards for safe drinking water. The water is initially delivered to an on-site storage tank, which accommodates fluctuations in usage and/or temporary outages of the off-site supply. A site distribution system delivers the water under pressure to interface connections at each building distribution system. The system pressure is $\sim 0.8 \text{ MPa}$.

The fire protection water system maintains a pressurised, plant-wide system which can supply water on demand for fire fighting to installed hydrants and sprinkler mains connecting to each building. It is also capable of filling and delivering water through a separate backup piping network which is normally dry. The system maintains an on-site inventory of fire fighting water able to operate for 24 hours of continuous fire fighting. The maximum flow rate is $0.4 \text{ m}^3\text{s}^{-1}$ at a pressure of 1.3 MPa. These conditions can be met at any ten delivery points (hydrants and sprinkling mains) at one time. The system is capable of drawing water from other sources such as the cooling tower basins after fire fighting water is exhausted. The fire protection water system is part of the overall ITER fire protection design which includes fire detection, the ITER Fire Department, local installed dry chemical or CO₂ fire fighting systems, and portable fire extinguishers located throughout the plant.

II.8.3.2.2 Steam, Condensate, and Demineralized Water

The steam, condensate system supplies and distributes steam to components and systems (including HVAC) which require auxiliary heating. The system also collects and returns condensate to the steam boiler. Steam is generated by the oil (or gas) fired saturated boilers (with a rating of ~ 0.5 MPa) from high quality condensate return water. The total system capacity is estimated at $15,000 \text{ kg h}^{-1}$. Makeup water to this system is supplied from the demineralized water system. Steam is distributed to the client systems through a steam pipe network. This network will be designed to meet interfacing system requirements at the interface location. To reduce the total flow, it is assumed that the HVAC systems have their own condensers. After distribution and use, hot condensed water is cooled to $\leq 100^\circ\text{C}$ and collected in collection tanks and/or the condensate storage tank. From there, condensate is fed to the boiler unit to generate steam.

The demineralized water system supplies and distributes demineralized water for process purposes and makeup to cooling systems. The system capacity is approximately $200 \text{ m}^3\text{d}^{-1}$ at a nominal pressure of 1 MPa. The system uses raw or potable water as a feed and employs filtration, de-ionisation and de-aeration equipment to achieve water quality of $1.0 \mu\text{Mhcm}^{-1}$ with dissolved oxygen and chlorine concentrations less than 0.1 ppm.

II.8.3.2.3 Sanitary and Industrial Sewage

The sanitary and industrial sewage system collects, monitors, treats and releases sewage to an off-site utility sewage system. Both systems consist of gravity flow sewer line networks which transport sewage from buildings to pretreatment facilities and holdup tanks located outside the east side of the ITER site.

The sanitary sewage system has a total capacity determined by a site population in operation of 1,000 and includes fluids drained from lavatories, drinking fountains, kitchens, showers, laundry facilities and floors in rooms where these services are located. The sanitary sewage system is not connected to drains where the possibility of radioactive contamination exists. Such drains are served by the radioactive liquid drain system. Nevertheless, the sanitary sewage system has monitoring and holdup capabilities to prevent unpermitted contaminants from entering the off-site sewage system. If necessary, the sanitary sewage system has enough storage capacity to receive and store drainage for at least 15 days ($3,000 \text{ m}^3$ hold-up tank).

The ITER sanitary sewage will be discharged to an off-site receiver pipeline. Depending on the site selection, a range of sanitary sewage pretreatments may be imposed by the off-site sewage system. However, there is space allocated for a minimum pretreatment system, should it be required. It is assumed that the minimum pretreatment will consist of primary filtration. The principal components are: a screen filter, an aeration and equalising tank, a hold-up tank, an equalising tank and a transfer pump and line to the offsite sewage system. Macerating equipment could be substituted for the screens if they are not acceptable. To hold 15 days capacity of sanitary sewage, it is necessary to have an aeration unit with the hold-up tank and in order to accept a steady flow during this period, an equalising tank is also necessary.

The industrial sewage system has a capacity of $200 \text{ m}^3\text{d}^{-1}$ and includes remaining non-radioactive floor and equipment drainage where there is no expectation of biological waste. The industrial drainage also includes cooling tower blowdown. Activities within the ITER plant are

designed to provide a high level of assurance that sanitary drains are not contaminated with oils, chemicals, or metals and that industrial drains are not contaminated with biological waste. The industrial waste system has monitoring and holdup capabilities with capabilities to de-toxify and separate out contaminants prohibited by local utility sewers. The hold-up capacity of the industrial sewage system is 3,000 m³.

As in the case of the sanitary sewage system, the ITER industrial sewage will be discharged to an off-site receiver pipeline. Depending on the site selection, a range of pretreatment requirements may be imposed by the utility sewage system. The same accommodation is made for the industrial sewage system as for the sanitary sewage system: space is allocated for the minimum pretreatment system. It is assumed that the minimum pretreatment will consist of primary filtration and oil removal. The principal components are: an industrial drain tank, oil separation unit, a transfer pump and line to the offsite sewage system.

II.8.3.3 Gaseous Systems

II.8.3.3.1 Compressed Air

The compressed air system has two subsystems, the instrument air system and the service air system. The instrument air system supplies clean, oil-free and dry air for control valve actuators, power operators and pneumatic controllers. The service air system supplies undried, unfiltered air to air-powered tools, air-blast cleaning equipment and aeration equipment. Both instrument air and service air are supplied at a nominal pressure 690 kPa(g). The pressure was selected on the basis of supplying air to a pneumatic air cylinder designed for 552 kPa(g) plus suitable margin for compressor control and line losses.

Both instrument and service air are supplied by seven compressed air stations located at convenient locations within the site with each station serving several buildings. The interface point is at the building connection. The buildings themselves have their own distribution network. Estimates for the design capacities and principal buildings served by the seven air stations are given in Table II.8-4.

Each station employs three 100% capacity air compressors. The compressors are of the water-cooled, oil-free rotary screw type, driven by 250 kW motors for subsystems with 4,500 std m³h⁻¹ capacity and 120 kW motors for subsystems with 1,200 std m³h⁻¹ capacity. The air from the compressor feeds into three air receivers. Service air is delivered directly from the receivers. Instrument air from the receivers discharges into two 100% capacity air dryer units prior to distribution.

Each station connects to a dedicated distribution system constructed of stainless steel pipe or tubing. Diaphragm isolating valves are provided at various locations for maintenance. Pressure regulators to maintain pressures lower than 690 kPa are provided. Compressed air requirements that must be supplied continuously for pressures greater than about 700 kPa are supplied by compressed air bottles with regulators set to the desired pressure.

Table II.8-4 Compressed Air Station Capacities

Station	Buildings Served	Instrument Air Capacity std m ³ h ⁻¹	Service Air Capacity std m ³ h ⁻¹
1	Tokamak Building	4,050	450
2	Tritium Building	1,080	120
3	Hot Cell Building	1,080	120
4	Cryoplant Building	1,080	120
5	Emergency Power Supply Building	1,080	120
6	Auxiliary Buildings	4,050	450
7	Site Services Building	1,080	120

II.8.3.3.2 Breathing Air

Breathing air is supplied to selected ITER plant locations at a nominal pressure of 520 kPa(g) by a single, centralised system of compressors with a distribution system. The locations are those where radioactive and/or hazardous materials are present. The centralised concept is justified on an economic basis because it eliminates duplication of breathing air system components, and controls are minimised.

Breathing air is used by personnel wearing plastic suits and respirators when entering contaminated areas. With plastic suits, about 80% of the air is used for suit cooling while the other 20% is for breathing. The system is designed large enough to accommodate leakage and other losses of up to 5-10%. The system capacity is designed to meet the maximum breathing air requirement of work in at least two ITER plant buildings (tokamak and tritium building) at the same time. The total breathing air capacity is that for up to 70 persons in plastic suits at one time (an exceptional situation) and each suit needing 50 std m³h⁻¹ air flow.

The breathing air system consists of three oil-free compressors, two non-cycling refrigerated dryers operating in parallel, and three air receivers, located in the plant services building.

II.8.3.3.3 Nitrogen, Helium, and Special Gases

The total site gas demands are given below. The helium cryoplant and liquid nitrogen system will be sources of the distributed supply of helium and nitrogen. Special gases include SF₆ for high voltage electrical equipment such as the neutral beam injector power feeds and high voltage switchgear. Demand rates are approximated in Table II.8-5.

SF₆ systems include recovery and purification equipment. The remaining gases have small demand rates and are supplied from outdoor bottle stations near the client system equipment.

Table II.8-5 Nitrogen, Helium and Special Gas Demands

Gas	Supply Capacity	Purity Specification
Industrial Nitrogen	100,000 std m ³ /month (max.) 45,000 std m ³ /month (avg.)	< 0.1% impurity
Industrial Helium	20,000 std m ³ /month (max.) 10,000 std m ³ /month (avg.)	< 0.1% impurity
SF ₆	6,000 kg initial fill; makeup at 60 kg/month	Industrial grade
Ultra-Pure Nitrogen	5 std m ³ /month	Ultra-high purity
Ultra-Pure Helium	5 std m ³ /month	Ultra-high purity
Deuterium	5 std m ³ /month	Ultra-high purity
Hydrogen	25 std m ³ /month	Laboratory Grade
Argon	10 std m ³ /month	Laboratory Grade
Neon	10 std m ³ /month	Laboratory Grade

II.8.3.4 Tunnels and Bridges

The ITER site employs an underground tunnel and/or bridge system for distribution of high voltage power cables and signal cables. Further, tunnels carry the cooling water from the heat sink area to the tokamak building, and the cryogenic cooling from the cryoplant to and from the tokamak building. Bridges are used to carry the electric power from the MPSSNB to the tokamak building. Additional tunnels are established for personnel convenience and for control system access (between the control building and the assembly hall, and to the emergency control system in the emergency power building).

II.8.3.5 Steady-state Electrical Power Network

The steady-state electric power network (SSEPN) provides power to all ITER plant electric loads except the magnet and the heating and current drive system loads which are supplied by the pulsed power supply.

The SSEPN receives power from two independent transmission lines. Each of these two lines is capable of supplying the entire plant maximum steady state load. Power from the grid is provided at 220 kV. This voltage is supplied to two step-down transformers with 11 kV secondary voltage for distribution. Four distribution busbars at 11 kV are combined in two groups. The busbars of each group are supplied by the two transformers and could be connected, in case of failure, to one incoming transmission line. Lower voltage loads receive power through additional step-down transformers at 3.3 kV and 0.4 kV. The emergency power supply is based on diesel generators. The loads are segregated into several areas, each serviced by a load centre. Class I and II (uninterruptible DC and AC supplies respectively - see Table I.1.5-2) battery system power supplies are located throughout the ITER plant and are included in the systems that they supply.

Table II.8-6 Power Demand by Plant Subsystem

WBS	System	Connected load				Class IV Power consumption POS, kW	KlxKs avr*
		Total kW	Cl.2 kW	Cl.3 kW	Cl.4 kW		
1.1	Magnet	45	45	45	0	43	1
1.5	Vacuum Vessel	6	6	6	0	6	1
1.6	Blanket	6	6	6	0	6	1
1.7	Divertor	3	3	3	0	3	1
2.3	Remote Handling Equipment	2999	165	281	2718	80	0.03
2.4	Cryostat	10	10	10	0	10	1
2.6	Cooling Water	46269	133	2311	43958	35736	0.77
2.7	Thermal Shields	13	2	13	0	13	1
3.1	Vacuum Pumping and Fuelling	1319	132	362	957	885	0.67
3.2	Tritium Plant and Detritiation	2074	32	1138	937	1730	0.83
3.4	Cryoplant and Cryodistribution	33866	21	21	33845	26674	0.79
4.1	Pulsed & Steady-state Power Supplies	1679	502	704	975	1214	0.72
4.5	Central Control, Data Acquisition, Interlock and Alarm	151	151	151	0	147	1
5.1	Ion Cyclotron H&CD	2837	37	37	2800	1754	0.62
5.2	Electron Cyclotron H&CD	582	38	38	544	355	0.61
5.3	Neutral Beam H&CD	21	21	21	0	20	1
5.4	Low Hybrid H&CD	229	33	33	196	175	0.76
5.5	Diagnostics	2000	400	400	1600	2000	1
5.6	Test Blankets	17	17	17	0	17	1
6.2	Buildings and Layout	12179	225	1365	10814	4217	0.35
6.3	Hot Cells and Waste Processing	1114	4	4	1110	393	0.35
6.4	Radiological & Environmental Monitoring	328	9	126	203	248	0.75
6.5	Liquid and Gas Distribution	2759	0	1001	1758	2070	0.75
Total		110507	1993	8094	102413	77796	0.70

*Load (demand) factor (Kl) is the ratio, expressed as a numerical value or as a percentage, of the maximum demand of an installation or a group of installations within a specified period, to the corresponding total installed load of installation(s).

Coincidence (simultaneous) factor (Ks) is the ratio, expressed as a numerical value or as a percentage, of the simultaneous maximum demand of a group of electrical appliances or consumers within a specified period, to the sum of their individual maximum demands within the same period.

Kl x Ks avr is the product of the load factor (Kl) and the coincidence factor (Ks) averaged per system.

The SSEPN distinguishes the real maximum power consumed by the plant from the total connected load. The total active power demand from the HV grid has been estimated considering the uncertainty and the growth factors. This assessment has allowed a substantial reduction of the site requirements for continuous power to 120 MW. The total load of the emergency diesel generators is about 6 MW, also including some margins for power uncertainty and future growth.

The SSEPN is divided into three subsystems: the steady-state electrical switchyard (SSES), the emergency power supply (EPS) and the steady-state electrical distribution system (SSEDs). The outline design of these subsystems leads to the loads described¹ in Table II.8-6.

II.8.4 Conclusions

II.8.4.1 Space Utilisation

The upper area of the tokamak hall is generally an “open-plan” arrangement, which provides space for equipment laydown, access preparation, maintenance, and other operational activities. This area is especially useful as it is almost all serviceable by the crane, and during construction and during assembly of in-vessel components. Current information concerning the NB cell power supplies and the bioshield roof does not allow for this open plan to be all at the same elevation, which would be even more convenient. However, attaining this feature is currently under study. Closing in this area of the tokamak hall, and incorporating the newly enclosed room into the vault volume would provide additional volume into which the steam from a LOCA could expand, which would also reduce the resulting over-pressure and, hence, reduce the potential stress on the structure.

There is not much space available within the tokamak building for routing of services and essential feeds to the magnet, such as waveguides, cryolines, vacuum lines, power and signal lines, HVAC ducts, cooling and chilled water lines, diagnostic lines, etc. This space limitation is mainly in, but not restricted to, the vertical direction dictated by VV port orientation.

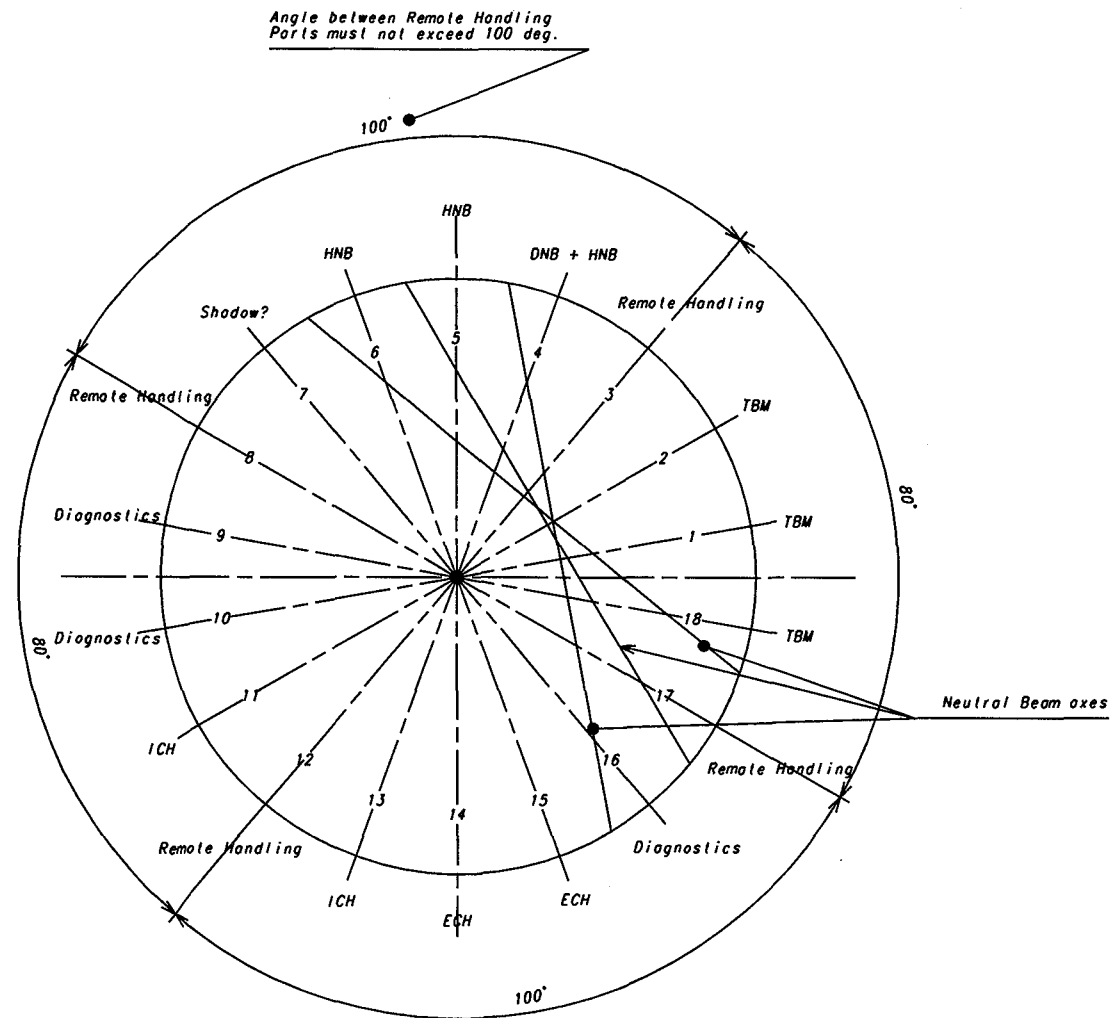
II.8.4.2 Future Work

A number of future actions are summarised below:

- detailed study of space that must be allowed for passage of services such as electrical power, cooling water, and movement of personnel and materials - access must be available for all phases of the project, including construction, operation, maintenance, and decommissioning;
- continuing study on the dual use of buildings, especially in the area of the assembly hall and RF heating;
- development of details of building operation, including HVAC and air flow parameters in each controlled zone, and other safety implications (such as safety escape routes), etc.;
- investigation into the allowable allocations of penetrations into the tokamak building;
- study on the bioshield roof to minimise height and maximise flexibility;
- study on crane tooling (with a crane supplier) to allow for the use of vertical space between the two cranes, to further minimise building height requirements;

¹ N 43 RI 4 99-11-30 W0.1 Britousov. “Steady State Electrical Power Network: Preliminary Design for ITER-FEAT”, Issue 1, 30 November 1999

- confirm design parameters for LOCAs, with and without baking;
- combine the tritium building and the tokamak building onto the same seismically qualified basemat;
- confirmation of dimensional and equipment layout aspects of the all of the buildings;
- detailed layout of the tunnels and bridges on the site;
- study of a one-level tokamak crane hall open concept;
- study of the requirements for a diagnostic hall on the west side of the tokamak building.



Equatorial Port Allocation

TITLE *ITER-FEAT EQUATORIAL PORT ALLOCATION*

DATE *15-NOV-99*

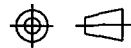
WORK BREAKDOWN STRUCTURE *1.0*

W.B.S. TITLE

Tokamak Basic Machine

DO NOT TAKE MEASUREMENTS
USE ONLY DIMENSIONS GIVEN

THIRD ANGLE
PROJECTION



BASELINE VERSION

1.A.M.-

DRAWING NUMBER

1.0007.2000.1

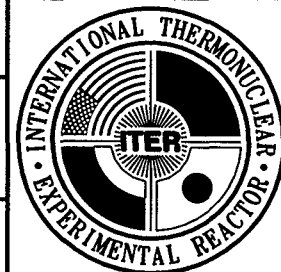
ITER-EDA

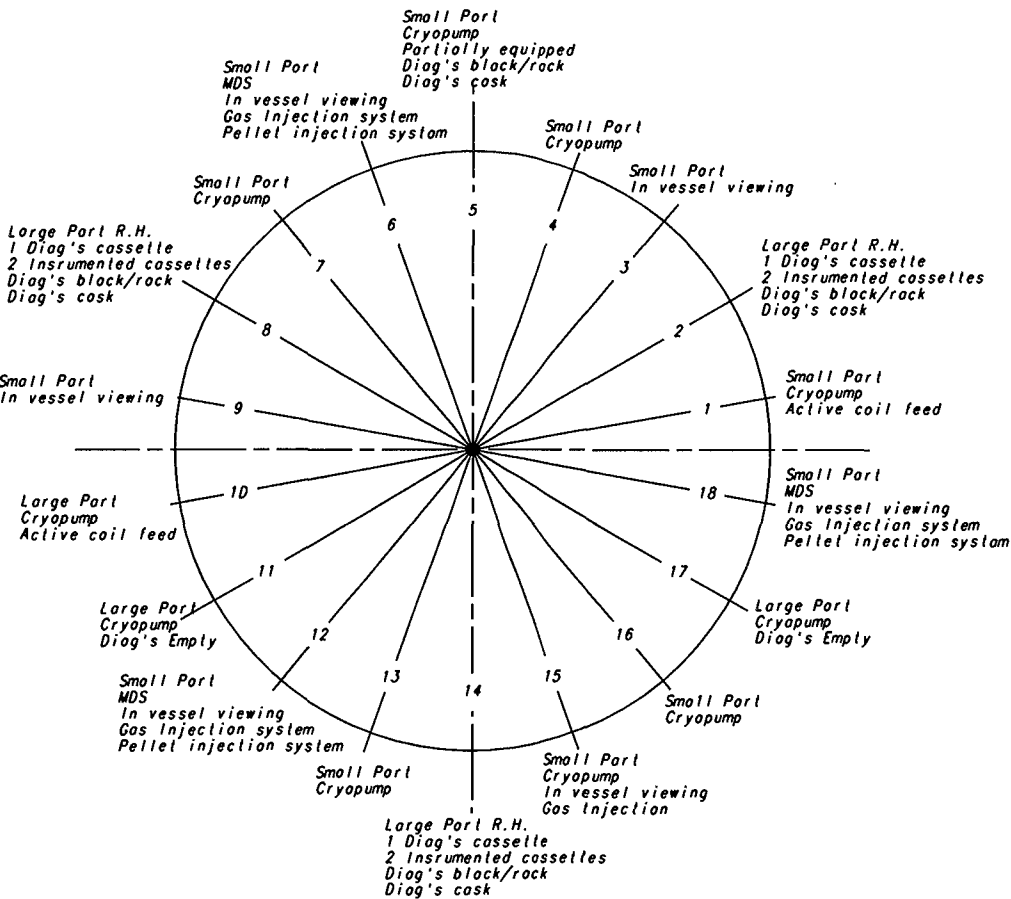
NOT FOR PUBLICATION

The information on this drawing is confidential under the terms of the ITER EDA agreement. This information shall not be transmitted to anyone who is not authorised to receive it

OBJECT TYP FORMAL REV WORKING REV STATUS

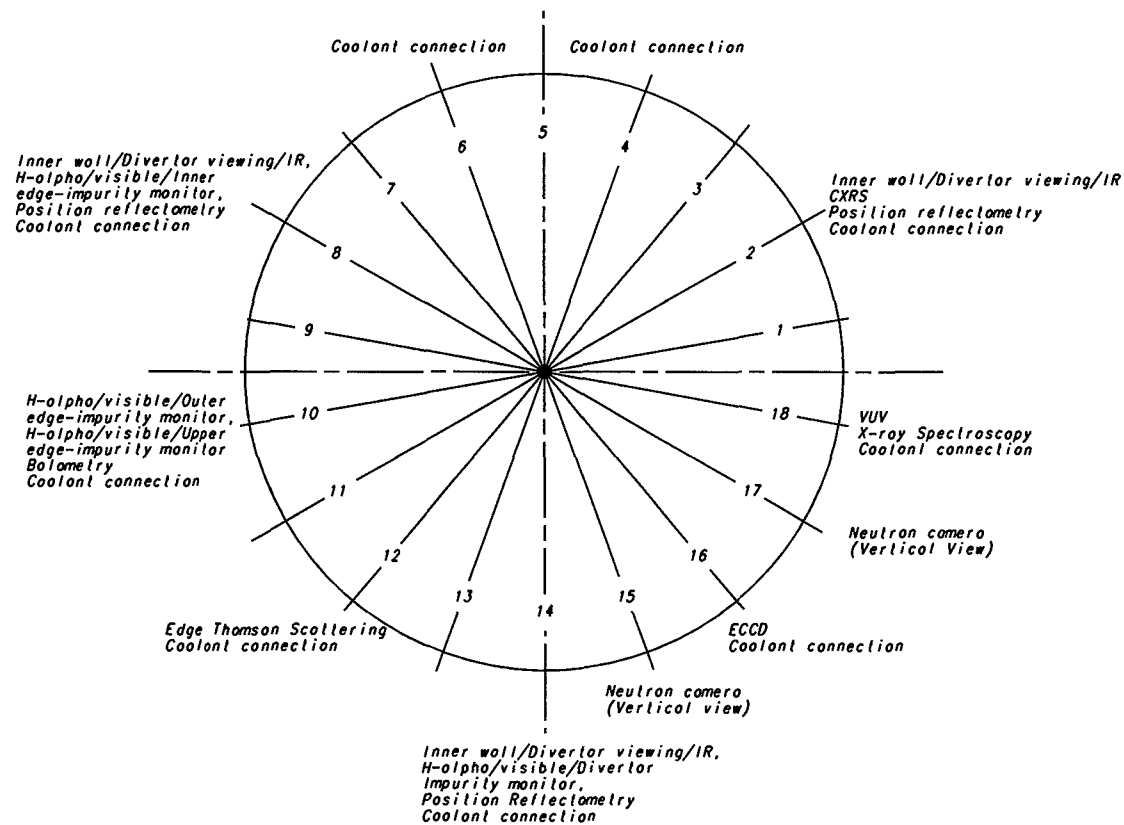
2.D 0.0 0.1 W





Divertor level Port Allocation

TITLE ITER-FEAT DIVERTOR LEVEL PORT ALLOCATION		DRG FRAME SIZE 420 x 297		ITER-EDA NOT FOR PUBLICATION The information on this drawing is confidential under the terms of the ITER EDA agreement. This information shall not be transmitted to anyone who is not authorised to receive it.				
DATE 15-NOV-99		WORK BREAKDOWN STRUCTURE 1.0					DRAWN D.O CHK'D D.O.M. MAM GDC GDC	
W.B.S. TITLE Tokamak Basic Machine		NAME OF ORGANISATION NAKA JWS					RESP. ENGR JWS CHK'D RESP. OFFR MAM --- RAR	
DO NOT TAKE MEASUREMENTS USE ONLY DIMENSIONS GIVEN		THIRD ANGLE PROJECTION					BASELINE VERSION I.A.M.-	
		DRAWING NUMBER 1.000.7.30.00.1		OBJECT TYP 2.D		FORMAL REV 0.00		
				WORKING REV 0.1		STATUS W		

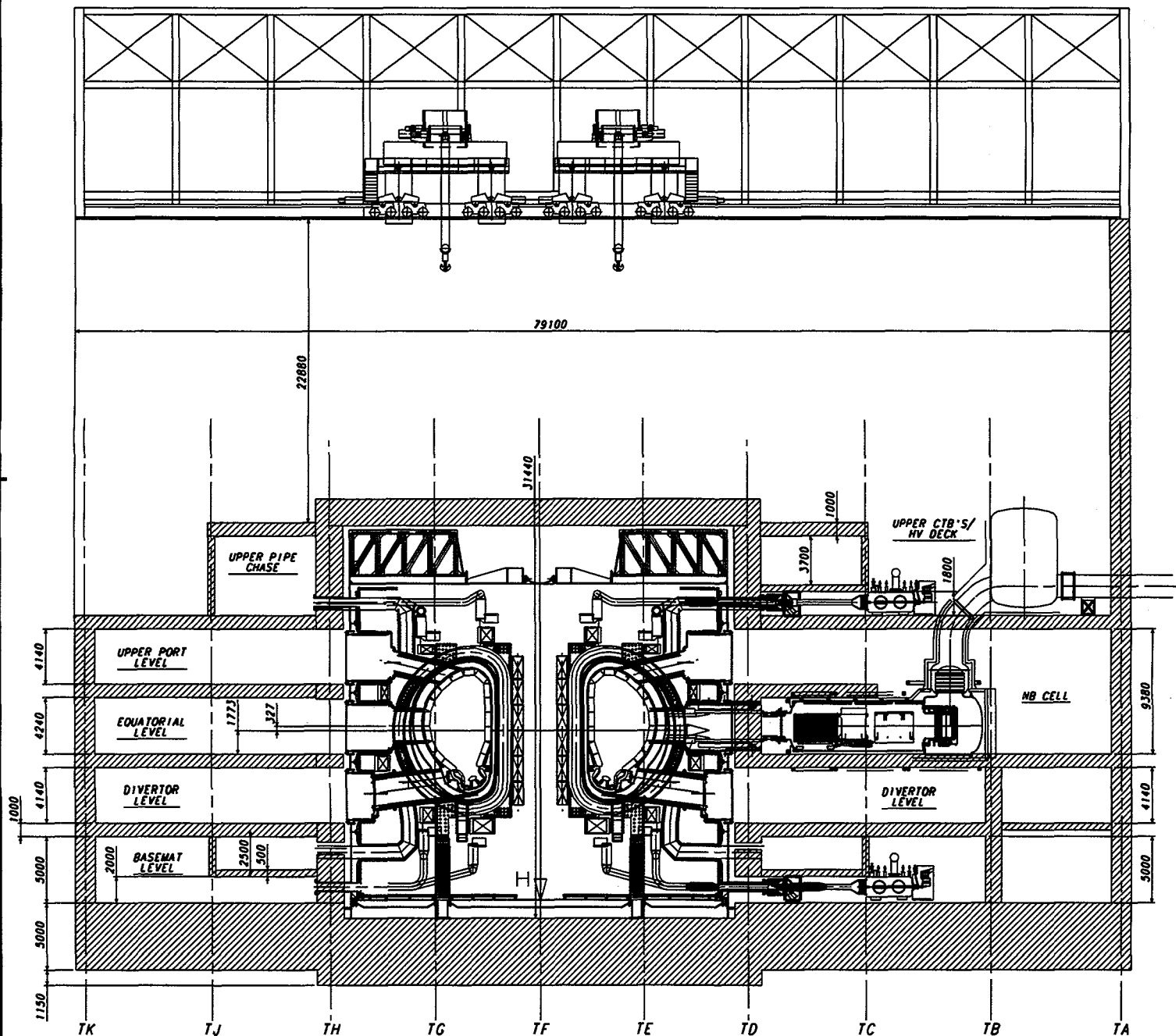


Upper Port Allocation

TITLE UPPER PORT ALLOCATION		DRG FRAME SIZE 420 x 297		ITER-EDA NOT FOR PUBLICATION The information on this drawing is confidential under the terms of the ITER EDA agreement. This information shall not be transmitted to anyone who is not authorised to receive it.			
		DRAWN D.O. CHK'D D.O.M.					
		MAM GDC GDC					
		RESP. ENGR JWS CHK'D RESP. OFFR					
DATE 19-NOV-99	WORK BREAKDOWN STRUCTURE 1.0	MAM --- RAR	NAME OF ORGANISATION				
	W.B.S. TITLE Tokamak Basic Machine	NAKA JWS					
DO NOT TAKE MEASUREMENTS USE ONLY DIMENSIONS GIVEN	THIRD ANGLE PROJECTION	BASELINE VERSION 1.A.M.-	DRAWING NUMBER 1.000.740.00.1	OBJECT TYP 2.D	FORMAL REV 0.0	WORKING REV 0.1	
				STATUS W			

V

355

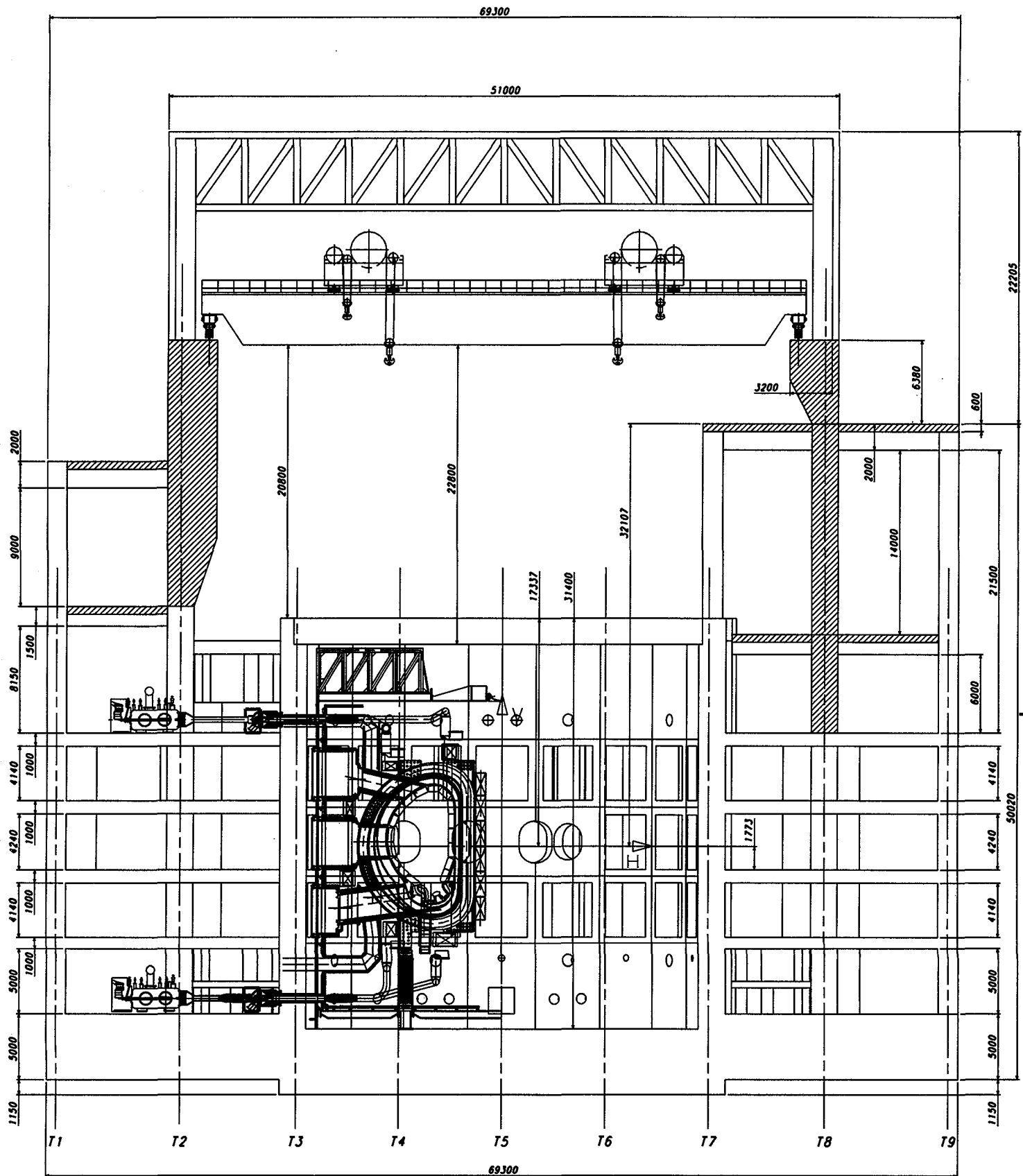


ITER-FEAT
TOKAMAK BUILDING
EQUIPMENT LAYOUT
NORTH-SOUTH SECTION
11-11-99

0 1000 5000 10000		ITER-Feat	
TITLE: ITER-FEAT TOKAMAK BUILDING EQUIPMENT LAYOUT NORTH SOUTH SECT'N		ITER-Feat	
DATE: 15-NOV-99	WORK DESCRIPTION: STRUCTURE 2.1	ITER-Feat	
D.S. TITLE: Machine Layout (Layout in Pit and G)		ITER-Feat	
DRAWN BY: NAKA JWS		ITER-Feat	
CHECKED BY: NAKA JWS		ITER-Feat	
NO NOT TAKE MEASUREMENTS USE ONLY DIMENSIONS GIVEN		ITER-Feat	
THIRD ANGLE PROJECTION		ITER-Feat	
I.A.M.-2100290001		ITER-Feat	
200001W		ITER-Feat	

356

DIMENSIONS RELATE TO ROOM TEMPERATURE (293K)



ITER-FEAT
TOKAMAK BUILDING
EQUIPMENT LAYOUT
EAST-WEST SECTION

11-11-99

0 1000 5000 10000

ITER-1M2 TOKAMAK BUILDING
EQUIPMENT LAYOUT EAST WEST SECTION

DATE 15-NOV-99

WORK DESCRIPTION STRUCTURE 2.1

P.E.S. TITLE Machine Layout (Layout in P11 and C)

DO NOT TAKE MEASUREMENTS
USE ONLY DIMENSIONS GIVEN

THIRD ANGLE PROJECTION

ITER-EDA

NOT FOR PUBLICATION

Any description on this drawing is subordinate
to the name of the ITER EDA system.
Any description must be in accordance with the
name of the ITER EDA system.

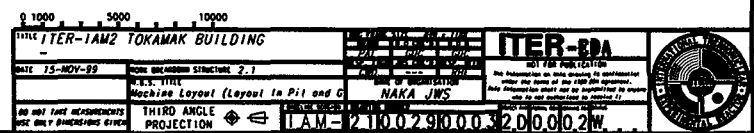
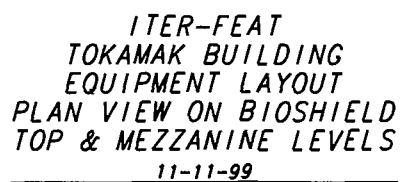
NAKA JWS

LAM-2100290002200002W

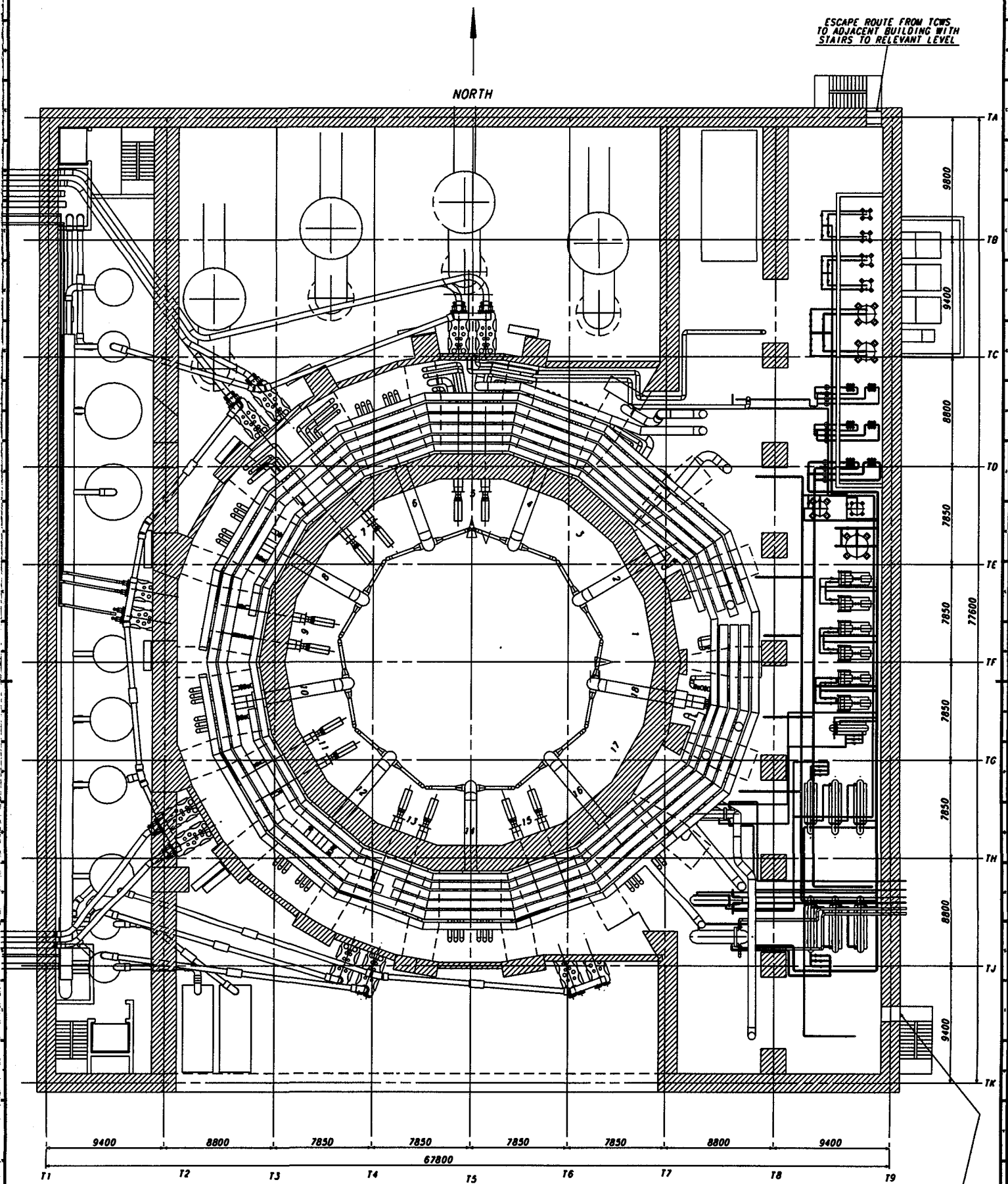
357



NORTH



DIMENSIONS RELATE TO ROOM TEMPERATURE (293K)

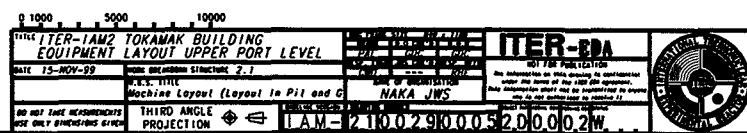


ITER-FEAT
TOKAMAK BUILDING
EQUIPMENT LAYOUT
TCWS LEVEL

11-11-99

[illegible]

NORTH



NORTH

ESCAPE ROUTE

ESCAPE ROUTE FROM
TCMS LEVEL


**ESCAPE ROUTE TO
ADJACENT BUILDING**

ESCAPE ROUTE

ESCAPE ROUTE
TO OUTSIDE

**ESCAPE ROUTE FROM
TCWS LEVEL TO GROUND**

11-11-99

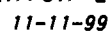
0 1000 3000 10000	
TITLE ITER-1AM2 TOKAMAK BUILDING EQUIPMENT LAYOUT EQUATORIAL LEVEL	
DATE 15-NOV-99	ENGINE ORIGINATOR STRUCTURE 2.1
	U.S. TITLE Machine Layout (Layout in Pil on
DO NOT TAKE MEASUREMENTS USE ONLY DIMENSIONS GIVEN	THIRD ANGLE PROJECTION  I AM

The photograph shows a document with a grid of numbers and text. The grid contains numbers like 2100290006 and 200002W. Text includes 'ITER-800', 'NOT FOR PUBLICATION', and 'NAKA JWS'.



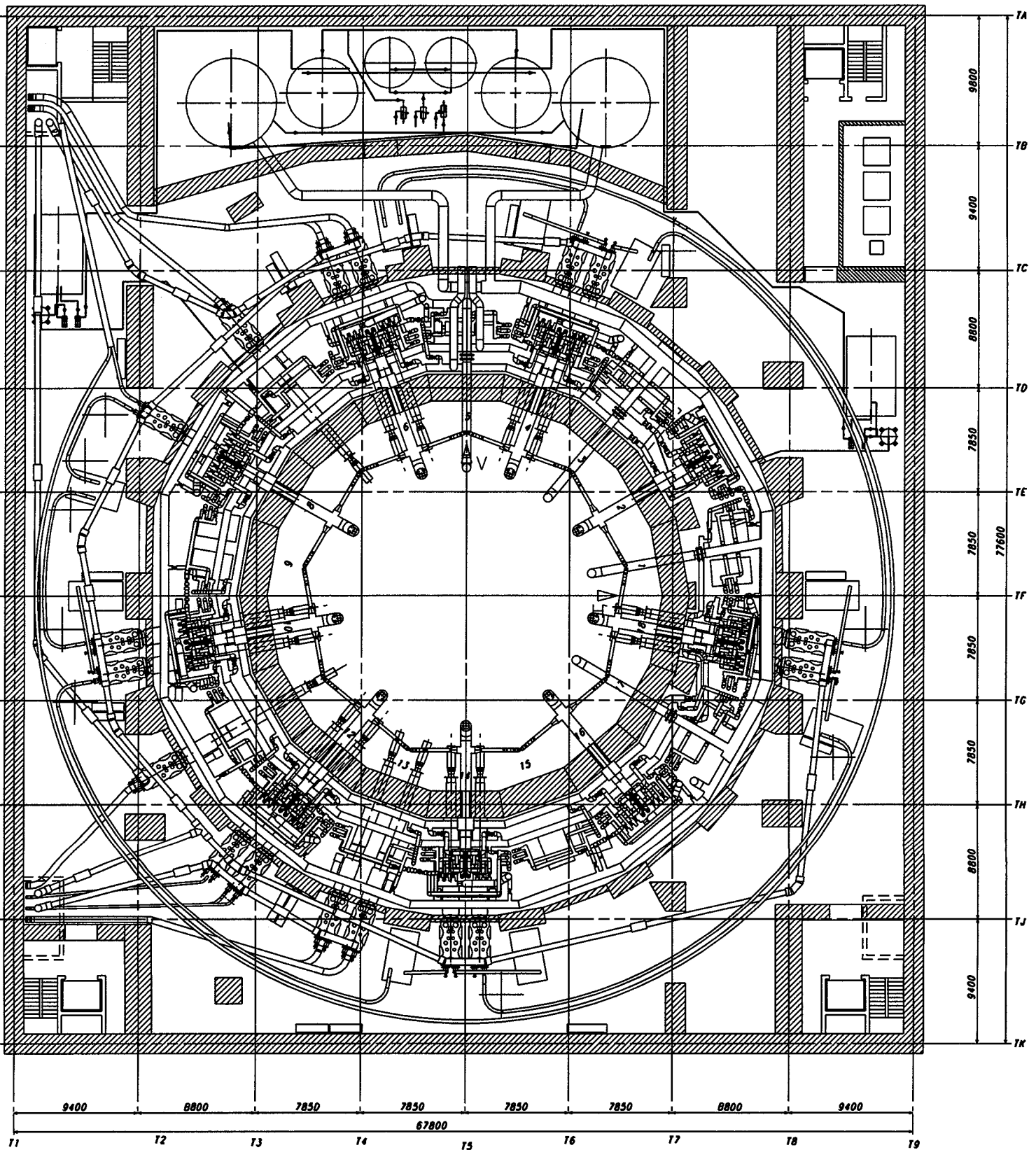
36

NORTH

[illegible]

DIMENSIONS RELATE TO ROOM TEMPERATURE (293K)

NORTH



ITER-FEAT
TOKAMAK BUILDING
EQUIPMENT LAYOUT
BASEMAT LEVEL
11-11-99

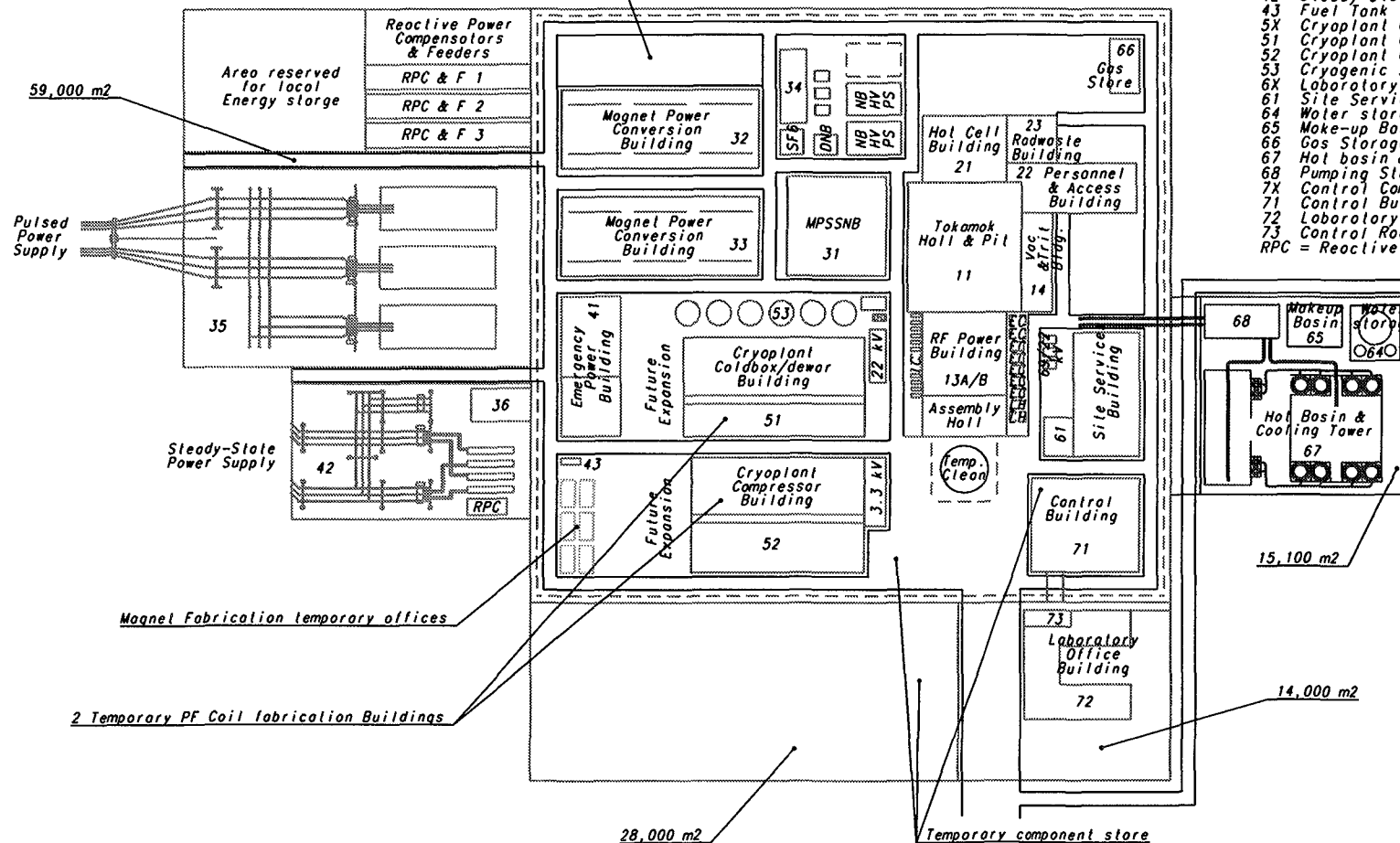
0 1000 5000 10000		ITER-Feat	
TITLE: ITER-Feat TOKAMAK BUILDING EQUIPMENT LAYOUT BASEMAT LEVEL		ITER-Feat	
DATE: 11-NOV-99		NOT FOR CONSTRUCTION	
ROOM: ONE AND TWO STRUCTURE 2.1		NAKA JWS	
P.E. TITLE: Machine Layout (Layout in Pit and C)		ITER-Feat	
DO NOT TAKE MEASUREMENTS USE ONLY DIMENSIONS GIVEN		THIRD ANGLE PROJECTION	
TAM-2100290008200002W		363	

301

KEY TO TOKAMAK BUILDINGS, AREAS & ACRONYMS

- 1X Tokamak Complex
- 11 Tokamak Hall & Pit
- 13 Assembly Hall/RF Power Building
- 14 Tritium & Vacuum Building
- 2X Hot Cell & Radwaste Complex
- 21 Hot Cell Building
- 22 Personnel & Access Building
- 23 Radwaste Building
- 3X Pulsed Power Supply Complex
- 31 Magnet Power Supply Switching Network Building
- 32 North Magnet Power Conversion Building
- 33 South Magnet Power Conversion Building
- 34 NBI Power Supply Switchgear Building
- 35 Pulsed Power Supply Switchgear Area
- 36 AC Distribution Building
- 4X Steady-State Power Supply Complex
- 41 Emergency Power Supply Building
- 42 Steady-State Power Supply switchgear Area
- 43 Fuel Tank
- 5X Cryoplant Complex
- 51 Cryoplant Coldbox / Dewar Building/PF Coil Fabrication
- 52 Cryoplant Compressor Building/PF Coil fabrication
- 53 Cryogenic Storage Tanks
- 6X Laboratory Support Complex
- 61 Site Services Building
- 64 Water storage
- 65 Make-up Basin
- 66 Gas Storage
- 67 Hot basin & Cooling Tower
- 68 Pumping Station
- 7X Control Complex
- 71 Control Building
- 72 Laboratory Office Building
- 73 Control Room & Vehicle Entry Perimeter Gatehouse
- RPC = Reactive Power Compensators

High Security area 141,000 m2



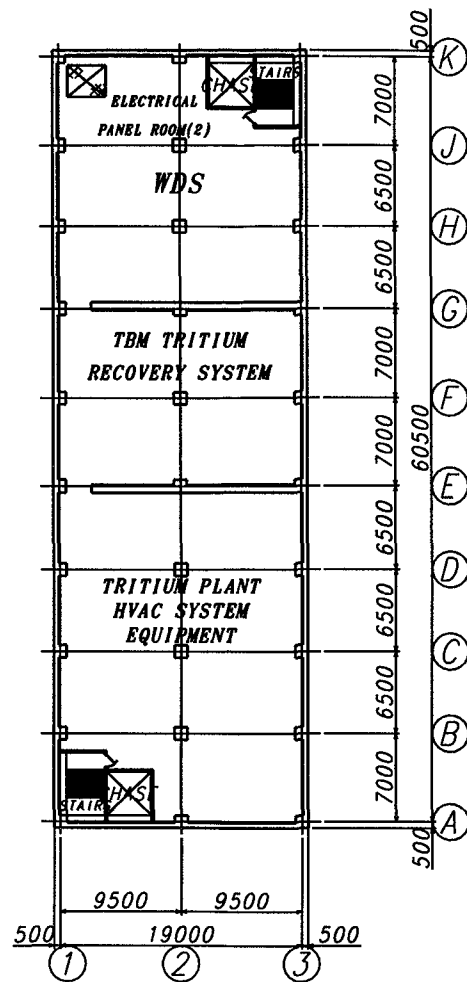
Compulsory area = 242,000 m2
Total area = 257,100 m2

0 10m 50m 100m

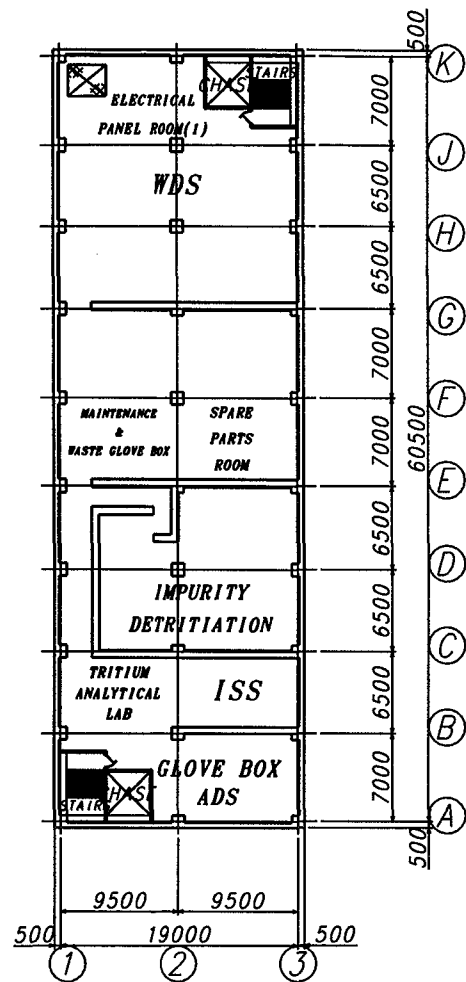
TITLE ITER-EDA SITE LAYOUT		ITER-EDA	
DATE 15-NOV-89	SCALE 1:1000	ITER-EDA	
NAME OF ORGANIZATION NAKA JWS	PROJECT NUMBER 16.110.0.0.210.0.0.12.D10.01W	ITER-EDA	
THIRD ANGLE PROJECTION	ITER-EDA		



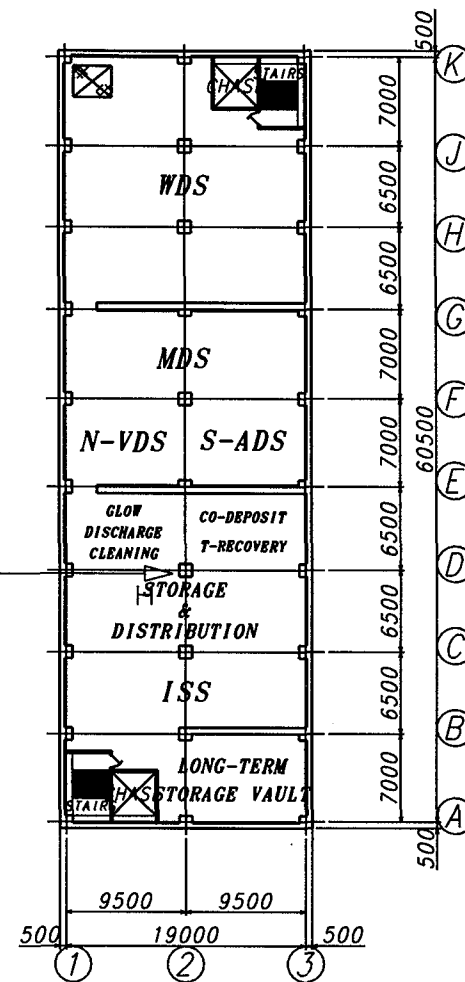
DIMENSIONS RELATE TO ROOM TEMPERATURE (293K)



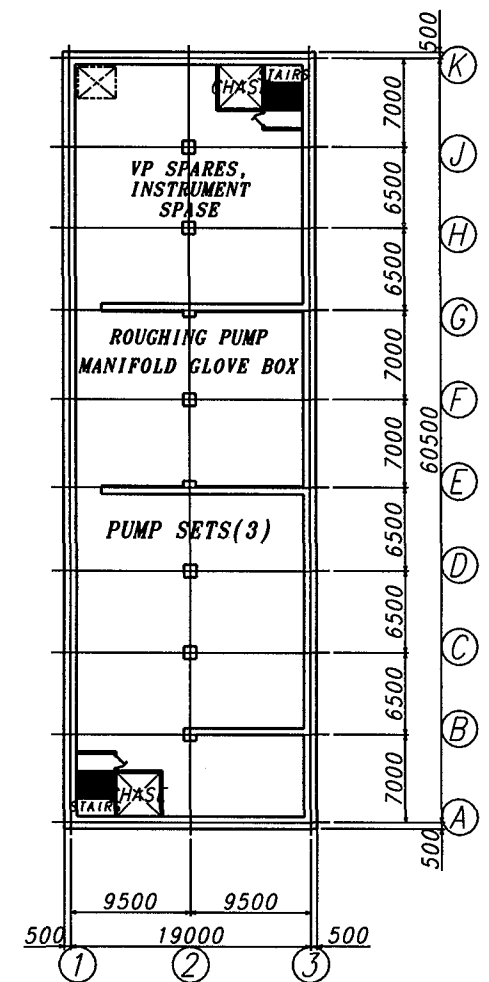
GL 14.2M



GL 7.2M



GL 0.2M

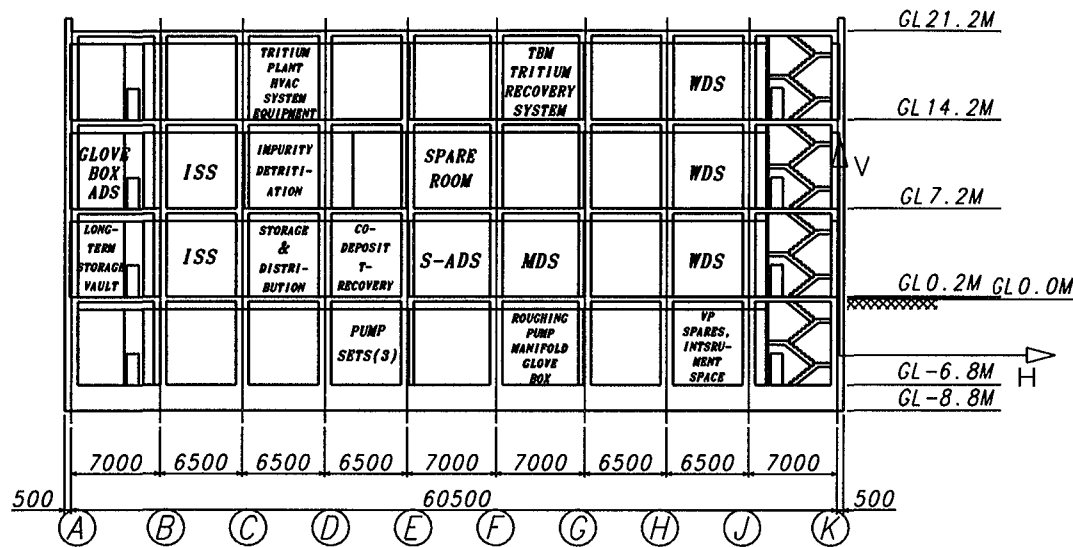


GL -6.8M

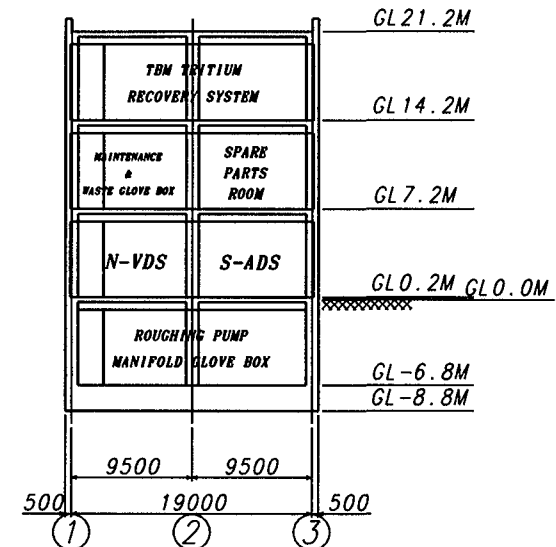
THE GENERAL ARRANGEMENT IN THE TRITIUM BUILDING
(PLAN VIEW)

THE GENERAL ARRANGEMENT IN THE TRITIUM BUILDING (PLAN VIEW)		ITER-BDA	
DATE: 17-NOV-99	ROOM: GROUND STRUCTURE 6.2.A.02	NOT FOR PUBLICATION	
P.S. TITLE: Tritium Building		No alterations to this drawing, its content or the data of any part of the equipment shall be made without the approval of the design office.	
DRAWN BY: NAKA JWS		No alterations to this drawing, its content or the data of any part of the equipment shall be made without the approval of the design office.	
THIRD ANGLE PROJECTION		TAM-6203340001200002W	

DIMENSIONS RELATE TO ROOM TEMPERATURE (293K)



NORTH-SOUTH SECTION



EAST-WEST SECTION

THE GENERAL ARRANGEMENT IN THE TRITIUM BUILDING
(ELEVATION)

TITLE THE GENERAL ARRANGEMENT IN THE TRITIUM BUILDING(ELEVATION)		ITER-EDA	
DATE 17-NOV-99	BOOK OREANSOM STRUCTURE 6.2.A.02	NOT FOR PUBLICATION	
P.E.S. TITLE Tritium Building		UNDER THE NAME OF THE ITER CONVENTION	
DATE OF ORIGIN 1999		ITER-EDA	
DO NOT TAKE MEASUREMENTS		THIRD ANGLE PROJECTION	
USE ONLY DIMENSIONS GIVEN		ITER-EDA	
ITER-EDA		ITER-EDA	

II.9 Initial Assembly

II.9.1	Introduction	1
II.9.2	Assembly Plan	1
II.9.2.1	Strategies	1
II.9.2.1.1	Strategy to Meet the Tolerance Requirements	1
II.9.2.1.2	Building Utilisation	3
II.9.2.2	Overall Assembly Sequence	4
II.9.2.3	Implications of the Design of the TF to VV Supports	8
II.9.3	Tooling and Facilities	8
II.9.4	Conclusions and Future Work	9

II.9.1 Introduction

The main issue for the assembly of the ITER tokamak is the tight installation tolerances required for the major components, considering the large size and weight of the components. To achieve the specified tolerances, the assembly plan must follow sequences and processes which minimise both deviations and the residual stresses in the components, and which allow for the correction of any deviations as they occur so that there is no need for subsequent corrective actions.

For the tokamak, therefore, specific assembly procedures and tooling must be developed. This is not the case for other parts of the plant, where conventional construction operations are foreseen. The overall assembly plan must also minimise the associated duration and cost.

II.9.2 Assembly Plan

II.9.2.1 Strategies

II.9.2.1.1 Strategy to Meet the Tolerance Requirements

With the alignment tolerances close to the limit of what is achievable, the accumulation of deviations is not acceptable. The assembly plan is therefore designed to correct alignment deviations at each step of the assembly sequence. This strategy relies on linking a sophisticated optical metrology system (OMS) to a CAD system, which can generate and analyse complex 3D models in near-real time, to provide a complete, evolutionary database of the as-built components. With respect to the major components, it is essential that most geometrical interfaces have the provision for adjustment (probably shimming) included in their design.

The strategy for controlling the dimensions of the tokamak build is illustrated in Figure II.9-1. Component installation will be preceded by a comprehensive survey of the tokamak pit; a best-fitting process will then be used to define the "tokamak assembly datum" (see Figure II.9-1) with respect to the as-built pit geometry. Prior to completion of the TF magnet, the large components will each be independently aligned with respect to these datums. In principle, the datums will be fixed for the duration of this part of the assembly, although, in practice, it may be advantageous to progressively modify these datums, as the assembly of the TF magnet would then proceed via a process of best-fitting (adjusting) of the datums to the as-built geometry of the TF magnet.

N 22 GR 1 99-12-06 F 3

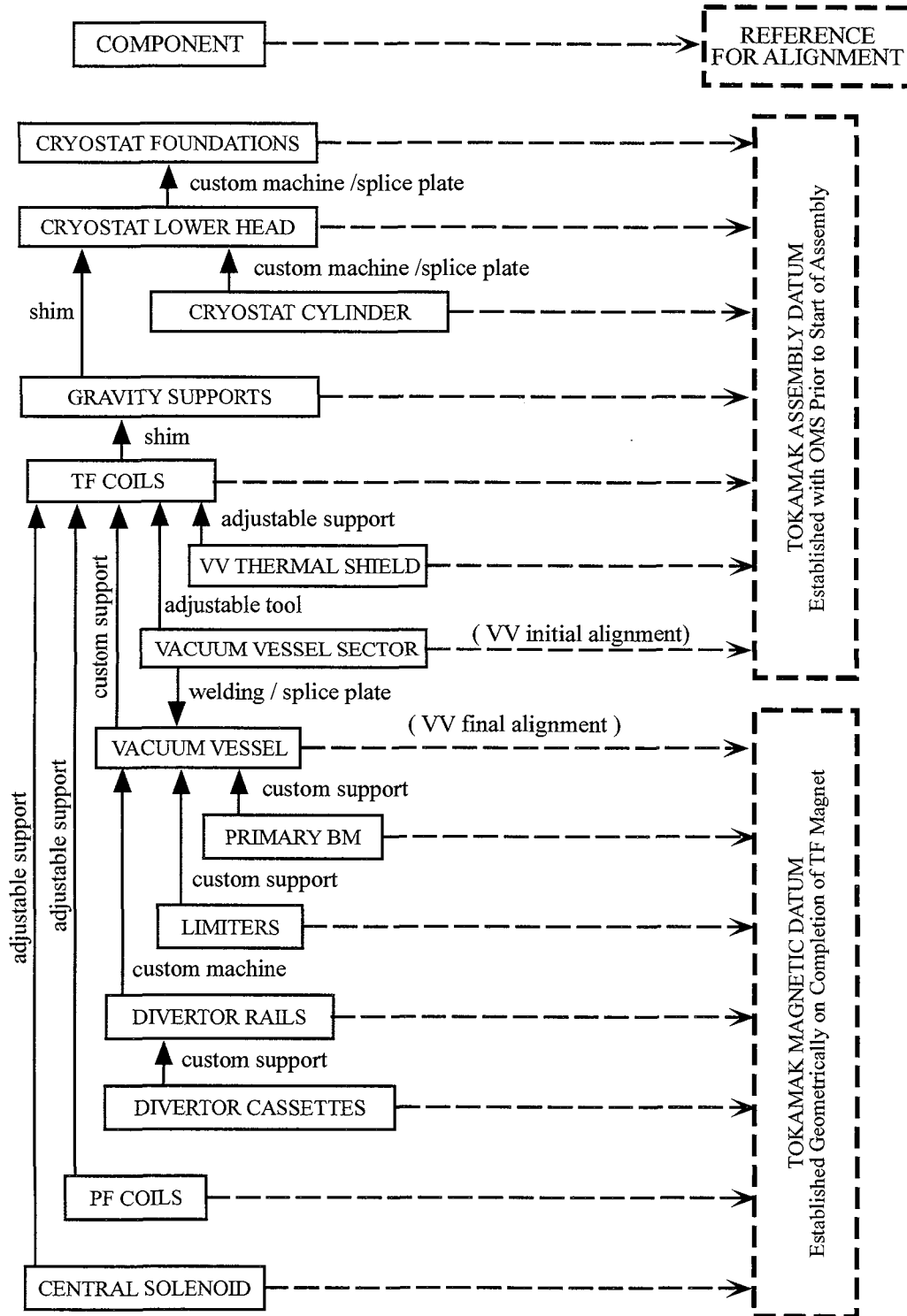


Figure II.9-1 Tokamak Alignment Strategy

On completion of the assembly of the TF magnet, a comprehensive survey of the TF coils will be combined with manufacturing dimensional control data to provide a geometrical estimate of the magnetic axis of the machine; this is referred to by the term "tokamak magnetic datum" in Figure II.9-1. Subsequent alignment operations, primarily on the components which are tightly toleranced, will be carried out relative to the tokamak magnetic datum.

Figure II.9-1 also identifies the proposed method of adjusting the component interfaces at each assembly step.

II.9.2.1.2 Building Utilisation

The assembly processes in the assembly hall are aimed at obtaining the maximum utility from the available layout.

A temporary area will be established outside the south end of the building complex (see Figure II.9-2) in which the large components will be cleaned before entry into the assembly hall. The routing of the components into and through the assembly hall will conform to the following basic plan.

Initial assembly phase:

- the sub-assembly tooling and workstations for the VV thermal shields (VVTs), TF coils and VV are cleaned, installed and tested in the assembly hall;
- the cryostat foundations, base sections and cylinder, and the lower, trapped PF coils, PF5 and PF6, are cleaned, and then prepared in the laydown area prior to installation in the pit (this may require lifting these components over the sub-assembly tooling and work stations).

This strategy will allow the TF/VV/VVTs sub-assembly operations to begin in parallel with the lower cryostat activities, see Figure II.9-3, thereby advancing the start of installation of the TF/VV/VVTs sectors in the pit.

TF, VV, and in-vessel components:

- the VV sectors, VVTs sectors and TF coils are cleaned, prepared, sub-assembled and controlled in the assembly hall;
- the blanket modules, divertor cassettes and other in-vessel components are cleaned, prepared and controlled in the hot cell, located to the north of the tokamak hall.

N 22 GR 2 99-11-22 F 2

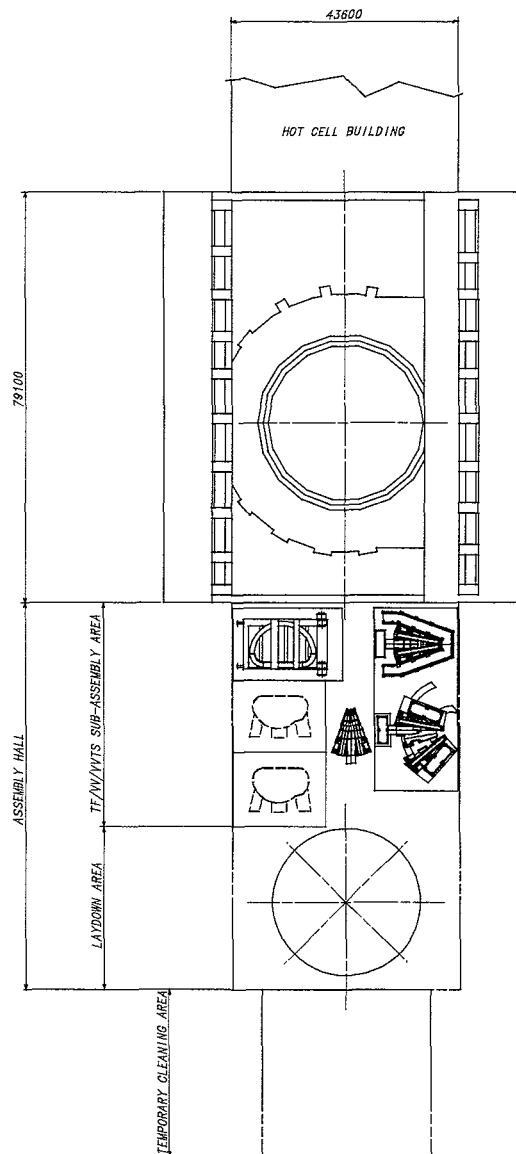


Figure II.9-2 Building Utilization for Machine Assembly

II.9.2.2 Overall Assembly Sequence

An outline procedure has been developed for the tokamak assembly, as the basis for determining the assembly schedule, manpower and tooling requirements and the associated cost. A high level summary of this procedure is provided by the logic diagram, Figure II.9-3. The overall sequence is divided into the following six main sub-sections:

- 2.2.A.1 Lower cryostat activities: the sub-section includes the assembly procedures for the bottom of the cryostat, the gravity supports, and the lower PF coils. This section covers activities from the initial assembly in this area up to the placement of the first TF/VV/VVTS sector;

- 2.2.A.2 TF/VV/VVTS sub-assembly: includes installation of the VVTS workstations, the upending tool, the TF/VV/VVTS sector sub-assembly jig, and the sector completion tool, in addition to the procedures necessary to sub-assemble each of the nine sectors. Each sector includes a pair of TF coils, a 40° segment of the VV and three VVTS parts, an inboard 40° sector and two outboard, opposite hand 20° sectors. The sub-assembly procedure is illustrated diagrammatically in Figure II.9-4;
- 2.2.A.3 Integrated TF/VV/VVTS assembly: covers the sequencing of the TF/VV/VVTS assembly in the cryostat;
- 2.2.A.4 Establish magnetic axis: this section includes the survey procedures by which the tokamak magnetic datum is geometrically established;
- 2.2.A.5 Ex-vessel activities: includes all assembly procedures for the components and systems external to the VV and ports, from the establishment of the magnetic datum to the preparation for commissioning. These activities occur in parallel with the in-vessel assembly procedures;
- 2.2.A.6 In-vessel activities: includes the welding of the final VV field joints (toroidal closure), and all assembly procedures specific to the VV and port internals, up to the preparation for commissioning.

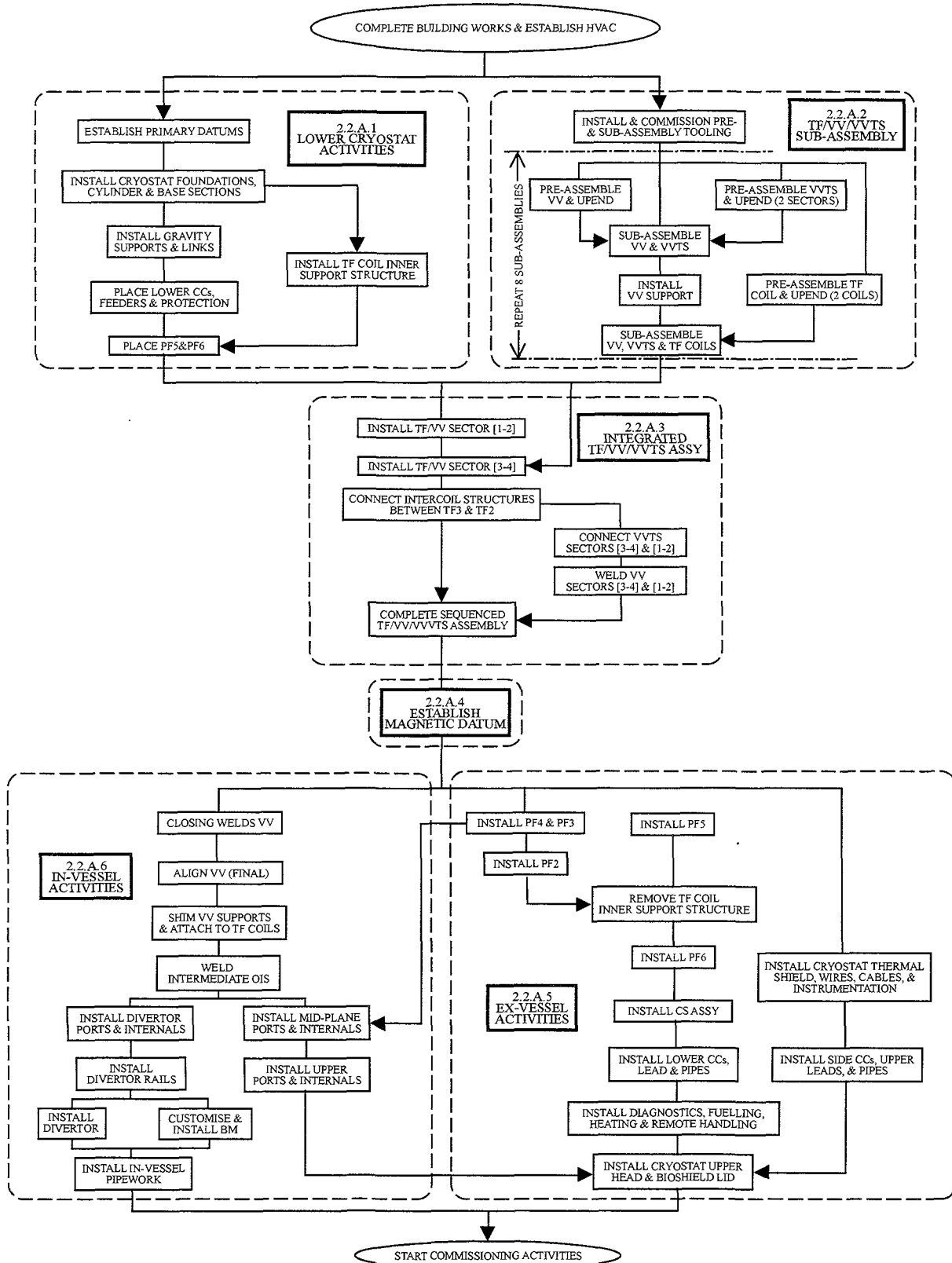


Figure II.9-3 Tokamak Assembly Sequence

N 22 GR 5 99-12-06 F 3

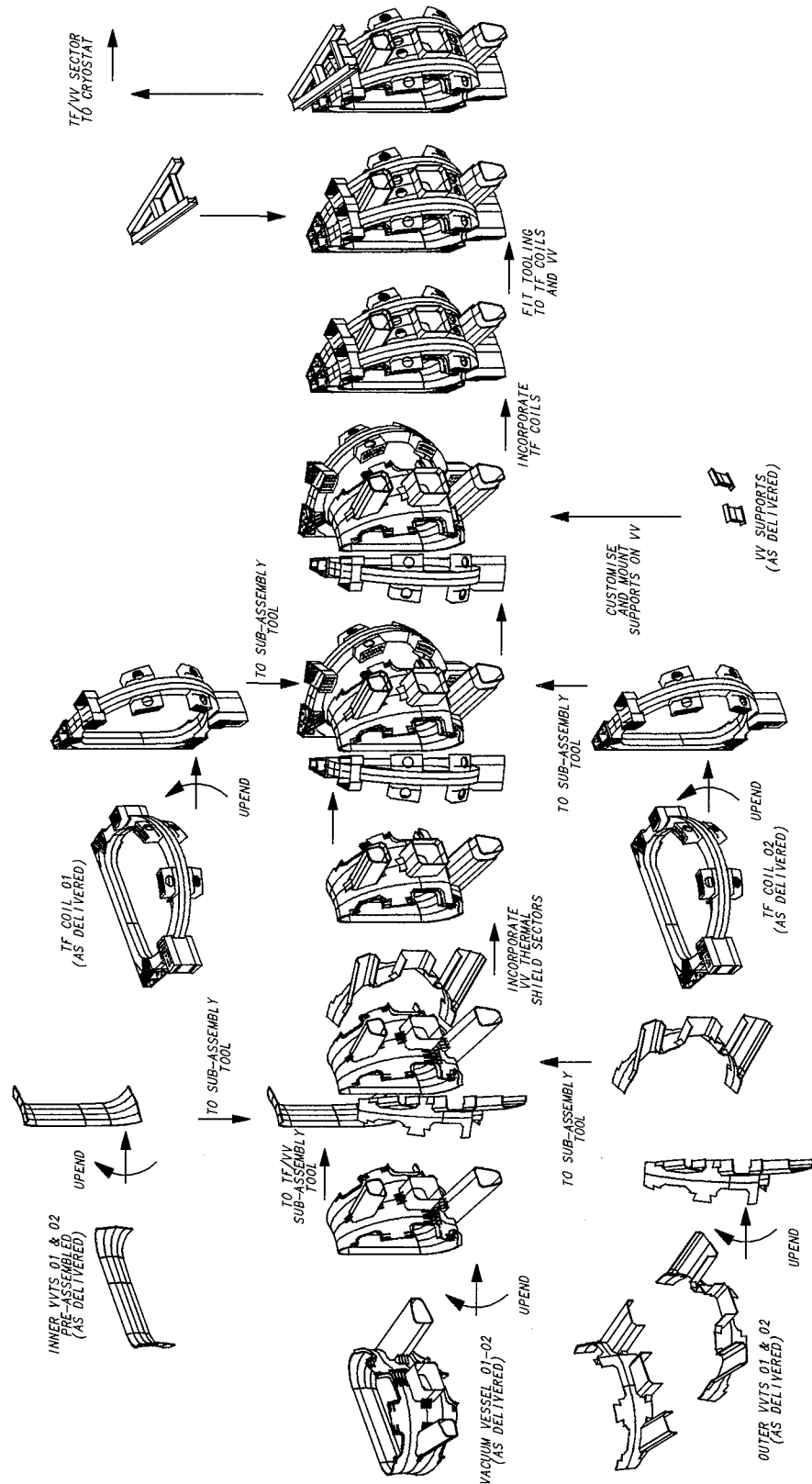


Figure II.9-4 Sub-assembly of TF/VV/VVTS using Separated Inboard and Outboard VVTS Sectors

II.9.2.3 Implications of the Design of the TF to VV Supports

The machine support system consists of two sets of plates that are arranged such that they are flexible in the radial direction, thereby allowing relative thermal displacement during cool-down and warm-up of the cold structures, but extremely stiff in all other directions. One set of 18 flexible supports connects the TF coils to the basemat, and the second set connects the VV to the TF coils.

The high toroidal stiffness of the TF to VV supports makes them unsuitable for use during assembly, prior to completion of the VV field joint welds, because the weld shrinkage (~ 12 mm, toroidally, per field joint) would subject them to large stresses. Thus, the VV will have to be supported via tooling until the final field joints have been welded, and the VV has been closed toroidally. Following toroidal closure of the VV, with the tooling supporting the weight of the VV, the individual flexible supports may be customised (e.g. shimmed), to guarantee an acceptable sharing of load, prior to being attached to the corresponding TF coil. At this stage the tooling may be used to adjust the position of the completed VV with respect to the magnetic datum, if required.

The TF to VV supports are located in an area which is difficult to access. In fact access for fastening or adjustment is feasible only through a vertical gap between the intermediate outer intercoil structures (OISs). This gap is closed by an OIS splice plate, which will be welded following completion of the VV assembly and installation of the TF to VV supports.

Conceptually, the assembly sequence will be an elaboration of the following:

- at the sub-assembly stage in the assembly hall, the TF-VV supports are inserted through the VVTS, shimmed and attached to the VV; the supports are not connected to the TF coil during sub-assembly and, thus, purpose-built tooling is required to support the VV independently during installation of the sector;
- after installation of a number of TF/VV/VVTS sectors inside the pit, the VV sectors are welded together, following a specific sequence to reduce the amount of accumulated deviations;
- following completion of the VV closing welds, the VV is aligned with the magnetic datum, and the TF-VV supports can then be accurately shimmed and fastened. Subsequently, the interface between the supports and the VVTS, which includes a thermal anchor in the flexible plates of the supports, is completed;
- the splice plates of the intermediate OIS are welded, thereby limiting further access to the TF-VV supports; subsequent to this operation, the position of the VV with respect to the TF coils is fixed and cannot be adjusted later.

II.9.3 Tooling and Facilities

In addition to the purpose-built tooling required for sub-assembly, assembly and handling of the components, the following temporary, or permanent, facilities will be established and maintained to support the assembly operations:

- cleaning area on the south end of the assembly hall;
- plant for storage, treatment and disposal of liquid waste;
- outdoor storage areas for tooling and components;
- temporary heavy lifting equipment in storage areas;

- on-site, or local, machining capability for finish machining small components, e.g. splice plates, shims, wedges and keys, etc. and for tooling modifications;
- clean grinding and machining capability in the assembly hall for sub-assembled and assembled components, e.g. for the correction of weld preparation on the VV port extensions;
- metrology and metallurgical laboratories to perform the required quality control tests;
- health physics and beryllium analysis laboratories to satisfy the site occupational health requirements.

II.9.4 Conclusions and Future Work

While a high level assembly plan has been established for ITER-FEAT, due to evolution in the design of the major components, the details of many assembly activities remain to be established, e.g. assembly of the TF to VV supports. This will also affect the design of the assembly tooling.

One issue which will affect the assembly strategy is the very accurate fit required for the mating surfaces between adjacent TF coils. The results of current structural analyses indicate that, in order to maintain acceptable operating stresses, it will be necessary to guarantee near complete contact over the full length of the inboard legs of the coils. This may necessitate lengthy and precise matching operations, e.g. shimming, and a significant impact on the assembly schedule should be anticipated, were the operations to be carried out on the ITER site. Accordingly, it has been proposed to have pairs of coils pre-assembled and, if required, pre-shimmed at the factory. Concepts and procedures for in-situ surveying and shimming have yet to be developed.

II.10 Tokamak Maintenance

II.10.1	Basic Maintenance Approach	1
II.10.2	In-vessel Maintenance	2
II.10.2.1	Divertor Maintenance	2
II.10.2.2	Blanket Maintenance	4
II.10.3	Port Handling	4
II.10.4	In-cryostat Repair	7
II.10.5	In-vessel Viewing/Metrology	8
II.10.6	Neutral Beam Injector Maintenance	9
II.10.7	TF/VV, CS, PF Disassembly/Re-assembly	9
II.10.8	Hot Cell	10
II.10.9	Remote Handling Equipment Test Stand	12
II.10.10	Conclusions and Future Activities	13

II.10.1 Basic Maintenance Approach

The strong requirement to reduce the investment cost for ITER-FEAT versus the 1998 ITER design, has led to a number of design changes of components with an associated impact on the design of remote handling (RH) equipment. Studies have also been carried out to investigate the possibility of reducing the cost of RH equipment, or at least to defer their procurement such that equipment would be procured on a “just-in-time” basis.

The general tokamak maintenance philosophy for ITER-FEAT is based on the following broad strategy:

- in-vessel interventions will generally be preceded by in-vessel inspection to obtain information on the extent of damage and maintenance activities required;
- maintenance of in-vessel components will generally consist of the replacement of components; the removed, activated and contaminated components will be transported to the hot cell for eventual repair and refurbishment, or, alternatively for preparations for disposal as waste;
- RH equipment will be introduced into the vacuum vessel from casks docked to dedicated ports (RH ports) of the vacuum vessel;
- casks are sealed, but not shielded, so that evacuation of personnel from the pit and gallery areas is required when casks are transported to and from the hot cell;
- the cask transporter is based on air cushion flotation;
- preparatory activities, prior to initial cask docking, will involve hands-on (assisted) operations, including gaining access to the bioshield plug, its removal, opening of the cryostat closure plate, etc;
- all components inside the cryostat must be designed to last the lifetime of the ITER machine, hence not requiring scheduled maintenance; should, however, components inside the cryostat require repair, then hands-on repair requiring human access is the reference procedure, with remote repair as a backup; the accessibility requirement may drive the shielding design of the ITER machine;

- gross failure of components inside the cryostat may require their replacement; the design and layout of components inside the cryostat and the building, as well as the design of the cryostat itself, must allow for the replacement of large components.

Individual RH procedures must be in accordance with a number of high level requirements and guidelines that include the following principles:

- (i) minimization of intervention time and waste volume as well as the risk of the spread of radioactive or hazardous contamination, and the minimization of the radiation exposure of personnel.
- (ii) standardization/modularization so as to reduce the cost and risk of RH equipment.
- (iii) segmentation of components to be handled should be based on achieving a very high degree of pre-testing of components (integrity tests as well as functional tests) prior to their (re)installation.
- (iv) hands-on (assisted) maintenance must be in accordance with ALARA guidelines and the workers' exposure is subject to legal dose limits (see Table I.1.3-2).

Tokamak maintenance is a prerequisite to a successful ITER experiment. This essential capability relies, simultaneously, on the detailed design of the components to be maintained or repaired, on the actual procedure to be followed during the maintenance process, and on the development of simple, robust and efficient remote handling equipment and tools.

II.10.2 In-vessel Maintenance

II.10.2.1 Divertor Maintenance

Divertor cassettes are RH Class 1 components. Repair or refurbishment requires removal from the VV through three radial RH ports, that are somewhat inclined to the horizontal, and transfer to the hot cell where the actual operations are carried out using dedicated and common remote work stations. After transfer to the hot cell, each divertor cassette is refurbished by replacing the high heat flux components. In order to minimize the cassettes inventory and the hot cell storage requirements, a just-in-time refurbishment strategy is being devised¹. This strategy is subject to a detailed logistics study.

A total of 54 cassettes are mounted in the ITER VV through the 3 RH ports. One port covers therefore 18 cassettes. Replacement of the cassettes requires radial movement of the central cassette combined with some rotational movement around its toroidal axis in order to maneuver it through the relatively narrow handling space inside the VV and through the RH port (see Figure II.10-1). All other cassettes require, in addition, toroidal movement to bring them opposite to the exit port. The cassettes are 3.2 m long, 1.86 m high, 0.4 – 0.78 m wide and weigh approximately 12 t. The handling equipment and transfer features are described below (see Table II.10-1).

Supports and rails: The position of the cassette supports and related toroidal rails is inboard and outboard of the cassettes. The cassettes are fastened to the rail by means of a locking device, using the cassette toroidal mover manipulator arm. Access from below the central cassette to lock its inboard support is difficult. The radial fixed reference of all cassettes is

¹ C. Damiani, G. Bertacci, M. Irving, et al; "R.H. Divertor Maintenance – The Divertor Refurbishment Platform", ISFNT5, Rome, 1999.

therefore the outboard support. The cassette inboard supports can accommodate the relative motions (thermal expansions, etc.) between cassette and vessel.

Radial cassette handling: This is based on a cantilever multifunctional mover (CMM) which grips and handles the cassette at its outboard end in a cantilevered manner. The CMM includes an articulated end-effector that allows the toroidal movement of the second cassette, i.e. the one adjacent to the central cassette, as well as a manipulator arm to perform locking/unlocking operations inside the RH port.

Toroidal cassette handling: With 3 RH ports the toroidal movers must cover a maximum of 120°. This may be accomplished by either two one-direction cassette toroidal movers or one bi-directional cassette toroidal mover. Cantilevering the cassette from the cassette toroidal mover as an alternative to lifting (using wheeled and jacking forks) is being investigated.

N 23 GR 160 99-11-22 W 0.1

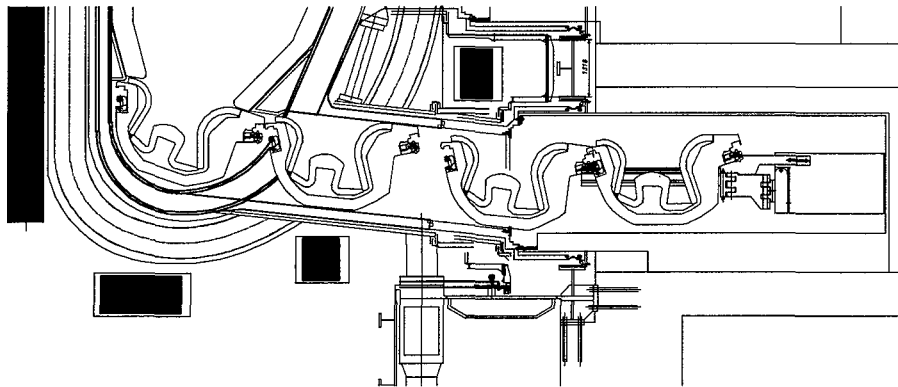


Figure II.10-1 Divertor RH port Cassette Handling

Table II.10-1 In-vessel RH Equipment for Divertor Cassette Handling

RH EQUIPMENT	NUMBER REQUIRED
RH ports	3
Toroidal movers	2 cassette toroidal movers
Radial movers	2 cantilever multifunctional movers
Welding/cutting tools	2 sets of crawler bore tools
Test stand	1 dummy RH port
Casks	1 transfer cask

II.10.2.2 Blanket Maintenance

The blanket maintenance requirements include the inspection of modules followed by replacement if they are found to need repair. In-situ repair will be used where possible, but replacement of modules will also be required. In addition, it is also planned later in operation to replace all outboard shield blanket modules with breeding blanket modules.

The main remote handling equipment used for these operations uses an in-vessel transporter (IVT) comprising a segmented rail (articulated) on which a vehicle with manipulator arm and additional attachments can be deployed inside the vessel. After maintenance campaigns the rail and vehicle are withdrawn from the vessel and stored inside a test stand facility. In order to reduce the cost of the blanket, its segmentation into modules has been minimized by making the modules as large as practical. The maximum payload of the IVT is determined by the maximum size of the RH port, the load on the main gear of the transporter that rotates the modules around the rail, and the kinematics inside the vacuum vessel (VV).

Conceptual designs for ITER-FEAT have been developed for an IVT to be deployed from casks. The in-vessel kinematics are shown in Figure II.10-2. The conceptual design of the IVT and associated equipment involve the following.

Rail deploying device: The IVT articulated rail deployment is achieved using a deploying device, a vehicle fixing arm, and a slide arm to support the vehicle fixing arm, as shown in Figure II.10-3. To deploy the carbon steel or titanium alloy rail inside the VV, an intermediate cask is attached to each of the four RH ports at the equatorial level to provide the umbilical cable handling interface between the VV and the pit area outside the bioshield. In addition, the intermediate cask contains a pin insertion device and a rail guide device to interconnect the individual rail links. The vehicle fixing device is supported by the slide arm that is remotely connected to it in the cask. The deployed rail is supported by four rail support devices inserted through the four RH ports which are spaced apart 80° or 100° from each other.

Blanket module handling equipment: The vehicle has a two-step, telescopic handling arm with an end-effector for in-vessel maintenance, a rack-and-pinion mechanism for controlling travel along the rail and a locking mechanism for locking the joints of the rail. A rack gear is installed on the inner side wall of the rail. The vehicle travels on the rail by driving a pinion gear installed on the vehicle. Each roller swings along the rail wall and is able to support load uniformly. The load capacity of the arm excluding the end-effector weight (1.0 t) is 4.5 t, sufficient for all handling requirements. The telescopic handling arm is also capable of handling the remote tools required for connection/dis-connection of the module to/from the vessel wall.

Refurbishment: Beryllium plasma spray (to repair minor first wall damage by erosion) and replacement of the separable first wall (in case of heavier damage) are planned for the refurbishment (performed in-line) of the blanket modules.

II.10.3 Port Handling

Port handling systems are provided to guarantee the safe transfer of components from the vacuum vessel to the hot cell and vice versa. In particular, the use of sealed (but unshielded) transfer casks avoids the spread of active contaminants to the building during component

replacement and transfer operations. The main port handling design criteria¹ place minimum size constraints on key RH system elements:

- a) building size relative to the transfer cask size (direct consequence of the size of components to be transported by the cask and of the components' cantilevered handling system). While the cask dimensions can vary depending on the size of the component to be transported (approximately WxLxH 2.5x8.5x3.6 m, except for special casks required for NB maintenance and IVT use) these dimensions are standardized as much as possible. In particular, the base of the cask (i.e. the part which is removeable and contains the cask air bearing transfer and air springs alignment systems) will be the same for all (except IVT and NB casks);
- b) vacuum vessel port position relative to the building (direct consequence of the minimum space requirements for the cask docking interface to the VV port and hot cell). This space envelope is dictated by the minimum size allowable for the double-seal door, by the cask docking mechanism and by the minimum size required for the locking and sealing of the port assembly (shielding plug, diagnostic equipment, etc.)². Figure II.10-4 shows a plug handling and transfer cask solution for the case of inclined ports.

N 23 GR 162 99-11-22 W 0.1

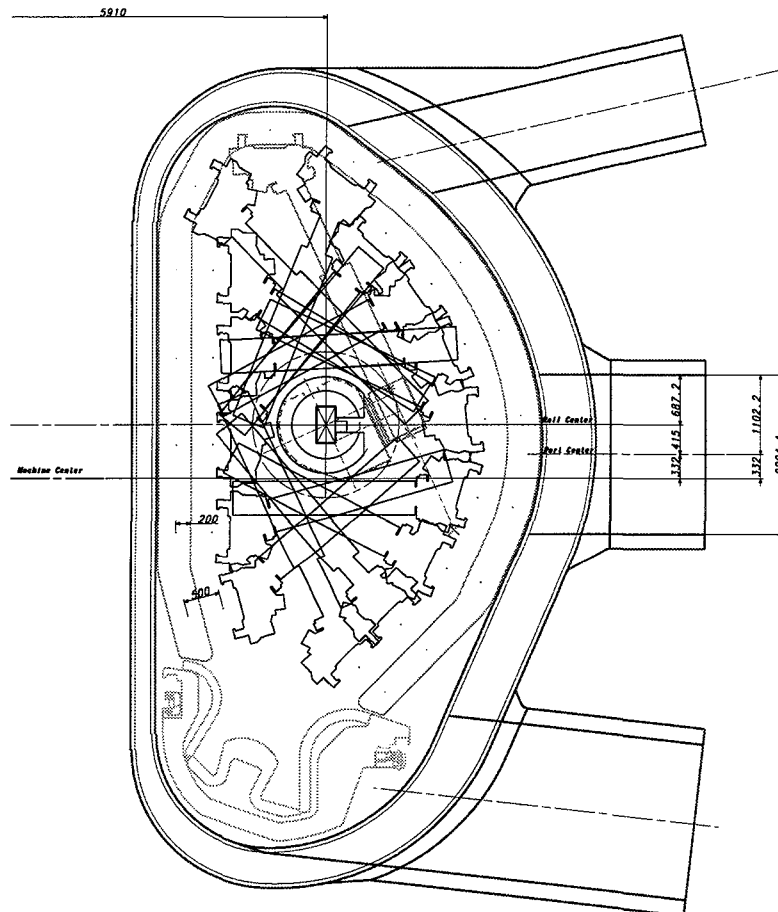


Figure II.10-2 The In-vessel Kinematics of the IVT

¹ N 23 DDD 22 98-06-15 W 0.3, "Remote Handling"

² N 23 MD 7 98-12-08 W 0.2, "Port Assembly Handling - Locking and Remote handling Maintenance Casks: RC ITER-Related Issues"

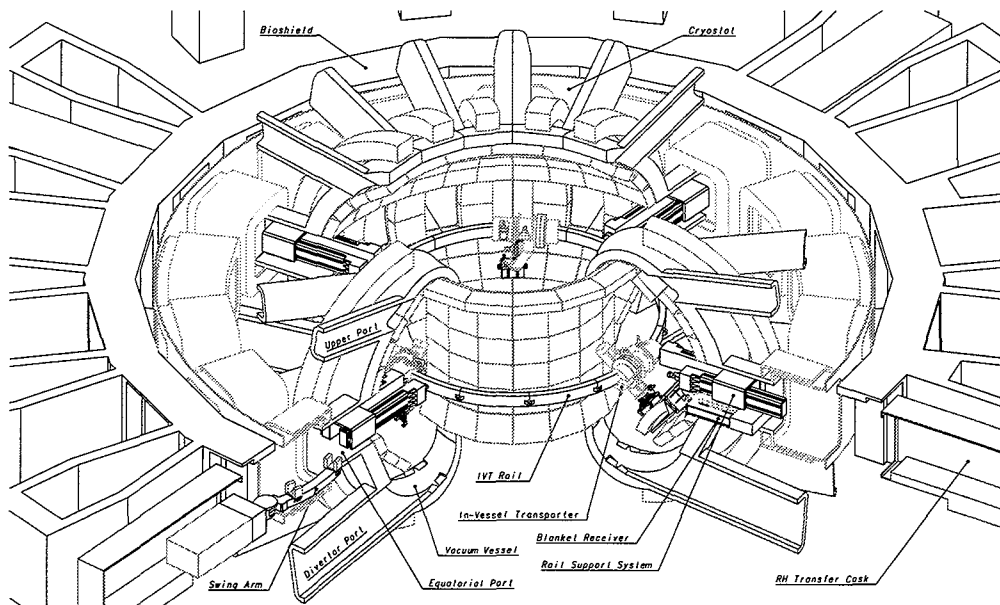


Figure II.10-3 In-vessel Transporter (Rail Mounted Vehicle System)

Double-seal door system: The double-seal door system design will be as common as possible to the various port locations (including the hot cell). This will result in a small inventory of doors and a relatively simple fabrication and maintenance. Double-seal doors are tilted up and backwards inside the cask. This allows the cask dimensions to be minimized and to position the cask payload along its longitudinal centerline.

Shielding: There is no gamma shielding associated with the door and the main cask body. Some shielding may be required to protect the cask transfer system.

Docking: This will be achieved by using pulling devices fitted on the cask, reacting on the building floor. The reference cask position, relative to the building, is horizontal at all port locations.

Sealing to the VV port: While the use of O-rings is the reference, the possibility of using inflatable seals (reduced contact forces, increased compliance) is being investigated.

System ports access frequency: There will be more than 2 to 5 openings if replacement other than for maintenance (i.e. upgrading) is considered. The frequency will form the basis for the design of welding lips that are partly consumable.

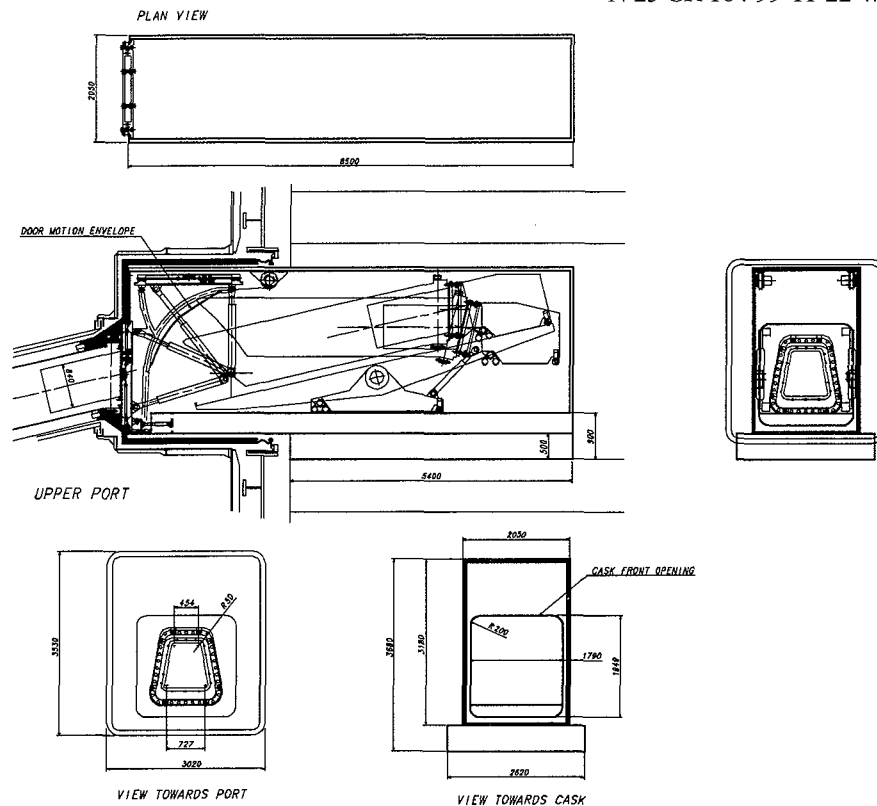


Figure II.10-4 Upper Port Plug Handling and Transfer Cask

II.10.4 In-cryostat Repair

Because of the congestion within the cryostat and the difficulty of gaining direct access to the machine components situated between the vacuum vessel and the cryostat, in-cryostat maintenance is, as much as possible, to be eliminated by design. All components inside the cryostat are regarded as RH Class 3. The strategy assumes that sufficient shielding will be provided to allow hands-on maintenance as the primary method of repair. Radiation received by maintenance personnel must be below the acceptable levels as per the ALARA guidelines (see Table I.1.3-2). Because unscheduled maintenance cannot be entirely ruled out, the possibility of remote backup operations for certain in-cryostat components is being developed.

Access for the hypothetical repair of magnet feed line components, including the termination boxes, break boxes, and module bypass joints for PF1 & 2 is from the upper central cryostat roof, for PF3 & 4 is from within the equatorial horizontal port ducts, and for PF5 & 6 is from below and at the divertor ports. TF1 through 18 are also accessed from the divertor ports. CS1 through 3 can be accessed from above, and access to CS4 through 6 is from below. The space constraint within the cryostat has created some location problems for the PF4 and PF5 terminal boxes, break boxes and module bypass joints. A minimum radial clearance of approximately 1 m is required to allow worker access to create a PF magnet module bypass. The limited height available between the ports requires that a worker operates in the crouched position. Failed lower, trapped PF5 & 6 coils rely fully on in-built redundancy or on in-situ rewinding of the coils.

II.10.5 In-vessel Viewing/Metrology

Initial investigations and 3D simulations¹ have shown that the inside of the VV, including the divertor legs, can be inspected by deploying probes through the divertor radial ports for which suitable locations are available at the side of the vacuum vessel. Every third divertor port out of 18 needs a viewing probe for complete coverage, i.e. a total of 6. The required viewing resolution of all points is 6 mm at points on the blanket module and divertor surfaces. Achievable resolution is defined in Table II.10-2.

Table II.10-2 In-vessel Viewing System Characteristics

Distance between object & tip of IVV (mm)	Resolution* for Periscope (mm)	Accuracy** for Metrology (mm)
500 to 3000	1	± 0.5
3001 to 5000	1.7	± 0.8
5001 to 8000	2.7	± 1.0

* for a surface normal to line from the IVV tip

** of measurement of the distance along a line from the IVV tip

The IVV has a straight optical transmission path from the in-vessel area to the service unit located outside the bioshield. The deployment of the viewing probe is along a straight inclined line. The IVV head protrudes into the vacuum chamber through a hole in the outboard leg of the divertor.

The IVV connections with its external service unit include heat removal, power and signals, as well as a structural interface. The diameters of the probe and its external deployment tube are limited to 150 and 300 mm respectively. The interface is shown schematically in Figure II.10-5. An elevation view of the VV with inserted viewing probe is shown in Figure II.10-6. The external service unit allows for the interchange of probes. This may allow the deployment of probes for different functions.

N 23 GR 165 99-11-23 W 0.1

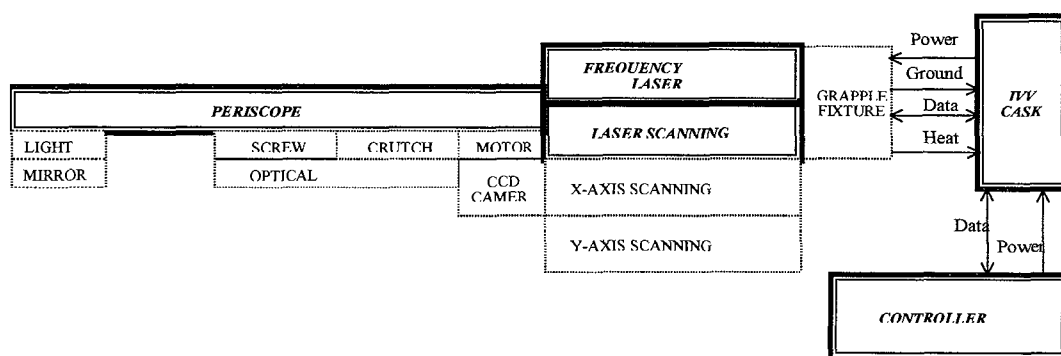


Figure II.10-5 Scheme of IVV Interfaces

¹ N 23 MD 9 99-06-09 W 0.1, Comparison study of viewing / metrology system deployment location

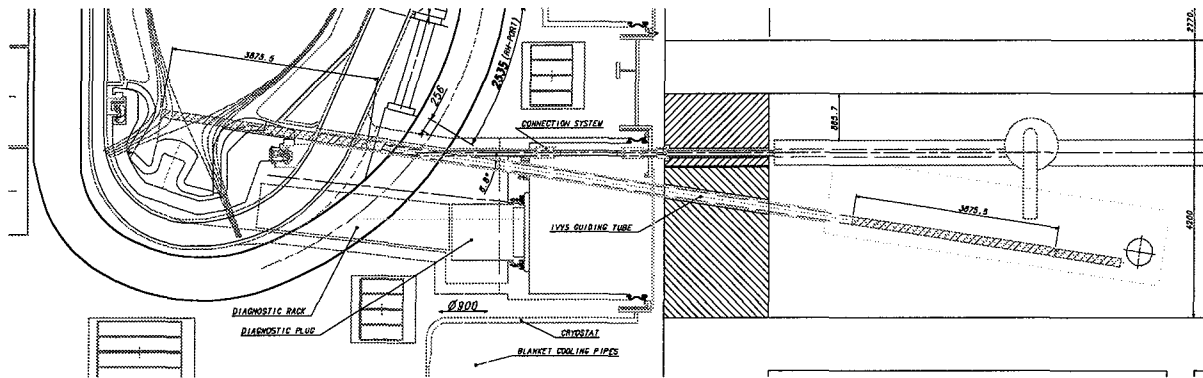


Figure II.10-6 Elevation Showing IVV Deployed Inside the VV

II.10.6 Neutral Beam Injector Maintenance

RH Class 1 maintenance of the NB injector is needed for the replacement of filaments and oven. RH Class 2, maintenance is expected for grids, decontaminating insulators by the removal of cesium and changing parts of the fast shutter. All other components are RH Class 3. The aim is to avoid removing the ion source for RH Class 1 and 2 operations. The sources are very large, have many, very complex interfaces and their removal would require non-standard, very large casks. The present status is that replacement of the filaments and the Cs oven can be done in-situ, while the in-situ removal of Cs is under consideration. Feasibility of the RH Class 2 operations without source removal is as yet doubtful.

II.10.7 TF/VV, CS, PF Disassembly/Re-assembly

The vacuum vessel, toroidal field coils, central solenoid coil and poloidal field coils repair or replacement are RH Class 3 operations. However, the feasibility of disassembly/re-assembly are basic requirements which affect the machine layout and building design. All three replacement operations are complex and require the cryostat lid to be fully or partly removed, together with the upper bioshield slab, which has been designed to be removable in sections. The strategy is to carry out repair in-situ by manned access into the cryostat. However, if replacement is necessary, the procedures aim at minimizing the radiation in the tokamak hall through the opening in the upper bioshield.

Toroidal field coils and vacuum vessel disassembly/ re-assembly

In case of TF coil failure, remote replacement of the TF/VV sector will be required. This complex operation entails the prior dismantling and removal of a large number of the components inside the cryostat using manned interventions, and remote removal of the relevant in-vessel components, followed by cutting the affected VV sector. This poses an additional problem in that the releasable activity contained within the VV (tritium and activated dust) must be contained within the VV sector that is replaced and in the VV itself when the replacement operation is carried out. Depending on the vessel and TF coil activation levels at the time of replacement, some form of local gamma shielding may be required. Using a cask into which the TF/VV sector is lifted provides such a possibility. However, the combined weight may exceed the lifting capacity of the main crane. Therefore, the use of a twin crawler crane is being considered.

Central solenoid disassembly/ re-assembly

The central solenoid can be repaired in-situ following a cryogenic line, electrical insulator fault or helium leak. Any other fault may require that the coil is removed from the machine. For this operation a lifting device is inserted from the top, after removing the central flange from the cryostat head, and the CS is lifted by the overhead crane. Set-down space is reserved in the assembly hall to receive the CS.

Poloidal field coils disassembly/ re-assembly

The PF coils can be repaired or replaced following a) a helium leak, b) an electric short circuit, c) a ground insulation fault. In case gross failure occurs requiring coil replacement, the upper coils can be removed and new coils installed. PF3 and 4 are trapped between radial ports. Their replacement would require a very large amount of preparatory work. For that reason, these coils have an increased amount of in-built redundancy. The lower coils PF5 and 6 are trapped beneath the VV. Replacement of a lower PF coil requires that a new coil is fabricated in-situ. The layout inside the cryostat has been configured such that this can be done.

II.10.8 Hot Cell

The proposed ITER-FEAT hot cell and hot cell systems provide space and facilities for receiving, decontamination, storage, repair, refurbishment and testing of highly radioactive and/or contaminated tokamak in-vessel components and materials. Facilities are also provided for the maintenance of remote handling tools and for radioactive waste processing and storage prior to disposal by the ITER host. A preliminary design is shown in Figure II.10-7. This design will be subject to modifications as a result of detailed studies on the refurbishment of components and the overall logistics.

As shown in Figure II.10-7, the hot cell consists of a series of areas which include: a) a casks docking area, where components withdrawn from the VV are received and offloaded into a cleaning cell to remove activated dust and possibly tritium, b) a main processing area for dedicated and general work stations, and c) a radwaste processing and storage area, where the waste is treated for tritium recovery, if required, and segmented and packaged for the ITER host organization. Direct-access docking from inside the NB cell is available for maintenance operations on NB ion sources, should this be required.

The open-plan, rectangular layout of the processing area provides flexibility to modify the internal work stations. For added space and layout flexibility, the shield walls north of the docking area and of the processing room are made of concrete blocks. Storage for activated components is provided in an annex area of the main processing room so that an intermediate shield wall can be installed allowing manned access to the main processing room after the removal of activated components and dust from this area.

It is assumed that the hot cell building is available during the initial installation phase of the tokamak in-vessel components, thereby providing a pre-assembly, Be-controlled area, and a loading facility for components into transfer casks or other form of transfer to the tokamak. Furthermore, a RH area could be integrated with the hot cell at this stage and used for the preparation of RH equipment used for initial machine assembly.

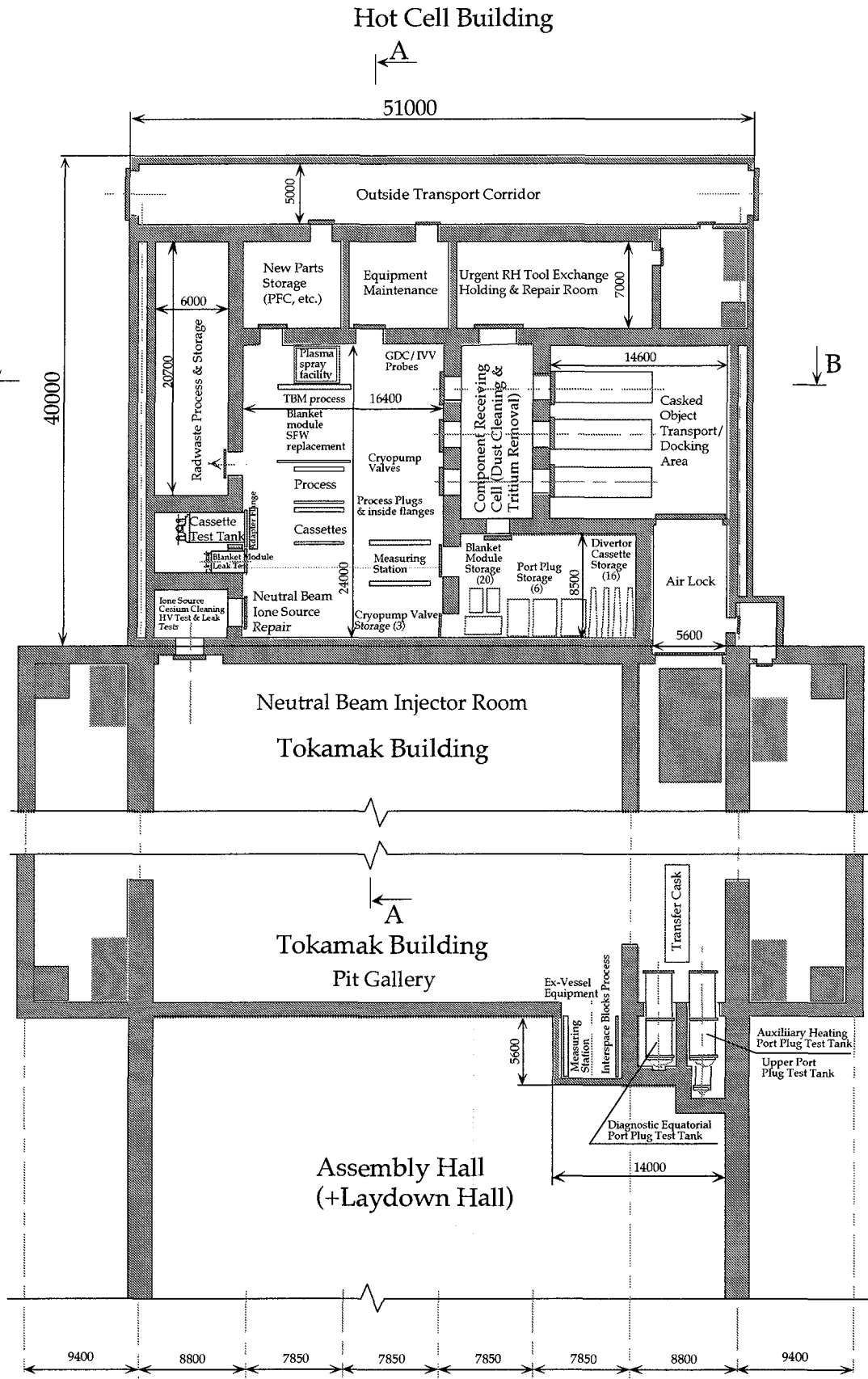


Figure II.10-7

Hot Cell Building – Preliminary Plan View

In order to minimize tritiated water generation from air in-leakage (about 1 air change per day), low humidity (dried) air is circulated through the air spaces around the hot cell. Thus, only dry air is subject to inleakage.

The main additional features of the hot cell are as follows:

- a) hot cell arrangement on one (ground) level;
- b) in-line repair and refurbishment concept;
- c) common in-vessel component refurbishment is used instead of dedicated cells;
- d) common in-vessel component storage is used instead of dedicated cells;
- e) common radioactive waste processing and storage area is used instead of dedicated cells.

South of the tokamak building, on the east side of the assembly hall, a test area is provided for the testing of port plugs after refurbishment in the hot cell. This arrangement simplifies the routing of the necessary power supplies, waveguides, etc.

II.10.9 Remote Handling Equipment Test Stand

Remote handling requires precise and well-rehearsed or automatic operations to repair an in-vessel component efficiently. To ensure this, even in situations going beyond previous experience, a RH equipment test facility as shown in Figure II.10-8 has been included in ITER-FEAT. The main functions of the test stand are the maintenance and repair of RH equipment followed by commissioning, operation training and commissioning of equipment before rescue interventions in the vessel, and storage of RH equipment. The RH equipment test stand is above the hot cell, i.e. near the pit, and makes use of the main component lift for the transfer of casks. It includes a part mock-up of the VV with ports allowing the deployment of the in-vessel RH equipment as well as port plugs using dummy port flanges, so that the transfer of contaminated equipment can occur into the mock-up VV without contaminating the surrounding area. The in-vessel area is therefore a Be and radiation zone allowing hands-on maintenance with respiratory protection, whereas the area external to the mock-up VV is contamination-free. In the latter area the casks are used for docking operations and the area is also used for cask storage that includes RH tools during plasma operation campaigns.

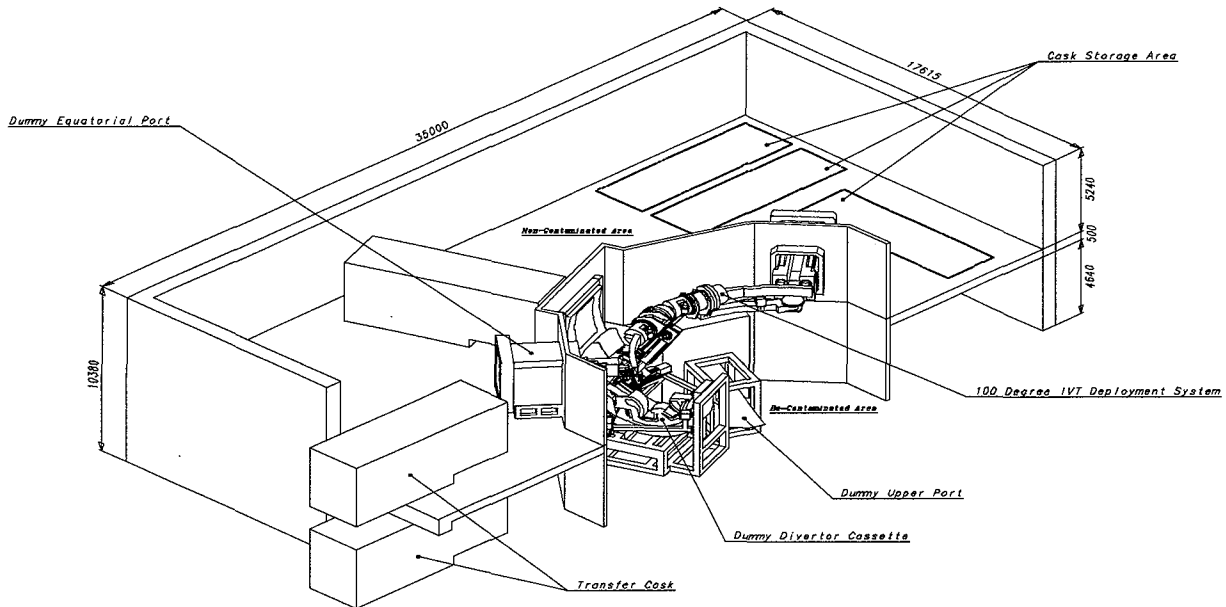


Figure II.10-8 RH Equipment Test Stand

II.10.10 Conclusions and Future Activities

The remote maintenance for ITER-FEAT takes full advantage of the design and R&D undertaken during the EDA. Cost savings are feasible for the divertor handling, due to a redesign that results in a smaller number of handling devices. For blanket handling, investment costs may be deferred by initially using not the full 360° rail system but only 180° sections of the in-vessel rail. The in-vessel viewing and metrology probes are accessed from divertor ports.

Handling concepts for divertor cassette and blanket module replacement are available for further detailing. The areas that still need considerable design and R&D input are port handling, in-cryostat repair activities and hot cell remote repair activities. In-cryostat procedures will need further development at the conceptual level to finalise the layout and design of components within the cryostat.



XA0102522

TAC
15 June 2000

ITER
TECHNICAL ADVISORY
COMMITTEE MEETING

25-27 June 2000
St Petersburg

**PROGRESS IN RESOLVING
OPEN DESIGN ISSUES
FROM THE ODR**

Report by the Director

Table of Contents

1. Introduction	4
2. Physics	5
2.1. Introduction	5
2.2. Inductive operation scenario of Q=10 and sensitivity analysis	5
2.2.1. Typical operation scenario	5
2.2.2. Effect of Sawteeth	9
2.2.3. Operation Boundaries	10
2.2.4. Impurity Effect	13
2.2.5. Density Profile Effect	15
2.2.6. Ion Heating Effect	16
2.2.7. Temperature Profile Effect	16
2.2.8. Effect of Degradation near the Greenwald Density	18
2.3. High-Q (~50) Operation and Possibility of Ignition	20
2.4. Long Pulse and Steady-state Operations	22
2.4.1. Long Pulse Operations	22
2.4.2. Steady-state Operation	24
2.5. Confinement Database	26
2.5.1. Present ELMy H-mode Confinement Database	26
2.5.2. Necessity of Dimensionless Transport Studies	30
2.5.3. Offset non-linear confinement scalings and edge pedestal	30
2.5.4. Predictions of ELM Energy Loads and their Control in ITER-FEAT	30
2.5.5. Probabilistic Performance Assessment using Different Confinement Scalings	40
2.5.6. A Dimensional Extrapolation Technique based on a System Code Applied to the ITER H-mode Energy Confinement Database	42
2.6. Progress in Divertor Modelling	45
2.6.1. SOL Width	45
2.6.2. Code Validation	47
2.6.3. Divertor Geometry Effects	48
2.6.4. Operational window for ITER-FEAT	51
2.7. NTM Suppression by ECCD	53
2.8. ITER Physics R&D	55
3. Magnets	58
3.1. Support of TF Coil Loads	58
3.1.1. Winding Pack Issues	58
3.1.2. Wedged support at the TF coil inboard legs	60
3.1.3. Intercoil Structure Redesign	61
3.2. Inductive Flux Generation	65
3.2.1. Choice of CS Jacket Material	65
3.2.2. Choice of the CS conductor cross-section: rectangular or square jackets	67
3.2.3. CS manufacture and compression structure and supports	69
3.3. Conductor Design Issues	70
3.3.1. Current Non-Uniformity	70
3.3.2. PF Conductor Design	71
3.4. Limits to Elongation/Triangularity	71
4. Vessel/In-Vessel	75
4.1. Manifolding of Blanket Coolant	75

4.2.	Vacuum Vessel Design Development	84
4.2.1.	Fabrication	84
4.2.2.	Vacuum Vessel Loads/Function vs 1998 ITER	86
4.2.3.	Structural Assessment of the Vacuum Vessel	93
4.3.	Design Implications of Divertor Material Choice	97
5.	<i>Buildings and Plant Services</i>	103
5.1.	Developments in Building/Services Design	103
5.2.	Hot Cell Building	108
5.2.1.	Building Size and Layout Requirements	108
5.2.2.	ADS/VDS Requirements	109
5.2.3.	Dose and Dust Requirements	109
5.2.4.	Design Outline	110
5.2.5.	Hot Cell Docking and Storage System	114
5.2.6.	Hot Cell Repair/Testing System	115
5.2.7.	Hot Cell Waste Processing and Storage System	115
5.2.8.	Hot Cell Radioactivity and Toxic Material Control System	116
6.	<i>Operation</i>	117
6.1.	Limits to Pulse Length	117
6.2.	Limits to Fusion Power	118
7.	<i>Safety</i>	119
7.1.	Methodological Improvements	119
7.2.	Design Changes due to Safety Considerations	121
7.3.	Safety Assessment	122

1. Introduction

In January 2000, the ITER Meeting *"accepted the ITER-FEAT Outline Design Report, taking note of the TAC Report and recommendations, and agreed to transmit the report to the Parties for their consideration and domestic assessment"*. It further *"agreed that the Outline Design Report provides the basis for continuing design work by JCT and Home Teams"*, and *"recognising the importance to optimise a single agreed design,... asked the Director and JCT to interact with the Parties during the course of their domestic assessments. The Parties should keep the Director informed of the findings of their domestic assessments with a view to optimising a design for approval, following TAC review, at the coming ITER Council Meeting, in the context of the planned Joint Assessment."*

The above-mentioned interaction has now taken place, and the Parties have transmitted to the JCT their domestic assessments. Given the parallel nature of the continuing design work in the JCT and HomeTeams, as well as the Parties' assessment, some issues raised remain to be addressed by the developing design: for the most part either because the available experimental results do not provide a good enough basis for a confident extrapolation (for example ELMS, NTM stabilisation, steady state, etc.), or because the R&D on questions specific to ITER, and clearly identified, are ongoing (for example tritium codeposition with graphite and its removal, etc.) Nevertheless, as agreed at the Meeting, it has been possible to prepare "a progress report which will briefly summarise the choices made for the few remaining design options" addressing, where sufficiently known, the concerns of the Parties.

This report therefore covers all those design features of ITER which result from a resolution of a choice of options. More details on other features of the design will be given in the Final Design Report for ITER-FEAT, after more detailed engineering studies. The report also takes the opportunity to address issues raised by the physics assessments of the Parties, in discussions of the operating scenarios, projection sensitivities, and divertor-edge physics. The object of this report is not to repeat the ODR information, but to concentrate on the specific open issues and the progress towards their resolution.

2. Physics

2.1. Introduction

This report summarises the Physics analysis activities since the last TAC meeting, in an effort to address some of the recommendations raised by TAC and HTs. Also the structure and goals of Physics Expert Group activities are briefly described.

Section 2.2 discusses inductive operation scenario and sensitivity analysis on effects of sawtooth, operation boundaries, impurity, density and temperature profile, ion heating and degradation near the Greenwald density. Section 2.3 presents the possibility of high Q (~ 50) and ignition operation with a short pulse heating. Section 2.4 presents recent analysis work on long-pulse and steady-state operation. Section 2.5 discusses the confinement and pedestal database used for projection. Section 2.6 addresses divertor physics. Section 2.7 discusses recent theoretical work on neoclassical tearing mode suppression by ECCD, and Section 2.8 the structure and goals of Physics Expert Group activities.

2.2. Inductive operation scenario of $Q=10$ and sensitivity analysis

2.2.1. Typical operation scenario

The performance of ELMy H-mode operation in ITER-FEAT is assessed by using 1.5 D transport codes PRETOR¹ and ASTRA². The transport coefficients are normalised in a way that the global confinement time is equal to that given by the scaling law. The confinement enhancement factor (H_H -factor) over ELMy H mode scaling³ IPB98(y,2) is used.

Figure 2.2-1 shows the time evolution of plasma parameters in a typical operation with the flat top current of 15 MA. The simulation is performed from X-point formation (XPF) to the end of burn (EOB). The average electron density is controlled by pre-programming. During the flat top, 33 MW of NB and 7 MW of RF heating are used and about 400 MW of fusion power is produced ($Q = 10$). The helium accumulation is calculated for the condition that $\tau_{He^*}/\tau_E = 5$. Argon (Ar) impurity up to 0.12% is seeded to keep the power to the divertor target about 30 MW, which gives less than 5 MW/m² on the divertor target. The corresponding effective charge is 1.69 and the helium contribution is about 0.16 with $f_{He} = 4.3\%$. The power across the separatrix is 86 MW. This power and the separatrix density of $0.3 \times 10^{20} \text{ m}^{-3}$ are given to 2-D divertor simulation code (see section 2.6 for details). Ar transport and its radiation are yet to be included in 2D divertor calculation. However, even without Ar radiation in the divertor plasma, the maximum heat load on the target is estimated to be 8 MW/m². Carbon impurity level at the separatrix is only 0.19 % from 2D divertor calculations, which is negligible compared with the effect of Ar in PRETOR. Recent experimental results suggest that wall impurity sources are as important as divertor sources. Therefore 2D divertor calculations provide an underestimate of impurity contamination. 2 % of beryllium is assumed in PRETOR as impurity from the wall. The helium level is also

¹ D. Boucher, *et. al.*, in Proc. 16h IAEA Fusion Energy Conference, Montreal, 1996 (IAEA, Vienna, 1997) 945.

² G. V. Pereverzev, *et. al.*, IPP 5/42 (1991).

³ ITER Physics Basis, Nucl. Fusion 39 (1999) 2137.

estimated to be much lower with the divertor code than with PRETOR. On this point, the PRETOR results give a conservative estimate. Efforts to improve consistency or resolve inconsistency of the analysis between PRETOR and 2-D divertor code is underway.

Figure 2.2-2 shows the detailed time trace in the starting phase. Plasma heating starts just after the current flat top. At this time, the electron density should be small enough to reduce the threshold power for H-mode transition and large enough to avoid shine through of neutral beams. In this case, NBI heating starts at 100s when $n_e = 4 \times 10^{19}/\text{m}^3$. In the simulation, H-mode transition occurs at 110s, when the second NB is injected.

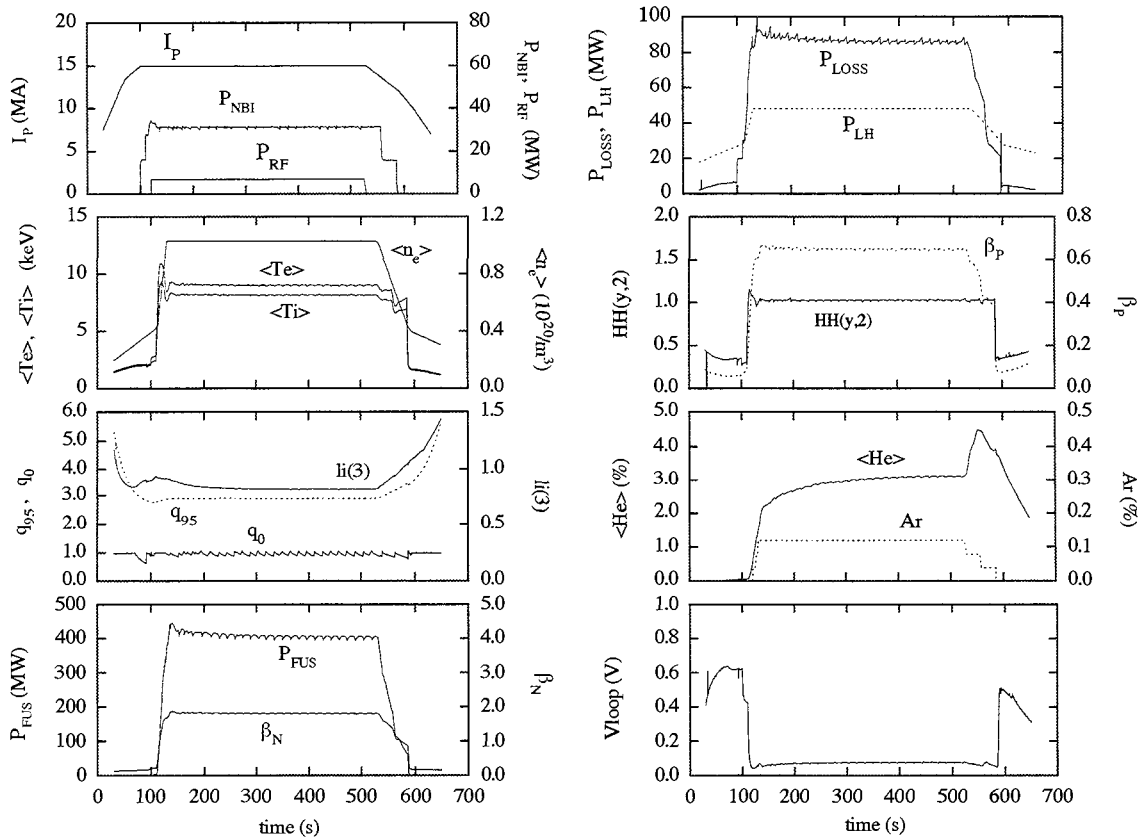


Figure 2.2-1: Time evolution of plasma parameters for 400MW operation without pre-heating during the current ramp up

In this simulation, the outermost flux surface is fixed during the simulation and the full size plasma is studied, and 2-D equilibrium is calculated consistently with the pressure change. The simulation for the growing phase to the full-size plasma, including the X-point formation, is done by using the DINA code⁴ with a simplified transport model. The PF-coil system is consistent with the whole phase of the plasma operation.

The requirement for plasma shut down in ITER-FEAT is eased since the transition to L-mode can be easily achieved by switching off the auxiliary heating power. The threshold power, however, decreases when the electron density is reduced, which is also necessary to decrease the fusion power. In the simulation, a threshold power reduction by 50% for the H-L transition is implemented to be conservative. The transition to L-mode occurs at 580s, when all the heating power is switched off in this case.

⁴ R.R. Khayrutdinov, V.E. Lukash, J. Comp. Physics 109 (1993) 193.

The loop voltage at the flat top is about 75mV and the burn time is estimated to 400s when the available flux is 30Vs. To prolong the operation pulse length, pre-heating during current ramp up can be used. In this case, 5 to 10 Vs is saved and the burn time is ~ 500 s.

Figure 2.2-3 shows the profiles of plasma parameters at the flat top. Here, a flat density profile is assumed for the reference scenario, to be conservative. Temperature profile is calculated by the RLWB energy transport model⁵ and the edge pedestal is created by reducing χ in the region $r/a > 0.9$. Helium accumulation level at the magnetic axis is about 4.2% and Z_{eff} at the axis is 1.69. The fraction of bootstrap current is about 15%. Main physics parameters at the flat top are summarised in Table 2.2-1. All major parameters such as beta, n_e/n_{GW} , divertor heat load, $\tau_{\text{He}}^*/\tau_E$ and Z_{eff} are in a reasonable range.

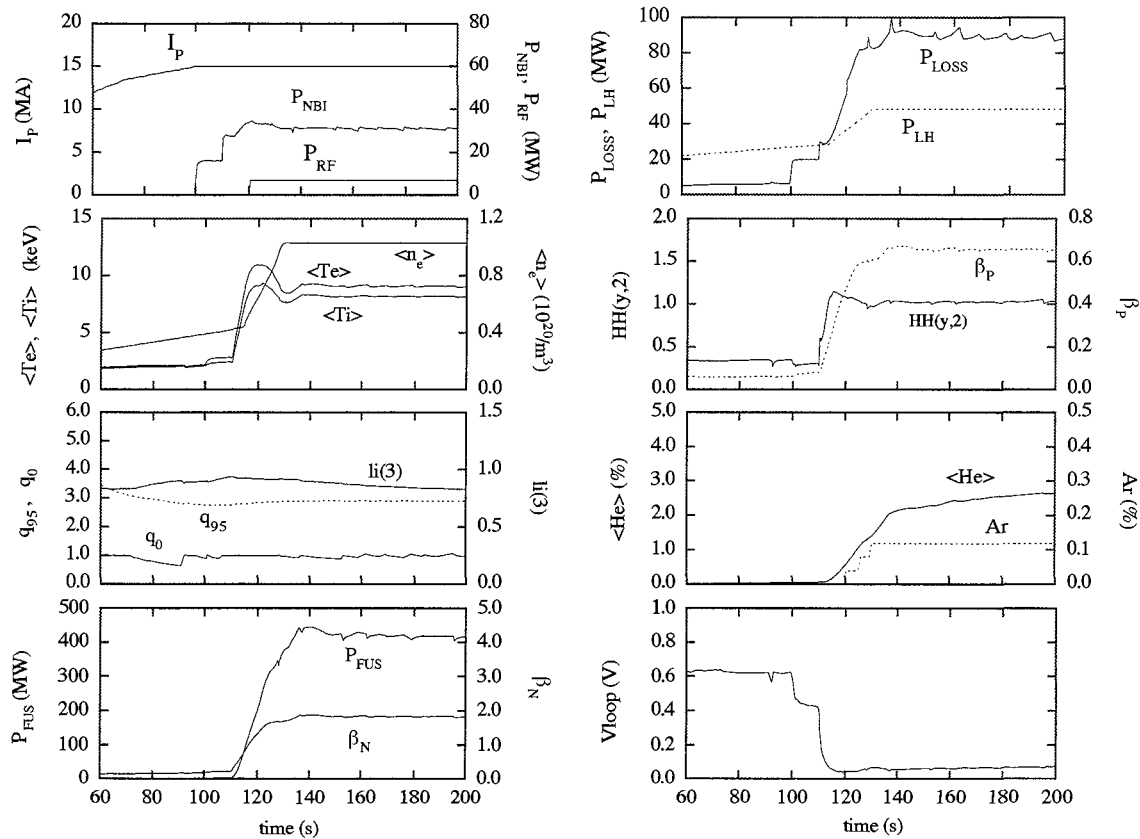


Figure 2.2-2: Time evolution of plasma parameters for 400MW operation (start-up)

⁵ D. Boucher and P.-H. Rebut, in Proc. IAEA TCM on Advances in Simulations of Modeling of Thermonuclear Plasmas, 1992, IAEA, Vienna (1993) 142.

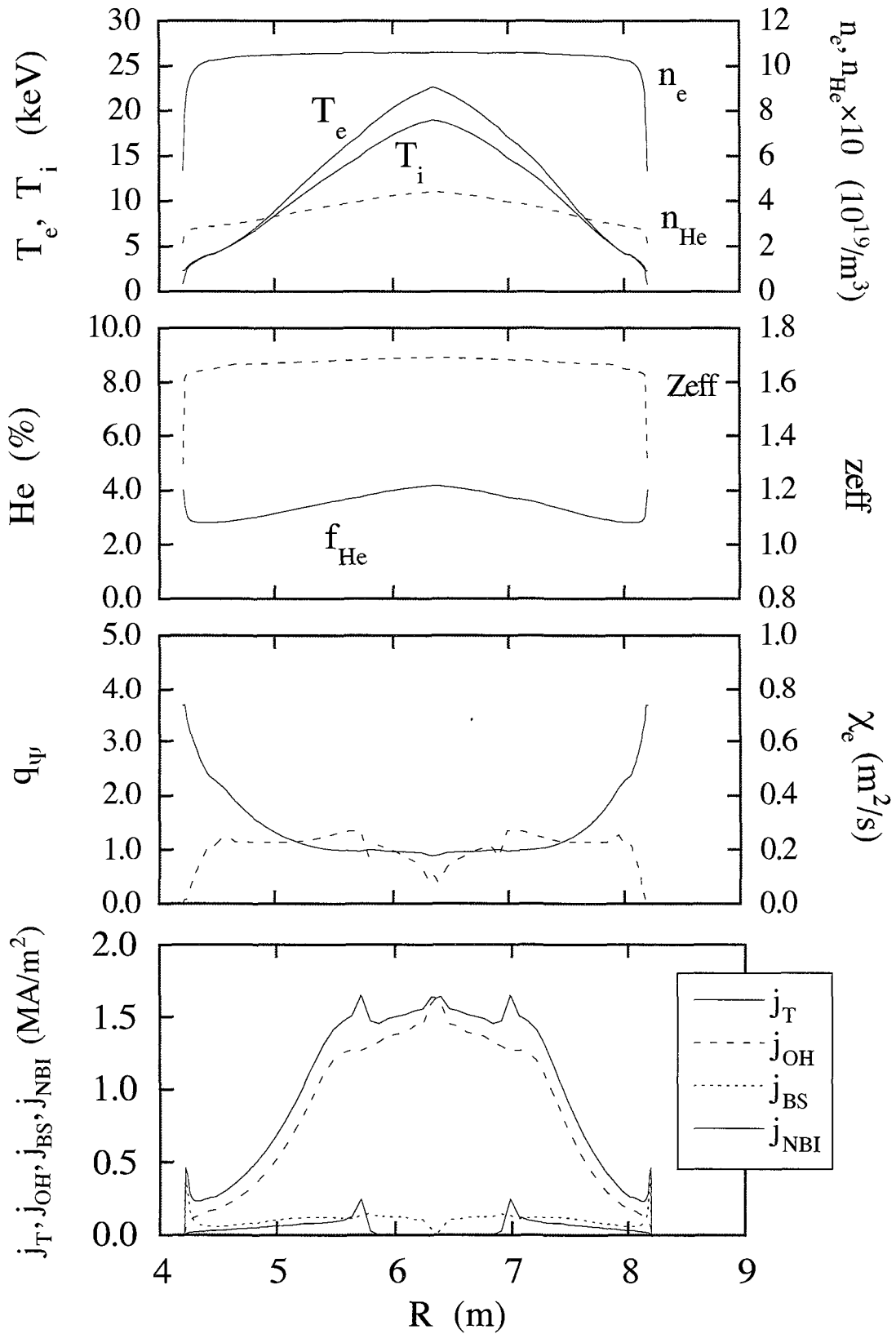


Figure 2.2-3: Profiles of plasma parameters. Here, $P_{FUS} = 400$ MW, $P_{NBI} / P_{RF} = 33$ MW / 7 MW and $H_H(y,2) = 1.0$, respectively

Table 2.2-1 Parameters of ITER-FEAT for typical inductive operation scenario

Parameter		Parameter	
R/a (m/m)	6.2/2.0	P _{OH} (MW)	1
Volume (m ³)	815	P _{TOT} (MW)	121
Surface (m ²)	673	P _{BRM} (MW)	22
Sep. length (m)	18.0	P _{SYN} (MW)	7
S _{cross-sect.} (m ²)	21.9	P _{LINE} (MW)	17
B _T (T)	5.3	P _{RAD} (MW)	46
I _p (MA)	15.0	P _{FUS} (MW)	400
κ _x /δ _x	1.84/0.5	P _{LOSS} /P _{LH}	86/48
κ ₉₅ /δ ₉₅	1.7/0.3	n _{e,sep} (10 ¹⁹ /m ³)	3
I _i (3)	0.82	q _{target} ^t (MW/m ²)	8
V _{loop} (mV)	75	Q	10
q ₉₅	3	τ _E (s)	3.7
β _N	1.81	W _{th} (MJ)	323
<n _e > (10 ¹⁹ /m ³)	10.2	W _{fast} (MJ)	31
n _e /n _{GW}	0.85	H _{H-IPB 98(y,2)}	1.0
<T _e > (keV)	9.1	τ _{He} [*] /τ _E	5.0
<T _i > (keV)	8.2	Z _{eff,axis}	1.69
<β _T > (%)	2.6	f _{He, axis} (%)	4.3
β _p	0.65	f _{Be, axis} (%)	2.0
P _α (MW)	80	f _{C, axis} (%)	0.0
P _{RF} +P _{NB} (MW)	7+33	f _{Ar, axis} (%)	0.12

2.2.2. Effect of Sawteeth

The PRETOR code is also used to evaluate the effects of sawteeth. In order to model the effects of the internal magnetic reconnection empirically, the temperature and pressure profiles within a mixing radius determined by the location of $q = 1$ surfaces are flattened when the perturbed magnetic energy reaches the threshold value. The present model is based on magnetic turbulence⁶ and the stabilizing effect due to fast alpha particles and trapped ions are included.

Figure 2.2-4 shows the detailed time trace of plasma parameters at the current flat top. Here, $T_e(0)$, $T_i(0)$, $q(0)$, P_α , P_{IN} and P_{FUS} denote the electron and ion temperatures, safety factor at the magnetic axis, alpha heating power, power across the separatrix and fusion power, respectively. By the present sawtooth model, the predicted sawtooth period is about 15s for full reconnection. A significant central temperature change is observed but the fusion power change at the crash is about 3%. The alpha heating power increases at the crash since the slowing down time of fast alpha particles becomes short when they are ejected to the peripheral region.

Figure 2.2-5 shows the profiles just before and after the sawtooth crash. In the present model, the inversion radius is relatively large ($\sim 0.6 \times r/a$). When the crash occurs, the power to the

⁶ D. Boucher and P.-H. Rebut, in Proc. IAEA TCM on Advances in Simulations of Modeling of Thermonuclear Plasmas, 1992, IAEA, Vienna (1993) 142.

SOL (P_{IN}) increases slightly due to the increase of alpha power (2MW in this case) and the formation of a steep temperature gradient. This effect, however, does not cause any severe impact on the first wall load, nor divertor target heat load.

The sawtooth prediction involves many uncertainties, but there are experimental and theoretical bases for controlling the sawtooth period by ECCD or ICH. The goal in ITER is to keep the sawtooth period short, to prevent problems such as impurity accumulation in the core and input to NTM seed islands.

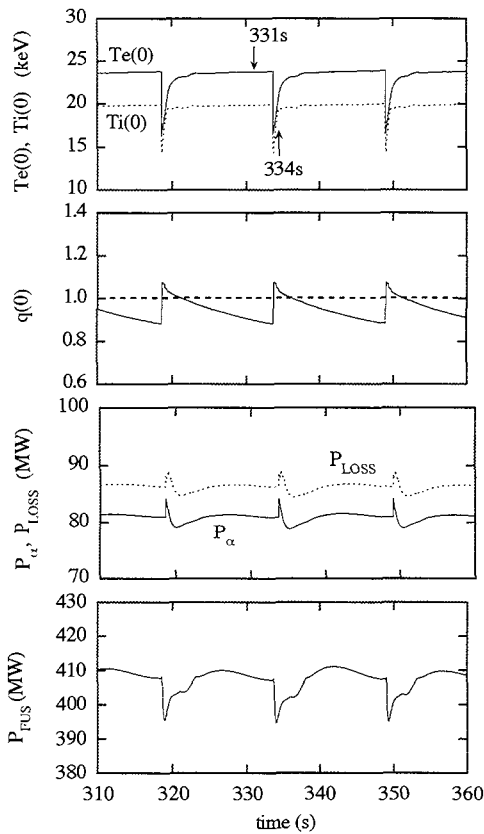


Figure 2.2-4 Time evolution of plasma after the sawtooth crash

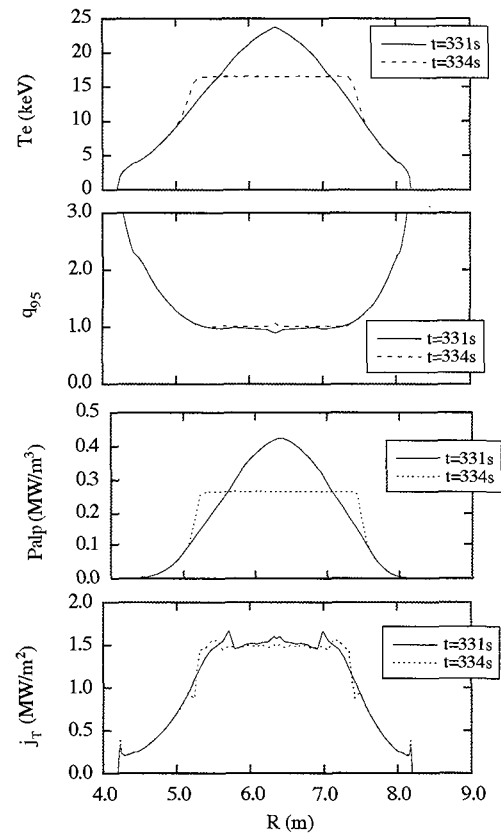


Figure 2.2-5 Plasma profiles before and parameters during flat top

2.2.3. Operation Boundaries

If the electron density is increased close to the Greenwald density n_{GW} , the fusion power increases to 580MW at $I_P = 15$ MA and $H_{H(y,2)} = 1.0$. In this case, the argon impurity should be increased to 0.15% to keep the power flux to the divertor region ≤ 30 MW and Z_{eff} goes up to 1.78. The normalised beta β_N increases to 2.2. Neoclassical tearing modes (NTM) may limit the achievable β_N and cause a degradation of confinement time. Control and suppression of NTMs by ECCD is planned to assure operation of the device at $\beta_N = 2.2$. Simulation predicts that NTMs with $m/n = 3/2$ and $2/1$ could be stabilised by 20 MW of ECCD power⁷. Requirements for fuelling, such as the high field side pellet injection will be studied.

⁷ G. Saibene, *et. al.*, 25th EPS Conference on Controlled Fusion and Plasma Physics, Praha (1998).

The operation would start from relatively low density, e.g. $n_e \sim 0.7 \times n_{GW}$. In this case, the fusion power is about 260 MW at $H_H(y,2) = 1.0$. Figure 2.2-6 shows the time evolution for these cases, with the parameters at the important moments summarised in Table 2.2-2. The poloidal field coil system is designed to cover these operation scenarios.

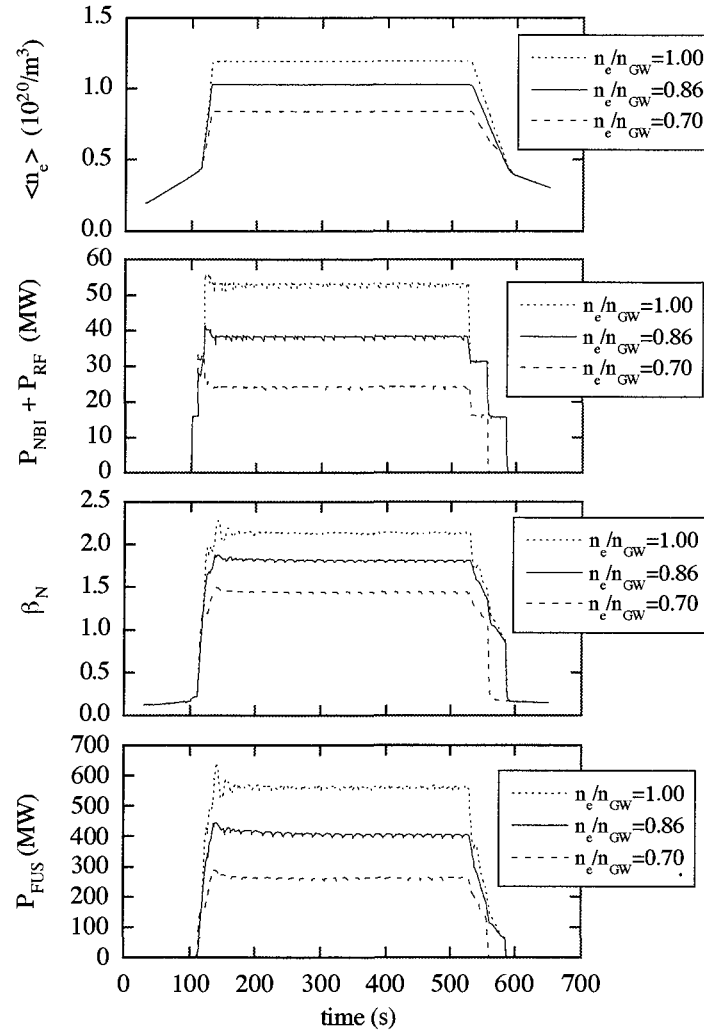


Figure 2.2-6 Time history for various electron density. Here, $H_H = 1.0$ and $Q = 10$

Table 2.2-2 Range of plasma parameters for inductive 15MA, Q = 10 scenario without heating during I_p ramp-up

phase	XPF	SOF/H	SOB	EOB	EOC
t, s	30	100	130	530	590
I_p , MA	7.5	15	15	15	12
q_{95}	5.3	3.0	3.0	3.0	3.0
q_0	1.0	1.0	1.0	1.0	1.0
nom. $\langle n_e, 20 \rangle$	0.2	0.4	1.02	1.02	0.5
min. $\langle n_e, 20 \rangle$	↑	↑	0.84	0.84	↑
max. $\langle n_e, 20 \rangle$	↑	↑	1.20	1.20	↑
nom. n_e/n_{GW}	0.20	0.40	0.85	0.85	0.43
min. n_e/n_{GW}	↑	↑	0.70	0.70	↑
max. n_e/n_{GW}	↑	↑	1.00	1.00	↑
nom. P_{fusion}	0	0	400	400	0
min. P_{fusion}	↑	↑	260	260	↑
max. P_{fusion}	↑	↑	580	580	↑
nom. P_{aux} , MW	0	0	40	40	0
min. P_{aux} , MW	↑	↑	26	26	0
max. P_{aux} , MW	↑	↑	60	60	0
nom. $Z_{eff, axis}$	1.3	1.3	1.69	1.69	1.4
min. $Z_{eff, axis}$	↑	↑	1.57	1.57	↑
max. $Z_{eff, axis}$	↑	↑	1.78	1.78	↑
nom. β_p	0.1	0.05	0.65	0.65	0.1
min. β_p	↑	↑	0.52	0.52	↑
max. β_p	↑	↑	0.79	0.79	↑
nom. β_N	0.1	0.2	1.81	1.81	0.2
min. β_N	↑	↑	1.45	1.45	↑
max. β_N	↑	↑	2.20	2.20	↑

*1 Minimum fusion power is defined by good ELMy-H mode ($P_{IN}/P_{LH} \geq 1.3$) and maximum fusion power by $n_e/n_{GW} \leq 1$.

*2 Burn time is calculated for nominal operation case ($V_{loop} = 75mV$).

*3 Burn time can be prolonged by heating during I_p ramp-up.

2.2.4. Impurity Effect

In surveys of operation scenarios of ITER-FEAT, 2% of beryllium is assumed as a main impurity, and helium accumulation is calculated for the condition that $\tau_{\text{He}}^*/\tau_E = 5$. The assumption of $\tau_{\text{He}}^*/\tau_E = 5$ is reasonable for ELMy H mode plasmas. In addition, argon (Ar) impurity up to 0.2% or carbon impurity up to 1.2% is considered. In this case, the corresponding effective charge, Z_{eff} , is 1.4 to 1.8.

Figures 2.2-7 and 2.2-8 show the plasma parameters with various impurity contents when the fusion power $P_{\text{FUS}} = 400$ MW, fusion gain $Q = 10$ and $H_{\text{H}}(y,2) = 1.0$. In the simulation, we assume $\tau_{\text{He}}^*/\tau_E = 5$.

When argon impurity is seeded, the line radiation increases significantly, while the increase of the required operation density is small. This means that the operation point is robust and the only effect is decrease of burn time due to the increase of loop voltage. In the case of carbon, the line radiation power is small. The increase of the operation density, however, is larger than that for argon case, and the resultant radiation loss power including bremsstrahlung loss power is almost same level as argon case.

The effective charge Z_{eff} in the present confinement database is shown in Figure 2.2-9. Here, the horizontal axis represents the scaling formula

$$Z_{\text{Scaling}} = 1 + 7 \times \frac{P_{\text{RAD}}(\text{MW})}{n_{e20}^2 S_p(\text{m}^2)}$$

where P_{RAD} is the radiation power, n_{e20} is electron density in 10^{20} m^{-3} , and S_p is the plasma surface area. If the data for similar conditions with ITER-FEAT ($\kappa > 1.4$, $q_{95} < 3.5$, $n_e/n_{\text{GW}} > 0.65$, $P_{\text{RAD}}/P < 0.5$) are selected, $1 < Z_{\text{eff}} < 2.1$ as is shown in Figure 2.2-10. In the figure, the symbol (+) denotes JET data. This figure means that Z_{eff} for high density plasmas with a Be first wall is relatively small and close to assumptions used in this report.

To summarise, the requirement from performance is that Z_{eff} should be smaller than 2.0. On the other hand, radiative cooling is such that the peak divertor heat load is lower than 8 MW/m^2 . According to calculations of divertor transport described in section 2.6, the peak power load can be lowered to 8 MW/m^2 at a separatrix density of $3.2 \times 10^{19} \text{ m}^{-3}$. At the same time Z_{eff} and helium concentration can remain at low values controlled by the divertor operation. These calculations suggest that the ITER FEAT divertor can exhaust heat and particles efficiently. However, this estimate is probably underestimating the impurity influx since it neglects the impurity flux from the first wall. Presently PRETOR is assuming 2 % of beryllium and helium concentrations, higher than 2D divertor calculation (4.3 % vs. 1.2 %), to be conservative.

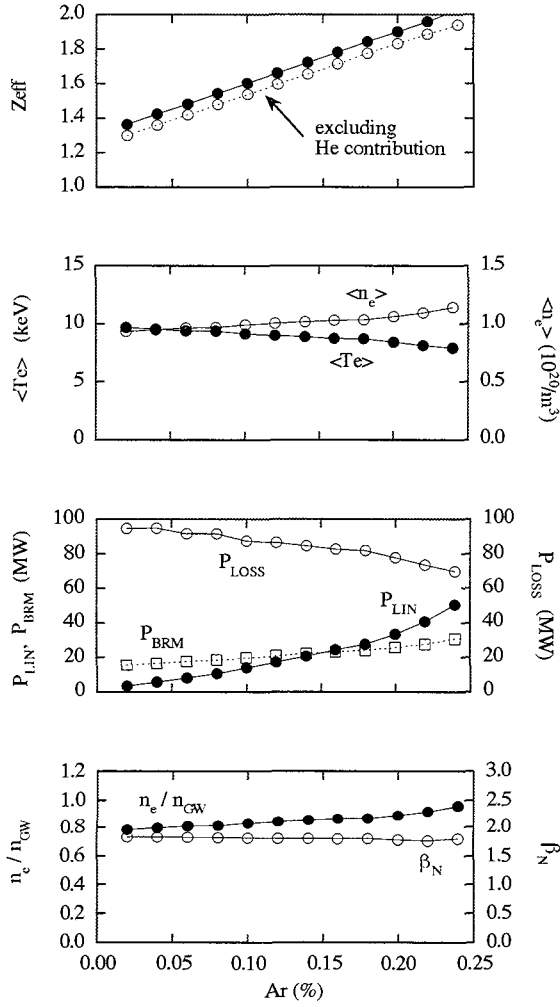


Figure 2.2-7 Plasma parameters for various Ar fractions. Here, $Q=10$, $H_H=1$ and $P_{FUS}=400\text{MW}$

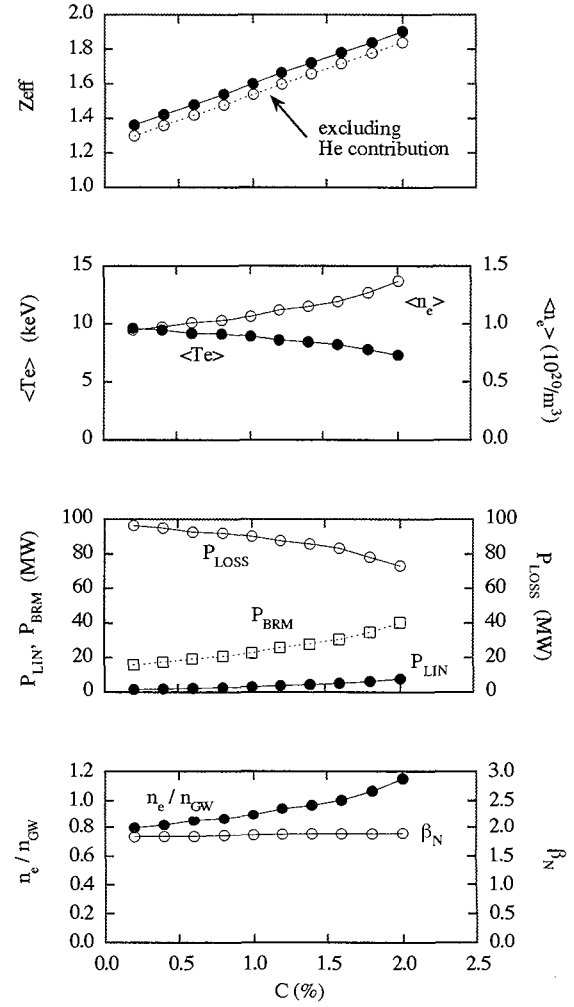


Figure 2.2-8 Plasma parameters for various C fractions. Here, $Q=10$, $H_H=1$ and $P_{FUS}=400\text{MW}$

DB3v5 : All observations with auxiliary heating

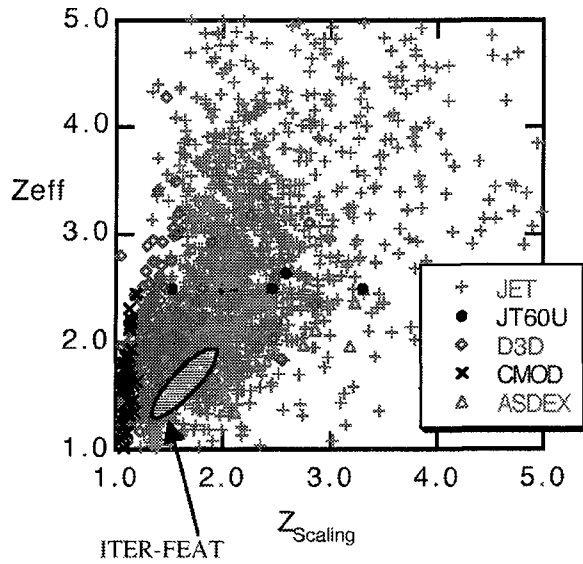


Figure 2.2-9 Z_{eff} for all shots in database DB3v5

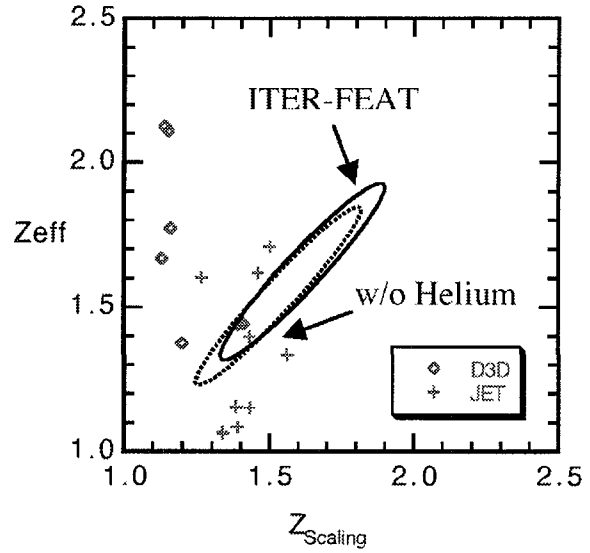
 $\kappa > 1.4$, $q_{95} < 3.5$, $n_e/n_{\text{GW}} > 0.65$, $P_{\text{RAD}}/P < 0.5$ 

Figure 2.2-10 Z_{eff} for shots with $\kappa > 1.4$, $q_{95} < 3.5$, $n_e/n_{\text{GW}} > 0.65$, $P_{\text{RAD}}/P < 0.5$

2.2.5. Density Profile Effect

In the reference scenario, a flat density profile is assumed. In general, peaked density profiles tend to produce larger fusion power for the same average density. Operation with peaked density profile due to the pinch effect has been examined using the PRETOR code. Figure 2.2-11 shows the density profiles when a pinch term proportional to the thermal diffusivity and to the magnetic shear is included with a different pinch coefficient V_p . The pinch effect is not significant in the core region ($r/a < 0.5$) where the shear is small. Figure 2.2-12 shows the fusion power for various pinch coefficients. Here, the ratio n_e/n_{GW} of average electron density to Greenwald density is fixed to 0.85.

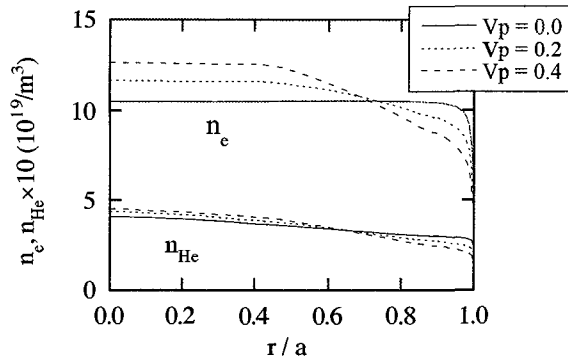


Figure 2.2-11 Density profiles for various pinch coefficients V_p ($n_e/n_{\text{GW}} = 0.85$)

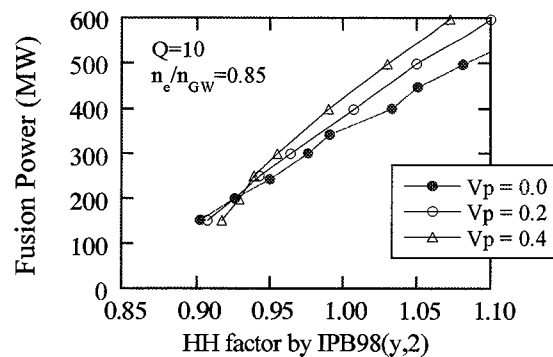


Figure 2.2-12 Dependence of fusion power on H_H factor for the pinch coefficients shown in Figure 2.2-11

Significantly higher fusion power is available in the nominal to high H_H -factor region, while the margin below 1.0 in H_H -factor is decreased from 10 to 8 % since the temperature decreases with the increase of density. Helium accumulation due to the pinch effect also degrades the performance. Deep fuelling by pellet injection from the high field side will be studied.

2.2.6. Ion Heating Effect

Strong ion heating by ICH is also favourable for the improvement of the confinement margin. Figure 2.2-13 shows the relation between the H_H -factor and fusion power for different ion heating fractions $P_I/(P_I + P_E)$ from PRETOR analysis. Here, heating power $P_I + P_E$ is adjusted to $Q = 10$ with $n_e/n_{GW} = 0.85$. Fusion power increases through the H_H range, and the lower H_H margin is improved from 10% to 12%. ICH power alone of 20MW would allow a fusion power of 200 - 300 MW.

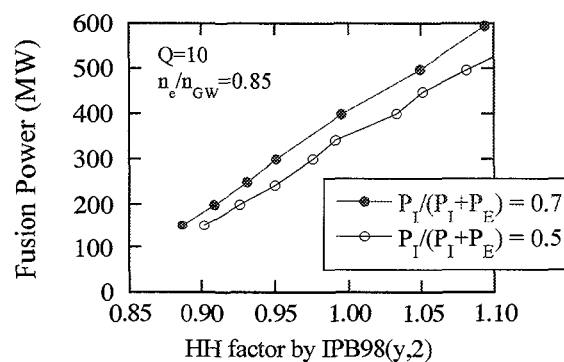


Figure 2.2-13 Dependence of Fusion Power on H_H Factor for Various Ion Heating Fractions.

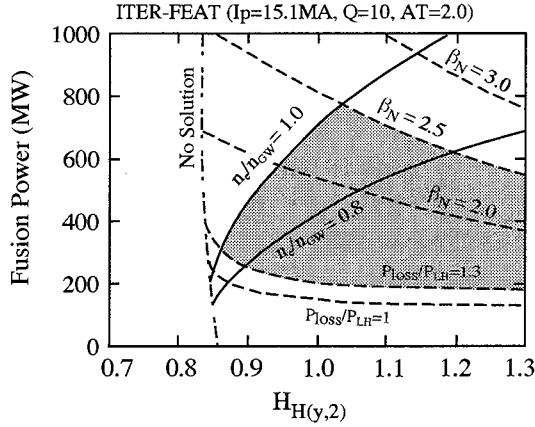
2.2.7. Temperature Profile Effect

In this section, operation domains for various temperature profiles calculated by a simple 0-D code are presented. A parabolic temperature profile $T(x) = T(0) (1-x^2)^{AT}$ is assumed with a parameter AT .

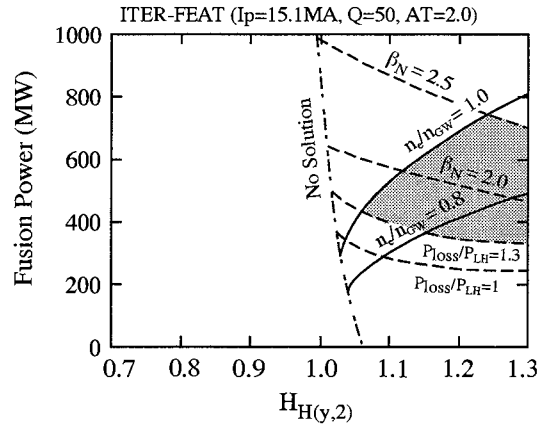
Figures 2.2-14 show the operation domain in H_H -factor and fusion power space when $Q = 10$. The confinement margin does not change significantly with the change of temperature profile. In higher fusion power region, however, the requirement for the density limit is mitigated and the confinement margin increases when the temperature profile becomes flat (AT decreases). There is no significant difference between the cases with $AT = 1.0$ and $AT = 1.5$ when $Q = 10$.

Figures 2.2-15 show the operation domain in H_H -factor and fusion power space when $Q = 50$. A similar tendency is seen.

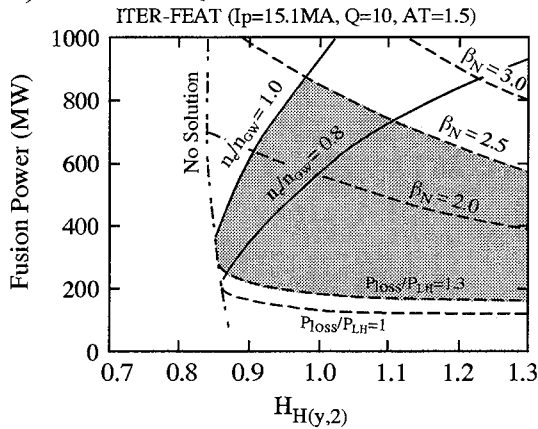
a) AT = 2.0, Q = 10



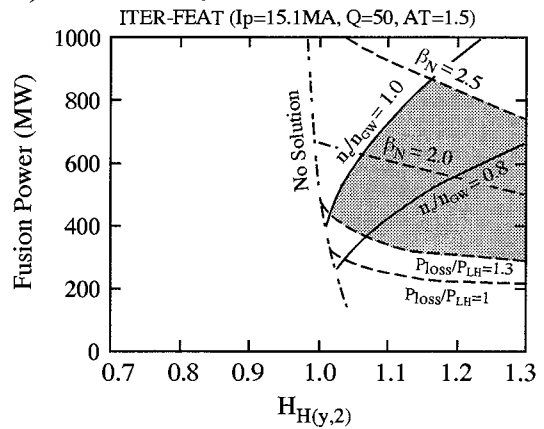
a) AT = 2.0, Q = 50



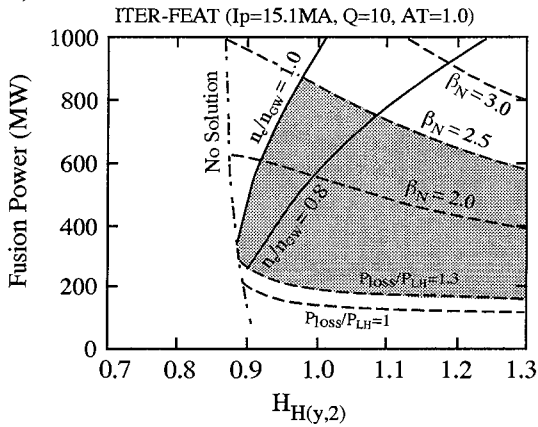
b) AT = 1.5, Q = 10



b) AT = 1.5, Q = 50



c) AT = 1.0, Q = 10



c) AT = 1.0, Q = 50

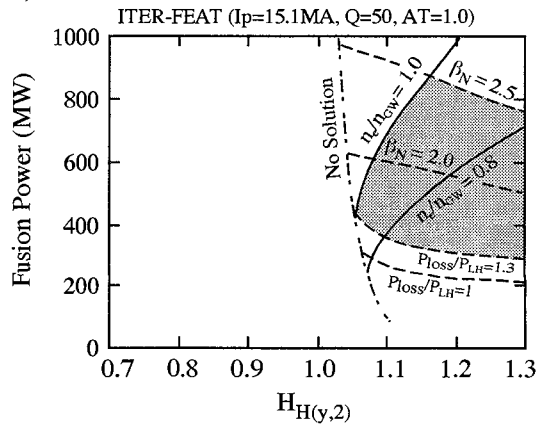


Figure 2.2-14 Operation space of ITER-FEAT when $I_p = 15.1\text{ MA}$ and $Q = 10$

Here, $T(x) = T(0) (1-x)^{2AT}$

a) AT = 2.0, b) AT = 1.5,

c) AT = 1.0

Figure 2.2-15 Operation space of ITER-FEAT when $I_p = 15.1\text{ MA}$ and $Q = 50$

Here, $T(x) = T(0) (1-x)^{2AT}$

a) AT = 2.0, b) AT = 1.5,

c) AT = 1.0.

2.2.8. Effect of Degradation near the Greenwald Density

Confinement time degradation near the operation boundary (especially near the density limit) is generally observed in experiments⁸. The deterioration can be mitigated by high triangularity. In JET, for example, with triangularities ~ 0.35 , good confinement is maintained up to $0.8 \times n_{GW}$. Furthermore, the confinement near the Greenwald density can be improved by high-field-side pellet injection. This area remains an intensive research subject, but one possible explanation can be given by the physics of the edge pedestal, which is described in section 2.5. In this section, the sensitivity of operation performance to confinement saturation is investigated by using a 0-D code. An example of confinement saturation is examined, in which the density dependence of confinement is neglected when the electron density is above $0.8 \times n_{GW}$. This is not a very conservative assumption, but it provides a sensitivity analysis.

Figure 2.2-16 shows the plasma parameters as functions of the normalised density. Here, CASE-A denotes the case with original IPB98(y,2) scaling and CASE-B corresponds to the case including the saturation of confinement time. The confinement time is constant above $0.8 \times n_{GW}$ and the corresponding H_H -factor decreases; therefore the fusion power saturates. In this case, a fusion power of 400 MW can be produced with $n_e \sim 0.95 \times n_{GW}$. Here, $Q = 10$, $\tau_{He^*}/\tau_E = 5$, $Be = 2\%$ and $Ar = 0.12\%$ to be conservative. (The fraction of Ar could be reduced in high density operation.) The density profile is flat and a temperature profile $T(x) = T(0)(1-x^2)^{AT}$ with $AT=2.15$ is used.

⁸ G. Saibene, *et. al.*, 25th EPS Conference on Controlled Fusion and Plasma Physics, Praha (1998).

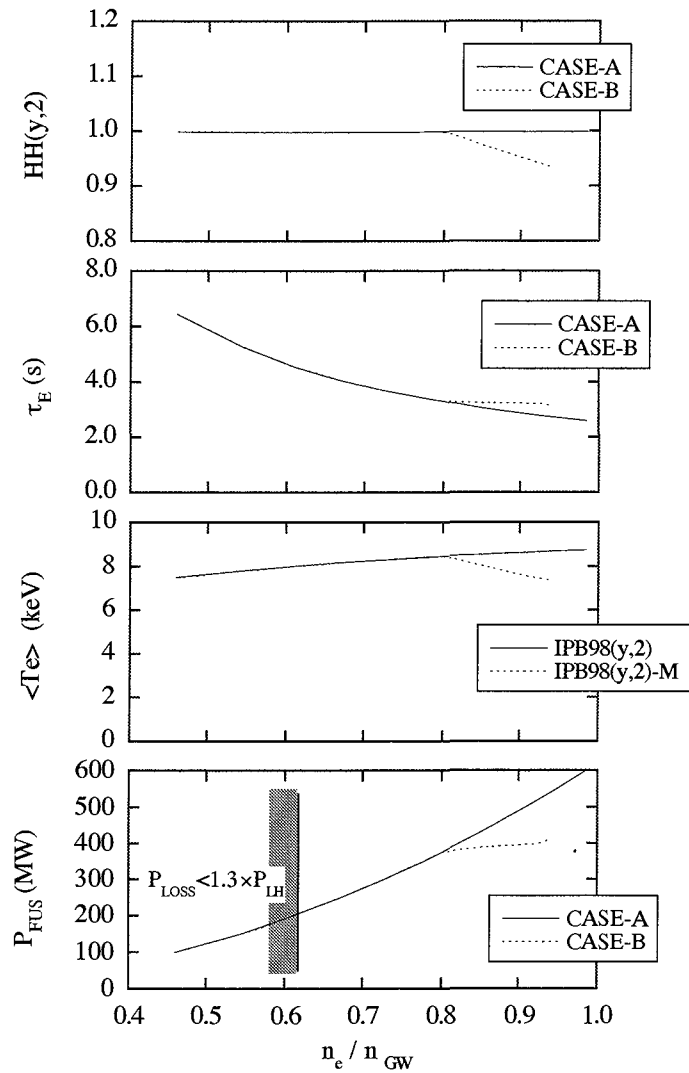


**Figure 2.2-16 : Operation parameters as a function of electron density normalised by Greenwald density n_{GW} . Here, $Q=10$, $\tau_{He^*}/\tau_E=5$, $Be=2\%$ and $Ar=0.12\%$ Density profile is flat and temperature profile $T(x)=T(0)(1-x^2)^{AT}$ with $AT=2.15$. CASE-A : IPB98(y,2) scaling
CASE-B : IPB98(y,2) scaling, but no density dependence when $n_e > 0.8 \times n_{GW}$.**

2.3. High-Q (~50) Operation and Possibility of Ignition

As described in the ODR⁹, high-Q (~50) operation is possible with $H_H = 1.0$ when the plasma current is 17 MA. In this section, the method to achieve such an operation is examined and the possibility of ignition is explored. Here, the current ramp-up and density build-up are not considered for simplicity.

Figure 2.3-1 shows the PRETOR simulation for high-Q operation when the plasma current is 17MA and the electron density is $1.1 \times 10^{20}/\text{m}^3$ ($\sim 0.81 \times n_{GW}$). Helium accumulation is calculated by assuming $\tau_{He^*}/\tau_E = 5$. At the flat top, auxiliary heating power (P_{AUX}) is 10 MW and about 450 MW ($Q = 45$) of fusion power (P_{FUS}) is produced. In this case, 73 MW of auxiliary heating power is added from 10s to 13.5s to achieve the H-mode transition. Here, P_{LH} is the threshold power for LH-transition and P_{LOSS} is the power across the H-mode edge pedestal. In the early phase of the discharge, thermal instability can be observed. This result implies that ignition is possible by turning off the auxiliary heating power for a short period.

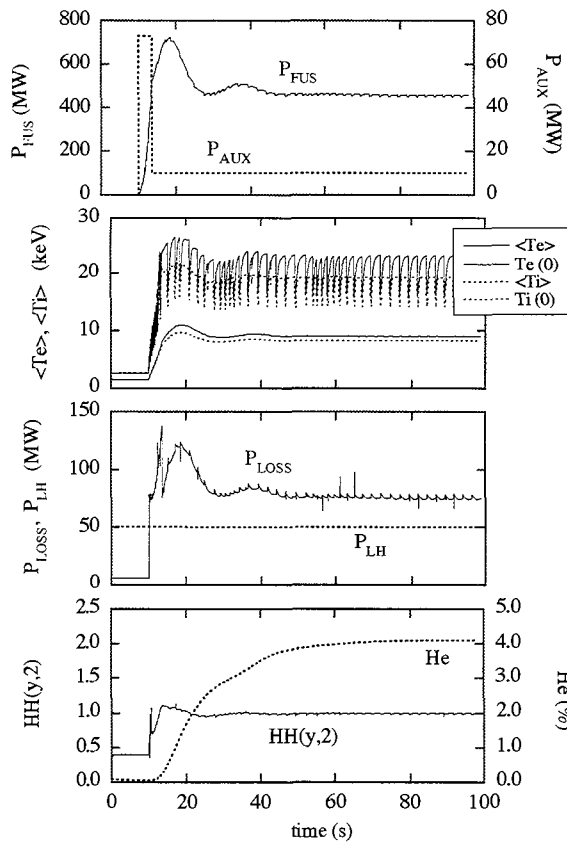


Figure 2.3-1 Time evolution of plasma parameters for transient ignition.
Here, $I_p=17$ MA, $\langle n_e \rangle = 1.1 \times 10^{20}/\text{m}^3$
($n_e/n_{GW}=0.81$) and $\tau_{He^*}/\tau_E=5$.

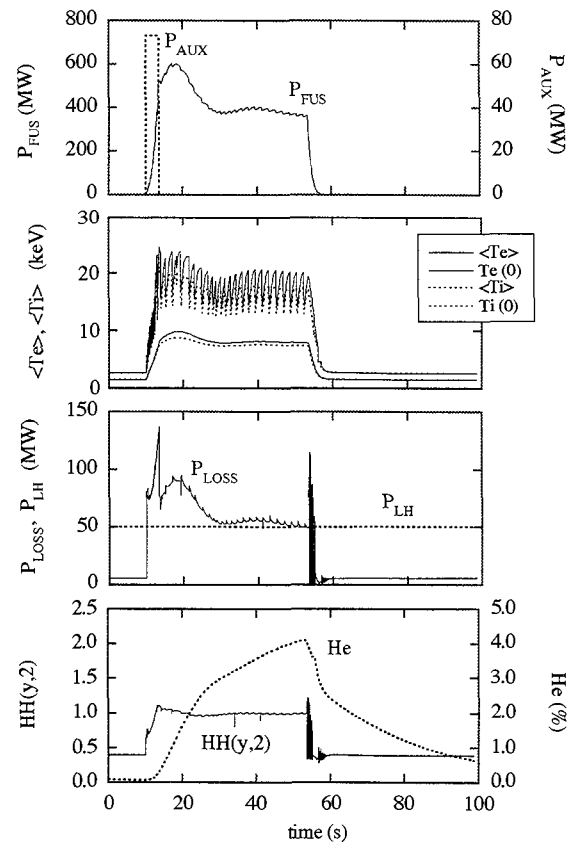


Figure 2.3-2 Time evolution of plasma parameters for high-Q operation.
Here, $I_p=17$ MA, $\langle n_e \rangle = 1.1 \times 10^{20}/\text{m}^3$
($n_e/n_{GW}=0.81$) and $\tau_{He^*}/\tau_E=5$.

Figure 2.3-2 shows the result for ignition. When the heating power is turned off at $t = 13.5$ s, the helium level is very small and the self-heating power is large enough to stay in H-mode.

⁹ Technical Basis for the ITER-FEAT Outline Design G A0 RI 2 00-01-18 R1.0.

Other assumptions are the same as Figure 2.3-1. In this case, the ignition state is maintained for about 40s and the L-mode transition occurs at $t = 55$ s. In this study, hysteresis for HL-transition is not assumed and dW/dt is not included in P_{LOSS} to be conservative.

Figure 2.3-3 shows the results for various helium accumulation levels. The ignition operation continues in steady state when $\tau_{He}^*/\tau_E \leq 4$. It is seen that a transient ignition experiment can be performed even for lower pumping efficiency ($\tau_{He}^*/\tau_E = 7$).

Figure 2.3-4 shows the results when the H_H -factor is improved by 10%. In this case, $\tau_{He}^*/\tau_E = 5$ is assumed but other assumptions are the same as previous figures. When $H_H = 1.1$, the fusion power increases by about 25% and the ignition continues as long as PF-coil flux (more than 100 s) is available even when $\tau_{He}^*/\tau_E = 5$.

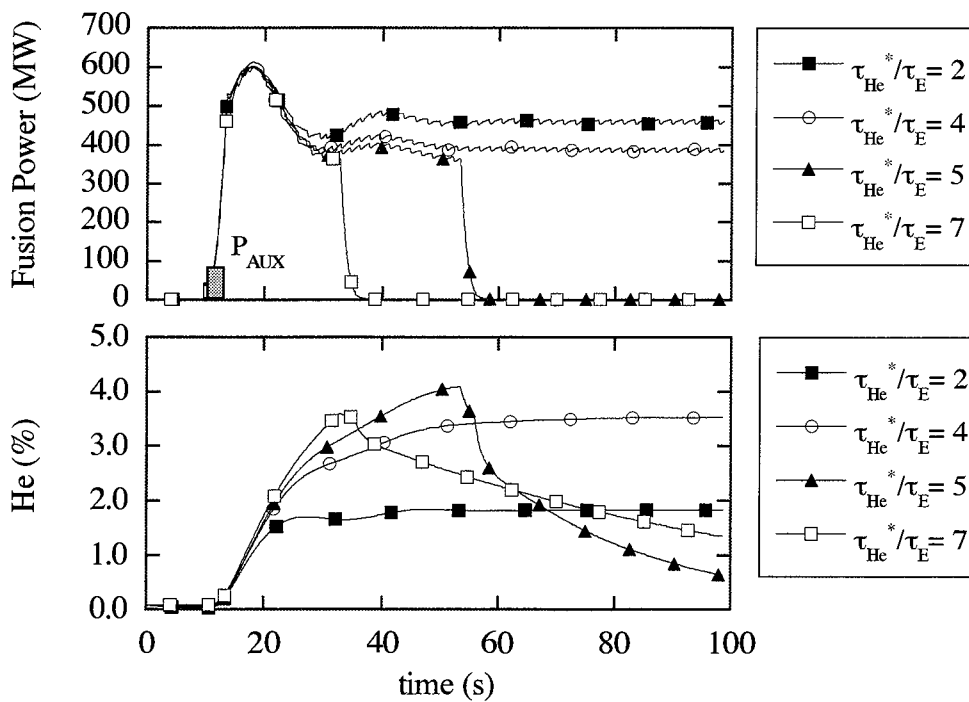


Figure 2.3-3: Time traces of fusion power and helium fraction for various τ_{He} assumptions. Here, $I_p = 17$ MA, $\langle n_{e20} \rangle = 1.1$ ($n_e/n_{GW} = 0.81$) and $P_{AUX} = 73$ MW from $t = 10$ s to $t = 13.5$ s. L-mode transition occurs when the loss power P_{LOSS} is less than P_{LH}

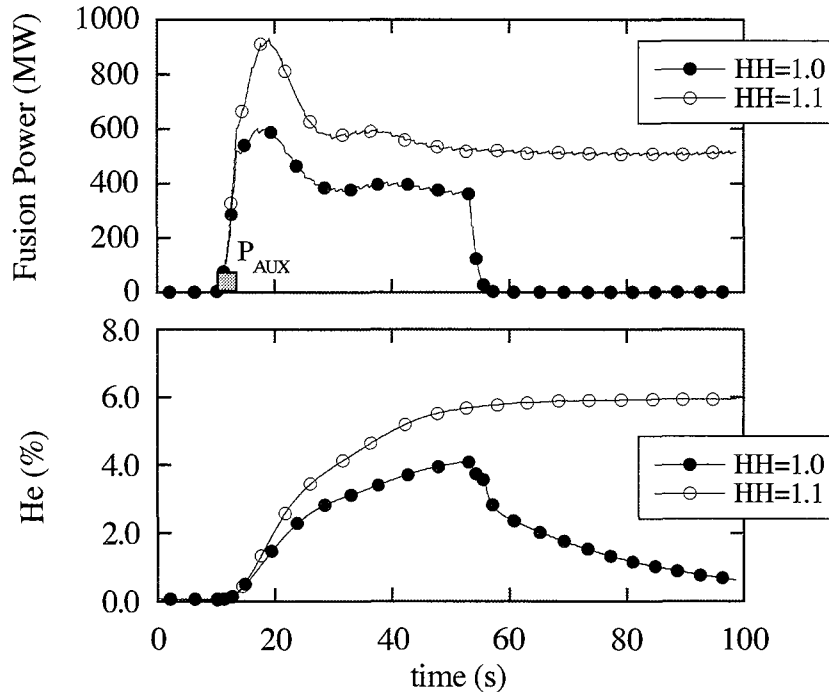


Figure 2.3-4: Time traces of fusion power and helium fraction when H_H -factor is improved. Here, $\tau_{He^*}/\tau_E = 5$, $I_p = 17$ MA, $\langle n_{e20} \rangle = 1.1$ ($n_e/n_{GW} = 0.81$) and $P_{AUX} = 73$ MW from $t = 10$ s to $t = 13.5$ s. L-mode transition occurs when P_{LOSS} is less than P_{LH} .

2.4. Long Pulse and Steady-state Operations

2.4.1. Long Pulse Operations

A hybrid mode of operation, in which a substantial fraction of the plasma current is driven by external CD power and the bootstrap current, is a promising route towards the establishment of true steady-state modes of operation. Table 2.4-1 shows two scenarios of hybrid operation, with plasma currents of 13.5 MA. These scenarios satisfy $Q \sim 5$ and burn time ~ 1000 s at $H_H = 1$. Both scenarios use the full size plasmas ($R/a = 6.2$ m/2.0 m). Scenario 1, with a fusion power of 400 MW, is compatible with the auxiliary heating power available in the initial phase (73 MW), while scenario 2, with a fusion power of 500 MW, requires a total auxiliary heating power of 100 MW. The advantage of high current (13.5 MA) scenario is that the requirements on β_N and density are very modest. These scenarios show that long pulse operation regimes are accessible to ITER-FEAT at a modest requirement, in particular at 400 MW – 1000 s.

Table 2.4-1 PRETOR simulation: Hybrid mode 400/500 MW

	1	2
R (m) / a (m)	6.2 / 2.0	(
$\kappa_{95} / \delta_{95}$	1.7 / 0.33	(
V_P (m ³)	814	(
B_T (T)	5.3	(
I_P (MA)	13.5	(
q_{95}	3.2	(
$\langle n_e \rangle$ (10 ¹⁹ m ⁻³)	9.3	10.0
n / n_{GR}	0.87	0.94
$\langle T_i \rangle$ (keV)	8.4	8.8
$\langle T_e \rangle$ (keV)	9.7	10.2
β_N	1.98	2.25
P_{FUS} (MW)	400	500
P_{NBI} (MW)	33	40
P_{RF} (MW)	40	60
$Q = P_{FUS} / (P_{NBI} + P_{RF})$	5.4	5.0
P_{loss} / P_{LH}	115/46	152/48
τ_E (s)	2.70	2.29
He (axis/ave) %	3.6 / 2.6	3.3 / 2.4
Ar (axis) %	0.17	0.20
Z_{eff} (ave)	1.79	1.88
P_{RAD} (MW)	51.9	65.1
β_p	0.79	0.90
l_i (3)	0.93	0.93
I_{CD} / I_P %	25	32
I_{BS} / I_P %	18	21
γ_{20NBI} (A/Wm ²)	0.24	0.23
γ_{20RF} (A/Wm ²)	0.30	(
γ_{20TOT} (A/Wm ²)	0.27	0.28
V_{loop} (mV)	60	52
H_{F-98} (y2)	1.0	←
τ_{α}^* / τ_E	5	←
Burn time (s)*	880	1020

2.4.2. Steady-state Operation

Here, the possibility of steady-state operation in ITER-FEAT is examined by using a 1.5-D transport code. In the simple analysis reported in the ODR¹⁰, it was shown that a relatively large H_H -factor is required to achieve steady-state operation with $Q = 5$, even with a somewhat high efficiency of current drive. In this section, an H_H -factor survey is performed for given current-drive power, and the achievable fusion power (and Q -value) is investigated. The current-drive efficiency of NBI is given by the Mikkelsen-Singer model¹¹ and the normalised current drive efficiency for RF is fixed to about $0.24 \times 10^{20} \text{ A/Wm}^2$. In this survey, 40 MW of RF power (5 MW on axis and 35 MW in the peripheral region) is used. Two cases (33MW and 60 MW) of NBI power are investigated.

Figure 2.4-2 shows the relation between H_H -factor and the achievable Q -value in non-inductive operation of ITER-FEAT. When the current-drive power is 73 MW (NBI 33 MW and RF 40 MW), the required H_H -factor is about 1.6 to achieve steady-state operation with $Q = 5$. In this case, $n_e/n_{GW} = 0.7$ and $\beta_N = 3.1$. When the current-drive power is 100 MW (NBI 60 MW and RF 40 MW), the required H_H -factor is about 1.4 to achieve steady-state operation with $Q = 5$. In this case, $n_e/n_{GW} = 0.65$ and $\beta_N = 3.2$. Further study is needed.

¹⁰ Technical Basis for the Outline Design of ITER-FEAT, G A0 RI 2 00-01-18 R1.0

¹¹ D. R. Mikkelsen and C. E. Singer, Nucl. Technol. /Fusion 4 (1983) 237.

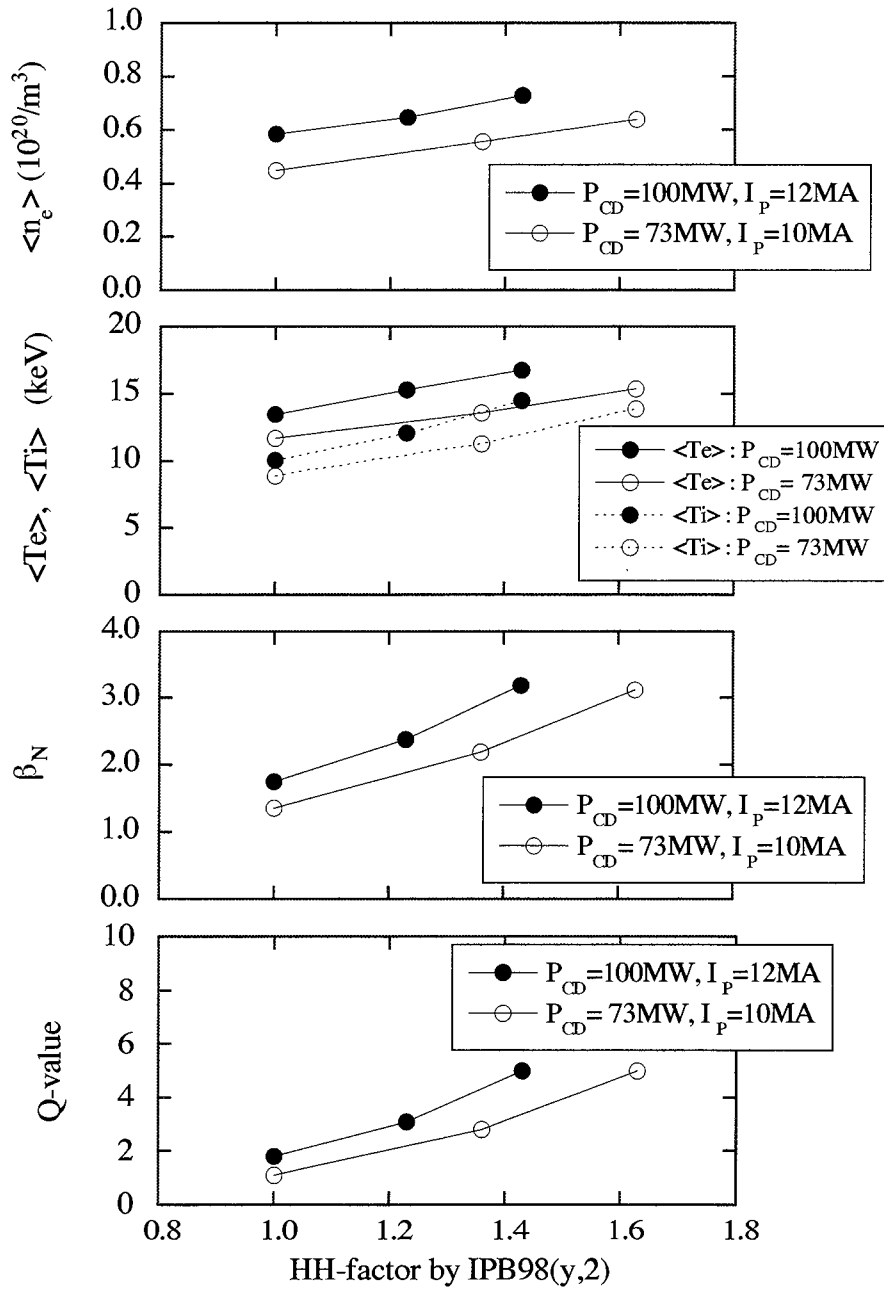


Figure 2.4-2 Steady-state operation parameters of ITER-FEAT.

2.5. Confinement Database

2.5.1. Present ELMMy H-mode Confinement Database

For information, the ITER-FEAT reference point is compared with the data from the H-mode confinement database DB3v5¹². The subset of the database for (y,2) scaling is used. The data represents a cloud of points in multi-dimensional space of different parameters. This cloud is projected onto the planes of $H_H(y,2)$ factor ($H_H(y,2) = \tau_{\text{exp}}/\tau_{y,2}$) versus the following parameters:

- β_N - normalised beta;
- κ_a - elongation calculated through area;
- δ_x - triangularity at separatrix;
- q_{95} - safety factor;
- P/P_{LH} - heating power related to predicted threshold power of L- to H-mode transition;
- ν^* - normalised collisionality;
- n/n_{GW} - plasma density related to Greenwald density.

The position of the ITER-FEAT reference point is indicated on the figures. All figures with $H_H(y,2)$ versus β_N , κ_a , δ_x , q_{95} , P/P_{LH} , ν^* demonstrate that the ITER-FEAT point lies in the interior of the cloud of experimental points, except for Figure 2.5-7: $H_H(y,2)$ versus n/n_{GW} . The ITER-FEAT reference point lies close to the boundary of the cloud of experimental points on this graph.

All of these graphs indicate that there are many experiments with $H_H(y,2) \sim 1$ at parameters relevant to ITER-FEAT, but (not evident in the graphs) there are only a few data points having simultaneously parameters relevant to ITER-FEAT and which give $H_H \sim 1$. However, the width of the distribution in H_H against all other parameters is not representative of a probability distribution against random values of the other parameters: distinct physical phenomena are acting, not all of which are identified and understood.

¹² ITER Physics Basis, Nucl. Fus. 39 (1999) 2175

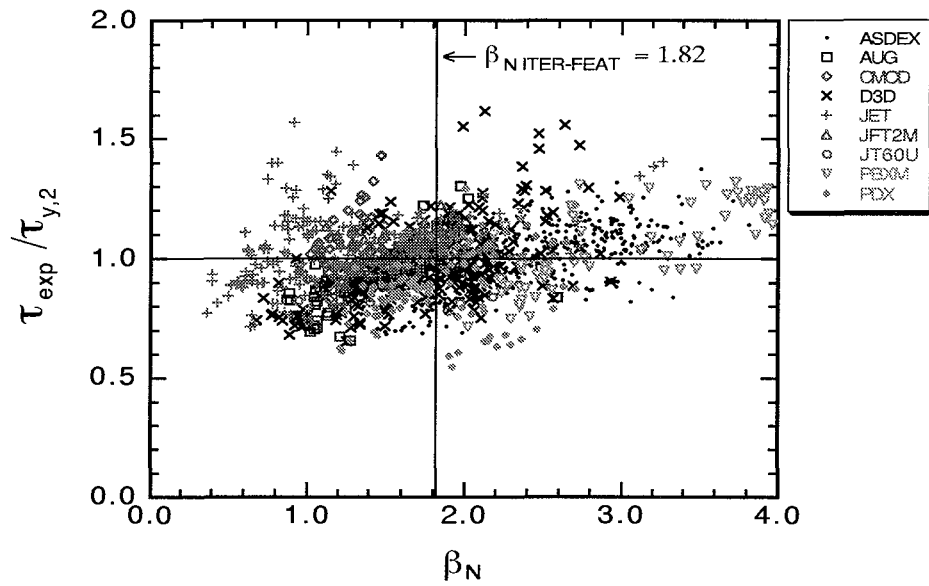


Figure 2.5-1 $H_H(y,2) = \tau_{\text{exp}}/\tau_{y,2}$ versus β_N .

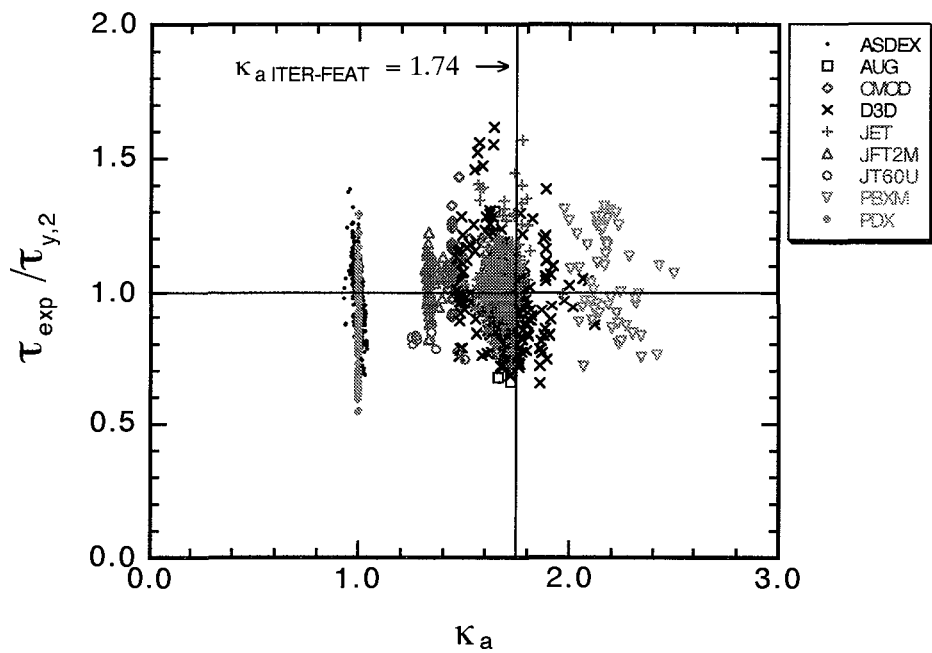


Figure 2.5-2 $H_H(y,2) = \tau_{\text{exp}}/\tau_{y,2}$ versus κ_a .

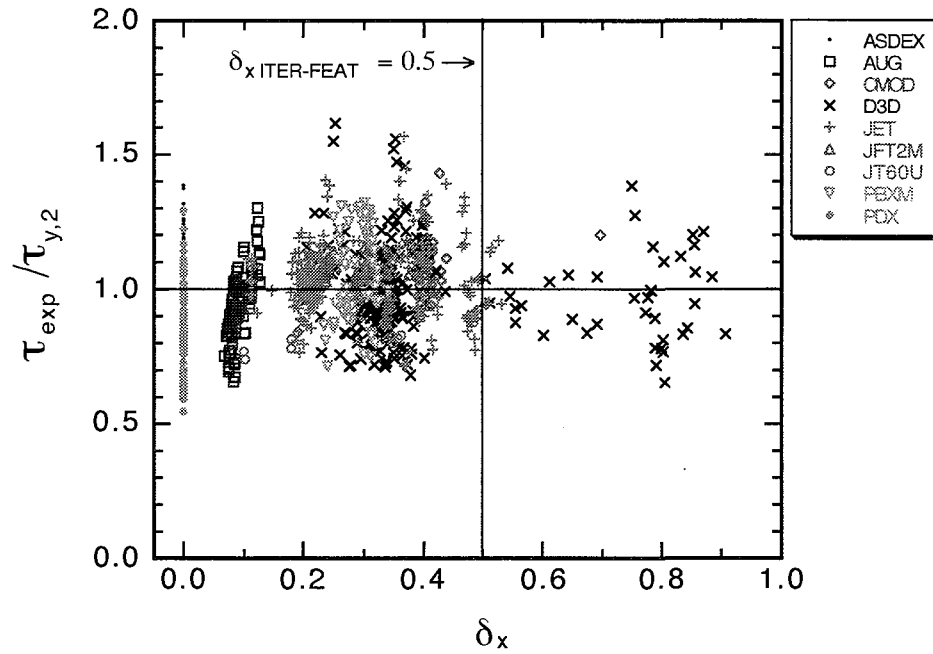


Figure 2.5-3 $H_H(y,2) = \tau_{\text{exp}} / \tau_{y,2}$ versus δ_x .

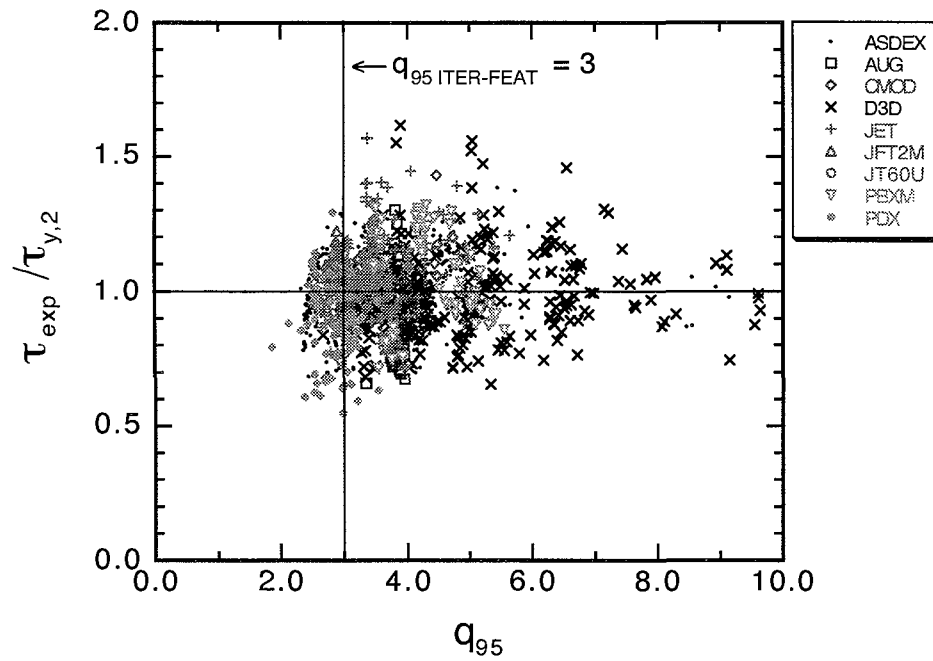


Figure 2.5-4 $H_H(y,2) = \tau_{\text{exp}} / \tau_{y,2}$ versus q_{95} .

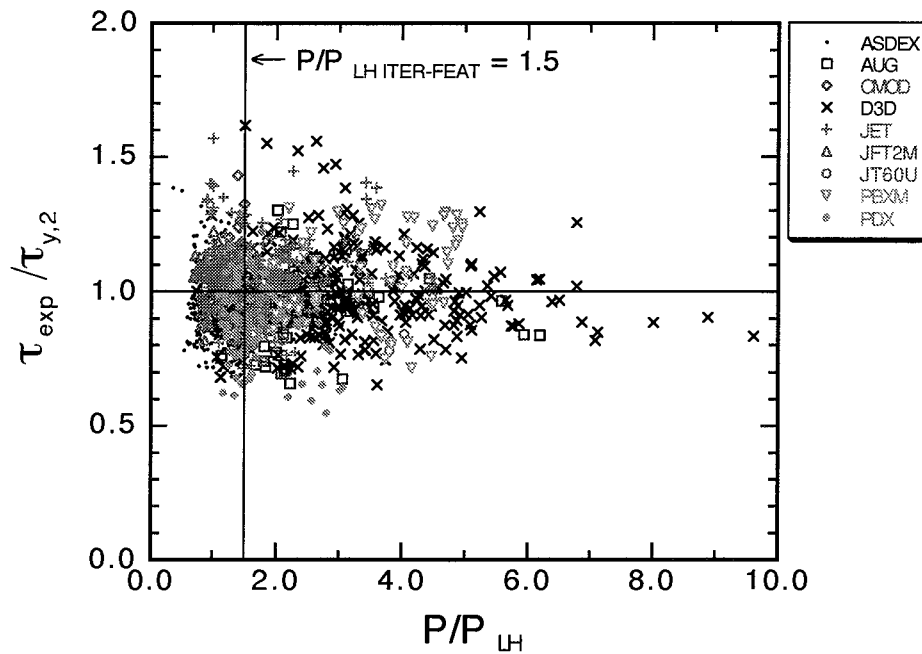


Figure 2.5-5 $H_{\text{H}}(y,2) = \tau_{\text{exp}} / \tau_{y,2}$ versus P/P_{LH} .

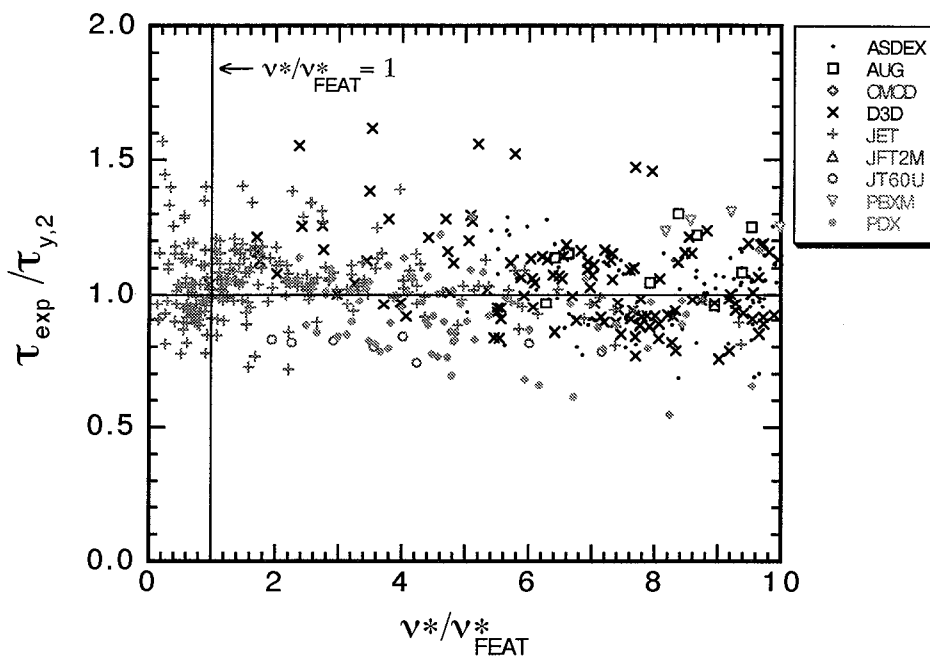


Figure 2.5-6 $H_{\text{H}}(y,2) = \tau_{\text{exp}} / \tau_{y,2}$ versus v^*/v^*_{FEAT} ,
points with $v^*/v^*_{\text{FEAT}} > 10$ are omitted.

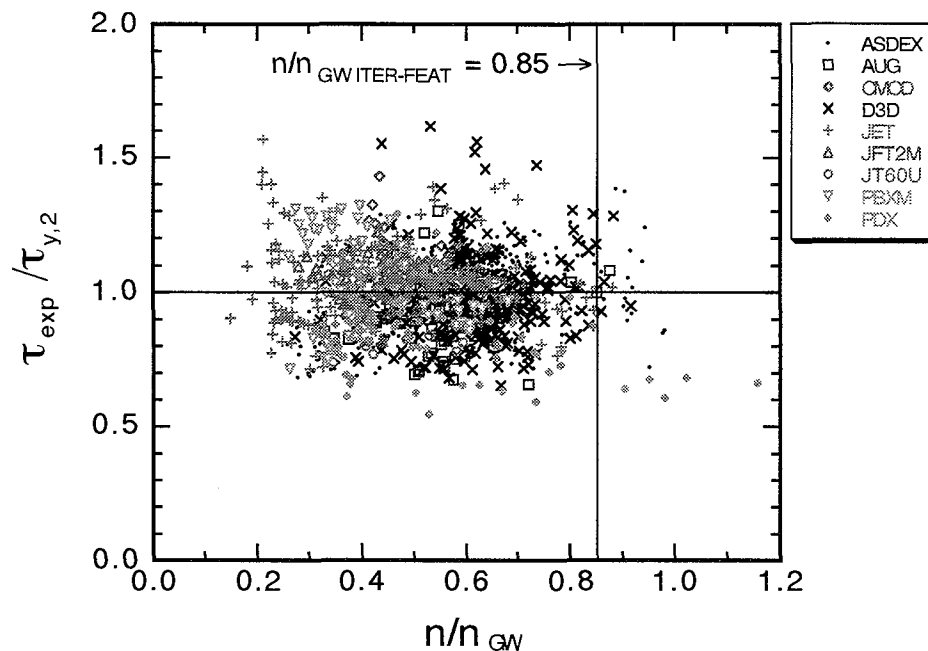


Figure 2.5-7 $H_H(y,2) = \tau_{exp}/\tau_{y,2}$ versus n/n_{GW} .

2.5.2. Necessity of Dimensionless Transport Studies

There are no data for the Dimensionless Transport Study for ITER-FEAT. New experiments in the present tokamaks are required.

2.5.3. Offset non-linear confinement scalings and edge pedestal

During recent years, increasing attention has been paid to development of the physics based on offset non-linear confinement scalings taking account of different transport properties of the core and edge plasmas. This activity is presently in its early stage and suffers mainly from the absence of a reliable model for the edge pedestal parameters. The next section provides one insight into this problem from a very different point of view.

2.5.4. Predictions of ELM Energy Loads and their Control in ITER-FEAT

During recent years a basic understanding of the relation between the H-mode pedestal and the core energy confinement has emerged¹³ which allows to understand e.g. the importance of

¹³ G. Janeschitz, Yu. Iglikhanov, M. Sugihara et al., 26 the EPS Conference on Contr. Fusion Plasma Physics, Maastricht, (1999) p 1445.

M. Sugihara, Y. Iglikhanov, G. Janeschitz, Pedestal Width Scaling, to be published in Nucl Fusion

high triangularity for good H-mode confinement at densities near the Greenwald density. The choice of relatively high triangularity ($\delta_{95\%} \sim 0.35$) of the ITER-FEAT equilibria is based on this knowledge and on experimental observations¹⁴. Based on these observations a minimum temperature at the top of the pedestal, is required in order to achieve good H-mode confinement (Figure 2.5-8a, 2.5-8b)¹⁵.

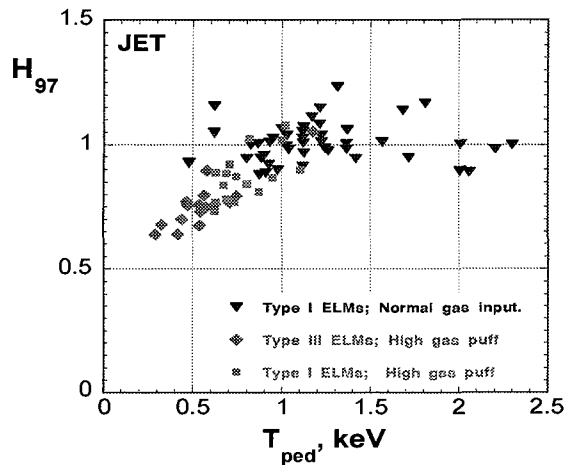


Figure 2.5-8a H-factor normalised to the H97 scaling versus the temperature on top of the pedestal (T_{ped}) for discharges with different gas puff scenarios and ELM types in JET. One can clearly see that the H factor in discharges with low pedestal temperature is proportional to T_{ped} (characteristic for stiff temperature profiles) while it becomes independent of T_{ped} at high pedestal temperatures (non-stiff branch).

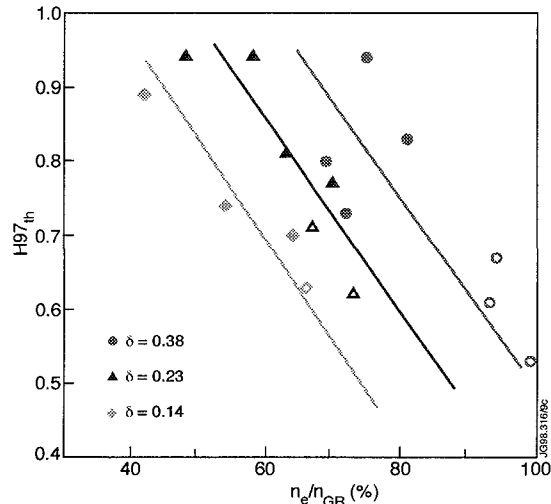


Figure 2.5-8b H-factor versus density normalised to the Greenwald density for JET discharges with different triangularities. From these data it can be clearly seen that at higher triangularity (higher pedestal pressure) the confinement degradation starts at higher density, i.e. the critical T_{ped} of Figure 2.5-8a (TPT) is reached at higher density.

However, the pedestal temperature decreases with increasing density due to the fact that the pedestal width, the maximum pressure gradient in the pedestal (ballooning limited) and thus the pressure on top of the pedestal is more or less constant for a given set of magnetic parameters (I_p , triangularity, etc). This is also true if one varies the heating power, because due to the pressure gradient limit and a more or less constant pedestal width only the ELM frequency increases without changing the average pressure on top of the pedestal when increasing the heat flux through the pedestal. Therefore, if one wants to operate with good confinement at high density a high pedestal pressures and thus high triangularity is needed resulting in a high pedestal energy content. The above considerations explain the degradation of energy confinement at high density and its dependence on triangularity (Figure 2.5-8b). Due to a large pedestal energy content in high triangularity Type I ELM scenarios (high

Kotchenreuter, M., et al, 16th IAEA Fusion Energy Conference, Montreal, Canada, (1996) IAEA-F1-CN-64/D1-5.

¹⁴ G. Saibene, L. D. Horton, R. Sartori, et al., Nucl. Fusion **39** (1999) 1133.

Stober J et al 1999 26th EPS Conference on Controlled Fusion and Plasma Physics, Maastricht, ECA **23J** 1401

O. Gruber, et al., 17th IAEA Fusion Energy Conference, Yokohama, Japan, IAEA-F1-CN-69/OV4/3 (1998).

Y. Kamada, et al., 17th IAEA Fusion Energy Conference, Yokohama, Japan, IAEA-F1-CN-69/CD2/EX9/2 (1998).

¹⁵ G. Janeschitz, Yu. Igitchanov, M. Sugihara et al., 26 the EPS Conference on Contr. Fusion Plasma Physics, Maastricht, (1999) p 1445.

pedestal pressure) larger energy losses during ELMs can be expected and are in fact observed¹⁶.

A possible model to quantify the pedestal energy content

The importance of high triangularity and thus of a high H-mode pedestal pressure and energy content can be understood by assuming stiff temperature profiles, which are related to Ion Temperature Gradient (ITG) driven turbulence¹⁷. In fact several machines observe such profile stiffness in their H-mode discharges, albeit, in some cases, only at medium to high densities (e.g. JET (Figure 2.5-8a), JT60U) while other machines are almost always in a stiff temperature regime (e.g. C-mod, ASDEX-UP, DIII-D)¹⁸. In cases where the stiffness of the temperature profiles disappears (above a certain edge – pedestal temperature) energy transport behaviour very different from ITG turbulence takes over¹⁹ and it is suspected that this transport behaviour is dominated by the electrons (assuming strong energy equipartition, i.e. higher densities). Based on these considerations, it is reasonable to assume that the above-defined TPT is an optimised operation point for good H-mode confinement (optimised for minimum ELM size and good energy confinement). In order to understand how this TPT scales with machine size and with plasma parameters a simple analytical model presented²⁰ is employed, which is able to explain the change over between stiff and non-stiff temperature profiles on machines in which both branches of confinement behaviour are observed (DIII-D, JET, JT60U). Recently also ASDEX-UP found a change of confinement behaviour (loss of stiffness)²¹ at a pedestal temperature predicted by the simple model (Figure 2.5-9a), giving some confidence for predicting a TPT for existing machines as well as for ITER-FEAT.

Applying this model to ITER-FEAT gives a TPT of ~ 3.5 keV (Figure 2.5-9b). While this temperature should be taken to be approximate rather than an accurate number, it is in the same range as the ones predicted to be required for good H-mode confinement by detailed transport code calculation based on ITG models²². A similar pedestal temperature for ITER-FEAT at the nominal operation point is predicted by a model for the pedestal width²³ when assuming a pressure gradient in the pedestal close to the ballooning limit.

¹⁶ Saibene G. et al, Nuclear Fusion 39, 1133 (1999)

Leonard, A., et al., J. Nucl. Materials 266-269 (1999) 109.

¹⁷ G. Janeschitz, Yu. Iglikhanov, M. Sugihara et al., 26 the EPS Conference on Contr. Fusion Plasma Physics, Maastricht, (1999) p 1445.

Kotchenreuter, M., et al, 16th IAEA Fusion Energy Conference, Montreal, Canada, (1996) IAEA-F1-CN-64/D1-5.

¹⁸ G. Janeschitz, Yu. Iglikhanov, M. Sugihara et al., 26 the EPS Conference on Contr. Fusion Plasma Physics, Maastricht, (1999) p 1445.

M. Sugihara, Y. Iglikhanov, G. Janeschitz, et al., 26 the EPS Conference on Contr. Fusion Plasma Physics, Maastricht, (1999) p1449.

¹⁹ G. Janeschitz, Yu. Iglikhanov, M. Sugihara et al., 26 the EPS Conference on Contr. Fusion Plasma Physics, Maastricht, (1999) p 1445.

²⁰ G. Janeschitz, Yu. Iglikhanov, M. Sugihara et al., 26 the EPS Conference on Contr. Fusion Plasma Physics, Maastricht, (1999) p 1445.

²¹ J. Stober, et.al., 7th IAEA Workshop on H-mode physics and Transport Barriers, Oxford 1999, to be published in PPCF

²² e.g Kotchenreuter, M., et al, 16th IAEA Fusion Energy Conference, Montreal, Canada, (1996) IAEA-F1-CN-64/D1-5.

²³ M. Sugihara, Y. Iglikhanov, G. Janeschitz, et al., 26 the EPS Conference on Contr. Fusion Plasma Physics, Maastricht, (1999) p1449.

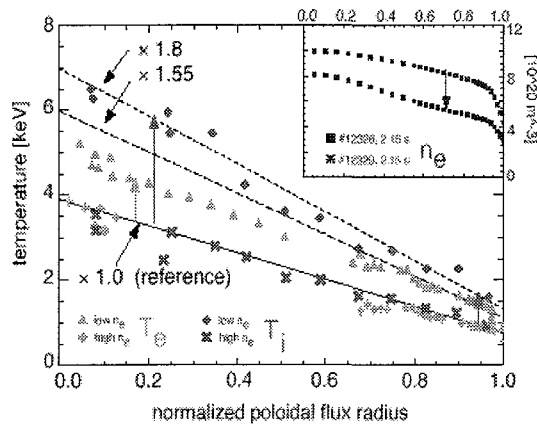


Figure 2.5-9a Electron (green) and ion (red) temperature profiles in ASDEX-UP for two discharges with different density²⁴. While at the higher density (low pedestal temperature) both temperature profiles seem to be stiff, the electrons deviate from a stiff behaviour at the lower density (high T_{ped}). This change happens at a TPT predicted by the analytic model²⁵. Due to the relatively low density the ions are decoupled from the electrons and continue thus to display a stiff behaviour which would not be the case at higher density, i.e. stronger energy equipartition.

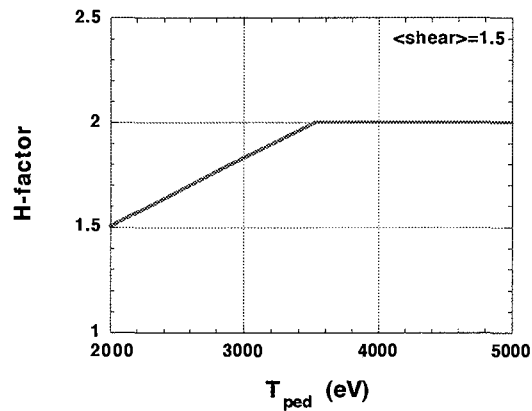


Figure 2.5-9b H-factor versus pedestal temperature predicted for ITER-FEAT by the analytic model. The two areas of confinement behaviour (stiff / non stiff) and the TPT of ~ 3.5 keV can be seen

By knowing the temperature ($T_{\text{PT}} \sim 3.5$ keV) and assuming that the density on top of the pedestal is 0.8 of the operation density ($0.8 n_{\text{average}}, \sim 0.8 \times 10^{20} \text{ m}^{-3}$), the energy content of the pedestal can be obtained. These considerations yield an energy stored in the pedestal of ITER-FEAT of ~ 107 MJ (53.5 MJ electron energy) which is $\sim 1/3$ of the total stored energy (stored energy ~ 350 MJ for the reference operation point at ~ 410 MW fusion power). Again this is in line with e.g. JET discharges with low gas puff at medium density and good H-mode confinement which also have pedestal energies in the order of $1/3$ of the total stored energy. Of course there are other ways than the one described here to obtain the pedestal temperature and/or the pedestal energy content (e.g. offset linear confinement scaling). However, when comparing all existing attempts to extrapolate the pedestal energy content to ITER-FEAT, only the considerations described here are consistent with all experimental observations (e.g. confinement behaviour, energy stored in pedestal on existing machines, etc.).

Fraction of the pedestal energy content lost during an ELM

Once the energy stored in the pedestal is known, one has to assess the fraction of this energy which is lost during an ELM. One way of extrapolating the fraction of stored energy lost per ELM from present machines to ITER is by empirical scaling using the ELM database²⁶ constructed from JET and DIII-D discharges at separatrix triangularities between 0.25 and 0.3. From this database analysis it was found that the energy loss per ELM is about $\sim 31\% \pm$

²⁴ J. Stober, et al., 7th IAEA Workshop on H-mode physics and Transport Barriers, Oxford 1999, to be published in PPCF

²⁵ G. Janeschitz, Yu. Igitkhanov, M. Sugihara et al., 26 the EPS Conference on Contr. Fusion Plasma Physics, Maastricht, (1999) p 1445.

²⁶ Leonard, A., et al., J. Nucl. Materials 266-269 (1999) 109.

5 % of the pedestal electron energy content. Assuming that the loss fraction will be the same in ITER-FEAT, the energy loss per ELM can be evaluated yielding an average energy loss per ELM of ~ 14 to 19 MJ which is 4% to 5.5% of the total stored energy. This result is in principle in line with observations on present machines²⁷, for low gas puff good energy confinement H-modes at < 0.5 of the Greenwald density.

The energy loss per ELM can be reduced by increasing the gas puffing rate. However, increasing the gas puffing rate and/or the density of a discharge significantly causes in many cases not only a reduction of the ELM size but also of energy confinement (Figure 2.5-10a). This loss of energy confinement can be understood from a reduction of the average pedestal pressure (ELMs are triggered early before maximum possible pressure is achieved) or by reducing the pedestal temperature below the TPT.

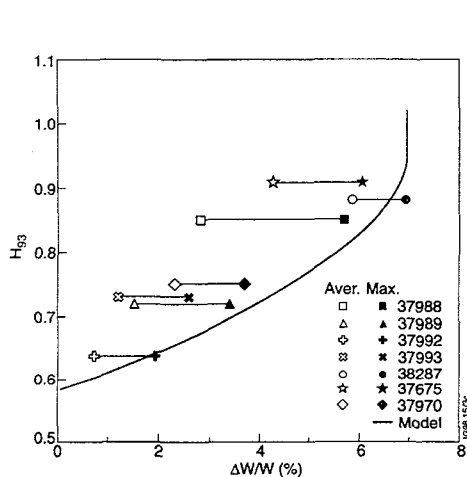


Figure 2.5-10a H-factor versus fraction of stored energy lost during an ELM in JET. In this series of discharges by increasing the gas puff (decreasing average pedestal energy content) the confinement decreases²⁸

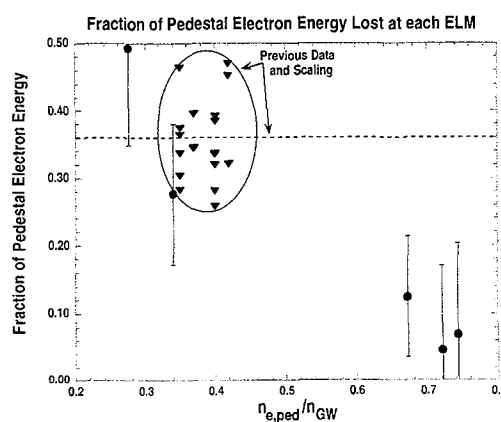


Figure 2.5-10b ELM electron energy loss fraction in DIII-D for standard medium density discharges (36%) and for discharges close to the Greenwald density ($< 10\%$) with relatively good energy confinement.

There are, however, several DIII-D discharges where the ELM energy losses were reduced by \sim factor 5 at high density (Figure 2.5-10b) when compared to low and medium density discharges with only moderately decreased energy confinement²⁹. These discharges are at present limited to low power operation (< 3 MW NBI-heating) and the physics mechanism, which allows to retain reasonably good H-mode confinement, is not yet fully understood and it is therefore not known whether these discharges can be extrapolated to ITER-FEAT.

Also in ASDEX-UP a lower fraction of the total stored energy than in JET and DIII-D is lost in Type I ELMs ($\sim 2\%$) even at comparable triangularities. The times during which this energy is deposited on the divertor plates varies also and tends to be longer in DIII-D and ASDEX-UP (< 350 μ s in medium densities and close to 1 ms in the very high density cases) when compared to JET and JT60U where the ELM energy deposition time at low to medium

²⁷ e.g. J. Stober, et.al., 7th IAEA Workshop on H-mode physics and Transport Barriers, Oxford 1999, to be published in PPCF

Fishpool, G.M., Nucl. Fusion **38** (1998) 1373.

²⁸ Fishpool, G.M., Nucl. Fusion **38** (1998) 1373.

²⁹ A. Leonard, et. al., Proceedings of the 14th PSI Conference, Rosenheim, May 2000

density is $\sim 150 \mu\text{s}$ to $180 \mu\text{s}$. These different observations suggest that a simple empirical scaling of the energy loss fraction and of the deposition time as a method to extrapolate to ITER-FEAT is at least questionable and should therefore be accompanied by some physics considerations.

The short deposition times reported by the larger machines suggest that there might be a collisionless transport of energy and particles to the divertor plates. In fact when assessing the collisionality in the SOL during an ELM for these machines, it is in the order of 0.1 (Figure 2.5-12a), based on the assumption that during an ELM the temperature and density at the separatrix are for a short period similar to the pedestal temperature and density and by taking the connection length from the midplane to the divertor into account. During an ELM, the bulk of the energy cannot travel faster than with the ion sound speed (ambipolarity, more than 50% of energy in the ions, low collisionality, no time for energy equipartition) which gives for a typical JET ELM a characteristic time of ~ 150 to $180 \mu\text{s}$. However, in high density low pedestal temperature discharges such as the high density discharges in DIII-D and also in some discharges in ASDEX-UP, the SOL can become collisional also during an ELM, resulting in even longer energy deposition times (can be up to 1 ms) (Figure 2.5-11b). When assessing the collisionality during an ELM for ITER-FEAT it will be similar to JET and JT60U discharges (Figure 2.5-12) and not as large as in the high density discharges of DIII-D and ASDEX (> 1.0). Thus a collisionless transport of energy with ion sound speed can be expected also for ITER-FEAT ELMs.

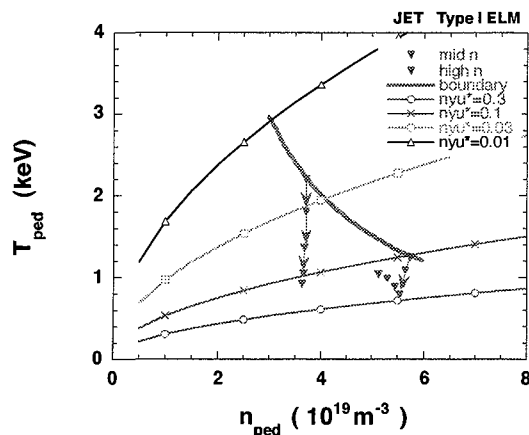


Figure 2.5-11a Pedestal $n - T$ diagram for typical JET discharges and the estimated collisionality (0.03 to 0.1) when assuming pedestal n and T values in the SOL. Trajectories for ELMs are also shown.

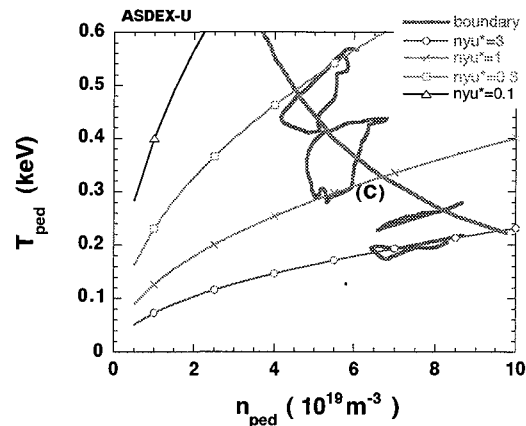


Figure 2.5-11b $n-T$ diagram for ASDEX-UP and the collisionality (at C $\sim 1.0 - 3.0$) in the SOL assuming pedestal plasma parameters during an ELM. Trajectories for ELMs are also shown

The following mechanism can possibly control the fraction of pedestal stored energy lost per ELM. If one assumes that an ELM occurs because a pressure gradient limit (e.g. ballooning) is exceeded and if the transport of energy and particles across field lines is due to turbulence similar to an avalanche effect, as reported for the core plasma in heat pulse experiments, the driving term (pressure gradient) and thus the turbulence should last only a few 10^{th} of μs , i.e. the gradient disappears on this fast timescale) Thus it becomes most likely shorter than the energy transport time along fieldlines when assuming ion convection is dominating there.

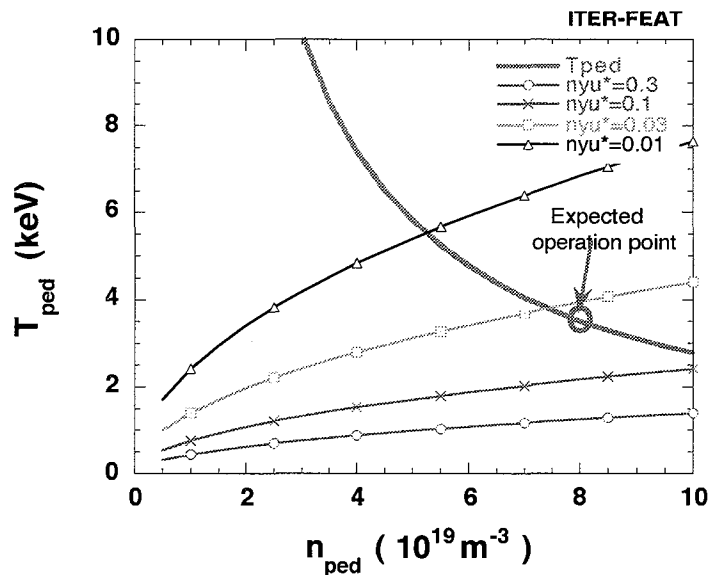


Figure 2.5-12 The expected n-T diagram for ITER-FEAT and the collisionality (~ 0.03) in the SOL assuming pedestal plasma parameters during an ELM.

This means that, with the assumed very short ELM avalanche, the maximum energy which can be lost during an ELM is determined by the characteristic loss time in the SOL and not by the pedestal physics. This loss time is in turn dependent on the temperature which exists in the SOL during an ELM and thus on the pedestal temperature. In order to apply such a scaling the ELM time (time of turbulence) and the fraction of stored energy which would be lost during an ELM without a transport limit in the SOL are unknowns. Therefore this model (idea) is an “ansatz” which has to be calibrated by data from one machine and can then be checked if it fits the observations on other machines.

A low and a very high density discharge of DIII-D have been taken for this calibration and the model then applied to JET, JT60U and ASDEX-UP. After the calibration on DIII-D the model predicts the observed energy loss fractions (compared to total stored energy) and as far as known also the correct deposition times in JET, JT60U and ASDEX-UP. It thus unifies the otherwise confusing observations with very different energy loss fractions and deposition times. While these considerations are very preliminary and must be checked in more detail, the good agreement of the model with data from existing machines encourages its use for extrapolation to ITER-FEAT as one possible way to assess an upper limit for the pedestal energy fraction lost during an ELM.

In ITER-FEAT the characteristic transport time in the SOL is $\sim 310 \mu\text{s}$ when considering a pedestal temperature of 3.5 keV and a pedestal density of $8.0 \times 10^{19} \text{m}^{-3}$ and thus twice as long as the one in JET and JT60U. This results in not quite a factor of 2 lower pedestal energy loss fraction than the one observed in JET and JT60U.

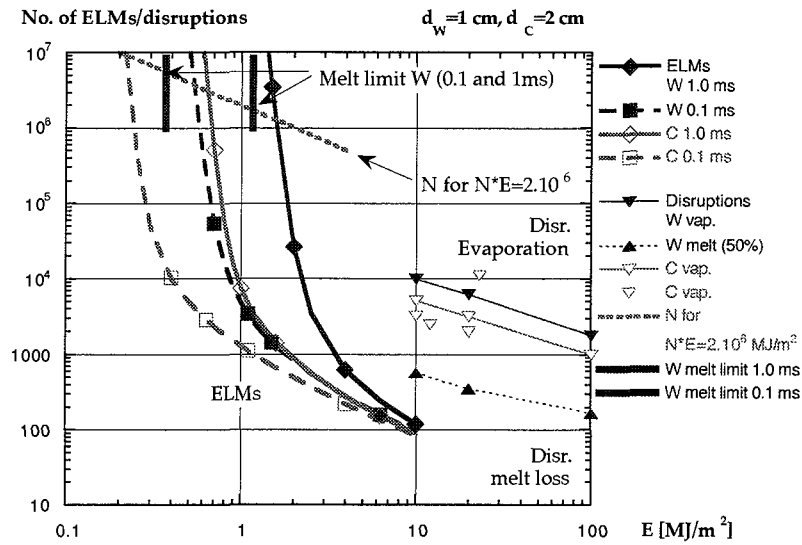


Figure 2.5-13 Divertor target lifetime in number of ELMs versus the energy deposited during an ELM for CFC and W clad targets

Table 2.5-1 Allowable Energy deposition on the divertor targets during ELMs

	C (0.3 ms)	W (0.3 ms)
Allowable energy deposition E (MJ/m ²) for 10 ⁶ ELMs, deposition time = 0.3 ms	0.4	0.93 (0.64)
Allowable W _{ELM} (MJ) for 10 ⁶ ELMs with deposition area S = S _{SS} = 8 m ²	3.2	7.44 (5.1)
Allowable W _{ELM} (MJ) for 10 ⁶ ELMs with deposition area S = 2xS _{SS} = 16 m ²	6.4	14.9 (10.2)

S_{SS} -. Strike zone Surface

() considering melting

In order to decide whether ELMs are tolerable for the divertor targets of ITER-FEAT one has to be aware that during a 400 sec long discharge approximately 1000 ELMs will occur and that the lifetime of the targets should be in the order of several 1000 discharges. Due to the large number of ELMs during the life of an ITER divertor target no evaporation or melting of the target material can be accepted (too large erosion per ELM) resulting in the power deposition limits reported³⁰ and in table 2 for CFC and W targets, respectively. From Figure 2.5-13 and Table 2.5-1 one can see that an energy load of only 0.4 MJm⁻² and 0.64 MJm⁻² is allowed for CFC and W targets, respectively, when assuming an energy deposition time of 0.3 ms. The total allowed energy loss from the plasma during an ELM depends also on the surface area which receives this load (see Table 2.5-2). From present day machines we know that there is either no broadening of the strike zones (S_{SS} in Table 2.5-2) or at most a factor 2 widening of the main power deposition area³¹.

Combining the energy deposition limits with the expected energy loss during ELMs in ITER-FEAT when using the physics based scaling and assuming 310 µs deposition time yields the results shown in Figure 2.5-14 for CFC (Figure 2.5-14a) and W targets (Figure 2.5-14b). The variation of the energy loss per ELM over fusion power in Figure 2.5-14 is obtained by using the assumed proportionality between fusion power and stored energy

³⁰ G. Federici, et. al., "Assessment of Erosion and co-deposition in ITER-FEAT", PSI 1999

³¹ Leonard, A., et al., J. Nucl. Materials **266-269** (1999) 109.

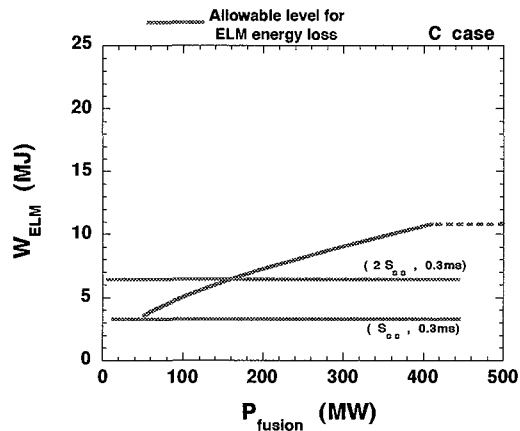


Figure 2.5-14a The predicted ELM energy loss) and the allowable pulsed energy load for a CFC target. The predicted ELM energy loss exceeds the allowable above 200 MW fusion power.

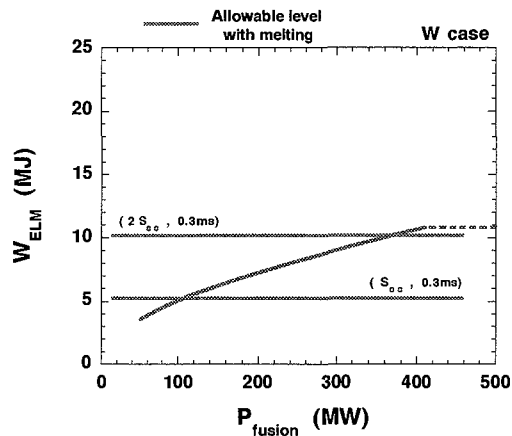


Figure 2.5-14b The predicted ELM energy loss and the allowable pulsed energy load for a W target (melt limits from Figure - 2.5-13 are assumed). The predicted ELM energy loss has some overlap with the limits defined by melting almost up to the reference operation point..

Figure 2.5-14 shows that the energy loss per ELM might exceed the allowable level for vaporisation of the divertor plates for CFC targets and might be more acceptable for a W target when considering a factor 2 widening of the deposition zone. It is assumed that the ELM energy loss does not increase above the reference operation point because the pedestal energy content does not increase anymore above the TPT. If the high density discharges reported by DIII-D³² could be directly extrapolated (same energy loss fraction) to ITER-FEAT, then a much larger overlap between allowable and expected ELM energy loss could be achieved. However, due to the different collisionality regimes between the ELMs in these DIII-D discharges and of the ones in ITER-FEAT, it is very questionable if such a direct extrapolation of the energy loss fraction to ITER is allowed.

Due to the fact that the error bars in all the above extrapolations are large and due to the fact that a model for the ELM itself does not exist, the predicted ELM energy loss in ITER-FEAT has certainly large error bars. Therefore, definitive conclusions cannot be reached at present. Nevertheless, it might be that a Type-I ELM regime without mitigation techniques for the ELM energy losses, which must not reduce the energy confinement, will only be marginally usable in ITER-FEAT

However, if it is possible to peak the density profiles and thus to reduce the pedestal density, at constant or even increased line-average density, the pedestal pressure and thus also the pedestal energy content can be decreased without a significant loss of confinement (pedestal temperature stays above TPT). This has been observed in pellet-fuelled discharges³³. A simple assessment for ITER-FEAT shows that with a density peaking factor of 2, a reduction in the ELM energy loss by \sim factor 2 (lower pedestal energy content), is feasible without a loss of confinement which would make Type-I ELMs most likely compatible with a W and a CFC target. While this example demonstrates that there is in principle some experimental

³² A. Leonard, et. al., Proceedings of the 14th PSI Conference, Rosenheim, May 2000

³³ O. Gruber, et al., 17th IAEA Fusion Energy Conference, Yokohama, Japan, IAEA-F1-CN-69/OV4/3 (1998).

flexibility which might allow Type-I ELM operation in ITER-FEAT, the situation remains marginal and alternative high energy confinement regimes need to be investigated for their applicability to ITER-FEAT.

An H-mode regime with high pedestal pressure, good confinement and small or no ELMs exists. It is called either grassy ELM³⁴, Type-II ELM³⁵ or Enhanced D-Alpha (EDA)³⁶ regime and might be a backup solution for the reference Type-I ELM regime in ITER-FEAT. However, based on present knowledge it can only be obtained at $q_{95\%} > 3.5$ and at high triangularity > 0.4 . Only if more data and a better understanding of this regime is available it will be possible to assess its applicability to an ITER like machine.

The RI mode is another possible high confinement regime and can in principle be understood in the same way as the pellet injection discharges from the high field side, i.e., the peaking of the density profile compensates the reduction of the pedestal pressure or in extreme cases the existence of an L-mode edge by directly improving the ITG caused transport³⁷. The relevance of this operation regime for ITER-FEAT must be demonstrated on large machines (e.g. JET, JT60U), before this scenario can be employed as a backup for the Type I ELMy H-mode.

2.5.5. Probabilistic Performance Assessment using Different Confinement Scalings

A probabilistic performance assessment has been made by assuming a normal distribution function for the H_H -factor with standard deviation σ . Under this assumption, the expectation of achieving a Q value of at least a specified value, Q_0 is estimated considering the beta $\beta_N \leq 2.5$, the L-H transition threshold power, P_{LH} , and the density $n_e/n_{GW} \leq 0.85$. In this section, results for various scaling formulae are shown. Here, IPB98(y,1) scaling, IPB98(y,2) scaling, IPB98(y,3), IPB98(y,4) scaling and IPB98(y) scaling are examined.

Figure 2.5-15 shows calculation results for the expectation of achieving $Q \geq Q_0$ for various scaling formulae when $\tau_{He^*}/\tau_E = 5$, $n_e/n_{GW} \leq 0.85$, $P_{LOSS}/P_{LH} \geq 1.0$ and the uncertainty for the scaling formula $\sigma = 20\%$. Here, the "maximised conditional probability (MCP)" is obtained by optimizing the heating power³⁸. When $\sigma = 20\%$, the MCPs of achieving $Q \geq 10$ are about 65-90%, and those of achieving $Q \geq 50$ is 25-60%. The MCPs for $Q \geq 10$ are not sensitive to the assumption for LH-transition power assumptions ($P_{LOSS}/P_{LH} \geq 1.3$ or 1.0).

Figure 2.5-16 shows the case when $\sigma = 10\%$. The MCPs of achieving $Q \geq 10$ are about 80-95%, and those of achieving $Q \geq 50$ is 10-70%.

³⁴ Y. Kamada, et al., 7th IAEA TCM on H-mode and Transport Barrier Physics, Oxford, Sep. 1999.

³⁵ T. Ozeki, et al., Nucl. Fusion **30** (1990) 1425.

³⁶ M. Greenwald, et al., 17th IAEA Fusion Energy Conference, Yokohama (1998) IAEA-F1-CN-69/EX1/4.

V. P. Baltanagar, et al., 18th EPS Conference on Controlled Fusion and Plasma Physics, vol. 1 (1991) p369.

³⁷ A. Messian, et al., Phys. Rev. Lett. **77** (1996) 2487.

³⁸ ITER EDA Document GA0RI199-02-12 W0.2 Study of RTO/RC ITER Options

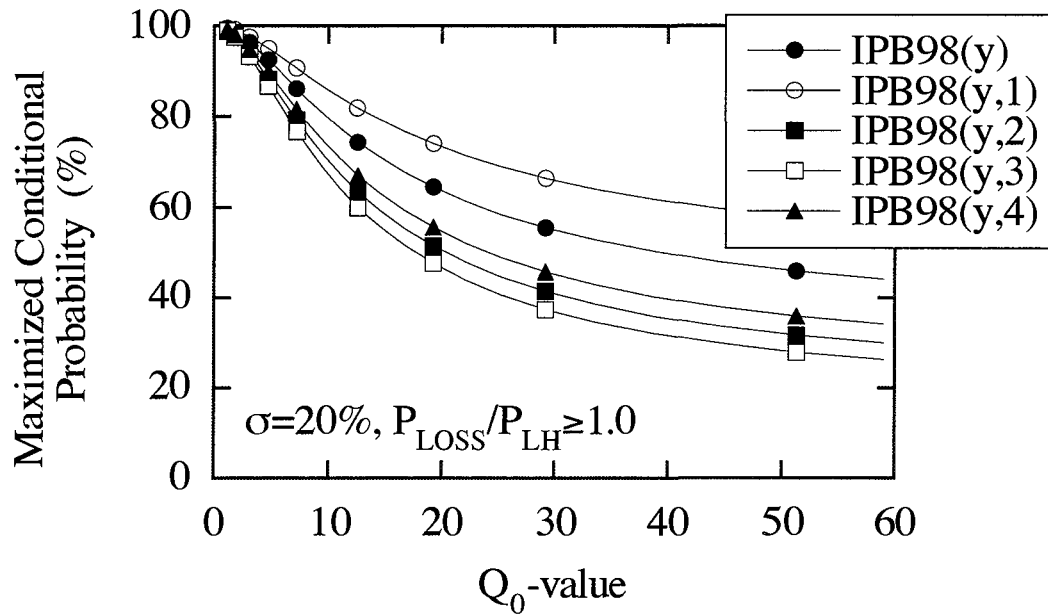


Figure 2.5-15 Expectation of achieving $Q \geq Q_0$ for various scaling formulae when $\tau_{\text{He}}^*/\tau_{\text{E}} = 5$, $n_e/n_{\text{GW}} \leq 0.85$, $P_{\text{LOSS}}/P_{\text{LH}} \geq 1.0$ and the uncertainty for the scaling formula $\sigma = 20\%$.

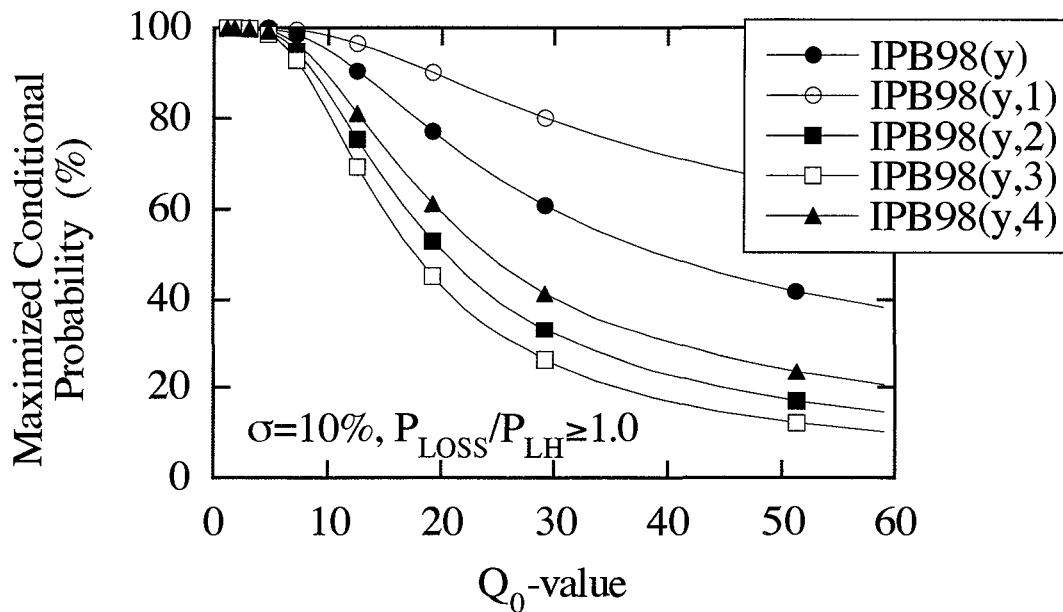


Figure 2.5-16 Expectation of achieving $Q \geq Q_0$ for various scaling formulae when $\tau_{\text{He}}^*/\tau_{\text{E}} = 5$, $n_e/n_{\text{GW}} \leq 0.85$, $P_{\text{LOSS}}/P_{\text{LH}} \geq 1.0$ and the uncertainty for the scaling formula $\sigma = 10\%$.

2.5.6. A Dimensional Extrapolation Technique based on a System Code Applied to the ITER H-mode Energy Confinement Database

[The content of this section was first presented at the last TAC meeting in Naka in December 1999 as a result of preliminary studies and was included in the final version of the ODR submitted to the Parties in January 2000. It is provided here with further elaboration for the benefit of TAC members.]

This novel approach tries, amongst other things, to overcome the difficulty associated with the simultaneous choice of non-dimensional parameters ($A = R/a$, κ , δ , q_{95} , β_N , n/n_{GW}) which, when close to their respective limits, may have some significant hidden interactions which affects the energy confinement. As an example, this is observable in the effect of shear (triangularity, q , κ , A) on confinement in high density discharges, or the effect of sawteeth on low edge safety factor discharges at high elongation and triangularity³⁹.

In addition, the proposed methodology addresses, in part, the fact that the enhancement factor H_H cannot be treated as a simple scalar because it may hide some additional variables as well as explicitly treated terms (in the energy confinement formula), for example the density or elongation, the influence of which on the energy confinement time may not be mathematically expressed in a simple monomial form within the empirical formula for energy confinement time. The employed procedure is as follows:

1. each shot in the database is evaluated by extracting all of its parameters and sizing by means of the system code (in accordance with the ITER criteria) for a $Q = 10$ machine with the same geometry (k , δ , $A=R/a$), q_{95} , and n/n_{GW} : these parameters are then assumed to come as a “package”;
2. the extrapolation in the energy confinement time is performed based on the empirical scaling coefficients applied only on the parameters not kept constant, and by using relative ratios. There is no need for H_H .

The energy confinement time empirical scaling then becomes:

$$\tau_{E,Q10} = \tau_{E,DBSHOT} \left(\frac{I_{Q10}}{I_{DBSHOT}} \right)^{\alpha_I} \left(\frac{P_{Q10}}{P_{DBSHOT}} \right)^{\alpha_P} \left(\frac{B_{Q10}}{B_{DBSHOT}} \right)^{\alpha_B} \left(\frac{R_{Q10}}{R_{DBSHOT}} \right)^{\alpha_R} \left(\frac{M_{Q10}}{M_{DBSHOT}} \right)^{\alpha_M} \left(\frac{n_{Q10}}{n_{DBSHOT}} \right)^{\alpha_n} \quad (1)$$

where :

- the subscript “Q10” refers to the $Q = 10$ machine designed from the shot in the H-mode database and indicated with the subscript “DBSHOT”.
- The α_i exponents are the same exponents found in the empirical scaling law for the correspondent parameters.

In addition, considering then the following relationships:

$$q = \frac{BR}{I} * f(\delta, \kappa, A) \quad ; \quad n_{GW} = \frac{I}{\pi a^2} \quad (2,3)$$

³⁹ Saibene G. et al, Nuclear Fusion 39, 1133 (1999)

Stober et al, 26th EPS conf. on controlled fusion, Maastricht (1999)

Kamada Y. et al, 14th. IAEA Conf. Plasma Physics, Wuerzburg (1992)

Horton L.D. et al, Nuclear Fusion, 39 993 (1999)

equation (1) further simplifies, because q_{95} , geometry, and normalised density are fixed in the extrapolation, to:

$$\tau_{E,Q10} = \tau_{E,DBSHOT} \left(\frac{P_{Q10}}{P_{DBSHOT}} \right)^{\alpha_P} \cdot \left(\frac{B_{Q10}}{B_{DBSHOT}} \right)^{\alpha_B + \alpha_n + \alpha_I} \cdot \left(\frac{R_{Q10}}{R_{DBSHOT}} \right)^{\alpha_R - \alpha_n + \alpha_I} \cdot \left(\frac{M_{Q10}}{M_{DBSHOT}} \right)^{\alpha_M} \quad (4)$$

Considering, for example, the IPB-98y2 empirical scaling law for ELMy H mode:

$$\tau_{E,th}^{IPB98(y,2)} = 0.0562 H_H I^{0.93} B^{0.15} P^{-0.69} n_{19}^{0.41} M^{0.19} R^{1.97} \epsilon^{0.58} K_a^{0.78} \quad (5)$$

then expression (4) becomes:

$$\tau_{E,Q10} = \tau_{E,DBSHOT} \left(\frac{P_{Q10}}{P_{DBSHOT}} \right)^{-0.69} \cdot \left(\frac{B_{Q10}}{B_{DBSHOT}} \right)^{1.49} \cdot \left(\frac{R_{Q10}}{R_{DBSHOT}} \right)^{2.49} \cdot \left(\frac{M_{Q10}}{M_{DBSHOT}} \right)^{0.19} \quad (6)$$

Of the more than a thousand shots in the ELMy H-mode database, less than half turn out to extrapolate to a $Q = 10$ machine whose major radius is smaller than 8 m, however about 70 extrapolate to a $Q = 10$ machine with $R < 6.2$ m.

Figure 2.5-17 shows the major radius of the extrapolated $Q = 10$ machine versus the edge safety factor q_{95} of the analyzed shots. It is apparent that there are a good number of shots, from DIII-D, JET, and ASDEX-U, which confirm the robustness of the ITER-FEAT design in reaching the $Q = 10$ objective on the basis of the existing experimental results. Of particular interest are those DIII-D shots which are capable of being extrapolated to a competitive $Q = 10$ device, even at a rather large edge safety factor. It is nevertheless clear that the choice of a safety factor of about 3 is sound.

As an even more general simplification to the proposed approach, the use of an empirical scaling formula for the energy confinement time can be completely avoided if the extrapolated device is sized based on a fusion power requirement and not on the amplification factor Q . In order to do so, the above-mentioned, non-dimensional parameters are chosen to be kept constant, based on the consideration that the most unpredictable, from first principles, turbulent, phenomena taking place in the plasma are mostly influenced by stability and even more so by the geometry of the magnetic field, q and shear profiles. In addition, in this second methodology, the value of β_N observed in the extrapolated experiment is also fixed. This last hypothesis implies that the magnetic and pressure profiles in the experiment in question and the larger extrapolated device are completely self similar. The pressure scales then as:

$$p \propto B^2 \quad (7)$$

And, for a DT experiment, the fusion power then scales approximately as:

$$P_f \approx p^2 \cdot V \propto B^4 R^3 \quad (8)$$

However, considering that the total fusion power is not exactly proportional to T^2 , it is in principle necessary, but not too important for the result, to choose an operating density. This can be taken assuming also in this case the same density normalised to the Greenwald density scaling as:

$$n \propto \frac{I}{a^2} \propto \frac{B}{R} \quad (9)$$

Figure 2.5-18 shows the machine major radius versus the safety factor at the edge. Also in this case, a number of shots extrapolate to a 500 MW device with a major radius smaller than the one of ITER-FEAT. In summary, also in accordance with this alternative design methodology, the ITER-FEAT design seems to be soundly based on the extrapolation of many high performance ELMy H-mode shots from JET, DIII-D, and ASDEX-U.

The procedure above thus enables the fusion power to be extrapolated but not the transport losses and thus the value of Q to be predicted. However, by considering that the temperature scales as:

$$T \propto \frac{P}{n} \propto BR \quad (10)$$

and assuming that τ_E scales as gyroBohm, we have:

$$\tau_{E, \text{GyroBohm}} \propto \frac{a^2}{\rho^* \chi_{\text{Bohm}}} = \frac{R^2}{\frac{\sqrt{MT}}{\epsilon RB} \left[\frac{T}{B} \right]} \propto R^{1.5} \cdot B^{0.5} \cdot M^{-0.5} \quad (11)$$

The inverse isotopic mass dependence, shown in equation (11) is not supported by the empirical scaling laws, which typically have a positive exponent. This could be because the positive mass dependence of the pedestal edge width shown in experiments⁴⁰ is neglected whereas it is thought that the edge pedestal width scales with a complex function of magnetic shear, machine size and thermal ion Larmor radius. Considering equation (11) for the evaluation of the energy confinement time, the lowest *cost* shots turn out to have a value of Q in the range between 4 and 15.

The scaling derived above can be compared with the different scaling laws expressed in the ITER Physics Basis⁴¹. By assuming the usual set of non-dimensional parameters equation (6) above becomes:

$$\tau_{E, Q10} = \tau_{E, \text{DBSHOT}} \cdot \left(\frac{B_{Q10}}{B_{\text{DBSHOT}}} \right)^{\frac{\alpha_B + \alpha_s + \alpha_I + 2\alpha_p}{1 + \alpha_p}} \cdot \left(\frac{R_{Q10}}{R_{\text{DBSHOT}}} \right)^{\frac{\alpha_R - \alpha_s + \alpha_I + 3\alpha_p}{1 + \alpha_p}} \cdot \left(\frac{M_{Q10}}{M_{\text{DBSHOT}}} \right)^{\frac{\alpha_M}{1 + \alpha_p}} \quad (12)$$

Figure 2.5-19 compares the various empirical laws with the one derived on the basis of gyroBohm scaling, all under the assumptions of freezing the same non-dimensional parameters (A , k , δ , q_{95} , β_N , n/n_{GW}) in the extrapolation. With the exception of the scaling IPB98(y,3), where a free fit without Kadomtsev constraint was performed, all scalings are very similar in the coefficients γ_B and γ_R . For a given engineering approach the relation between R and B is, to a first approximation, one of proportionality, when aspect ratio and elongation are constant. This means that the sum $\gamma_B + \gamma_R$ is the single most important coefficient in the scaling. When compared with eq. (11), the scalings 98(y), 98(y,1) give a more favourable size/field effect whereas scaling 98(y,2), 98(y,3), and 98(y,4) yield the opposite result.

⁴⁰ Cordey J et al, JET P98(53), Submitted to Nuclear Fusion.

⁴¹ ITER Physics Basis, Nucl. Fus. 39 (1999)

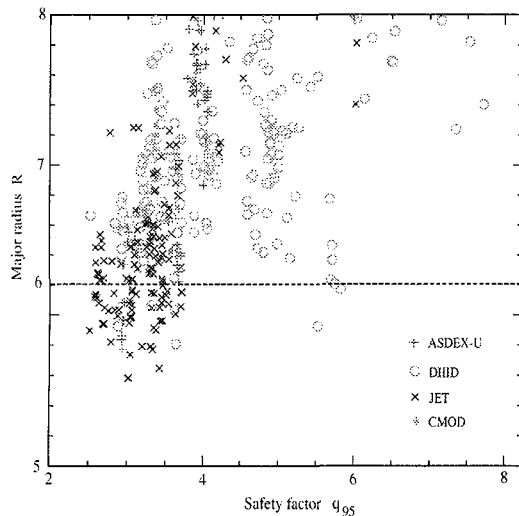


Figure 2.5-17 Major Radius of $Q = 10$ Machine vs. q_{95} Obtained with Dimensional Extrapolation Methodology

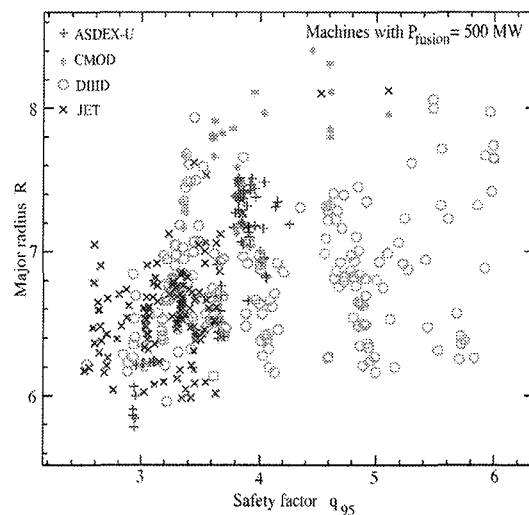


Figure 2.5-18 Major Radius of 500 MW Fusion Power Device versus Safety Factor in the Database under the Assumption of Constant Beta

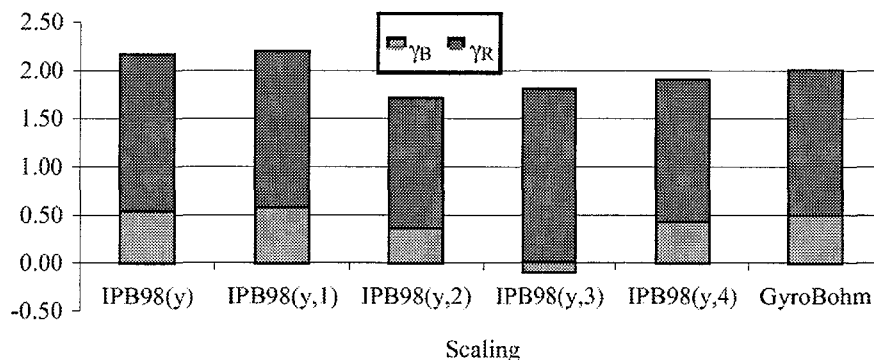


Figure 2.5-19 Comparison of Gyrobohm scaling versus IPB empirical scalings at constant n/n_{GW} , β_N , and magnetic field geometry.

2.6. Progress in Divertor Modelling

2.6.1. SOL Width

Extrapolation of the SOL width to a reactor-scale machine is one of the primary concerns for the divertor design. At present, experiments show a narrow power SOL (well below 1 cm) and, according to the common physical picture developed some 20 years ago⁴², it should become even narrower when the power increases. Indeed, the SOL width is determined by a competition between the cross-field and parallel transport. If the cross-field transport stays approximately constant, then an increase of power causes an increase of the plasma temperature at the separatrix and the parallel transport gets significantly faster, making the

⁴² Harrison, M., et al., Nucl. Technology/Fusion **3** (1983) 432

SOL narrower. Experiments generally confirm this trend, especially in L-mode discharges, see e. g. Figs.2.6–1, 2.6–3. However, the trend is opposite in the high-power H-mode experiments⁴³ which show some increase of the SOL width with power, Fig.2.6–2. Increase of the SOL width with the input power for H-mode can also be seen from the JET data, Fig.2.6–3, if one considers only the points with power greater than 8 MW. A formal statistical fit over the whole power range is simply misleading here.

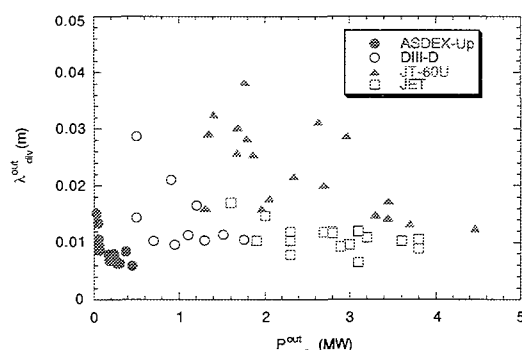


Figure 2.6–1 Width of power deposition profiles in L-mode for different machines (experiment)⁴⁴

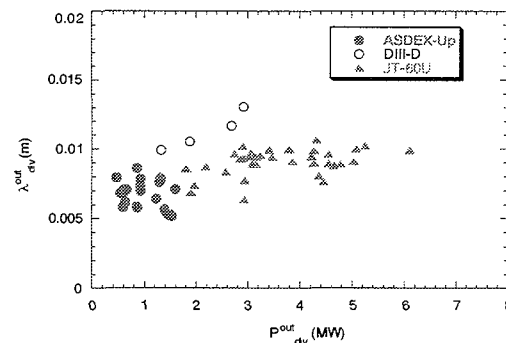


Figure 2.6–2 The same in H-mode

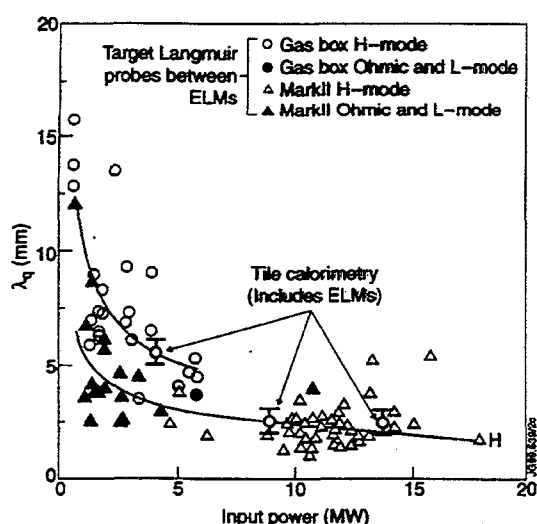


Figure 2.6–3 Width of power deposition profiles from JET (experiment)⁴⁵

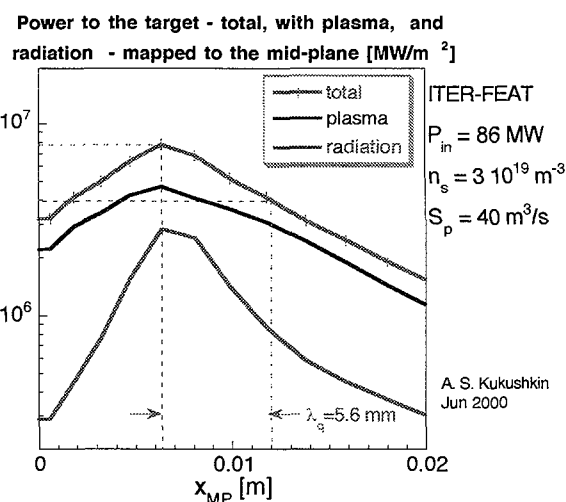


Figure 2.6–4 Typical power deposition profiles on the outer target of ITER-FEAT, mapped to the mid-plane.

Detailed profile measurements on ASDEX Upgrade⁴⁶ between ELMs have shown that the temperature gradients in high-power H-mode stay constant, corresponding to the ballooning limit, and continue smoothly across the separatrix. This allows the proposition of a model where the cross-field transport coefficients increase when the gradients approach the

⁴³ Loarte, A., et al., J. Nucl. Mater. **266-269** (1999) 587
Herrmann, A., et al., Proc. 23rd EPS Conf. Contr. Fusion Plasma Phys., Vol. 20C, Part II (1996) d-039.
Buchenauer, D., et al., J. Nucl. Mater. **196-198** (1992) 133.
Itami, K., et al., J. Nucl. Mater. **196-198** (1992) 755.
⁴⁴ Jaquinot, J., TAC meeting, Dec. 1999, Naka; Matthews, G., Expert Group meeting, Dec. 1999, Naka
⁴⁵ Jaquinot, J., TAC meeting, Dec. 1999, Naka; Matthews, G., Expert Group meeting, Dec. 1999, Naka
⁴⁶ Neuhauser, J., et al. 26th EPS Conf. Contr. Fusion Plasma Phys., Maastricht, 1999. Paper P4.040

ballooning limit⁴⁷. Such a model produces a qualitatively correct dependence of the SOL width on power, and it is consistent with interpretative modelling done for ASDEX Upgrade⁴⁸ where an increase of the fitted transport coefficients for H-mode discharges at high power was reported.

In ITER modelling, $\chi_{\perp} = 1 \text{ m}^2/\text{s}$ is normally used. This value may appear strongly overestimated in a plain comparison with the coefficients used to fit the experimental profiles in H-mode at low power (typically, below $0.1 \text{ m}^2/\text{s}$). However, the SOL width predicted for ITER-FEAT with the reference coefficient is around 5 mm, Figure 2.6-4, and, in line with the previous ASDEX Upgrade results, is consistent with the pressure gradient at the plasma edge in ITER-FEAT being close to the ballooning limit. The choice of the cross-field transport coefficients $\chi_{\perp} = 1 \text{ m}^2/\text{s}$ used in ITER-FEAT divertor modelling is therefore reasonable.

2.6.2. Code Validation

The models used for predictions of the divertor performance in ITER-FEAT are validated against the data from a variety of experiments and their predictive capability is probably higher than that for the core plasma models. Detailed model validation is mostly done by the Home Teams. In particular, the B2-Eirene code package has been extensively validated against the data from ASDEX Upgrade⁴⁹ and JET⁵⁰. The code had been used to analyse the “Lyra” divertor performance in ASDEX Upgrade before the experiments started, and the results show remarkable accuracy in the predictions of the divertor power load, radiation distribution, and helium and neon compression (see Figures 2.6-5 and 2.6-6). The codes are still unable to reproduce fully the experimentally observed in-out asymmetries – probably because of the lack of adequate description of the drifts and currents in the SOL. Work is being done on the model improvement in this direction⁵¹. From a broader perspective, many essential features of plasma detachment (e.g. low plasma temperature, importance of volumetric recombination) were first predicted by modelling and then confirmed by experiment. Also some apparently minor but potentially important effects like the self-sustained oscillations in the divertor plasma⁵² had been predicted long before they were identified in experiments. The generally good agreement of the modelling results with existing experiments and the proven predictive capability give confidence for predicting the performance of the ITER-FEAT divertor.

⁴⁷ Kukushkin, A. S., et al. Proc. 7th PET Workshop, Tajimi, Japan, 1999. To be published in “Contributions to Plasma Phys.”

⁴⁸ Coster, D., et al., *ibid.*

⁴⁹ Schneider, R., et al. Fusion Energy 1998 (Proc. 117th Conf., Yokohama, 1998) IAEA, Vienna, 1999, p.1525

⁵⁰ Loarte, A., et al. J. Nucl. Mater., **266-269** (1999) 146

⁵¹ Chankin, A., et al. Contributions to Plasma Phys. **40** (2000) 288
Schneider, R., *ibid.*

⁵² Krasheninnikov, S. I., et al. Nucl. Fusion **27** (1987) 1805
Loarte, A., et al. Phys. Rev. Lett. **83** (1999) 3657

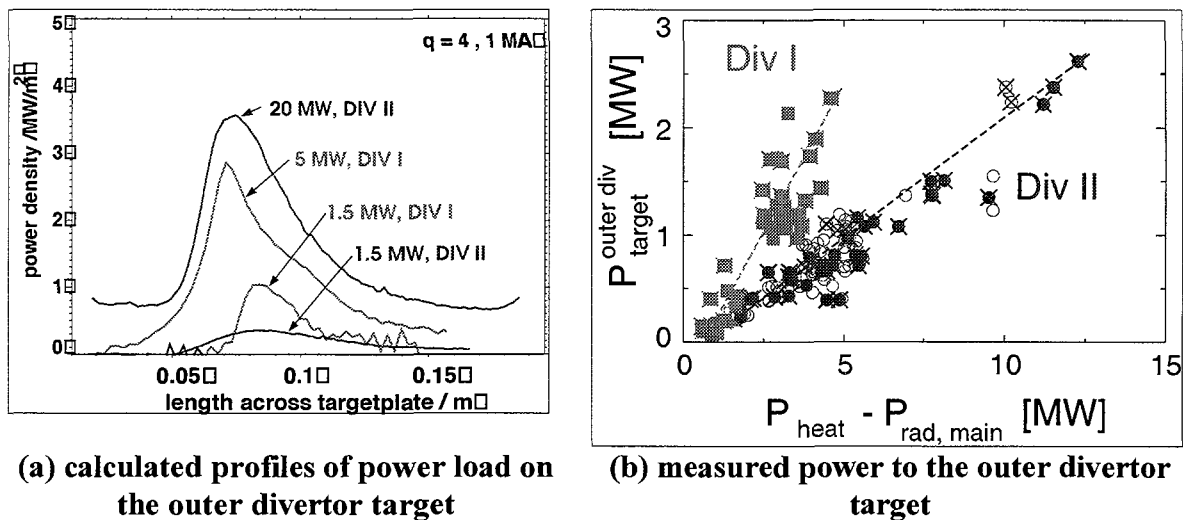


Figure 2.6-5 Predicted reduction of power load by a factor 2 to 3 in Divertor II (“Lyra”) of Asdex Upgrade, as compared to Divertor I, is clearly seen in the experiment⁵³.

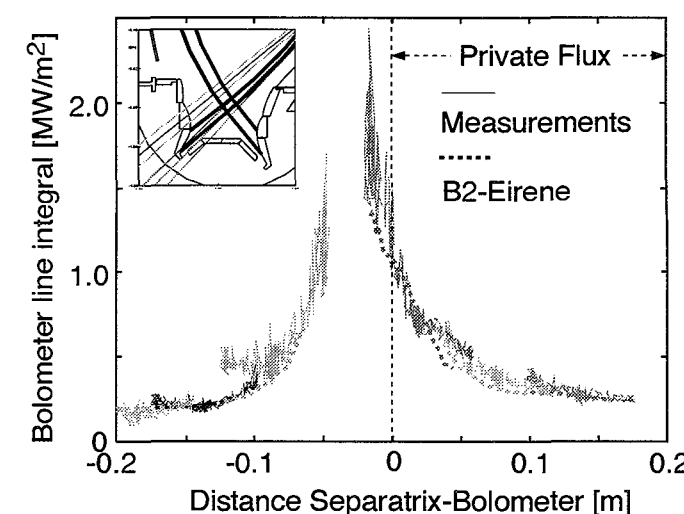


Figure 2.6-6 Comparison of predicted and measured bolometer signals for Divertor II of Asdex Upgrade⁵⁴.

2.6.3. Divertor Geometry Effects

Design studies undertaken in the last 2 years and aimed at a reduction of the cost (i. e., of the size) of ITER have resulted in ITER-FEAT. These studies have involved a broad variation of the divertor geometry retaining the vertical target plates in the divertor. From the point of view of divertor modelling, the ODR was based on the results obtained for the earlier versions (LAM, IAM, etc.). The most significant difference in the divertor geometry between FEAT and earlier versions, which was not understood at that time, was in abandoning the dump target, Figure 2.6-7a. The effect of dump target, or the V-shaped divertor bottom near the strike point, has recently been analysed⁵⁵. It is shown that this “V” is beneficial for

⁵³ Schneider, R., et al. Fusion Energy 1998 (Proc. 17th Conf., Yokohama, 1998) IAEA, Vienna, 1999, p.1525

⁵⁴ Schneider, R., et al. Fusion Energy 1998 (Proc. 17th Conf., Yokohama, 1998) IAEA, Vienna, 1999, p.1525

⁵⁵ Kukushkin, A. S., et al., 14th PSI Conference, Rosenheim, May 2000. To be published in J. Nucl. Mater.

reduction of the peak power loads primarily because it keeps high neutral density near the strike point and furthers the partial detachment. A similar effect was previously reported from JET experiments where the separatrix was swept across the divertor targets in both Mark I and Mark II divertors⁵⁶.

Figure 2.6-8 shows the comparison of the peak power load for one of the previous modifications (LAM) and different variants of the FEAT divertor geometry for the same input power of 100 MW. In these calculations, besides DT and He, the C ions are present in the plasma and they ensure the necessary radiation level. The source of carbon is mostly chemical sputtering of the target surfaces with a constant yield of 1 %, although physical sputtering is also taken into account. The divertor geometries for the compared cases are shown in Figure 2.6-7. The striking difference between the baseline FEAT and LAM can be attributed to the different target shape: the straight target originally proposed for FEAT is less efficient in assisting the plasma detachment around the strike point, whereas the pronounced “V” with the strike point almost in the corner does this job for the LAM. Minor variations of the divertor shape for FEAT (“V-out” and “V-in”) also show significant reduction of the peak power, Figure 2.6-8, although in these studies, plugging the “V” by plasma was less efficient than in the LAM cases. Another important parameter which could explain the remaining difference between the V-shaped FEAT divertor and LAM divertor is the pumping speed. It was about 60 m³/s for the LAM and 75 m³/s for FEAT calculations shown here, and reduction of the pumping speed increases the neutral pressure in PFR and facilitates the partial detachment near the strike point⁵⁷, thus lowering the divertor target load (Figure 2.6-9) without increasing too much the He density at the separatrix.

A V-shaped configuration of the target and divertor floor is beneficial for divertor performance. It provides a considerable reduction of the peak power loads on the target without spoiling the helium removal. The effect is mostly due to accumulation of neutrals near the strike point when the “V” is plugged by plasma, as confirmed by the available experimental data from JET. Such a configuration could also be useful for transients such as ELMs, providing some shielding for the targets. It can however negatively affect the operational flexibility of the machine since the freedom of positioning the strike point is reduced. As a result of these studies, it is recommended to keep a V-shaped target configuration in ITER-FEAT.

⁵⁶ Loarte, A., Nucl. Fusion **38** (1998) 587.

Monk, R., et al., Proc. 24th EPS Conf. Contr. Fusion Plasma Phys., Berchtesgaden, 1997, Vol. 21A, p. 117.

⁵⁷ Kukushkin, A. S., et al., 14th PSI Conference, Rosenheim, May 2000. To be published in J. Nucl. Mater.

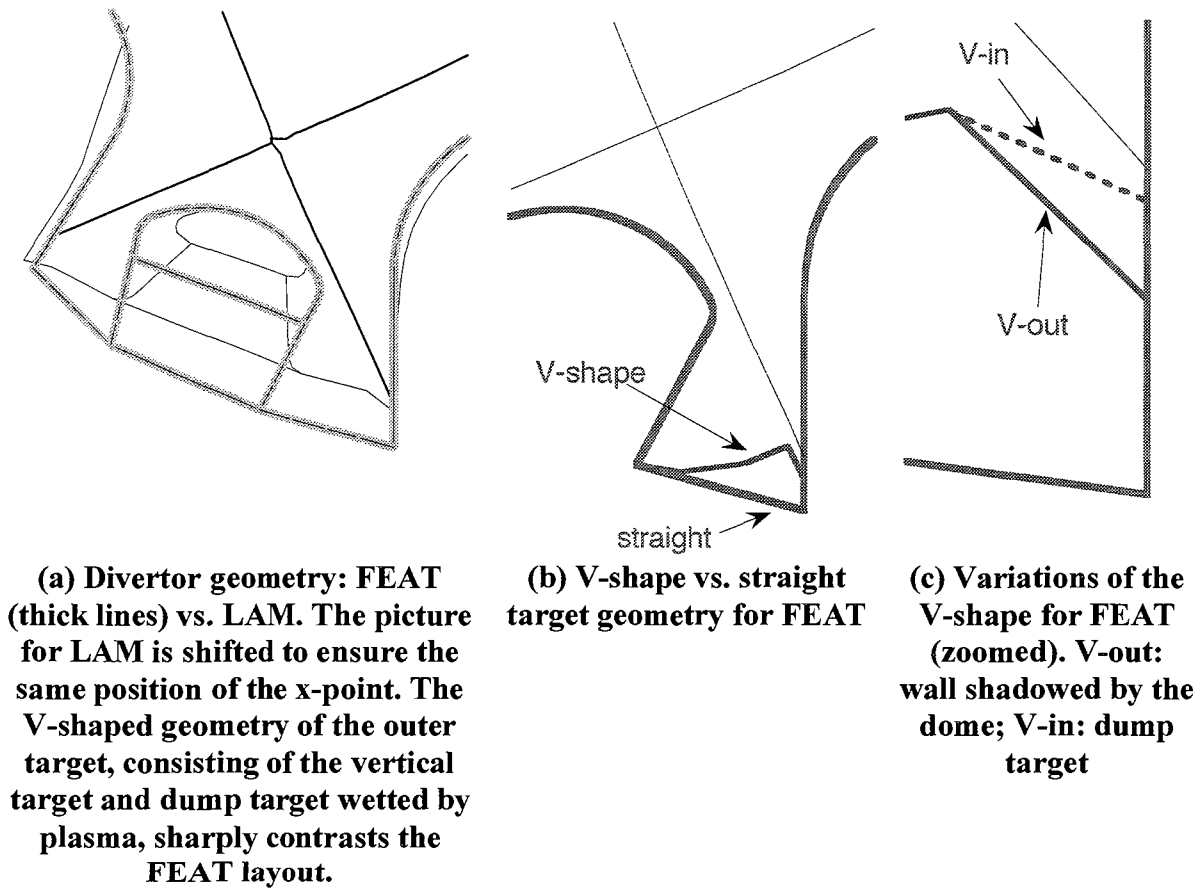


Figure 2.6-7 Variations of the divertor geometry used for modelling presented in Figure 2.6-8

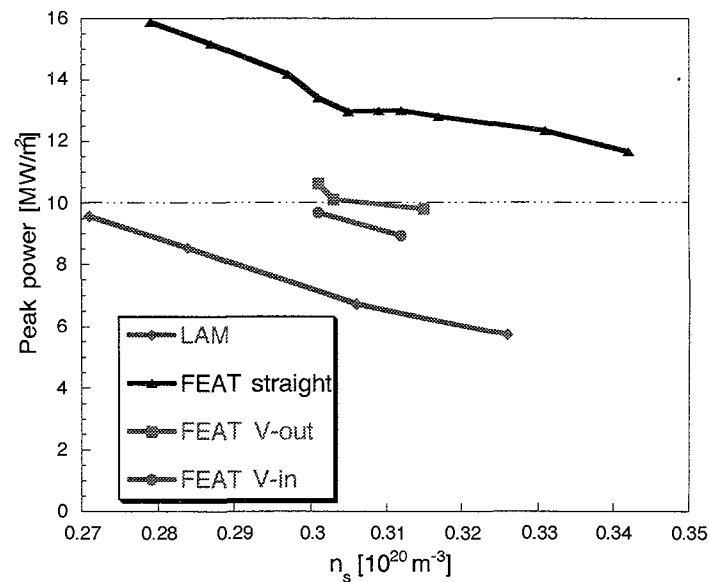


Figure 2.6-8 Peak power load q_{pk} vs. upstream plasma density at the separatrix n_s for different divertor geometry. The total power entering the SOL region is 100 MW. The variation of the divertor geometry is shown in Figure 2.6-7.

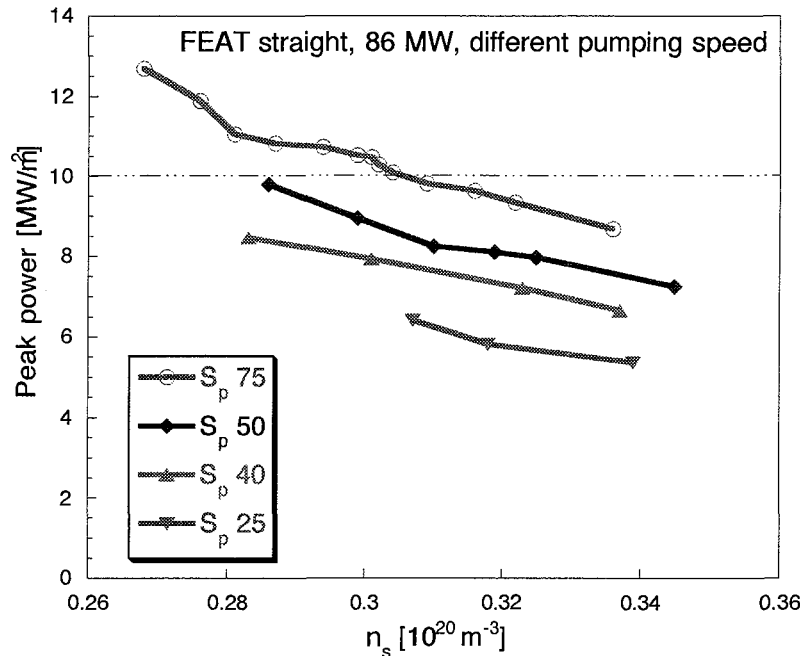


Figure 2.6-9 Peak power load q_{pk} vs. upstream plasma density at the separatrix n_s for different pumping speed (75, 50, 40, and 25 m^3/s), with 86 MW input power, straight target geometry (see Figure 2.6-7)

2.6.4. Operational window for ITER-FEAT

The window for divertor operation in ITER is delimited by several constraints, summarised in Table 2.6-1, arising from core plasma and technology requirements⁵⁸. Several different means of controlling the operational point of the ITER-FEAT divertor in this 6-dimensional window have been considered⁵⁹ and the results are briefly summarised as following.

For the baseline ITER-FEAT divertor, without V-shaped geometry, at full pumping speed of 75 m^3/s and without additional impurity seeding, there is no window for the input power above approximately 80 MW. At higher powers, 86 MW and above, whenever the peak power load is brought low enough, the particle throughput and eventually the upstream density become too high. There is however a considerable margin in Z_{eff} and some margin in c_{He} .

Impurity seeding (in addition to the automatically-produced carbon) can permit the window to be extended somewhat. However, neon seeding is not appropriate. Instead of adding to carbon, neon largely replaces carbon as the radiator, radiating further away and thereby reducing the peak heat load, but it produces higher Z_{eff} . It does not radiate much below 20 eV. Seeding with a different impurity having radiation efficiency higher than carbon could be more effective – the tradeoff here is between the radiation and Z_{eff} .

Reducing the pumping speed opens the window for 86 and 100 MW. It leads to higher c_{He} at the same upstream density, but somewhat lower c_{He} at the same throughput.

⁵⁸ Janeschitz, G., et al., 14th PSI Conference, Rosenheim, May 2000. To be published in J. Nucl. Mater.

⁵⁹ Kukushkin, A. S., et al., 14th PSI Conference, Rosenheim, May 2000. To be published in J. Nucl. Mater.

For the same pumping speed of 75 m³/s, the V-shaped geometries show much better performance than the straight one: the 100 MW curve lies at the corner of the window in q_{pk} , and Γ_{DT} , and the 86 MW points investigated lie just outside the Γ_{DT} limit implying that acceptable solutions exist at somewhat lower n_s . Reduction of the pumping speed should then increase the available operational space, and the margin in Z_{eff} suggests that impurity seeding can also be used here. Helium removal does not deteriorate with V-shaped target configurations.

An operational window in 6-dimensional phase space for ITER-FEAT is shown in Figure 2.6-10. Only points which satisfy all the constraints and which are produced using the different means of divertor operation control discussed above are shown, demonstrating that powers up to 100 MW can be accommodated. Reduction of the upstream plasma density below $2.5 \cdot 10^{19} \text{ m}^{-3}$, which may be needed for non-inductive operation, does not however look feasible. Variation of the pumping speed and fuelling rate in combination with impurity seeding provides control of the operational point within the window. Further exploration of these control means is in progress.

Table 2.6-1 Limits of the operational window of the ITER-FEAT divertor

Peak power load on the targets	$q_{pk} \leq 10 \text{ MW/m}^2$
D-T particle throughput	$\Gamma_{DT} \leq 200 \text{ Pa} \cdot \text{m}^3/\text{s}$
Core fuelling	$0 \leq \Gamma_{core} \leq 100 \text{ Pa} \cdot \text{m}^3/\text{s}$
Upstream plasma density	$n_s \leq 0.33 \cdot 10^{20} \text{ m}^{-3}$
Helium concentration in the core plasma	$c_{He} \leq 0.06$
Z_{eff} in the core plasma	$Z_{eff} \leq 1.6$

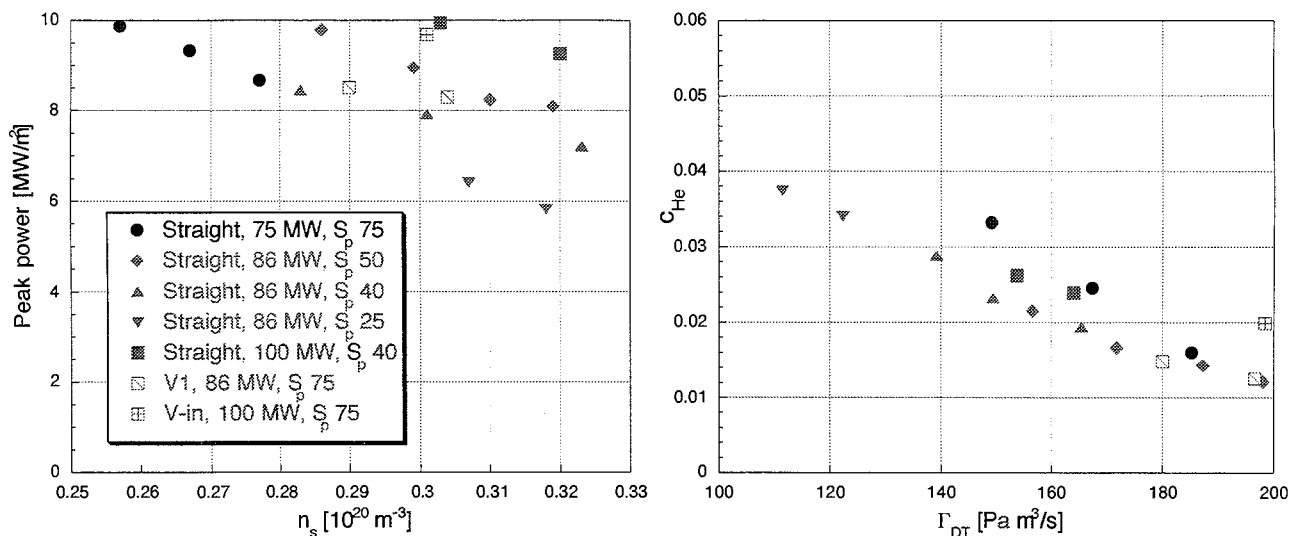


Figure 2.6-10 2 cross-sections of the 6D operational window for the FEAT divertor. Only acceptable points within window and without neon seeding are shown. V1 is a slight modification of the V-out geometry.

2.7. NTM Suppression by ECCD

Optimisation of ECCD has been carried out⁶⁰ in frequency, poloidal (θ_p) and toroidal (θ_t) injection angle and injection position (defined by the poloidal angle χ_i) from the equatorial plane, solving ray-tracing and using the relativistic Fokker-Planck equation. The calculation has been carried out for ITER-FEAT-like parameters ($R/a = 6.2 \text{ m}/1.9 \text{ m}$, $n_{e0} = 1.17 \times 10^{20} \text{ m}^{-3}$, $T_{e0} = 30 \text{ keV}$, $Z_{\text{eff}} = 2$) but with slightly higher B field (5.5 T). The density profile is assumed to be flat ($\sim(1-\psi/\psi_s)^{0.15}$) and the temperature profile is assumed to be parabolic ($\sim(1-\psi/\psi_s)$). Figure 2.7-1 shows that for off-axis current drive, optimal injection position is ~ 70 degrees, and the frequency is 180 GHz ($\sim 170 \text{ GHz}$ for $B=5.3\text{T}$). Figure 2.7-2 shows the sensitivity to optimal toroidal injection angle, indicating the need for accurate control of injection angle. In this figure, at each frequency and each injection position, values for the toroidal and poloidal angles are chosen to have the maximum efficiency at a given radius ρ . The figure shows, for 190 GHz and for this angle $\chi_i = 70^\circ$, the variation of these angles θ and the current density and efficiency, when the radius is varied. Other key points include:

- (1) control of both poloidal and toroidal angles is essential for tangential resonance, which is the condition of optimisation;
- (2) it is also essential to avoid the second harmonic resonance;
- (3) estimated required power for stabilisation of NTM is several MW under the condition that the driven current is localised within 3% of minor radius from the optimised resonance point.

Modelling of modulated ECCD stabilisation of NTMs has been done for FEAT equilibria and the required EC power has been determined⁶¹. Equatorial and upper port launching has been considered. It has been shown that NTM detection in the early stage of evolution allows the requirements on EC power to be eased. A reasonable island size to be detected $w/a=0.04$ ($w \sim 10\text{cm}$) allows the power required for stabilisation of both 3/2 and 2/1 NTMs to be reduced from 28 to 18MW for upper launching and from 35 to 22MW for equatorial launching. For small islands the polarisation current term in Rutherford's equation is essential, so an accurate model for this term is desirable.

Theoretical investigation⁶² of NTM suppression has shown recently that the polarisation current is stabilising not only for subdrift island propagating in the ion drift direction ($0 < \omega/\omega_{*i} < 1$) but also for islands propagating in the electron drift direction with a sufficiently low rotation velocity ($0 < -\omega/\omega_{*i} < k^* \sim 0.118$).

Clearly, some experimental verification of models in present experiments is required, before a definite conclusion can be drawn with confidence.

⁶⁰ K. Hamamatsu, private communication and in preparation for publication.

⁶¹ Zvonkov(Kurchatov)

⁶² Mikailovskii et al.(Kurchatov)

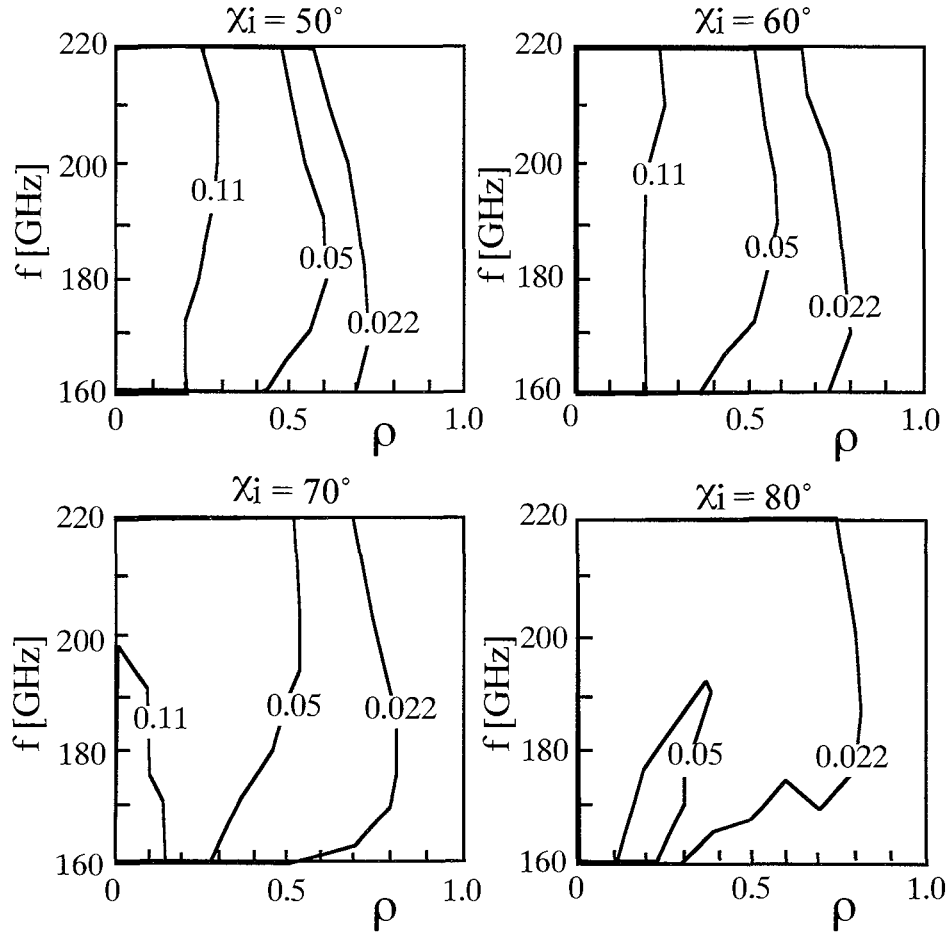


Figure 2.7-1 Contours of driven current density (in MA/m² per MW input) (frequency f vs. normalised radius ρ) for different poloidal injection angles χ_i .

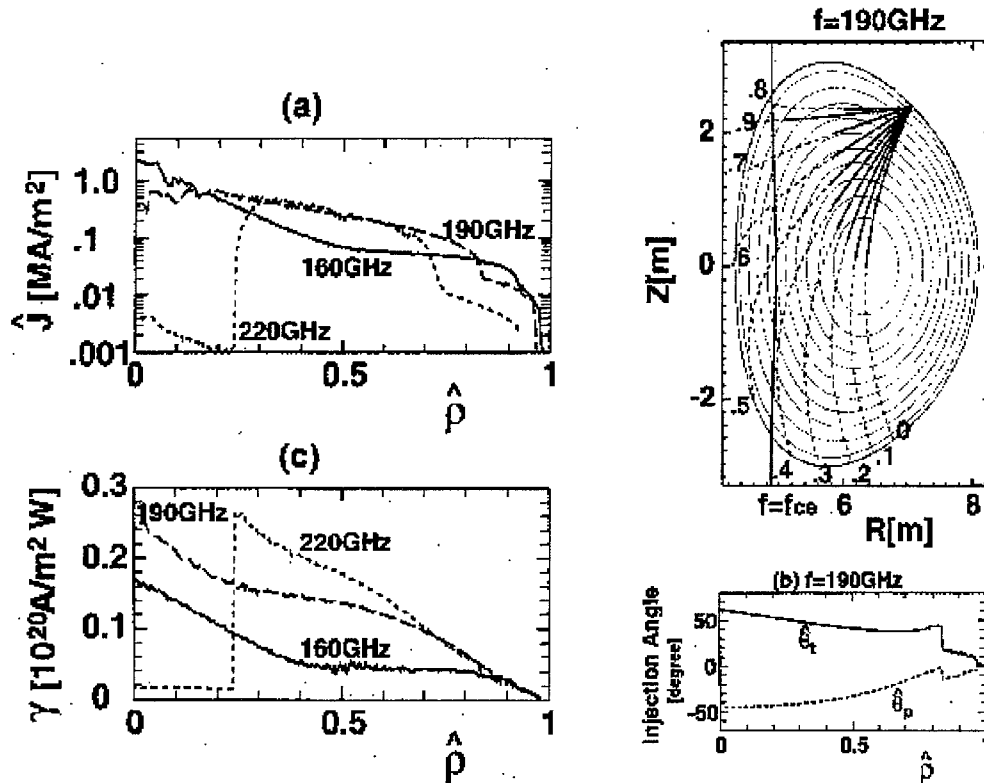


Figure 2.7-2 Current density per MW of injected power (a) with the optimum choice of injection angles, at one frequency (b) versus normalised radius. Global efficiency is shown in (c) for the same conditions

2.8. ITER Physics R&D

The projections of ITER performance require extrapolations from present experience and these must rest on established theory and experimental results from the leading laboratories, facilities and universities that together pursue the Parties' fusion science programmes.

The Parties undertake their Physics work for ITER on a voluntary basis outside of the framework of task assignments established for ITER Tasks in technology R&D and Design. Nonetheless the Parties' various efforts are undertaken in a structure designed to offer coherence and co-ordination of the voluntary contributions. An ITER Physics Committee comprising the Director and the Parties' designated persons for ITER Physics exercises oversight and is supported by seven Physics Expert Groups in the areas of

- Diagnostics
- Scrape-off-layer and Divertor Physics
- Edge and Pedestal Physics
- MHD, Disruption and Control
- Energetic Particles, Heating and Steady State Operation
- Transport and Internal Barrier Physics
- Confinement, Database and Modelling

Expert Groups meet up to twice a year and communicate their recent results to the ITER JCT, and they assist JCT via recommending physics basis and methodologies for physics design calculations to be used for ITER-FEAT. The results are reported to Physics Committee held once a year, and research priorities are determined from the perspective of addressing ITER-relevant problems most efficiently using the facilities and resources available to the Parties. Table 2.8-1 shows the Urgent and High-Priority Research Areas for the year 2000.

With the support and commitment of individuals and organisations throughout the Parties, this structure has proved to be extremely effective in providing the necessary physics support to the ITER design activities, the results of which have been published in the December 1999 edition of the Nuclear Fusion Journal. At the same time, ITER has proved a catalyst to general progress in tokamak physics through the discipline and focus required to identify and address efficiently the main challenges of establishing the ITER Physics Basis.

After the withdrawal of U.S. from ITER Expert Group activities, a decision was made in July 1999 at the Program Directors' Meeting to arrange as much as possible a 'pre-Meeting' or international workshop/conference, where generic issues will be discussed including the U.S. scientists, in conjunction with the Expert Group Meeting. Considerable efforts have been made successfully to involve U.S. scientists in voluntary physics activities by combining Expert Group Meetings with international meetings (U.S.-Japan Workshop, IAEA TCM, etc.).

Table 2.8-1 Urgent (Bold) and High Priority Physics Research Areas

Research Areas	Issues
Finite- β effects	Tolerable ELMs ($dW/W < 2\%$) with good confinement alternate to type-I ELMs (e.g. type II, Type III+core confinement) Stabilisation of neoclassical islands and recovery of β
Plasma termination and halo currents	Runaway electron currents: production and quenching, e.g. at low safety factor
Sol and divertor	Achievement of high n_{sep} and relation of $n_{sep}/\langle n_e \rangle$ in ELMy H-modes Carbone Chemical sputtering and deuterium retention/cleaning methods
Diagnostics	Determine requirements for $q(r)$ and assess possible methods that can be applied to ITER Determine life-time of plasma facing mirrors and optical elements (incl. Those in divertor) Reassessment of measurement requirements in divertor region + recommendation of diagnostic techniques
Core confinement	Non dimensional scaling and identity experiments; effect of finite β and flow shear Determine dependence of τ_E upon shaping, density peaking etc.
Internal transport barrier properties	ITB power thresholds vs n , B , q , T_e/T_i , Vrotation etc. for strong reversed shear ($q_{min} > 3$), moderate reversed shear ($q_{min} > 2$), and weak shear ($q_{min} > 1$).
H-mode power threshold	H-mode accessibility in ITER-FEAT, Data scatter
Density limit physics	Confinement degradation onset density; its dependence on aspect ratio, shape and neutral source
Pedestal physics	Scaling of pedestal properties and ELMs Effects of plasma shape on pedestal and ELMs

3. Magnets

3.1. Support of TF Coil Loads

3.1.1. Winding Pack Issues

Two options have been considered for the TF coil winding pack configuration:

- the radial plate design where the TF conductors use a thin circular jacket and are placed in spiral grooves machined on steel radial plates;
- the square conductor design where the conductor uses a thick-walled square jacket.

The advantages and drawbacks of these options are reviewed and the rationale for a choice is outlined.

Insulation

For both designs, radial plates and square conductors, the recommended procedure for the application of the conductor insulation is to follow the method used for the CS Model Coil. After heat treatment, the conductor is wrapped with insulation tapes (pre-impregnated glass and polyimide) and the insulation is cured. This allows a full visual inspection and voltage testing of the conductor insulation and gives a good guarantee that there is no pre-existent defect. The conductor is then either transferred to the radial plate or reformed into a double pancake. An insulating layer is then built up around each radial plate (or double pancake) and this assembly is filled with epoxy resin in a single impregnation step. The plates (or double pancakes) are bonded together to form a winding pack with ground insulation in a final impregnation step.

The radial plate and square conductor designs use therefore similar insulation manufacturing procedures. Even though the manufacturing procedures are similar, there are differences in the conductor geometry and operation conditions which give to the radial plate configuration major advantages in terms of the conductor insulation long term quality and reliability.

- 1) The jacket with a circular outer cross section is the optimum shape to apply the glass and polyimide insulation tapes. The result is an insulation which is uniform in thickness and also uniform in the relative glass/polyimide/epoxy content. This insulation is robust since it can contain a high density of glass and polyimide film.
- 2) During the magnet operation, the Lorentz forces acting on each conductor are transferred to the plate, without accumulation of forces on the conductor and its insulation. As a result, almost no primary load is applied to the conductor insulation and there is no degradation leading to damage due to mechanical cycling.
- 3) With circular conductors in radial plates, the insulation is not subject to the stress concentration effects which are always present at corners of square conductors.
- 4) With circular conductors in radial plates, delamination between the conductor insulation and the radial plate is of no consequence and has no impact on the mechanical behaviour of the winding pack.

In summary, the insulation of a circular conductor in radial plates is expected to be highly reliable. It is also expected to be very robust and able to easily stand the full coil ground voltage thus providing a second line of defense in the case of a ground insulation fault.

Another advantage of the radial plate configuration is that it provides a “double insulation” with two independent barriers and the capability to detect impending faults.

- 1) The conductor and ground insulations are independent and physically separated by the radial plate. It is therefore impossible for a single insulation fault to affect both conductor and ground insulations.
- 2) A single conductor insulation fault can be detected by monitoring the resistance between conductor and radial plate. In the event of such a fault, action taken before a second fault induces severe damage to the coil system.

The considerations above indicate that, with the radial plate design, faults internal to a TF coil and leading to coil damage are avoided by design.

There is, however, the possibility that faults external to a TF coil, for example at the TF coil terminal or along the coil feeders, may lead to a full coil short. The ITER design ensures that this type of fault does not occur: the TF coil terminals are separated by steel separator plates, and bus-conductors from one coil are routed in separate feeder tubes.

It can be concluded that, with radial plates, TF coil shorts are avoided by design. This is a very important statement in view of the severe thermal and mechanical damage induced by a TF coil short.

By contrast, the square conductor insulation is subject to large primary stress due to the in-plane and out-of-plane (cyclic) loads and to stress concentrations at corners of conductors. In particular, the square conductors show local tension regions in the insulation, which would cause local debonding at the corners extending in the worst case to about 20% of the jacket surface. With the square conductor design, the conductor and ground insulations are not separated and there is no possibility to detect impending faults in a TF coil. The occurrence of an insulation fault leading to significant damage cannot, therefore, be excluded.

Cost and radial build

Although the radial plates allow the use of a highly reliable turn insulation, they cannot be used without a cost penalty due to the radial plate manufacture and additional coil manufacturing steps to transfer conductors onto the plates. The cost difference between the radial plate and square conductor design options has been estimated using the 1998 ITER design unit costs. It has been found that the total TF coil cost with radial plates is about 8% more expensive than with square conductors when there is an identical radial build.

Some design and R&D activities have been requested in the EU and JA Home teams to study methods to reduce the manufacturing cost of the radial plates.

The radial plate design implies also a radial build penalty. The stress analysis of the TF coil inboard leg indicates that at similar stress levels in the case and radial plate (or square conductor jacket), the radial plate design requires a radial build which is 30 – 50 mm thicker than with square conductors.

Other considerations

Turn insulation voltage

With radial plates, each plate is connected (through a resistor) to the conductor cross-over. The turn insulation voltage is therefore 425 V for a coil terminal voltage of 5 kV. With square conductors, the turn to turn voltage is 35 v and the voltage between pancakes is 850 V.

The higher turn insulation voltage, in the case of the radial plate design, is not seen as a disadvantage in view of the high insulation reliability of this design.

Fast discharge and recool time:

- Radial plate design: In the event of a fast discharge of the TF system, eddy currents flow in the case and the radial plates. Heat conduction causes a quench of the superconductor after about 12 s. The radial plate temperature rises to about 60K and the conductor temperature to $\sim 40 - 60\text{K}$. During such an event, the helium in the TF coils is expelled and is collected in a cold (LN2 temperature) pressure vessel (volume of about 1800 m^3 and pressure of 1.8 MPa). Recooling and recharge of the TF magnet is expected to take less than 2 days.
- Square conductor design: In this case, the TF coil case temperature rises but this is not expected to cause a conductor quench. Recooling of the case is expected to take about half a day.
- Fast discharges are expected to be very infrequent and the difference in time to recool the magnet is not considered as a significant element in the choice.

Conclusions

The evaluation of the two winding pack configurations requires a balanced judgement between considerations of totally different nature such as insulation quality, radial build, cost, etc..

This judgement is therefore somewhat subjective since it critically depends on the weight and priority given certain aspects of the design.

Considering that insulation faults are the most probable cause of magnet failure and considering the difficulties involved in the replacement of a TF coil in ITER, the considerations on insulation reliability during operation have been given a high, overriding, priority over other considerations. This is the basis for the use of radial plates in the ITER TF coils.

3.1.2. Wedged support at the TF coil inboard legs

All along their inboard legs, the coil cases are wedged over their full radial thickness. About half of the centring force is reacted through the winding pack part of the coil, while the other half is reacted by the case.

The wedging surfaces must be accurately matched to achieve the required magnetic alignment and reduce stress peaks under the large wedging pressure. Precision machining of the wedging surfaces will be required as well as accurate surveying techniques to verify that deviations from the theoretical shape are within allowed limits.

Machining will ensure that deviations from flatness involve only long wavelengths and do not result in localized peak stress. Systematic errors, in particular on the wedge angle, could result in significant stress intensification and must be kept within tolerable limits, if necessary by using shims. Insulating shims are, in any case, necessary to avoid eddy currents flowing between adjacent coils. Analysis is underway to evaluate the effects of dimensional deviations and specify the acceptable range of tolerances.

It is assumed that the TF coil cases will be finish machined, surveyed and fitted with insulated shims before delivery.

3.1.3. Intercoil Structure Redesign

The main design driver for the inner intercoil structure (which is situated immediately above and below the inner straight leg of the TF coils) has been the requirement to achieve acceptable tensile stresses in the curved part of the coil in these regions. The allowable stresses are driven by cyclic fatigue considerations and, depending on the case material, fabrication history and welding procedures, are expected to be in the range 450-500MPa. Although the outer intercoil structure (forming four toroidal bands around the outboard curved regions of the coil) has only a small influence on the stresses in the inner curved region (due to the relatively high flexibility of the coils), the configuration of the inner intercoil structure can have a significant impact on the load conditions of the outer intercoil structures.

Many configurations of inner intercoil structure have been analysed with a detailed finite element model but the only one that gives acceptable stresses in the coil case, combined with an acceptable stress distribution within the structure (and especially the keys/bolts associated with the structure), is a set of poloidal keys between the coils. The intercoil structure itself is absorbed into the coil case, so that (at least at assembly) the wedged region of the coils extends into the curved regions by a thickening of the toroidal width of each coil case. The keys run in between the coils in these curved regions, normal to the coil centreline, extending to the inner (plasma facing) surface. A set of three or four in the poloidal direction appears adequate. The keys provide full support between the coils and prevent the development of torsion of the case which can make a large contribution to the case tensile stresses. At the same time, the flexibility of the case in bending gives a uniform poloidal distribution of load on the 3 or 4 keys. The poloidal keys are shown in Figure 3.1-1.

In this curved region away from the central vault, the coil cases tend to separate on charging due to the overall expansion of the coil. The radial movement is small compared to the radial outward movement at the outer equator but is still sufficient to create an extra toroidal gap of about 0.5 mm between key and key slot. During plasma operation, the shear loads acting on the keys increase this gap to more than 1 mm. Key shapes which can tolerate this sort of "breathing" without losing contact have to be square or rectangular and produce high stress concentrations in the keyways. Detailed evaluations of the key and key slot stresses are still underway but at present the preferred solution is to use circular cross-section keys. The shear

loads acting on these create an extra de-wedging force which increases the gap between key and slot to more than 1mm. It is intended to suppress the breathing movement plus the extra de-wedging force by an upper and lower precompression ring. This ring is attached to each TF coil (and therefore requires eddy current barriers) in the upper and lower curved regions and is put into tension on assembly. The TF coils are therefore put into toroidal compression in the upper and lower curved regions (effectively, the wedged region of the central vault is extended above and below the inner straight leg) and toroidal separation in the key region is much reduced. The impact of the ring is summarised in Table 3.1-1 and 3.1-2

Table 3.1-1 Peak Tensile Stresses in the TF Coil Case

	Maximum Tensile Stress MPa	Min/Max Stress (R value)	Allowable Stress (LEFM with fixed initial defect - MPa)
With Ring			
Bottom of straight leg	516	0.65	560
In front of first key	342	0.42	440
Without Ring			
Bottom of straight leg	493	0.58	520
In front of first key	439	0.38	425

Table 3.1-2 Maximum Poloidal Key Shear Loads (4 Keys) in MN

	First Key (nearest inner leg)	Last Key
With Ring	16.2	14.4
Without Ring	19.5	14.7

To be effective, these precompression rings need to have a significantly lower elastic modulus than that of the case, so that the precompression is not sensitive to assembly tolerances. A thermal contraction coefficient larger than that of the case is also advantageous. The space available for the precompression rings between the CS and the inner PF coils is limited and a material that can provide the necessary hoop force within that space is a unidirectional glass fibre-epoxy composite. Any solution based on metallic materials would require a much larger (almost a factor of two larger) cross-sectional area than the glass fibre solution: aluminium wound as strips would offer the required elasticity and higher thermal contraction. The rings need to be placed close to the curved part of the coil, as extensive flange connections tends to rapidly reduce the effectiveness of the rings due to the flexibility of the flanges. The precompression is applied by tightening radial bolts between ring and the back of the coil case in the upper and lower curved regions (see Figure 3.1-1). The stresses in the rings are dominated by the precompression at room temperature. The material is stronger at 4K and there are no significant extra stresses due to out-of-plane movement of the TF coils (this is very small as the rings are close to the poloidal shear keys that restrain any coil rotation).

Table 3.1-3 summarises the main requirements for the rings for two of the most promising materials. On the basis of this, glass fibre is selected as the reference.

Table 3.1-3 Stresses in Precompression Rings at RT

Material	Allowable RT Tensile stress MPa	Cross-sectional Area of Ring m²	Radial Displace- ment to Apply Precompression mm
Glass fibre	650	0.22	10
Aluminium Alloy	250	0.34	30

The use of the precompression rings has a significant impact on the outer intercoil structures (OIS) due to the changes in the radial expansion of the outer coil leg under the magnetic loads. It appears that the upper and lower structure rings are practically redundant. The poloidal keys carry the out-of-plane loads previously carried by the upper and lower OIS and the precompression rings cause the hoop tension (previously caused by the radial expansion of the coil) to drop to zero. The upper and lower OIS are maintained because they are used for coil positioning during assembly but they have no structural function (although the TF coil radial expansion creates significant key loads in these upper and lower OIS sections). Their extent can be reduced and their poloidal position can be flexible.

The outer intercoil structures directly above and below the equator are still required to support the out-of-plane forces on the outer part of the coil, and the out-of-plane loads are not much affected by the inner intercoil structures. However, the precompression rings cause a significant reduction (by a factor of more than 3) in the hoop tension carried by these structures due to the radial expansion of the coil cases. The key loads are summarised in the Table 3.1-4.

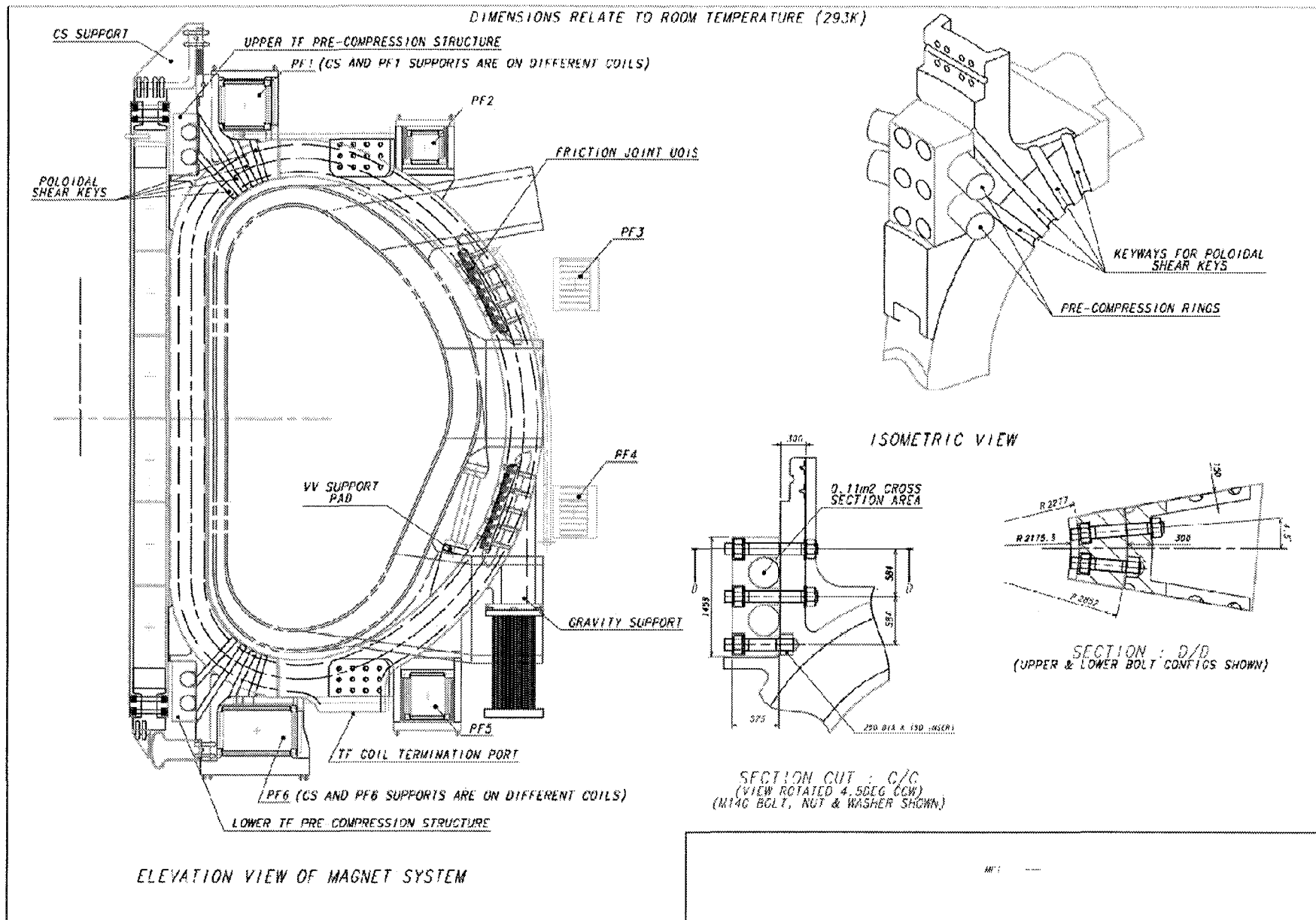
Table 3.1-4 Tensile (Toroidal) Bolt Loads on the Equatorial OIS Sections in MN

	Upper Equatorial OIS	Lower Equatorial OIS
With Rings	7.9	1.9
Without Rings	22.8	17.7

The poloidal extent of the two equatorial OIS belts is determined by the out-of-plane loads and cannot be much reduced. There is some flexibility to position the belts to suit the requirements of the equatorial access gaps. A further major constraint on the design arises from the requirement for access to the vacuum vessel gravity supports (which connect to the TF coil cases) during assembly. The supports are placed behind the lower equatorial OIS ring and, in previous designs of this ring, are inaccessible once the ring is in place. The access requirement for the vacuum vessel supports has resulted in the choice of a "friction joint" type of OIS. This OIS is assembled after the TF coils (and the vacuum vessel supports) have been installed, by welding to the TF coil case on each side. The use of the inner precompression ring has reduced the toroidal load requirements on the equatorial OIS belts and the designs are now being reassessed to see if a prewelded and keyed/bolted box structure (with a removable central part to allow access to the vacuum vessel supports) can provide adequate out-of-plane support, eliminating in-situ welding.

454

Figure 3.1-1



3.2. Inductive Flux Generation

3.2.1. Choice of CS Jacket Material

The main function driving the design of the central solenoid is the generation of inductive flux to ramp up and maintain the plasma current. Flux generation in the solenoid is improved by:

- (i) the choice of a maximum field compatible with the variation of the superconducting strand current density with field
- (ii) the use of the highest allowable tensile stresses in the jacket material

The requirements for the CS conductor jacket material in the FEAT ITER are primarily a high fatigue resistance to stress cycling. The jacket material can also affect the performance of Nb₃Sn superconductor due to differential contraction with the strands from the heat treatment temperature. This is a significant factor but not the main reason for choosing a jacket material.

Fatigue resistance can be assessed based on one of two procedures.

- a) Fatigue life (S-N curves) measurements for the jacket, both base metal and weld
- b) Linear Elastic Fracture Mechanics (LEFM) which requires the definition of an 'initial defect' and measurement of the material fatigue crack growth rate (FCGR). The initial defect is usually taken as the smallest defect that can be reliably detected in the material and welds during the fabrication inspections.

As indicated in the ODR, there are two basic design options for the CS jacket.

1. The use of an extruded jacket with a square outer section where the structural material goes through the Nb₃Sn heat treatment. The possible jacket materials are Incoloy 908, as developed for the CS Model Coil, or a 'modified' stainless steel if such a steel can be developed to meet the fatigue life requirements after heat treatment.
2. A double armour option involving the use of an inner titanium circular jacket (which undergoes the Nb₃Sn heat treatment and which matches the thermal contraction of the Nb₃Sn) reinforced by two outer U-channels which are applied after the heat treatment of the conductor. In this case, the steel can be selected for optimum mechanical properties, without consideration of the degradation caused in steel by the heat treatment.

In the case of option 1 above, the possible jacket materials are Incoloy 908 and a 'modified' SS.

The problems of Incoloy 908 are well known:

- a) it is highly sensitive to stress accelerated grain boundary oxidation (SAGBO) during the Nb₃Sn heat treatment, which requires very strict control of the heat treatment atmosphere ($O_2 < 0.1$ ppm)
- b) the welding procedure was not adequately developed by USHT in the EDA period. The welds suffer from local hot cracking due to Nb precipitation with multi-pass welding. The effect on fatigue is unknown but presumably not acceptable. A possible solution was identified towards the end of the EDA by USHT, using a low-Nb weld wire. This wire was never qualified by USHT but this work is now being undertaken by EUHT. (recent results indicate that the new wire solves the hot cracking issue).

There are two significant advantages of Incoloy. It is a precipitation hardened superalloy with (in the base metal) a very high fatigue resistance, and the thermal contraction matches Nb₃Sn. It was selected for the ITER CS reference on the basis that the weld problems can be solved and that process for heat treatment of Incoloy has been well established in the CSMC fabrication. Difficulties have been encountered by the EU in the heat treatment of an Incoloy pancake. This occurred with a thin circular TF jacket (not the CS square type) and the heat treatment was performed in an oven well outside the ITER specification.

The 'stainless steel' issues are less clear because 'stainless steel' is a generic term and does not define either the specific alloys required to withstand the Nb₃Sn heat treatment without embrittlement due to carbide precipitation, or those that have good cryogenic properties. For example, the JK2 proposed as the material for the second ITER reference option is a stainless steel that cannot withstand the Nb₃Sn heat treatment and which has a coefficient of thermal contraction close to Nb₃Sn between room temperature and 4K. As a result of R&D in EU and JA, several steels are known which seem to withstand the heat treatment without degradation of properties. The EU has manufactured 3 variants (all low carbon, high nitrogen modifications of the standard 316LN), one from Boehler, one from Valinox and one from Sandvik.

The measured FCGR (fatigue crack growth rate) performance of the Boehler and Valinox steels is extremely poor, about x5 higher than usually expected for high quality stainless steel (and x5 higher than measured for JK2). This may be due to the poor quality level of these steels (no electroslag refining) but this is not known definitely. The most recent supply, from Sandvik, was used for the TFMC. The EU has a task agreement (since 1996) which includes the fatigue characterisation (S-N and FCGR) of this steel but this has never been performed.

For fatigue life assessments based on FCGR, the assumed initial defect size is critical. The selection of an initial defect for use in an LFM assessment is not only based on what can be 'seen' in an X-ray photograph but also on what is present, determined by destructive sectioning, and cannot be seen. The EU has referred to defect sizes of 0.1 mm 'detected' during the fabrication of CS coil jackets. However, it is known from subsequent investigations on the CSMC jackets that defects were present that were not detected by inspections but later became visible after winding operations. The defect size stated by the EUHT of 0.1 mm is not much larger than the material grain size (0.04 mm) and is unlikely to be supportable in a proper qualification procedure.

The use of realistic defects sizes (the JCT reference value is 0.5 mm² for a crack area) together with the available FCGR data for Boehler and Valinox steels would lead to an unacceptable CS design. Not only are the allowable stresses low (about 300 MPa compared to 400 MPa for Incoloy 908) but the thermal contraction coefficient causes degradation of the Nb₃Sn properties. In addition, the use of a steel jacket reduces the vertical precompression that can be applied to the CS and may bring some limitation in achievable plasma shaping.

Alternative fatigue assessment procedures (S-N curves) may be appropriate for application to the jacket welds as they can take into account the stress cycles needed to initiate a crack from a defect. At present this is not possible as almost no data is available for any of the 3 EU steels, base metal or weld (and generally S-N data for austenitic stainless steels at low temperature is very limited. It is not certain that this alternative procedure would allow higher

operating stresses as conventional safety factors with fatigue life predictions are higher than with FCGR-based predictions.

The JCT action in this situation has been as follows:

- a) select Incoloy 908 as the provisional reference solution and Ti- stainless steel (JK2, without heat treatment) as an alternative solution;
- b) try to establish with JAHT task agreements to demonstrate the JK2 fatigue properties and establish the Ti-JK2 fabrication route (the application of U channels after heat treatment is a complicated process);
- c) place a task agreement with EUHT to provide S-N data on Valinox base and weld metal;
- d) try to establish another task agreement with EUHT to manufacture and qualify a steel variant properly optimised for good fatigue performance after Nb₃Sn heat treatment.

3.2.2. Choice of the CS conductor cross-section: rectangular or square jackets

The qualitative reasons for choosing square CS conductors have been presented both to the Concept Improvement and Design Integration Task Forces in 1999 and to TAC. In view of the comments received from the EUHT on the possible use of rectangular conductors, this has now been quantified, confirming the original JCT judgment.

Stress Analysis

It is clear from simple geometric considerations that a vertically elongated jacket will provide better support to the vertical forces (for the same jacket area) than a square one. However, the difference between the two jacket configurations become negligibly small in the case of the CS winding pack because of the large fraction of structural material which is required to support the hoop stress.

The JCT has performed a stress analysis, using two CS winding packs with identical structural material fractions. One winding pack has the reference square conductor plus co-wound strip, the other has a rectangular conductor with an aspect ratio of 2.5 plus cowound strip. The results are given in the table.

	Toroidal Hoop Stress MPa	Tresca Stress MPa	Vertical Stress MPa
<i>Stress Limits</i>	400	867	N.A.
Square Conductor	392	546	-302
Rectangular Conductor	395	476	-269

The toroidal hoop stress is almost identical to the maximum principal tensile stress as it occurs on the inner surface of the jacket where the shear stress is zero. The cross-section of structural material in the CS conductor is determined by mechanical fatigue which depends on the toroidal hoop stress. The rectangular conductor design does not present any advantage in this respect.

Cable Performance and Supporting Data

Conductors with a rectangular cable will not achieve higher current densities than conductors with a circular cable unless the final substage wrap of inconel foil (used to control AC losses) is omitted.

Based on present knowledge, the following comments can be made on such rectangular cables.

- a) AC losses would be unacceptable without an Inconel wrap. Although the rectangular shape helps reduce AC losses due to field changes parallel to the long side, the rectangular shape also gives a better contact between the final cable units than the circular shape with units arranged around a central hole.
- b) The AC losses of cables with substage wraps are dominated by the last but one substage and the shape (rectangular or circular) has almost no impact.
- c) Because of the different cable contact distribution and AC loss behaviour, the use of a rectangular conductor would require the AC loss characterisation work to be repeated.
- d) When submitted to transverse changing fields, the round shape offers symmetry and hence the best conditions to provide uniform current distribution among sub-cables and strands. Predictive analysis of non-uniform current distributions and their effects on conductor performance is difficult and is more likely to be successful when applied to a symmetrical configuration.
- e) The circular cable can be produced with a minimum size hole in the centre for short unit lengths. For coils with long unit lengths that require a greater cooling flow, the hole diameter can easily be increased without changing the cable concept.

Joints

It has been claimed that a rectangular conductor joint in the CS occupies less radial space than the square. This claim seems to be based on the assumptions that the joint is an overlap type, that the toroidal length in each case is the same, and that the top or bottom side of the conductor (the narrow side for the rectangular) is used as the contact surface.

Two comments can be made on this question.

- a) For the same circumferential length of the joint, a rectangular conductor has a lower contact resistance area than a circular. This reduction in area has a very significant impact on the current distribution into the individual strands, as fewer of them come into contact with the copper sole plate of the joint. The rectangular joint could be made longer but this has a drastic impact on the joint AC losses in the CS.
- b) If a rectangular joint with lower contact surface area is acceptable, the circular cable can be given a similar shape locally in the joint region. The overall compaction of the cable in the joint gives vertical space for such an adjustment.

Manufacture

The selection of a circular cross section for the cable was made at the beginning of EDA. Advantages in the manufacture of the cable and the jacketing process were important reasons of that choice.

- A circular cable is made of typically 6 identical sub-cables in a symmetrical configuration. This geometry minimizes the amount of deformation of the sub-cables

during the production of the cable and during the subsequent jacketing operation. As a result strand damage is also minimized.

- It has been verified that a circular cable can be pulled through a seamless jacket which has been fully inspected (X-ray, liquid penetrant, ..) and leak tested before the insertion of the cable. This gives the best guarantee of the jacket quality.

By contrast, rectangular conductors require a large deformation of the cable which probably sets an undesirable lower limit to the void fraction. It is not clear if a rectangular cable can be pulled through the jacket as cable torsion can create extra friction. The jacket is also subject to large cold work deformation especially at the corners and may not be able to be produced as seamless tubing.

Overall R&D Database

The entire conductor and magnet R&D effort of all ITER Parties since 1992 has been focused on circular conductors. The development has covered all aspects of conductor manufacture (cabling, jacketing) and performance evaluation (AC losses, short sample and joint performance) and culminates now in integrated performance testing of model coils. The circular conductor concept is common to all ITER coils (TF, CS and PF).

The use of a rectangular conductor would require to repeat many items of this development. It would also convey the message that EDA R&D has not been useful.

3.2.3. CS manufacture and compression structure and supports

The CS is pancake wound. In the current design, a single conductor length of 820 m is adequate for six pancakes. This "hexa-pancake" winding arrangement minimizes the number of joints at the outer diameter and, therefore, it reduces the complication associated with the joint configuration which includes the joint itself with its mechanical clamps, the helium pipes and the tie plates which carry the mechanical hoop tension. These components must fit in a narrow space between the CS and TF coils. On the other hand, this configuration requires more complicated manufacturing processes and tools, in particular for the winding of a conductor when the winding starts from the outer diameter. A preliminary study on the CS manufacture has been performed by industry and indicated a possible process to make hexa-pancakes with some conceptual design of tooling. The design of the cooling inlets at the high field cross-over point of each pancake is another issue that requires R&D to resolve. The use of the hexa-pancakes makes positioning of prepared jacket penetrations (formed before the cable is put in the jacket) very difficult, and forming them in-situ is complicated, with potential for strand damage and the introduction of weld defects. A more conventional double pancake winding is of course possible and is kept as a backup option, but it requires three times as many joints.

The CS consists of a stack of six electrically independent modules. The field curvature at the ends of the CS creates vertical forces on the modules. At IM (initial magnetization) and EOB (end of burn), these forces are towards the centre of the stack, whereas at some intermediate equilibrium configurations the end modules carry opposite currents to the central ones and are repelled. This means that a vertical support structure is required. This structure applies axial pre-compression to the coil stack so that the modules remain in contact during all operating conditions. To obtain uniform compression, tie plates running axially along the CS are provided at both inside and outside diameters and connect to pressure plates at top and bottom. This structure is designed so that it can restrain the maximum vertical separating load

of 75 MN acting on the end modules of the stack. The required axial tension in the structure is achieved partly by pretensioning at room temperature and partly by differential contraction during cool-down. This requires a jacket material of the CS conductor with a lower contraction coefficient than the tie plates which use stainless steel.

The whole CS stack is hung from the top of the TF coils through the precompression structure. The top supports consists of flexible plates which provide axial and toroidal registration of the CS but allow relative radial motion between the CS and the TF coils. At the bottom of the CS stack, springs provide a radial centering force.

3.3. Conductor Design Issues

3.3.1. Current Non-Uniformity

It is now widely recognised that the current in a cable made of parallel-connected strands is most unlikely to be uniformly distributed in each strand. The non-uniformity can be driven by resistive variations in the strands at the joints, or by inductive coupling variations between strands along the cable length. Transition between these two drivers is controlled by the time constant of circulating currents in the cable, which is of the order of 1000 to 10000s. In the ITER coils, the CS and PF coils are expected to have inductance-dominated current distributions and the TF to have resistance-dominated.

Current non-uniformity is not a problem in itself: only if it leads to degradation of the thermal stability level of the cable does it need to be avoided. In some coils (which are not typical of the ITER coil design), current non-uniformity has caused such phenomena as the 'ramp rate limit'. The ITER coils have various levels of current uniformity control:

- The cables are designed to be fully transposed with the strands in predictable positions around a central annulus, so that a uniform inductance can be expected.
- The joints are designed to give uniform contact resistances at the level of the final substage (one sixth of the cable, with about 150-200 strands). This avoids gross mal-distribution in the cable and is within the current capability of joint manufacturing technology to achieve. Current non-uniformity is dominated by current variations within the strands of each of the final subunits.
- The cables have a minimum level of transverse conductance between the strands in each of the final substages. This conductance has to be carefully controlled through the cable void fraction (and hence through the jacket manufacturing tolerances). Too high a conductance leads to a high AC loss, too low and fast current redistribution of current during thermal disturbances cannot occur.

The CSMC was designed to test the impact of both resistive and inductive current distributions in full-size ITER cables. The results so far (including steady and pulse tests of the main module up to 13T) show no sign of any performance degradation due to current non-uniformity. Numerical analysis of current non-uniformity is also being developed and verifies the ITER choice of design criteria (these criteria, updated from the 1998 ITER design, were discussed and agreed in March 1998 at a meeting attended by all HTs, and will be included in the ITER FEAT FDR at the end of this year.

3.3.2. PF Conductor Design

The PF conductor design rationale has been presented to the HTs in recent working documents⁶³. These contain a detailed discussion on the factors controlling the design of the PF conductors and the reason that three or four grades should be chosen (to reduce cost).

The PF conductors have been designed in accordance with the criteria agreed with all HT. The copper: non-copper ratio is derived from the usual combination of requirements from the limiting current (Stekly), temperature margin and hot spot criteria, and (to achieve the lowest cost, most compact cable design) all three limits are satisfied at the design point. The highest field conductor (PF1 and 6 under back-up conditions, at 6.4T and 4.7K) requires a low Cu:nonCu ratio of about 1.6. The performance of NbTi rapidly improves with lower field so that the Cu:nonCu ratio rises to 6.75 for the PF2,3 and 4 conductors at 4T and 5K.

3.4. Limits to Elongation/Triangularity

Several analyses⁶⁴ have shown that the strong reverse (negative) shear plasmas (“*long pulse*”) modelled in the recent RTO/RC ITER studies pose less demand on the vertical stabilization system than the nominal (positive) shear counterparts (“*high current*”). In fact, although the plasma elongation (κ) is typically larger for the reverse shear equilibria, the vertical field decay index⁶⁵ is smaller than in the negative shear case⁶⁶. Moreover, the reverse shear plasmas are better coupled with the passive stabilization structures. As a result, the stability margin (m) and growth time (τ_g) of the negative shear plasmas (see box) are, typically, 50-100% larger than in the positive shear equilibria⁶⁷. Because of these facts the stabilization system is designed for the “the most demanding” positive shear plasma and - a posteriori - checked to ensure that the reverse shear plasma can indeed be stabilized by a feedback loop designed for the negative shear case⁶⁸. It turns out that the positive shear, Start Of Flat-top (SOF) equilibrium is the most demanding equilibrium as far as vertical stabilization is concerned⁶⁹.

The “plasma disturbances” considered at present to test the performance of the vertical stabilization system *in normal operation condition* are already quite severe (e.g. $\delta l_i \approx -0.1 l_{i,ref}$). In this respect, using internal coils to stabilize plasma equilibria in the presence of even larger disturbances would not be consistent with the assumptions made on the design of other systems for the normal operation condition (e. g. maximum divertor heat loads in normal operation⁷⁰).

For the case of positive shear plasma equilibrium at Start Of Flattop, an increase in κ leads to

⁶³ Basic Design Package for Analysis (BDPA) 2000 version2, 6 March 2000

⁶⁴ Report of RTO/RC-ITER Concept Improvement Task Force, 2 July 1999, N A0 RI 99-07-19 F1.

A. Kavin, “Study of Reversed Shear Plasmas in ITER-FEAT”, ITER Naka JWS, February 2000.

⁶⁵ Therefore also the de-stabilizing force from the applied quadrupole field.

⁶⁶ A. Portone, “Plasma shape control and vertical stability”, Point Design Review Meeting, Naka, 13 October 1998.

⁶⁷ Report of RTO/RC-ITER Concept Improvement Task Force, 2 July 1999, N A0 RI 99-07-19 F1.

⁶⁸ A. Kavin, “Control of Plasma with Strong Reversed Shear”, Design Task Review Meeting, ITER Garching JWS, 9-10 March 2000.

⁶⁹ ITER-FEAT Outline Design Report, January 2000.

⁷⁰ ITER-FEAT Outline Design Report, January 2000.

a reduction of stability margin and growth time. Studies⁷¹ have shown that up to $\kappa_{95} \approx 1.7$ the outer PF coils can be used to control the plasma. For $\kappa_{95} > 1.7$ (see Table 3.4-1 and Figure 3.4-1 and -2) the stability margin drops below $m \approx 0.4$, the growth time drops below $\tau_g \approx 80$ ms and internal control coils becomes essential to allow reliable plasma stabilization and to limit the installed power necessary for control⁷². Therefore *internal coils are essential for plasma control as soon as $\kappa_{95} > 1.7$* . The question now is *how much we can increase κ_{95} by using internal coils for stabilization*. From Figure 3.4-1 it appears that above $\kappa_{95} \approx 1.8$ the stability margin drops below $m \approx 0.3$ and the growth time below $\tau_g \approx 50$ ms. For reliable vertical stabilization (reduction of disruption rate during operation⁷³) *we assume as design criterion $m > 0.3$* . To achieve $m \approx 0.3$ for $\kappa_{95} > 1.8$ it is necessary to design the in-vessel components to increase their passive stabilization capability. This can be obtained⁷⁴, for example, by attaching copper strips to the blanket modules to allow eddy currents flow along low resistance paths close to the plasma⁷⁵.

The use of internal coils to improve plasma stabilization at high plasma triangularity (for the same elongation) is not justifiable, the maximum δ achievable being limited by the PF equilibrium currents (and cost) rather than by the vertical stabilization capability of the out-of-vessel as opposed to the in-vessel coils.

In conclusion therefore, above $\kappa_{95} \approx 1.7$ internal control coils are needed to allow prompt control at the cost of relatively low installed power (typically < 300 MVA). Above $\kappa_{95} \approx 1.8$ internal control coils must be aid by copper stabilizers in the blanket that improve passive stabilization (in the CDA, for example, twin loops allowed $\kappa_{95} \approx 2$). Therefore, the use of the internal control coils "per se" does not allow substantial increases in vertical elongation ($\approx 5\%$). Larger increases of plasma elongation (for example⁷⁶, $\approx 20\%$) can be achieved only provided that the in-vessel components (in particular, the blanket) are designed to keep $m > 0.3$.

Table 3.4-1⁷⁷

design	I_p (MA)	R_p (m)	a (m)	β_p	I_i	$\kappa_{95\%}$	m	τ_g (ms)
IAM	13.3	6.20	1.90	0.10	0.85	1.66	0.47	95
HK1	13.4	6.02	1.86	0.10	0.85	1.76	0.36	66
HK2	13.4	5.85	1.81	0.10	0.85	1.86	0.20	31

⁷¹ Report of RTO/RC-ITER Concept Improvement Task Force, 2 July 1999, N A0 RI 99-07-19 F1. ITER-FEAT Outline Design Report, January 2000.

⁷² Report of RTO/RC-ITER Concept Improvement Task Force, 2 July 1999, N A0 RI 99-07-19 F1.

⁷³ J.B. Lister, et Al., "Stability Margins of Elongated Plasmas in TCV and Implications for ITER", 26th EPS Conference on Controlled Fusion and Plasma Physics, Maastricht, 1999, European Conference Abstracts, Vol. 23J (1999) 1073-1076.

⁷⁴ ITER Poloidal Field System, ITER Documentation Series, No. 27, IAEA, Vienna, 1991.

⁷⁵ Such current flow is always present on the "inductive time scale" and, strictly speaking, the stability margin - defined in terms of "inductive mode current distribution" - increases as a result of this. However, for the reference blanket modules, the eddy currents decay very quickly (<10ms) and are not useful in increasing the passive stabilization features of the metallic structures.

⁷⁶ ITER Poloidal Field System, ITER Documentation Series, No. 27, IAEA, Vienna, 1991.

⁷⁷ R. Albanese et Al., CREATE Report, 31 May 1999, Issue 2.

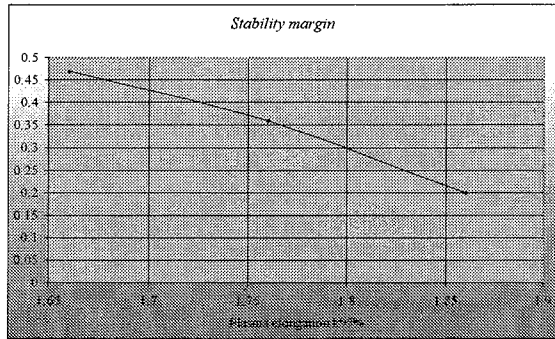


Figure 3.4-1 Stability margin vs. plasma elongation

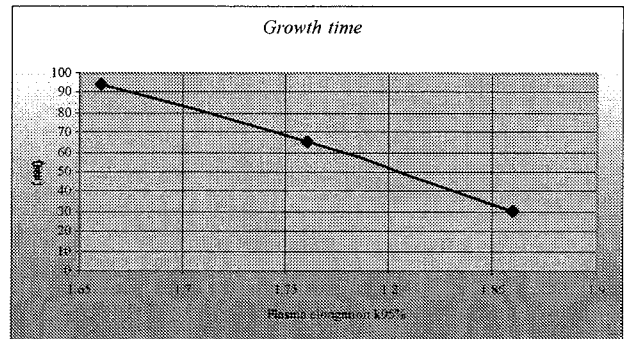


Figure 3.4-2 Instability growth time vs. plasma elongation

Stability margin and instability growth time

Background

The stability margin m is a measure of how far from the Alfvén's unstable regime is the plasma equilibrium configuration under study. If $m < 0$ any perturbation to the plasma vertical position will grow on the μs -time scale related to the plasma inertia and the instability growth time τ_g will scale as $\tau_g \propto \sqrt{m_p}/F_{dest}$ where F_{dest} is the destabilizing force from the equilibrium field and m_p is the plasma mass. On the other hand, if $m > 0$ the growth time increases of several order of magnitude up to the ms time scale related to the L/R decay time of the image currents induced by any plasma displacement in the surrounding metallic structures and $\tau_g \propto m L/R$.

Discussion and conclusions

The stability margin m is defined as $m \equiv (F_{stab}^{ideal} / F_{dest}) - 1$ where the stabilizing force acting on the plasma is given by the passive structures considered as ideally conducting. For the one-mode approximation to the eddy current distribution in the metallic structures and neglecting the plasma mass, the Kirchhoff's voltage law and the plasma momentum equation can be combined to give:

$$m\tau_e dz/dt - z = 0 \Rightarrow \tau_g = m\tau_e \quad (1)$$

where τ_e is the L/R decay time constant of the (one mode distribution) current in the passive structures. From (1) it follows that if the plasma parameters vary (for example, the plasma current density profile quantified by l_i) leading to a variation of the stability margin δm , the relative variation in the growth time $\delta\tau_g/\tau_g$ scales as:

$$\delta\tau_g/\tau_g = \delta m/m \quad (2)$$

To avoid that small variations in the (quite unpredictable) plasma current density profile may lead to large variations in the growth time and complications to the plasma stabilization, m should be "as large as possible" (see (2)).

In case of out-of-vessel control coils several studies⁷⁸ have shown that $m \approx 0.5$ and $\tau_g \approx 100$ ms lead to satisfactory control effort and robustness. Plasma variations up to $\delta m \approx -0.1$ (i.e. $m \approx 0.4$) leading to $\tau_g \approx 80$ ms are still controllable but with strong closed-loop degradation.

In case of in-vessel control coils the closed-loop system is more robust to plasma degradation. On the other hand⁷⁹, above $\kappa_{95} \approx 1.8$ m the stability margin drops below $m \approx 0.3$, the growth time drops (rapidly) below $\tau_g \approx 50$ ms and – more importantly – large relative variations in τ_g may result from small variations in the plasma parameters. For example, at $m \approx 0.2$ an error of $\approx 5\%$ in the quadrupole field due, for instance, to the limited accuracy of the PF coils current control system, the relative variation of growth time could be as large as $\delta\tau_g/\tau_g \approx 30\%$.

⁷⁸ Report of RTO/RC-ITER Concept Improvement Task Force, 2 July 1999, N A0 RI 99-07-19 F1.

⁷⁹ A. Portone, "Effects of Plasma Elongation on Vertical Stabilization Parameters", Plasma & Field Control Division, N 47 RI 29 99-05-14 F1, Naka JWS, 14 May 1999.

4. Vessel/In-Vessel

4.1. Manifolding of Blanket Coolant

The removal of the backplate has simplified the load assembly of ITER FEAT and reduced the inboard thickness with respect to the 1998 ITER design. Some functions, like the blanket module support and the plasma stabilisation, can only be transferred to the vessel. However, the supply of the coolant to the blanket modules can be achieved either by passages built inside the vessel wall or by separate ducts mounted between or behind the modules. Both solutions have been considered and their advantages and disadvantages have been presented⁸⁰.

To improve the leak detection procedure for the blanket requires an increase in the number of cooling manifolds to reduce the number of modules per parallel loop. The simplification of the double wall vessel and the ability to use standard welding techniques increases by removing many independent cooling passages. These facts, and recent design improvements, have led the separate manifolds to be now adopted as the reference design for ITER FEAT.

Inboard and outboard basic layout

In the inboard region (Figure 4.1-1), from the divertor cassette to the upper port opening, the blanket is segmented into 8 rows of 18 modules (toroidal span 20°) wedged towards the centre axis and covering the field joints. Since there are no gaps between the modules, the cooling manifolds are located in special grooves machined in the back of the modules. Behind each module there is an inlet and an outlet cooling manifold. The flexible branch pipes of the hydraulic connection are mounted between the manifolds over the 40 cm space. The single curvature plane manifolds are 20 cm either side of the field joint of the vacuum vessel, for 9 modules out of 18.

In the outboard region, from the upper port to the divertor port, the blanket is segmented into 9 rows of 36 modules (toroidal span 10° apart the port regions). The modules are rectangular parallelepipeds for assembly reasons which leaves triangular voids between the modules. The cooling manifolds are located in these voids and act as filler shield. Often they need more space than available (2-10 cm width increasing from the first wall towards the vessel) and cut outs are needed in the corner of the modules. Toroidally alternate manifolds are used for coolant inlet and outlet.

⁸⁰ Technical basis for the ITER-FEAT Outline Design , G A0 RI 2 00-01-18 R1.0 Section II.2.2

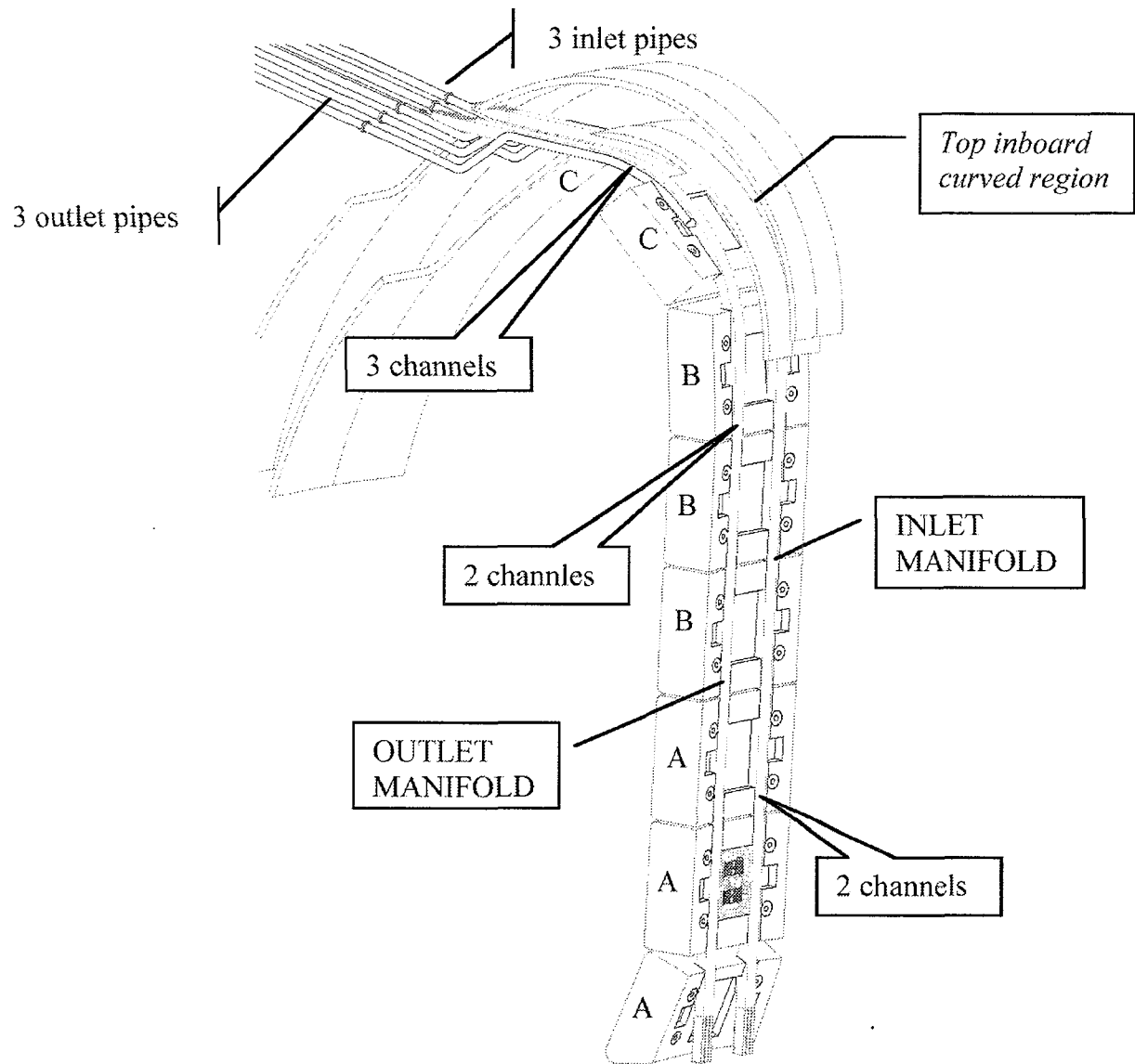


Figure 4.1 -1 – Cooling manifolds for inboard blanket, typical 20° sector.
(see also the cross section in Figure 4.1-4)

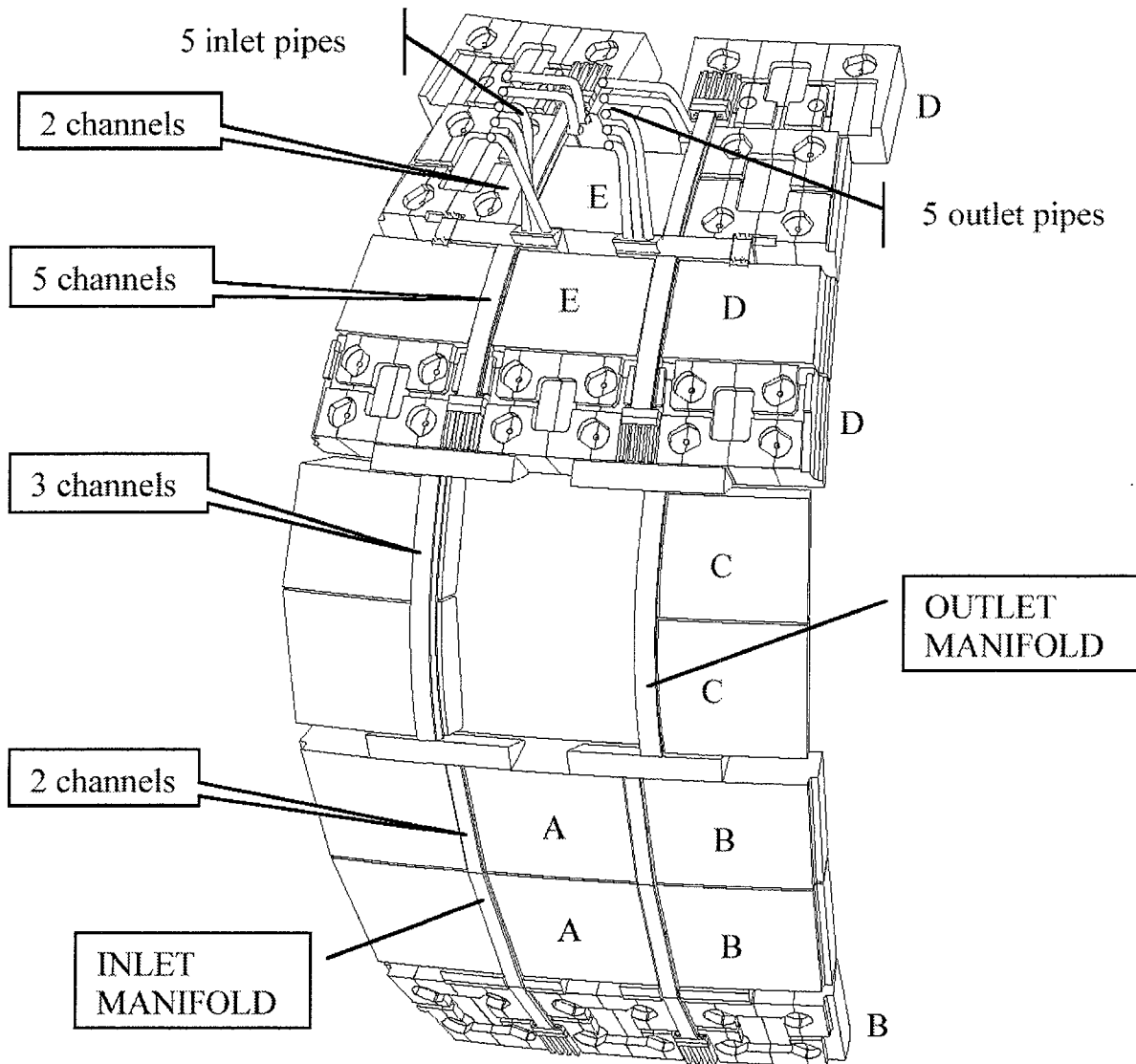


Figure 4.1-2 – Cooling manifolds for outboard blanket, 20° periodic arrangement
(see manifold cross sections in Figure 4.1-9)

Multiple loops per circuit

Each inboard manifold includes 3 independent cooling passages feeding separately the 8 modules in groups of 3-3-2, from the bottom up (see positions A, B and C in Figure 4.1-1).

Each outboard manifold includes 5 independent cooling passages feeding separately the 15 modules in groups of (see positions in Figure 4.1-2):

3-3, below the equatorial ports: centre (A) and adjacent (B)

2, between the equatorial port (C)

3-4, above the equatorial port: centre (E) and adjacent (D), including the module in between the upper ports.

The cooling loops are kept separate up to the heat transfer system room where they group into the 3 cooling circuits of the blanket. In this room individual cooling loops can be isolated from each other by ice plugs (if valves are not used) and be checked progressively for leaks with tracer elements.

Upper port allocation and diagnostics

All inboard and outboard manifolds end in the proximity of the upper port and are fed through it by circular pipes arranged in two ranks near to the side walls. The pipes are 2.5" and occupy 14 cm space including support clamps and welding access. There are 8 pipes on either side of all upper ports.

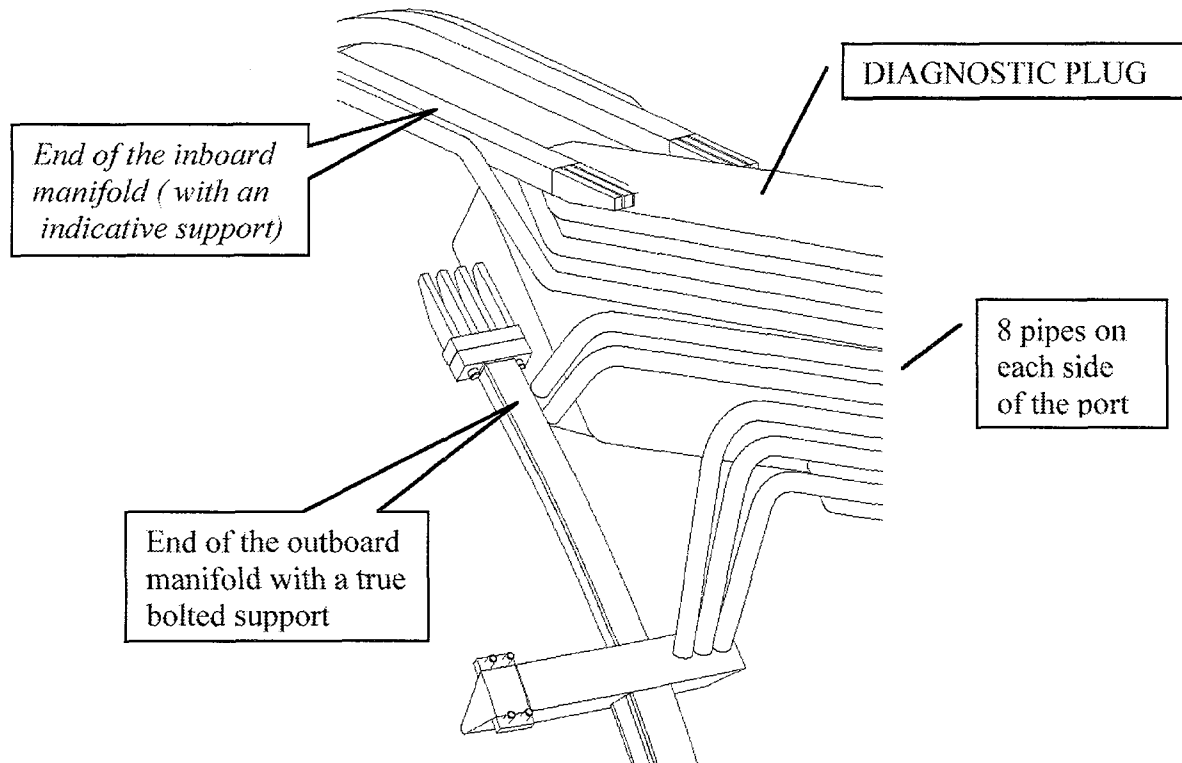


Figure 4.1-3 – Typical arrangement in the 18 upper ports (port duct omitted)

The access through the trapezoidal port is 58 cm wide on the top and 88 cm on the bottom. It is still adequate for EC antennas and diagnostic plugs. The permanent pipes should not cross the flange of the port and thus they are channelled upwards from the port duct before the flange through special twin chimneys built symmetrically either side of the split field joint.

The in-vessel diagnostics have few interferences with the separate cooling manifolds in the inboard blanket because the gap between the modules is free also for the passage of the cables. Outboard of the plasma the passages of the cables and the diagnostic positions need integration with the filler shields, as in the 1998 ITER design, and require ad-hoc cuts in the modules. Local modifications are required, but are feasible.

Manifold cross section design

The cross section of the manifolds is typically sized for 3 blanket modules, each needing a coolant flowrate of 8 kg/s in average. The coolant velocity derives from the pressure drop allowed in the manifolds, 1 bar over the 5 assumed in total, and the range is 6-9 m/s.

The manifolds have a rectangular cross-section to match better the modules and avoid gaps in the nuclear shielding. The restraint on the vessel is also easier than for circular cross-section pipes.

the system is large. Undercooling of the inlet manifolds is possible in operation within the above excursions. A number of more extreme accidental excursions are acceptable within the fatigue limit of the materials, i.e. the welded joints.

Support design

The typical longitudinal support is formed by a bracket on the vessel and a flange with two bolts at the end of the manifold. The bracket is welded to the vessel by a set of webs which distribute the reaction force (typically 750 kN) on a wide surface, decreasing the shear stress applied to the wall at 25 MPa. The manifolds are connected to the bracket by high strength M36 bolts, which can react also in tension the typical compressive load of the flange. These bolts are made of Inconel 718 and are similar to those of the module supports.

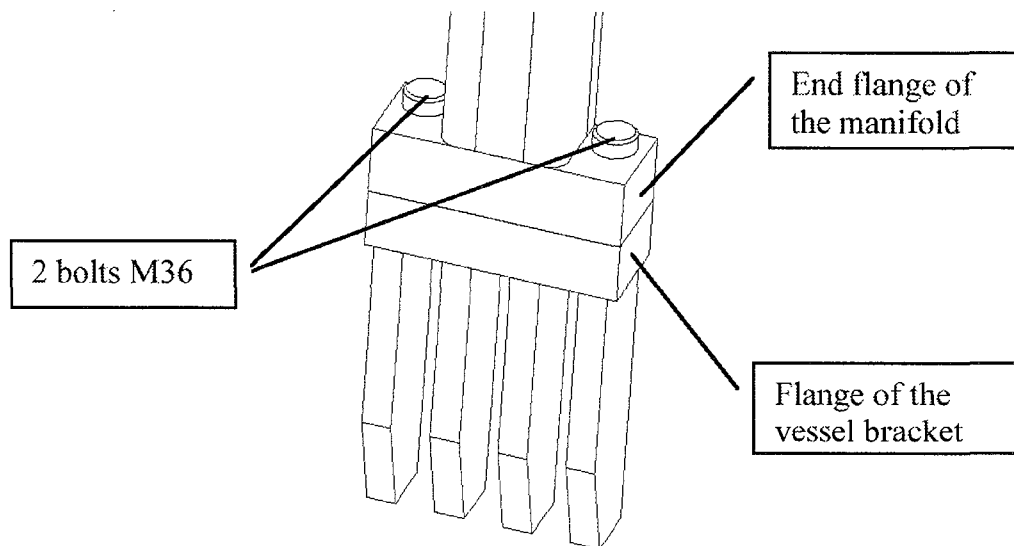


Figure 4.1-5 – The bolted lower end supports of the outboard manifolds.

Mechanical connection has been preferred to a strong weld because it reduces the possible vessel distortions during the initial assembly, it improves the disassembly of the manifolds for repair, and helps the separate manufacturing of the manifolds. However, the bolted flange is larger than a welded one and needs more material to be cut away in the back of the modules locally.

A welded connection has been preferred for the radial/toroidal supports which are small and distributed every 50 cm along the manifolds. These supports are formed by a thin socket applied to the vessel and a retention collar, made from 4 mm bent sheets welded with a fillet to the vessel wall. The manifolds sit inside the socket and cannot move toroidally.

Thermal stress analysis

The inboard manifolds are plane and their compressive force 750 kN is balanced by the two end supports. In the top inboard curved region they generate a pushing force of 450 kN/m poloidal towards the vessel. The straight part relies on the toroidal restraints to prevent buckling.

The outboard manifolds have an arc profile in the vertical plane and include two 15 cm offsets corresponding with the equatorial port, whose width is larger than the 10° toroidal span of the modules in the outboard blanket. The restraints at both ends of the toroidal filler shields provide the reaction torque which balances the offset between the compressed

manifold segments. The outboard manifold cross-section decreases from the top to the bottom because the row of modules are different and do not need to have the same cut outs as in the inboard blanket. To take account of the variation of the number of channels and thus of the compressive force, an intermediate support is located above the equatorial port. The efficiency of the support system and the stress condition of the manifolds has been verified with a 3D finite element model. The pushing force of the arc manifold towards the vessel is typically 250 kN/poloidal m radially.

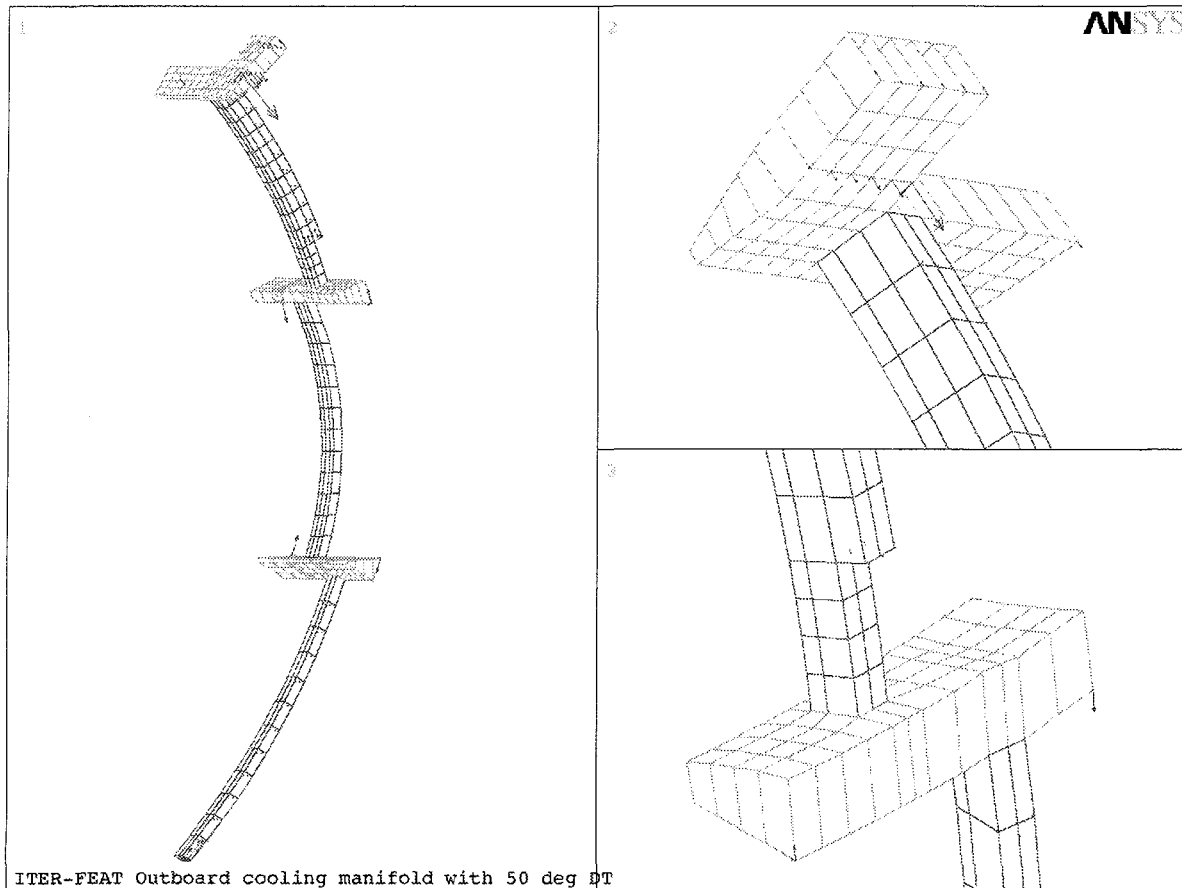


Figure 4.1-6 – Control of the reaction force distribution with a 3D finite element model (the upper manifold extension is missing).

Impact on the blanket module

In the inboard blanket modules narrow prismatic keys are located in between the flexible supports, to leave some vertical corridors free for the manifolds. A third smaller key is located in the middle of the module for centring. For alignment with the upper port the manifolds require the installation of the modules over the field joint in 9 cases out of 18. Therefore some centre key and some sockets of the electrical strap are located on the splice plate. The hydraulic connection is pre-assembled on the vessel and the two ends of the branches are welded to the manifolds. The modules on the inboard cylindrical vacuum vessel are similar because the manifold maintains the same size even if some channels end. The space they vacate is occupied by the remaining channels getting larger.

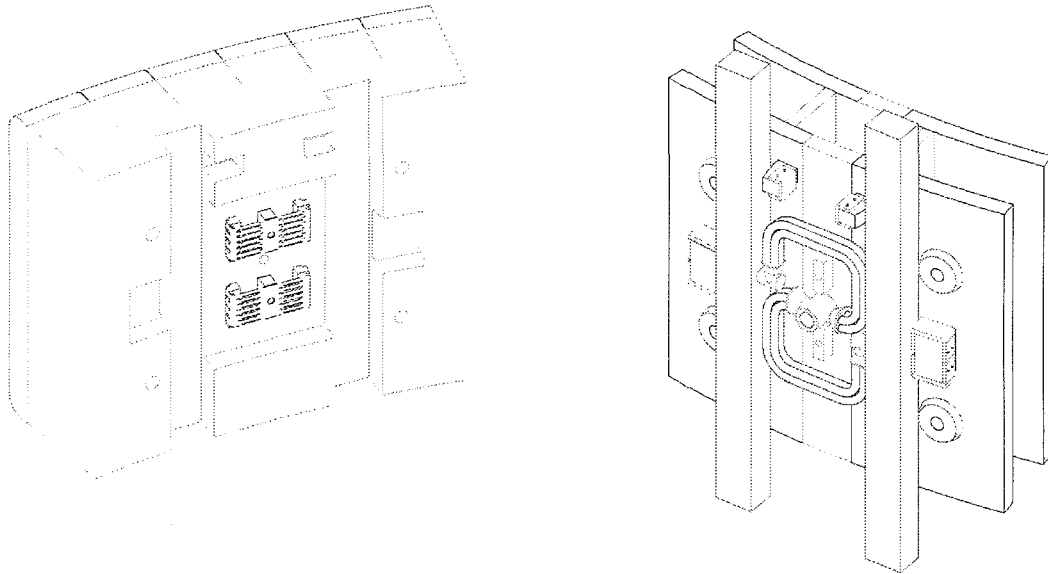


Figure 4.1-7 – Typical attachment of the inboard blanket modules.

In the outboard blanket, stub keys are used, because the space is large enough and they minimise the interface with the vessel. Modules mounted over the field joint need only electrical strap sockets on the splice plate. The branch pipes are mounted between the manifolds which need a tubular extension from the side to the centre of the modules.

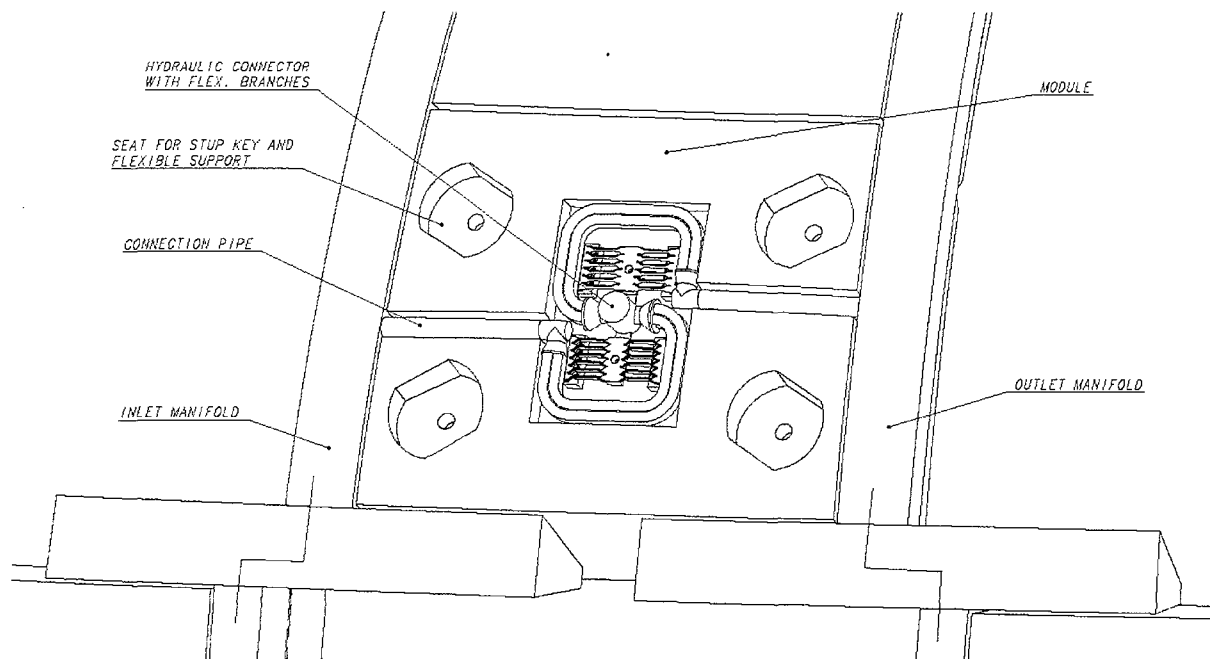


Figure 4.1-8 – Typical attachment of the outboard blanket modules.

Since in a row of modules the inlet/outlet manifolds occupy alternate positions, the coaxial nozzle of the hydraulic connection is inverted 180° to deliver/return the coolant to the module always in the same direction.

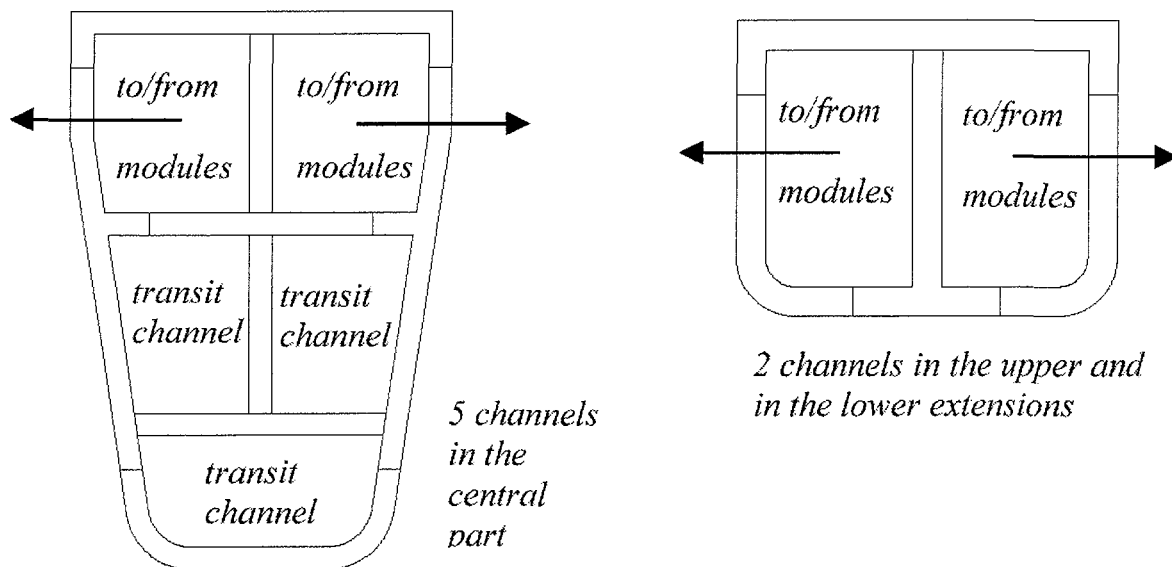


Fig. 4.1-9 – The variable cross section of the outboard manifolds.

Leak detection and repair

In the case of a leak in the blanket, the cooling loop including 2-4 modules is identified by tracer elements injected in the coolant. After that the loop is drained and dried and prepared for He leak testing, which may be necessary to check the hydraulic connections and to identify the faulty module, when the damage is not evident. The vacuum vessel is opened and the RH vehicle is prepared near to the leaking group of modules.

A previous study has shown that most of the water coolant in a loop is entrained upward through the manifolds by a strong gas stream. If this result were not confirmed, a drainage system should be installed.

In that case a siphon pipe reaches the lowest point inside the outlet manifold channel. These pipe are small, typically 16 mm in diameter and 1 mm thick, and hosted inside the manifold to avoid new vacuum boundaries. They will emerge from the manifolds inside the upper port. From here onward the pipes are routed separately and leave the pipe bore free for any crawler tool. There are 8 drain lines per port.

Electromagnetic loads

Significant electromagnetic loads arise in the manifolds from the poloidal currents induced by changes of the toroidal flux during the thermal quench of the plasma or the fast discharge of the TF coils. The former produces the pulling force which is reacted by the welded sheet clamps, the later pushes the manifolds against the support sockets on the vessel. The small radial field generates minor toroidal forces reacted by the indentation of the sockets.

In the inboard region a thermal quench produces a pulling force of 120 kN/m poloidal and a toroidal force 7.5 kN/m poloidal. The TF coil fast discharge produces a pushing force of 40 kN/m poloidal.

The horizontal filler shields integrated with the cooling manifolds have end supports which are electrically insulated and exclude radial currents to/from the vessel. All bolts use washers coated with ceramic insulation to prevent thread seizure by current flow.

Conclusions

Recent design evolutions show that the separate blanket cooling manifolds can be thick, robust and reliable. They can be repaired inside the vessel and are compatible with the diagnostic plugs and the EC antenna in the upper ports.

Since the separate manifolds avoid any vessel coolant contamination and improve the leak testing of the blanket they are adopted as the reference design for ITER FEAT.

4.2. Vacuum Vessel Design Development

4.2.1. Fabrication

The Vacuum Vessel (VV) is a torus-shaped, double-wall structure with shielding and cooling water between the shells. The double-wall structure is made from SS 316L(N)-IG, with stiffening ribs between the shells to give the required mechanical strength. The inner and outer shells are both 60 mm plates and the stiffening ribs 40 mm plate. The space between the shells will be filled with plates made of SS 304 containing 2% boron (SS 30467), and the ferromagnetic SS 430.

To minimize the final assembly time on site, and to deliver the vessel structure with a higher quality, the VV is to be fabricated in the factory as 9 sectors each spanning 40° and to be transported to the site. The practicality of transporting a large sector from the factory to the site is an important factor in the manufacture of the vessel and must be assessed after the site is selected. Each sector includes a full set of ports at the toroidal centre of the sector and a set of half ports (split on the port centre) on each side. The port stubs on the lateral sides of the sector are not installed in the factory. This allows the TF coils to be installed in the assembly area.

Due to the addition of blanket supports in the VV double wall structure, stiffening ribs between the shells are partially replaced by flexible support housings for the blanket module support. Currently, the VV design details are under development, taking account of the optimization of the layout of the ribs and support housings, the structural integrity of the VV, and the detailed fabrication procedure. One of the current design efforts is to reduce the number of the ribs to minimize the associated fabrication cost.

The shielding blocks are installed at the factory before shipment to the site for all circuits except in the area of the field joints. In addition, most of the instrumentation is to be installed at the factory.

Two concepts have been considered for the sector fabrication scheme. One is to complete the inner shell first because it forms the first confinement boundary. Butt weld joints can be fully applied to the inner shell and inspection can be easily performed. Next, all ribs and support housings would be welded to the inner shell. After shield blocks have been installed, parts of the outer shell would be welded (access is from the rib side and through the open space). The remaining parts of the outer shell would be welded (with a one-sided weld). Another concept is to utilize poloidal segments of a double wall structure, which are fabricated first then welded together to form a sector. This scheme was employed for the full-scale vessel sector fabrication in the L-3 R&D project.

The development of full base metal stress capability requires assurance of complete penetration at the weld root opening. To achieve complete penetration at the root, considering the specific configuration and assembly requirements for the VV, similar but slightly different weld details will be used for various areas of the shells, shell closure sections, and ports. Where access to the root side of the joint is not possible, a joint design is required that assures the root side is smooth and uniform which will allow it to be reliably inspected. This is required to achieve the full design allowances as specified by the welding codes.

Actual manufacturing welding process selection is influenced by various factors including material type, thickness, component design and intended service-specific requirements. A vessel of the size and complexity of the ITER vessel can be expected to utilize a combination of weld processes depending upon the type of weld joint, accessibility, and volumetric examination required. Both automated and manual welding are expected to be used during the actual vessel manufacturing.

All conventional manual, automatic, and most advanced welding processes are suitable for use on SS 316 L(N)-IG. ITER specifications identify inert gas tungsten arc welding (TIG) as the preferred process to be used for the vessel and port welds but other processes such as metal inert gas (MIG) welding, metal active gas (MAG) welding, and electron beam (EB) welding are also acceptable and will be considered as ways to increase welding productivity and decrease distortion. Welding procedures are to be qualified in accordance with an accepted code. Specified material properties at the weld joints, such as ferrite content in the deposited metals, must be assured.

Most weld joints are to have conventional configurations and to be radiographically inspected to assure 100% weld efficiency. It is considered that they could be easily code/standard qualified. However, the one-sided weld joints between the outer shell and the ribs and the field joints cannot be radiographically inspected and will be inspected by UT (ultrasonic testing). In this case, a special code case will be required. The current approach of the weld joint designs is to minimize the code cases.

To reduce the VV fabrication cost, a forged and/or cast structure has been investigated⁸¹. The region of the VV gravity support is a highly-stressed region, requiring numerous reinforcements. Instead of an all-welded shell structure, a forged structure would reduce the fabrication cost and improve the fabrication tolerances there. In addition, a large number of the housings in the VV for the blanket module support that have a relatively small and simple structure can be manufactured by precision casting for cost saving. A preliminary comparison of the fabrication costs between the forged/precision cast structures and the welded structures shows a cost benefit for the forged/precision cast structure. Powder HIPing is also being considered for further cost reduction.

The most important VV R&D performed so far during the EDA was associated with the fabrication of a sector. The Full Scale Sector Model, fabricated and tested as a part of the L-3 project, provided critical information related to fabrication technology required to produce a high quality sector, and the magnitude of welding distortions and achievable tolerances. Since the basic design of the ITER-FEAT VV is the same as the fabricated sector

⁸¹ "Improvement of VV fabrication method for RC-ITER" - JAHT report, INT-9022 - June 11, 1999 and "EU contribution to the task force report, Section VI.5 Improvement of manufacturing processes for cost reduction," EUHT report, June 14, 1999.

model (i.e., the material, the basic torus shape, and the double wall structure with shielding and cooling water between the shells), this R&D also validated the fundamental feasibility of the ITER-FEAT double wall design. Additional R&D, such as the fabrication of a partial VV sector model, may be required to confirm the improved fabrication technology and associated tolerances, as a first step to be done by the industrial firm chosen for manufacturing the vacuum vessel.

4.2.2. Vacuum Vessel Loads/Function vs 1998 ITER

The primary functions of the ITER-FEAT Vacuum Vessel (VV) are the same as for the 1998 ITER design. These functions are to provide a high quality vacuum for the plasma, as well as the first confinement barrier of radioactive materials and a second barrier (after the cryostat) for the separation of air. The total decay heat can be removed by the water in the VV cooling system, even when all the in-vessel cooling loops are not functioning. The vessel still supports the blanket and divertor components, however the blanket modules are attached directly to the VV since the back plate has been eliminated. In addition, a tight fitting configuration of the VV aids the plasma vertical stability, and the ferromagnetic material in the VV reduces the toroidal field ripple. Along with other in-vessel components, the VV provides radiation shielding in particular for the magnets, and even more so to reduce the post shutdown radiation level in the cryostat.

The water flow velocity and flow rate for normal operation needs to cope with the nuclear heating rate in the VV, and keep thermal stresses in the VV structure at acceptable levels. Table 4.2-1 summarizes the VV cooling and baking conditions for the VV. The required water flow condition for normal operation is forced turbulent flow. In order to maintain stresses at acceptable levels for the separate manifold under the current design, it is necessary for the VV cooling water inlet temperature to be similar to the blanket water inlet temperature which is 100°C. Capability of natural convection cooling is provided to remove the decay heat of both the VV and blanket during off-normal events, e.g., the event of a multiple cooling pump trip.

Table 4.2-1 Cooling/Baking Conditions of the Vacuum Vessel

Parameters	Unit	Value
Maximum Total Heat Removal	MW	~10
Water Parameters		
- Normal Operation		
- Inlet / Outlet Temperatures	°C	~100 / ~ 104
- Inlet Pressure	MPa	~ 1.1
- Flow Velocity	m/s	0.04
- Total Flow Rate for Parallel Cooling System	kg/s	~ 950
- Baking Operation		
- Inlet Temperature	°C	200
- Inlet Pressure	MPa	~ 2.4

As was the case for the 1998 ITER, the ITER-FEAT VV must withstand many individual and combined loading conditions during both normal and off-normal operation (see box⁸²). For normal operating conditions (category I and II events), the most severe loads are caused by the coolant pressure, VV and in-vessel component weights, seismic events, plasma

⁸² Annex to ITER Design Requirements & Guidelines Level 1 (DRG1) G A0 GDRD 2 W0.2

disruptions and VDEs, and the TF coil fast discharge (TFCFD). The loads that will most likely drive the design are due to the centred disruption, VDE, and TFCFD. A summary of VV loads is shown in Table 4.2-2.

Load combinations

A set of rules are being used across the ITER design to establish event combinations and to classify them. A fundamental question is to establish the probability of one condition triggering another loading event. In fact, after an initiating condition, other additional conditions may occur.

- *Conditions are here called “likely” to occur if their conditional probability is higher than 1%.*
- *Conditions are here called “unlikely” to occur if their conditional probability is smaller than 1%.*

Whenever lacking a more comprehensive probabilistic analysis, conditions are categorized as follows:

- *Category I, for a combination of:*
 - *All category I conditions when occurring at the same time or likely to be triggered by the initiating condition.*
- *Category II, for a combination of:*
 - *The above category I combinations with other category I conditions also when they are unlikely to be triggered by the initiating condition.*
 - *A category II condition with other category I and II conditions which are present or likely to be triggered by the initiating condition.*
- *Category III, for a combination of:*
 - *The above category II combinations with other category II and I conditions also when they are unlikely to be triggered by the initiating condition.*
 - *A category III condition with other category I, II, and III conditions which are present or likely to be triggered by the initiating condition.*
- *Category IV, for a combination of:*
 - *The above category III combinations with other category III, II and I conditions also when they are unlikely to be triggered by the initiating condition.*
 - *A category IV condition with other category I, II, III, and IV conditions which are present or likely to be triggered by the initiating condition.*

Following the above general considerations, the following table shows the typical combinations for the definition of seismic events SL-1 and SL-2. The subsequent box gives the definition of Disr. I & II plasma disruptions and VDE I, II & III vertical displacement events.

Load Combinations and Their Categories

<i>Pressr</i>	<i>Seism</i>	<i>Plasma</i>	<i>Magnet</i>	<i>Others CatI</i>	<i>Others CatII</i>	<i>Others CatIII</i>	<i>Others CatIV</i>	<i>Cat</i>	<i># of cycles</i>
		VDE I		L				I	150
		Disr. I		L				I	3000
		Disr. I	F.Disc	L				I	50
		L	L	I				I	-
LOCAII		Disr. I						II	50
		VDE I		U				II	-
		Disr. I		U				II	-
		Disr. I	F.Disc	U				II	-
		U	U	I				II	-
LOCAII		Disr. II		L	L			II	300
LOCAII		VDE II		L	L			II	15
	SL-1	Disr. I		L	L			II	-
	SL-1	VDE I		L	L			II	-
		L	L	L	I			II	-
LOCAIII		Disr. II		U	U			III	-
LOCAIII		VDE II		U	U			III	-
		Disr. II	F.Disc	U	U			III	-
		U	U	U	I			III	-
	SL-1	Disr. II	F.Disc	U	U			III	-
	SL-1	VDE II	F.Disc	U	U			III	-
LOCAIII		VDE III		L	L	L		III	-
		L	L	L	L	I		III	-
LOCAIV		Disr. I						IV	-
LOCAIV		VDE III		U	U	U		IV	-
		U	U	U	U	I		IV	-
	SL-2	VDE I		L	L	L	L	IV	-
	SL-2	Disr. I		L	L	L	L	IV	-
		L	L	L	L	L	I	IV	-

Disruption Definitions

Type I - a normal worst case fast disruption. Its characteristics are:

Initial Plasma State	EOB
Condition category	I: Normal
Initial Plasma current	15 MA
Total duration to zero plasma current	54 ms
Peak Plasma current	~16 MA
Expected number of events	3000

Type II - an upset worst case fast disruption. Its characteristics are:

Initial Plasma State	EOB
Condition category	II: Likely
Initial Plasma current	15 MA
Total duration to zero plasma current	27 ms
Peak Plasma current	~16 MA
Expected number of events	300

VDE Type II. In this worst case scenario:

1. the plasma remains in a healthy (full beta and plasma current) configuration until it becomes a limiter plasma when a fast thermal quench takes place (loss of beta).
2. the plasma continues to drift vertically without current quench until q_{edge} reaches the critical value of 1.5. At that time a slow plasma disruption is initiated.
3. slow disruptions are thought to give rise to higher vertical loads on the passive structure since they allow additional plasma vertical drift into the destabilizing quadrupolar field.
4. halo currents will develop and will contribute to the global vertical equilibrium. They will start developing as soon as the plasma becomes limiter-like.

The above VDE scenario followed by a slow current quench (VDE/S) can be summarized by:

Definition of type III VDE followed by slow current quench

	VDE/S type III
Initial Plasma State	EOB
Condition category	III: Unlikely
Current Quench initiator	$q=1.5$
Plasma Current quench duration	~100 ms
Direction of movement	Up / down
Expected number of events	-
Peak ($I_{halo} * P_f / I_{plasma}$) ⁽¹⁾	0.58
Peak total net horizontal load [MN]	25
⁽¹⁾ P_f = Toroidal peaking factor of the halo currents	

Disruption Definitions (continued)

Type II VDE

For these slow VDEs (VDE/S), the assumption is that they will occur 15 times in the lifetime of the machine and that they will generate a load equal to 75% of the Type III VDE/S. Their Category is II.

Type I VDE

For these slow VDEs (VDE/S), the assumption is that they will occur 150 times in the lifetime of the machine and that they will generate a load equal to 60% of the Type III VDE/S. Their Category is I.

VDE's followed by fast current quench (VDE/F)

Type I, II, and III VDE's are particularly severe for the intensity of the net vertical loads and their impact on the Vacuum Vessel.

An equal number of VDE's of all types (I, II, and III), followed by a fast current quench are considered in the design with the assumption of a toroidal peaking factor as well as a net horizontal load equal to half of what is assumed for the VDE/F.

Definition of type III VDE followed by fast current quench

	<i>VDE/F type III</i>
<i>Initial Plasma State</i>	<i>EOB</i>
<i>Condition category</i>	<i>III: Unlikely</i>
<i>Current Quench initiator</i>	<i>$q=1.5$</i>
<i>Plasma Current quench duration</i>	<i>as Disrupt type II</i>
<i>Direction of movement</i>	<i>Up / down</i>
<i>Expected number of events</i>	<i>-</i>
<i>Peak ($I_{halo} * P_f / I_{plasma}$) ⁽¹⁾</i>	<i>$0.58/2=0.29$</i>
<i>Peak total net horizontal load [MN]</i>	<i>$25/2=12.5$</i>
<i>(1) P_f = Toroidal peaking factor of the halo currents</i>	

The major changes in the loads for the ITER-FEAT VV with respect to the 1998 ITER VV result from design modifications in the following areas.

1. Changes related to the smaller machine size, the lower plasma current and the new magnetic configuration. These changes tend to reduce VV loads.
2. The elimination of the back plate which results in; (a) increased induced and halo currents, (b) direct loads from the blanket modules to the VV, and (c) increased nuclear heating to the VV. These changes tend to increase VV loads.

Table 4.2-2 VV Load Summary

	ITER Load Category	1998 ITER	ITER-FEAT*
Water pressure (Normal operation/Baking operation) (MPa)	I	0.4/1.8	1.1/2.4
Gravity load (MN)	I	190	100
Plasma current quench			
- EM pressure on inboard/outboard VV wall due to induced currents (MPa)	II	1.2/0.6	1.2/0.6
Centered disruption			
- Maximum radial moment on a module at the inboard wall (MNm)	II	-1.25	-0.65
- Maximum poloidal moment on a module at the inboard wall (MNm)	II	0.77	0.61
VDE followed by a fast current quench (Fast VDE)			
- Maximum radial moment on a module at the inboard wall (MNm)	III	-1.74	-0.88
- Maximum poloidal moment on a module at the inboard wall (MNm)	III	1.0	0.76
VDE followed by a slow current quench (Slow VDE)			
- Maximum EM pressure on the VV wall due to halo current (MPa)	III	2.8	3.9
- Poloidal force on a module (MN)	III	1.0	1.0
- Radial force on a module (MN)	III	1.3	0.4
- Maximum total net vertical force on VV and blanket for downward/upward slow VDE (MN)	III	-150/ 80	-71/52
- Maximum total net horizontal force on the VV and blanket (plasma tilting and shifting) (MN)	III	50	25
TF coil fast discharge			
- EM pressure on the VV inboard wall due to the poloidal induced current (MPa) [Current quench time (sec)]	I	2.1 [15]	1.6 [11]

*: According to the most recent assessment⁸³ for 15 MA plasma operation. Load values on blanket modules may vary depending on the blanket module design.

A preliminary assessment of the electromagnetic loads on the VV and on the blanket module has been made for the case of 17.4 MA plasma operation. Assuming that the toroidal field remains constant in comparison with the 15 MA operation case, the electromagnetic loads on the blanket modules due to the induced currents coupled with the toroidal field, the loads on the VV and the blanket modules due to halo currents coupled with the toroidal field increase linearly with the plasma current (by a factor of 1.16). The electromagnetic pressure on the inboard and outboard wall, mainly caused by the interaction of the induced toroidal current due to the plasma quench and the poloidal field, increases proportionally to the square of the ratio of the plasma currents (a factor of 1.33). The electromagnetic pressure due to the TF coil fast discharge remains the same.

⁸³ G 73 MD 34 00-04-19 W 0.1, "FEAT category III fast/slow downward/upward VDE simulation" and G 16 MD 280 00-05-22 W 0.1, "EM loads on modules for the ITER-FEAT."

4.2.3. Structural Assessment of the Vacuum Vessel

The most severe loading conditions for the VV are the toroidal field coil fast discharge (TFCFD) and the load combination with electromagnetic loads due to a plasma vertical instability. In this load combination a high compressive stress occurs in the VV inboard wall and the VV structure has to withstand buckling instability. A non-linear analysis has to be performed assuming the worst possible geometrical imperfection.

The direct attachment of the blanket modules to the VV shell produces local stress and geometrical discontinuities of the VV shells. Detailed analyses have been performed to assess the stress level in locations of geometrical discontinuities and where concentrated loads are applied.

The location of the VV supports has an impact in the stress distribution and local stress and influences the VV deformation and dynamic behaviour. A comparison of the results obtained with different support locations has been performed.

Toroidal field coil fast discharge

In the case of a TFCFD, the induced poloidal currents in the VV interact with the toroidal magnetic field causing compressive stress in the VV inboard wall. Elastic buckling analysis⁸⁴ has shown that the critical elastic buckling pressure is much larger than the pressure causing a stress level above the yield.

The inelastic buckling analysis requires the definition of the initial imperfection of the VV geometry. Different shapes of the VV geometrical imperfections have been considered⁸⁵. The type of geometrical imperfection that has the minimum critical inelastic pressure is the radial misalignment of adjacent sectors. An assessment performed assuming a VV geometry similar to the present ITER FEAT VV design has given a critical buckling pressure of 6.6 MPa (misalignment of adjacent sectors = ± 5 mm).

Following, for example, the recommendations from a code, e.g. RCC-MR, and assuming a load factor (ratio between the inelastic buckling and the operating load) of 2.5, the maximum allowable electromagnetic pressure value on the inboard wall is 2.64 MPa (the estimated pressure for ITER FEAT in case of TFCFD is 1.6 MPa). An analysis on the reduction of the total double wall thickness at the inboard wall of 100 mm (from 388 mm to 288 mm) has given a relatively small reduction of the critical pressure ($\sim 5\%$) (ITER FEAT VV inboard wall is 338 mm). Also the increase of the initial imperfection of the VV geometry from ± 5 mm to ± 10 mm causes a reduction of the critical pressure of $\sim 4\%$.

Load combination : TFCFD and Plasma VDE

To reduce the primary stress in the VV, the inboard wall can be reinforced by making the triangular support frame that holds the lower modules of the blanket at the inboard wall toroidally continuous. This solution gives also advantages for the plasma stability. Three

⁸⁴ G Sannazzaro - G 15 MD 144 99-04-27 W0.1 - Elastic buckling of the RTO-RC ITER VV inboard wall due to TFC fast current discharge - 15 June, 1999.

⁸⁵ G Sannazzaro - G 15 MD 149 99-06-15 W0.1 - Inelastic buckling of the RTO/RC ITER VV inboard wall due to TFC fast current discharge - 15 June, 1999.

design options of the support frame shape and size have been considered⁸⁶: 1) large frame (1.6m high), 2) small frame (0.9m high) and 3) no frame.

Table 4.2-3 summarizes the results obtained for the following load conditions:

- Loads conditions :
- 1) TFCFD : 1.6 MPa at the inboard wall
 - 2) TFCFD (1.6 MPa) + Downward VDE I (2.3 MPa)
 - 3) TFCFD (1.6 MPa) + Downward VDE II (2.8 MPa)

Table 4.2-3 Summary of Primary Membrane Stress Results for TFCFD and VDE Events

Static analysis results : Primary membrane stress intensity (MPa) and stress safety margin in brackets ⁽¹⁾ in the VV inboard wall for the 3 design options					
Load case	Load category	Allowable (MPa)	Large frame (1.6m)	Small frame (0.9m)	No frame model
TFCFD	I	137	62 (2.2)	62 (2.2)	62 (2.2)
TFCFD + VDE I	II	137	100 (1.37)	121 (1.13)	131 (1.05)
TFCFD + VDE II	III	164	114 (1.44)	137 (1.20)	147 (1.12)

⁽¹⁾ The stress safety margin is the ratio between the allowable stress and the calculated stress.

The non-linear buckling analyses⁸⁷ have given the following results for the 3 types of reinforcements.

Table 4.2-4 Summary of Non-linear Buckling Analyses

Buckling safety margin for the 3 design options – Geometrical imperfection type : sector misalignment +/-5 mm				
Load case	Allowable safety margin (RCC-MR)	Large frame model	Small frame model	No frame model
TFCFD	2.5			4.1
TFCFD + VDE I	2.5	2.9	2.5	2.4
TFCFD + VDE II	2.0	2.5	2.2	2.1

The present design of the ITER FEAT VV has adopted the “small frame option”. For this option the buckling load does not exceed the allowable value, but is very close to it.

Stress in the VV due to the direct attachment of the blanket modules to the VV

The VV has to provide support to the blanket modules. At the attachment points the VV needs to be reinforced to avoid large local stresses. The main loads from the blanket modules to the VV are caused by fast plasma disruption. The induced currents in the blanket modules

⁸⁶ TAC Meeting – Presentation by K Ioki – Naka, December, 1999.

⁸⁷ TAC Meeting – Presentation by K Ioki – Naka, December, 1999.

generate poloidal and radial moments. Each module is radially supported by 4 flexible cartridges that transfer the poloidal moments to the VV shells. The flexible cartridges are recessed inside the VV wall, rather than in the blanket module. This solution has the advantage that the nuclear heat generation on the flexible cartridges is strongly reduced, and the design of the blanket module is simpler. On the other hand, the continuity of the inner VV shell is lost and stress concentration is generated at the holes required to locate the flexible supports.

Several designs have been studied to limit the induced currents and the poloidal moment on the blanket modules and to minimize the stress in the VV. Present evaluations (studies are still in progress) show that the poloidal moment can be reduced to a maximum value of ~ 0.6 MNm and the consequent membrane + bending stress in the VV shell can be limited to 90 MPa.

Two different design options to support the radial moment (the moment along the axis normal to the module first wall) applied to the module in case of plasma disruption and VDE have been considered: stub keys and shear keys. (Stub keys are extensions of the cylindrical housings for the flexible attachments that engage into the back of the blanket modules, whereas the shear keys are solid blocks welded to the vessel shell).. In an analysis performed on the modules attached to the inner VV wall⁸⁸ (EM loads on these modules are larger than those on the outboard wall) large stresses have been found in case the radial moment is reacted by the stub keys; therefore the “shear key” design option, with an appropriate reinforcement, has been selected for the modules at the inboard wall.

Operation at 17.4 MA plasma current

The increase of the electromagnetic loads from 15 MA to 17.4 MA operation reduces the stress safety factor for primary loads to values very close to 1. Table 4.2-5 summarizes the comparison between the results for the two operation scenarios at 15 and 17.4 MA. Preliminary buckling analysis has shown that for the present VV design the buckling safety factor is 2.3 for the load case combination TFCFD + VDE I in case of 17.4 MA operation, which is slightly smaller than the allowable value (following the RCC-MR code the allowable value is 2.5). Therefore, a more accurate analysis is still to be performed, reviewing the assumed conditions, which may be conservative. If its results do not improve the buckling safety factor, the requirement to allow operation at 17 MA will lead to make the current VV structure stronger against buckling at the location of the lower inboard wall, to satisfy the code requirement (for example, by adding a locally continuous toroidal reinforcement).

⁸⁸ G Sannazzaro - G 15 MD 135 98-11-13 W0.1 - Primary Stress in the VV Inboard Wall due to the Module Direct Attachment (RC-ITER IAM Configuration - Short Flexible)

**Table 4.2-5 Comparison of Results from 15 MA and 17.4 MA
Plasma Current Operation**

Primary membrane (Pm) stress intensity (MPa) and stress safety factor in brackets ⁽¹⁾ in the VV inboard wall + buckling safety factor for the 2 operational scenarios: 15 and 17.4 MA						
	Pm (MPa)			Buckling safety factor ⁽²⁾		
Load case	Ip=15 MA	Ip=17.4 MA	Limit	Ip=15 MA	Ip=17.4 MA	Limit ⁽³⁾
TFCFD	62 (2.2)	62 (2.2)	137	4.1	4.1	2.5
TFCFD + VDE I	121 (1.13)	127 (1.08)	137	2.5	2.3	2.5
TFCFD + VDE II	137 (1.20)	149 (1.10)	164	2.2	2.0	2.0

⁽¹⁾ The stress safety factor is the ratio between the allowable stress and the calculated stress.

⁽²⁾ Ratio inelastic buckling load/operational load

⁽³⁾ The limits are based on RCC-MR

VV support location

The ITER FEAT VV supports have been modified with respect to the 1998 ITER design. A study has been performed to estimate the effect on the stress in the VV of the location of the VV vertical supports from static vertical loads⁸⁹. Three possible locations have been considered: 1) bottom of the VV (same as 1998 ITER design), 2) between the equatorial ports, and 3) top of the VV.

The analysis of the VV behaviour for vertical static loads for the 3 support options, shows that there is not a great difference in the stress values in the main VV structure. The support option 2 generates a slightly larger stress in the VV main shells at the inboard wall mainly due to a larger stress in the poloidal direction. Some localized stress occurs in the support case options 1 and 3 in the poloidal ribs, but these stress values can be reduced by local reinforcements. Vertical displacements of the inboard wall are much larger for support option 2 (equatorial), but the overall value is relatively small (3.8 mm for 80 MN vertical static load due to downward VDE). On the other end, in this case the displacement of the ports, especially the equatorial port, is smaller than in the other two cases.

A design of the VV support made of flexible plates (similar to the 1998 ITER design backplate supports) located between the equatorial port has been developed. The structural analysis⁹⁰ has shown that these supports can withstand the envisaged loads on the VV, including seismic and thermal loads.

In comparison to the ITER 1998 design (where the horizontal supports were located at the equatorial port near the port extension) this solution has the advantage that the horizontal stiffness of the overall VV structure is increased. Therefore the first horizontal natural frequency is expected to increase giving a smaller dynamic factor for horizontal seismic loads.

⁸⁹ G Sannazzaro - G 15 MD 162 99-10-04 W0.1 - Stress in the RTO/RV ITER VV for different vertical support locations - 4 October, 1999

⁹⁰ F Elio - G 16 MD 248 99-10-13 - Peripheral flexible plate supports for the vacuum vessel and the magnets

Overall assessment

The VV must withstand many individual and combined loading conditions during both normal and off-normal operation. Analyses done to date are those considered for the most severe loading cases which will most likely drive the basic design of the VV structure. Although further analyses are required for numerous loading conditions to confirm the structural integrity of the VV, based on the analyses performed to date, the VV appears structurally capable of withstanding the loads to which it can be expected to be subjected

4.3. Design Implications of Divertor Material Choice

The plasma facing material selection for the divertor has been made largely on the basis of lifetime. However, other considerations that have to be taken into account are the generation and control of dust, which is a safety issue, and the chemical trapping of tritium with carbon, which is both a safety and an operational issue. In order to simplify the complex interrelated issues associated with armour choice for the divertor, the discussion below has been broken down into three sections; armour selection, tritium inventory and control, and dust and management of dust.

From the candidate armours for the divertor (Be, C & W), carbon has been selected for the strike point regions of the scrape-off layer (SOL) on the lower vertical target, and tungsten for the upper vertical target/baffle, gas box liner and dome PFCs. Carbon is the choice around the strike points, since beryllium would have an inadequate life-time and W would melt during high power transients and could form surface irregularities that might later form hot spots in normal steady-heat flux operation. Elsewhere, W has been selected because it has the lowest sputter yield in regions where erosion is dominated by charge-exchange (CX) sputtering. However, with the above material selection, of particular concern is the co-deposition of tritium with carbon, which could severely limit the operational availability of ITER by trapping the entire allowable inventory in co-deposited layers. The prospects of using tungsten in the region of the strike point are improving and the divertor design, which offers the possibility of routine remote exchange of the divertor cassettes, lends itself to a change to an all tungsten armoured divertor prior to, or during, the D-T phase.

Armour Selection

The choice of armour for the divertor is a compromise which takes into account power handling capability, armour lifetime, plasma compatibility, tritium retention, activation etc. In terms of lifetime and sustaining the heat flux, the most demanding component is the lower target, where the goal is to survive the following:

- 3000 full power discharges of 400 sec, with a steady state heat flux $\sim 10 \text{ MW.m}^{-2}$;
- one in ten discharges to include a slow transients ($\sim 10 \text{ sec}$), where the normal semi-detached operation of the divertor is interrupted and the full power of the SOL is assumed to strike the target (20 MW.m^{-2});
- one in ten discharges to end in a disruption;
- occasional giant ELMs and a significant number of small ELMs.

During the EDA, the silver-free joining of carbon to copper has advanced to a level where armoured plasma facing components can routinely operate with heat loads of 20 MW/m^2 , and following a relatively short development period, W armoured prototypes already promise to be as reliable, at similar heat flux, as their carbon armoured counterparts⁹¹.

With regard to erosion lifetime, this is maximised if the cladding is as thick as allowed by the predicted steady-state power load (e.g. $\sim 10 \text{ mm Be}$, $\sim 20 \text{ mm W}$, $\sim 20 \text{ mm CFC}$) and can be improved further if the threshold for sputtering is higher than the particle energy. The latter consideration favours high Z plasma facing materials such as W (sputtering threshold for D and T are $\sim 210 \text{ eV}$ and 140 eV , respectively), in particular for the parts of the divertor where CX sputtering is dominant (no ion sheath acceleration). Hence, W is the armour choice for the dome and upper vertical target. CFC is chosen near the strike-points because it sublimates, rather than melts during disruption thermal quenches or giant ELMs, thereby avoiding surface irregularities that might later form hot spots in normal steady-heat flux operation.

Apart from the issues of high heat flux capability and erosion lifetime, the final armour choice also depends on the plasma compatibility and the effect on tritium inventory of the armours. Plasma compatibility is a strong concern for the high Z plasma facing material, such as tungsten. However, ASDEX Upgrade (W)⁹² and C-Mod (Mo)⁹³ have provided evidence that high-Z walled devices can operate, at least in certain modes, without plasma contamination, and further evidence should be provided as ASDEX Upgrade increases, in stages, the W coverage of the first wall⁹⁴.

Tritium Inventory

There are concerns over tritium inventory because carbon is considered as a plasma facing material. During D-T operation the co-deposition of tritium with carbon has the potential to trap the entire allowable tritium inventory for ITER-FEAT in a few hundred pulses. Estimates range from 1 to 5 g tritium/pulse⁹⁵, the lower value based on physical sputtering alone, and the higher value including both physical and chemical sputtering. The codeposition rate that may result from Be wall erosion is estimated to be $< 0.5 \text{ g-T/pulse}$. Even though the divertor is designed to allow the strike point of the SOL to be swept across the vertical target in order to release the T trapped during normal operation, unless specific measures are taken the T will be trapped in the private region of the separatrix and the pumping ducts. In an attempt to mitigate this, controlling the temperature of the private region PFCs is being studied and may provide a workable solution. The design proposal is to employ a "hot" liner. To achieve high operating temperatures, it is proposed to use the

⁹¹ M. Merola, et al., Manufacturing and Testing of a Prototypical Divertor Vertical Target for ITER, 9th Int. Conf. on Fusion Reactor Materials, October 10-15, 1999, Colorado Springs, to appear in J. Nucl. Materials. G. Vieider, et al; European Development of Prototypes for ITER High Heat Flux Components, ISFNT-5, Rome, 1999.

A. Makhankov et.al. Development and Optimization of Tungsten Armour Geometry for ITER Divertor. Proceed. of 20 Symposium on Fusion Technology, Marseille, September 1998, p.267-270

R.E.Nygren, et al; "Heat sinks armoured with tungsten rods" ISFNT-5 Rome, Sept. 1999

⁹² Krieger, K., Maier, H., Neu, R., and the ASDEX Upgrade Team, J. Nucl. Mater. **266-269** (1999) 207

⁹³ Greenwald, M., H Mode confinement in Alcator C-MOD, Nuclear Fusion, 37 (1997) 793

⁹⁴ Neu, R., et al., Plasma operation with tungsten tiles at the central column of ASDEX Upgrade, presented at the 14th International PSI Conference, Rosenheim, May 2000, to appear in J. Nucl. Mater.

⁹⁵ G. Federici, et al., Assessment of Erosion and Tritium Codeposition in ITER-FEAT, presented at the 14th International PSI Conference, Rosenheim, May 2000, to appear in J. Nucl. Mater.

radiated power from the divertor channel to heat radiatively cooled, tungsten tiles⁹⁶. These tiles are shaped in such a way as to prevent or minimise line-of-sight from the plasma to the cassette body and to create a labyrinth through which the helium ash, hydrogen isotopes, and other impurities are pumped from the divertor channels, while providing sufficient length for the hydrocarbons entrained in the gas stream to undergo many collisions with the hot surface of the liner.

In support of this design, laboratory experiments have been carried out at the Institute for Physical Chemistry (IPC) in Moscow. These are aimed at understanding the chemistry of carbon deposition on the hot liner and on the cold surfaces of the divertor and vessel beyond the liner. Although, somewhat preliminary and the subject of ongoing further verification, the main conclusions from these studies can be summarised as follows⁹⁷: 1) the 'hot' liner (to be operated in a range of 800-1000°C) converts a large fraction of active radical carbon species impinging onto the surfaces of the private region to stable volatile molecules which are pumped away without residual deposits; 2) the remaining fraction of active radicals, although small has a relatively low sticking coefficient and passes through the liner where it leads to the formation of thin, soft, hydrogenated films on the relatively cold (< 150°C) structures behind the liner. One way of overcoming the deposition of these films is to ensure that the pumping duct behind the liner is kept hot enough ($T > 300^\circ\text{C}$) in order to minimise the sticking of radicals in regions inside the divertor private region. However, in itself this is not enough and an ancillary 'cold' catcher plate must be added to the design, to minimise the formation of tritium-bearing films on cold surfaces downstream of the divertor and all over the vessel. This catcher plate would concentrate active hydrocarbon species escaping through the liner, from where the T could be reclaimed by occasional heating of the catcher to release the T in the form of stable gas molecules, or alternatively by mechanically removing T-bearing flakes to an ex-vessel reclamation facility (e.g. by using a conveyor).. In addition to codeposition on and behind the liner, there will be tritium in the films forming on the surface of the tiles located in the area of net-deposition in the divertor and in the gaps and crevices of the numerous castellations of the plasma-facing components. The deposits on surfaces exposed to the plasma are expected to be recycled, but the films building up in gaps are of concern and need the same attention as those in the private region.

R&D is in progress that will contribute to the to the liner design. IPC experiments use RF and magnetron sources in conjunction with methane, but there are still large uncertainties in the applicability of the results to the ITER divertor. Tests carried out in IPP-Garching⁹⁸ and a test with more relevant plasma chemistry to be carried out in the Berlin Plasma Linear Simulator (PLI), should allow, by the end of 2000, better insights into the functioning of the liner. It is important to determine the sticking coefficients versus temperature of the CH radicals found in the divertor exhaust gas stream. Additionally, possible mixed-material effects need further investigation.

⁹⁶ A. Makhankov, et. al; "Design of a Radiative Semi-transparent Liner for the ITER Divertor Cassette", ISFNT-5 Rome 1999

⁹⁷ I. Arkhipov, et al., to be presented at the 14th International Conference on Plasma Surface Interactions, Rosenheim, Germany, May 22-26, 2000, to appear in J. Nucl. Mater.

⁹⁸ von Keudell, A., et al., *Surface reactions of hydrocarbon-radicals: suppression of the redeposition in fusion experiments via a divertor liner*, presented at the 14th International PSI Conference, Rosenheim, May 2000, to appear in J. Nucl. Mater.

Although it is unreasonable to expect the co-deposition of carbon with tritium to be stopped altogether. However, reduction by one to two orders of magnitude in the rate will reach the anticipated erosion lifetime of the target, when the tritium trapped in the divertor can be reclaimed by baking in the hot cell.

The only methods proven effective for removing tritium so far involve (1) oxidation of the codeposited layers (e.g., thermo-oxidative erosion $> 250^{\circ}\text{C}$, or O plasma discharges) or (2) physical removal. For carbon codeposited films, oxidation rates strongly depend on the microstructure of the layers. Mixing of materials shows that higher temperatures might be required for erosion of the films and release of the retained hydrogenic-species⁹⁹. Therefore, although baking at 240°C may remove soft films, due to the variability of film properties, a baking capability at temperatures greater than 300°C . would be required. However, frequent use of oxygen bakes raises collateral issues of damage on other reactor vessel components, as well as recovery time for normal plasma operation.

Dust and Dust Management

Dust will be composed of Be (first wall), W (divertor) and C (divertor strike point) causing a significant safety problem associated with hazards of chemical explosion (Be and C dust) and radiological contamination (W and C dust). The definition of dust is somewhat uncertain, but particle sizes $< 100\ \mu\text{m}$ can be considered as dust. It is anticipated that the tritium bearing co-deposits will build up on cold surfaces in the divertor and in some areas, these films will become thick enough to detach and produce carbon flakes. These flakes ($> 100\ \mu\text{m}$), although not strictly dust, are likely to dominate the total mass of dust in the divertor.

There is a large uncertainty in the prediction of the production rate of dust for ITER-FEAT, which have been derived from tokamak experience and code simulations. However, the dust may well require routine removal and will in any case require monitoring in order to guarantee that the levels do not breach the specified safety limits. Two in-vessel dust limits are specified. The first limit is for the dust held on hot surfaces, which has the potential to generate hydrogen during an accident when steam is in contact with the dust. Potentially the worst case is for beryllium dust, which has an exothermic and hence, self-sustained reaction with steam. The limit in this case for particles $\ll 10\ \mu\text{m}$, that are highly reactive because of their relatively large surface area, is in the range 10 – 20 kg. The second limit is the overall amount of dust that can be mobilised during an accident and, hence, escape into the environment causing a radiological hazard. This is set at a few hundred kg. Within a machine the scale of ITER-FEAT, with an in-vessel surface well in excess of $1000\ \text{m}^2$, these limits represent values that will be difficult to guarantee.

At first sight the limit of 10 - 20 kg on the hot surfaces appears the hardest to fulfil. It is reasonable to assume that dust cannot exist on the hot surfaces directly exposed to the plasma and so fortunately, the critical reservoirs for 'hot' dust are limited to the grooves of the horizontal surface of the dome, and the divertor baffle. These grooves or castellations in the tungsten armour are an essential feature of the design and must remain in order to relieve stresses during cyclic loading with high heat flux, thus maximising the fatigue lifetime of the armour to heat-sink joint. Initial analysis shows that the volume of dust that can be contained in these grooves is of a similar order to the 'administrative' limit (10 – 20 kg). Hence, the present design of the plasma-facing surfaces is being optimised to minimise dust

⁹⁹ M. Balden, ICFRM-9 – 1999, to appear in J. Nucl. Mater.

accumulation (e.g., by decreasing the number and dimensions of the grooves). If the total quantity of chemically reactive dust on 'hot' PFCs can be maintained below the 'administrative' limit, and the authorities responsible for safety can be convinced of this argument, then there will be no need to have reliable methods to measure accumulation of chemically reactive dust in the grooves. What may help further is that the self-sustainable reactivity of beryllium dust with steam may be inhibited, because steam access is restricted to much of the material confined in the grooves. An R&D activity has been launched to study this possibility.

This leaves the rest of the dust (and flakes), not residing on hot surfaces. The majority of this is expected to collect in and beneath the divertor, and based on the experience gained from existing tokamaks, the majority of this will accumulate beneath the inner vertical target, carried there by a combination of grad B drift and gravity. A cross-section of the divertor shows that there is scope for introducing dust handling systems that can either remove dust on-line or during the interval between pulses. Two separate regions are potentially available for this use within the divertor. Firstly the space between the underside of the divertor cassettes and the vacuum vessel, and secondly, the region between the dome PFC and the cassette body.

An R&D activity has been launched¹⁰⁰ that that has manufactured artificial tokamak dust based on measurements of actual tokamak dust, and this will be used to study the transport of dust during accidents, as well as developing means to extract the dust from the vessel. Within this task the effectiveness of various dust removal methods will be studied, ranging from the global, such as removing dust suspended by gas re-circulation or liquid wash, to the local, such as vibratory conveyors. In addition, it is hoped that, with better knowledge of the behaviour of the dust, the quantity remaining can be lowered to levels that require infrequent interventions.

Conclusions

Bearing in mind all the above, the prudent position remains initially to install carbon as armour on the targets, which is forgiving when exposed to disruptions and is acceptable from a plasma contamination viewpoint, and to maintain the option to switch to a more reactor-relevant all tungsten armoured targets prior to D-T operation, when tritium inventory becomes an issue. The decision to make this change will depend on the progress made in controlling the plasma, in particular, on the frequency and severity of disruptions and, on the other hand, the success achieved in mitigating the effects of T co-deposition.

In addition to replacing the targets, it may be necessary to thoroughly clean the carbon from all in-vessel surfaces, since the residual layers will continue to have the potential to collect T by isotope exchange. Hence, even if carbon is considered only for the H and D phases, methods need to be developed that can adequately remove the carbon deposits. Apart from mechanical methods of removing the carbon deposits, baking in the presence of a partial pressure of oxygen has been shown to be effective in removing the soft hydrogenated carbon layers responsible for retaining most of the tritium. This bake, at a temperature to be better determined, may take many days to be effective, but has the potential to reach all the in-vessel surfaces of the machine and may be worthwhile as a one-off event prior to a switch to all tungsten armour.

¹⁰⁰ Eu report on dust.

In summary, D-T operation with carbon poses many problems and in the end these may prove impractical to overcome, but pending the results of on-going R&D with both carbon and tungsten, carbon remains the armour choice for the strike point region of the vertical targets. Tungsten is the choice for all other plasma facing surfaces of the divertor.

5. Buildings and Plant Services

5.1. Developments in Building/Services Design

TAC has questioned some aspects of the design of the buildings for ITER-FEAT.

- With regard to the tokamak building general layout, there was a general question on the available access for services and vertical distribution, particularly the use of the vertical pipe shafts connecting the upper and lower pipe chases.
 - The concept of combining the tokamak and tritium building onto a common basemat, as was indicated to be a possibility in the ODR.
 - The concept of the diagnostic hall, as its concept and description in the ODR was limited.
- These three concerns are addressed below.

Vertical Access in the Tokamak Building

The ITER-FEAT tokamak building is considerably more compact than it was for 1998 ITER design. The current building measures 69.5 meters from east to west, and 77.8 meters from north to south. The building has been redesigned since the 1998 ITER design, and has more challenges to accommodate all the equipment and services required to make ITER-FEAT functional. A particular challenge was to provide access from the bottom of the vessel to the top, as there would be only one area for the heat transfer system. It was decided early on in the reduced cost study to investigate and, if feasible, adopt the idea of using vertical pipe shafts connecting two donut shaped pipe chases, one at the top and the other at the bottom, of the vacuum vessel. These pipe shafts are located outside the bioshield, so that the radiation fields that the contents are exposed to is minimized. These pipe chases collect and deliver cooling water lines to each port for blanket, divertor, and vacuum vessel cooling, as well as providing for system drainage. The biggest user of these pipe shafts is the heat transfer piping. In addition to the piping, the vertical shafts allow for vertical connections of cryolines, which are required to be in close proximity to the vessel to minimize their costs and layout problems. Further, they can be used for conductors, as in cabling and wiring, where the radiation and insulation properties are compatible. There is some, but limited, access available into these pipe shafts during maintenance, so that components and lines can be inspected, monitored and, if necessary, repaired.

Another function of these vertical pipe shafts is to provide a relatively easy and non-restrictive path for accommodating the pressure rise that results from an ex-vessel LOCA (see section 0). The LOCA overpressure is confined to the upper and lower pipe chases, the TCWS vault, and the NB cell. The vertical pipe shafts connect the upper and lower pipe chases at 18 positions around the machine, making such connections relatively unrestricted and providing relatively uniform pressure distribution in this event. The four vertical pipe shafts (see Figure 5.1-1 (a) and (b)) in the north end of the building on the equatorial level (at ports 3, 4, 5, and 6) have no concrete walls, but open directly to the NB cell. In a similar fashion, the seven vertical pipe shafts (at ports 1,2,3 and 15, 16, 17, and 18) on the east side have no concrete walls, but open directly to the TCWS vault.

In addition to these vertical pipe shafts, the ITER-FEAT tokamak building provides limited vertical communication in the four corners of the building,. At these positions are located the stairways, the personnel lifts, the HVAC duct chase (which is used for other vertical access but is limited by available size).

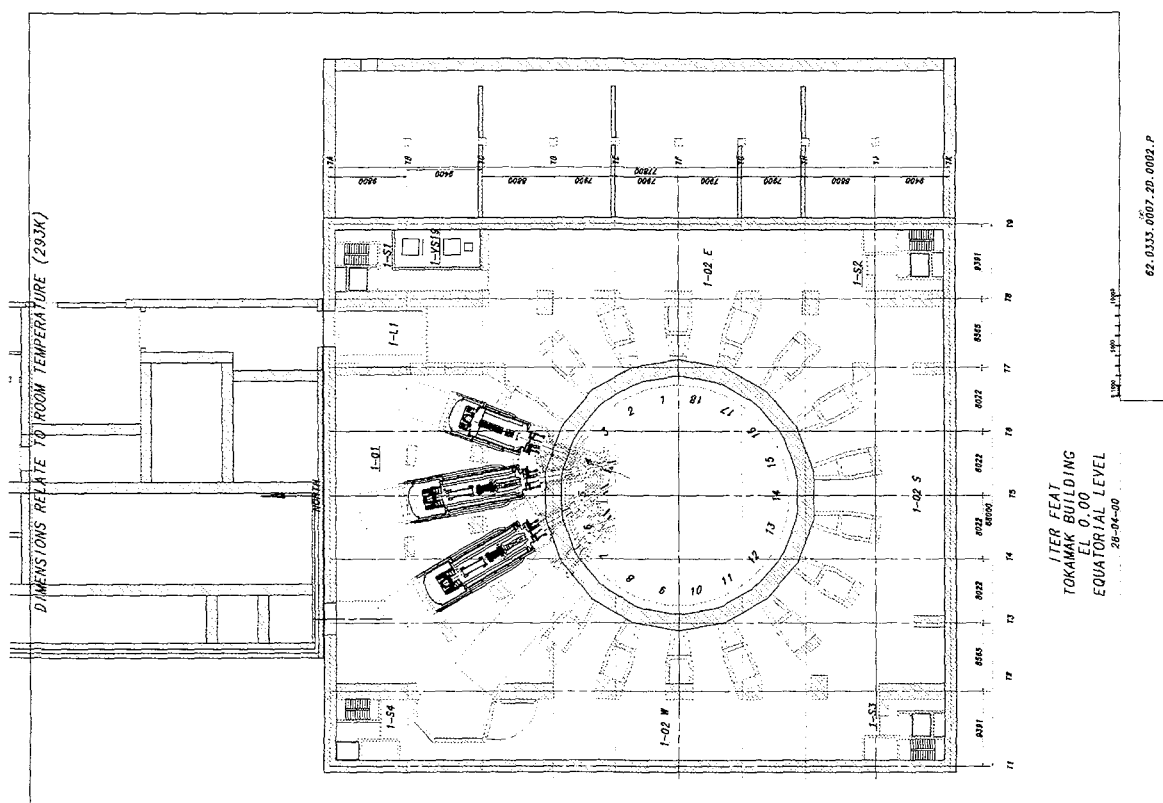


Figure 5.1-1(a) Tokamak Building Floor Plan at Equatorial Port Level Showing Vertical Penetrations.

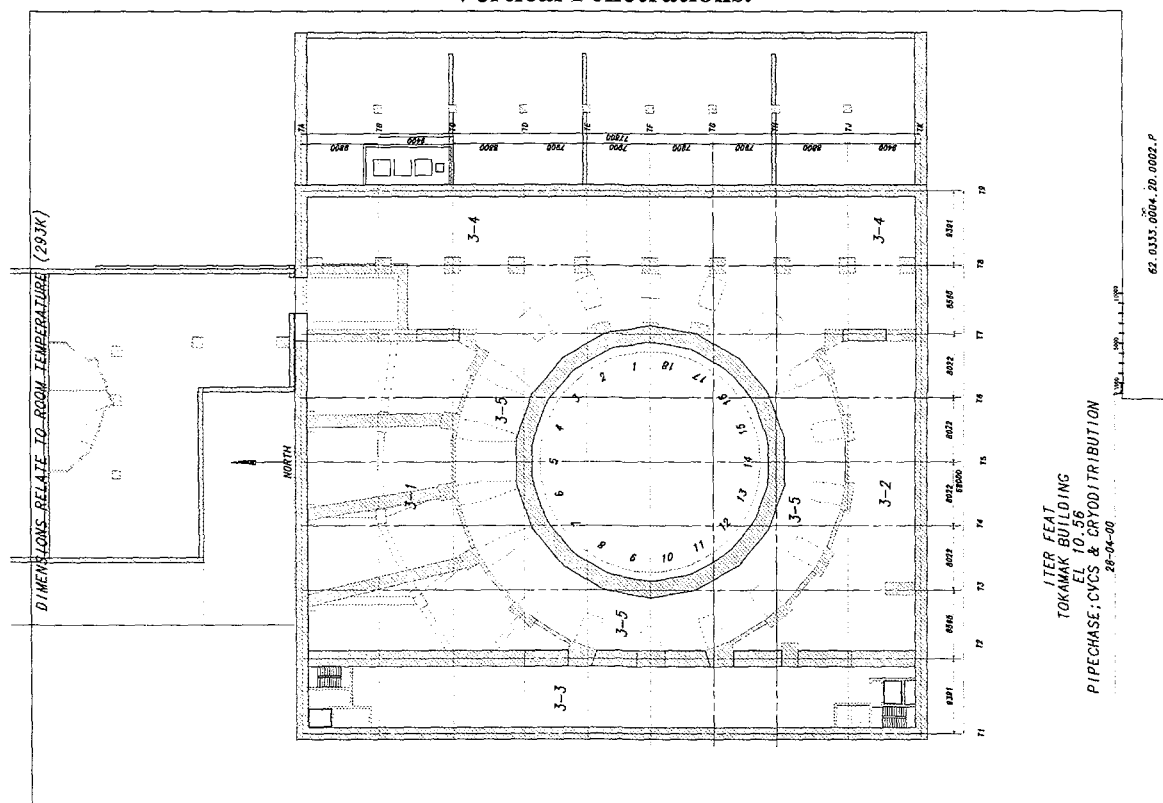


Figure 5.1-1(b) Tokamak Building Floor Plan at the TCWS Level Showing Vertical Penetrations.

These studies have so far not identified any problems and have relieved previous concerns on the ability to achieve the necessary vertical access.

Combined Tokamak and Tritium Building on a Common Basemat

In examining the layout of the tokamak building and the tritium building, and in reviewing the connections that are required between these buildings, it became apparent that there was a significant advantage in locating them on a common basemat. The first reason was safety and in consideration of the seismic event that safety systems and hazardous systems are required to be designed for. Placing the two buildings on a common basemat allows us to ignore the "seismic gap" that would otherwise be required between such buildings to allow for insertion of sufficient length of flexible connections such that they would survive the design basis earthquake. This gap would have to be of the order of 500 mm to 1500 mm, depending on the nature of the connecting components, whether it was a small diameter pipe, a large HVAC or VDS duct, or cables or power supplies. Further, once the combined building is on a common basemat, there is much more flexibility in the design of the tokamak building services, especially the HVAC and various detritiation systems, and it allows for expansion of tokamak building-related services where required. Also, a common basemat reduces the complexity of analyzing the structures.

This feature is shown in Figure 5.1-2.

Diagnostic Hall

In a continuing effort to simplify and combine functions of buildings and to minimize costs, the Diagnostic Hall has been added to the west side of the tokamak building. The diagnostic hall is 20 m by 63 meters, and has a number of floors dedicated to diagnostic instrumentation and cubicles. In addition, the building also houses the TF coil fast discharge resistors and capacitors, and also serves as the electrical busbar feed to the tokamak building. Figure 5.1-3 show the proposed layout of the diagnostic hall. There is ample room in this building for air conditioning units as well as for load centres. The main components of the diagnostic hall are the diagnostic instrumentation, and these are tied to the tokamak building as shown in the following figure.



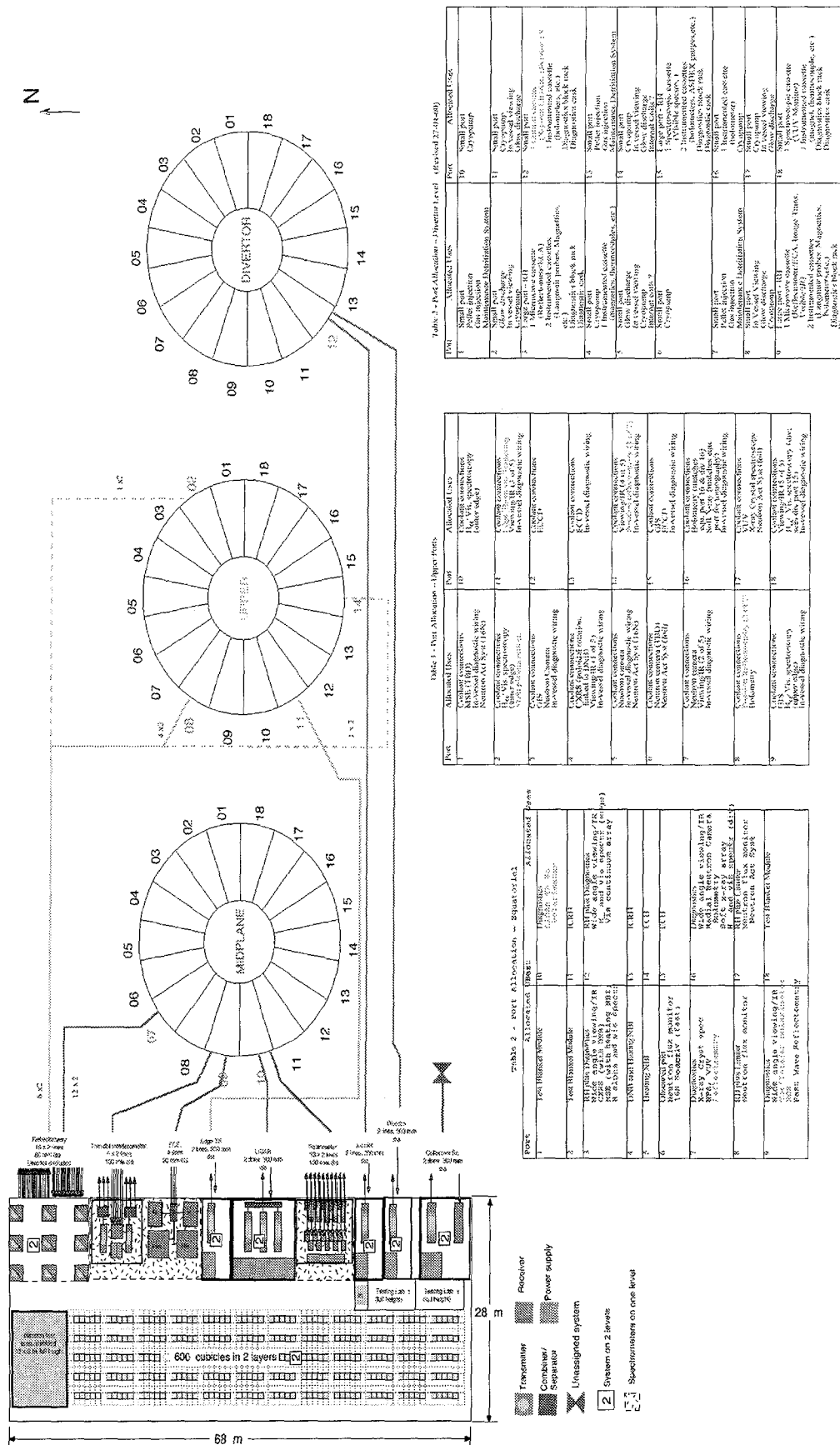


Figure 5.1-3 Diagnostic Hall Showing Links to Tokamak Building

5.2. Hot Cell Building

5.2.1. Building Size and Layout Requirements

The rationale for the conceptual hot cell building layout and size (Figure 5.2-1, 5.2-2 and 5.2-3) are determined by the maintenance requirements and by a few main design features which have evolved from a number of studies and reviews which particularly aimed at simplification of the remote processes. The main features and requirements for space are given below:

- (a) hot cell arrangement on one (ground) level;
- (b) in-line (i.e. during maintenance shutdown) repair and refurbishment concept (assumption for the present layout);
- (c) common in-vessel component refurbishment area is used instead of dedicated hot cells;
- (d) common in-vessel component storage is used instead of dedicated cells;
- (e) common radioactive waste processing and storage area is used instead of dedicated cells;
- (f) common repair/test area for all diagnostic and RF heating port plugs including interspace blocks;
- (g) component receiving/dust cleaning cell with required three docking ports that, together with current dimensions of transfer casks, determine the size of hot cell transportation/docking area;
- (h) RH tool exchange holding and repair/storage area;
- (i) RH equipment test stand and transfer cask storage area on top of the hot cell building;
- (j) new parts and components receiving and storage area;
- (k) cranes/manipulators and transportation devices retraction/maintenance space;
- (l) ADS/VDS/HVAC space (see below);
- (m) load center area for services such as lighting and power supply;
- (n) biological shielding, air locks, access and escape routes for personnel.

The sizing of the hot cell receiving room, processing room and storage space is based on meeting the requirements for maximum allowable maintenance duration. The sizing of the hot cell receiving room is based on unloading and loading of three casks during the same shift. The process room size is based on simultaneous refurbishment of one divertor cassette and one blanket module. In parallel, port plugs can be refurbished and tested by insertion in special port interfaces. The storage space is based on simultaneous storage of 24 blanket modules, 16 divertor cassettes and 6 port plugs. The detailed refurbishment procedures and the necessary RH equipment are still under detailed study. It may therefore be expected that further design optimization will be applied.

Most of the other room sizes are a logical consequence of their functional requirements, i.e., space needed for casks to maneuvering, space for equipment, e.g., HVAC, etc.

The wall thickness is based on the shielding and structural requirements. The current maximum thickness of 1.35 cm (normal concrete of 2.35 g/cm³ density) for the walls that

separate access zone D from access zone B was defined for the 1998 ITER design¹⁰¹, and need to be checked for ITER-FEAT.

5.2.2. ADS/VDS Requirements

The required hot cell ADS capacity is based on in-vessel component tritium release rate and derived air concentration (DAC) within the hot cells. Based on the tritium release rate best estimate of 6 TBq/hr (3 TBq/hr for the divertor and 3 TBq/hr for the other in-vessel components) of the "cold" torus with some dust and co-deposited tritium cleaning, it was found that the tritium off-gassing rate per cassette is 1.5 Ci/hr and ~ 0.2 Ci/hr per blanket module.

Taking into account the tokamak maintenance logistic design study, no more than 11 divertor cassettes can be within the hot cells at the same time, giving a tritium out-gassing rate of 16.5 Ci/hr. There also could be two port plugs or 6 blanket modules at the same time, giving an additional 1.2 Ci/hr. In total the tritium out-gassing rate within the hot cells (receiving, storage, refurbishment, waste processing) is ~18 Ci/hr as basis value for ADS capacity calculation. The ADS design capacity of 4500 m³/hr provides a DAC value of 500.

A VDS design capacity of 500 m³/hr is proposed based on a 100% volume/day in-leakage rate for all rooms of the hot cell building. A normal VDS capacity of 316 m³/hr is determined by 100% volume/day air in-leakage rate for the 4 zone D hot cells and their total volume of 7630 m³.

The standby VDS capacity depends on the following scenarios:

1. accidental tritium release,
2. work with temporary localized secondary enclosures,
3. purge and detritiation of contaminated equipment.

The standby VDS capacity of 160 m³/hr was calculated based on 100% volume/day air in-leakage rate and the volume of 4 zone B rooms which may simultaneously require VDS.

5.2.3. Dose and Dust Requirements

The expected surface contact dose levels of tokamak components stored within the storage cell, are listed in Table 5.2-1 (1998 ITER design):

¹⁰¹ "Hot Cell Building Shielding Criteria." ITER Task D230-C5. January 1996. IBERTEF.

Table 5.2-1. Hot Cell Component Surface Contact Dose Levels
(Dose in Sv/h)

Component	Time After Shutdown			
	30 days	90 days	150 days	1 year
Limiter Module	1.4E+03	9.2E+02	6.6E+02	3.1E+02
IBB Module	9.5E+02	6.2E+02	4.4E+02	2.1E+02
OBB Module	1.4E+03	9.2E+02	6.6E+02	3.1E+02
Divertor Body & Dome	9.5E+02	6.2E+02	4.4E+02	2.1E+02
Divertor HHFC Stainless Steel	9.5E+02	6.2E+02	4.4E+02	2.1E+02
Divertor HHFC Copper	4.1E+02	3.6E+02	3.3E+02	2.7E+02
Divertor HHFC Tungsten	2.0E+02	1.4E+02	9.4E+01	2.8E+02

Even though the tokamak will include provisions for dust removal, it is assumed that considerable amounts of dust on components (mainly divertor cassettes) can be delivered to the hot cell area. Therefore, the receiving cell fulfils a double function as component cleaning facility, in order to minimize the amount of activated dust inside the hot cell processing and storage areas.

5.2.4. Design Outline

The HCB is organized on two main levels, with the main hot cell functions on the ground floor, include in-vessel component docking, dust cleaning, storage, repair/testing, remote handling (RH) tools exchange/ maintenance, waste processing and waste storage/shipping, and new parts/ components receiving/storage. Upper level functions include RH equipment test, transfer casks storage, atmosphere confinement control and atmosphere detritiation equipment.

The hot cell building is available during the initial installation phase of the tokamak in-vessel components to provide a pre-assembly, Be-controlled area and a facility for loading components into transfer casks.

The hot cell building is designed such that it can be expanded to meet future increased processing capacity needs, e.g., for the decommissioning phase of ITER.

Port plugs requiring refurbishment will not normally be off-loaded into the HC receiving cell but instead be installed inside the special docking ports, to allow remote refurbishment from inside the HC and hands-on maintenance at the front side of the plug, including functional testing, if required.

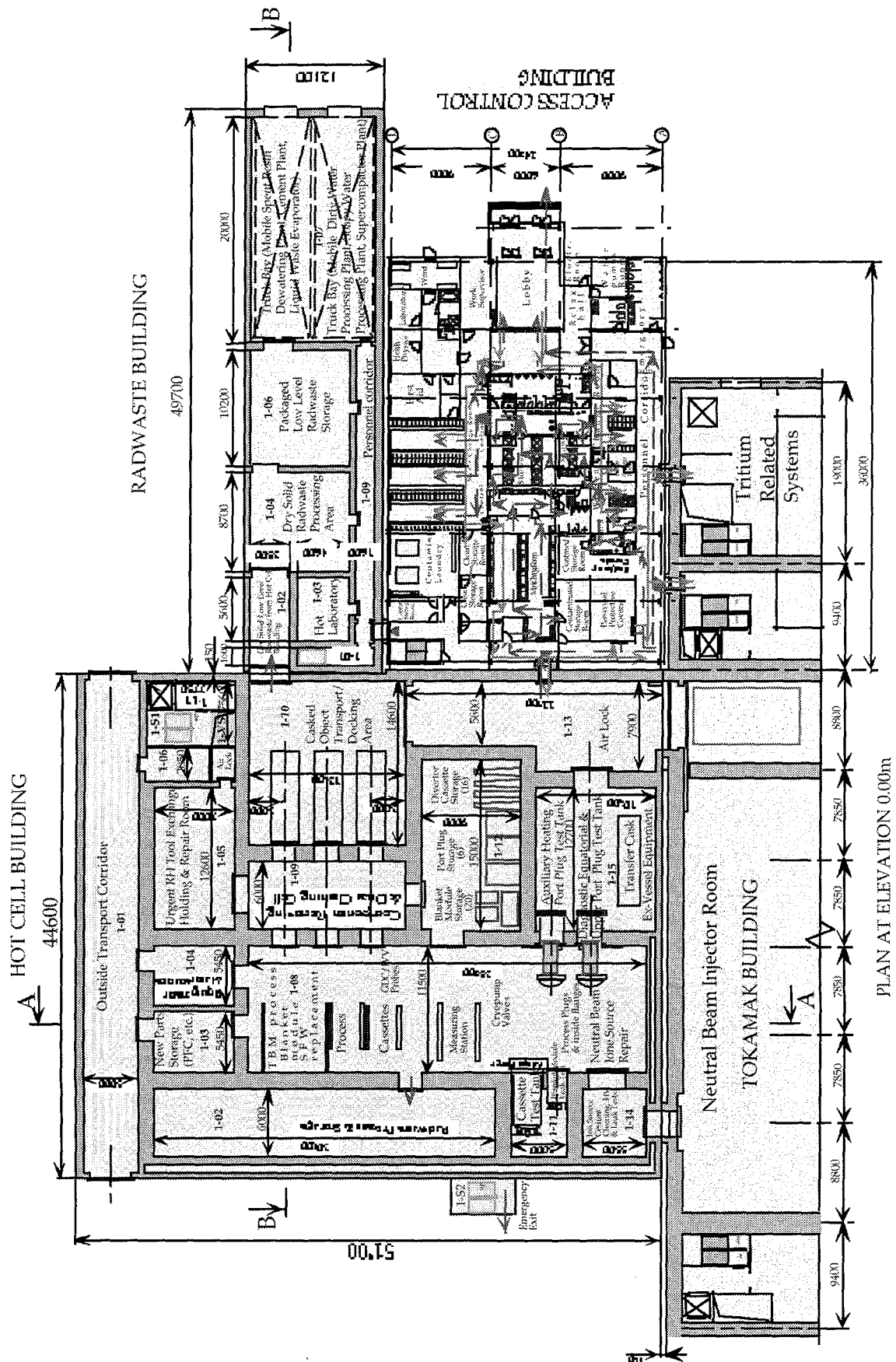


Figure 5.2-1 Hot Cell Building Ground Floor Plan

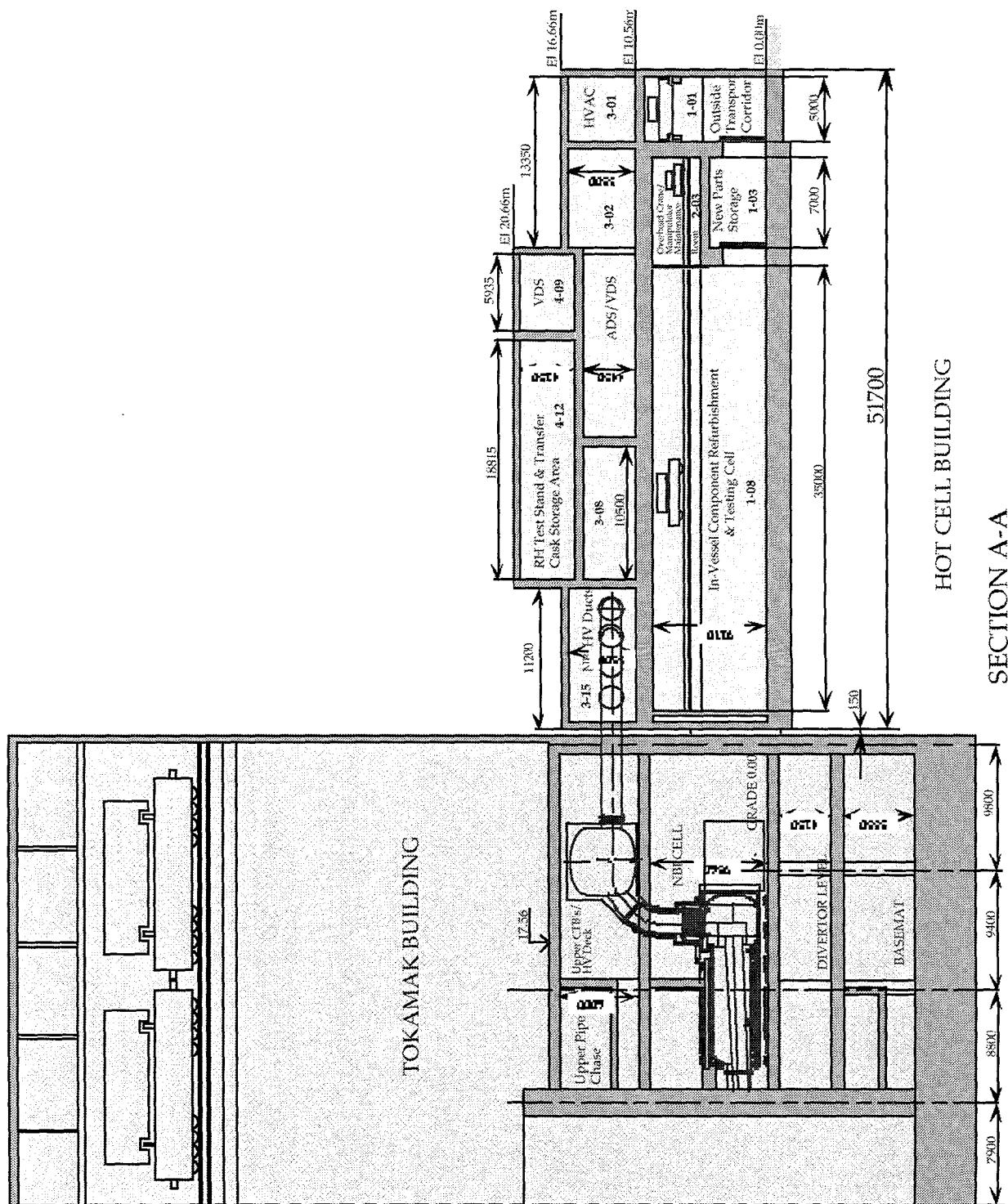


Figure 5.2-2 Hot Cell Building Horizontal Section AA in Figure 5.2-1

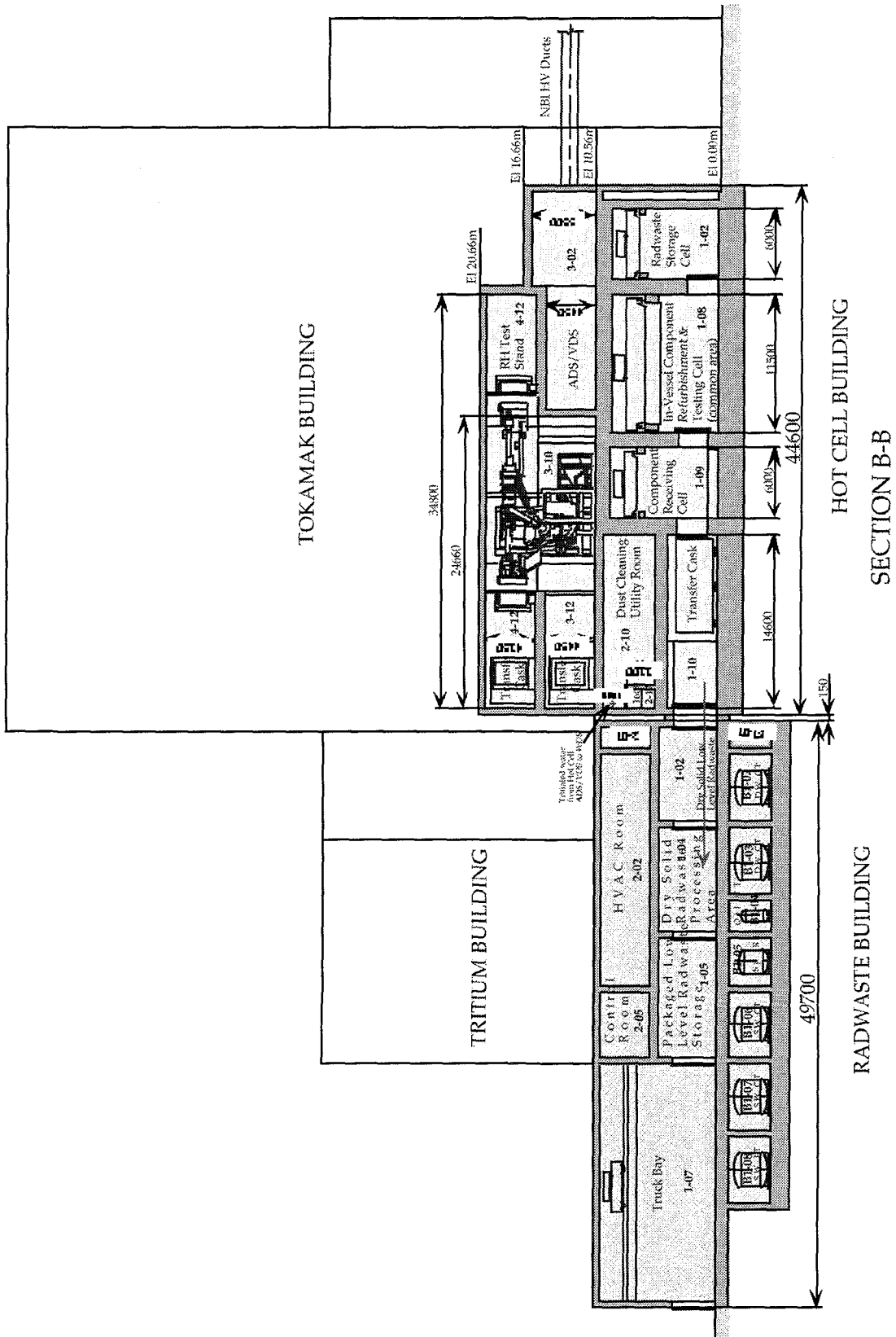


Figure 5.2-3 Hot Cell Building Vertical section BB in Figure 5.2-1

5.2.5. Hot Cell Docking and Storage System

The hot cell docking and storage system consists of six major subsystems as described below.

Docking Sub-System

The cask transportation system provides the passage of transfer casks from the tokamak building to the hot cell docking ports and provides the appropriate rotations of the transfer casks in the docking area (transport corridor). The docking ports, which have identical double-seal door systems to the corresponding docking ports in the tokamak pit, provide hermetical connection of the transfer casks to the receiving cell. The receiving cell with three docking ports connects to three cells, namely: in-vessel component storage cell, in-vessel component repair/ refurbishment cell, and urgent remote handling tools exchange holding and repair cell. Within the receiving cell, dust cleaning operations for all received objects are carried out.

The docking ports have exchangeable docking adapters, which enable a port to receive different types of tokamak components (except a NB ion source) during a maintenance campaign. There is a dedicated docking port for the NB ion source transfer cask. Direct-access docking from inside the tokamak NB cell is available for maintenance operations on NB ion sources, should this be required.

Dust Cleaning Sub-System

This sub-system provides the clean up of dust on components and RH tools delivered by transfer casks from the tokamak to the receiving cell. Although the tokamak will include provisions for dust removal, it is assumed that dust on components (mainly divertor cassettes) can be delivered to the hot cell area. To prevent contamination from spreading, dust is thoroughly removed from components. The dust recovered by the primary collector is enclosed in the dust canister. The cap of the canister is equipped with a porous sintered metal filter to enable baking the canister for further detritiation, should this be required.

Nitrogen Purge Sub-System

After transfer cask undocking, the atmosphere in the transfer cask must be purged with nitrogen.

Storage Sub-System

The sub-system acts as a buffer between tokamak remote maintenance operations and hot cell repair/waste operations. Objects such as divertor cassettes are withdrawn from the tokamak and then delivered to the hot cell storage sub-system, which places them into storage locations before repair/waste processing. All transportation and storage functions are performed remotely within shielded cells in the hot cell building.

In order to support the process operations a storage cell is provided. This storage cell is dedicated to in-vessel components, which are expected to be changed several times during the life of the ITER plant.

Remote Handling Tool Storage/Repair Sub-System

A storage cell is provided for urgent RH tools, which are immediately needed for exchanging without undocking the transfer cask from the receiving cell during a tokamak maintenance campaign. Rotation of the RH tools within this cell corresponds to the operational sequence of the object replacement schedule.

After dust cleaning of RH tools (if needed) inside the receiving cell, the repair activities within the RH tool storage/repair cell can be carried out by "hands-on" procedures. Access for workers into this cell could be provided through an air-lock.

Control, interlock and monitoring

All hot cell systems and equipment status, as well as environmental conditions and interlock system status are provided to the supervisory control system.

5.2.6. Hot Cell Repair/Testing System

The hot cell repair/testing system processes components which have become activated by neutron exposure and/or contaminated with tritium or activated dust particles and which have been removed from the tokamak for repair or refurbishment and testing prior to return to service. Remote handling tools and equipment, which are used for removal /installation of tokamak components are also repaired and returned to service.

The processing includes examination, preparation of service plans, preparation of samples for material evaluation, evaluation and segregation of parts into those which can be reused and those which must be replaced, disassembly, replacement of parts, re-assembly, and inspection/testing. Components, which enter the system for repair, may be diverted, following evaluation, to the hot cell waste processing system. The system includes equipment for monitoring and control of all repair/testing operations.

The system comprises the following processing stations and system elements:

- 1) Divertor cassettes plasma facing components (PFCs) replacement workstation
- 2) Blanket module separable first wall (SFW) replacement workstation
- 3) Equatorial and upper port plugs repair/test tanks (ICH&CD, ECH&CD and diagnostic plugs)
- 4) Cryopump valves repair
- 5) NB ion source repair/testing
- 6) Two testing tanks for divertor cassettes and blanket modules, respectively
- 7) New parts/sub-components storage room
- 8) Transporters
- 9) Equipment maintenance facility

5.2.7. Hot Cell Waste Processing and Storage System

The hot cell waste processing and storage system processes and stores solid radioactive materials which have been removed from the tokamak and which will be discarded. The hot

cell waste processing and storage system is designed to process discarded tokamak materials, which have become activated by neutrons, and/or contaminated with dust/tritium.

Waste processing includes disassembly, cutting, preparation of samples for material evaluation, containerization of radwaste, and recovery of tritium from plasma-facing components and T-contaminated dust, if required. The hot cell waste processing and storage system provides up to 2 months storage of radioactive waste. The specific waste processing and storage operations are determined by the nature of the component, its state of degradation, the extent and nature of its radioactivity, the level of tritium contamination, and the host country regulations for processing and packaging radwaste for final disposal.

5.2.8. Hot Cell Radioactivity and Toxic Material Control System

The hot cell radioactivity and toxic material control system provides high level radiation shielding, as well as airborne tritium and radioactive/toxic dust confinement. The necessity to address tritium and toxic Be dust distinguishes the ITER hot cell from most other hot cells.

Three access control zones are utilized, which regulate access according to exposure conditions and contamination levels. The hot cell atmosphere is controlled by dividing the work areas into ventilation groups according to the hazard level of airborne tritium. Assignment of work areas to specific ventilation groups is based on the DAC of HTO. Areas with the highest tritium levels are assigned the lowest room pressure, so that the leakage is always from lower to higher tritium concentrations.

To minimize tritiated water generation from air in-leakage, low humidity (dried) air is circulated through the air spaces around the hot cells. Thus, only dry air is subject to inleakage. In this way the generation of tritiated water is minimised.

Tritiated water is transferred from the hot cell atmosphere detritiation system (ADS) and vent detritiation system (VDS) into the water detritiation system (WDS) of the tritium building.

6. Operation

6.1. Limits to Pulse Length

The ITER-FEAT pulse length is limited by:

- 1) the available inductive flux or current drive power installed;
- 2) the number of torus cryopumps installed;
- 3) the heat rejection capacity of the site cooling water system;
- 4) the processing capability of the tritium plant.

In the design of the TF conductor, nuclear heating has been considered as a steady state heat load. Therefore, the TF coils are compatible with steady state operation at 15 MA without any modification of the cooling conditions.

For cooling water equipment, the critical system is the heat rejection system, e.g. the basin size and cooling tower capacity. The other systems have no limitation because they have full steady state capacity for a fusion power of 500 MW plus 100 MW of additional heating.

The cooling tower design considers the temperature levelling effect in the hot basin and is sized for the maximum allowable temperature in the hot basin with a flat top of 500 s and the worst atmospheric conditions (highest air temperature and humidity). Any increase in pulse length leads therefore to a higher temperature in the cold basin which feeds the tokamak components.

The temperature levelling effect in the basins and the cooling tower characteristics under the worse air condition and cooler condition has been evaluated¹⁰². The allowable pulse duration with 500 MW of fusion power and 100 MW of additional heating power, in the case of the worst atmospheric (nominal) conditions, are:

- ~2000 s in the case of full mixing in the hot basin only;
- ~4000 s in the case of full mixing in both hot and cold basins.

Full mixing may require additional investment.

In the case that the air temperature is lower than 26.1 °C (winter case), studies¹⁰³ have shown that an infinite pulse duration can be accommodated.

For the T-plant, the design scenario assumed was that the 6 cryopumps would pump all exhaust gas throughout the full pulse length (~ 450 s) and be sequentially regenerated during the dwell time. The processing capacity of the T-plant could therefore be limited to approximately 30% of the fuelling rate. This has considerable cost advantages and reduces the loop inventory. The storage onto cryopumps is limited by the total inventory in the VV as well as by the deflagration limit of the hydrogen stored on cryopumps. The latter limit is generally reached before the former. Increasing the burn time significantly beyond the inductive limit, requires the regeneration of pumps during plasma operation, and the installation of 10 pumps so that some may be under regeneration during the burn.

There are two ways, or a mix of the two, to upgrade the T-plant for long pulse operation.

¹⁰² Technical basis for the ITER-FEAT Outline Design Report G A0 RI 2 00-01-18 R1.0 Chapter II.5

¹⁰³ Y. Kataoka, "Cooling tower design and operable duration under steady state condition"

- (i) Increase the processing capacity to allow full steady state operation. Using simple engineering cost scaling factors, this would roughly double the cost of the front-end permeators, impurity processing and isotope separation system (ISS). Moreover, it would also significantly increase the inventory in the loop, particularly in the ISS.
- (ii) Replace intermediate storage on cryopumps with intermediate storage on hydride beds. This would require an increase in the capacity of the front-end permeator and the addition of some 10 (or more) hydride beds. The exact number of additional beds depends on a number of factors that are under study. This upgrade would also significantly increase the tritium inventory in the fuel cycle loop.

Method (ii) can, in principle, be added at a later stage to the plant. It is likely to be cheaper than (i), but this needs confirmation. The main drawback of method (ii) is that the unloading of the hydride beds used for interim storage of the tokamak exhaust, after passing through the front-end permeator, and preparations for reloading, take considerable time, and requires the processing of the large batch of exhaust gas with up to ~780 g of tritium. Therefore, if long pulse operation should be envisaged as routine operation or as a frequently used scenario, method (i) would be the natural choice.

6.2. Limits to Fusion Power

The TF coils can tolerate, in steady state conditions, the nuclear heating associated with the 17 MA scenario by increasing the cryogen mass flow rate in the conductors from 8 to 10 g/s.

The cryoplant can accommodate steady state operation with a fusion power of 700 MW. This assessment is based on the current values of the heat loads.

When a larger fusion power, but with much shorter burn time (typically 100 s), is considered, a proper transient thermohydraulic analysis is required. In this analysis, the heat capacity of the TF coil metal parts (case, radial plate) plays a role to limit the rate of rise of the conductor temperature, and the electrical insulation layers (turn and ground) act as thermal barriers to slow down the diffusion of heat into the conductor. Requirements on mass flow rates are expected to be reduced as compared to those found for steady state conditions.

For the ex-vessel portion of the water cooling system, the maximum pulse duration with 700 MW of fusion power has been evaluated¹⁰⁴. The maximum pulse duration is limited by the allowable maximum inlet temperature for the in-vessel components. The higher fusion power results in an increase of the inlet temperature due to the mismatch between the heat load and the heat which can be rejected through the heat exchanger.

The results show that the allowable pulse duration varies between ~60 s (nominal case) and ~260 s (winter case). From these results, it is concluded that ~700 MW is the maximum power when a pulse duration longer than 100 s is required.

¹⁰⁴ Y. Kataoka, "Study on allowable duration of high-beta operation for heat removal systems"

7. Safety

7.1. Methodological Improvements

In December 1999 the TAC recommended that:

"comprehensive and integrated safety assessments should be conducted in future to be consistent with the detailed design work, with particular attention paid to the licensability of ITER/FEAT. Further refinement on the estimation of source terms arising from the radioactive inventory is to be encouraged in order to characterise the nuclear aspects of ITER and improve the safety and licensing process in the Parties"

If the releasable inventory can be kept below a value such that dose limits in a Host Country are not exceeded even if the entire amount is released, it is expected that the licensing process will be simplified because the details of the accident sequence become much less important in demonstrating that dose limits are met. Tritium and in-vessel dust inventories were reviewed at the Point Design Meeting (Naka, February 2000). Aggressive targets for tritium inventories for in-vessel and the fuel cycle were set (subject to confirmation of feasibility) based on a review of Japanese and Canadian dose limits and typical site characteristics.

Tritium Inventory Guidelines

Tritium Inventory	Guideline
Maximum mobilisable inventory within the vacuum vessel [g]	≤ 450 (working guideline subject to confirmation of feasibility)
Maximum mobilisable inventory in the pumping and fuelling systems and the tritium plant [g]	≤ 450 (working guideline subject to confirmation of feasibility)
Long-term storage [g]	≤ 450 per independent storage area
Maximum mobilisable in hot cell [g]	≤ 250

Key issues of in-vessel dust and tritium removal and monitoring are addressed in section 4.3.

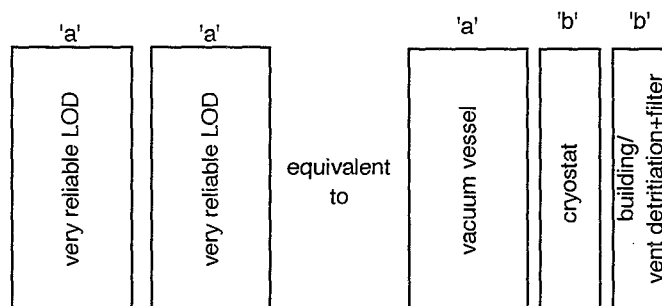
The extensive analysis base available in NSSR-2 is being used to improve the implementation of safety in the design. Specifically, the confinement approach is being reviewed and refined to obtain a balance of safety requirements imposed on the systems with confinement functions. Safety-related specifications for a system or component comprise two parts:

- minimum performance specifications assumed in the safety analyses (e.g. leak tightness, detritiation efficiency, heat removal capacity, etc.)
- level of assurance, reliability, or degree of confidence required from the system or component to be consistent with the assumptions in the safety analyses.

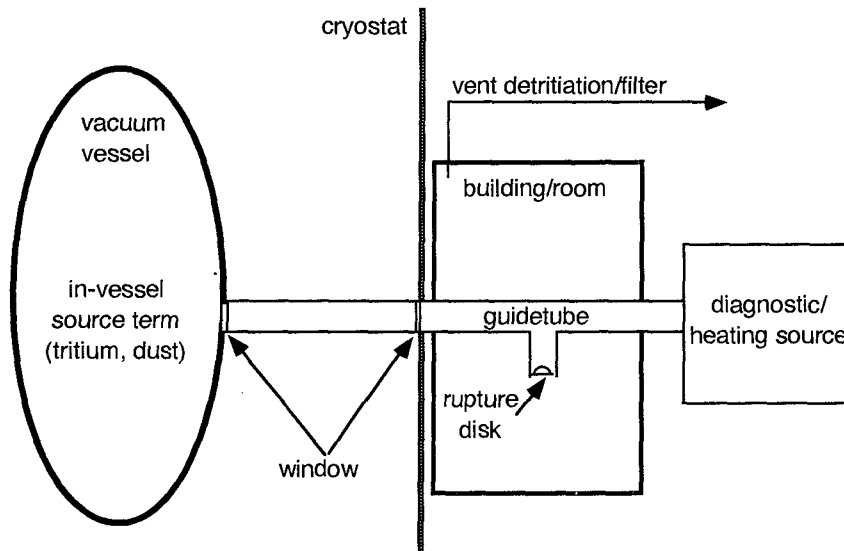
An initial set of minimum performance specifications have been developed in the Plant Safety Requirements. It is expected that as the design progresses and the ITER-FEAT safety analysis results become available, there will be changes in specifications.

The pre-1998 ITER safety design approach used the idea of "two strong barriers" for confinement and placed nearly equal weight on all safety functions (i.e. confinement, heat removal, control of chemical energy, control of magnetic energy, control of coolant enthalpy, etc.). For ITER-FEAT, having the detailed results from NSSR-2 available as background, the safety design focuses on confinement as THE safety function; the others being recognised as required to protect confinement barriers. A "lines-of-defence" (LOD) methodology is being used to provide the initial identification of systems providing confinement. The benefit of the LOD approach is that it provides a systematic method to obtain the required level of safety while balancing the requirements imposed on systems and components. The number and characteristics of an approach depends upon the inventory at risk. Two types of lines of defence and an equivalence rule are considered.

- A **very reliable LOD** (type 'a') results from robustness, redundancy, conservatism, and inherent or passive features. These lines of defence would be analogous to systems characterised by an unavailability of less than 10^{-3} - 10^{-4} per demand or by a failure rate (or occurrence rate) less than 10^{-3} - 10^{-4} per year.
- A **reliable LOD** (type 'b') does not have the same degree of conservatism that is characteristic of a type 'a' LOD. These lines of defence would be analogous to systems characterised by an unavailability of less than 10^{-1} - 10^{-2} per demand or by a failure rate (or occurrence rate) less than 10^{-1} - 10^{-2} per year.
- Multiple, diverse/independent type 'b' LODs can be considered equivalent to a type 'a' LOD if their combined reliability is consistent with the reliability of a type 'a' LOD.



The general confinement approach being implemented for systems that penetrate the vacuum vessel and cryostat, such as diagnostics, is to provide a pair of windows or isolation valves (e.g. windows are considered a type 'b' line of defence) capable of withstanding the pressures, temperatures, forces, radiation conditions, etc., and a means (e.g. rupture disk or perforated wave guide) to ensure venting into a room where the discharge can be filtered, detritiated and monitored, in the case of an in-vessel accident with failure of the windows. A system by system review is being carried out by the safety group and designers to ensure an acceptable design.



7.2. Design Changes due to Safety Considerations

As noted in the Outline Design Report, detailed analysis of the design is needed to clarify the conditions under which the technical need for a stack for ITER-FEAT can be avoided. The dependence on a high stack may reduce the safety attractiveness of ITER-FEAT for siting and fusion in general. For NSSR-2 it was assumed that a 100 m stack existed in determining the appropriate release guidelines to use as acceptance criteria. In all but a couple of accident sequences, releases were orders of magnitude below release guidelines. If inventories are kept to reasonable values or reduced (as noted in section 7.1), confinement improvements are implemented to avoid or mitigate "bypass events" (as noted in section 7.1), and estimates of operational losses are reduced (in progress), then a tall stack is not needed to meet project release guidelines. A controlled, monitored release point is still needed, and the height could be increased if needed for Host Country licensing.

The TCWS vault, pipe chases to the vault, and the NB cell provide part of the confinement barrier for the in-vessel and TCWS source terms. The TCWS vault and NB cell are designed to be leaktight and withstand pressures following coolant spills. Exhaust from these areas can be treated by filters and detritiation systems and is directed to the monitored plant exhaust.

It is only during pulsed operation of the plasma (coolant temperatures $\sim 150^{\circ}\text{C}$) that an ex-vessel LOCA can lead to in-vessel failures and hence potentially release the in-vessel source term (tritium, dust) into the TCWS vaults. The stainless steel piping used in the TCWS piping is ductile, and incipient failures will be revealed by leaks before any crack reaches a critical crack size. For such materials and with a reasonable leak detection system, double-ended guillotine failures can be considered "hypothetical events". Nonetheless, the TCWS vault and its connected volumes can also confine the pressure caused by any pipe failure during plasma operation up to and including a double-ended guillotine rupture. A pressure of ~ 200 kPa(a) is adequate to confine such a release with a margin to allow for computational uncertainty. In addition, the TCWS vaults are designed to confine the pressures resulting from a leak in the TCWS piping under any foreseen operating conditions. Due to the higher

temperatures, a leak during machine baking conditions (coolant temperatures $\sim 240^{\circ}\text{C}$) is limiting. A pressure of ~ 200 kPa(a) is also adequate to confine such a leak.

In assessing the ultimate safety margins of ITER-FEAT, "cliff edge effects", where the consequences increase significantly if some parameter increases, should be avoided. In the case of the TCWS vault, a failure of the vault due to overpressure is avoided by having the pressure relieved by blow out panels to the environment. The releases would be limited to tritium and activated corrosion products (ACP) in the TCWS loop which are below Category IV (Extremely Unlikely Event) release guidelines.

This approach of confining breaks even up to double-ended guillotine failures during plasma operation adds margin to the design and decreases the importance to public safety of being able to correctly predict critical crack sizes and leak rates and of having a sensitive leak detection system capable of working under transient conditions such as during a pulse.

An important issue for water-cooled plasma-facing components with beryllium is the beryllium steam reaction that can occur during accidents when there is an ingress of coolant into the vacuum vessel. This reaction is exothermic and leads to production of hydrogen. The approach in ITER-FEAT is to limit the potential production of hydrogen by controlling the amount of reactive dust on hot surfaces and limiting long term temperatures under accident conditions. Of particular concern is the consequence of a problem with heat removal from plasma facing components while the plasma continues. To mitigate the potential for Be-steam reactions after ex-vessel loss of cooling accident a design study will be done with the objective to develop pockets of liquids (e.g. water) which will burst into the plasma chamber at high temperature (about 400°C) and terminate the plasma burn. The estimated water amount needed in these pockets is a few cm^3 . The pockets will be in the shadow of the plasma about 5-10 cm away from the first wall surface. Two pockets will be installed per cooling loop (preferably on equatorial modules), i.e. a total of 6 modules will be equipped with these pockets. If successfully developed, the need for safety credit of the fusion power shutdown system may vanish.

7.3. Safety Assessment

The initial assignment of Safety Importance Classification (SIC) to all ITER-FEAT systems and components has been completed taking into account issues identified in the 1998 ITER design and safety assessment, and the above methodology. The implications of an assigned Safety Importance Classification in terms of design, fabrication, testing, operation, etc. is also being addressed in more detail. The assignment of Safety Importance Classification, and implementation in the design, is being refined as the design progresses and ITER-FEAT safety analysis becomes available.

The Generic Site Safety Report (GSSR) will document the safety assessment of ITER-FEAT, and it will follow the structure and content of the previous Non-Site-Specific Safety Report (NSSR-2) produced for the 1998 ITER design:

Volume I	Safety Approach
Volume II	Safety Design
Volume III	Radiological and Energy Source Terms
Volume IV	Normal Operation
Volume V	Radioactive Materials and Waste

Volume VI	Occupational Safety
Volume VII	Analysis of Reference Events
Volume VIII	Ultimate Safety Margins
Volume IX	External Hazards Assessment
Volume X	Sequence Analysis
Volume XI	Safety Models and Codes

In addition to providing evidence to the Parties that the design of ITER is sound, the GSSR is intended to assist potential Host Countries in the preparation of regulatory submissions for siting. Regulatory submissions must be prepared by experts from the Host Country familiar with the regulatory requirements and regulator's expectations. At this stage in the Project, the GSSR can support siting decisions, but further design detail and Host-Country-specific safety assessments are likely to be needed to obtain regulatory approval for construction.

At the Technical Meeting on Safety and Environment held in Garching, February 2000, the contents of GSSR, and in particular, changes from NSSR-2, were reviewed and agreed with Home Team safety experts, including representatives from Japan and Canada who are in discussions with their regulators about licensing ITER. The detailed contents of each volume were discussed, and the tasks to provide the underlying analysis agreed by the JCT and Home Teams. In particular, the extent of update needed for the sequence analysis, the set of reference events, and the scope of analysis for ultimate safety margins, were agreed upon.

Maintaining consistency between the evolving design and the safety assessments is facilitated through the use of bounding assessments to accommodate design evolution and the use of a Safety Analysis Data List and Analysis Specifications for each volume used by all contributors to GSSR. These will be updated periodically to reflect the latest safety-relevant design parameters. This approach was proven successful in producing NSSR-2.